



VNIVERSITATĪ DE VALÈNCIA

Facultad de Química

Departamento de Química Analítica

Doctoral Programme in Chemistry (R.D. 1999/2011)

Enantioseparations with polysaccharide-based chiral stationary phases in HPLC. Application to the enantioselective evaluation of the biodegradability of chiral drugs in activated sludge from a Valencian waste water treatment plant.



**Ph.D. Thesis presented by:
Mireia Pérez Baeza**

Supervised by:

María José Medina Hernández, Ph.D.

Laura Escuder Gilabert, Ph.D.

Valencia, May 2023



VNIVERSITATĪ VALÈNCIA

 Facultat de Química

Doctoral Programme in Chemistry (R.D. 1999/2011)

Enantioseparations with polysaccharide-based chiral stationary phases in HPLC. Application to the enantioselective evaluation of the biodegradability of chiral drugs in activated sludge from a Valencian waste water treatment plant.

Ph.D. Thesis presented by:

Mireia Pérez Baeza

Supervised by:

María José Medina Hernández, Ph.D.

Laura Escuder Gilabert, Ph.D.

Valencia, May 2023

Programa de Doctorado 3154 en Química (R.D. 99/2011)

Facultad de Química

Universitat de València

Doctoranda

Mireia Pérez Baeza

Graduada en Química

Máster en Técnicas Experimentales en Química

Universitat de València

Directoras

Dra. M^a José Medina Hernández

Catedrática de Universidad

Departamento de Química Analítica. Facultad de Química

Universitat de València

Dra. Laura Escuder Gilabert

Profesora Titular de Universidad

Departamento de Química Analítica. Facultad de Química

Universitat de València



VNIVERSITATIS VALÈNCIAE

D^a. MARÍA JOSÉ MEDINA HERNÁNDEZ, Catedrática de Universidad del Departamento de Química Analítica de la Universitat de València, y D^a. LAURA ESCUDER GILABERT, Profesora Titular de Universidad del Departamento de Química Analítica de la Universitat de València,

CERTIFICAN:

Que la presente Memoria titulada "Enantioseparations with polysaccharide-based chiral stationary phases in HPLC. Application to the enantioselective evaluation of the biodegradability of chiral drugs in activated sludge from a Valencian waste water treatment plant.", realizada en el Departamento de Química Analítica de la Universitat de València, constituye la Tesis Doctoral de D^a. MIREIA PÉREZ BAEZA.

Asimismo, certifican haber dirigido y supervisado los distintos aspectos del presente trabajo, así como su redacción, y dan el visto bueno para su depósito y autorizan su presentación para optar al Título de Doctora con Menció Internacional por la Universitat de València.

Y para que conste a los efectos oportunos, firman el presente certificado en Valencia, en mayo de 2023.

Dra. María José Medina Hernández

Dra. Laura Escuder Gilabert

ACKNOWLEDGMENTS

I would like to thank all those people who, in one or another way, have been part of this stage of my life. Especially, I would like to thank my Thesis supervisors, Prof. María José Medina Hernández and Prof. Laura Escuder Gilabert. Thank you for the dedication you have given me during my Doctoral Thesis and throughout my research period, as well as for your guidance, advices and friendship. And above all, thank you for having trusted me by giving me the opportunity to be part of this project. Likewise, I would like to thank the rest of the research group (GAMM, multivariate and multicomponent analysis), Yolanda and Salva, for their attention, affection and for always solving all my doubts. I have learned a lot working with each of you. All this would not have been possible without your support. You will always have a place in my heart.

Thanks also to Professors J.J. Baeza Baeza and M.C. García-Alvarez-Coque for helping me with part of my Thesis (Paper IV), patiently explaining things to me and being there when I needed them.

Nor can I forget the students who have passed through this research group to carry out their TFGs, TFMs, internships or work placements, with whom I have shared laboratory and good moments. Thank you very much. You have also given me the opportunity of learning some things from you.

Of course, I would like to thank Dr. Paola Peluso and the rest of the colleagues (Roberto, Barbara, Alessandro, Paola, Valeria, Antonella, Luigi, etc.) I had during my research stay at the Istituto di Chimica Biomolecolare of the Consiglio Nazionale delle Ricerche (ICB-CNR) in Sardinia, Italy. Thanks for having welcomed me and making my stay more enjoyable. You have taught me to look at things in a different way.

I would also like to thank the Generalitat Valenciana and the European Social Fund for their financial support (ACIF/2019/158 research contract and BEFPI/2021/073 research stay), which have allowed me to develop my Ph.D. project.

Finally, this Thesis is also the result of the affection of the people around me, so I would like to highlight the support of my parents, Paco and Rosa; my sister, Meritxell; my partner in life, Miguel; and the rest of my family. I would also like to thank all my friends. Thank you all very much for your patience, your encouragement, for being always there, for loving me and taking care of me, for supporting me in my decisions and for believing in me.

"Water is the driving force of all nature"

– Leonardo da Vinci (1452-1519) –

LIST OF ORIGINAL PUBLICATIONS

This Doctoral Thesis is presented in the "Compendium of publications" modality, as considered in the Regulations for assessment and deposit of doctoral theses (ACGUV 29-XI-2011. Amended: ACGUV 28-II-2012, ACGUV 29-X-2013, ACGUV 28-VI-2016 and ACGUV 31-X-2017) of the Universitat de València. In addition, the Ph.D. student applies for the mention "International Doctor".

The publications included in this Thesis are listed below. The journal impact factor (JIF) as considered in the Journal of Citation Reports (JCR) Science Edition, together the JIF rank and JIF quartile in the corresponding category for the year of publication is also included.

SECTION	PAPER REFERENCE
IV.1 VI.- Paper I	<p><u>Mireia Pérez-Baeza</u>, Laura Escuder-Gilabert, Yolanda Martín-Biosca, Salvador Sagrado, María José Medina-Hernández</p> <p>Comparative modelling study on enantioresolution of structurally unrelated compounds with amylose-based chiral stationary phases in reversed phase liquid chromatography-mass spectrometry conditions</p> <p>Journal of Chromatography A, 1625 (2020) 461281</p> <p>https://doi.org/10.1016/j.chroma.2020.461281</p> <p>JIF (2020): 4.759</p> <p>Category: Analytical Chemistry JIF rank: 17/87 JIF quartile: Q1</p>
IV.2 VI.- Paper II	<p><u>Mireia Pérez-Baeza</u>, Laura Escuder-Gilabert, Yolanda Martín-Biosca, Salvador Sagrado, María José Medina-Hernández</p> <p>Comparative study on retention behaviour and enantioresolution of basic and neutral structurally unrelated compounds with cellulose-based chiral stationary phases in reversed phase liquid chromatography-mass spectrometry conditions</p> <p>Journal of Chromatography A, 1673 (2022) 463073</p> <p>https://doi.org/10.1016/j.chroma.2022.463073</p> <p>JIF (2021): 4.601</p> <p>Category: Analytical Chemistry JIF rank: 20/87 JIF quartile: Q1</p>
IV.3 VI.- Paper III	<p><u>Mireia Pérez-Baeza</u>, Yolanda Martín-Biosca, Laura Escuder-Gilabert, María José Medina-Hernández, Salvador Sagrado</p> <p>Artificial neural networks to model the enantioresolution of structurally unrelated neutral and basic compounds with cellulose tris(3,5-dimethylphenylcarbamate) chiral stationary phase and aqueous-acetonitrile mobile phases</p> <p>Journal of Chromatography A, 1672 (2022) 463048</p> <p>https://doi.org/10.1016/j.chroma.2022.463048</p> <p>JIF (2021): 4.601</p> <p>Category: Analytical Chemistry JIF rank: 20/87 JIF quartile: Q1</p>

SECTION	PAPER REFERENCE
IV.4 VI.- Paper IV	<p><u>M. Pérez-Baeza</u>, L. Escuder-Gilabert, M.J. Medina-Hernández, J.J. Baeza-Baeza, M.C. García-Alvarez-Coque</p> <p>Modified Gaussian models applied to the description and deconvolution of peaks in chiral liquid chromatography</p> <p>Journal of Chromatography A, 1625 (2020) 461273</p> <p>https://doi.org/10.1016/j.chroma.2020.461273</p> <p>JIF (2020): 4.759</p> <p>Category: Analytical Chemistry JIF rank: 17/87 JIF quartile: Q1</p>
IV.5 VI.- Paper V	<p>Laura Escuder-Gilabert, Yolanda Martín-Biosca, <u>Mireia Perez-Baeza</u>, Salvador Sagrado, María José Medina-Hernández</p> <p>Trimeprazine is enantioselectively degraded by an activated sludge in ready biodegradability test conditions</p> <p>Water Research, 141 (2018) 57-64</p> <p>https://doi.org/10.1016/j.watres.2018.05.008</p> <p>JIF (2018): 7.913</p> <p>Category: Water Resources JIF rank: 1/91 JIF quartile: Q1</p> <p>Category: Environmental Sciences JIF rank: 9/251 JIF quartile: Q1</p>
IV.6 VI.- Paper VI	<p>Laura Escuder-Gilabert, Yolanda Martín-Biosca, <u>Mireia Perez-Baeza</u>, Salvador Sagrado, María José Medina-Hernández</p> <p>Direct chromatographic study of the enantioselective biodegradation of ibuprofen and ketoprofen by an activated sludge</p> <p>Journal of Chromatography A, 1568 (2018) 140-148</p> <p>https://doi.org/10.1016/j.chroma.2018.07.034</p> <p>JIF (2018): 3.858</p> <p>Category: Analytical Chemistry JIF rank: 15/84 JIF quartile: Q1</p>
IV.7 VI.- Paper VII	<p><u>Mireia Pérez-Baeza</u>, Laura Escuder-Gilabert, Yolanda Martín-Biosca, Salvador Sagrado, María José Medina-Hernández</p> <p>Reversed phase liquid chromatography for the enantioseparation of local anaesthetics in polysaccharide-based stationary phases. Application to biodegradability studies</p> <p>Journal of Chromatography A, 1625 (2020) 461334</p> <p>https://doi.org/10.1016/j.chroma.2020.461334</p> <p>JIF (2020): 4.759</p> <p>Category: Analytical Chemistry JIF rank: 17/87 JIF quartile: Q1</p>

OTHER ORIGINAL RESEARCH PAPERS (NOT INCLUDED IN THIS THESIS) PUBLISHED DURING THE Ph.D. STUDIES

Yolanda Martín-Biosca, Laura Escuder-Gilabert, Mireia Pérez-Baeza, Salvador Sagrado, María José Medina-Hernández

Monod-based 'single-data' strategy for biodegradation screening tests

Environmental Chemistry, 17(3) (2019) 278-288

<https://doi.org/10.1071/EN19171>

JIF (2019): 1.910

Category: Analytical Chemistry

JIF rank: 24/87

JIF quartile: Q2

Yolanda Martín-Biosca, Laura Escuder-Gilabert, Mireia Perez-Baeza, Salvador Sagrado, María José Medina-Hernández

Biodegradability features of fluoxetine as a reference compound for monitoring the activity of activated sludges in drug biodegradation studies

International Journal of Advanced Research in Chemical Science (IJARCS), 6(1) (2019) 16-23

<http://dx.doi.org/10.20431/2349-0403.0601003>

Alessandro Dessì, Barbara Sechi, Roberto Dallochio, Bezhan Chankvetadze, Mireia Pérez-Baeza, Sergio Cossu, Victor Mamane, Patrick Pale, Paola Peluso

Comparative enantioseparation of planar chiral ferrocenes on polysaccharide-based chiral stationary phases

Chirality, 34(4) (2022) 609-619

<https://doi.org/10.1002/chir.23417>

JIF (2021): 2.183

Category: Analytical Chemistry

JIF rank: 64/87

JIF quartile: Q3

Mireia Pérez-Baeza, Laura Escuder-Gilabert, Yolanda Martín-Biosca, Salvador Sagrado, María José Medina-Hernández

Potential of sodium dodecyl sulfate micellar solutions as eluents in magnetic dispersive micro-solid phase extraction with polydopamine-coated magnetite nanoparticles. Application to antidepressant drugs

Journal of Chromatography A, 1680 (2022) 463430

<https://doi.org/10.1016/j.chroma.2022.463430>

JIF (2021): 4.601

Category: Analytical Chemistry

JIF rank: 20/87

JIF quartile: Q1

WORKS SUBMITTED TO NATIONAL OR INTERNATIONAL CONFERENCES

XI International Workshop on Sensors and Molecular Recognition (IWOSMOR XI). Valencia, Spain, 06-07/07/2017

María José Medina-Hernández, Laura Escuder-Gilabert, Yolanda Martín-Biosca, Emilio Bonet-Domingo, [Mireia Pérez-Baeza](#), Salvador Sagrado

Bacterial recognition of emergent contaminants: Biodegradation screening of β -blocker drugs
Poster 23

María José Medina-Hernández, Laura Escuder-Gilabert, Yolanda Martín-Biosca, Emilio Bonet-Domingo, [Mireia Pérez-Baeza](#), Salvador Sagrado

Bacterial recognition of emergent contaminants: Biodegradation screening of antihistamine drugs
Poster 56

María José Medina-Hernández, Laura Escuder-Gilabert, Yolanda Martín-Biosca, Emilio Bonet-Domingo, [Mireia Pérez-Baeza](#), Salvador Sagrado

Bacterial (enantio)recognition of emergent contaminants: Propranolol biodegradation evaluation
Poster 63

María José Medina-Hernández, Laura Escuder-Gilabert, Yolanda Martín-Biosca, Emilio Bonet-Domingo, [Mireia Pérez-Baeza](#), Salvador Sagrado

Bacterial (enantio)recognition of emergent contaminants: Metoprolol biodegradation evaluation
Poster 98

XXI Reunión de la Sociedad Española de Química Analítica (SEQA2017). Valencia, España. 05/09/2017-07/09/2017

Mireia Pérez-Baeza, Yolanda Martín-Biosca, María José Medina-Hernández, Laura Escuder-Gilabert, Emilio Bonet-Domingo, Salvador Sagrado

Fluoxetine as reference compound for inoculum control in biodegradation studies
Poster PO-MA-21

XII International Workshop on Sensors and Molecular Recognition (IWOSMOR XII). Valencia, Spain, 05-06/07/2018

María José Medina-Hernández, Laura Escuder-Gilabert, Yolanda Martín-Biosca, Emilio Bonet-Domingo, [Mireia Pérez-Baeza](#), Salvador Sagrado

Bacterial enantiorecognition of ketoprofen: ready biodegradability test
Poster P-11

María José Medina-Hernández, Laura Escuder-Gilabert, Yolanda Martín-Biosca, Emilio Bonet-Domingo, [Mireia Pérez-Baeza](#), Salvador Sagrado

Bacterial enantiorecognition of emergent contaminants: peak area-based biodegradability models
Poster P-12

María José Medina-Hernández, Laura Escuder-Gilabert, Yolanda Martín-Biosca, [Mireia Pérez-Baeza](#), Salvador Sagrado

Bacterial recognition: Relevant time outputs derived from a single screening biodegradability assay data
Poster P-31

WORKS SUBMITTED TO NATIONAL OR INTERNATIONAL CONFERENCES (continued)

María José Medina-Hernández, Laura Escuder-Gilabert, Yolanda Martín-Biosca, Mireia Pérez-Baeza, Salvador Sagrado

Enantiorecognition of organic contaminants: Modelling the enantioresolution of stationary phases in RPLC

Poster P-38

María José Medina-Hernández; Laura Escuder-Gilabert; Yolanda Martín-Biosca; Mireia Pérez-Baeza; Salvador Sagrado

Bacterial recognition: Models comparison, accuracy, reliability and diagnostic plots

Poster P-63

XIII International Workshop on Sensors and Molecular Recognition (IWOSMOR XIII). Valencia, Spain, 04-05/07/2019

Mireia Pérez-Baeza, María José Medina-Hernández, Laura Escuder-Gilabert, Yolanda Martín-Biosca, Yeray Pallás-Tamarit, Salvador Sagrado

Potencial of modified magnetic nanoparticles with CTAB for preconcentration of acidic compounds by dispersive solid phase extraction

Oral communication O-11

María José Medina-Hernández, Laura Escuder-Gilabert, Yolanda Martín-Biosca, Mireia Pérez-Baeza, Yeray Pallás-Tamarit, Salvador Sagrado

Bacterial recognition: improved accuracy of environmental relevant parameters estimates

Poster P-56

María José Medina-Hernández, Laura Escuder-Gilabert, Yolanda Martín-Biosca, Mireia Pérez-Baeza, Salvador Sagrado

Modelling the (bio)degradability of organic contaminants from structure

Poster P-57

XXII Reunión de la Sociedad Española de Química Analítica (SEQA2019). Valladolid, Spain, 17-19/07/2019

Mireia Pérez Baeza, Laura Escuder Gilabert, María José Medina Hernández, María Celia García Álvarez-Coque, Juan José Baeza Baeza

Estudio de picos cromatográficos de compuestos quirales utilizando funciones gaussianas modificadas

Poster TSE-P04

4th International Mass Spectrometry School. Sitges, Spain, 15-20/09/2019

Mireia Pérez-Baeza, María José Medina-Hernández, Laura Escuder-Gilabert, Yeray Pallás-Tamarit, Yolanda Martín-Biosca, Salvador Sagrado

Chiral HPLC-MS assessment of enantio-biodegradability of bupivacaine and omeprazole in WWTPs

Poster P-57

WORKS SUBMITTED TO NATIONAL OR INTERNATIONAL CONFERENCES (continued)

25th Latin-American Symposium on Biotechnology, Biomedical, Biopharmaceutical, and Industrial Applications of Capillary Electrophoresis and Microchip Technology (LACE2019). Alcalá de Henares, Spain, 29/09/2019-02/10/2019

Y. Martín-Biosca, M. Pérez-Baeza, R. Muñoz-Espí, L. Escuder-Gilabert, S.Sagrado, M. J. Medina-Hernández

Dispersive micro solid phase extraction using modified magnetite nanoparticles with ionic surfactants

Poster PP-9

27th International Symposium on Electrophoretic and Liquid Phase Separation Techniques. Nanjing, China, 02-04/11/2020 (virtual congress)

M. Pérez-Baeza, L. Escuder-Gilabert, M.J. Medina-Hernández, J.J. Baeza-Baeza, M.C. García-Álvarez-Coque

Calculation of the enantiomeric fraction through deconvolution of chromatographic peaks

On-line poster

XIV International Workshop on Sensors and Molecular Recognition (IWOSMOR XIV). Valencia, Spain, 08-09/07/2021

Ángela Recuenco Cava, Mireia Pérez-Baeza, María José Medina-Hernández, Laura Escuder-Gilabert, Yolanda Martín-Biosca, Salvador Sagrado, Francisco F. Pérez Pla

Dispersive micro-solid phase extraction using polydopamine coated magnetite nanoparticles for preconcentration of antidepressants

Poster P-41

Mireia Pérez-Baeza, María José Medina-Hernández, Laura Escuder-Gilabert, Yolanda Martín-Biosca, Salvador Sagrado

Modelling the enantioresolution of basic and neutral compounds using cellulose chiral stationary phases by HPLC

Poster P-42

Sara Ballester Gómez, Mireia Pérez-Baeza, María José Medina-Hernández, Laura Escuder-Gilabert, Yolanda Martín-Biosca, Salvador Sagrado, Rafael Muñoz Espí

Solid phase extraction using polydopamine coated magnetite nanoparticles for directly analysis of food additives

Poster P-43

Sofía Rodrigo Bustos, Mireia Pérez-Baeza, María José Medina-Hernández, Laura Escuder-Gilabert, Yolanda Martín-Biosca, Salvador Sagrado

Retention behaviour of neutral and basic compounds using cellulose chiral stationary phases and aqueous-organic mobile phases

Poster P-44

WORKS SUBMITTED TO NATIONAL OR INTERNATIONAL CONFERENCES (continued)

7es Jornades d'Innovació Educativa. Innovar per a transformar: el repte de la innovació educativa en la universitat, Valencia, Spain, 20-21/07/2021 (virtual congress)

Yolanda Martín Biosca, Mireia Pérez Baeza, Laura Escuder Gilabert, María José Medina Hernández, Salvador Sagrado

El laboratorio de análisis químico del grado en CTyA en tiempos COVID: adaptación a la docencia híbrida

Poster AP-20

Workshop 'Enantioselective Chromatography and Electromigration Techniques: Theory, Mechanisms, and Applications'. Sassari, Italy, 19/11/2021

Mireia Pérez-Baeza, Laura Escuder-Gilabert, Yolanda Martín-Biosca, Salvador Sagrado, María José Medina-Hernández

Anticipating the enantioresolution with polysaccharides-based chiral stationary phases and hydroorganic mobile phases of structurally unrelated compounds

Oral communication

II Workshop for Young Researchers in Chemistry (YRChem2022). Valencia, Spain, 19-20/05/2022

Mireia Pérez-Baeza, Laura Escuder-Gilabert, Yolanda Martín-Biosca, Salvador Sagrado, María José Medina-Hernández

Retention behavior and enantioresolution with polysaccharide-based chiral stationary phases and hydroorganic mobile phases of basic and neutral structurally unrelated chiral compounds

Oral communication OC23

XV International Workshop on Sensors and Molecular Recognition (IWOSMOR XIV). Valencia, Spain, 11-12/07/2022

Mireia Pérez-Baeza, María José Medina-Hernández, Laura Escuder-Gilabert, Yolanda Martín-Biosca, Salvador Sagrado

Artificial intelligence applied to study the enantio recognition and enantioresolution of structurally unrelated chiral compounds with a cellulose chiral selector

Oral communication O-09

Mireia Pérez-Baeza, María José Medina-Hernández, Laura Escuder-Gilabert, Yolanda Martín-Biosca, Salvador Sagrado

Polysaccharide-based chiral stationary phases with hydroorganic mobile phases. Effect of the polysaccharide backbone on the retention and enantioresolution of structurally unrelated basic and neutral chiral compound

Poster P-66

FUNDING FROM PUBLIC COMPETITIVE CALLS

RESEARCH PROJECTS

Estudio de la biodegradación enantioselectiva de contaminantes emergentes quirales. Implicaciones y riesgos para la salud y el medio ambiente (Project CTQ2015-70904-R, MINECO/FEDER, UE)

Spanish Ministerio de Economía, Industria y Competitividad (MINECO) and European Regional Development Fund (FEDER)

Programa Estatal de Investigación, Desarrollo e Innovación Orientada a los Retos de la Sociedad, in the framework of the Plan Estatal de Investigación Científica y Técnica y de Innovación 2013-2016

01/01/2016 - 31/12/2019

GRANTS

Ayudas para la iniciación a la investigación para estudiantes de la Universitat de València que cursan estudios oficiales en centros propios de esta universidad (764336)

Servei d'Informació i Dinamització (SeDI)

Universitat de València

Curso 2017 – 2018

Subvenciones para la contratación de personal investigador predoctoral (ACIF/2019/158)

Conselleria d'Educació, Investigació, Cultura i Esport de la Generalitat Valenciana and FEDER

Programa para la promoción de la investigación científica, el desarrollo tecnológico y la innovación en la Comunitat Valenciana

01/09/2019 – 09/12/2022

Subvenciones para estancias de contratados predoctorales en centros de investigación fuera de la Comunitat Valenciana (BEFPI/2021/073)

Conselleria d'Innovació, Universitats, Ciència i Societat Digital de la Generalitat Valenciana and FEDER

Programa para la promoción de la investigación científica, el desarrollo tecnológico y la innovación en la Comunitat Valenciana

20/08/2021 – 20/12/2021

The research stay was carried out in the research group led by Ph.D. Paola Peluso in the Istituto di Chimica Biomolecolare - Consiglio Nazionale delle Ricerche (ICB-CNR), Sassari, Italy

RESUMEN AMPLIO

(artículo 7.2, Reglamento ACGUV 29-XI-2011, última modificación ACGUV 31-X-2017)

La naturaleza quiral de los sistemas vivos tiene implicaciones evidentes para los compuestos quirales biológicamente activos que interactúan con ellos. A nivel molecular, la quiralidad representa una propiedad intrínseca de los componentes esenciales de la vida, como los aminoácidos y los azúcares, y, por tanto, de péptidos, proteínas, enzimas, carbohidratos, nucleósidos y una serie de alcaloides y hormonas. En consecuencia, los procesos mediados por los sistemas biológicos son sensibles a la estereoquímica, y un par de enantiómeros puede tener efectos diferentes en los organismos vivos.

La quiralidad tiene implicaciones en distintos campos científicos, como el farmacéutico, el alimentario y nutricional, el clínico y el medioambiental.

La comunidad científica lleva más de un siglo estudiando las implicaciones de la quiralidad para la vida. Hoy en día, sigue siendo un área activa de investigación y debate debido al gran número de moléculas quirales que forman parte de los organismos vivos y de nuestra vida cotidiana. En este contexto, las metodologías analíticas para la separación de los enantiómeros de las moléculas quirales desempeñan un papel crucial.

Sin duda, el uso de fases estacionarias quirales (CSPs) en cromatografía de líquidos de alta resolución (HPLC) es la opción preferida para la separación de enantiómeros. Prueba de ello es el gran número de CSPs disponibles en el mercado. Hoy en día, aproximadamente el 90 % de las separaciones quirales se realizan por HPLC utilizando CSPs de derivados de polisacáridos, principalmente de derivados de celulosa y de amilosa, debido a su amplia capacidad de reconocimiento quiral que les confiere una amplia aplicabilidad para una gran diversidad estructural de compuestos y a que son compatibles con todos los regímenes de fases móviles: orgánicas apolares en cromatografía de fase normal (NPLC), hidro-orgánicas en cromatografía en fase inversa (RPLC) y de interacción hidrofílica (HILIC); y orgánicas polares en cromatografía orgánica polar.

Las separaciones quirales suponen uno de los mayores retos de todas las separaciones analíticas. La interacción entre dos especies quirales no garantiza la separación de sus enantiómeros. Algunas CSPs han demostrado una amplia aplicabilidad; sin embargo, no existe una CSP de aplicabilidad universal.

A pesar del gran número de aplicaciones analíticas de las CSPs en HPLC, los mecanismos fundamentales responsables de las separaciones quirales no se comprenden completamente debido a la complejidad inherente de estos sistemas cromatográficos. De hecho, hoy en día, la búsqueda de la combinación adecuada de CSP/fase móvil para la separación de los enantiómeros de un compuesto quiral determinado se lleva a cabo mediante procedimientos de ensayo y error, lo que se traduce en

un enorme coste y esfuerzo experimental. Por lo tanto, la predicción de la capacidad de un sistema cromatográfico dado, para saber si es posible una separación quiral, sería de gran utilidad.

Para dilucidar el mecanismo de reconocimiento quiral de las CSPs, se han utilizado técnicas analíticas de separación en combinación con técnicas espectroscópicas y estrategias de modelización molecular. Dentro de estas últimas, caben destacar las denominadas relaciones cuantitativas estructura-propiedad (QSPRs). En ellas se relacionan propiedades estructurales de compuestos quirales (p. ej., descriptores moleculares) con parámetros cromatográficos relacionados con su enantioseparación (p. ej., factor de selectividad (α), factor de retención de los enantiómeros (k) y en menor medida la enantio-resolución (R_s)) obtenidos en un sistema cromatográfico dado. Para el análisis de estos conjuntos de datos se requiere el uso de técnicas quimiométricas multivariantes, como las técnicas de regresión multivariante –por ejemplo, regresión lineal múltiple (MLR), regresión por mínimos cuadrados parciales (PLS), redes neuronales artificiales (ANNs)– o técnicas de clasificación multivariante como mínimos cuadrados parciales discriminantes (DPLS) y árboles de clasificación y regresión (CART). Los modelos QSPRs permiten extraer información valiosa sobre el reconocimiento molecular.

La mayoría de los modelos QSPRs publicados se han desarrollado para compuestos relacionados estructuralmente, éstos han demostrado ser útiles para averiguar qué descriptores moleculares de los compuestos quirales influyen más en su retención y enantioseparación, y para dilucidar los mecanismos de enantio-reconocimiento que operan en el caso (compuestos y sistema cromatográfico) estudiado; sin embargo, muestran una aplicabilidad limitada. En cambio, los modelos QSPRs para compuestos no relacionados estructuralmente, son preferibles para una selección racional de un sistema cromatográfico (combinación CSP/fase móvil) para separar los enantiómeros de cualquier compuesto nuevo.

Cuando no es posible experimentalmente conseguir la resolución completa de los picos de los enantiómeros de un compuesto quiral es posible lograr la resolución matemática mediante la aplicación de técnicas de deconvolución de picos solapados. Ello requiere la aplicación de modelos matemáticos capaces de describir adecuadamente el perfil de los picos cromatográficos de cada uno de los enantiómeros del compuesto quiral.

Por otra parte, la concienciación sobre la protección del medio ambiente ha aumentado notablemente en los últimos años, debido a los efectos adversos que los contaminantes pueden producir no sólo en el medio ambiente sino también en la salud humana. Entre los contaminantes emergentes, los fármacos son probablemente la principal preocupación de las autoridades reguladoras debido a su enorme consumo. Los fármacos, sus metabolitos y sus productos de degradación pueden llegar al medio ambiente debido principalmente a los bajos índices de eliminación en las estaciones depuradoras de aguas residuales (EDAR) y a la eliminación inadecuada de los medicamentos no utilizados. Sin embargo, a pesar de los grandes esfuerzos realizados por las

autoridades reguladoras y la comunidad científica, no se sabe mucho sobre el impacto de este tipo de compuestos sobre el medio ambiente y la salud humana. La mayoría de los fármacos actualmente disponibles son compuestos quirales (56 %) y, aunque el uso de enantiómeros puros ha aumentado durante las últimas décadas, muchos de ellos se comercializan como mezclas racémicas. Sin embargo, los enantiómeros de los contaminantes quirales pueden estar presentes en el medio ambiente en proporciones diferentes como resultado de la excreción enantioselectiva de los seres vivos, la bioacumulación en compartimentos medioambientales y la biodegradación microbiana durante el proceso de tratamiento de aguas residuales.

La biodegradabilidad, definida como la capacidad de una molécula de ser degradada por microorganismos formando productos finales más simples, es un parámetro esencial para conocer el riesgo que supone la dispersión de un compuesto en el medio ambiente. Esta propiedad depende de la estructura química del compuesto, así como de las condiciones fisicoquímicas en las que tiene lugar el proceso de degradación. Los ensayos de biodegradabilidad están diseñados para probar una sustancia química como única fuente de carbono en un inóculo mixto. Los ensayos de biodegradabilidad inmediata de la Organización para la Cooperación y Desarrollo Económico (OECD) se han concebido como métodos de cribado para determinar si una sustancia química es potencialmente biodegradable, lo que contribuye a adquirir conocimientos en el campo de la investigación sobre el agua y el medio ambiente.

Por todo lo expuesto, y debido al hecho de que los enantiómeros pueden tener propiedades toxicológicas y ecotoxicológicas diferentes entre sí, la cuantificación de las fracciones enantioméricas (*EF*) durante el proceso de biodegradación es esencial para la evaluación del riesgo medioambiental. Sin embargo, no se ha investigado mucho sobre este tema.

Esta Tesis Doctoral tiene dos **objetivos** principales claramente diferenciados:

- i.- Contribuir al conocimiento de la cromatografía líquida quiral con CSPs de derivados de polisacáridos y fases móviles hidro-orgánicas. El interés se centra en las CSPs comerciales de polisacáridos más utilizadas: tres derivados de amilosa (Am1: tris(3,5-dimetilfenilcarbamato) de amilosa; Am2: tris(5-cloro-2-metilfenilcarbamato) de amilosa; Am3: tris(3-cloro-5-metilfenilcarbamato) de amilosa inmovilizada) y cinco derivados de celulosa (Cell1: tris(3,5-dimetilfenilcarbamato) de celulosa; Cell2: tris(3-cloro-4-metilfenilcarbamato) de celulosa; Cell3: tris(4-metilbenzoato) de celulosa; Cell4: tris(4-cloro-3-metilfenilcarbamato) de celulosa; Cell5: tris(3,5-diclorofenilcarbamato) de celulosa inmovilizada). Como fases móviles se utilizaron disoluciones acuosas de acetonitrilo (ACN) y metanol (MeOH) compatibles con matrices acuosas y detección con espectrometría de masas (MS). Para la consecución de este objetivo, se han planteado los siguientes objetivos específicos:

- Contribuir a una selección racional del sistema cromatográfico para separar los enantiómeros de un determinado compuesto. Para ello, se compara la retención y enantio-resolución de un conjunto de aproximadamente 60 compuestos quirales estructuralmente no relacionados (fármacos y pesticidas básicos y neutros) en todos los sistemas cromatográficos de amilosa (**apartado IV.1, Artículo I**) y celulosa (**apartado IV.2, Artículo II**) arriba indicados. Además, se pretende elaborar modelos QSPR para describir y predecir parámetros relacionados con la enantio-resolución obtenidos en Am1 y Am3 (**apartado IV.1, Artículo I**), así como en Cell1 (**apartado IV.3, Artículo III**), utilizando fases móviles acuosas ACN.
 - Explorar el uso de la deconvolución de picos solapados para lograr la resolución matemática cuando no puede alcanzarse experimentalmente una enantio-resolución completa (**apartado IV.4, artículo IV**). Para ilustrar el potencial de esta estrategia, se considera la enantioseparación de bupivacaína, flurbiprofeno, ibuprofeno, ketoprofeno, metoprolol, omeprazol, propranolol y trimepricina en CSPs de derivados de polisacáridos (Cell1, Cell2, Cell3, Cell5 y Am2) y fases móviles hidro-orgánicas de ACN o MeOH a diferentes temperaturas de separación.
- ii.- Contribuir a la evaluación de los riesgos y peligros de los contaminantes quirales. Para ello, se realizan ensayos de biodegradabilidad inmediata de acuerdo con la guía de la OECD utilizando todos activados de una EDAR valenciana (Quart Benàger) para algunos fármacos quirales de uso extendido: trimepricina (**apartado IV.5, Artículo V**), ibuprofeno y ketoprofeno (**apartado IV.6, artículo VI**), y cuatro anestésicos locales (bupivacaína, mepivacaína, prilocaína y propanocaína; **apartado IV.7, artículo VII**). A continuación, se lleva a cabo la separación y determinación de los enantiómeros del compuesto intacto mediante métodos de RPLC quirales (con CSPs de derivados de amilosa o celulosa y fases móviles de ACN o MeOH compatibles con matrices acuosas y detección con MS) desarrollados para tal fin.

A continuación, se incluye un resumen de los objetivos concretos, la metodología, los principales resultados y conclusiones de cada uno de los estudios realizados en esta Tesis Doctoral.

Como se ha comentado anteriormente, las CSPs de derivados de polisacáridos son las CSPs más utilizadas en HPLC. Estas CSPs pueden utilizarse en NPLC, RPLC, HILIC y con fases móviles orgánicas polares. Aunque en la mayoría de las aplicaciones descritas en la bibliografía se ha utilizado NPLC, las fases móviles utilizadas en esta modalidad de trabajo no son adecuadas para la separación quiral de compuestos polares, para el análisis de muestras acuosas y para la detección por MS. En estas situaciones, son preferibles las condiciones de RPLC, sin los aditivos no volátiles habituales que son incompatibles con la detección por MS. Además, en la mayoría de los métodos cromatográficos quirales descritos, la retención es demasiado grande para el trabajo en análisis de rutina.

Los estudios realizados en este trabajo se encaminaron a la consecución de dos objetivos principales. Por un lado, se pretende realizar un estudio comparativo del comportamiento de retención y enantio-resolución de 53 compuestos estructuralmente no relacionados (fármacos y pesticidas) utilizando tres CSPs de derivados de amilosa (Am1, Am2 y Am3). Para las separaciones cromatográficas se utilizaron fases móviles hidro-orgánicas compatibles con la detección por MS consistentes en mezclas de ACN y NH_4HCO_3 (5 mM, $\text{pH} = 8.0$), en proporción variable (10-80 % en volumen de ACN). El valor máximo de los factores de retención se fijó en 15 para obtener condiciones prácticas para los análisis de rutina. Por otro lado, este trabajo también tiene como objetivo comparar y describir las capacidades de enantioseparación de estas CSPs. Con este fin, se pretende desarrollar modelos QSPR para predecir/anticipar la enantio-resolución categórica (CRs) a partir de 57 variables estructurales y propiedades fisicoquímicas de los compuestos para cada CSP. Se utiliza DPLS1 (DPLS para una variable respuesta) para la selección de variables (FS) y modelización. Hasta donde sabemos, éste es el primer intento de modelizar parámetros relacionados con la enantio-resolución para un gran conjunto de datos de compuestos estructuralmente no relacionados en condiciones cromatográficas realistas desde un punto de vista práctico.

En las condiciones experimentales ensayadas, se observó un comportamiento de retención RPLC típico (la retención disminuye al aumentar el contenido de ACN) para los 53 compuestos quirales estructuralmente no relacionados estudiados. Adicionalmente, las CSP Am1 y Am3 permitieron la enantioseparación parcial o completa para un número similar de compuestos ($Rs \geq 1.5$: 11 compuestos en ambas CSPs; $0 < Rs < 1.5$: 16 y 14 compuestos en Am1 y Am3, respectivamente), pero mostraron enantioselectividades diferentes. La CSP Am2 proporcionó los peores resultados ($Rs \geq 1.5$: 4 compuestos; $0 < Rs < 1.5$: 9 compuestos), y su selectividad apenas complementó a la de las otras CSPs. De hecho, Phenomenex ya no comercializa la CSP Am2.

Empleando una nueva estrategia de FS-DPLS1, se seleccionó un conjunto reducido de variables estructurales (de las 57 variables predictoras iniciales), con contribuciones positivas y

negativas a la *CRs* en las CSPs de Am1 y Am3. Se concluyó que la presencia de grupos carbonilo directamente enlazados al carbono quiral (C*) y de grupos aromáticos en los compuestos son características estructurales clave de los compuestos que favorecen su enantioseparación en los sistemas cromatográficos estudiados, lo que pone de manifiesto que las interacciones enantiómero-CSP de tipo π - π y de enlaces de hidrógeno pueden desempeñar un papel crucial.

Se observó que, la enantio-resolución en la CSP de Am1 puede estar favorecida o desfavorecida por la posición y naturaleza química de los sustituyentes en el anillo aromático. Además, la presencia de aminas terciarias (aceptores de enlaces de hidrógeno) en un grupo cíclico alifático puede mejorar la enantioseparación. En el caso de la CSP Am3, la presencia de anillos condensados también mejora la enantio-resolución, probablemente debido a la rigidez que confieren a la molécula.

Por último, la presencia de anillos aromáticos con nitrógeno en los compuestos también resultó ser importante para su enantioseparación, con una contribución favorable para Am3 y desfavorable para Am1. Esta selectividad opuesta de Am3 en comparación con Am1 podría explicarse por la combinación de las interacciones enantiómero-CSP de tipo π - π y de enlaces de hidrógeno, junto con la formación de aductos de Lewis entre los átomos de N de tipo piridina (bases de Lewis) y el átomo Cl (ácido de Lewis) en la CSP Am3, o el átomo H del grupo carbamato de la CSP Am3 (cuyo carácter dador de enlaces de hidrógeno se ve exaltado por la sustitución 3-cloro en la fracción fenilcarbamato).

Para avanzar en el conocimiento sobre las CSPs de polisacáridos, en este trabajo se realiza un estudio comparativo sobre el comportamiento de retención y la enantio-resolución de 54 compuestos neutros y básicos no relacionados estructuralmente (prácticamente los mismos que en el Artículo I) utilizando cinco CSPs comerciales de derivados de celulosa (Cell1, Cell2, Cell3, Cell4 y Cell5) y fases móviles hidro-orgánicas compatibles con MS. Las fases móviles empleadas fueron mezclas binarias de NH_4HCO_3 (5 mM, $\text{pH} = 8.0$) con MeOH o ACN en proporción variable (30-90 % en volumen de MeOH; 10-98 % en volumen de ACN).

Los enantiómeros de 38 de los 54 compuestos quirales estudiados se separaron totalmente en al menos uno de todos los sistemas cromatográficos ensayados. Sólo se obtuvieron valores de $R_s = 0$, en cualquiera de los sistemas cromatográficos estudiados, para tres compuestos.

En las condiciones experimentales ensayadas, para todos los compuestos y CSPs, con fases móviles MeOH: NH_4HCO_3 se observó un comportamiento de retención típico de RPLC (la retención disminuye al aumentar el contenido de disolvente orgánico). Mientras que para las fases móviles ACN: NH_4HCO_3 se distinguieron dos dominios diferentes según el contenido de agua en la fase móvil y el comportamiento de retención: (i) el dominio RPLC, para fases móviles con un contenido de agua del 20-90 % (contenido de ACN inferior al 80 %), en el que prevalece el comportamiento RPLC; y (ii) el dominio HILIC, para una proporción de agua en la fase móvil inferior al 20 % (contenido de ACN del 80-98 %), en el que prevalece el comportamiento de retención HILIC (la retención aumenta al aumentar el contenido de disolvente orgánico). Este comportamiento de retención dual HILIC/RPLC se observó para todos los compuestos y todas las CSPs. Sin embargo, la magnitud de los cambios de retención fue diferente para cada compuesto y cada CSP. El comportamiento HILIC fue más notable para los compuestos hidrófilos con todas las CSPs.

El uso de fases móviles MeOH: NH_4HCO_3 o ACN: NH_4HCO_3 condujo a diferentes enantioselectividades y grados de enantio-resolución. Para la mayoría de los compuestos, en todas las CSPs, se obtuvieron valores de R_s mucho mayores con fases móviles ACN: NH_4HCO_3 que los obtenidos con fases móviles MeOH: NH_4HCO_3 . Este efecto fue menos acusado en el sistema cromatográfico MeOH-Cell3. Los sistemas cromatográficos MeOH-Cell1 y MeOH-Cell5 mostraron una capacidad de enantioseparación muy pobre. La menor capacidad de resolución de los sistemas cromatográficos MeOH: NH_4HCO_3 podría atribuirse a la competición del MeOH con el enantiómero por las interacciones de enlace de hidrógeno con la CSP.

En el caso de las fases móviles ACN: NH_4HCO_3 , se obtuvo una enantio-resolución mucho mejor en el dominio RPLC para la mayoría de los compuestos. Excepto los enantiómeros de prometacina, los enantiómeros de todos los compuestos que se resolvieron en HILIC, también lo hicieron en RPLC.

Entre todos los sistemas cromatográficos ensayados, el sistema ACN-Cell2 permitió la separación de los enantiómeros del mayor número de compuestos quirales ($R_s \geq 1.5$: 21 compuestos; $0 < R_s < 1.5$: 17 compuestos). Las CSPs de tipo fenilcarbamato (Cell1, Cell4 y Cell5) no mostraron una enantioselectividad claramente complementaria a la de Cell2 con fases móviles de ACN:NH₄HCO₃. Comparando la enantio-resolución de Cell2 frente a Cell4 (CSPs con una estructura similar; la única diferencia entre ellas es que los sustituyentes metilo y cloro en la posición (3,4) del grupo fenilo están intercambiados), puede concluirse que la posición de los sustituyentes, aunque no ejerce un efecto marcado sobre la enantioselectividad de la CSP, sí afecta al grado de enantio-resolución en fases móviles de ACN:NH₄HCO₃, pero no en las de MeOH:NH₄HCO₃.

Por otro lado, comparando la enantio-resolución de Cell1 frente a Cell5 (CSPs que sólo difieren en la naturaleza de los sustituyentes: dos grupos metilo en Cell1 y dos átomos de cloro en Cell5; no en su posición: (3,5) en el grupo fenilo), se puede concluir que la naturaleza de los sustituyentes de la CSP tiene un efecto significativo en la resolución con fases móviles de ACN:NH₄HCO₃.

La CSP Cell3 (de tipo benzoato) fue la única CSP que mostró una enantioselectividad claramente complementaria a la de Cell2, principalmente con fases móviles de MeOH:NH₄HCO₃.

A partir de los resultados obtenidos, para intentar separar los enantiómeros de un nuevo compuesto quiral básico o neutro en las CSPs de celulosa estudiadas, se recomendó utilizar el sistema cromatográfico ACN-Cell2 en el dominio RPLC como primer intento, después MeOH-Cell3, ACN-Cell5 y ACN-Cell1 (ambos en el dominio RPLC) y, finalmente, otros sistemas.

En este trabajo para avanzar en el conocimiento de la selección racional del sistema cromatográfico para separar los enantiómeros de un determinado compuesto, uno de los objetivos de esta Tesis Doctoral, se utilizan ANNs para intentar estimar cuantitativamente la enantio-resolución de moléculas quirales a partir de su información estructural.

Las ANNs son técnicas de aprendizaje automático robustas y flexibles que pueden modelar relaciones entre las variables predictoras (**X**) y la(s) variable(s) respuesta (**y** o **Y**) complejas y/o no lineales. Una ANN aprende a partir de un conjunto de datos de aprendizaje hasta que mejora su capacidad predictiva para un conjunto de datos de validación. La arquitectura de una ANN consta de neuronas interconectadas dispuestas en múltiples capas que deben optimizarse. En el método *feed-forward*, la arquitectura de la ANN tiene: (i) una capa de entrada (primera capa) en la que las variables **X** se organizan en las N_v neuronas, (ii) una capa de salida, la capa final, en la que también se organizan la(s) variable(s) de respuesta conocida(s) (**y** o **Y**) y (iii) en el medio deben disponerse las denominadas capas ocultas. Durante el proceso de aprendizaje, los pesos (W_i) que conectan todas las neuronas se ajustan mediante funciones lineales o no lineales (funciones de activación). Una vez optimizada la arquitectura, la ANN está lista para estimar la(s) respuesta(s) de nuevos compuestos.

Debido a la complejidad interna de las ANN, la relación **y-X** no es fácil de conocer. Esta falta de transparencia se conoce como la "caja negra". Aunque se han propuesto varios métodos para estimar la importancia de las variables **X** en la predicción de respuestas, no están exentos de limitaciones. Además, actualmente no existen medios para verificar la calidad de dichas estimaciones.

La metodología de las ANNs tiene un gran número de aplicaciones en diversas áreas de investigación. Sin embargo, hasta donde sabemos, en la bibliografía sólo existen cuatro aplicaciones de ANNs para la modelización de QSPR en HPLC quiral. Estos modelos QSPR se han derivado para compuestos estructuralmente relacionados.

El objetivo de este trabajo fue diseñar, por primera vez, una estrategia basada exclusivamente en ANNs para FS y obtención de modelos QSPR de valores cuantitativos de enantio-resolución de compuestos quirales estructuralmente no relacionados en un sistema cromatográfico dado. La estrategia propuesta se probó para la predicción de los valores de resolución máxima (R_s *max*) de 56 compuestos quirales de 14 familias químicas diferentes cromatografiados en la CSP Cell1 y fases móviles acuosas de ACN (casi los mismos compuestos y fases móviles de ACN estudiados en el Artículo II) a partir de información estructural seleccionada. También se sugirió una aproximación de la importancia relativa de las variables seleccionadas para predecir cuantitativamente la R_s *max*.

Los 56 compuestos estudiados se dividieron en tres bloques: (i) el bloque de entrenamiento para el aprendizaje con 49 compuestos, (ii) el bloque de validación para el control del sobreajuste con 7 compuestos que cubrían un intervalo representativo de valores de *Rs max*, y (iii) el bloque test, para mejorar la robustez, que incluía 9 conjuntos de 5 compuestos de entrenamiento diferentes utilizados para la validación cruzada y también como compuestos de prueba.

Se propuso una estrategia basada en un nuevo indicador de calidad (*Q*), calculado a partir de 9 parámetros proporcionados por la ANN, que se diseñó para adaptarse a la complejidad de los datos y al tamaño limitado del conjunto de datos a efectos de modelización con ANNs. Esta estrategia permitió: (i) seleccionar una arquitectura de ANN sencilla (con una sola capa oculta de siete neuronas) que presentó una capacidad predictiva adecuada, y (ii) un proceso de FS-ANN secuencial (variable a variable) que dio lugar a la selección de ocho variables predictivas.

Por último, el estudio de la importancia relativa de las ocho variables seleccionadas en el modelo QSPR, que combinó estimaciones de dos enfoques diferentes, sugirió que la tensión superficial (contribución positiva a la *Rs max*) y el número de grupos aminas secundarias en la molécula (contribución negativa a la *Rs max*) eran las características estructurales más importantes de los compuestos para la predicción de la enantio-resolución en las condiciones experimentales ensayadas.

La descripción de los perfiles de los picos cromatográficos se ha estudiado ampliamente, para ello se han propuesto un gran número de funciones matemáticas. Entre ellas, se ha destacado la precisión alcanzada con los modelos gaussianos modificados que describen la desviación de un pico gaussiano ideal como un cambio en la varianza o desviación estándar del pico a lo largo del tiempo. Estos modelos son, de hecho, una familia de funciones de diferente complejidad con gran flexibilidad para ajustar picos cromatográficos con una gran variedad de asimetrías y formas. Sin embargo, puede producirse un comportamiento incontrolado de la señal fuera de la región que se está ajustando, lo que obliga a utilizar diferentes estrategias para resolver este problema.

En este trabajo se comparó el rendimiento de los modelos LMG (*Linear modified Gaussian*), PVMG (*Parabolic variance modified Gaussian*) y PLMG (*Parabolic-Lorentzian modified Gaussian*) con variantes obtenidas mediante la combinación de los modelos gaussianos modificados con una ecuación que añade una cola exponencial y con otras funciones que limitan el crecimiento de la variable independiente. El comportamiento de las aproximaciones se comprobó mediante el ajuste simultáneo de picos enantioméricos que presentan un amplio rango de características (p. ej., diversos valores de asimetría, tiempos de retención, R_s y EF), obtenidos en la separación de ocho fármacos quirales (bupivacaína, flurbiprofeno, ibuprofeno, ketoprofeno, metoprolol, omeprazol, propranolol y trimepracina) por HPLC utilizando diferentes CSPs, fases móviles, temperaturas y valores de pH . El estudio también se llevó a cabo con el fin de realizar la deconvolución de los picos de los enantiómeros, cuando éstos no están completamente resueltos, para evaluar la fracción enantiomérica.

Los modelos de picos gaussianos modificados estudiados permitieron el ajuste de picos cromatográficos con una amplia gama de propiedades. El modelo LMG obtuvo los peores resultados, sólo proporcionó ajustes adecuados para picos suficientemente simétricos. El modelo PVMG proporcionó ajustes satisfactorios para la mayoría de los picos, siendo el modelo elegido para compuestos que presentan perfiles convencionales. El modelo PLMG proporcionó los mejores ajustes (con errores inferiores al 1% para la mayoría de los compuestos y significativamente menores que los obtenidos con los modelos LMG y PVMG), aunque en algunas situaciones pueden surgir problemas de sobreajuste o de colas insatisfactorias.

Para establecer correctamente la forma del pico en picos solapados, es necesario restringir los modelos. Si los modelos se aplican sin ninguna restricción, tienden a sobreajustarse y a transferir una fracción de área de un pico a otro si esto conduce a un mejor ajuste. La aplicación de colas exponenciales puede eliminar eficazmente los problemas de cola, pero no mejora sustancialmente los ajustes. La aplicación de la función sigmoideal es una opción adecuada, presenta resultados aceptables y es más fácil de aplicar.

La deconvolución de los picos enantioméricos de un compuesto quiral dado, cuando éstos están insuficientemente separados, también es posible si dicha resolución no es demasiado baja. Se compararon los modelos que mostraron los mejores resultados en el ajuste de picos cromatográficos (PLMG y PVMG). Ambos modelos generaron un buen ajuste de los picos, con áreas totales similares. Cuando la enantio-resolución fue suficiente ($R_s > 1.0$), todos los enfoques dieron valores de EF similares. Sin embargo, para resoluciones más bajas la variabilidad fue mayor. Dicha variación fue apreciablemente mayor para el modelo PLMG que para el modelo PVMG.

Deberían realizarse más estudios para resolver los problemas encontrados, p.ej. limitando la variación de la forma de los picos. También debería desarrollarse un procedimiento para mantener constante la EF en el procedimiento de deconvolución y los modelos propuestos deberían seguir siendo probados cuando la EF esté lejos de ser racémica ($EF = 0.5$).

Como ya se ha comentado anteriormente, a pesar de la reconocida importancia de la estereoquímica en farmacología, a menudo se ha ignorado en el campo de la investigación medioambiental. La enantioselectividad en los procesos de ecotoxicidad y biodegradación es evidente y paralela a la observada en los ámbitos médico y biomédico.

Trimepracina es un antihistamínico tricíclico que suele emplearse como antiemético para prevenir el mareo, o como antihistamínico en combinación con otros medicamentos para aliviar la tos y el resfriado.

El objetivo de este trabajo fue estudiar, por primera vez, la posible biodegradación enantioselectiva de los enantiómeros de trimepracina mediante ensayos de biodegradabilidad inmediata en condiciones similares a las recomendadas en los ensayos de la OECD. Otros objetivos planteados fueron: (i) conectar la biodegradación enantioselectiva con el crecimiento microbiano; (ii) aplicar un método de ajuste de curvas para los datos de concentración (S), biodegradación (BD) y, también, por primera vez, de EF a lo largo del tiempo para ampliar la utilidad de los resultados; (iii) realizar un estudio de precisión sobre los datos de S y EF en condiciones de precisión intermedia, por primera vez.

Los experimentos se llevaron a cabo en modo discontinuo utilizando un medio salino con un inóculo de lodo activado procedente de una EDAR local al que se le adicionó *rac*-trimepracina a tres niveles de concentración (4.8, 9.0 and 18.0 mg L⁻¹). Las muestras se incubaron con agitación (150 rpm) a 20 °C bajo ciclos de luz natural durante 23 días. Para la monitorización de las concentraciones de los enantiómeros de trimepracina a diferentes tiempos de incubación prefijados se desarrolló un método de RPLC quiral que utiliza Cell1 como CSP y una mezcla ACN:NaClO₄ 0.5 M (40:60, v/v) como fase móvil.

Los valores de EF calculados constituyen la primera evidencia de biodegradación enantioselectiva de la trimepracina. La enantioselectividad máxima observada (valor mínimo de EF) fue de 0.44. El crecimiento de la biomasa (establecido indirectamente mediante medidas de la densidad óptica a 600 nm, OD_{600}), sugirió que el proceso de biodegradación enantioselectiva se produce durante la fase estacionaria (más que en la etapa de crecimiento exponencial).

El ajuste de curvas mediante una aproximación tipo Michaelis-Menten (modelo Monod simplificado) proporcionó curvas $S-t$ que se ajustaron bien a los datos experimentales. Estas curvas permitieron obtener curvas $BD-t$ y, por primera vez, $EF-t$. A partir de las curvas ajustadas $BD-t$ se estimaron los tiempos de semivida: $t_{1/2} \sim 4.5$ días para ambos enantiómeros en el nivel de concentración estudiado más alto; $t_{1/2} \sim 4.5$ y ~ 6 en el nivel de concentración intermedio para el enantiómero menos (E1) y más (E2) retenido, respectivamente; y $t_{1/2} \sim 5$ días para E1 en el nivel

de concentración más bajo, no se pudo estimar $t_{1/2}$ para E2 porque nunca alcanzó $BD = 50\%$. La similitud entre las curvas $EF - t$ para los tres niveles de concentración ensayados indicó que la enantioselectividad es independiente de la concentración.

Se observó una imprecisión moderada en los valores de S (en condiciones de repetibilidad) y, por primera vez, en EF (en condiciones de precisión intermedia). Esta imprecisión debería tenerse en cuenta en trabajos futuros al emplear modelos cinéticos de Monod o modelos alternativos.

Los resultados obtenidos en este trabajo sugieren que trimepricina posee una biodegradación enantioselectiva moderada potencial en EDARs. Los resultados de este estudio sugieren que trimepricina presenta degradación potencial en diversos entornos, de acuerdo con las directrices de la OECD. Sin embargo, no se recomienda la extrapolación de estos resultados directamente a escalas medioambientales o de tratamiento de aguas residuales.

De forma similar al artículo anterior, en el presente trabajo pretende contribuir al avance del conocimiento de los riesgos y peligros de los contaminantes quirales. En concreto, en este trabajo se estudia la biodegradación enantioselectiva de ibuprofeno y ketoprofeno, antiinflamatorios no esteroideos quirales de uso muy extendido.

Ibuprofeno y ketoprofeno presentan propiedades antiinflamatorias y analgésicas. Los beneficios terapéuticos de estos fármacos se atribuyen principalmente a sus enantiómeros *S*. Pese a ello, suelen comercializarse como mezclas racémicas.

Existe cierta controversia sobre la biodegradación enantioselectiva de ibuprofeno y ketoprofeno en EDARs y ensayos de laboratorio. Las variaciones encontradas en los valores de *EF* de ibuprofeno y ketoprofeno durante la biodegradación se han atribuido no sólo a la degradación más rápida de un enantiómero en comparación con la del otro (degradación enantioselectiva), sino también a la existencia de inversión quiral por parte de enzimas, o debido a la combinación de ambos procesos.

El objetivo de este trabajo fue la evaluación de la biodegradación de los enantiómeros de ibuprofeno y ketoprofeno mediante ensayos de biodegradabilidad inmediata, compatibles con las directrices de la OECD. El procedimiento seguido fue similar al utilizado en el Artículo V. Las concentraciones ensayadas fueron 15.6 mg L⁻¹ de *rac*-ibuprofeno y 18.0 mg L⁻¹ de *rac*-ketoprofeno. Para separar los enantiómeros de ibuprofeno y ketoprofeno, se ensayaron CSPs de derivados de celulosa y amilosa (Am2, Cell1, Cell3 y Cell5) y mezclas binarias de ácido fórmico (0.1 %, v/v) con ACN o MeOH en proporciones variables (25-80 % en volumen de ACN; 75-92 % en volumen de MeOH). Se ensayaron temperaturas de separación comprendidas entre 15 y 25 °C.

Otro objetivo de este trabajo es el desarrollo de una nueva estrategia para estimar parámetros significativos relacionados con el proceso de biodegradación utilizando las áreas de los picos cromatográficos de los enantiómeros en lugar de su concentración. Esta estrategia se diseñó para eliminar la incertidumbre asociada a la etapa de calibración y para reducir el esfuerzo y el coste experimentales. Adicionalmente, se propusieron ecuaciones nuevas para modelar las curvas *BD-t* y *EF-t* utilizando las áreas de pico de los enantiómeros como variables dependientes. La eficacia de esta estrategia se comparó con la de los modelos convencionales.

Los sistemas cromatográficos seleccionados para monitorizar los enantiómeros de los antiinflamatorios no esteroideos estudiados en los ensayos de biodegradabilidad fueron: Cell3, MeOH:HCOOH (0.1 %, v/v), 80:20 (v/v), 25 °C para ibuprofeno; Am2, ACN:HCOOH (0.1 %, v/v), 35:65 (v/v), 15 °C para ketoprofeno. Estos métodos fueron rápidos (tiempos de retención inferiores

a 10 min) y permitieron la separación completa de los enantiómeros de ambos analitos ($R_s = 2.8$ para ibuprofeno y $R_s = 1.6$ para ketoprofeno).

El ensayo de biodegradabilidad inmediata mostró que los enantiómeros de ibuprofeno y ketoprofeno eran fácilmente biodegradables con una degradación abiótica no significativa. Estos resultados sugieren que estos fármacos presentan una degradación potencial en diversos entornos, de acuerdo con las directrices de la OECD. Sin embargo, no se recomienda la extrapolación de estos resultados directamente a escalas medioambientales o de tratamiento de aguas residuales.

Se observó que ibuprofeno presenta una biodegradabilidad enantioselectiva, siendo la BD de (R)-ibuprofeno mayor que la BD de (S)-ibuprofeno. No se observó una biodegradación enantioselectiva para ketoprofeno.

Los valores máximos de OD_{600} se obtuvieron al quinto día de las pruebas de biodegradación para ambos analitos. Durante la fase estacionaria de crecimiento, se observó el comportamiento diferencial de los enantiómeros de ibuprofeno.

Las nuevas ecuaciones propuestas utilizando las áreas de los picos cromatográficos proporcionaron estimaciones similares a las obtenidas utilizando datos de S . Sin embargo, el uso de áreas eliminó la incertidumbre asociada a los cálculos derivados de curvas de calibración y proporcionó estimaciones más precisas de BD y EF .

El uso de los valores de área de pico permitió estimar parámetros significativos relacionados con el proceso de biodegradación: (i) para (R)-ibuprofeno y (S)-ibuprofeno se estimaron valores de $t_{1/2}$ de 18 y 25 días, respectivamente, mientras que para ambos enantiómeros de ketoprofeno se estimaron valores de $t_{1/2}$ de 12 días; (ii) se requirieron 60-80 días para alcanzar valores de BD próximos al 100 % para los enantiómeros de ibuprofeno, mientras que se precisaron 25 días para los enantiómeros de ketoprofeno; (iii) el valor de EF de ibuprofeno disminuyó a aproximadamente 0.4 a los 28 días y el valor mínimo esperado es de aproximadamente 0.2 a los 60 días.

De forma similar a los artículos V y VI, en el presente trabajo se estudia la biodegradación enantioselectiva de bupivacaína, mepivacaína, prilocaína y propanocaína, anestésicos locales de amplio uso en hospitales.

Los anestésicos locales son analgésicos de uso común que bloquean temporalmente la producción y transmisión de señales de dolor en el tejido nervioso. Se han descrito diferencias en las propiedades farmacocinéticas, farmacodinámicas y toxicológicas de los enantiómeros de los anestésicos locales quirales. Por ejemplo, el enantiómero (*R*)-bupivacaína es más potente y tóxico que el enantiómero (*S*)-bupivacaína.

Se ha detectado la presencia de mepivacaína, lidocaína, bupivacaína, prilocaína, procaína y benzocaína en muestras de aguas residuales en concentraciones del orden de ng L^{-1} . Sin embargo, hasta nuestro conocimiento, no existen estudios que aborden la posible biodegradación enantioselectiva de estos compuestos.

Uno de los objetivos de este artículo fue realizar un estudio exhaustivo sobre la retención y resolución de los enantiómeros de bupivacaína, mepivacaína, prilocaína y propanocaína utilizando cinco CSPs de derivados de celulosa (Cell1, Cell2, Cell3, Cell4 y Cell5) y tres derivados de amilosa (Am1, Am2 y Am3) y mezclas binarias de NH_4HCO_3 (5 mM, $\text{pH} = 8.0$) con MeOH o ACN en proporciones variables (30-90 % en volumen de MeOH, 10-100 % en volumen de ACN) como fases móviles. También se ensayaron diferentes temperaturas de separación comprendidas entre 15 y 40 °C. Los resultados del estudio se utilizaron para proponer las condiciones cromatográficas experimentales óptimas para determinar los enantiómeros de los anestésicos en estudio en muestras acuosas utilizando detección por MS, con el fin de realizar, por primera vez, ensayos de biodegradabilidad inmediata, compatibles con las directrices de la OECD. El procedimiento seguido fue similar al utilizado en los Artículos V y VI. Las concentraciones ensayadas fueron 19.8 mg L^{-1} para *rac*-bupivacaína, 20.6 mg L^{-1} para *rac*-mepivacaína, 21.0 mg L^{-1} para *rac*-prilocaína y 21.0 mg L^{-1} para *rac*-propanocaína. Para estimar los parámetros significativos relacionados con el proceso de biodegradación se utilizó el enfoque cromatográfico directo propuesto en el Artículo VI.

El estudio del comportamiento de retención de los enantiómeros de bupivacaína, mepivacaína, prilocaína y propanocaína en cinco CSPs derivados de celulosa (Cell1, Cell2, Cell3, Cell4 y Cell5) y tres CSPs derivados de amilosa (Am1, Am2, Am3) reveló que para las fases móviles hidro-orgánicas que contienen MeOH, los compuestos mostraron un comportamiento típico de RPLC. Mientras que para las fases móviles que contienen ACN, los compuestos mostraron un comportamiento HILIC o RPLC, en función del contenido de agua en la fase móvil, tal y como se comentó en el Artículo II.

La enantioselectividad de las CSPs ensayadas hacia los enantiómeros de bupivacaína, mepivacaína, prilocaína y propanocaína fue diferente. La CSP Cell2 permitió la resolución completa de los enantiómeros de mepivacaína, prilocaína y propanocaína, mientras que las CSP Cell1, Am2 y Am3 no permitieron la enantio-resolución de los compuestos estudiados. La CSP Cell4 permitió la resolución de los enantiómeros de prilocaína y propanocaína, mientras que las CSPs Cell3, Cell5 y Am1 sólo proporcionaron la enantio-resolución completa para uno de los anestésicos locales (bupivacaína, mepivacaína y prilocaína, respectivamente).

Los sistemas cromatográficos seleccionados para monitorizar los enantiómeros de los anestésicos locales estudiados en los ensayos de biodegradabilidad fueron: Cell3, MeOH:NH₄HCO₃ (5 mM, pH = 8.0), 70:30 (v/v), 0.50 mL min⁻¹, 40 °C, para bupivacaína; Cell5, ACN:NH₄HCO₃ (5 mM, pH = 8.0), 50:50 (v/v), 0.75 mL min⁻¹, 25 °C para mepivacaína; Cell4, ACN:NH₄HCO₃ (5 mM, pH = 8.0), 40:60 (v/v), 1.00 mL min⁻¹, 25 °C para prilocaína y propanocaína. Estos métodos fueron rápidos (tiempos de retención inferiores a 14 min) y permitieron la separación completa de los enantiómeros de los analitos (*R_s* = 1.5, 2.0, 1.8 y 2.0 para bupivacaína, mepivacaína, prilocaína y propanocaína, respectivamente).

La degradación estimada a los 28 días de incubación para los ensayos biótico y abiótico de los enantiómeros de bupivacaína y mepivacaína fue inferior al 20 %; por consiguiente, de acuerdo con las directrices de la OCDE, bupivacaína y mepivacaína pueden considerarse como compuestos potencialmente persistentes. Estos resultados deberían confirmarse mediante ensayos de simulación o de biodegradabilidad inherente.

En cambio, para los enantiómeros de prilocaína, la degradación microbiológica y fisicoquímica a los 28 días de incubación fue incompleta pero notable (~69 % y 23 % para los ensayos bióticos y abióticos, respectivamente). En el caso de los enantiómeros de propanocaína se observó una biodegradación próxima al 100 % en tres días. En cuanto a los ensayos abióticos, la degradación fisicoquímica de propanocaína no fue significativa (< 20 %) hasta los 14 días y alcanzó el ~ 53 % tras 28 días de incubación. Según las directrices de la OCDE, los enantiómeros de prilocaína y propanocaína muestran una biodegradabilidad aeróbica inherente. Para ambos compuestos, los valores de *EF* se aproximaron a 0.5 durante el transcurso del ensayo de biodegradabilidad, lo que indica la ausencia de mecanismos enantioselectivos en los procesos de biodegradación.

ABBREVIATIONS, ACRONYMS AND SYMBOLS

Abbreviations and acronyms

AAD:	antiarrhythmic drug
ACD:	anticholinergic drug
ACN:	acetonitrile
ACO:	anticoagulant
AD:	antidepressant
AF:	antifungal
AGP:	α_1 -acid glycoprotein
AH:	antihistamine
Am1:	coated amylose tris(3,5-dimethylphenylcarbamate)
Am2:	coated amylose tris(5-chloro-2-methylphenylcarbamate)
Am3:	immobilised amylose tris(3-chloro-5-methylphenylcarbamate)
ANAL:	analgesic
ANOVA:	analysis of variance
ANN:	artificial neural network
ANP:	antineoplastic
APCI:	atmospheric pressure chemical ionisation
APD:	antipsychotic drug
BB:	β -blocker
BD:	bronchodilator
BSA:	bovine serum albumin
BUPI:	bupivacaine
CaB:	calcium channel blocker
CART:	classification and regression tree
CBH:	cellobiohydrolase
CD:	cyclodextrin
CEC:	capillary electrochromatography
Cell1:	coated cellulose tris (3,5-dimethylphenylcarbamate)
Cell2:	coated cellulose tris(3-chloro-4-methylphenylcarbamate)
Cell3:	coated cellulose tris(4-methylbenzoate)
Cell4:	coated cellulose tris(4-chloro-3-methylphenylcarbamate)
Cell5:	immobilised cellulose tris(3,5-dichlorophenylcarbamate)
COFs:	covalent-organic frameworks
CoMFA:	comparative molecular field analysis
CoMSIA:	comparative molecular similarity indexes analysis
CSPs:	chiral stationary phases
CSR:	combined squared roots
CSs:	chiral selectors
DAD:	diode array detector
DEA:	diethylamine

Abbreviations and acronyms

DL:	discrimination level
DPLS:	discriminant partial least squares
DPLS1:	discriminant partial least squares on one single response
EEO:	enantiomer elution order
EKC:	electrokinetic chromatography
EMG:	exponentially modified Gaussian
ESI:	electrospray ionisation
ETA:	extended topochemical atom
EtOH:	ethanol
EVA:	normal mode eigenvalues
E1:	least retained enantiomer
E2:	most retained enantiomer
FDD:	fractional factorial design
FLU:	flurbiprofen
FS:	feature selection
FS-ANN:	artificial neural networks-feature selection
FS-DPLS1:	discriminant partial least squares-feature selection
GA:	genetic algorithm
GC:	gas chromatography
GETAWAY:	geometry, topology, and atom-weights assembly
GEX:	generalized exponential
HILIC:	hydrophilic interaction liquid chromatography
HPLC:	high performance liquid chromatography
HSA:	human serum albumin
IBU:	ibuprofen
i.d.:	internal diameter
KET:	ketoprofen
LA:	local anaesthetic
LMG:	linear modified Gaussian
LOD:	limit of detection
LOQ:	limit of quantification
MeOH:	methanol
MEPI:	mepivacaine
MET:	metoprolol
MI:	mutual information
MIA:	multivariate image analysis
MIPs:	molecular imprinted polymers
MLR:	multiple linear regression
MOFs:	metal-organic frameworks
MoRSE:	molecule representation of structures based on electron diffraction
MP:	mobile phase

Abbreviations and acronyms

MS:	mass spectrometry
MSM:	minimal salts medium
NMR:	nuclear magnetic resonance
NPLC:	normal phase liquid chromatography
NSAID:	non-steroidal anti-inflammatory drug
OECD:	Organisation for the Economic Cooperation and Development
OLS:	ordinary least squares
OME:	omeprazole
OVM:	ovomucoid
PA:	preservative agent
PCA:	principal component analysis
PEMG:	polynomial-exponential modified Gaussian
PLMG:	parabolic Lorentzian modified Gaussian
PLS:	partial least squares
PMG:	polynomial modified Gaussian
PPI:	proton pump inhibitor
PRILO:	prilocaine
PRO:	propranolol
PROPA:	propanocaine
PVMG:	parabolic variance modified Gaussian
QSERR:	quantitative structure-enantioselective retention relationship
QSPR:	quantitative structure-property relationship
QSRR:	quantitative structure-retention relationship
RDF:	radial distribution function
RF:	random forest
ROI:	retention order index
RPLC:	reversed-phase liquid chromatography
SFC:	supercritical fluid chromatography
SIM:	selected ion monitoring
SVM:	support vector machines
TIC:	total current ion chromatogram
TLC:	thin layer chromatography
TRI:	trimeprazine
UV:	ultraviolet
VolSurf:	volume and surface
WHIM:	weighted holistic invariant molecular
WWTP:	waste water treatment plant

Structural descriptors and physicochemical properties

<i>Abc</i> :	aromatic bond count, number of aromatic bonds in the molecule
<i>abc</i> :	aliphatic bond count, number of non-aromatic bonds in the molecule excluding bonds of hydrogen atoms
<i>ACA</i> :	number of moieties Ar-C-Ar (Ar is aromatic ring)
<i>ACH3</i> :	number of methyl groups bonded to an aromatic ring in the molecule
<i>ACl</i> :	number of chlorine atoms bonded to an aromatic ring in the molecule
<i>ACOOR</i> :	number of ester groups bonded to an aromatic ring in the molecule
<i>ANHCOR</i> :	number of amide groups bonded to an aromatic ring in the molecule
<i>AOH</i> :	number of hydroxy groups bonded to an aromatic ring in the molecule
<i>AOR</i> :	number of ether groups bonded to an aromatic ring in the molecule
<i>Arc</i> :	aromatic ring count, number of aromatic rings in the molecule
<i>arc</i> :	aliphatic ring count, number of rings in the molecule that have non-aromatic bonds
<i>A12</i> :	number of aromatic groups with 1,2 substitution
<i>A123</i> :	number of aromatic groups with 1,2,3 substitution
<i>A14</i> :	number of aromatic groups with 1,4 substitution
<i>A124</i> :	number of aromatic groups with 1,2,4 substitution
<i>bc</i> :	bond count, number of bonds in the molecule including hydrogens
<i>Bi</i> :	Balaban index
<i>C*</i> :	chiral carbon atom
<i>C*A</i> :	number of aromatic groups bonded to the chiral carbon
<i>C*a</i> :	number of aliphatic groups bonded to the chiral carbon
<i>C*C=O</i> :	number of carbonyl groups bonded to the chiral carbon
<i>C*H</i> :	number of hydrogen atoms bonded to the chiral carbon
<i>C*hA</i> :	number of aromatic heterocycles groups bonded to the chiral carbon
<i>C*X</i> :	number of heteroatoms bonded to the chiral carbon
<i>C*XH</i> :	number of hydroxy or amine groups bonded to the chiral carbon
<i>C</i> :	number of carbon atoms in the molecule
<i>Cl</i> :	number of chlorine atoms in the molecule
<i>Crc</i> :	carbo ring count, number of rings in the molecule that contain carbon atoms only
<i>F</i> :	number of fluorine atoms in the molecule
<i>fArc</i> :	fused aromatic ring count, number of aromatic rings having common bonds with other rings
<i>frc</i> :	fused ring count, number of fused rings in the molecule (having common bonds)
<i>fsp3</i> :	number of sp ³ hybridized carbons divided by the total carbon count
<i>HArc</i> :	heteroaromatic ring count, number of aromatic heterocycles in the molecule
<i>Harc</i> :	heteroaliphatic ring count, number of aliphatic heterocycles in the molecule
<i>HBA</i> :	number of hydrogen bond acceptors in the molecule
<i>HBD</i> :	number of hydrogen bond donors in the molecule
<i>HOMO</i> :	highest occupied molecular orbital
<i>Hrc</i> :	hetero ring count, number of rings in the molecule that contain hetero atoms
<i>iP</i> :	number of isopropyl groups in the molecule

Structural descriptors and physicochemical properties

$\log D$:	logarithm of the distribution coefficient at a given pH
$\log P$:	logarithm of the <i>n</i> -octanol/water partition coefficient
LUMO:	lowest unoccupied molecular orbital
MR :	molecular refractivity
M_r :	molecular mass
MSA :	molecular surface area
MV :	molar volume
NA :	number of nitrogen aromatic groups
NHR :	number of secondary amine groups in the molecule
NRc :	number of tertiary amines in aliphatic cycles
$NR2$:	number of tertiary amine groups in the molecule
O :	number of oxygen atoms in the molecule
OEC^* :	orbital electronegativity of the chiral carbon
OH :	number of hydroxyl groups in the molecule
pK_a :	minus logarithm of the acidity constant
PSA :	polar surface area
Rbc :	ring bond count, number of ring bonds
Rc :	ring count, number of rings in the molecule
ROR :	number of ether groups in the molecule
Rsc :	ring system count, number of disjunct ring systems
S :	number of sulphur atoms in the molecule
Sc :	number of sulphur atom in cycles
$Srss$:	smallest ring system size, number of rings in the smallest ring system
ST :	surface tension
tB :	number of tert-butyl groups in the molecule
$zmax$:	maximal z length
$zmin$:	minimal z length

Chromatographic parameters

α :	selectivity factor
ϕ :	percentage of organic modifier in the mobile phase
σ :	peak standard deviation (or related parameter)
σ_G and t_G :	coefficients of the precursor Gaussian signal
τ :	time constant
A :	peak area
A_0 :	initial peak area at $t = 0$ days
a and b :	left and right, respectively, half-width related parameters
B/A :	asymmetry factor where A is the left half-width and B is the right half-width
CRs :	categorical enantioresolution
h_0 or H_0 :	height at the peak maximum

Chromatographic parameters

$h(t)$:	peak height at a given time t
k :	retention factor
k_1 :	retention factor for the least retained enantiomer
k_2 :	retention factor for the most retained enantiomer
k_{w2} :	k_2 extrapolated to a 100 % aqueous mobile phase
M_0 :	peak area
m/z :	mass/charge ratio
N :	efficiency
Rs :	enantioresolution
$Rs\ max$:	maximum enantioresolution
S :	eluent strength from Snyder equation
t_R :	retention time
t_{R1} :	retention time for the least retained enantiomer
t_{R2} :	retention time for the most retained enantiomer
t_0 :	gross hold-up time
t_1 and t_2 :	parameters related to the peak position
t_i :	initial time
w :	peak width at 50 % peak height

Biodegradation related parameters

μ_m :	maximum specific growth rate
AD :	abiotic degradation
BD :	microbial degradation (biodegradation)
BD_{7d} :	biodegradation after seven days of incubation
D :	degradation value obtained in a 28-day test
D_{10w} :	degradation value in a 10-day window within a 28-day test
EF :	enantiomeric fraction
k :	first-order rate constant
K_s :	half saturation constant for growth or Monod constant
OD_{600} :	optical density at 600 nm
S :	substrate concentration
S_0 :	initial substrate concentration at $t=0$ days
$t_{1/2}$:	half-life time
V_m :	maximum specific growth rate (maximal rate)
X :	biomass concentration
X_0 :	initial biomass concentration
Y :	yield coefficient: mass of biomass per mass of substrate

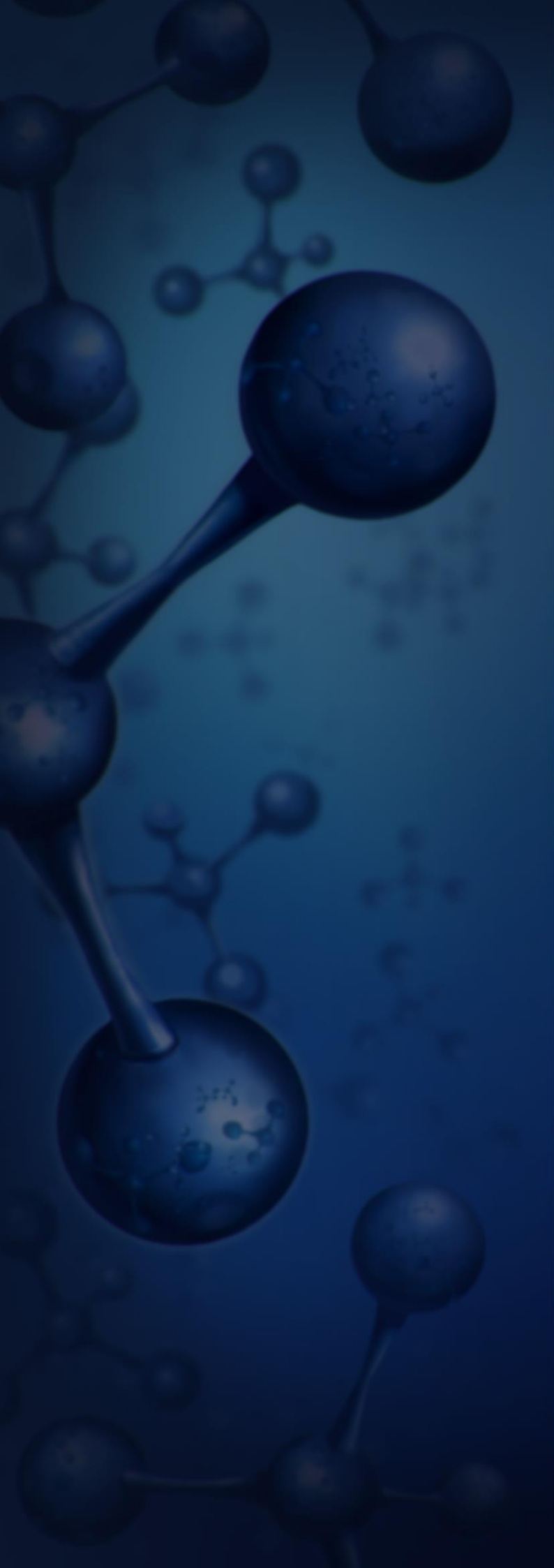
Statistical parameters

b_0 :	intercept of calibration curve
b_1 :	slope of calibration curve
dD :	discriminant distance
dD_{cv} :	discriminant distance in cross validation
k, kk :	number of neurons in the hidden layers
MSE :	mean squared error
MS_r :	residual mean square
MS_{run} :	between-run mean square
$mUrb$:	mean of the relative uncertainty
No :	numbered order
Nr :	number of replicates
Ns :	number of series (incubation times)
Nv :	number of structural variables
$pMSE$:	penalised mean squared errors
Q :	quality target indicator
R :	correlation coefficient
R^2 :	determination coefficient
RSD :	relative standard deviation
RSD_r :	relative standard deviation in repeatability conditions
RSD_{run} :	between-run relative standard deviation
s :	standard deviation
s_{mean} :	standard deviation of the grand mean
s_r :	standard deviation in repeatability conditions
s_{run} :	between-run standard deviation
SS_{class} :	sum of squares for the difference between predicted and actual discriminant level values
TI :	target indicator
Wi :	inner weights
\mathbf{X} :	predictor matrix
\mathbf{y} or \mathbf{Y} :	response vector or matrix
$\hat{\mathbf{y}}$:	estimated response vector

TABLE OF CONTENTS

I.- INTRODUCTION	1
I.1.- Significance of chirality	3
I.2.- Separation of enantiomers of chiral compounds	4
I.2.1.- Chiral stationary phases in HPLC	5
I.2.1.1.- Small organic molecule-based CSPs	6
I.2.1.2.- Macromolecule-based CSPs	14
I.3.- Modelling approaches for enantioseparations in HPLC with CSPs	21
I.4.- Deconvolution of peaks in chiral liquid chromatography	31
I.4.1.- Peak models	31
I.5.- Chiral pollutants	37
I.5.1.- Biodegradation: concept and evaluation	39
I.5.2.- Evaluation of the enantioselective biodegradability of chiral pollutants	43
II.- OBJECTIVES	45
III.- METHODOLOGY	49
III.1.- Instrumentation	51
III.2.- Chemicals and solutions	52
III.3.- Experimental procedures	62
III.3.1.- Chiral columns conditioning	62
III.3.2.- Chromatographic conditions	62
III.3.3.- Biodegradability tests	67
III.4.- Software and calculations	67
IV.- SUMMARY OF THEMATIC, RESULTS AND CONCLUSIONS	69
IV.1.- Comparative modelling study on enantioresolution of structurally unrelated compounds with amylose-based chiral stationary phases in reversed phase liquid chromatography-mass spectrometry conditions. Paper I	71
IV.1.1.- Brief introduction and objectives	71
IV.1.2.- Results and discussion	72
IV.1.2.1.- Retention behaviour and enantioresolution studies	72
IV.1.2.2.- Structure-categorical enantioresolution relationships in amylose-based CSPs	75
IV.1.3.- Conclusions	80
IV.2.- Comparative study on retention behaviour and enantioresolution of basic and neutral structurally unrelated compounds with cellulose-based chiral stationary phases in reversed phase liquid chromatography-mass spectrometry conditions. Paper II	81
IV.2.1.- Brief introduction and objectives	81
IV.2.2.- Results and discussion	82
IV.2.2.1.- Retention behaviour study	82
IV.2.2.2.- Enantioresolution study	84
IV.2.3.- Conclusions	88

IV.3.- Artificial neural networks to model the enantioresolution of structurally unrelated neutral and basic compounds with cellulose tris(3,5-dimethylphenylcarbamate) chiral stationary phase and aqueous-acetonitrile mobile phases. Paper III	89
IV.3.1.- Brief introduction and objectives	89
IV.3.2.- Results and discussion	90
IV.3.2.1.- ANN architecture optimisation, feature selection and predictive ability	91
IV.3.2.2.- Importance of variables	93
IV.3.3.- Conclusions	94
IV.4.- Modified Gaussian models applied to the description and deconvolution of peaks in chiral liquid chromatography. Paper IV	95
IV.4.1.- Brief introduction and objectives	95
IV.4.2.- Results and discussion	95
IV.4.2.1.- Fitting performance	95
IV.4.2.2.- Peak deconvolution	98
IV.4.3.- Conclusions	99
IV.5.- Trimeprazine is enantioselectively degraded by an activated sludge in ready biodegradability test conditions. Paper V	100
IV.5.1.- Brief introduction and objectives	100
IV.5.2.- Results and discussion	101
IV.5.2.1.- Chiral chromatographic analysis	101
IV.5.2.2.- Enantioselective biodegradation results	101
IV.5.2.3.- Kinetic assessment of the data. Curve fitting	103
IV.5.2.4.- Precision study under intermediate precision conditions	104
IV.5.3.- Conclusions	105
IV.6.- Direct chromatographic study of the enantioselective biodegradation of ibuprofen and ketoprofen by an activated sludge. Paper VI	106
IV.6.1.- Brief introduction and objectives	106
IV.6.2.- Results and discussion	107
IV.6.2.1.- Chiral chromatographic separation	107
IV.6.2.2.- Biodegradation assays and chromatographic information	107
IV.6.3.- Conclusions	111
IV.7.- Reversed phase liquid chromatography for the enantioseparation of local anaesthetics in polysaccharide-based stationary phases. Application to biodegradability studies. Paper VII	112
IV.7.1.- Brief introduction and objectives	112
IV.7.2.- Results and discussion	112
IV.7.2.1.- Chiral chromatographic separation	112
IV.7.2.2.- Biodegradability assays	115
IV.7.3.- Conclusions	117
V.- GENERAL CONCLUSIONS AND FUTURE STUDIES	119
VI.- REFERENCES	125
VII.- APPENDIX: PUBLICATIONS	149



I.- INTRODUCTION

I.1.- Significance of chirality

Chirality is a structural property of a molecule whereby is able to exist in two asymmetric forms, which are mirror images. Usually, chirality is caused by chiral carbon atoms, but also by sulfur, phosphorus or nitrogen atoms. The chiral nature of living systems has obvious implications for the biologically active compounds that interact with them. At the molecular level, chirality represents an intrinsic property of the essential building blocks of life, such as amino acids and sugars, and therefore, of peptides, proteins, enzymes, carbohydrates, nucleosides and a number of alkaloids and hormones. Consequently, processes mediated by biological systems are stereochemistry-sensitive, and a pair of enantiomers can have different effects on living organisms [1].

Chirality has implications in different scientific fields, mainly in the pharmaceutical field, but also in other such as the food and nutrition, clinical and environmental fields. For instance, the presence of D-amino acids in food, originated in food processing or resulting from microbiological sources, can lead to nutritionally poorer and less safe products [2]. Furthermore, the detection of filbertone (the main flavour component of hazelnuts) can be an indication of adulteration of extra virgin olive oil [3]. An example of chiral clinical applications is the determination of 2-hydroxy acids in urine that can be useful for the diagnosis of the maple syrup urine disease [4]. Other examples are chiral nanomaterials which are promising strategies for anti-tumour therapy [5].

The pharmaceutical industry has been the main contributor to the development of chirality research. Several reviews on this issue have been reported in the literature [6,7]. Great attention has been paid to the development of safer and more effective drugs. When a given racemic mixture of a drug is administered and enters into the human body, there are some pharmacodynamic, pharmacokinetic and toxicological processes that may exhibit a certain degree of enantioselectivity, so it could result in different pharmacological activity of the enantiomers. In some cases, pharmacological activity exists in one enantiomer (eutomer) whereas the other one (distomer) might be inactive, or less potent, or present a different pharmacological activity or even be a toxic enantiomer [6,8-10]. There are a lot of examples of chiral drugs whose enantiomers exhibit this differential behaviour [7,11]. Everyone is aware of the tragic episode with the administration of thalidomide racemate to pregnant women in the 1960s, which led to multiple congenital abnormalities in new-born babies that were attributed to the (*S*)-enantiomer. Other example is naproxen, (*S*)-(+)-naproxen is used to treat arthritis pain, but (*R*)-(–)-naproxen has no analgesic effect and causes liver poisoning [12]. A more recent example can be found in the accelerated research of new drugs in the Covid-19 pandemic. During this search it was argued that (*S*)-chloroquine and (*S*)-hydrochloroquine could potentially have a higher response against SARS-CoV-2 than their (*R*)-enantiomers [13].

Nearly 50 % of drugs are chiral [14]; however, until the beginning of 21st century, regulatory authorities could just encourage the pharmaceutical industries to commercialise single enantiomer of drugs, although most of them were commercialised as racemates [15]. Nowadays, two-thirds of the

drugs in development are chiral, and 51 % of them will be launched on the market as a pure enantiomer. In addition to these drugs, many other drugs initially marketed as racemic mixtures have been re-launched on the market as pure enantiomers. In both cases, regulatory agencies require rigorous drug characterisation, including pharmacodynamic and pharmacokinetic profiles of individual enantiomers and their combinations [6].

In spite of the well-established role of stereochemistry in pharmacological processes, it has often been ignored in environmental research. More than 1500 chiral pollutants are present in the environment, but, unfortunately, there is no regulation for controlling them [16]. The enantioselectivity in ecotoxicity and biodegradation processes is evident and comparable to the events in medical/biomedical fields [17,18]. There are a lot of examples to illustrate the role of chirality in environmental toxicology. It has been reported differences in the toxicities of the enantiomers of chiral pollutants. In addition, biological transformation (uptake, metabolism, and excretion) of the chiral pollutants can be also stereoselective. Chiral pollutant metabolites are often chiral as well. In addition, some achiral pollutants have chiral metabolites [19]. For instance, it has been found that α -HCH enantiomers show different carcinogenic potencies and growth stimulation in primary rat hepatocytes [20]. Other example is heptachlor and 2-chloroheptachlor pesticides and some cyclodiene pesticides that have different enantioselective toxicities on cockroach species [21,22].

For all the aforementioned reasons, there is a special interest in analytical methodologies for the separation of the enantiomers of chiral molecules that allow to control the enantiomeric purity and to evaluate the differential biological behaviour of the enantiomers of a chiral compound.

I.2.- Separation of enantiomers of chiral compounds

For the separation of enantiomers of a chiral compound it is necessary to create a chiral environment using chiral selectors (CSs). CSs can be classified according to their origin into natural (e.g., saccharides, amino acids, oligosaccharides, mucopolysaccharides, macrocyclic antibiotics and proteins), semi-synthetic (modified oligosaccharides and polysaccharides, such as cyclodextrin (CD) derivatives and phenylcarbamate or benzoate polysaccharide derivatives) and synthetic (e.g., chiral surfactants, crown ethers, molecular imprinted polymers (MIPs) , metal-organic frameworks (MOFs) and covalent-organic frameworks (COFs)) CSs [23-27].

CSs form the corresponding diastereoisomers with the enantiomers of a chiral compound, either through covalent bonds or by the formation of transient enantiomer-CS complexes. The former is the basis for the so-called indirect methods and the latter, for the direct methods [28,29].

In indirect methods, optical pure CSs are used and the separation of the enantiomers of the chiral compound can be achieved by exploiting the differences in the physical and chemical properties of the diastereoisomers using non-enantioselective separation techniques (e.g., crystallisation,

distillation or non-chiral chromatography) and subsequently releasing the CS. These methods are used on a preparative scale [28,29].

In direct methods, most widely used from the analytical point of view, the separation of enantiomers can be achieved by the interaction of the chiral compound with a CS found in the separation system. Hydrophobic and electrostatic interactions, hydrogen bonding, van der Waals forces and inclusion phenomena contribute to the chiral recognition process [30].

The most commonly used analytical techniques for the separation of enantiomers of chiral compounds are high performance liquid chromatography (HPLC) [27,30-32], thin layer chromatography (TLC) [33,34], gas chromatography (GC) [35,36], supercritical fluid chromatography (SFC) [37,38], electrokinetic chromatography (EKC) and capillary electrochromatography (CEC) [39-42].

In chiral chromatographic and electrophoretic techniques, the CS can be used in solution, i.e., added to the liquid mobile phase or electrophoretic buffer, or adsorbed or immobilised on a support in the so-called chiral stationary phases (CSPs) [31]. HPLC using CSPs is by far the most used technique for the separation of enantiomers. This is due to several reasons; on the one hand, because of the inherent characteristics of HPLC, mainly its robustness and wide range of applicability (analytes, samples and sensitivity). On the other hand, the high consumption of CSs as additives in the mobile phase together with their high cost limits their applicability.

I.2.1.- Chiral stationary phases in HPLC

The first application of chiral liquid chromatography was reported by Henderson and Rule in 1938, involving separation of *D,L-p*-phenylenebisiminocamphor enantiomers using a column packed with lactose as CSP [43]. Since then, many CSPs for chromatographic enantioseparation have been developed. Figure I.1 shows a rough classification of the CSPs most used in HPLC attending on the type of CS used in the CSP. As can be observed, these CSPs could be roughly classified into chiral small organic molecule-based CSPs and macromolecule-based CSPs. The main features and applications of these CSPs is briefly discussed thereafter.

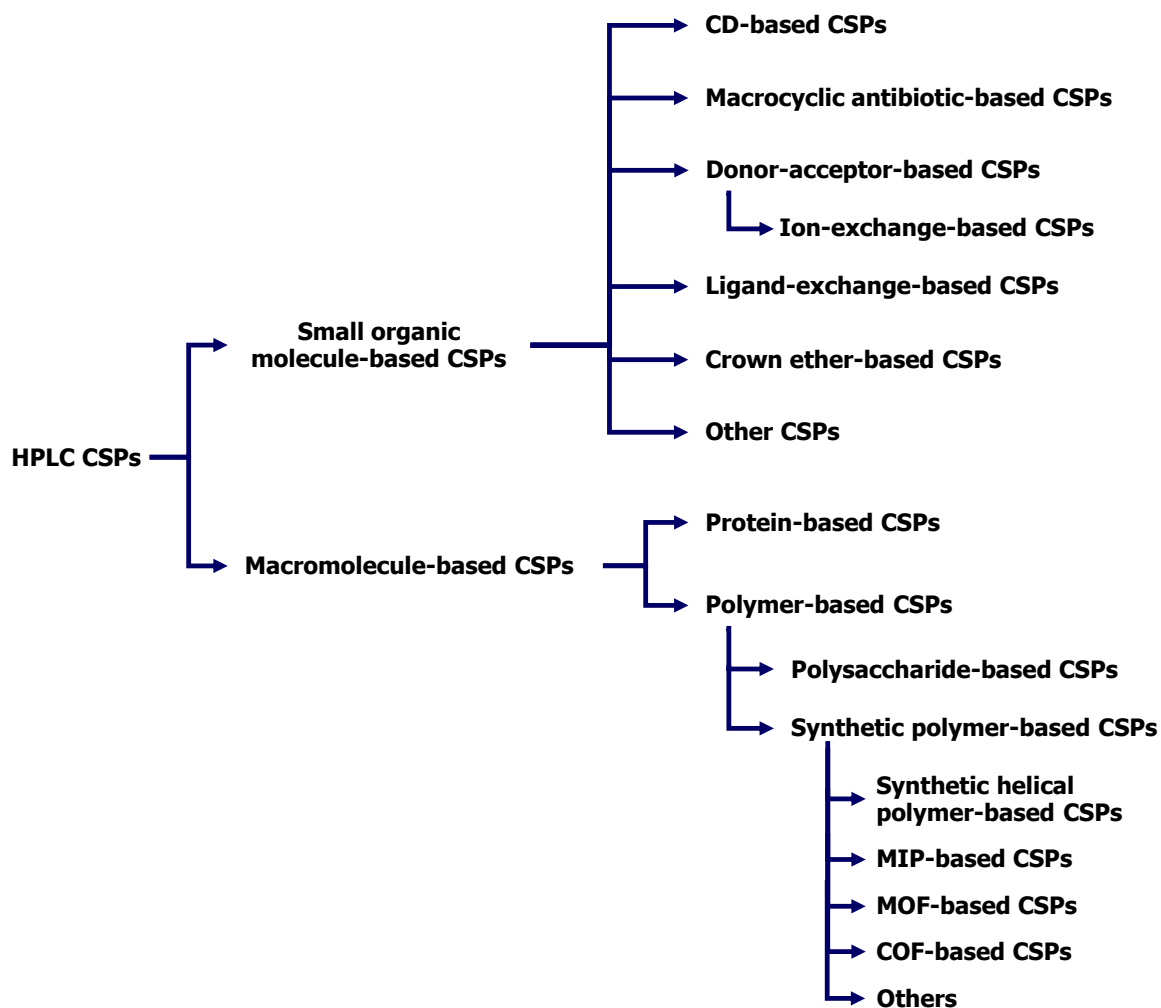


Figure I.1.- General overview of the most used CSPs in HPLC.

I.2.1.1.- Small organic molecule-based CSPs

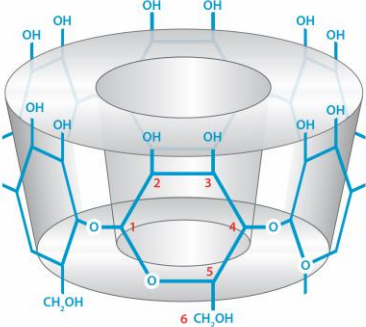
Small organic molecule-based CSPs include CDs, macrocyclic antibiotics, donor-acceptor, ion-exchange, ligand-exchange and crown ether CSs, among other CSs (see Figure I.1).

CD-based CSPs are one of the most used chiral small molecule-based CSPs. CDs are macrocyclic oligosaccharides linked by α -1,4-glycosidic bonds. Native CDs (α -, β -, and γ -CDs) are oligosaccharides consisting of 6, 7 and 8 D-(+)-glucopyranose units, respectively, containing 30-40 chiral centres. CDs have a toroidal structure (truncated cone-shaped) with a hydrophilic outside and a hydrophobic inner cavity. Their structure and cavity size allow the formation of inclusion complex with chiral guest molecules. To modulate their physicochemical properties and molecular recognition ability, hydroxyl groups in native CDs have been chemically modified resulting in a large number of derivatives. The main interactions involved in enantiomer-CD complex formation are believed to be hydrophobic, van der Waals and hydrogen bonding interactions, as well as steric factors. Electrostatic interactions must also be taken into account in the case of charged CDs, and π - π interactions with

CD derivatives containing aromatic substituents [44,45]. Chemical interactions that lead to chiral separations occur on both the exterior and interior surfaces of the cyclodextrin toroid.

It must be pointed out that CDs are by far the most used CS in EKC [46]. Although in a lesser extent, CDs have been also used as mobile phases additives in HPLC enantioseparations. In 1978, Harada *et al.* achieved the first chiral separation in liquid chromatography using CD-based CSPs [47]. Since then, home-made or commercial CD-based CSPs (containing native or derivative CDs) have been used in HPLC, GC, SFC and CEC. Examples of commercial CD-based CSPs used in HPLC are Astec® Cyclobond™ (Merck), ChiraDex® (Merck), Ultron ES-CD® (Shinwa), AZYP CDSshell-RSP® (Regis Technologies), Reprosil Chiral series (Dr. Maisch HPLC) and Sumichiral OA-7000 series (Sumika Chemical Analysis Service, Ltd.) [26]. One of the important aspects of the CD-based CSPs is that they operate in most of the mobile phase systems: reversed-phase HPLC (RPLC, using water or aqueous buffers containing methanol (MeOH) or acetonitrile (ACN)), normal phase HPLC (NPLC, using non-polar organic mobile phases) and polar organic HPLC (using mixtures consisting of ACN and/or MeOH and polar organic additives). Table I.1 summarises the main features of Astec® Cyclobond™ CD-based CSPs.

Table I.1.- Astec® Cyclobond™ CD-based CSPs for HPLC and SFC.

Theoretical structure of a CD molecule	CD	Derivative (2- and 3-position hydroxyls)	Trademark
	β-CD	None (native)	Astec CYCLOBOND I 2000
	β-CD	Acetyl	Astec CYCLOBOND I 2000 AC
	β-CD	Dimethyl	Astec CYCLOBOND I 2000 DM
	β-CD	3,5-Dimethylphenylcarbamate	Astec CYCLOBOND I 2000 DMP
	β-CD	2,6-Dinitro-4-trifluoromethyl phenyl ether	Astec CYCLOBOND I 2000 DNP
	β-CD	(<i>S</i>)-Hydroxypropyl ether	Astec CYCLOBOND I 2000 SP
	β-CD	(<i>R,S</i>)-Hydroxypropyl ether	Astec CYCLOBOND I 2000 RSP
	β-CD	(<i>R,S</i>)-Hydroxypropyl ether	Astec CYCLOBOND I 2000 HP-RSP
	γ-CD	None (native)	Astec CYCLOBOND II
	γ-CD	Acetyl	Astec CYCLOBOND II AC
Number of D-(+)-glucopyranose units			
β-CD	7		
γ-CD	8		

Macrocyclic antibiotic-based CSPs or macrocyclic glycopeptide-based CSPs are probably the most used small organic molecule-based CSPs. Macrocyclic glycopeptides are macrocyclic antibiotics that were introduced as CS by Armstrong *et al.* [48]. They have been frequently applied in HPLC, SFC, EKC and CEC [49]. Typical CSs in this family are vancomycin, teicoplanin, teicoplanin aglycone, avoparcin, ristocetin A and eremomycin. These CSs are composed of three or four

interconnected amino acid-based macrocycles containing two aromatic rings and a peptide sequence. Due to the different functional groups in these CSs, they are able to interact with enantiomers in different ways, such as inclusion, electrostatic, dipole-dipole, π - π and hydrophobic interactions, as well as hydrogen bonding and steric effects [27]. As an example, Figure I.2 shows the structure of vancomycin together with the main types of molecular interactions involved in the enantioselective process.

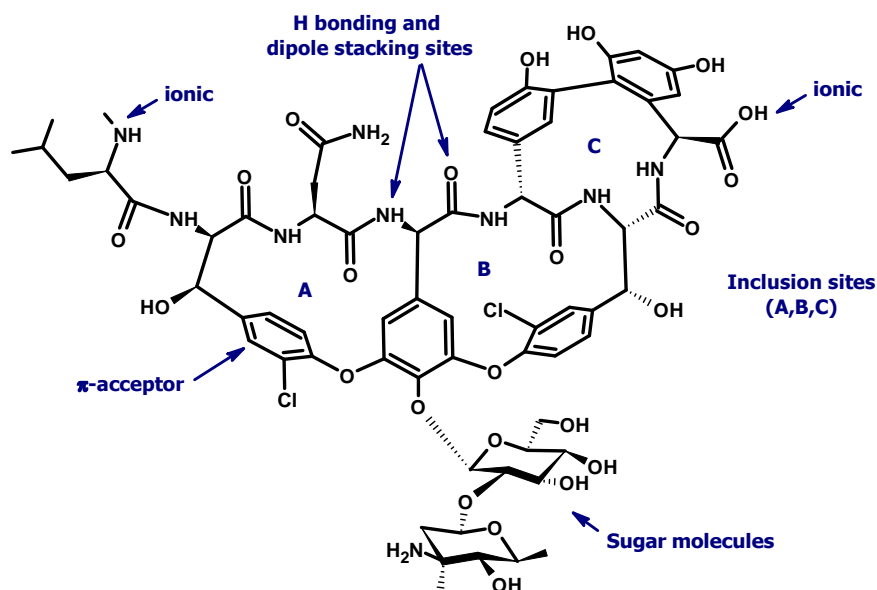


Figure I.2.- Structure of vancomycin showing different types of enantioselective molecular interactions.

In HPLC, these CSs have been used as mobile phases additives, but mainly as CSPs. These CSPs are multimodal, they can be used in NPLC, RPLC and polar organic modes. Examples of commercial macrocyclic antibiotic-based CSPs include the Astec® CHIROBIOTIC® family (see Table I.2), as well as VancoShell® and TeicoShell® CSPs from AZYP, and ReproSil Chiral-TAG CSP from Dr. Maisch HPLC.

Table I.2.- Main features of Astec® CHIROBIOTIC® macrocyclic antibiotic-based CSPs.

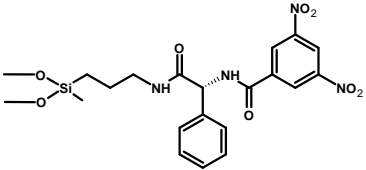
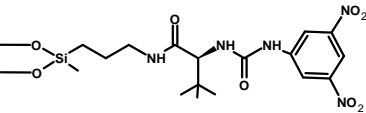
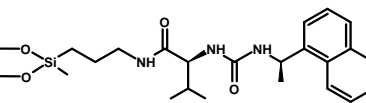
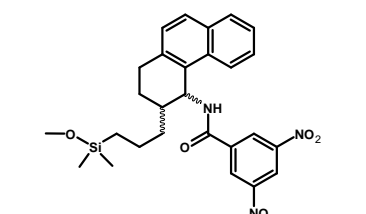
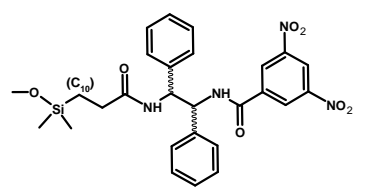
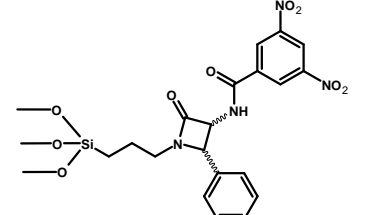
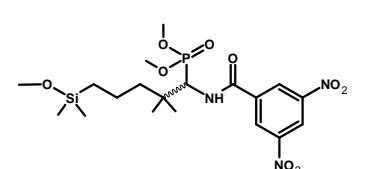
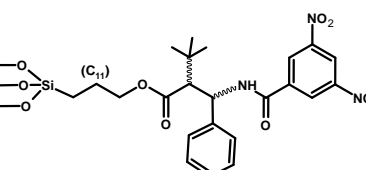
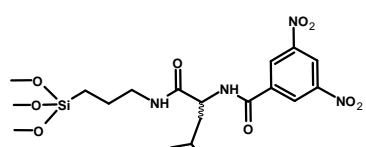
CHIROBIOTIC® CSP	Macrocyclic antibiotic	Chiral centres	Sugar groups	Inclusion cavities	pH range
CHIROBIOTIC® V and V2	Vancomycin	18	2	3	3.5 - 7.0
CHIROBIOTIC® T and T2	Teicoplanin	23	3	4	3.8 - 6.8
CHIROBIOTIC® TAG	Teicoplanin aglycone	8	0	4	3.0 - 6.8
CHIROBIOTIC® R	Ristocetin A	38	6	4	3.5 - 6.8

Donor-acceptor-based CSPs, also called brush-type or Pirkle-type CSPs, are prepared by covalent binding of low molecular mass CSs (e.g., amino acid, amino alcohol, small peptides, small sugars...) on a chromatographic support. These CSPs were introduced by W.H. Pirkle in HPLC [50]. CSs used in donor-acceptor-based CSPs have more than one of the following moieties near the chiral centre [27,49,51]:

- Aromatic groups capable of acting as electron acceptors or electron donors in face-to-face or face-to-edge π - π interactions
- Hydrogen bond acceptors or donors
- Electronegative groups for dipole-dipole interactions
- Bulky non-polar groups for other possible van der Waals interactions and/or steric hindrance

In 1980, Regis Technologies, along with Professor W.H. Pirkle introduced the Pirkle-type CSPs. Chirex® from Phenomenex, ReproSil Chiral series from Dr. Maisch HPLC and Sumichiral series from Sumika Chemical Analysis Service, Ltd. are also commercial donor-acceptor-based CSPs. Table I.3 shows some of these commercial CSPs. These CSPs can be used in both, NPLC or RPLC mode, although NPLC is most common.

Table I.3.- Examples of commercial donor-acceptor-based CSPs.

Donor-acceptor-based CSP	CS	Trademark
	(<i>R</i>)-Phenylglycine and 3,5-dinitrobenzoic acid amide linkage	Chirex [®] 3001 ^a Sumichiral OA-2000 ^b
	(<i>S</i>)- <i>tert</i> -Leucine and 3,5-dinitroaniline urea linkage	Chirex [®] 3011 ^a Sumichiral OA-3200 ^b
	(<i>S</i>)-Valine and (<i>R</i>)-1-(α -naphthyl)ethylamine urea linkage	Chirex [®] 3014 ^a Sumichiral OA-4100 ^b
	1-(3,5-Dinitrobenzamido)-1,2,3,4-tetrahydrophenanthrene	WHELK-O [®] 1 (<i>R,R</i>) ^c WHELK-O [®] 1 (<i>S,S</i>) ^c
	3,5-Dinitrobenzoyl derivative of diphenylethylenediamine	ULMO (<i>S,S</i>) ^c ULMO (<i>R,R</i>) ^c
	3-(3,5-Dinitrobenzamido)-4-phenyl- β -lactam	Pirkle 1-J (<i>3R</i> , <i>4S</i>) ^c Pirkle 1-J (<i>3S</i> , <i>4R</i>) ^c
	<i>N</i> -3,5-Dinitro-benzoyl- α -amino-2,2-dimethyl-4-pentenyl phosphonate	α -Burke 2 (<i>R</i>) ^c α -Burke 2 (<i>S</i>) ^c
	<i>N</i> -3,5-Dinitrobenzoyl-3-amino-3-phenyl-2-(1,1-dimethylethyl)-propanoate	β -GEM 1 (<i>R,R</i>) ^c β -GEM 1 (<i>S,S</i>) ^c
	3,5-Dinitrobenzoyl leucine	D-Leucine ^c L-Leucine ^c ReproSil Chiral L-Leucin ^d

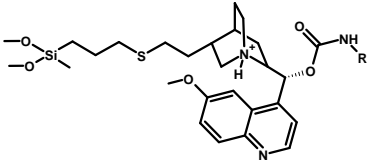

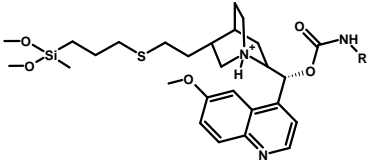
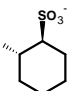
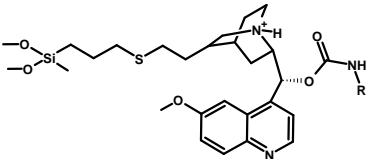

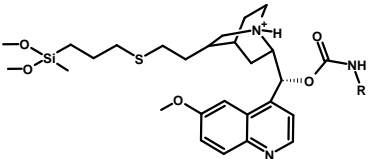
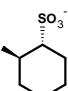
Supplier: ^a Phenomenex. ^b Sumika Chemical Analysis Service, Ltd. ^c Regis Technologies. ^d Dr. Maisch HPLC.

Ion-exchange-based CSPs are included as a subgroup of donor-acceptor CSPs. These CSPs were introduced by Rosini *et al.* in 1985 [52], but most of their applications were reported by Lindner group [53]. This type of CSPs can be divided into three different categories [26,49,54]:

- Anionic CSPs, such as *Cinchona* alkaloid-based quinine and quinidine CSPs used for the separation of enantiomers of acidic compounds (e.g., *N*-derivatised amino acids and phenols)
- Cationic CSPs, containing carboxylic or sulfonic acid groups, used for the chiral separation of basic compounds
- Zwitterionic CSPs, such as underivatised amino acids and small peptides, used for the chiral separation of acid, basic, and zwitterionic compounds

These CSPs can be used in NPLC, polar organic or RPLC modes. Some examples of commercial ion-exchange CSPs are shown in Table I.4.

Table I.4.- Examples of commercial ion-exchange-based CSPs.

Ion-exchange-based CSP	R	CS	Trademark
		<i>O</i> -9-(<i>tert</i> -Butylcarbamoyl) quinine	Chiralpak® QN-AX ^a ProntoSIL Chiral AX QN-1 ^b
		Quinine with (1 <i>S</i> ,2 <i>S</i>)-cyclohexyl-1-amino-2-sulfonic acid linked via a carbamoyl group	Chiralpak® ZWIX(+) ^a
		<i>O</i> -9-(<i>tert</i> -Butylcarbamoyl) quinidine	Chiralpak® QD-AX ^a ProntoSIL Chiral AX QD-1 ^b
		Quinidine with (1 <i>R</i> ,2 <i>R</i>)-cyclohexyl-1-amino-2-sulfonic acid linked via a carbamoyl group	Chiralpak® ZWIX(-) ^a

Supplier: ^a Daicel Chiral Technologies. ^b Bischoff Chromatography.

Ion-exchange CSPs interact with ionisable chiral compounds through electrostatic interactions, although π - π interactions and hydrogen bonding have to be also considered [49,51,54]. As an example, Figure I.3 shows the structure of an ion-exchange CSP together with the main types of molecular interactions involved in the enantiorecognition process.

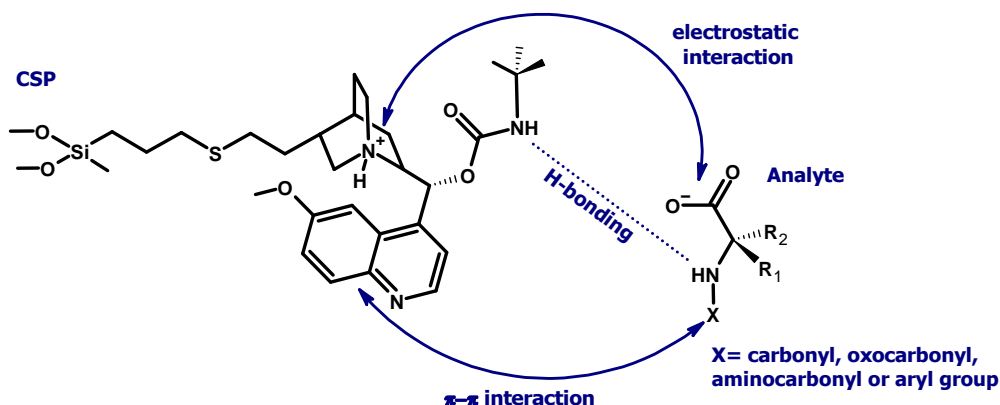


Figure I.3.- Structure of a quinine derivative ion-exchange CSP showing different types of enantioselective molecular interactions.

Ligand-exchange-based CSPs are another type of small molecule-based CSPs that were introduced in liquid chromatography by Davankov and Rogozhin [55]. From then on, different ligand-exchange CSs have been developed. Its basic principle is based on the coordination between the reversible chelate of a chiral compound and a metal ion (e.g., Cu²⁺, Zn²⁺, Ni²⁺ or Mn²⁺), which in turn forms a complex with a CS (e.g., amino acid derivatives, hydroxy acids or amino sugar derivatives), resulting in a selectand-metal ion-CS complex. Chiral separations using this type of CSs are limited to compounds with two or more electron-donating functional groups (e.g., hydroxy acids, α -amino acids, amino alcohols and diols). In HPLC, these CSs have been used as mobile phases additives or adsorbed/immobilised on a solid support as CSPs (see Table I.5). The metal ion can be included in the CSP or added to the aqueous mobile phase. These CSPs can also tolerate mobile phases containing MeOH (or other alcohols) and ACN as organic modifiers [26,49,56].

Table I.5.- Examples of commercial ligand-exchange-based CSPs.

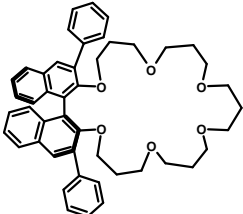
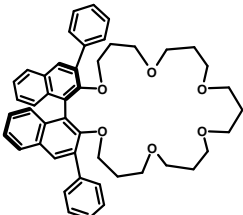
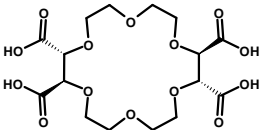
Ligand-exchange-based CSP	CS	Trademark
	<i>N,N</i> -Dioctyl-L-alanine	Chiralpak® MA(+) ^a
	D-Penicillamine	Chirex® (D)-penicillamine ^b Sumichiral OA-5000 ^c

Supplier: ^a Daicel Chiral Technologies. ^b Phenomenex. ^c Sumika Chemical Analysis Service, Ltd.

Finally, **crown ether-based CSPs** are also considered as small molecule-based CSPs and were introduced as CSPs by Dotsevi *et al.* [57]. Crown ethers are macrocyclic polyethers with a cavity, which contains binaphthyl or tartaric acid moieties [57-59]. Crown ether CSPs have been used in HPLC for the chiral separation of α -amino acids, primary and secondary amines, as well as amides. The application of these CSPs is limited because the chiral separation is achieved through the formation of complexes between the protonated amines of the analyte and the oxygen atoms of the macrocyclic polyether by hydrogen bonds. Although other interactions (e.g., π - π interactions and dipole-dipole interactions) and steric hindrance may also contribute to the formation of the complex [26,31,59].

Some examples of commercial CSPs for HPLC are shown in Table I.6. These coated or immobilised CSPs can be used in both NPLC or RPLC modes.

Table I.6.- Examples of commercial crown ether-based CSPs.

Crown ether-based CSP	Trademark
 <p>(3,3'-Diphenyl-1,1'-binaphthyl)-25-crown-6</p>	Crownpak® CR(+) ^a Crownpak® CR-I(+) ^a
 <p>(3,3'-Diphenyl-1,1'-binaphthyl)-25-crown-6</p>	Crownpak® CR(-) ^a Crownpak® CR-I(-) ^a
 <p>(18-Crown-6)-2,3,11,12-tetracarboxylic acid</p>	ChiroSil® RCA(+) ^b ChiroSil® SCA(-) ^b ChiroSil ME® RCA(+) ^b ChiroSil ME® SCA(-) ^b

Supplier: ^a Daicel Chiral Technologies. ^b Regis Technologies.

I.2.1.2.- Macromolecule-based CSPs

Macromolecule-based CSPs use proteins and chiral polymers as CSs (see Figure I.1). Proteins contain multiple chiral centres and binding sites that favour numerous interactions with small molecules [31]. The well-known enantioselectivity of serum proteins inspired their application as CS in enantioseparation techniques. The first application of **protein-based CSPs** was reported in 1973 by Stewart and Doherty that used a bovine serum albumin (BSA) CSP [60]. Since then, many other protein-based CSPs have been investigated, mainly those consisting of human serum albumin (HSA), α_1 -acidglycoprotein (AGP), ovomucoid (OVM) and cellobiohydrolase I (CBH I) as CSs, but also other protein-based CSs have been proposed (e.g., trypsin, lysozyme, pepsin, fatty acid-binding protein, avidin, riboflavin binding protein, or immunoglobulin G antibody) [31,61].

Home-made or commercial protein-based CSPs have been used for the separation of the enantiomers of a large number of acidic, basic and neutral chiral compounds [31]. In these CSPs, diverse molecular interactions such as hydrogen bonding, π - π interactions, ionic interactions, dipole-dipole interactions, hydrophobic interactions and steric effects contribute to the chiral separation [26,61].

Coated or immobilised protein-based CSPs are used in the RPLC mode; however, these CSPs have limited stabilities due to the possible denaturation of proteins, which limits the working temperature and *pH*, ionic strength, and the nature and concentration of the organic modifier used in the mobile phase. To overcome these problems, new immobilisation and entrapment techniques as well as new solid supports for protein are being developed. Currently, the most used supports are silica and polymer particles or monoliths [31,61]. Figure I.4 shows some examples of protein linkage to silica supports proposed in the literature [61].

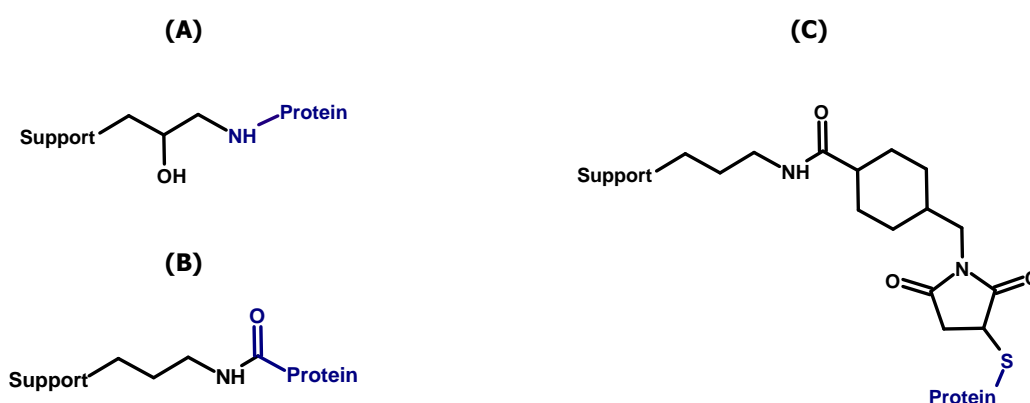


Figure I.4.- Examples of linkages supports for protein-based CSP. The immobilisation of proteins and glycoproteins onto functionalised silica supports can be conducted via their **(A)** amino, **(B)** carboxy, and **(C)** sulfhydryl groups.

Some examples of commercial protein-based CSPs are Chiralpak® columns (AGP, HSA and CBH from Chiral Technologies or Regis Technologies); Resolvosil® BSA (Macherey & Nagel); Sumichiral columns (AGP, HSA and CBH from Sumika Chemical Analysis Service, Ltd); Reprosil Chiral columns (AGP and HSA from Dr. Maisch HPLC); and Ultron® columns (ES-OVM and Pepsin from Shinwa Chemical or Agilent Technologies).

Nowadays, approximately 90 % of the chiral separations are performed by HPLC using **polymer-based CSPs** [62]. The most used CSs in polymer-based CSPs are natural polysaccharide derivatives, but also other chiral synthetic polymers have been used (see Figure I.1).

The first enantioseparation dealing with **polysaccharide-based CSPs** was reported by Kotake *et al.* in 1951. The authors enantioresolved several amino acids using cellulose as CS in paper chromatography [63]. Since then, several natural polysaccharides and their derivatives were assayed as CSPs, but they exhibited limited resolution ability. In 1980s, Y. Okamoto research group from Osaka University and the Daicel company pioneered the contemporary polysaccharide-based CSPs [62,64-70]. Several different polysaccharides (e.g., amylose, cellulose, chitin, chitosan, curdlan, dextran, galactosamine, inulin and xylan; see Figure I.5) derivatives were investigated. Amylose and cellulose derivatives (e.g., phenylcarbamates) were found to be the most useful CSPs because of their wide enantioselectivity, pure form availability and simplicity of processing. It is worth mentioning, that some other polysaccharide derivatives (particularly chitin phenylcarbamates) exhibited good enantioselectivity for some chiral compounds. Today, the most popular commercial polysaccharide-based CSPs are phenylcarbamate or benzoate derivatives of cellulose and amylose. Some examples of commercial coated or covalently immobilised amylose or cellulose derivative CSPs are shown in Table I.7. Among them, the most used are from Chiral Technologies (Chiralcel® and Chiralpak® series) and Phenomenex (Lux® series). It is worth mentioning that cellulose tris(3,5-dimethylcarbamate) and amylose tris(3,5-dimethylcarbamate) CSPs account for approximately 2/3 of the research papers dealing with polysaccharide-based CSPs.

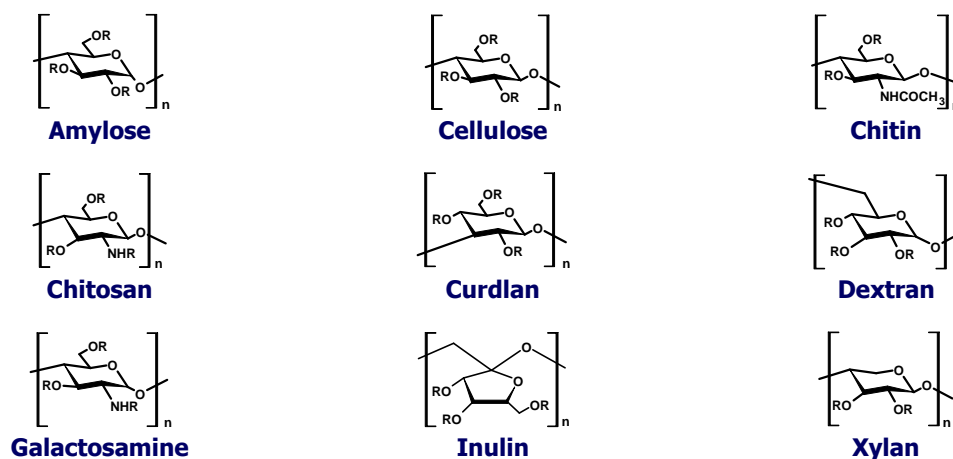
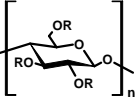
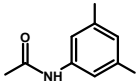
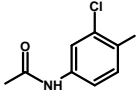
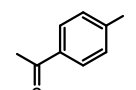
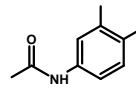
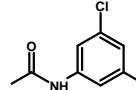
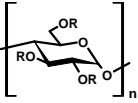
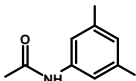
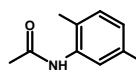
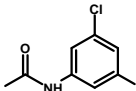


Figure I.5.- Structures of different types of polysaccharides used as CSPs.

Table I.7.- Examples of commercial cellulose- and amylose-based CSPs.

Polysaccharide-based CSP	R	CS	Trademark
		Cellulose tris(3,5-dimethylphenylcarbamate)	Chiralcel® OD ^a Chiralpak® IB ^a Lux® Cellulose-1 ^b ReproSil® Chiral-OM ^c Reflect™ C-Cellulose B ^d Reflect™ I-Cellulose B ^d CHIRAL ART Cellulose-C ^e CHIRAL ART Cellulose-SB ^e Kromasil® CelluCoat® ^f
		Cellulose tris(3-chloro-4-methylphenylcarbamate)	Chiralcel® OZ ^a Lux® Cellulose-2 ^b ReproSil® Chiral-ZM ^c Reflect™ I-Cellulose Z ^d
		Cellulose tris(4-methylbenzoate)	Chiralcel® OJ ^a Lux® Cellulose-3 ^b ReproSil® Chiral-JM ^c Reflect™ I-Cellulose J ^d CHIRAL ART Cellulose-SJ ^e
		Cellulose tris(4-chloro-3-methylphenylcarbamate)	Chiralcel® OX ^a Lux® Cellulose-4 ^b ReproSil® Chiral-XM ^c
		Cellulose tris(3,5-dichlorophenylcarbamate)	Chiralpak® IC ^a Lux® i-Cellulose-5 ^b ReproSil® Chiral-MIC ^c Reflect™ I-Cellulose C ^d CHIRAL ART Cellulose-SC ^e
		Amylose tris(3,5-dimethylphenylcarbamate)	Chiralpak® AD ^a Chiralpak® IA ^a Lux® Amylose-1 ^b Lux® i-Amylose-1 ^b ReproSil® Chiral-AM ^c ReproSil® Chiral-MIA ^c Reflect™ C-Amylose A ^d Reflect™ I-Amylose A ^d CHIRAL ART Amylose-C ^e CHIRAL ART Amylose-SA ^e Kromasil® AmyCoat® ^f
		Amylose tris(5-chloro-2-methylphenylcarbamate)	Chiralpak® AY ^a Lux® Amylose-2 ^b ReproSil® Chiral-YM ^c
		Amylose tris(3-chloro-5-methylphenylcarbamate)	Chiralpak® IG ^a Lux® i-Amylose-3 ^b

Supplier: ^a Daicel Chiral Technologies. ^b Phenomenex. ^c Dr. Maisch HPLC. ^d Regis Technologies. ^e YMC. ^f Nouryon.

As can be observed in Figure I.5 and Table I.7, amylose- and cellulose-based CSPs are linear helical polymers, which are composed of D-glucose units with α (1 \rightarrow 4) or β (1 \rightarrow 4) glycosidic linkages, respectively. The derivatisation of glucose molecules is made from their hydroxyl groups usually with benzoate or phenylcarbamate moieties, as indicated above. In addition, these moieties are able to accept different substituents (e.g., methyl and/or chlorine groups) in different positions of the aromatic ring. Finally, these CSPs contain chiral helical grooves and cavities, with different shapes and sizes that depend on the polysaccharide backbone and the nature of the substituents of the aromatic ring. All these possibilities yield a large variety of derivatives with different selectivities and applications [45,62,71].

In cellulose- and amylose-based CSPs, a complex steric environment is created, and a large number of interactions contribute to chiral separation that occur in the chiral grooves and cavities formed from the backbone and side chains. Only some formed chiral grooves and cavities can identify the enantiomers of a chiral compound depending on its structure, shape, and size [72]. The formation of enantiomer-CS complexes can be promoted by hydrogen bonds involving the CO or NH groups of the carbamate moieties, π - π interactions with the phenyl rings, van der Waals interactions, and steric factors [45,62,73-76]. It has also been described that halogen bonds contribute to selector-selectand complexation as electrostatic interactions [77,78]. Recently, chalcogen and π -hole interactions have been also explored in HPLC environment [79]. All this variety of interactions confers them a high chiral recognition ability and, therefore, a wide applicability for a great diversity of compounds.

On the other hand, polysaccharide-based CSPs are multimodal, i.e., they have been used in NPLC, RPLC and polar organic modes as other above mentioned CSPs, but also in hydrophilic interaction liquid chromatography (HILIC) [62,71,74,80,81]. The mobile phase in these CSPs strongly modulates the chiral recognition process. Different chromatographic behaviours, including inversions in the enantiomer elution order (EEO), are observed depending on the nature and composition of the mobile phase (e.g., the addition of additives, the organic modifier or the water content), as a consequence of the changes produced in the intramolecular hydrogen bonds of the polysaccharide structure [71,74,81-85]. Hydro-organic mobile phases are of special importance for [86-88]:

- Polar compounds that are poorly soluble in alkanes, low molecular weight alcohols and ACN
- Aqueous matrix samples (e.g., biological and environmental samples)
- Mass spectrometry (MS) detection. Most of the additives used in RPLC conditions to improve resolution, and to control the ionic strength and the pH of the mobile phase, are non-volatile (e.g., hexafluorophosphate or phosphate buffers) or suppress analyte response (e.g., diethylamine), becoming incompatible with MS detection. Hydro-organic mobile phases improve the analyte ionisation, and therefore, the sensitivity in MS detection

Other aspect to be taken into account when using hydro-organic mobile phases is that the retention of compounds with polysaccharide-based CSPs may follow a dual behaviour (RPLC and HILIC behaviours) depending on the protic or aprotic character of the organic solvent and the water content in the mobile phase [81,84,89-91]. It has been proposed that the balance between hydrophilic (hydrogen-bond interactions with carbamate or ester moieties) and hydrophobic (with phenyl moieties) enantiomer-CSP interactions can explain this dual behaviour [81,84,90-92].

Protic solvents, such as MeOH, compete with the analyte for hydrogen-bonding interactions with the polysaccharide-based CSP. So, the addition of water to the mobile phase does not alter hydrophilic interactions but promotes hydrophobic interactions between the analyte and the polysaccharide CSPs. This fact may increase the analyte retention (RPLC behaviour) and eventually lead to an enhancement of enantioseparation [81,84,91,92].

For aprotic solvents, such as ACN, the addition of water to the mobile phase has two opposed effects. As above, it increases analyte-polysaccharide hydrophobic interactions leading to an increase in retention (RPLC behaviour). But as water competes with analytes for hydrogen-bonding interactions with polysaccharide-based CSPs, there is also a decrease in hydrophilic interactions. The latter effect reduces analyte retention (HILIC behaviour) and may decrease enantioresolution. The overall effect observed is the sum of both contributions. The first contribution prevails in mobile phases with high water content and the second one in mobile phases with low water content [81,84,91,92]. This behaviour has been reported for chlorinated polysaccharide-based CSPs which show a great ability to form strong hydrogen bonds [90].

The type of the union of the polysaccharide onto the silica surface (either coated or covalently immobilised) can also affect to the chiral recognition process. In general, coated CSPs have a slightly higher chiral recognition capacity than immobilised CSPs, but the latter reduce the problems related to the solvent limitations of coated CSPs, allowing the use of other solvents, which can provide new enantioselectivities [71,73,74,93].

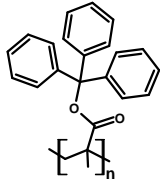
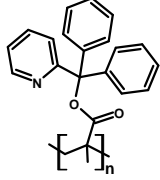
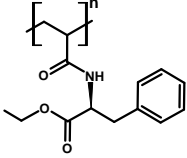
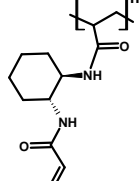
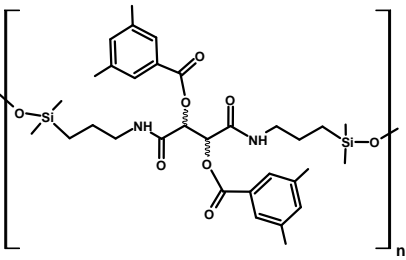
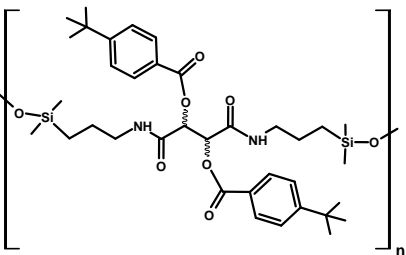
New trends in polysaccharide-based CSPs to improve the chiral recognition ability and the solvent stability include the study of new coating or immobilisation methodologies, the synthesis of new cellulose and amylose derivatives, and the search for new supports (e.g., monoliths, core-shell particles, and microspheres of silica as well as new hybrid materials) alternative to the classical spherical silica particles [27,31,81,82].

The CSs used in **synthetic polymer-based CSPs** include synthetic helical polymers, MIPs and chiral porous material-based CSPs (e.g., MOF- and COF-based CSPs).

Polyacrylamides, polymethacrylates, polyacetylenes, polystyrenes, polyurethanes, and polyisocyanides are some examples of CSs used in **synthetic helical polymer based-CSPs**. These CSs consist of chiral monomers that form stereoregular polymers with a defined helical conformation, which is the key in the chiral recognition process [62,94]. The mechanism of chiral separation using

this type of CSs is mainly based on hydrogen bonding, π - π interactions and steric factors [26,31]. Some examples of commercial synthetic polymers based CSPs are shown in Table I.8. These CSPs can be used in NPLC, polar organic as well as RPLC modes.

Table I.8.- Examples of commercial synthetic polymer-based CSPs.

Synthetic polymer-based CSP	CS	Trademark
	Triphenyl-methyl-methacrylate polymer	Chiralpak® OT(+) TM
	Diphenyl-(2-pyridyl)methyl-methacrylate polymer	Chiralpak® OP(+) TM a
	Poly(<i>N</i> -acryloyl-(<i>S</i>)-phenylalanine ethyl ester)	ChiraSpher® NT ^b
	(<i>R,R</i>) and (<i>S,S</i>) Poly(<i>trans</i> -1,2-cyclohexanediamine-bis-acrylamide)	Astec® P-CAP TM c
	<i>O,O'</i> -bis(3,5-Dimethylbenzoyl)- <i>N,N'</i> -diallyl-L-tartar diamide polymer	Kromasil® CHI-DMB ^d
	<i>O,O'</i> -bis(4- <i>tert</i> -Butylbenzoyl)- <i>N,N'</i> -diallyl-L-tartar diamide polymer	Kromasil® CHI-TBB ^d

Supplier: ^a Daicel Chiral Technologies. ^b MilliporeSigma. ^c Supelco. ^d Nouryon.

Efficient syntheses are still being developed to better control the stereoregularity of polymers [62]. The use of monoliths, nanoparticles and hybrid organic-inorganic materials is also being investigated. In addition, smart polymers have also aroused interest, they can dynamically and reversibly alter their properties depending on external chemical and physical stimuli such as temperature, *pH*, type of solvent, presence of ions or light. The inclusion of different responsive groups produces multi-responsive smart polymers, having a huge potential as CSPs, while its high-order structure is maintained [94].

MIPs-, MOF- and COF-based CSPs are not yet commercialised. **MIPs** are formed by polymerisation from functional monomers, cross-linking agents and the help of a template (i.e., a target compound with good chemical stability and functional groups that are easy to complex with the monomers). The chiral recognition ability of MIPs is due to the spatial distribution resulting from the template and the polymer, obtaining chiral cavities with chiral recognition ability for the target compounds. MIPs have a high specific chiral recognition ability that is illustrated in high enantioselectivity, marked substrate-specificity, and foreseeable elution order (i.e., the more retained enantiomer is the one used as template). MIP-based CSPs are template-dependent, limiting its use as CS. The main advantage and drawback of MIP-based CSPs is their marked "substrate-specificity". However, just this template-dependent enantioselectivity limits its applicability as CS [95].

The chiral separation using MOF- and COF-based CSPs is still in the process of maturing. These porous materials have been investigated as CSs due to their uniform and adjustable pore structures, high surface areas, selective adsorption capacities, and excellent thermal and chemical stabilities [27].

MOF-based CSPs are microporous crystalline materials, containing metal ions or clusters (nodes) linked by stereochemically pure chiral organic ligands as rigid spacer connectors through coordination bonds (rods) that extend networks to 1D, 2D or 3D and control the pore size [26,27]. **COF-based CSPs** are also crystalline materials but COFs consist of organic polymers with uniform porosity formed by pure organic building blocks through robust covalent bonds [27]. The chiral separation of MOF- and COF-based CSPs mainly depends on the pore size and channel shape of the framework. Although other different molecular interactions (e.g., hydrogen bonding, π - π interactions, hydrophobic interactions, van der Waals forces or dipole-dipole interactions) between the analyte and the chiral channels of CS can also contribute to the chiral separation [96].

As can be deduced from this section, there are a large number of CSPs commercially available (more than a hundred CSPs, of which approximately 20–30 CSPs are the most used). However, cellulose and amylose polysaccharide derivatives coated or immobilised on the stationary support represent, by far, the most used CSPs in HPLC, as well as SFC and CEC [45,62,82]. These polysaccharide-based CSPs are the used in this Thesis.

I.3.- Modelling approaches for enantioseparations in HPLC with CSPs

Chiral separations are considered one of the most challenging of all analytical separations. The interaction between two chiral species does not guarantee the separation of their enantiomers. Some CSPs have shown wide applicability; however, there is not a universal CSP [97].

Despite the large number of analytical applications of CSPs in HPLC, the fundamental mechanisms responsible for chiral separations are not fully understood due to the inherent complexity of these chromatographic systems. In fact, nowadays, the search for the right CSP/mobile phase combination for the separation of enantiomers of a given chiral compound is conducted using expensive and time-consuming trial-and-error procedures. Therefore, predicting the ability of a given chromatographic system to know whether a chiral separation is possible would be of great benefit. However, relatively few papers address this important issue in the development of chiral HPLC methods.

In order to elucidate the chiral recognition mechanism of CSPs, analytical separation techniques in combination with spectroscopic techniques (e.g., nuclear magnetic resonance spectroscopy, infrared spectroscopy, vibrational circular dichroism techniques, X-ray crystallography, etc.) have been used [26,30,98]. This is a very difficult task because of the structural complexity of CSPs that present different binding sites with varying affinities for the enantiomers; in addition, the structure of CSPs in the solid state differs from that in solution.

Molecular modelling strategies are often used to complement or as an alternative to spectroscopic techniques [99]. These approaches can provide a justification of why analytical separation occurs (i.e., a fundamental insight into the mechanism of chiral recognition is obtained). In addition, molecular modelling may also be helpful for predicting parameters of chiral separations. Two types of models can be distinguished in molecular modelling [99]:

- Atomistic models. These models, such as molecular docking and molecular dynamics, quantify the energetics of all the interactions between the atoms in the enantiomer and a given CSP [100-103].
- Empirical fitting procedures. These models relate structural properties of chiral compounds (e.g., molecular descriptors) with chromatographic parameters related to their enantioseparation (e.g., selectivity factor (α) and enantioresolution (R_s)) [104] in a given chromatographic system using multivariate techniques. In the literature, these models are called quantitative structure-property relationships (QSPR) or quantitative structure-retention relationships (QSRR) or quantitative structure-enantioselective retention relationships (QSERR) as well. Some authors use the acronym QSERR only when chiral descriptors are involved. Chemometric methods are applied to build multivariate models and to extract valuable information on molecular recognition.

Table I.9 shows a summary of some examples of QSPR models for chiral separations using HPLC with different CSPs [105-134]. As can be observed, the most studied CSPs are the donor-acceptor- and polysaccharide-based CSPs (both, 43 %). In most of the studies, the chiral separations are obtained in NPLC mode (~ 77 %), being the models constructed in RPLC conditions very reduced (~ 23 %) due the complexity of interactions solute-mobile phase in the last case.

As can be observed in Table I.9, to develop the multivariate QSPR models, different molecular descriptors have been used as predictor variables (**X** matrix) and retention time (t_R) [130] and retention factor (k) [105-117,120-122,127,128,132,134] related parameters, as well as categorical or numerical α [105-108,111,113,116,118,119,121-127,131,134] and R_s [123,129,133] related data have been used as **response variable (y)**.

As far as **predictor variables** is concerned, different molecular descriptors that describe hydrophobic, electronic, or steric properties of the molecule, among others, have been used to model the response variable [135]. There are simple molecular descriptors, usually called 0D- and 1D-descriptors, derived from the molecular formula by counting some atom types or structural fragments in the molecules –e.g., number of hydrogen bond acceptors (*HBA*) and donors (*HBD*) [109,119,120], ether groups [125] or heteroatoms linked to the chiral carbon (*C*X*) [133]– as well as physicochemical and bulk properties such as molar mass [114,119-121,134], logarithm of the *n*-octanol water partition ($\log P$) [114-117] or distribution ($\log D$) [133] coefficient. Other molecular descriptors (referred to as topological or 2D-descriptors) are derived from algorithms applied to a topological representation (e.g., connectivity indices [107,114,123,129]). Geometrical or 3D-descriptors consider the overall spatial configuration of molecule atoms (i.e., spatial (x, y, z)-coordinates of the atoms in the molecule). Examples of this type of descriptors are steric properties, total/molecular surface area (*MSA*) [121,133,134], volume related parameters [114,119-121,132,134], Balaban index [114], weighted holistic invariant molecular (WHIM) descriptors [123,129], among others. Another class of molecular descriptors, referred to as 4D-descriptors, result from interactions of the molecule with groups probes characterising their surrounding space. GRID [121,124,134], volume and surface (VolSurf) [121,134], comparative molecular field analysis (CoMFA) [105,106,116,118,127] and comparative molecular similarity indexes analysis (CoMSIA) [118] are methods based on molecular interaction fields to obtain 4D-descriptors.

ADAPT, CODESSA, DRAGON, Hyperchem, MolConnZ and OASIS are some of the most commonly used software for descriptor calculation. These programs calculate hundreds of descriptors for a single molecule, from SMILES, 2D-graphs to 3D- (x, y, z) -coordinates [135]. The analysis of these broad data sets requires the use of **multivariate chemometric techniques** including multivariate regression techniques –e.g., multiple linear regression (MLR) [107,109-117,119,120,122,123,128-130,132], partial least squares (PLS) regression [105,106,108,116,118,121,123-125,130,134], artificial neural networks (ANNs) [111,116,127,129], and support vector machine (SVM) [125]– or multivariate classification techniques such as random

forest (RF) [131], discriminant partial least squares (DPLS) [133], and classification and regression tree (CART) [123]. However, some of them (e.g., MLR) are unable to deal with data containing more variables than objects. Another well-known drawback of MLR technique is that the possible multicollinearity of \mathbf{X} variables can lead to over-fitted QSPR models and unreliable predictions of the response variable. All these problems can be solved by using feature selection (FS) techniques to reduce the number of \mathbf{X} variables by selecting just the most relevant ones. In addition, the knowledge of the most important variables enables an easier interpretation of the QSPR model, i.e., it can be used to explain the major operating forces in the modelled chiral chromatographic system. PLS does not have the previously mentioned problems of MLR. However, both MLR and PLS are essentially designed to model linear \mathbf{y} - \mathbf{X} relationships, although PLS is able to adjust for a certain degree of non-linearity. ANNs are a flexible machine learning approach capable of modelling complex/non-linear relationships between input and response variable(s) [136,137]. On the other hand, FS strategies can also improve the descriptive and predictive ability of PLS and ANN QSPR models.

Some authors use chromatographic data from ChirBase Database to establish QSPRs [124,126,131]. ChirBase [138] contains information for approximately 307000 chiral HPLC/SFC separations taken from the literature, as well as, from patents. However, these data should be used with caution as it is difficult to extract homogenous data, i.e., the chiral separations were obtained under different experimental conditions (mobile phase composition, temperature, column length, ...) and not all molecules were tested in all CSPs.

Finally, most of the reported QSPR models have been developed for **structurally related compounds** (83 %, e.g., oxadiazolines, arylcarboxylic acids, phenylalanine derivatives, etc.) that share close interaction modes with the CSP. To the best of our knowledge, only five papers comprise structurally unrelated compounds [117,124,126,131,133]. QSPRs for structurally related compounds have proven to be helpful to figure out which molecular descriptors of chiral compounds most influence their retention and enantioseparation, and to elucidate the enantio-recognition mechanisms operating in the case (compounds and chromatographic system) under study. However, they show limited applicability, i.e., they are only useful for the prediction of the response variable for a new compound whose structure is close to that of the compounds included in the model. In contrast, for **structurally unrelated compounds**, the main molecular descriptors affecting retention and enantioseparation, and therefore, the enantio-recognition mechanisms are more difficult to be established. Nevertheless, QSPR models derived from structurally unrelated compounds would be preferable for a rational selection of a chromatographic system (CSP/mobile phase combination) to separate the enantiomers of any new compound.

Table I.9.- Summary of some examples of QSPRs for chiral separations using HPLC with different CSPs found in the literature. When several predictor variables or chemometric techniques are tested, just those providing the best results are shown.

Compounds	CSP	HPLC mode	Predictor variables	Response variable	Chemometric technique	[Ref]
21 Alkyl aryl sulfoxides	DACH-DNB ^a	NPLC	2: Steric and electrostatic CoMFA fields	$\log \alpha$	PLS	[105]
9-18 α -Alkyl α -aryloxy acetic acid methyl esters (= $f(\mathbf{y})$)	DACH-DNB ^a	NPLC	1: Hansch hydrophobic constant 1: Charton parameter 2: Steric and electrostatic CoMFA fields	$\log k_2$ $\log k_2$ $\log \alpha$	OLS PLS	[106]
17 Hydantoin	β -CD	Polar organic	2: Charge index and connectivity index	$\log k_1$	MLR	[107]
15 α -Amino acids derivatives	α -CD	RPLC	3: Charge indices	$\log k_1$		
14 Arylamides	1-(α -Naphthyl) ethylamine	NPLC	3: 1 Geometrical index, and 2 connectivity indices 3: 1 charge index, and 2 connectivity indices	$\log k_1$ $\log \alpha$		
25-27 Oxadiazolines (= $f(\mathbf{y})$)	(<i>R,R</i>)-DACH-DNB ^a	NPLC	7: 3 Hansch hydrophobic constants, 3 Hammett constants, and 1 Verloop parameter 6: 3 Hammett constants, and 3 Charton parameters 3: <i>HBA</i> , <i>HBD</i> , and degree of aromaticity	$\log k_2$ $\log \alpha$ $\ln k_1, \ln k_2$	PLS MLR	[108] [109]
26 α -Alkylarylcarboxylic acids	Chiralpak [®] AD	NPLC		$\ln k_1, \ln k_2$	MLR	[110]
12 Mexiletines	Chiralpak [®] AD	NPLC	3: 2 Fragmental hydrophobicity of substituents, and total aromatic excess charge 3: 2 Fragmental hydrophobicity of substituents, and submolecular polarity	$\ln k_1$ $\ln k_2$	MLR	[111]
26-29 Aromatic acids and amides (= $f(\text{CSP})$): 21-23 (train); 5-6 (test)	Chiralpak [®] AD Chiralpak [®] AS ^b Chiralpak [®] AR ^c	NPLC	4: LUMO energy, molecular electrostatic potential, molecular lipophilic potential, and total dipole moment	$\ln k_1, \ln k_2, \alpha$	ANN	[111]
12 Arylcarboxylic acids	HSA	RPLC	2: Molecular lipophilic potential, and total energy 3: Molecular electrostatic potential, molecular lipophilic potential, and electronic state sum	$\ln k_1$ $\ln k_2$	MLR	[112]

Table I.9. - Continued

Compounds	CSP	HPLC mode	Predictor variables	Response variable	Chemometric technique	[Ref]
5 Benzoyl amides	CSP1: Chiralpak® AD CSP2: Chiralpak® AS ^b CSP3: Chiralpak® AR ^c	NPLC	1: Length of alkyl side chain	$\ln k_1, \ln k_2$	OLS	[113]
6 α -Methyl arylamides	CSP1		1: x Component of dipole moment 1: Total dipole moment	$\ln k_1$ $\ln k_2$		
	CSP2		1: 3 rd Order Kappa alpha connectivity index 1: x Component of dipole moment	α $\ln k_1, \ln k_2$		
	CSP3		1: Heat of formation 1: 3 rd Order valence-corrected cluster molecular connectivity index 1: Minimum molecular electrostatic potential	α $\ln k_1, \ln k_2$ α		
20-23 Sulfoxides (= f (CSP))	Cellulose trisphenyl/carbamate	NPLC	1: Balaban index 3: Balaban index, total dipole, and MV 4: $\log P, M_r, 0^{\text{th}}$ order Randić connectivity index, and polarizability shape index 4: $\log P, M_r, 0^{\text{th}}$ order Randić connectivity index, and directional dimension 4: Total dipole, $\log P$, topological information index, and distribution descriptor	$\log k_1$ $\log k_2$ $\log k_1$ $\log k_2$ $\log k_1$	OLS or MLR (PCA for FS)	[114]
	Cellulose tris(3,5-dimethylphenyl/carbamate)					
	Amylose trisphenyl/carbamate					
	Amylose tris(3,5-dimethylphenyl/carbamate)		4: Kier molecular connectivity index, Kappa shape index, $\log P$, and bond information index 4: 2 Carbosimilarity indices, 0 th order Randić connectivity index, and topological information index	$\log k_1$ $\log k_2$		
14 <i>O</i> -Ethyl <i>O</i> -phenyl <i>N</i> -isopropyl phosphoroamiditoates	Sumichiral OA4700 ^d	NPLC	3: $\log P$, LUMO energy, and total energy	$\ln k_1, \ln k_2$	Stepwise MLR	[115]

Table I.9.- Continued

Compounds	CSP	HPLC mode	Predictor variables	Response variable	Chemometric technique	[Ref]
9-13 <i>N</i> -3,5-Dinitrobenzoyl amino acids (= $f(\text{CSP}, \mathbf{y})$)	6 Quinine carbamates: CSP1: 9- <i>O</i> -(<i>n</i> -propylcarbamoyl) CSP2: 9- <i>O</i> -(<i>i</i> -propylcarbamoyl) CSP3: 9- <i>O</i> -(cyclohexylcarbamoyl) CSP4: 9- <i>O</i> -(<i>tert</i> -butylcarbamoyl) CSP5: 9- <i>O</i> -(1-adamantylcarbamoyl) CSP6: 9- <i>O</i> -(tritylcarbamoyl)	RPLC	4: Taft's steric parameter for selectand, and Taft's steric parameter for chiral selector, and their square terms	$\log \alpha$	MLR	[122]
41-47 Hydantoin (= $f(\mathbf{y})$): 30-32 (train); 11-15 (test)	(3 <i>R</i> ,4 <i>S</i>)-Whelk-O® 1	NPLC	4: Taft's steric parameter for selectand, and Taft's steric parameter for chiral selector, and their square terms 2: Hansch hydrophobic parameter, and Taft's electronic parameter for aliphatic substituents	$\log k_2, \log \alpha$ $\log k_1$	CART (PLS and stepwise MLR for FS)	[123]
175 Structurally unrelated compounds: 142 (train); 33 (test)	Whelk-O® 1	NPLC	119: GRID descriptors (e.g., acceptor-acceptor, donor-donor, lipophile-lipophile, acceptor-donor, acceptor-lipophile, and donor-lipophile)	$\ln \alpha$	PLS	[124]
67 Hydantoin: 40 (train); 27 (test)	Urea-linked α -arylkilaminine derivatives (CSP1, CSP2, CSP3)	NPLC	7 (for CSP1): 5 parameters related to the number of certain types of moieties (e.g., ester and ether), edge adjacency index, and Lipinski alert index 4 (for CSP2): 2 parameters related to the number of certain types of moieties (e.g., ether and CHR ₂ X), 9 th mean topological charge index, sum of geometrical distances between N..P, and a drug-like index 5 (for CSP3): 2 parameters related to the number of certain types of moieties (e.g., ester and ether), rotatable bond fraction, and a drug-like index	α	SVM (MI for FS)	[125]

Table I.9. - Continued

Compounds	CSP	HPLC mode	Predictor variables	Response variable	Chemometric technique	[Ref]
175 Structurally unrelated compounds: 157 (train); 18 (test)	Whelk-O® 1	NPLC	4: Atomic count at bonds distances 6, 7 and 8 from the C*, and H count at bond distance 4 from the C*	Categorical α	Decision trees (algorithms for FS)	[126]
17 1-Phenylethanol pure enantiomer pairs: 20 enantiomers (train); 14 enantiomers (test)	Chiralcel® OB-H ^e	NPLC	6: COMFA descriptors	ROI $\log\alpha$	ANN (GA for FS)	[127]
15 Pyrrolidin-2-ones pure enantiomer pairs: 11 (train); 4 (test)	Chiralpak® IA	NPLC	4-5: HOMO energy and COMFA descriptors (= $f(\text{MP})$) 3: <i>PSA</i> , LUMO energy, and categorical indicator descriptor (+1 for the 1 st and -1 for the 2 nd eluted enantiomers)	$\log k$ (joint data from $\log k_1$ and $\log k_2$) $\log k$ (joint data from $\log k_1$ and $\log k_2$)	MLR (GA for FS)	[128]
58 Aryloxyaminopropanols MLR: 44 (train); 14(test) ANN: 30 (train); 14 (validation); 14 (test)	Chirobiotic® T	Polar organic	5: 2D-autocorrelation, lipophilicity, WHIM, 3D-MoRSE, and NMR descriptors 12: 2 2D-autocorrelation, 5 NMR, edge adjacent index, and 4 categorical structural descriptors	R_s	ANN (GA and for FS)	[129]
Chirobiotic® V			8: 2 2D-autocorrelation, 1 lipophilicity, 1 WHIM, 3 3D-MoRSE and 1 GETAWAY descriptors 13: 1 2D-autocorrelation, 3 topological, 3 3D-MoRSE, 1 GETAWAY, 2 RDF, and 1 ETA descriptors		Stepwise MLR (GA and for FS)	

Table I.9. - Continued

Compounds	CSP	HPLC mode	Predictor variables	Response variable	Chemometric technique	[Ref]
13 1-(2-Naphthyl)-1 ethanol esters pure enantiomer pairs; 20 enantiomers (train); 6 enantiomers (test)	Chiralcel® OD	NPLC	NA: Structural descriptors 812: MIA descriptors	k_r (joint data from k_{r1} and k_{r2}) k_r (joint data from k_{r1} and k_{r2})	PLS (GA for FS) PLS	[130]
> 100 Structurally unrelated compounds	34 CSPs: 4 CDs 4 macrocyclic antibiotics 8 donor-acceptors 2 ligand-exchange CSPs (e.g., Chiralpak® ZWIX) 1 crown ether 2 proteins (e.g., Chiralpak® BSA), 1.1 polysaccharides (e.g., Chiralpak® IA) 3 synthetic helical polymers (e.g., Kromasil® CHI-DMB)	NA	NA: Topological descriptors generated by RDKit layer fingerprints	Categorical α	RF	[131]
10-14 Coumarins (= $f(\mathbf{Y})$)	Chiralpak® IA	Polar organic	1: Hammett substituent constant 3: $\log k_1$, van der Waals volume, and categorical indicator variable (+1 for <i>meta</i> and 0 for <i>para</i> substituents) 2: van der Waals volume, and categorical indicator variable (+1 for <i>meta</i> and 0 for <i>para</i> substituents)	$\log k_1$ $\log k_2$ $\log \alpha$	OLS MLR MLR	[132]
38 Structurally unrelated compounds; 34 (train); 4 (test)	CHIRAL ART Cellulose-SC	RPLC	9: C^*X , C^*hA , Arc , $zmin$, MSA , OEC^* , ST , $\log D$, and molar total charge	Categorical R_s	DPLS1 (PLS algorithms for FS)	[133]

Table I.9. - Continued

Compounds	CSP	HPLC mode	Predictor variables	Response variable	Chemometric technique	[Ref]
50 Arylhydantoin (train)	Whelk-O [®] 1 (<i>S,S</i>)	NPLC	78: GRID/VolSurf descriptors (e.g., total volume, total surface, energy minima, balances of the hydrophilic-hydrophobic interactions, amphiphilic moment, critical packing, molecular polarizability, and M_f)	$\log k_1, \log k_2$	PLS (FDD for FS)	[134]
38 (train); 12 (test)			38: GRID/VolSurf descriptors (e.g., total volume, total surface, volume of interaction with the H ₂ O probe, distances between the energy minima, and integrity moment)	$\log \alpha$		

^a DACH-DNB: 3,5-dinitrobenzoyl derivative of 1,2-diaminocyclohexane (donor-acceptor-based CSP), ^b Chiralpak[®] AS: amylose tris(*S*)- α -methylbenzylcarbamate (polysaccharide-based CSP), ^c Chiralpak[®] AR: amylose tris(*R*)-phenylethylcarbamate (polysaccharide-based CSP), ^d Sumichiral OA-4700: (*S*)-tert-Leucine and (*R*)-1-(α -naphthyl)ethylamine urea linkage (donor-acceptor-based CSP), ^e Chiralcel[®] OB-H: cellulose tribenzoate (polysaccharide-based CSP). The rest of the CSPs named in the table are described in the previous tables (section I.2).

Abbreviations: = f (CSP) (depending on the chiral stationary phase); = f (MP) (depending on the mobile phase); = f (\mathbf{y}) (depending on the response variable); α (enantioselectivity); ANN (artificial neural network); Arc (aromatic ring count); C^* (chiral carbon atom); C^*hA (aromatic heterocycles linked to the C^*); C^*X (heteroatoms linked to the C^*); CART (classification and regression trees); CoMFA (comparative molecular field analysis); CoMSIA (comparative molecular similarity indices analysis); DPLS1 (discriminant partial least squares for one response categorical variable); ETA (extended topochemical atom); EVA (normal mode eigenvalues); FDD (fractional factorial design); FS (feature selection); GA (genetic algorithm); GETAWAY (geometry, topology, and atom-weights assembly); HBA (hydrogen bond acceptor); HBD (hydrogen bond donor); HOMO (highest occupied molecular orbital); k (retention factor); k_1 (retention factor for the least retained enantiomer); k_2 (retention factor for the most retained enantiomer); k_{w2} (retention factor extrapolated to a 100% aqueous mobile phase for the most retained enantiomer); $\log D$ (logarithm of the distribution coefficient); $\log P$ (logarithm of the *n*-octanol/water partition coefficient); LUMO (lowest unoccupied molecular orbital); MI (mutual information); MIA (multivariate image analysis); MLR (multiple linear regression); MoRSE (molecule representation of structures based on electron diffraction); MP (mobile phase); MR (molecular refractivity); M_r (molecular mass); MSA (molecular surface area); MV (molar volume); NA (non-available); NMR(nuclear magnetic resonance); NPLC (normal phase HPLC); OEC^* (orbital electronegativity of the C^*); OLS (ordinary least squares); PCA (principal component analysis); PLS (partial least squares); $P54$ (polar surface area); RDF (radial distribution function); RF (random forest); ROI (retention order index); RPLC (reversed-phase HPLC); R_S (enantioresolution); S (Snyder equation eluent strength); $S7$ (surface tension); SVM (support vector machines); test (test set); t_R (retention time); t_{R1} (retention time for the least retained enantiomer); t_{R2} (retention time for the most retained enantiomer); train (training set); WHIM (weighted holistic invariant molecular); $zmin$ (minimal z length).

I.4.- Deconvolution of peaks in chiral liquid chromatography

The description of the chromatographic peak profiles has been studied extensively. For this purpose, a great number of mathematical functions has been proposed. These peak models, among other applications, allows the deconvolution of the overlapping peaks to achieve the mathematical resolution. This is particularly useful when the complete peak resolution cannot be achieved experimentally. These peak models have been widely investigated in achiral chromatography [139]. However, very few papers undertake the use of deconvolution methods for chiral chromatography separations [140-144]. In these studies, deconvolution methods have been used to estimate parameters related to the enantiomeric composition of chiral compounds (e.g., the enantiomeric fraction, EF , Eq. I.1) in several kinds of samples.

$$EF = \frac{S_{E1}}{S_{E1} + S_{E2}} \quad (\text{Eq. I.1})$$

where S_{E1} and S_{E2} usually refers to the estimated concentration of the most and least retained enantiomers, respectively.

The main aspects of mathematical functions used to describe the chromatographic peak profiles are described thereafter.

I.4.1.- Peak models

Chromatographic peak profiles (see Figure I.6) are the result of different types of interactions in the chromatographic system (e.g., adsorption/desorption and size exclusion processes within the column, intra-columns effects such as diffusive migration, and extra-column effects such as injection plug).

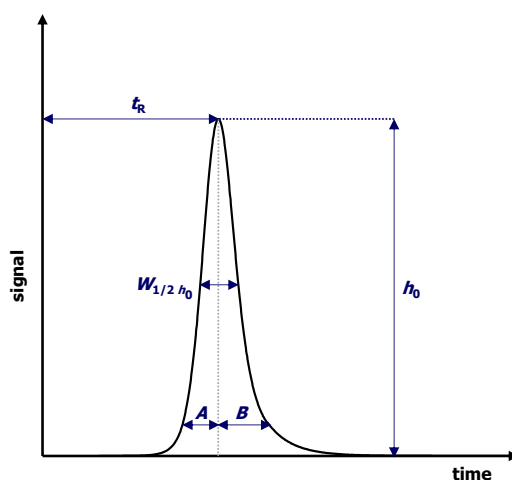


Figure I.6.- Some examples of chromatographic peak parameters: height at the peak maximum (h_0), half-width at 50 % peak height ($W_{1/2 h_0}$), retention time (t_R) and left (A) and right (B) half-widths.

For symmetrical and non-overloaded chromatographic peaks, the Gaussian model (see Eq. I.2) can describe well the elution profiles.

$$h(t) = h_0 e^{-\frac{1}{2} \left(\frac{t-t_R}{\sigma} \right)^2} \quad (\text{Eq. I.2})$$

where h_0 is the peak maximum, t_R is the retention time at the peak maximum, and σ is the peak standard deviation. It is usual to relate the peak width to the standard deviation of a Gaussian peak as a function of height. For example, 1σ at 88 % of maximum height, 2σ at 61 %, 4σ at 14 % and 4.6σ at 7 %.

However, non-ideal peaks (i.e., non-symmetrical peaks with fronting or tailing) are often obtained in practice. The asymmetry of peak favours the overlapping of neighbouring peaks since more solute is placed in the lower area of the peak than around the maximum of the peak. In addition, non-symmetrical peaks cannot be described well using simple functions. For this reason, there are so many theoretical and empirical mathematical functions for the description of chromatographic peak profiles [145,146]. Among all the existing theoretical and empirical mathematical functions, the **modified Gaussian models** (see Table I.10) are the most frequently used.

Table I.10.- Examples of some peak models proposed for Gaussian modified models [139].

Model	Equation ^a
Bi-Gaussian	$h(t) = h_0 e^{\left[-\frac{1}{2}\left(\frac{t-t_R}{\sigma_1}\right)^2\right]} \text{ for } t < t_R \quad (\text{Eq. I.3})$ $h(t) = h_0 e^{\left[-\frac{1}{2}\left(\frac{t-t_R}{\sigma_2}\right)^2\right]} \text{ for } t \geq t_R$
Gram-Charlier series	$h(t) = h_0 e^{\left[-\frac{1}{2}\left(\frac{t-t_R}{w}\right)^2\right]} \left[1 + \sum_{i=3}^n (-1)^i \frac{c_i}{i!} H_i(t) \right] \quad (\text{Eq. I.4})$ <p style="text-align: center;">being $H_i(t)$ the member of the Hermite polynomial</p>
Exponentially modified Gaussian (EMG)	$h(t) = \frac{M_0}{2\tau} e^{\left[\frac{\sigma_G^2}{2\tau^2} - \frac{t-t_G}{\tau}\right]} \left[1 - \text{erf}\left(\frac{\sigma_G}{\sqrt{2}\tau} - \frac{t-t_G}{\sqrt{2}\sigma_G}\right) \right] \quad (\text{Eq. I.5})$
Polynomial modified Gaussian (PMG)	$h(t) = h_0 e^{\left[-\frac{1}{2}\left(\frac{t-t_R}{\sigma_0+c_1(t-t_R)+c_2(t-t_R)^2+\dots}\right)^2\right]} \quad (\text{Eq. I.6})$ <p>where:</p> $\sigma_0 = 0.932 \frac{A_{0.1}B_{0.1}}{A_{0.1} + B_{0.1}} \quad \text{and} \quad c_1 = 0.466 \frac{B_{0.1} - A_{0.1}}{A_{0.1} + B_{0.1}}$
Mixed exponential (PEMG)	$h(t) = h_0 e^{\left[-\frac{1}{2}\left(\frac{t-t_R}{\sigma_0+c_1(t-t_R)}\right)^2\right]} \quad (\text{Eq. I.7})$ <p>Exponential decays:</p> $h = k_{1, \text{left}} e^{\{k_{2, \text{left}}(t-t_R)\}} \text{ for } t < t_R - A_{0.1}$ $h = k_{1, \text{right}} e^{\{k_{2, \text{right}}(t-t_R)\}} \text{ for } t > t_R + B_{0.1}$ <p>where:</p> $k_{1, \text{left}} = 0.1h_0 e^{(k_{2, \text{left}}A_{0.1})}; \quad k_{2, \text{left}} = \frac{\sigma_0 A_{0.1}}{(\sigma_0 - c_1 A_{0.1})^3}$ $k_{1, \text{right}} = 0.1h_0 e^{(k_{2, \text{right}}B_{0.1})}; \quad k_{2, \text{right}} = \frac{\sigma_0 B_{0.1}}{(\sigma_0 + c_1 B_{0.1})^3}$
Parabolic variance modified Gaussian (PVMG)	$h(t) = h_0 e^{\left[-\frac{1}{2}\frac{(t-t_R)^2}{\sigma_0^2+c_1(t-t_R)+c_2(t-t_R)^2}\right]} \quad (\text{Eq. I.8})$ <p>where:</p> $c_1 = \frac{B_{0.1} - A_{0.1}}{A_{0.1}B_{0.1}} s_0^2 \quad \text{and} \quad c_2 = 0.217 - \frac{s_0^2}{B_{0.1}A_{0.1}}$
Parabolic-Lorentzian modified Gaussian (PLMG)	$h(t) = h_0 e^{\left[-\frac{1}{2}\frac{1+c_3(t-t_R)+c_4(t-t_R)^2}{\sigma_0^2+c_1(t-t_R)+c_2(t-t_R)^2}(t-t_R)^2\right]} \quad (\text{Eq. I.9})$ <p>where:</p> $\sigma_0^2 = \frac{4}{1+c_0^2} \frac{A_{0.6}^2 B_{0.6}^2}{(A_{0.6}+B_{0.6})^2} \quad c_4 = \frac{c_3^2}{4} + c_5^2$ $c_1 = \frac{\sigma_0^2(B_{0.6} - A_{0.6})}{A_{0.6}B_{0.6}} + c_3 A_{0.6} B_{0.6} + c_4 A_{0.6} B_{0.6} (B_{0.6} - A_{0.6})$ $c_2 = 1 - \frac{\sigma_0^2}{A_{0.6}B_{0.6}} + c_3(B_{0.6} - A_{0.6}) + c_4 \frac{A_{0.6}^3 + B_{0.6}^3}{A_{0.6} + B_{0.6}}$

^a h_0 (maximal height or related parameter), t_R (time at the peak maximum), σ (standard deviation or related parameter), M_0 (peak area), σ_G and t_G (coefficients of the precursor Gaussian signal), τ (time constant), and c_0, c_1, c_2, \dots (fitting coefficients).

The bi-Gaussian model uses two half-Gaussians functions with different widths for the left and right peaks regions and a common maximum. However, this model does not describe well long tailing or fronting peaks because the front and the back of the peaks quickly achieve null values [147]. The Gram-Charlier series is a highly complex function that try to provide asymmetry to the Gaussian by multiplying it with different polynomials. It depends on the maximum peak asymmetry and the number of terms in the series are defined in terms of the statistical moments and cumulant coefficients [148]. The exponentially modified Gaussian (EMG) model is obtained by the convolution of the Gaussian function and an exponential decay function. EMG model is probably the most popular model since it usually offers good fittings for moderately asymmetric peaks [149]. The polynomial modified Gaussian (PMG) models describe the deviations from an ideal Gaussian peak as a change in the standard deviation with time according to a polynomial function. Linear modified Gaussian (LMG) is the simplest PMG model. LMG model easily relates the peak parameters with the half-widths, and it is adequate for peaks with moderate asymmetry. However, a more complex model is needed for more accurate fitting of chromatographic peaks, namely, higher degree polynomials create more flexible models, and then, they have a better chance of fitting the experimental data [147,150]. Parabolic and cubic functions can describe the most chromatographic peaks. However, when the polynomial takes zero or even negative values, the function does not work suitably. In addition, it is also possible that the predicted signal may grow outside the peak region after reaching a minimum value [150]. A polynomial-exponential modified Gaussian (PEMG) model perfectly solves the problem by substituting at a given point of the PMG model each outer peak region with an exponential decay, so that the derivatives of both PMG and exponential functions coincide [151]. Another simplest alternative is the parabolic variance modified Gaussian (PVMG) model. However, the assumption of a parabolic trend does not allow full recovery of baseline, leaving a small residual value that may be significant for peaks with high asymmetry [152]. PVMG model problem was overcome using a parabolic Lorentzian modified Gaussian (PLMG) model. In a PLMG model, the parabolic component describes the non-Gaussian region of the peak profile (i.e., the variance changes in the peak region), and the Lorentzian component annuls the increase in variance outside the elution region (i.e., it decreases the variance growth out of the peak region). Although PLMG model has demonstrated the best performance in the fitting of isolated asymmetric peaks, the use of this model may not converge if the initial values used to fit the model are far from the optimal values. Its high flexibility makes the optimisation process difficult and then, the results obtained need to be controlled to ensure that the best parameters derived by the software make physical sense [150,153]. Several semiempirical functions using half-width values at different peak height were proposed to solve this problem.

Other functions based on **non-Gaussian models** (see Table I.11) have also been proposed.

Table I.11.- Examples of some peak models proposed for non-Gaussian basis models [139].

Model	Equation ^a	
Extreme value	$h(t) = h_0 e^{\left[-e^{\left(\frac{t-t_R}{w}\right)} - \frac{t-t_R}{w} + 1\right]}$	(Eq. I.10)
Log-normal	$h(t) = h_0 e^{\left[-\frac{\ln 2}{\alpha^2} \left[\ln\left(\frac{2\alpha(t-t_R)}{w} + 1\right)\right]^2\right]}$	(Eq. I.11)
Generalised exponential (GEX)	$h(t) = h_0 \left(\frac{t-t_1}{t_R-t_1}\right)^{c_1} e^{\left\{\frac{c_2}{c_1} \left[1 - \left(\frac{t-t_1}{t_R-t_1}\right)^{c_2}\right]\right\}}$	(Eq. I.12)
	for $c_1 > 0$, $c_2 > 0$ and $t > t_1$	
Pap-Pápai	$h(t) = h_0 e^{\left\{\left(\frac{4}{\alpha^2} - 1\right) \left[\ln\left(1 + \frac{2\alpha(t-t_R)}{\sigma(4-\alpha^2)}\right) - \frac{2\alpha(t-t_R)}{\sigma(4-\alpha^2)}\right]\right\}}$	(Eq. I.13)
Losev	$h(t) = \frac{h_0}{e^{\left(-\frac{t-t_1}{a}\right)} + e^{\left(\frac{t-t_1}{b}\right)}}$	(Eq. I.14)
Li	$h(t) = \frac{h_0}{\left[1 + c_1 e^{\left(\frac{t_1-t}{a}\right)}\right]^{c_2} + \left[1 + c_3 e^{\left(\frac{t-t_2}{b}\right)}\right]^{c_4} - 1}$	(Eq. I.15)
Combined square roots (CSR)	$h(t) = \frac{h_0}{2} \left(\sqrt{\left(\frac{t-t_R}{a} + 1 + c_1\right)^2 + c_2^2} + \sqrt{\left(\frac{t-t_R}{b} - 1 - c_3\right)^2 + c_4^2} - \frac{a+b}{ab} \sqrt{(t-t_R)^2 + c_5^2} - c_1 - c_3 \right)$	(Eq. I.16)
Baker	$h(t) = \frac{h_0}{1 + c_1(t-t_R)^2 + c_2(t-t_R)^3 + c_3(t-t_R)^4}$	(Eq. I.17)
Giddings	$h(t) = \frac{h_0}{2w} \sqrt{\frac{t_1}{t}} I_1 \left(2 \sqrt{\frac{t_1}{w}} \right) e^{\left(-\frac{t+t_1}{w}\right)}$	(Eq. I.18)

$$\text{being } I_1 \text{ a modified Bessel function: } I_1(t) = \sum_{k=0}^{\infty} \frac{1}{k!(k+1)!} \left(\frac{t}{2}\right)^{2k+1}$$

^a h_0 (maximal height or related parameter), t_R (time at the peak maximum), w (parameter related to the peak width), α (parameter related with the asymmetry), t_1 (initial time), t_1 and t_2 (parameters related to the peak position), a and b (parameters related to the left and right half-widths), and c_0, c_1, c_2, \dots (fitting coefficients).

The extreme value, log-normal, generalised exponential (GEX) and Pap-Pápai models are inspired by statistical distribution functions. The use of log-normal, GEX, and Pap-Pápai models involve adopting restrictions to avoid logarithms of negative numbers and negative fractional exponential numbers [154-157]. Losev and Li models are empirical functions that divide the peak into fronting and tailing parts, each one described with a sigmoidal function. Combined squared roots (CSR) model is the sum of squared roots and it has shown satisfactory performance to describe peaks with high asymmetry. Losev, Li and CSR models need many parameters to fit properly any peak [158-160]. Baker model uses a modified Lorentzian that has a less pronounced decay than the Gaussian function, but it is not suitable for chromatography [161]. Giddings model considers asymmetric peaks in which left and right peak half-widths depend linearly on retention time, but the complexity of the model makes it less attractive [162-164]. Except for Baker model, the rest of models mentioned in

the Table I.11 can fit tailing peaks with good results, but only Losev, Li and CSR models can also fit fronting peaks. However, these functions do not allow the direct estimation of the half-widths.

Mathematical functions can be used to calculate peak parameters (e.g., area, mean, variance, skewness, number of theoretical plates, maximum height, retention time, width, and asymmetry factor) by fitting the experimental data. However, the most frequent applications of these mathematical functions are the prediction of chromatographic peak profiles at different retention times, the evaluation of peak overlapping, and the deconvolution of partially resolved peaks [139]. For this reason, the accuracy in describing the chromatographic peak profiles is necessary to extract reliably information from these isolated or overlapped peaks signals.

For example, in the case of the peak resolution optimisation, where optimal chromatographic conditions are searched, the use of models that can describe the solute retention and peak profile with changes in the experimental factors is useful. These models will tend to maximise the peak resolution, or at least to find the conditions in which the peaks are minimally overlapped. Although other objectives such as short analysis times can also be considered. In addition, when the peak shape is used in the optimisation process, it is necessary to take into account that sometimes the peaks are not symmetric (i.e., Gaussian model cannot describe well the peak profile) and that the efficiency of the peak depends as much on the solute nature and the experimental conditions. Therefore, a complete knowledge of the peak profiles is necessary for a reliable prediction. So, a estimation of the degree of overlap between peaks requires the knowledge of the position, size, and profile of each peak in the chromatogram [139].

As another example, when the complete peak resolution cannot be achieved experimentally, the use of peak models allows the deconvolution of the overlapping peaks to achieve the mathematical resolution. Deconvolution obtains the parameters of the function that each individual peak describes, giving rise to the whole signal by linear combination [139,151]. The deconvolution is possible, even with simple chemometrics, when working with moderately overlapping peaks. However, when working with higher overlapping, the results become ambiguous due to the possible collinearity between parameters, which produces poorly defined error surfaces. The results can be improved by enriching the chromatogram information through hyphenated techniques.

For all mentioned above, the application of these models to the description of the peaks obtained in a chiral separation is an important challenge since the peak characteristics for the enantiomers can be very different and their overlapping degree variable. Therefore, an adequate and practical mathematical model is needed to describe this type of chromatographic peaks.

I.5.- Chiral pollutants

Water is a limited natural resource, indispensable for life, which has suffered an alarming deterioration as a consequence of economic development and improper use. For decades, research on water pollution has focused on pollutants classified as hazardous or priority pollutants listed in legislation, in particular the persistent organic pollutants. These **priority substances** include heavy metals, pesticides, flame retardants and polycyclic aromatic hydrocarbons; known to be toxic, bioaccumulative and persistent in the environment [165].

The consumption habits of our society are generating a series of waste products and pollutants that may represent a new environmental problem. These substances, known as **emerging pollutants**, include biologically active compounds such as pharmaceuticals, drugs of abuse, personal hygiene products, household products or products of agricultural and industrial origin that have been released into the environment without regard for the possible consequences. An important characteristic of these pollutants is that they do not need to be persistent in the environment to cause negative effects, as their transformation and/or removal rates are compensated by their continuous introduction into the environment [165,166]. Emerging pollutants are not included in regulatory frameworks for the control and prevention of environmental pollution [166].

The main pathways for pollutants occurrence in the aquatic environment (see Figure I.7) are urban, industrial, agricultural and livestock wastewater as a result of anthropogenic activities [167,168].

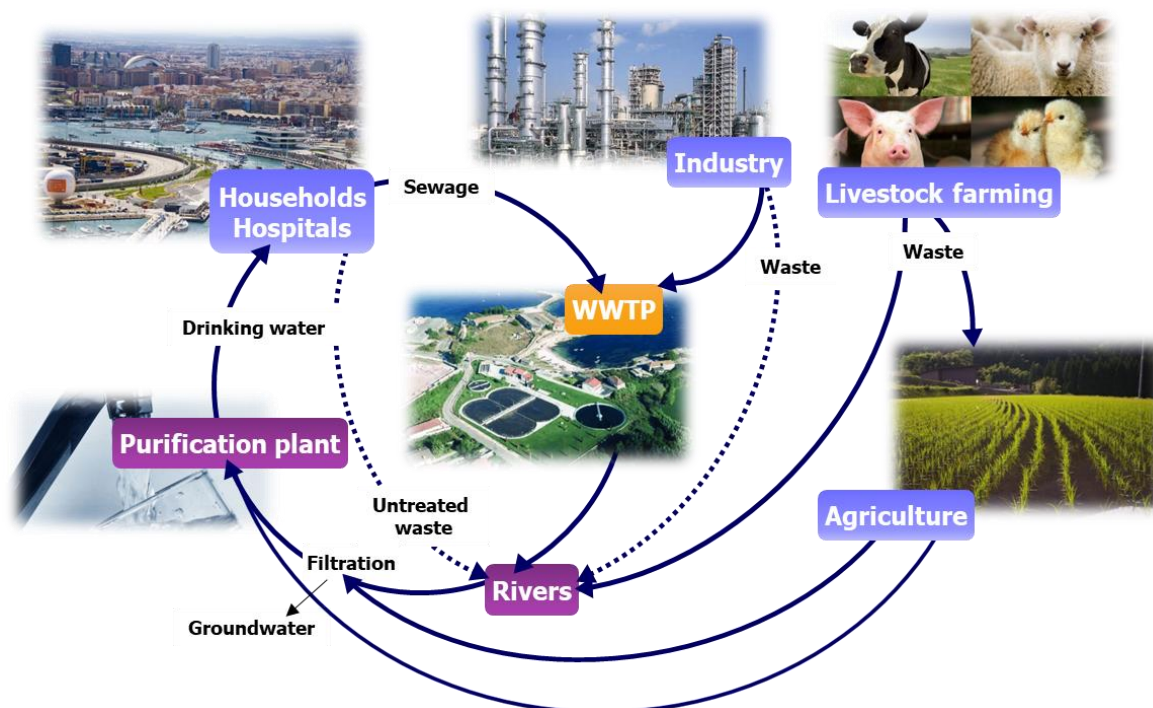


Figure I.7.- Water cycle: main pathways for pollutants occurrence in the aquatic environment.

Degradation of many of pollutants by the conventional treatment systems used in waste water treatment plants (WWTPs) is low or non-significant, so they easily reach natural aquatic systems, mainly coastal waters and rivers. In addition, it has been shown that some of these compounds can be transformed into toxic products in WWTP treatments [169-172]. The main health and environmental effects/risks of these compounds are due to their:

- Persistence (resistance to photochemical, biological, or chemical degradation)
- Bioaccumulation (greater affinity for living tissues than for water)
- Transformation (metabolites may be more toxic than the parent compounds)
- Synergy (multiplication of effects if compounds share mechanisms of action)
- Endocrine disruption (behave like hormones, altering the endocrine system)

As indicated in section I.1, despite the well-established role of enantioselectivity in pharmacodynamic, pharmacokinetic and toxicological processes, stereochemistry has often been neglected in environmental research [17,173]. There are about 1500 **chiral pollutants**, e.g., around 30 % of pesticides, 37 % of polychlorinated biphenyls, 27 % of brominated flame retardants, 10 % of polycyclic aromatic hydrocarbons and 56 % of drugs are chiral compounds. The presence of chiral pollutants, especially drugs, in the environment is also becoming a cause for concern because of the different properties occurring between enantiomers and their potential impact not only on human health, but also on the environment [166,174].

There are multiple references on the occurrence of chiral pollutants, their metabolites and degradation products in various environmental compartments [166,174-178]. They have been detected at levels of ng L^{-1} or $\mu\text{g L}^{-1}$ in surface water, groundwater and even in drinking water. In soils and sediments, where they can persist for a long time, they reach levels of g kg^{-1} . However, despite the great efforts made by regulatory authorities and the scientific community, not much is known about the impact of such compounds on the environment and human health [17,179,180].

Once introduced into the environment, chiral pollutants are subject to several processes:

- Abiotic processes (adsorption, photochemical transformation, and water-air or soil-air distribution processes) that are non-stereoselective since the enantiomers have the same physicochemical properties.
- Biotic processes (biodegradation by microorganisms) that can be stereoselective due to the possible differential interaction of the enantiomers of chiral pollutants with chiral substances present in living organisms (e.g., enzymes and biological receptors). This can result in an enrichment/reduction of the enantiomeric composition of chiral pollutants [17].

Thus, the enantiomers of chiral pollutants can be present in the environment in different proportions as a result of the enantioselective living being excretion (as indicated in section I.1), bioaccumulation in environmental compartments and the microbial biodegradation during the wastewater treatment process.

I.5.1.- Biodegradation: concept and evaluation

Biodegradation is the process by which organic compounds are decomposed by microorganisms into simpler products that are usually less toxic than the original compounds. According to the Organisation for the Economic Co-operation and Development (OECD), primary biodegradation, also known as biotransformation, is “*the structural change of a chemical substance by microorganisms resulting in the loss of chemical identity*” and ultimate aerobic biodegradation is “*the breakdown of a chemical substance by microorganisms in the presence of oxygen to carbon dioxide, water and mineral salts of any other elements present (mineralisation) and the production of new biomass and organic microbial biosynthesis products*” [181].

Biodegradability is defined as the ability of molecules to be degraded by microorganisms. This property depends on the physicochemical conditions under which the degradation process takes place and on the chemical structure of the compound. Biodegradability is an essential parameter for understanding the risk that involves the occurrence of substances into the environment. It is a determining parameter of the environmental behaviour of chemicals and a desirable property of products that are released in huge quantities into the environment [182]. To estimate this property, several biodegradability tests have been designed and standardised to quantify the persistence of chemical compounds in natural or industrial environments. There are tests that simulate soils, surface water or activated sludge processes, generally in the presence of oxygen.

In the scheme established by the OECD Guidelines for the Testing of Chemicals [181], the biodegradability of a substance is determined using three successive levels of testing: the tests for ready [183], inherent [184] and simulation [185] biodegradability tests (see Figure I.8). In this testing strategy, tests are conducted with increasing complexity, environmental realism and cost, in order to obtain appropriate information for environmental decision-making, but at the same time to minimise testing costs.

Firstly, the OECD recommends for economic and time reasons to perform **ready biodegradability tests**. Ready biodegradability tests are performed under aerobic conditions using high concentrations of the test compound ($\sim 2\text{-}100\text{ mg L}^{-1}$) in the presence of an inoculum (e.g., domestic sewage, activated sludge or secondary effluent) as a source of microorganisms. The inoculum should not have been pre-adapted to the degradation of the chemical (i.e., it must not have been previously exposed to the chemical or structurally related chemicals). A positive result in a ready biodegradability test (i.e., degradation above 70 % in a 10-day window within a 28-day test) can be considered as indicative of rapid and ultimate degradation in most environments including WWTPs [183]. A negative result in a ready biodegradability test does not necessarily mean that the chemical compound is not biodegradable, but that further studies are needed to assess its biodegradability. In this case, the OECD recommends performing simulation and/or inherent biodegradability tests.

In an **inherent biodegradability test**, low test substance to biomass ratios and with or without pre-adapted inocula are used. In these tests, biodegradation results above 20 % or 70 % may be considered as evidence of inherent primary or ultimate biodegradability, respectively. In the last case, the substance has a potential for degradation under favourable conditions (e.g., in well-operated WWTPs). Conversely, when a negative result is obtained (biodegradation below 20 %), the substance is potentially persistent in the environment and an evaluation of the potential adverse effects of transformation products should be performed. An alternative is to evaluate ultimate biodegradation at environmentally realistic conditions in a simulation test [181,184].

Simulation tests are intended to assess the biodegradation of chemicals, which do not biodegrade in OECD ready and inherent biodegradability tests. These tests aim to mimic realistic environmental concentrations ($\sim 1\text{-}100 \mu\text{g L}^{-1}$) of the test substance, as well as realistic conditions (e.g., pH , temperature, microbial community, the presence and concentration of other substrates). This guideline consists of five simulation tests in different scenarios (e.g., sewer systems, activated sludge, anaerobic digester sludge...), whose main objectives are the measurement of the primary biodegradation rate, the measurement of the mineralisation rate and the monitoring of the formation and decomposition of the main transformation products when appropriate [181,185].

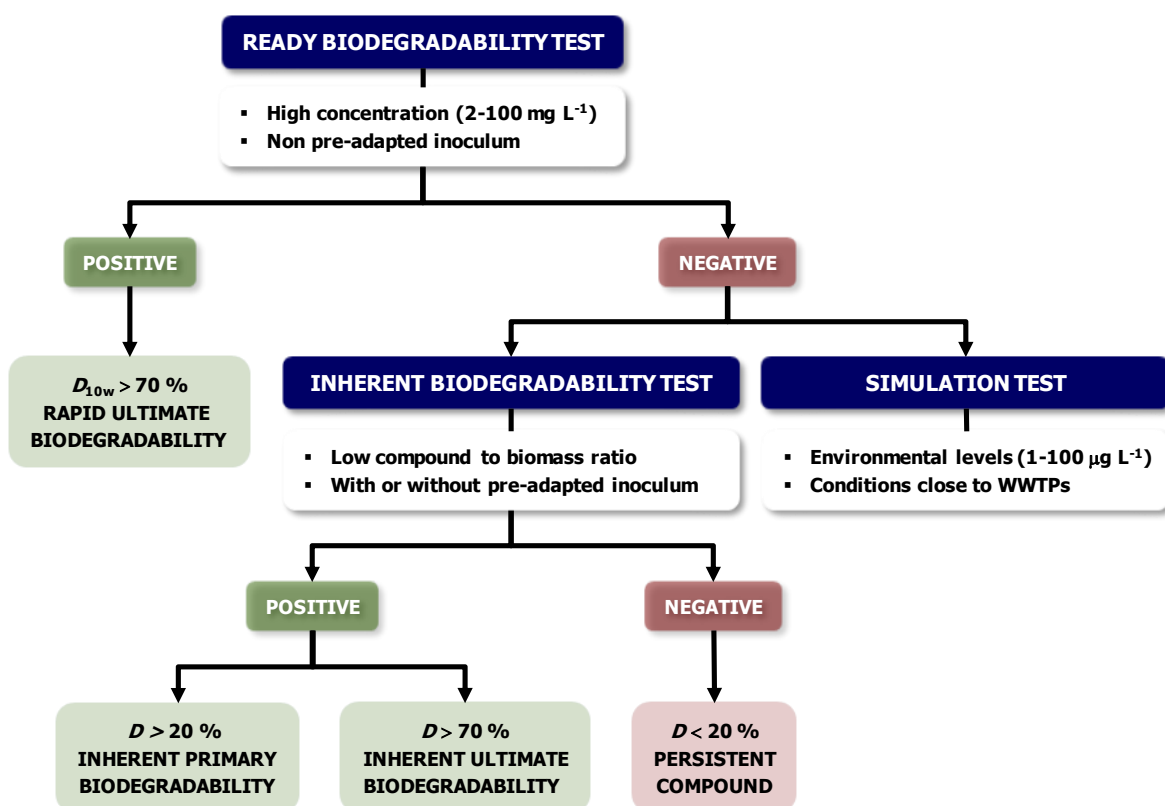


Figure I.8.- Scheme established by the OECD Guidelines for the Testing of Chemicals (Section 3 Environmental fate and behaviour) for biodegradability tests. D : degradation value obtained in a 28-day test. D_{10w} : degradation value in a 10-day window within a 28-day test.

The variation of the concentration (S) of the organic compound (substrate) along time (t) obtained from the above mentioned biodegradability tests can be adjusted to different **biodegradation kinetic models** in order to obtain additional information about the biodegradation process. Table I.12 summarises the biodegradation kinetic models (Eq. I.19–I.26) used for substrates exposed to pure microorganism strains or microbial populations from the natural environment [186–193].

The Monod equation (Eq. I.19, Table I.12) has been extensively utilised when microbial growth and substrate degradation rates are related (i.e., microbial growth-linked biodegradation of substrate). In contrast, the Michaelis-Menten-like (Eq. I.21, Table I.12) and the first order models (Eq. I.24, Table I.12) are derived from simplifications of Monod model. These simplified models are applicable in no-growth biodegradation situations (i.e., the concentration of the organism remains essentially constant even when the substrate is degraded) [186].

Kinetic parameters are key to understand the biodegradation phenomenon, to predict the performance of biological treatment systems, and for the hazard assessment (persistence) of substrate. So, accurate and reliable estimates are needed to avoid pitfalls in environmental and health risk assessment. It has been proven that the model selected for kinetic parameter estimation has a huge impact on their accuracy and reliability. However, the selection of the correct model for the case under study is not an easy task. *A priori*, simple experimental indicators of possible microbial growth-linked biodegradation (e.g., optical density at 600 nm measurements, OD_{600}) could be used for model selection. However, several factors (e.g., the presence of additional carbon sources and the use of substrate concentrations causing toxicity to the microorganisms) could lead to an incorrect selection of the model [186 and references therein]. Common pitfalls (e.g., good determination coefficient, R^2) involved in biodegradation kinetic parameters estimation have been outlined and anticipative strategies to reduce the impact of such pitfalls have been proposed [186].

It is worth mentioning that, regardless of the accuracy and reliability of the kinetic parameter estimates, Monod and Michaelis-Menten-like models provide curves with a good fit (e.g., high R^2) to the experimental S - t data in most cases. These curves can be very useful to estimate the half-life time ($t_{1/2}$) as well as to derive other related curves; for instance, to describe the variation of the percentage of biodegradation (BD , Eq. I.27) over time (BD - t curves) and the enantiomeric fraction course over time (EF - t curves) in the case of the biodegradation of a chiral compound.

$$BD = \frac{S_0 - S}{S_0} 100 \quad (\text{Eq. I.27})$$

where S_0 is the substrate concentration at the beginning of the experiment ($t = 0$ days).

Table I.12.- Biodegradation kinetic models used in the literature [186].

Model	Mathematical solutions	Comments
Monod	Eq. I.19 may be integrated [187], resulting in: $t = \frac{1}{\mu_m} \left\{ \left[\frac{K_s Y + S_0 Y + X_0}{Y S_0 + X_0} \ln \frac{Y(S_0 - S) + X_0}{X_0} \right] - \left[\frac{K_s Y}{Y S_0 + X_0} \ln \frac{S}{S_0} \right] \right\}$ (Eq. I.19) where: $Y(S_0 - S) + X_0 = X$	<ul style="list-style-type: none"> Microbial growth-linked biodegradation of substrate model Eq. I.20 is mathematical inconsistent (explicit in t). The distributed error is assumed to be in t (dependent variable), whereas it is experimentally in S [188] Lack of uniqueness (multiple solutions) in the first-order region ($S_0 < K_s$) due to the high $\mu_m - K_s$ correlation [187,189]
Michaelis-Menten-like (Monod simplified)	Eq. I.21 may be integrated [190], resulting in: $t = \frac{1}{V_m} \left(K_s \ln \frac{S_0}{S} + S_0 - S \right)$ (Eq. I.21) Eq. I.22 may be rearranged as [191]: $S = K_s W \left(\frac{S_0}{K_s} e^{-\frac{S_0 - V_m t}{K_s}} \right)$	<ul style="list-style-type: none"> No-growth biodegradation model ($X \sim X_0$, constant): $(X/Y)\mu_m = V_m \sim (X_0/Y)\mu_m = \text{constant}$ [189,190] (Eq. I.22) Eq. I.23 is explicit in S (avoids the mathematical inconsistencies of Eq. I.20) An offset term can be added (if the $S-t$ curve does not reach 0) [193] (Eq. I.23)^a
First-order	Eq. I.24 may be integrated [191], resulting in: $S = S_0 e^{-k t}$ Eq. I.25 may be rearranged as: $\ln \frac{S}{S_0} = -k t$	<ul style="list-style-type: none"> No-growth biodegradation model First-order region ($S_0 < K_s$): $k = V_m/K_s$ [187,189]. The assumption cannot be verified (K_s is usually unknown) Half-life time: $t_{1/2} = \ln 2/k$

^a Complete expression of Eq. I.23:

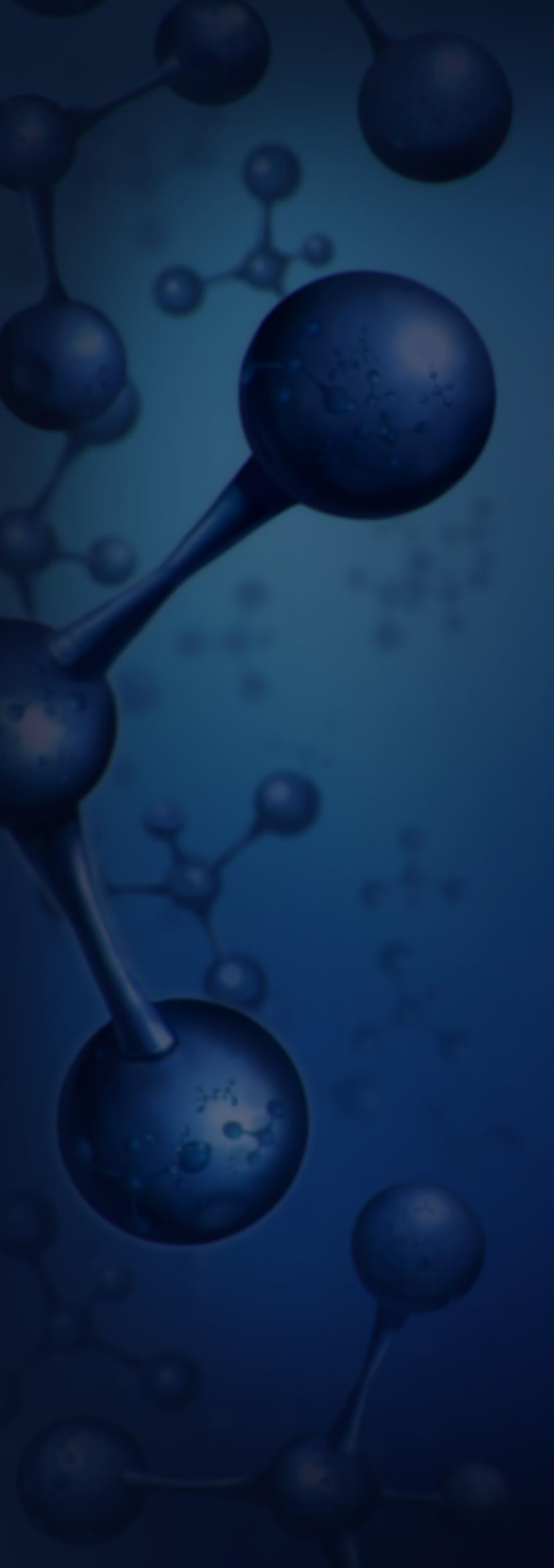
$$S = K_s \ln \left(1 + \frac{S_0}{K_s} e^{-\frac{S_0 - V_m t}{K_s}} \right) \left\{ 1 - \frac{\ln \left[1 + \ln \left(1 + \frac{S_0}{K_s} e^{-\frac{S_0 - V_m t}{K_s}} \right) \right]}{2 + \ln \left(1 + \frac{S_0}{K_s} e^{-\frac{S_0 - V_m t}{K_s}} \right)} \right\}$$

Abbreviations: μ_m (maximum specific growth rate); k (first-order rate constant); K_s (half-saturation or Monod constant); S (substrate concentration); S_0 (initial S value); t (time); V_m (maximal rate); X (biomass concentration); X_0 (initial X value); Y (yield coefficient: mass of biomass per mass of substrate).

I.5.2.- Evaluation of the enantioselective biodegradability of chiral pollutants

As has been indicated previously, biodegradation of chiral pollutants during the wastewater treatment process in WWTPs can lead to differences in the concentrations of the enantiomers ($EF \neq 0.5$). Therefore, the enantioselective evaluation of the biodegradability of the enantiomers of chiral pollutants is essential for their reliable environmental risk assessment. However, in the literature there are few papers that address this important issue.

Some papers have addressed the quantification of EF in influent and effluent from WWTPs [178,194-203]. In other papers, biodegradability tests have been performed, with subsequent separation and determination of the individual enantiomers of the parent compound (or its metabolites) in the test solution by chiral analytical techniques [204-221], mainly HPLC (in NPLC, RPLC and polar organic modes) using CSPs. These studies include antibiotics [204], amphetamine-based compounds [205,206], antidepressants [208-211], β -blockers [211-213], non-steroidal anti-inflammatory drugs [214], and miscellaneous drugs [207] and pesticides [215-221]. In these papers, first order kinetic models [204,209-213,215,216,218-221] are the most used.



II.- OBJECTIVES

The scientific community has been studying the implications of chirality for life for more than a century. Today, it remains an active area of research and debate because of the large number of chiral molecules that are part of living organisms and of our everyday life. In this framework, analytical methodologies for the separation of the enantiomers of chiral molecules play a crucial role.

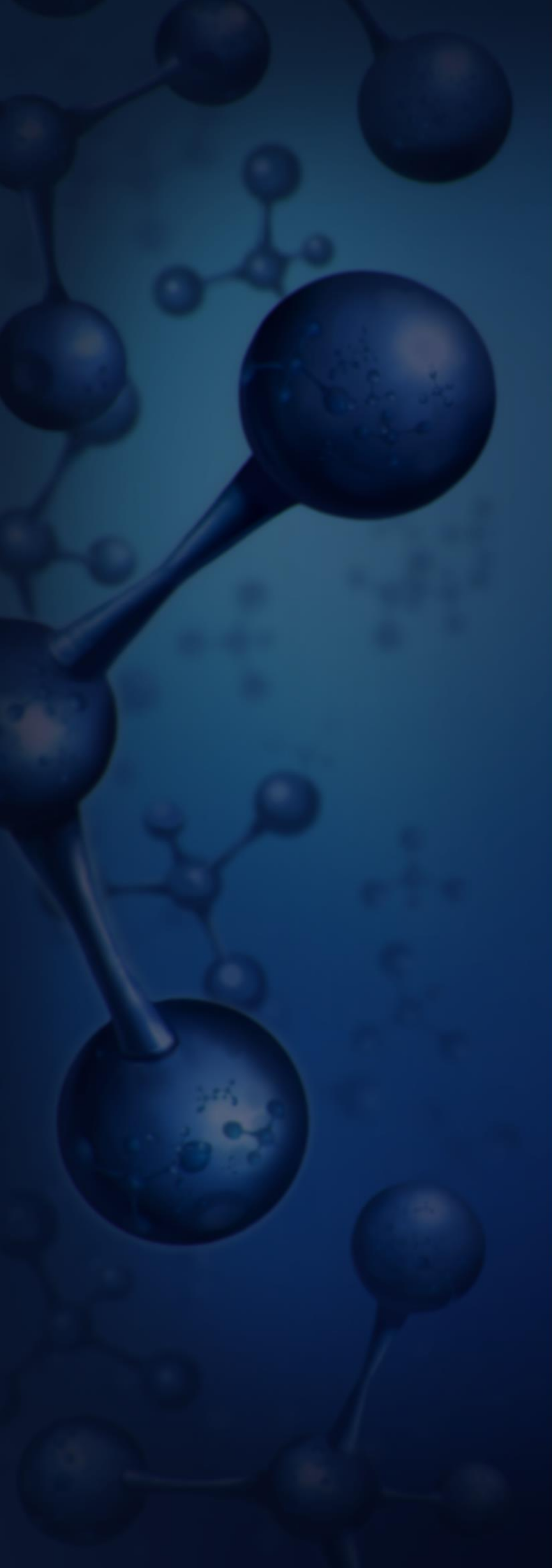
Undoubtedly, the use of CSPs in HPLC is the preferred choice for enantioseparations. This is evidenced by the huge number of CSPs available on the market. This fact, together with the trial-and-error methodologies commonly used for the selection of the most suitable chromatographic system (CSP/mobile phase combination) for a given enantioseparation, results in an enormous cost and experimental effort. This makes it necessary to develop strategies to simplify this important task.

This Doctoral Thesis has two clearly differentiated main objectives:

- i.- To contribute to the knowledge of chiral liquid chromatography with polysaccharide-based CSPs, the most exploited CSPs, and hydro-organic mobile phases. Interests are focused on the most popular commercial polysaccharide-based CSPs: three amylose derivatives (Am1: amylose tris(3,5-dimethylphenylcarbamate); Am2: amylose tris(5-chloro-2-methylphenylcarbamate); Am3: immobilised amylose tris(3-chloro-5-methylphenylcarbamate)) and five cellulose derivatives (Cell1: cellulose tris(3,5-dimethylphenylcarbamate); Cell2: cellulose tris(3-chloro-4-methylphenylcarbamate); Cell3: cellulose tris(4-methylbenzoate); Cell4: cellulose tris(4-chloro-3-methylphenylcarbamate); Cell5: immobilised cellulose tris(3,5-dichlorophenylcarbamate)). Mobile phases assayed comprise ACN and MeOH aqueous solutions compatible with aqueous matrices and MS detection. To this end, the following specific objectives have been set out:
 - To contribute to a rational selection of the chromatographic system to separate the enantiomers of a given compound. For this purpose, the retention and enantioresolution of a large dataset of structurally unrelated chiral compounds (approximately 60 basic and neutral drugs and pesticides) in all the amylose (section IV.1) and cellulose (section IV.2) chromatographic systems above indicated is compared. Moreover, QSPRs models for enantioresolution related data obtained in Am1 and Am3 (section IV.1) as well as in Cell1 (section IV.3) using ACN aqueous mobile phases are intended.
 - To explore the use of deconvolution of overlapping peaks to achieve the mathematical resolution when the baseline resolution cannot be achieved experimentally (section IV.4). To illustrate the potential of this peak model strategy, the enantioseparation of bupivacaine, flurbiprofen, ibuprofen, ketoprofen, metoprolol, omeprazole, propranolol and trimeprazine in polysaccharide-based CSPs (Cell1, Cell2, Cell3, Cell5 and Am2) and ACN or MeOH hydro-organic mobile phases at different separation temperatures is considered.

ii.- To contribute to the advancement of knowledge of the risks and hazards of chiral pollutants. To this end, OECD biodegradability tests using activated sludge from a Valencian WWTP (Quart Benàger) are performed for some common chiral pharmaceutical pollutants: trimeprazine (section IV.5), ibuprofen and ketoprofen (section IV.6), and four local anaesthetics (bupivacaine, mepivacaine, prilocaine and propanocaine; section IV.7). Next, the resolution and determination of the enantiomers of the intact compound is performed by means of chiral RPLC methods (with amylose- or cellulose-based CSPs and ACN or MeOH hydro-organic mobile phases compatible with aqueous matrices and MS detection) developed for that purpose.

The particular goals of each study are detailed in the corresponding sections.



III.- METHODOLOGY

III.1.- Instrumentation

Two Agilent Technologies 1100 chromatographs (Palo Alto, California, USA) were used. One of them was equipped with a quaternary pump, a column thermostat, an UV–visible variable wavelength detector, and an autosampler. Data acquisition and processing were performed using the ChemStation software (A.09.03 [1417], ©Agilent Technologies 1990-2002). The other chromatograph consisted of a binary pump, a column thermostat, an UV–visible diode array detector, a mass spectrometer with electrospray and atmospheric pressure chemical ionisation (ESI/APCI) sources and single quadrupole, and an autosampler. In this chromatograph, the LC/MSD ChemStation software (B.04.02 SP1 [208], ©Agilent Technologies 2001-2010) was used for data acquisition and processing.

For achiral analysis, an Halo C₁₈ column (2.7 μm, 75×4.6 mm i.d.) from Advanced Materials Technology (Wilmington, Delaware, USA) was used. For the separation of the enantiomers of all drugs and pesticides under study, eight polysaccharide-based CSPs were tested:

- Cell1: cellulose tris(3,5-dimethylphenylcarbamate); 3 μm, 150×4.6 mm i.d.
- Cell2: cellulose tris(3-chloro-4-methylphenylcarbamate); 3 μm, 150×4.6 mm i.d. (and 150×2.0 mm i.d. in section IV.4).
- Cell3: cellulose tris(4-methylbenzoate); 3 μm, 150×4.6 mm i.d.
- Cell4: cellulose tris(4-chloro-3-methylphenylcarbamate); 3 μm, 150×4.6 mm i.d.
- Cell5: immobilised cellulose tris(3,5-dichlorophenylcarbamate); 3 μm, 150×4.6 mm i.d.
- Am1: amylose tris(3,5-dimethylphenylcarbamate); 3 μm, 150×4.6 mm i.d.
- Am2: amylose tris(5-chloro-2-methylphenylcarbamate); 3 μm, 150×2.0 mm i.d.
- Am3: immobilised amylose tris(3-chloro-5-methylphenylcarbamate); 3 μm, 150×4.6 mm i.d.

All CSPs were purchased from Phenomenex (Torrance, California, USA). Cell5 was also purchased from YMC Separation Technology Co., LTD (Tokyo, Japan) (Chiral ART Cellulose-SC, used in sections IV.4, IV.5 and IV.6).

For the preparation of aqueous and buffer solutions, ultrapure water from Ultra Clear TWF UV system (SG Water, Barsbüttel, Germany) was used. A Crison MicropH 2000 pHmeter from Crison Instruments (Barcelona, Spain) was used to adjust the *pH* of the buffer solutions. Before their use, mobile phases were vacuum-filtered through 0.22 μm Nylon[®] membranes from Micron Separations (Westborough, Massachusetts, USA) and degassed in an Elmasonic S60 ultrasonic bath from Elma Schmidbauer GmbH (Singen, Germany).

For the preparation of sample mixtures used in biodegradability assays, 15 mL conical sterile polypropylene tubes from Deltalab S.L. (Barcelona, Spain) and disposable sterile filter pipette tips from CAPP (Odense, Denmark) were used. A WiseCube[®]Wis-30 shaking incubator with temperature control from Witeg Labortechnik GmbH (Wetheim, Germany) was also used. Before microbial growth monitoring, the incubated samples were shaken in a vortex mixer from Velp Scientifica Srl (Usmate

Velate, Italy). For microbial growth monitoring, the optical density of the cultures at 600 nm (OD_{600}) was measured with an Epoch 2 microplate reader from Biotek Instruments Inc. (Vermont, USA) and 96-well plates with UV-transparent flat bottom from Corning Inc. (Kennebunk, ME, USA). Finally, samples were stored at -80 °C in an U570 Premium ultra-low temperature freezer from New Brunswick Scientific Co., Inc. (Herts, United Kingdom) until chromatographic analysis.

Prior to injection into the chromatographic system, analyte solutions (standards and samples) were filtered through disposable 0.22 μm Nylon[®] syringe filters from Análisis Vínicos S.L. (Tomelloso, Ciudad Real, Spain).

III.2.- Chemicals and solutions

All chemicals were of analytical grade. Ammonium formate; diethylamine (DEA); potassium hexafluorophosphate; and potassium perchlorate were from Acros (Acros Organics, Geel, Belgium). Copper(II) sulfate pentahydrate; sodium molybdate dihydrate; and zinc sulfate heptahydrate were from Merck (Merck Sharp & Dohme, Madrid, Spain). Calcium chloride dihydrate; disodium hydrogen phosphate anhydrous; iron(II) sulfate dihydrate; manganese(II) sulfate monohydrate; potassium dihydrogen phosphate; and sodium sulfate were from Panreac (ITW Reagents, Barcelona, Spain). ACN [®]Multisolvant HPLC grade; ammonium hydroxide; ammonium acetate; ammonium bicarbonate; ammonium sulfate; ethanol (EtOH); ethylenediaminetetraacetic acid disodium salt dihydrate; formic acid 98 %; hydrochloric acid 37 %; magnesium sulfate heptahydrate; MeOH [®]Multisolvant HPLC grade; sodium azide; sodium dihydrogen phosphate monohydrate; sodium hydroxide; sodium perchlorate monohydrate; and sulfuric acid 98 % were from Scharlab S.L. (Barcelona, Spain). ACN and MeOH, HPLC/LC-MS grade, were also purchased from VWR International Eurolab (Avantor, Barcelona, Spain). The compounds studied in this Thesis are summarised in Table III.1.

Table III.1.- Name, family, structure and commercial supplier of the compounds studied in this Thesis.

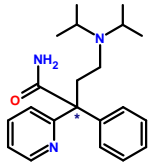
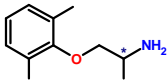
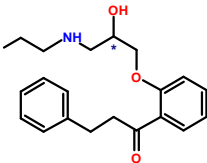
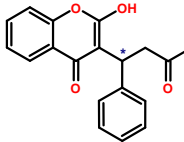
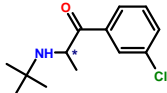
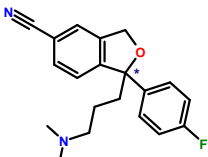
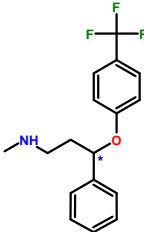
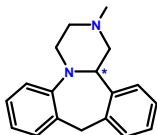
Chemical	Family ^a	Structure ^b	Supplier ^c	Section
Disopyramide	AAD		MP Biomedicals	IV.1 - IV.3
Mexiletine hydrochloride	AAD		Acros	IV.1 - IV.3
Propafenone hydrochloride	AAD		Abcam	IV.1 - IV.3
Warfarin	ACO		Cayman Chemical Co.	IV.1, IV.3
Bupropion hydrochloride	AD		Sigma-Aldrich	IV.1 - IV.3
Citalopram hydrobromide	AD		Tokyo Chemical Industry	IV.1 - IV.3
Fluoxetine hydrochloride	AD		Alter ^d	IV.1 - IV.3, IV.6, IV.7
Mianserin hydrochloride	AD		Alfa Aesar	IV.1 - IV.3

Table III.1.- Continued.

Chemical	Family ^a	Structure ^b	Supplier ^c	Section
Nomifensine maleate	AD		Sigma-Aldrich	IV.1 - IV.3
Trimipramine maleate	AD		Cayman Chemical Co.	IV.1 - IV.3
Viloxazine hydrochloride	AD		Astra Zeneca ^d	IV.1 - IV.3
Benalaxyl	AF		Dr. Ehrenstorfer GmbH	IV.1 - IV.3
Hexaconazole	AF		Dr. Ehrenstorfer GmbH	IV.1 - IV.3
Imazalil	AF		Dr. Ehrenstorfer GmbH	IV.1 - IV.3
Metalaxyl	AF		Dr. Ehrenstorfer GmbH	IV.1 - IV.3
Myclobutanil	AF		Dr. Ehrenstorfer GmbH	IV.1 - IV.3
Penconazole	AF		Dr. Ehrenstorfer GmbH	IV.1 - IV.3

Table III.1.- Continued.

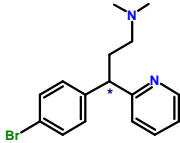
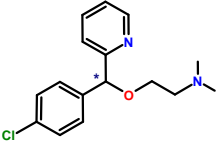
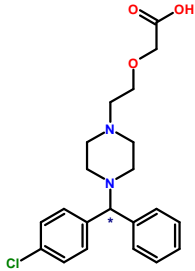
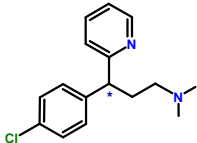
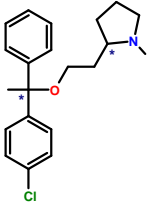
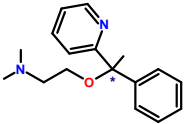
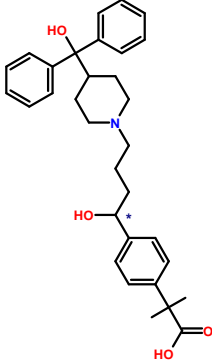
Chemical	Family ^a	Structure ^b	Supplier ^c	Section
Brompheniramine maleate	AH		Sigma-Aldrich	IV.1 - IV.3
Carbinoxamine maleate	AH		Sigma-Aldrich	IV.1 - IV.3
Cetirizine hydrochloride	AH		Cayman Chemical Co.	IV.1 - IV.3
Chlorpheniramine maleate	AH		Sigma-Aldrich	IV.1 - IV.3
Clemastine fumarate	AH		Sigma-Aldrich	IV.1
Doxylamine succinate	AH		Sigma-Aldrich	IV.1 - IV.3
Fexofenadine hydrochloride	AH		Sigma-Aldrich	IV.1, IV.3

Table III.1.- Continued.

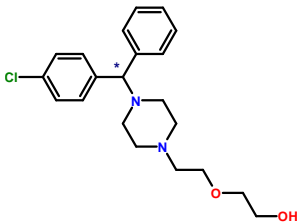
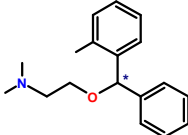
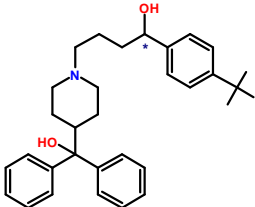
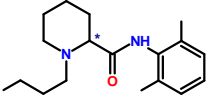
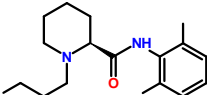
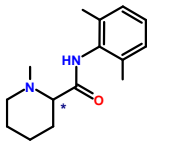
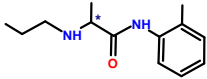
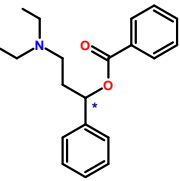
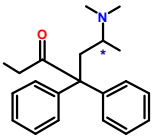
Chemical	Family ^a	Structure ^b	Supplier ^c	Section
Hydroxyzine hydrochloride	AH		Guinama	IV.1 - IV.3
Orphenadrine hydrochloride	AH		Sigma-Aldrich	IV.1 - IV.3
Terfenadine	AH		Sigma-Aldrich	IV.1 - IV.3
Bupivacaine	LA		Cayman Chemical Co.	IV.1 - IV.4, IV.7
(S)-Bupivacaine hydrochloride	LA		Sigma-Aldrich	IV.7
Mepivacaine hydrochloride	LA		Inibsa ^d	IV.1 - IV.3, IV.7
Prilocaine hydrochloride	LA		Inibsa ^d	IV.2, IV.3, IV.7
Propanocaine	LA		Seid Lab ^d	IV.1 - IV.3, IV.7
Methadone hydrochloride	ANAL		Sigma-Aldrich	IV.1 - IV.3

Table III.1.- Continued.

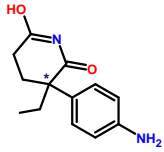
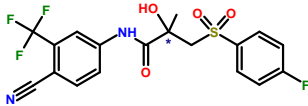
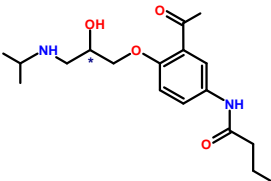
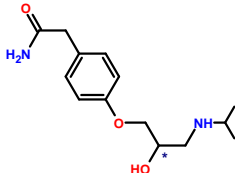
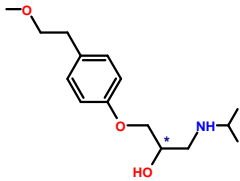
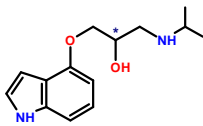
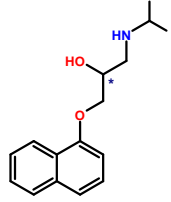
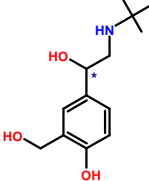
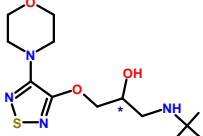
Chemical	Family ^a	Structure ^b	Supplier ^c	Section
Aminoglutethimide	ANP		Alfa Aesar	IV.1 - IV.3
Bicalutamide	ANP		Sigma-Aldrich	IV.1 - IV.3
Acebutolol hydrochloride	BB		Alfa Aesar	IV.1 - IV.3
Atenolol	BB		Acros	IV.2, IV.3
Metoprolol tartrate	BB		Alfa Aesar	IV.1 - IV.4
Pindolol	BB		Sigma-Aldrich	IV.1 - IV.3
Propranolol hydrochloride	BB		Acros	IV.2 - IV.4
Salbutamol sulfate	BB+BD		Alfa Aesar	IV.1 - IV.3
Timolol maleate	BB		Merck Sharp & Dohme ^d	IV.1 - IV.3

Table III.1.- Continued.

Chemical	Family ^a	Structure ^b	Supplier ^c	Section
Bambuterol hydrochloride	BD		Cayman Chemical Co.	IV.1 - IV.3
Clenbuterol hydrochloride	BD		Sigma-Aldrich	IV.1 - IV.3
Isoprenaline hydrochloride	BD		Acros	IV.1 - IV.3
Orciprenaline sulfate	BD		EDQM	IV.1 - IV.3
Terbutaline hemisulfate	BD		Abcam	IV.1 - IV.3
Cilnidipine	CaB		Acros	IV.1 - IV.3
Felodipine	CaB		EDQM	IV.1 - IV.3

Table III.1.- Continued.

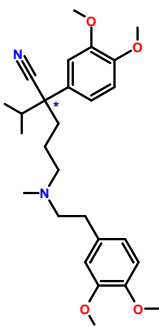
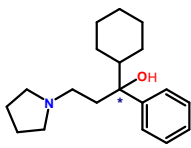
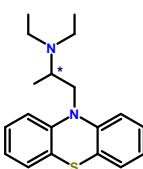
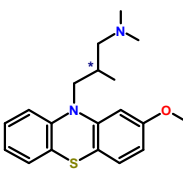
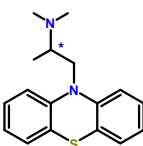
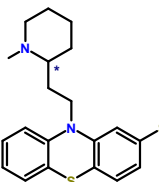
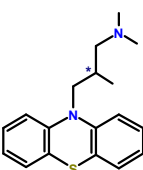
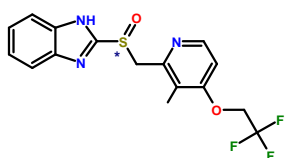
Chemical	Family ^a	Structure ^b	Supplier ^c	Section
Verapamil hydrochloride	CaB		Sigma-Aldrich	IV.1 - IV.3
Procyclidine hydrochloride	ACD		Sigma-Aldrich	IV.1 - IV.3
Ethopropazine hydrochloride	APD		Sigma-Aldrich	IV.1 - IV.3
Methotrimeprazine maleate	APD		Sigma-Aldrich	IV.1
Promethazine hydrochloride	APD		Sigma-Aldrich	IV.2, IV.3
Thioridazine hydrochloride	APD		Sigma-Aldrich	IV.1 - IV.3
Trimeprazine hemi(+)-tartrate	APD		Sigma-Aldrich	IV.1 - IV.5
Lansoprazole	PPI		Sigma-Aldrich	IV.2, IV.3

Table III.1.- Continued.

Chemical	Family ^a	Structure ^b	Supplier ^c	Section
Omeprazole	PPI		Acros	IV.4
Pantoprazole sodium	PPI		Sigma-Aldrich	IV.1 - IV.3
Rabeprazole sodium	PPI		Sigma-Aldrich	IV.1 - IV.3
Flurbiprofen	NSAID		Sigma-Aldrich	IV.4
Ibuprofen	NSAID		Sigma-Aldrich	IV.4, IV.6
(S)-(+)-Ibuprofen	NSAID		Sigma-Aldrich	IV.6
Ketoprofen	NSAID		Sigma-Aldrich	IV.4, IV.6
(S)-(+)-Ketoprofen	NSAID		Sigma-Aldrich	IV.6
Benzoic acid	PA		Panreac	IV.5

^a AAD (antiarrhythmic drug), ACO (anticoagulant), AD (antidepressant), AF (antifungal), AH (antihistamine), LA (local anaesthetic), ANAL (analgesic), ANP (antineoplastic), BB (β -blocker), BD (bronchodilator), CaB (calcium channel blocker), ACD (anticholinergic drug), APD (antipsychotic drug), PPI (proton pump inhibitor), NSAID (non-steroidal anti-inflammatory drug), and PA (preservative agent).

^b Non-salt form.

^c Abcam (Cambridge, United Kingdom); Acros (Acros Organics, Geel, Belgium); Alfa Aesar (Thermo Fisher Scientific Inc., Karlsruhe, Germany); Alter (Madrid, Spain); AstraZeneca (Cheshire, United Kingdom); Cayman Chemical Co. (Ann Arbor, USA); Dr. Ehrenstorfer GmbH (LGC Standards, Augsburg, Germany); EDQM (European Directorate for Quality of Medicines & Health Care, Strasbourg, France); Guinama (Valencia, Spain); Inibsa (Barcelona, Spain); Merck Sharp & Dohme (Merck KGaA , Darmstadt, Germany); MP Biomedicals (Irvine, USA); Panreac (ITW Reagents, Barcelona, Spain); Seid Lab (Barcelona, Spain); Sigma-Aldrich (Merck KGaA , Darmstadt, Germany); and Tokyo Chemical Industry Co., Ltd. (Tokyo, Japan).

^d Kindly donated by the indicated supplier.

Mobile phases were usually binary mixtures of aqueous or buffer solutions and different percentages of ACN or MeOH (10-98 % in volume of ACN or 30-90 % in volume of MeOH). Ternary mixtures of aqueous or buffer solutions, ACN or MeOH and 0.1 % (v/v) formic acid or DEA were occasionally used as mobile phases.

Solutions of 10 mM ammonium acetate ($pH = 8.0$), 5 mM and 20 mM ammonium bicarbonate ($pH = 8.0$), 10 mM ammonium formate ($pH = 3.0$) and 10 mM sodium dihydrogen phosphate monohydrate ($pH = 8.0$), were prepared by dissolving the appropriate amount of solid in ultrapure water. 1 M ammonium hydroxide or 2.5 M sodium hydroxide were used to adjust the pH to 8.0, and 1 M hydrochloric acid or formic acid was used to adjust the pH to 3.0.

Aqueous solutions of 100 mM potassium hexafluorophosphate, 500 mM potassium perchlorate and 500 mM sodium perchlorate were prepared by dissolving the appropriate amount of salts in ultrapure water or in the mobile phase. Aqueous solution of formic acid (0.1 % (v/v), $pH = 3.0$), was prepared by dilution of the appropriate volume of formic acid in ultrapure water.

The minimal salts medium (MSM) solution used in the biodegradability assays had the following composition per litre [211,212]: 2.1 g Na_2HPO_4 ; 1.4 g KH_2PO_4 ; 0.5 g $(\text{NH}_4)_2\text{SO}_4$; 0.2 g $\text{MgSO}_4 \cdot 7\text{H}_2\text{O}$, and 10 mL of a trace elements solution with the following composition per litre: 12.0 g $\text{Na}_2\text{EDTA}_2 \cdot 2\text{H}_2\text{O}$; 10 g Na_2SO_4 ; 2.0 g NaOH ; 1.4 g $\text{FeSO}_4 \cdot 2\text{H}_2\text{O}$; 1.3 g $\text{CaCl}_2 \cdot 2\text{H}_2\text{O}$; 0.7 g $\text{ZnSO}_4 \cdot 7\text{H}_2\text{O}$; 0.3 g $\text{MnSO}_4 \cdot \text{H}_2\text{O}$; 0.1 g $\text{Na}_2\text{MoO}_4 \cdot 2\text{H}_2\text{O}$; 0.1 g $\text{CuSO}_4 \cdot 5\text{H}_2\text{O}$; and 0.5 mL H_2SO_4 (98 %).

Stock standard solutions of 1000 mg L^{-1} of each compound under study were prepared by dissolving 10 mg of the chemical in 10 mL of MeOH. For chiral separation studies, 100 mg L^{-1} working solutions were prepared by dilution of the stock standard solutions in MeOH. All the solutions were stored under refrigeration at $4 \text{ }^\circ\text{C}$ until usage.

For biodegradability assays, 20 mg L^{-1} working solutions of each tested compound – *rac*-bupivacaine (*rac*-BUPI); *rac*-ibuprofen (*rac*-IBU), *rac*-ketoprofen (*rac*-KET), *rac*-mepivacaine (*rac*-MEPI), *rac*-prilocaine (*rac*-PRILO), *rac*-propanocaine (*rac*-PROPA), and *rac*-trimeprazine (*rac*-TRI); as well as *rac*-fluoxetine and benzoic acid– were prepared by dilution of the 1000 mg L^{-1} stock solution in the MSM. In addition, for *rac*-TRI, working solutions of 5 and 10 mg L^{-1} of in MSM were also prepared. For each drug, 100 mg L^{-1} stock solutions were obtained by dilution of the corresponding 1000 mg L^{-1} stock solution in MSM. Calibration standards in the concentration range $2\text{-}30 \text{ mg L}^{-1}$ were prepared by dilution of the corresponding stock solution of 100 mg L^{-1} in the MSM. 10 mg L^{-1} (*S*)-BUPI, (*S*)-IBU and (*S*)-KET solutions in MSM were prepared for the identification of the enantiomer peaks. All the solutions were stored under refrigeration at $4 \text{ }^\circ\text{C}$ until usage.

The activated sludge used in the biodegradability assays was kindly donated by General de Análisis Materiales y Servicios S.L. (GAMASER S.L., Valencia, Spain). It was collected in plastic flasks from the aerated tanks of Quart-Benàger WWTP (Valencia, Spain). This municipal WWTP receives domestic, agricultural, livestock, and industrial wastewater ($30318 \text{ m}^3/\text{day}$) from eight Valencian

towns with a surface area of 164171 ha and approximately 1 million inhabitants. Activated sludge was stored (less than 24 h) at 4-5 °C until usage.

III.3.- Experimental procedures

III.3.1.- Chiral columns conditioning

The CSPs are commercially acquired with *n*-hexane:2-propanol (90:10, v/v) as shipping solvent. For their use with hydro-organic or polar organic mobile phases, according to the manufacturers recommendations, the following procedure was used:

- A MeOH:EtOH (90:10, v/v) mobile phase was pumped for at least 10 column volumes (i.e., approximately 30 min at 1.0 mL min⁻¹ for the CSPs tested).
- Then, a ACN:H₂O (60:40, v/v) mobile phase was pumped for another 10 column volumes.
- Finally, the selected mobile phase was pumped for at least 10 column volumes to ensure stabilisation of the chromatographic system.

A flow rate of 1.0 mL min⁻¹ was used in all CSPs, except for Am2 CSP where a flow rate of 0.5 mL min⁻¹ was used. From a practical point of view, when pressure and detector signal are steady, the column is ready for use.

At the end of the working session, the column was stored in ACN or MeOH using following procedure: first changing the mobile phase to ACN:H₂O (60:40, v/v) to remove buffer, salts and sample; and finally to 100 % organic solvent (ACN or MeOH). A pressure in the chromatographic system of approximately 50 bar with ACN (or 80 bar with MeOH) using a flow rate of 1.0 mL min⁻¹ (or 0.5 mL min⁻¹ for Am2 CSP) at 25 °C is indicative that there is no blockage in the chromatographic system.

III.3.2.- Chromatographic conditions

The experimental conditions used for the chiral HPLC methods developed in this Doctoral Thesis are depicted in Table III.2.

Table III.2.- Experimental conditions of the chiral HPLC methods used in this Doctoral Thesis.

Section IV.1	
CSP	Am1, Am2, Am3
Mobile phase	<ul style="list-style-type: none"> ▪ Warfarin: ACN:HCOOH (0.1 %, v/v), 10:90 - 80:20, v/v ▪ Other compounds: ACN:NH₄HCO₃ (5 mM, pH = 8.0), 10:90 - 80:20, v/v
Flow rate	<ul style="list-style-type: none"> ▪ Am2: 0.5 mL min⁻¹ ▪ Other CSPs: 1.0 mL min⁻¹
Separation temperature	25 °C
Injection volume	2 µL
UV Detection	<ul style="list-style-type: none"> ▪ ADPs: λ = 254 nm ▪ Other compounds: λ = 220 nm
Section IV.2	
CSP	Cell1, Cell2, Cell3, Cell4, Cell5
Mobile phase	<ul style="list-style-type: none"> ▪ ACN:NH₄HCO₃ (5 mM, pH = 8.0), 10:90 - 98:2, v/v ▪ MeOH:NH₄HCO₃ (5 mM, pH = 8.0), 30:70 - 90:10, v/v
Flow rate	1.0 mL min ⁻¹
Separation temperature	25 °C
Injection volume	2 µL
UV Detection	<ul style="list-style-type: none"> ▪ ADPs: λ = 254 nm ▪ Other compounds: λ = 220 nm
Section IV.3	
CSP	Cell1
Mobile phase	ACN:NH ₄ HCO ₃ (5 mM, pH = 8.0), 10:90 - 98:2, v/v
Flow rate	1.0 mL min ⁻¹
Separation temperature	25 °C
Injection volume	2 µL
UV Detection	<ul style="list-style-type: none"> ▪ ADPs: λ = 254 nm ▪ Other compounds: λ = 220 nm
Section IV.4	
Bupivacaine (BUPI)	
CSP	Cell3
Mobile phase	MeOH:NH ₄ HCO ₃ (20 mM, pH = 8.0), 70:30, v/v, + DEA (0.1 %, v/v ^a)
Flow rate	1.0 mL min ⁻¹
Separation temperature	40 °C
Injection volume	2 µL
UV Detection	λ = 220 nm
MS Detection ^b	<i>m/z</i> = 100-500 (TIC ^c); 289.2 (SIM ^d)
Flurbiprofen (FLU)	
CSP; separation temperature; flow rate	<ul style="list-style-type: none"> ▪ Am2; 25 °C; 0.5 mL min⁻¹ ▪ Cell1; 15 °C; 1.0 mL min⁻¹
Mobile phase	ACN:HCOONH ₄ (10 mM, pH = 3.0), 40:60, v/v, + NaClO ₄ (500 mM ^a)
Injection volume	2 µL
UV Detection	λ = 220 nm
Ibuprofen (IBU)	
CSP; mobile phase; flow rate	<ul style="list-style-type: none"> ▪ Am2; ACN:HCOONH₄ (10 mM, pH = 3.0), 40:60, v/v, + NaClO₄ (500 mM ^a); 0.5 mL min⁻¹ ▪ Cell3; MeOH:HCOONH₄ (10 mM, pH = 3.0), 80:20 - 85:15, v/v; 1.0 mL min⁻¹
Separation temperature	25 °C
Injection volume	2 µL
UV Detection	λ = 220 nm

Table III.2.- Continued.

Ketoprofen (KET)	
CSP	Am2
Mobile phase	ACN:HCOOH (0.1 %, v/v), 35:65 - 60:40, v/v
Flow rate	0.5 mL min ⁻¹
Separation temperature	15 °C
Injection volume	2 µL
UV Detection	λ = 220 nm
Metoprolol (MET)	
CSP	Cell1
Mobile phase	ACN:CH ₃ COONH ₄ (10 mM, pH = 8.0), 30:70 - 40:60, v/v
Flow rate	1.0 mL min ⁻¹
Separation temperature	15 °C
Injection volume	2 µL
UV Detection	λ = 220 nm
Omeprazole (OME)	
CSP; mobile phase; flow rate	<ul style="list-style-type: none"> ▪ Cell2; ACN:NH₄HCO₃ (20 mM, pH = 8.0), 50:50, v/v; 0.5 mL min⁻¹ ▪ Cell5; ACN:CH₃COONH₄ (10 mM, pH = 8.0), 35:65, v/v, + DEA (0.1 %, v/v^a); 1.0 mL min⁻¹
Separation temperature	25 °C
Injection volume	2 µL
UV Detection	λ = 220 nm
MS Detection^b	Cell2: <i>m/z</i> = 100-500 (TIC ^c); 346.4 (SIM ^d)
Propranolol (PRO)	
CSP; mobile phase; flow rate	<ul style="list-style-type: none"> ▪ Am2: ACN:CH₃COONH₄ (10 mM, pH = 8.0), 40:60, v/v, + DEA (0.1 %, v/v^a); 0.5 mL min⁻¹ ▪ Cell1; ACN:CH₃COONH₄ (10 mM, pH = 8.0), 40:60, v/v; 1.0 mL min⁻¹ ▪ Cell1; ACN:NaClO₄ (500 mM), 40:60, v/v; 1.0 mL min⁻¹
Separation temperature	25 °C
Injection volume	2 µL
UV Detection	λ = 220 nm
Trimeprazine (TRI)	
CSP; mobile phase; separation temperature	<ul style="list-style-type: none"> ▪ Cell1; ACN:KClO₄ (500 mM), 40:60, v/v; 25 °C ▪ Cell1; ACN:KPF₆ (100 mM), 40:60, v/v; 15 °C ▪ Cell5; ACN:CH₃COONH₄ (10 mM, pH = 8.0), 45:55, v/v, + DEA (0.1 %, v/v^a); 25 °C
Flow rate	1.0 mL min ⁻¹
Injection volume	2 µL
UV Detection	λ = 254 nm
Section IV.5	
Tested conditions for TRI	
CSP	Am2, Cell1, Cell3, Cell5
Mobile phase	<ul style="list-style-type: none"> ▪ ACN:CH₃COONH₄ (10 mM, pH = 8.0), 60:40, v/v, + DEA (0.1 %, v/v^a) ▪ ACN:KPF₆ (100 mM), 40:60, v/v ▪ ACN:NaClO₄ (500 mM), 40:60, v/v
Flow rate	<ul style="list-style-type: none"> ▪ Am2: 0.4 mL min⁻¹ ▪ Other CSPs: 1.0 mL min⁻¹
Separation temperature	25 °C
Injection volume	2 µL
UV Detection	λ = 254 nm

Table III.2.- Continued.

Selected conditions for TRI	
CSP	Cell1
Mobile phase	ACN:NaClO ₄ (500 mM), 40:60, v/v ACN:KPF ₆ (100 mM), 40:60, v/v
Flow rate	1.0 mL min ⁻¹
Separation temperature	25 °C
Injection volume	2 µL
UV Detection	λ = 254 nm
Benzoic acid	
Stationary phase	C ₁₈
Mobile phase	ACN:HCOONH ₄ (10 mM, pH = 3.0), 30:70, v/v
Flow rate	1.0 mL min ⁻¹
Separation temperature	25 °C
Injection volume	2 µL
UV Detection	λ = 220 nm
Section IV.6	
Tested conditions for IBU and KET	
CSP	Am2, Cell1, Cell3, Cell5
Mobile phase	<ul style="list-style-type: none"> ▪ MeOH:HCOOH (0.1 %, v/v), 75:25 - 92:8, v/v ▪ ACN:HCOOH (0.1 %, v/v), 25:75 - 80:20, v/v
Flow rate	<ul style="list-style-type: none"> ▪ Am2: 0.5 mL min⁻¹ Other CSPs: 1.0 mL min⁻¹
Separation temperature	15 - 35 °C
Injection volume	2 µL
UV Detection	<ul style="list-style-type: none"> ▪ IBU: λ = 220 nm ▪ KET: λ = 240 nm
Selected conditions for IBU	
CSP	Cell3
Mobile phase	MeOH:HCOOH (0.1 %, v/v), 80:20, v/v
Flow rate	1.0 mL min ⁻¹
Separation temperature	25 °C
Injection volume	2 µL
UV Detection	λ = 220 nm
Selected conditions for KET	
CSP	Am2
Mobile phase	ACN:HCOOH (0.1 %, v/v), 35:65, v/v
Flow rate	0.5 mL min ⁻¹
Separation temperature	15 °C
Injection volume	2 µL
UV Detection	λ = 240 nm
Fluoxetine	
Stationary phase	C ₁₈
Mobile phase	ACN:NaH ₂ PO ₄ (10 mM, pH = 8.0), 70:30, v/v
Flow rate	1.0 mL min ⁻¹
Separation temperature	25 °C
Injection volume	2 µL
UV Detection	λ = 220 nm

Table III.2.- Continued.

Section IV.7	
Tested conditions for BUPI, mepivacaine (MEPI), prilocaine (PRILO) and propanocaine (PROPA)	
CSP	Am1, Am2, Am3, Cell1, Cell2, Cell3, Cell4, Cell5
Mobile phase	<ul style="list-style-type: none"> ▪ ACN:NH₄HCO₃ (5 mM, pH = 8.0), 10:90 - 100:0, v/v ▪ MeOH:NH₄HCO₃ (5 mM, pH = 8.0), 30:70 - 90:10, v/v
Flow rate	<ul style="list-style-type: none"> ▪ Am2: 0.5 mL min⁻¹ ▪ Cell3, Cell4, Cell5: 0.5 - 1.0 mL min⁻¹ ▪ Other CSPs: 1.0 mL min⁻¹
Separation temperature	<ul style="list-style-type: none"> ▪ Cell3, Cell4, Cell5: 15 - 40 °C ▪ Other CSPs: 25 °C
Injection volume	2 µL
UV Detection	λ = 220 nm
Selected conditions for BUPI	
CSP	Cell3
Mobile phase	MeOH:NH ₄ HCO ₃ (5 mM, pH = 8.0), 70:30, v/v
Flow rate	0.5 mL min ⁻¹
Separation temperature	40 °C
Injection volume	2 µL
MS Detection ^b	<i>m/z</i> = 100-500 (TIC ^c); 289.2 (SIM ^d)
Selected conditions for MEPI	
CSP	Cell5
Mobile phase	ACN:NH ₄ HCO ₃ (5 mM, pH = 8.0), 50:50, v/v
Flow rate	0.75 mL min ⁻¹
Separation temperature	25 °C
Injection volume	2 µL
MS Detection ^b	<i>m/z</i> = 100-500 (TIC ^c); 247.2 (SIM ^d)
Selected conditions for PRILO	
CSP	Cell4
Mobile phase	ACN:NH ₄ HCO ₃ (5 mM, pH = 8.0), 40:60, v/v
Flow rate	1.0 mL min ⁻¹
Separation temperature	25 °C
Injection volume	2 µL
MS Detection ^b	<i>m/z</i> = 100-500 (TIC ^c); 221.2 (SIM ^d)
Selected conditions for PROPA	
CSP	Cell4
Mobile phase	ACN:NH ₄ HCO ₃ (5 mM, pH = 8.0), 40:60, v/v
Flow rate	1.0 mL min ⁻¹
Separation temperature	25 °C
Injection volume	2 µL
MS Detection ^b	<i>m/z</i> = 100-500 (TIC ^c); 312.2 (SIM ^d)
Fluoxetine	
Stationary phase	C ₁₈
Mobile phase	ACN:HCOONH ₄ (10 mM, pH = 8.0), 60:40, v/v
Flow rate	1.0 mL min ⁻¹
Separation temperature	25 °C
Injection volume	2 µL
UV Detection	λ = 220 nm

^a Total concentration in the mobile phase

^b Positive electrospray ionisation (ESI) mode was used under the following experimental conditions: voltage = 3000 V, nebuliser pressure = 35 psig, N₂ flow = 12 L min⁻¹, drying temperature = 350 °C

^c Total current ion chromatogram

^d Selected ion monitoring at *m/z* values of the [M+H]⁺ ion

III.3.3.- Biodegradability tests

Biodegradability tests were performed by duplicate (two independent samples for each incubation time studied) in batch mode at approximately 20 mg L⁻¹ of each racemic compound under study (*rac*-BUPI, *rac*-IBU, *rac*-KET, *rac*-MEPI, *rac*-PRILO, *rac*-PROPA, and *rac*-TRI). For *rac*-TRI, 3 concentration levels (5, 10 and 20 mg L⁻¹) were assayed. To ensure aeration of the cultures, all samples were prepared in sterile tubes of 5-fold the sample volume. For biotic tests, 3000 μL of test compound solution were inoculated with 100 μL of the activated sludge, using tubes of a volume five-fold superior to guarantee the aeration of the cultures. Simultaneously, abiotic degradation tests were also performed using ultrapure water or 0.1 % (w/v) sodium azide (to prevent non-desirable microbial growth) instead of the activated sludge.

The samples were kept in a shaking incubator (150 rpm, 20 °C) under natural light cycles. At predefined incubation times (from 0 to 28 days), two test tubes for each compound and for each concentration level assayed were collected and samples were diluted up to 3100 μL with ultrapure water to compensate solvent evaporation. Next, samples were vortex-shaken and 200 μL of each tube were used to measure the OD_{600} . In addition, in this step, sodium azide was added to stop the microbial growth and then, they were frozen at -80 °C until HPLC analysis. Prior to HPLC analysis, samples were thawed at 4 °C, centrifugated and the supernatant was filtered. In parallel, biotic and abiotic biodegradability assays for fluoxetine or benzoic acid at 20 mg L⁻¹ were also performed to control inoculum activity.

III.4.- Software and calculations

To calculate the retention factor, the expression used was the following:

$$k = \frac{t_R - t_0}{t_0} \quad (\text{Eq. III.1})$$

where t_R is the gross retention time and t_0 is the gross hold-up time estimated from the first perturbation in the chromatogram.

The enantioresolution was calculated as follows:

$$R_S = 1.18 \frac{t_{R2} - t_{R1}}{w_1 + w_2} \quad (\text{Eq. III.2})$$

where subscripts 1 and 2 denote the first and second eluted enantiomer, respectively, and w is the peak width at 50 % peak height.

In section IV.4, R_S was estimated using Eq. III.3:

$$RS = \frac{t_{R2} - t_{R1}}{B_1 + A_2} \quad (\text{Eq. III.3})$$

where B_1 is the right half-width at 10 % peak height for the first eluted enantiomer and A_2 is the left half-width at 10 % peak height for the second eluted enantiomer.

The selectivity factor (α), plate number (N) and asymmetry factors (B/A) values were calculated using the following equations:

$$\alpha = \frac{k_2}{k_1} \quad (\text{Eq. III.4})$$

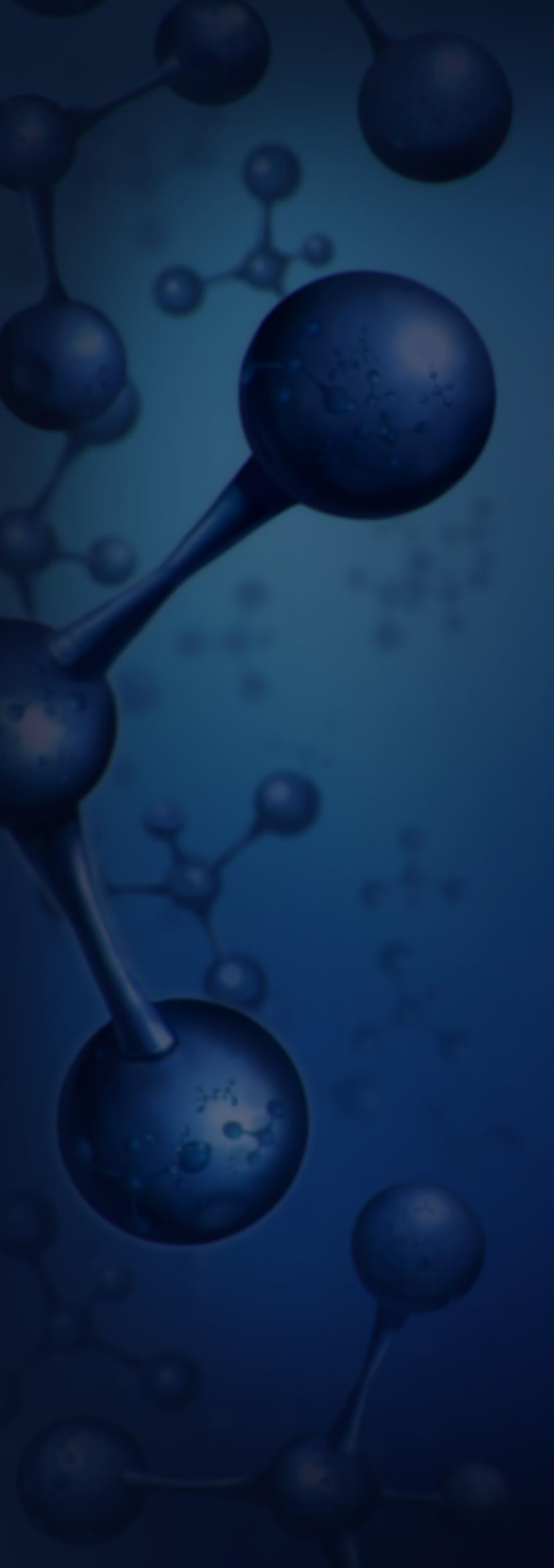
$$N = 5.54 \frac{t_R^2}{w^2} \quad (\text{Eq. III.5})$$

$$\text{Asymmetry factor} = \frac{B}{A} \quad (\text{Eq. III.6})$$

where A and B correspond to left and right half-widths at 10 % peak height (Foley-Dorsey asymmetry), respectively.

For data treatment and calculations, the following software was used:

- **ChemSketch**[®] (©Advanced Chemistry Development, Inc.; 2020.2.0 version): for drawing chemical structures.
- **Grapher** (©Golden Software, LLC; 3.03 version): for data representation.
- **MarvinSketch**[®] (©ChemAxon Ltd.; 21.8.0 version): for calculating chemical properties (e.g., pK_a , $\log P$, PSA , etc.).
- **Matlab**[®] (©The MathWorks, Inc.; R2016b and R2019a version): for kinetic and QSPRs modelling using informatics algorithms developed by Prof. Ph.D. S. Sagrado (Department of Analytical Chemistry, Universitat de València).
- **Microsoft Excel**[®] (©Microsoft 365 MSO; 2207 version): for data collecting, processing, and representation.
- **QB64**: for the description of the profiles of chromatographic peaks using informatics algorithms developed by Prof. Ph.D. J.J. Baeza-Baeza (Department of Analytical Chemistry, Universitat de València).
- **Statgraphics**[®] **Plus** for Windows (©Statistical Graphics Corp., 5.1 version): for obtaining the regression statistics of the calibration curves.
- **Unscrambler**[™] (©Aspen Technology, Inc., v.9.2 version): for multivariate analysis.



IV.- SUMMARY OF THEMATIC, RESULTS AND CONCLUSIONS

IV.1.- Comparative modelling study on enantioresolution of structurally unrelated compounds with amylose-based chiral stationary phases in reversed phase liquid chromatography-mass spectrometry conditions. Paper I

IV.1.1.- Brief introduction and objectives

As previously indicated in section I.2, the most commonly employed analytical technique for the separation of enantiomers of chiral compounds is HPLC using CSPs. Of the many CSPs used in HPLC, amylose and cellulose polysaccharide derivatives are unequivocally the most widely used (see section I.2.1.2). The nature and position of substituent(s) on the phenyl moiety of polysaccharides as well as the polysaccharide backbone are key factors in chiral recognition. Enantiomers are separated by the formation of transient complexes with the polysaccharide-based CSPs. Hydrophobic, electrostatic, hydrogen bonding, van der Waals forces and steric factors are involved in complex formation. Furthermore, these CSPs can be used with non-polar, polar organic and hydro-organic mobile phases.

Despite the widespread use of these CSPs in HPLC, the underlying mechanisms of chiral separations remain unclear due to the complexity of these chromatographic systems. Currently, finding the optimal CSP/mobile phase combination for separating the enantiomers of a specific chiral compound requires expensive and time-consuming trial-and-error methods. So, being able to predict the potential for chiral separation in a given chromatographic system would greatly improve this challenging task.

The studies carried out in this work are aimed at achieving two main objectives. On one hand, this paper is aimed at performing a comparative study on the retention behaviour and enantioresolution of 53 structurally unrelated compounds (drugs and pesticides) using three amylose-based CSPs (Am1, Am2 and Am3; see section III.1). Hydro-organic mobile phases compatible with MS detection consisting of mixtures of ACN and NH_4HCO_3 (5 mM, $\text{pH} = 8.0$), in varying proportion (10-80 % in volume of ACN), were used for the chromatographic separations. See Table III.2 for additional information. The maximum value for the retention factors was set at 15 to give practical conditions for routine analysis. On the other hand, this paper is also aimed at comparing and describing the enantioresolution capabilities of these CSPs. To this end, QSPR models to predict/anticipate a categorical enantioresolution (CR_s) from 57 structural and physicochemical properties of the compounds for each CSP are intended. DPLS1 (DPLS for one response variable) is used for FS and modelling purposes. To the best of our knowledge, this is the first attempt to model enantioresolution-related parameters for a large dataset of structurally unrelated compounds under realistic chromatographic conditions from a practical point of view (see Table I.9 in section I.3).

IV.1.2.- Results and discussion

IV.1.2.1.- Retention behaviour and enantioresolution studies

The compounds studied are 47 drugs from 13 different therapeutic families and six pesticides (see Table III.1). These compounds present a varying degree of hydrophobicity ($-1.6 \leq \log D \leq 5.2$) and most of them exhibit net positive charge at operational pH .

For all the compounds studied and CSPs, in the experimental conditions assayed (see Table III.2), a usual RPLC behaviour was found (i.e., retention decreased as the ACN content in the mobile phase increased from 10 to 80 %). On the other hand, when comparing retention data obtained in each CSP using the same mobile phase, Am3 presented the highest k values for most compounds (see Figure IV.1). This behaviour could be attributed to the distinct electronic properties of the CSPs, as well as the use of immobilised or coated amylose derivatives in the CSP.

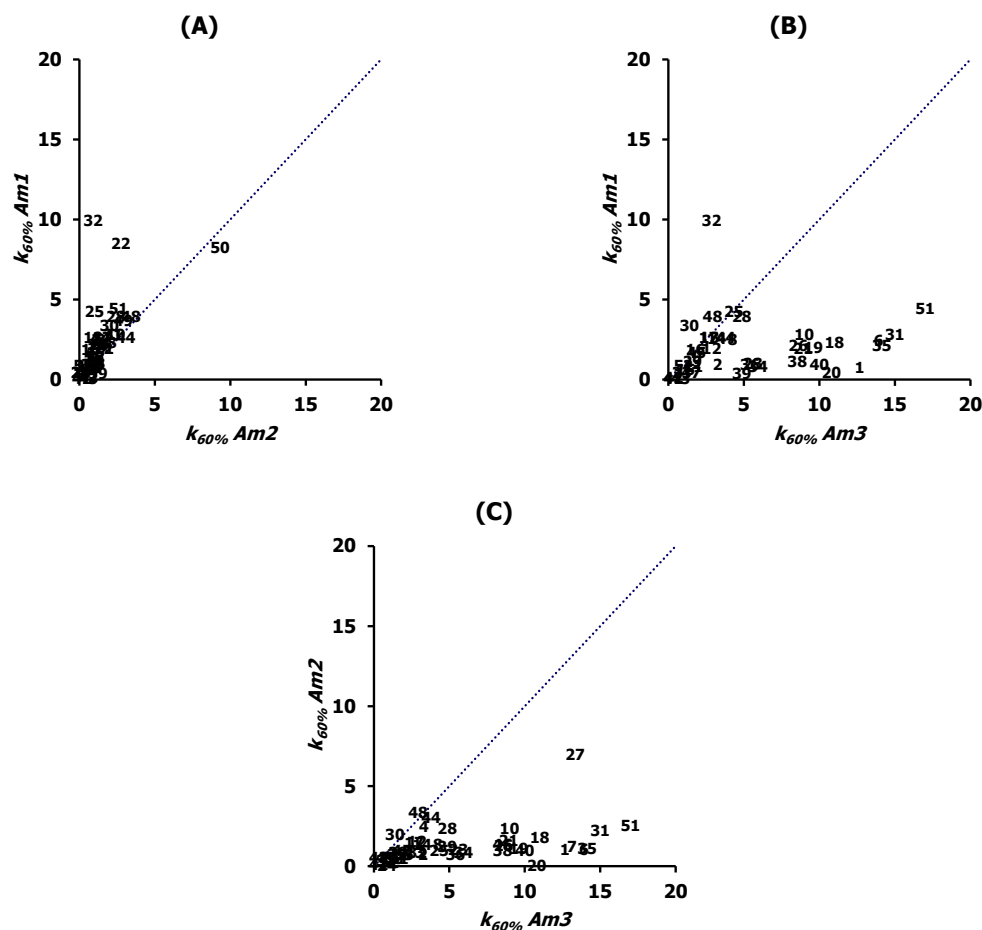


Figure IV.1.- Comparison of the retention factor (k) values for the first eluted enantiomer of compounds obtained in the different CSPs studied using ACN: NH_4HCO_3 (5 mM, $pH = 8.0$), 60:40 (v/v), as mobile phase. **(A)** Am1 vs. Am2, **(B)** Am1 vs. Am3, **(C)** Am2 vs. Am3. (.....) Identity line (i.e., slope = 1; intercept = 0). See compound number in section VII (Paper I, Table 1).

Regarding enantioresolution, the enantiomers of 16 of the 53 (30 %) tested compounds were baseline enantioresolved and 19 (36 %) were partially enantioresolved in at least one of the chromatographic systems assayed. Taking into account R_s data from all mobile phases assayed, Am1 and Am3 CSPs presented some extent of enantioresolution ($R_s > 0$) for a similar number of compounds (baseline enantioresolution: 11 compounds in both CSPs; partial enantioresolution: 16 and 14 compounds for Am1 and Am3, respectively). Am2 CSP provided the worst results (the lowest R_s values for most compounds and the lowest number of compounds exhibiting some extent of enantioresolution: 4 and 9 compounds with baseline and partial enantioresolution, respectively).

Figure IV.2 shows a comparison of the maximum enantioresolution values ($R_s \text{ max}$) obtained in each CSP. As can be observed, the highest $R_s \text{ max}$ values were found for mianserin ($No = 8$) in Am1 ($R_s \text{ max} = 8.3$), propafenone ($No = 3$) in Am2 ($R_s \text{ max} = 4.0$), and nomifensine ($No = 9$) in Am3 ($R_s \text{ max} = 8.4$). Bicalutamide ($No = 33$; $R_s \text{ max} = 3.7$ in Am1, $R_s \text{ max} = 3.3$ in Am2, and $R_s \text{ max} = 2.4$ in Am3) and rabeprazole ($No = 53$; $R_s \text{ max} = 2.6$ in Am1, $R_s \text{ max} = 2.0$ in Am2, and $R_s \text{ max} = 5.1$ in Am3) were baseline enantioresolved in all assayed amylose-based CSPs. Warfarin ($No = 4$; $R_s \text{ max} = 5.5$ in Am1, and $R_s \text{ max} = 5.3$ in Am3), bupropion ($No = 5$; $R_s \text{ max} = 6.7$ in Am1, and $R_s \text{ max} = 2.4$ in Am3), mianserin ($No = 8$; $R_s \text{ max} = 8.3$ in Am1, and $R_s \text{ max} = 3.0$ in Am3), nomifensine ($No = 9$; $R_s \text{ max} = 3.0$ in Am1, and $R_s \text{ max} = 8.4$ in Am3), and benalaxyl ($No = 12$; $R_s \text{ max} = 4.1$ in Am1, and $R_s \text{ max} = 6.6$ in Am3) were baseline enantioresolved in both Am1 and Am3 CSPs. For the other compounds studied, all CSPs exhibited differences in their enantioselectivities, which suggests differences in their enantio recognition mechanisms (i.e., differences in the enantiomer-CSP interactions).

It is worth mentioning that under the experimental conditions tested, Am2 (see Figure IV.2.A and IV.2.C) was the only CSP that allowed baseline enantioresolution of the enantiomers of brompheniramine ($No = 18$; $R_s \text{ max} = 1.2$ in Am1, $R_s \text{ max} = 1.6$ in Am2, and $R_s \text{ max} = 1.4$ in Am3), chlorpheniramine ($No = 21$; $R_s \text{ max} = 0.9$ in Am1, $R_s \text{ max} = 2.0$ in Am2, and $R_s \text{ max} = 1.3$ in Am3), and cilnidipine ($No = 44$; $R_s \text{ max} = 0$ in Am1, $R_s \text{ max} = 1.5$ in Am2, and $R_s \text{ max} = 0$ in Am3). The enantiomers of all the other compounds studied that were baseline enantioresolved in Am2 CSP also did in Am1 or Am3 CSPs. In fact, Phenomenex is currently no longer supplying Am2 CSP.

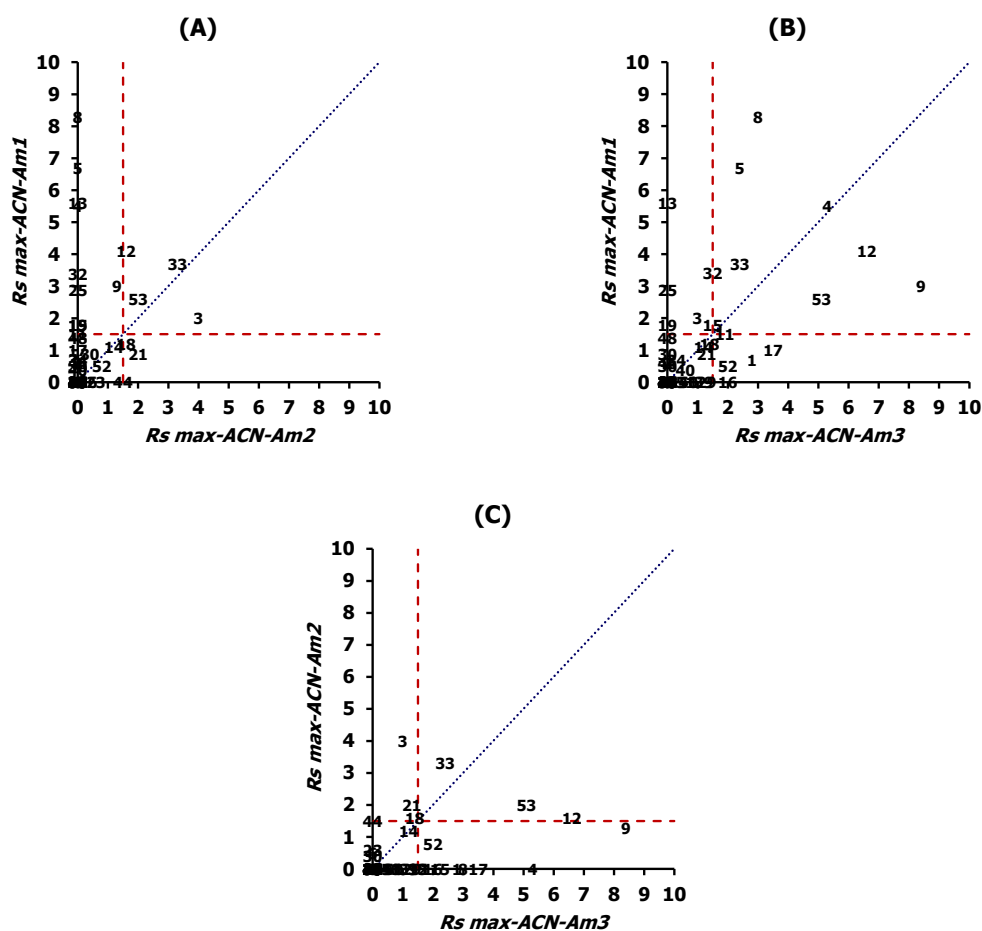


Figure IV.2.- Comparison of the maximum enantioresolution values (R_s max) obtained in the different CSPs studied using ACN:NH₄HCO₃ (5 mM, pH = 8.0) mobile phases. **(A)** Am1 vs. Am2, **(B)** Am1 vs. Am3, **(C)** Am2 vs. Am3. (·····) Identity line (i.e., slope = 1; intercept = 0). (- - - -) R_s max = 1.5.

Concerning the effect of the ACN percentage in the mobile phase on the enantioresolution, as the ACN content decreased (i.e., when the retention increased), there was generally an improvement in the R_s values. Nevertheless, for certain compounds (e.g., brompheniramine) higher R_s values were obtained in all the assayed CSPs when higher ACN percentages in the mobile phase were used. These opposite behaviours could be attributed to the prevalence of kinetic or thermodynamic processes on enantioresolution. For certain compounds, the increase in retention leads to higher selectivity factors, indicating that thermodynamics prevails over kinetics. However, for other compounds, the kinetic contribution is more important than the thermodynamic one, resulting in a decrease in efficiency as the retention increases.

IV.1.2.2.- Structure-categorical enantioresolution relationships in amylose-based CSPs

QSPR models to evaluate/anticipate the enantioresolution ability of Am1 and Am3 CSPs in aqueous ACN mobile phases for a given chiral compound from its structural parameters were intended. QSPR models for Am2 were not intended due to the low number of compounds showing baseline enantioresolution in this CSP. It must be pointed out that selectivity and retention factor related parameters are the most investigated response variables in QSPRs (see Table I.9 in the introduction section). Enantioresolution related parameters are more complex since they are affected by thermodynamic and kinetic factors, but in our opinion, they are more useful/realistic parameters for evaluating the separation between chromatographic peaks for practical purposes.

DPLS1 was used for modelling purposes. To build the QSPR models, the experimental R_s values were categorised as follows: (i) $CRs = 1$ (class-1) for compounds showing clear baseline enantioresolution ($R_s \max \geq 2.0$); (ii) $CRs = 0$ (class-0) for the rest of compounds. CRs values were used as response variable (\mathbf{y}) in the QSPR models. As \mathbf{X} matrix, 57 structural and physicochemical parameters of the studied compounds (see Paper I and Table S2 in section VII) were tested as predictor variables. These variables include chiral carbon (C^*) related parameters (C^* -parameters), and molecular descriptors and topological parameters predicted by software calculation. Autoscaled $\mathbf{y-X}$ data were used for DPLS1 modelling. Leave-one-out cross-validation was used.

To reduce the number of \mathbf{X} variables and simplify the interpretation of the QSPR model (see section I.3), a new FS strategy based on DPLS1 outputs (FS-DPLS1) was proposed. In the FS-DPLS1 process, the least informative variables (i.e., those with the worst descriptive and predictive ability) are eliminated sequentially (one-by-one) using a new target indicator (TI). The variable whose elimination results in the highest TI value is eliminated in the subsequent run. Eq. IV.1 shows the TI function introduced for the FS-DPLS1 process:

$$TI = W1 \ dD + (1 - W1) \ dDcv - W2 \ mUrb - W3 \ SSclass \quad (\text{Eq. IV.1})$$

where $W1$, $W2$ and $W3$ are parameters in the 0-1 range that have to be optimised; dD is the lowest discriminant distance between class-1 and class-0 γ estimates; $dDcv$ is the dD value for the γ estimates in the cross-validation step of the QSPR DPLS1 model; $mUrb$ is the mean value of the relative uncertainties of the DPLS1 model regression coefficients; and $SSclass$ is the sum of squares of the differences between the predicted discrimination level (DL) and actual γ values (CRs). DL are γ estimates that were categorised as follows: (i) $DL = 1$ (class-1) for compounds with γ estimates equal or higher than the highest γ estimate for class-0 compounds; (ii) $DL = 0$ (class-0) for compounds with γ estimates equal or lower than the lowest γ estimate for class-1 compound; (iii) $DL = 0.5$ for the rest of compounds.

Positive dD or $dDcv$ values indicate that the model correctly discriminates between all compounds in class-1 and class-0. Thus, $dD > 0$ and $dDcv > 0$ are an indication of acceptable descriptive and predictive ability of the model, respectively. Low $mUrb$ values mean high reliability of the model regression coefficients, and therefore, high reliability of the variables included the model; and low $SSclass$ values indicate high classification ability, the descriptive ability of the model is enhanced by both of these aspects.

Figure IV.3 shows the progress of FS-DPLS1 for the Am1 QSPR DPLS1 model just for illustrative purposes. As can be observed, the highest dD and $dDcv$ values were obtained after eliminating 35 variables (vertical dashed line). The resulting final QSPR DPLS1 model with 22 variables exhibited $dD > 0$, indicating acceptable descriptive ability, although their predictive ability was limited ($dDcv < 0$).

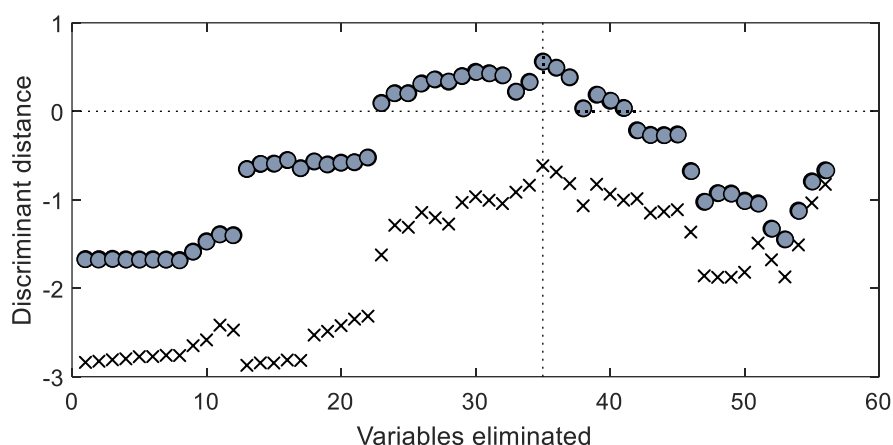


Figure IV.3.- Feature selection (FS-DPLS1) progress for Am1 model. (●) Discriminant distance (dD) and (×) discriminant distance in cross-validation ($dDcv$). The vertical dotted line shows the variables eliminated in the final model. The horizontal dotted line indicates discriminant distance equal to 0.

For both CSPs, the final models obtained using just the selected variables (22 for Am1 and 16 for Am3) after FS-DPLS1 showed better descriptive ($dD > 0$, and lower $mUrb$ values) and predictive ability (lower $dDcv$ values) than the initial ones obtained using all the 57 variables tested in matrix **X**. Although all the models (using all the variables or just the selected ones for both CSPs) showed limited predictive ability ($dDcv < 0$) (see Table IV.1).

Table IV.1.- Comparison of the descriptive and predictive ability of the DPLS1 models obtained for Am1 and Am3 CSPs.

CSP	DPLS1 model	Variables selected	$mUrb$	dD	$dDcv$	Descriptive ability	Predictive ability
Am1	Initial	57	10.9	-1.67	-2.85	Poor	Limited
	Final	22	1.2	0.56	-0.62	Acceptable	Limited
Am3	Initial	57	4.2	-0.88	-1.31	Poor	Limited
	Final	16	1.2	0.22	-0.67	Acceptable	Limited

W parameters of Eq. IV.1: $W1 = 0.53$, $W2 = 0.49$, $W3 = 0.48$ for Am1; $W1 = 1.00$, $W2 = 0.09$, $W3 = 0.62$ for Am3.

The regression coefficients derived from the final DPLS1 QSPR (see Figure IV.4) models can be used to explain the major operating forces in the modelled chromatographic systems. The absolute values of these coefficients reflect the relative importance of the corresponding variables in discriminating between class-1 and class-0 compounds, while their sign shows their positive or negative contribution to CRs . Consequently, for a given compound in a specific chromatographic system, the balance of these contributions determines its enantioresolution in that particular system.

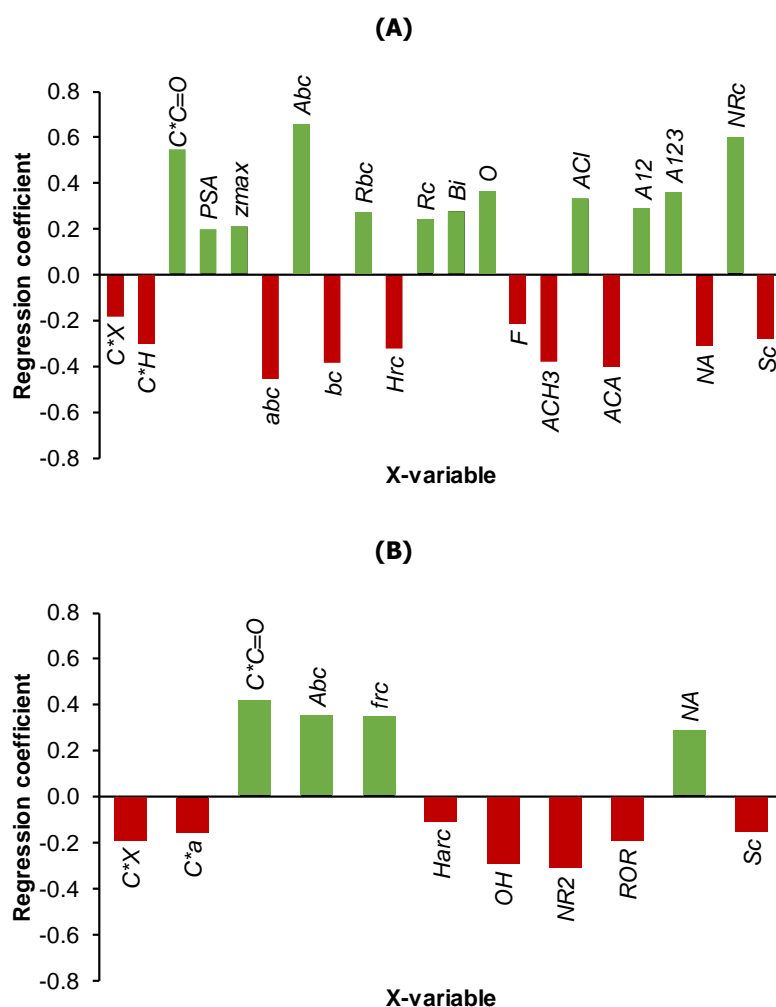


Figure IV.4.- Regression coefficients (scaled) values obtained for the selected variables in the final DPLS1 QSPR models (after FS-DPLS1). **(A)** Am1, **(B)** Am3. (■) Positive and (■) negative contribution to enantioresolution.

Variables (see further details in section VII: Paper I and Table S2):

Chiral carbon (C*) related parameters (C*-parameters): number of aliphatic groups (C*a), carbonyl groups (C*C=O), heteroatoms (C*X), and hydrogen atoms (C*H), directly bonded to C*.

Other molecular topological parameters: Balaban index (Bi), number of non-aromatic bonds (abc), aromatic groups with 1,2 substitution (A12), aromatic groups with 1,2,3 substitution (A123), aromatic bonds (Abc), Ar-C-Ar moieties (ACA), -CH₃ groups bonded to an aromatic ring (ACH3), Cl atoms bonded to an aromatic ring (ACI), bonds (bc), F atoms (F), fused rings (frc), aliphatic heterocycles (Harc), heterocyclic rings (Hrc), nitrogen aromatic groups (NA), -NR₂ groups (NR2), tertiary amines in aliphatic cycles (NRC), O atoms (O), -OH groups (OH), ring bonds (Rbc), rings (Rc), R-O-R (ROR), and S atoms in aliphatic cycles (Sc).

Other parameters: polar surface area (PSA), and maximal z length (zmax).

As can be observed in Figure IV.4, the DPLS1 QSPR models for Am1 and Am3 CSPs share some common features. In fact, in the DPLS1 QSPR models for both Am1 (Figure IV.4.A) and Am3 (Figure IV.4.B) CSPs, $C^*C=O$ is the most important variable favouring enantioresolution among the C^* -parameters studied; therefore, carbonyl groups in amides, ketones, and esters linked to the C^* play a crucial role in enantioresolution. Examples of this are bupropion ($No = 5$), benalaxyl ($No = 12$), aminoglutethimide ($No = 32$) and bicalutamide ($No = 33$) (see Table III.1 and Figure IV.2.B). The atoms of O, C, and N in amides are part of a conjugated system that involves molecular orbitals with delocalised electrons. As a result, these compounds can participate in π - π interactions with the CSPs. Additionally, amides, esters, and ketones are capable of acting as hydrogen bond acceptors, allowing them to take part in hydrogen bonding interactions with the CSPs.

Furthermore, Abc is also one of the most important variables in both DPLS1 QSPR models, which indicates that aromatic bonds in the molecule (e.g., warfarin, $No = 4$, in Figure IV.2.B) allowing enantiomer-CSP π - π interactions, also enhance enantioresolution in Am1 and Am3 CSPs. However, the absence of aliphatic bonds (e.g., abc and bc) in the molecule or aliphatic substituents in C^* (C^*a) promotes enantioresolution in Am1 and Am3, respectively. In both CSPs, the absence of heteroatom substituents in C^* (C^*X) also enhances enantioresolution.

On the other hand, NA is also one of the most important variables in both DPLS1 QSPR models. However, it has an opposite contribution to the enantioresolution in each CSP (i.e., unfavourable and favourable contribution in Am1 and Am3, respectively). Examples of compounds for which Am1 and Am3 display these opposite contributions to their enantioresolution are disopyramide ($No = 1$), myclobutanil ($No = 16$), and penconazole ($No = 17$), which have pyridine-like N atoms (basic aromatic rings); as well as pantoprazole ($No = 52$) and rabeprazole ($No = 53$), which are compounds with pyridine-like and pyrrole-like N atoms (non-basic aromatic rings) in their structure. The lone pair of electrons of the pyrrole-like N atom is part of the aromatic system, promoting π - π interactions between the CSP and the enantiomer molecules. Pyridine-like N atoms act as hydrogen bonding acceptors since their lone pair of electrons is not involved in the aromatic system. Moreover, the inverse selectivity of the Am3 CSP relative to Am1 may arise from the formation of Lewis adducts between pyridine-like N atoms, which act as Lewis bases, and either the Cl atom at 3-position of the phenylcarbamate moiety in the Am3 CSP, acting as Lewis acid, or the acidic H atom of the carbamate moiety of Am3, whose hydrogen-bond donor ability is enhanced by the 3-chloro substitution.

Other of the major contributions to enantioresolution in Am1 CSP is the absence of hydrogen substituents (C^*H) in C^* that also enhances enantioresolution. The nature and position of substituents in the aromatic ring can either diminish (e.g., $ACH3$ and ACA) or enhance (e.g., ACI , $A12$, and $A123$) enantioresolution. Lastly, the presence in an aliphatic cyclic moiety of a tertiary amino group (NRc) also promotes enantioresolution in the Am1 CSP. In the case of Am3 CSP, the

presence of fused rings (*frc*) in the molecule is also another major contribution improving enantioresolution.

IV.1.3.- Conclusions

Under the experimental conditions tested, which involved three commercially available amylose-based CSPs (Am1, Am2, and Am3) and ACN:NH₄HCO₃ (5 mM, pH = 8), 10:90 - 80:20 (v/v), mobile phases, typical RPLC retention behaviour was observed for all 53 structurally unrelated chiral compounds studied.

Am1 and Am3 CSPs provided baseline enantioresolution for a similar number of compounds but exhibited different enantioselectivities. Am2 provided the worst results, and its selectivity scarcely complemented the other CSPs. In fact, Phenomenex is currently no longer supplying Am2 CSP.

A reduced set of structural variables (from 57 initial predictor variables), with positive and negative contributions to categorical enantioresolution in Am1 and Am3 CSPs, was selected by FS-DPLS1 QSPR modelling. The presence of carbonyl groups directly bonded to the C* and aromatic bonds in the compounds were identified as key structural features favouring their enantioresolution in Am1 and Am3 CSPs, indicating that enantiomer-CSP π - π and hydrogen-bond interactions may play a crucial role.

The enantioresolution in Am1 CSP was also found to be influenced by both the position and chemical nature of substituents in the aromatic ring, which can either favour or disfavour it. Furthermore, the presence of a hydrogen-bond accepting ternary amine in an aliphatic cyclic group can enhance enantioresolution. For Am3 CSP, the presence of fused rings was also found to improve enantioresolution, probably due to the rigidity they confer to the molecule.

Finally, the presence of nitrogen in aromatic rings was also found to be important for enantioresolution, with a favourable contribution for Am3 and unfavourable contribution for Am1 CSP. This opposite selectivity of Am3 compared to Am1 could be explained by the combination of enantiomer-CSP π - π and hydrogen bonding interactions, along with the formation of Lewis adducts between the pyridine-like N atoms (Lewis bases) and either the Cl atom (Lewis acid) in Am3, or the H atom of the carbamate moiety of Am3 (whose hydrogen-bond donor character is exalted by the 3-chloro substitution in the phenylcarbamate moiety).

IV.2.- Comparative study on retention behaviour and enantioresolution of basic and neutral structurally unrelated compounds with cellulose-based chiral stationary phases in reversed phase liquid chromatography-mass spectrometry conditions. Paper II

IV.2.1.- Brief introduction and objectives

As previously mentioned in section I.2.1.2, in the polysaccharide-based CSPs the nature and composition of the mobile phase strongly modulates the chiral recognition mechanism.

It has been observed that in these CSPs, when using hydro-organic mobile phases containing aprotic organic solvents (e.g., ACN), compounds may exhibit dual retention behaviour (RPLC and HILIC) depending upon the water concentration. In such mobile phases, enantiomers can undergo hydrophobic interactions with the phenyl moieties of the CSP, as well as hydrophilic (hydrogen bond) interactions with the carbamate or ester moieties of the CSP. The addition of water to these mobile phases enhances hydrophobic interactions, resulting in an increase in the analyte retention (RPLC behaviour), but it also decreases hydrophilic interactions, leading to a decrease in the analyte retention (HILIC behaviour). The net effect observed is the balance of both contributions, with the first contribution dominating in mobile phases with high water content and the second contribution being more important in mobile phases with low water content. This behaviour has been observed for chlorinated polysaccharide-based CSPs due to their strong hydrogen bonding ability.

In contrast, in these CSPs when using hydro-organic mobile phases containing protic organic solvents (e.g., MeOH) only RPLC retention behaviour has been observed, since only analyte-CSP hydrophobic interactions can occur.

In this section, to deepen the understanding of polysaccharide-based CSPs, a comparative study on the retention behaviour and enantioresolution of 54 structurally unrelated compounds (nearly the same compounds studied in section IV.1 and Paper I) using five cellulose-based CSPs (Cell1, Cell2, Cell3, Cell4 and Cell5; see section III.1) was performed. Hydro-organic mobile phases compatible with MS detection consisting of mixtures of NH_4HCO_3 (5 mM, $pH = 8.0$) and ACN or MeOH, in varying proportion (10-98 % in volume of ACN and 30-90 % in volume of MeOH) were used for the chromatographic separations. See Table III.2 for additional information. The existence of RPLC and HILIC retention behaviour domains was also explored.

IV.2.2.- Results and discussion

IV.2.2.1.- Retention behaviour study

For all the compounds studied and CSPs in hydro-organic mobile phases containing MeOH (see Table III.2), a usual RPLC behaviour was found. However, in hydro-organic mobile phases containing ACN (see Table III.2), a U-shaped retention behaviour was observed indicating the coexistence of two retention domains as a function of the water content in the mobile phase: (i) the RPLC-domain for mobile phases with a water content higher than 20 % (< 80% ACN) and (ii) the HILIC-domain for mobile phases with a water content lower than 20 % (~ 80-98 % ACN). The magnitude of the differences in retention upon varying the water content in the mobile phase depended significantly on the nature of the compound and the CSP used. In all CSPs, these differences were higher for the most hydrophobic and hydrophilic compounds in the RPLC- and HILIC-domains, respectively. As an example, Figure IV.5 shows the k values corresponding to the least retained enantiomer obtained in the different chromatographic conditions assayed for atenolol ($N_o = 33$; the most hydrophilic compound studied: $\log D = -1.41$; Figure IV.5.A) and BUPI ($N_o = 25$; one of the most hydrophobic compounds studied: $\log D = 3.99$; Figure IV.5.B).

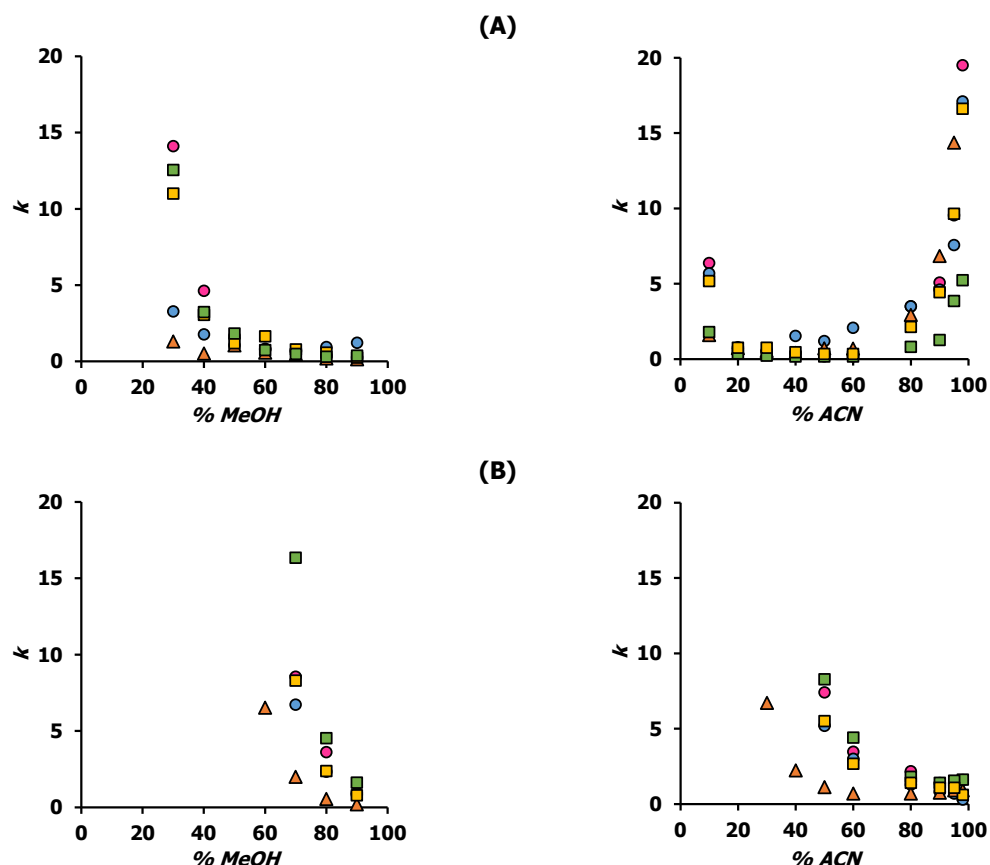


Figure IV.5.- Values of the retention factor (k) in the different chromatographic systems studied obtained for: **(A)** atenolol and **(B)** BUPI. CSPs: (●) Cell1, (●) Cell2, (▲) Cell3, (■) Cell4 and (■) Cell5. Mobile phases: MeOH: NH_4HCO_3 (5 mM, pH 8.0) 30:70-90:10 (v/v) (left part) and ACN: NH_4HCO_3 (5 mM, pH 8.0) 10:90-98:2 (v/v) (right part).

On the other hand, when comparing the k values for the first eluted enantiomer of compounds obtained in each CSP using mobile phases containing 50 % ACN ($k_{50\%}$), it was found that most CSPs (except Cell2 and Cell4) exhibited clear differences in their selectivities and retention extent (Figure IV.6). The similarity between the $k_{50\%}$ values obtained in Cell2 and Cell4 (Figure IV.6.A) is due to their close structure (i.e., the sole difference between them is the interchange of methyl and chlorine substituents at the 3,4 position of the phenyl moiety). However, the nature of substituents (methyl and chlorine in Cell1 and Cell5, respectively) at the 3,5 position of phenyl moiety did had effect on retention (Figure IV.6.E). However, it should be noted that in such cases, the impact of utilising coated (Cell1) or immobilised (Cell5) CSPs must also be considered. On the other hand, the $k_{50\%}$ values for most compounds were lower in benzoate-type CSPs (Cell3) than in phenylcarbamate-type (e.g., Cell4) CSPs (Figure IV.6.C).

Finally, when comparing the k values for the first eluted enantiomer of compounds obtained in a given CSP using mobile phases containing the same MeOH or ACN percentage in the RPLC-domain, it was observed that similarly to achiral RPLC, ACN has higher eluent strength than MeOH.

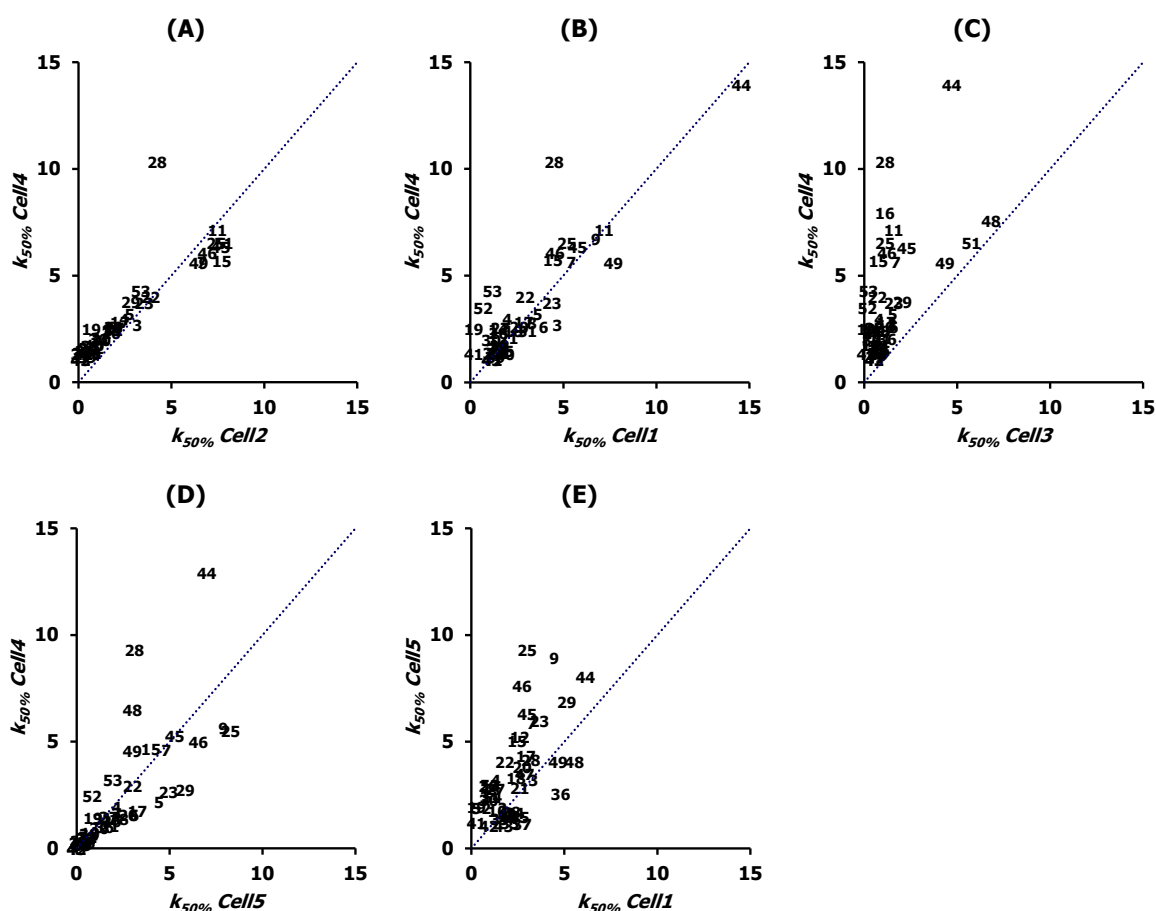


Figure IV.6.- Comparison of the retention factor (k) values for the first eluted enantiomer of compounds obtained in the different CSPs studied using ACN: NH_4HCO_3 (5 mM, $\text{pH} = 8.0$), 50:50 (v/v), as mobile phase. (A) Cell4 vs. Cell2, (B) Cell4 vs. Cell1, (C) Cell4 vs. Cell3, (D) Cell4 vs. Cell5, (E) Cell5 vs. Cell1. (.....) Identity line (i.e., slope = 1; intercept = 0). See compound number in section VII (Paper II, Table 1).

IV.2.2.2.- Enantioresolution study

Baseline enantioresolution was achieved for the enantiomers of 38 out of 54 (70 %) compounds studied, while partial enantioresolution was obtained for 13 compounds (24 %) in at least one of the chromatographic systems assayed. For three compounds (brompheniramine, $No = 17$; acebutolol, $No = 32$; and salbutamol, $No = 37$) null enantioresolution ($Rs = 0$) was obtained in all the tested chromatographic systems. The highest enantioresolution value ($Rs_{max} = 9.4$) was obtained for aminoglutethimide ($No = 30$) in the 90 % MeOH-Cell3 chromatographic system.

Regarding the effect on enantioresolution of the nature of the organic solvent used to prepare the mobile phase, chromatographic systems comprising MeOH/NH₄HCO₃ mobile phases provided distinct enantioresolution degrees and enantioselectivities to those observed with ACN/NH₄HCO₃ mobile phases (see Figure IV.7). For most compounds, the use of ACN/NH₄HCO₃ instead of MeOH/NH₄HCO₃ mobile phases provided higher Rs_{max} values for all CSPs, and allowed baseline enantioresolution for a higher number of compounds ($Rs_{max} \geq 1.5$ for 34 and 24 compounds in ACN/NH₄HCO₃ and MeOH/NH₄HCO₃, respectively). This lower enantioresolution ability of MeOH/NH₄HCO₃ mobile phases could be due to their capacity to displace the enantiomer from the enantiomer-CSP complex by exerting hydrogen bonds. From a practical standpoint, MeOH/NH₄HCO₃ mobile phases are only clearly advantageous for the baseline enantioresolution of $No = 51$ (TRI).

Concerning the effect on enantioresolution of the organic solvent percentage used to prepare the mobile phase, for the majority of compounds and CSPs, enantioresolution improved when the organic solvent percentage decreased using both MeOH/NH₄HCO₃ and ACN/NH₄HCO₃ mobile phases in the RPLC-domain. However, distinct patterns were observed for enantioresolution in the ACN HILIC-domain.

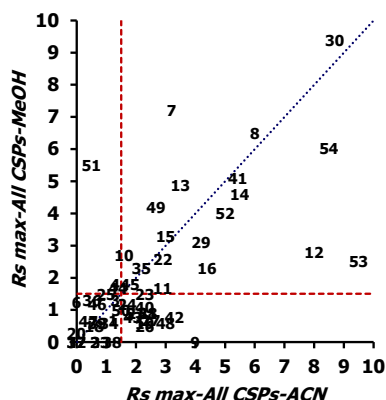


Figure IV.7.- Comparison of the maximum enantioresolution values (Rs_{max}) for the ACN:NH₄HCO₃ (5 mM, $pH = 8.0$) and MeOH:NH₄HCO₃ (5 mM, $pH = 8.0$) mobile phases studied taking into account all CSPs data jointly. (.....) Identity line (i.e., slope = 1; intercept = 0). (- - - -) $Rs_{max} = 1.5$.

On the other hand, approximately twice the number of compounds were baseline enantioresolved within the ACN RPLC-domain compared to the ACN HILIC-domain (32 and 17 compounds, respectively; see Figure IV.8). In addition, for most compounds, the R_s max values obtained in the RPLC-domain were higher than in the HILIC-domain for all CSPs. Only the enantiomers of $No = 49$ (promethazine) were baseline enantioresolved in the HILIC-domain, while they were only partially resolved in the RPLC-domain using ACN/ NH_4HCO_3 . However, MeOH/ NH_4HCO_3 mobile phases did allow their baseline enantioresolution. Finally, it is worth mentioning that only three (pindolol, $No = 35$; PRO, $No = 36$; and isoprenaline, $No = 41$) out of the 30 compounds studied that exhibited certain enantioresolution degree in HILIC conditions had $\log D$ values lower than 1.0.

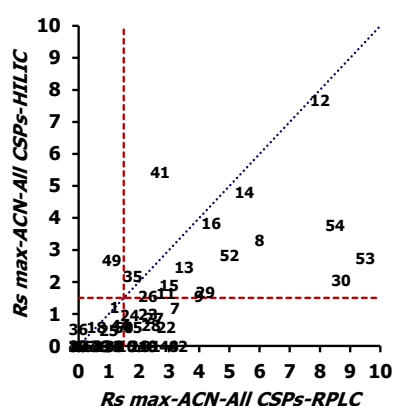


Figure IV.8.- Comparison of maximum enantioresolution values (R_s max) obtained for the HILIC and RPLC domains using ACN: NH_4HCO_3 (5 mM, $pH = 8.0$) mobile phases taking into account all CSPs data jointly. (·····) Identity line (i.e., slope = 1; intercept = 0). (- - - -) R_s max = 1.5.

As far as the effect on enantioresolution of the nature of the CSP is concerned, using ACN/ NH_4HCO_3 mobile phases, Cell2 was found to be the CSP that enabled baseline and partial enantioresolution for the largest number of chiral compounds, then Cell4, next Cell3, Cell5, and Cell1 (see Figure IV.9). Additionally, ACN-Cell2 was the chromatographic system that allowed baseline enantioresolution of the highest number of compounds (21) among all the tested systems, including MeOH/ NH_4HCO_3 systems.

On the other hand, phenylcarbamate-type CSPs (Cell1, Cell4 and Cell5; see Figures IV.9.A, IV.9.C-IV.9.E) did not exhibit clear complementary enantioselectivity to that of Cell2 when using ACN/ NH_4HCO_3 mobile phases.

When comparing the enantioresolution obtained in Cell2 and Cell4 CSPs, it was observed that the position of the substituents on the phenyl group, while not having a significant effect on the enantioselectivity of the CSP, did influence the enantioresolution degree in ACN/ NH_4HCO_3 mobile phases (see Figure IV.9.C), though not in MeOH/ NH_4HCO_3 mobile phases. In this way, the

enantiomers of the majority of the compounds that were baseline or partially enantioresolved in the ACN-Cell4 systems also did so in the ACN-Cell2 systems. From a practical standpoint, the ACN-Cell4 systems were found to be preferable to ACN-Cell2 in separating only the enantiomers of $No = 11$ (benalaxyl) and $No = 31$ (bicalutamide), which exhibited baseline enantioresolution only in ACN-Cell4 (although they did in other systems as well).

In practical terms, ACN-Cell1 (see Figure IV.9.A) and ACN-Cell5 (see Figure IV.9.D) systems were clearly advantageous over the ACN-Cell2 systems and also over all the systems studied to achieve baseline enantioresolution of the enantiomers of just a few compounds –ACN-Cell1 for $No = 23$ (orphenadrine); ACN-Cell5 for $No = 24$ (terfenadine) and $No = 43$ (terbutaline)–. Moreover, upon comparing the enantioresolution obtained in the ACN-Cell1 and ACN-Cell5 systems (see Figure IV.9.E), it was observed that they exhibited nearly orthogonal enantioselectivity, underlining the significant influence of the nature of substituents in the CSP phenyl moiety on the enantioresolution.

On the other hand, out of all the CSPs tested with ACN/ NH_4HCO_3 mobile phases, only Cell3 (a benzoate-type CSP; see Figure IV.9.B) displayed distinct complementary enantioselectivity compared to Cell2 and the remaining CSPs.

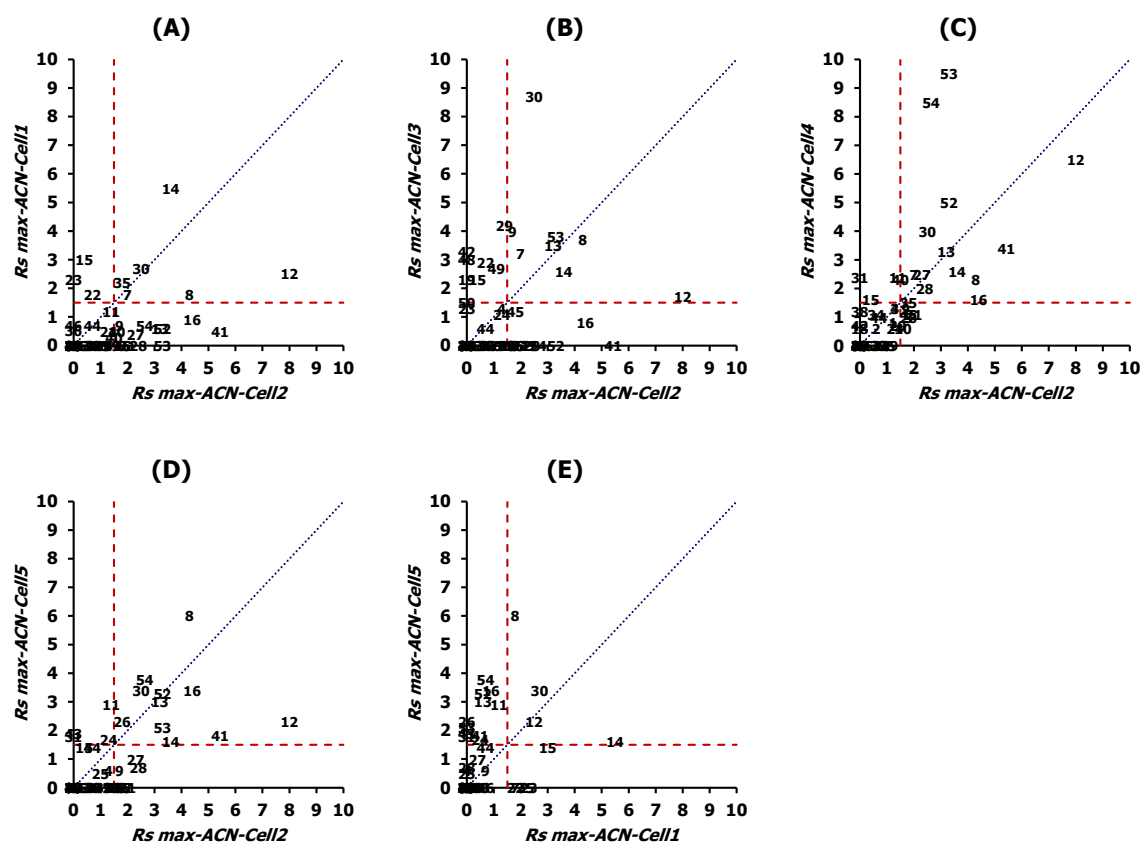


Figure IV.9.- Comparison of maximum enantioresolution values ($R_s \max$) obtained in the different CSPs studied using ACN: NH_4HCO_3 (5 mM, $pH = 8.0$) mobile phases. **(A)** Cell1 vs. Cell2, **(B)** Cell3 vs. Cell2, **(C)** Cell4 vs. Cell2, **(D)** Cell5 vs. Cell2, **(E)** Cell5 vs. Cell1. (.....) Identity line (i.e., slope = 1; intercept = 0). (- - - -) $R_s \max = 1.5$.

Using MeOH/NH₄HCO₃ mobile phases, Cell2 was found to be the CSP that enabled baseline enantioresolution for the largest number of chiral compounds, then Cell3, next Cell4, Cell5, and Cell1. MeOH-Cell3 and MeOH-Cell2 chromatographic systems exhibited nearly orthogonal enantioselectivity (see Figure IV.10.A). Furthermore, MeOH-Cell2 and MeOH-Cell4 systems exhibited comparable enantioselectivities and enantioresolution degrees (see Figure IV.10.B). Finally, the MeOH-Cell1 and MeOH-Cell5 systems showed nearly negligible enantioresolution ability (see Figure IV.10.C).

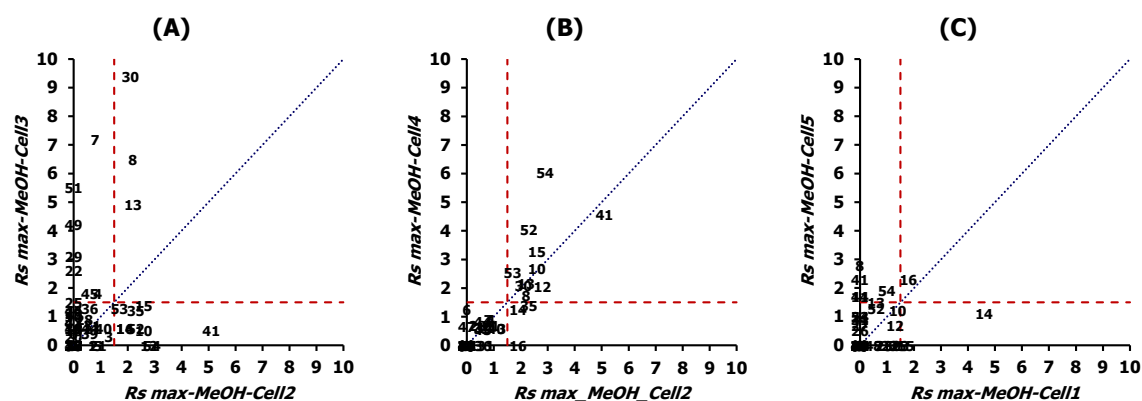


Figure IV.10.- Comparison of maximum enantioresolution values ($R_s \max$) obtained in the different CSPs studied using MeOH:NH₄HCO₃ (5 mM, pH = 8.0) mobile phases. **(A)** Cell3 vs. Cell2, **(B)** Cell4 vs. Cell2, **(C)** Cell5 vs. Cell1. (·····) Identity line (i.e., slope = 1; intercept = 0). (- - - -) $R_s \max = 1.5$.

Taking into account all the above considerations, we suggest following this order of chromatographic systems while attempting to enantioresolve a new neutral or basic chiral compound in the assayed cellulose-CSPs: (i) ACN-Cell2, (ii) MeOH-Cell3, (iii) ACN-Cell5, (iv) ACN-Cell1, and (v) other systems.

IV.2.3.- Conclusions

All the studied compounds and CSPs displayed the characteristic RPLC retention behaviour in MeOH/NH₄HCO₃ mobile phases under the tested experimental conditions. However, in ACN/NH₄HCO₃ mobile phases, the U-shaped retention behaviour observed depending on their H₂O content proved the existence of two retention domains: the RPLC-domain, for mobile phases containing from 20 % to 90 % H₂O (< 80 % ACN); and the HILIC-domain, where the H₂O percentage in the mobile phase was below 20 % (80-98 % ACN). All the studied compounds and CSPs (both chlorinated and non-chlorinated) exhibited this dual HILIC/RPLC retention behaviour. Nonetheless, the magnitude of the differences in retention upon varying the H₂O content in the mobile phase depended significantly on the nature of the compound and the CSP used. In all CSPs, hydrophilic compounds exhibited more noticeable HILIC behaviour.

The chromatographic systems exhibited differing enantioresolution degrees and enantioselectivities when MeOH/NH₄HCO₃ or ACN/NH₄HCO₃ were employed as mobile phases. MeOH/NH₄HCO₃ provided worse enantioresolution than ACN/NH₄HCO₃ mobile phases for the majority of the compounds with all CSPs studied. This could be due to competition between MeOH and the enantiomer for hydrogen bonding interactions with the CSP.

ACN/NH₄HCO₃ mobile phases yielded significantly better enantioresolution in the RPLC-domain as compared to the HILIC-domain for nearly all compounds. With the exception of promethazine enantiomers, all compounds that had complete enantioresolution in the HILIC domain had it in the RPLC domain as well.

The ACN-Cell2 chromatographic system enabled the separation of the enantiomers of the largest amount of chiral compounds compared to the other tested systems. Only Cell3 CSP exhibited a significant complementary enantioselectivity to Cell2, being nearly orthogonal with the use of MeOH/NH₄HCO₃ mobile phases.

When comparing the enantioresolution obtained in Cell2 and Cell4 CSPs, it is possible to conclude that the position of the substituents on the phenyl moiety, while not having a significant effect on the enantioselectivity of the CSP, did influence the enantioresolution degree in ACN/NH₄HCO₃ but not in MeOH/NH₄HCO₃ mobile phases. On the other hand, the nature of the CSP substituents played a significant role in the enantioresolution with ACN/NH₄HCO₃ mobile phases as can be concluded from the comparison of the enantioresolution obtained in Cell1 and Cell5. The use of MeOH/NH₄HCO₃ mobile phases with these CSPs was found to be unsuitable as these systems almost lose their enantioresolution capability.

To assist in achieving optimal enantioresolution results and reducing the experimental effort for the enantioseparation of a new basic or neutral chiral compound, the following screening sequence was recommended: (i) ACN-Cell2 in the RPLC-domain; (ii) MeOH-Cell3; (iii) ACN-Cell5 in the RPLC-domain; (iv) ACN-Cell1 in the RPLC-domain; (v) other chromatographic systems.

IV.3.- Artificial neural networks to model the enantioresolution of structurally unrelated neutral and basic compounds with cellulose tris(3,5-dimethylphenylcarbamate) chiral stationary phase and aqueous-acetonitrile mobile phases. Paper III

IV.3.1.- Brief introduction and objectives

In this work to advance in the knowledge of the rational selection of the chromatographic system to separate the enantiomers of a given compound, one of the objectives of this Doctoral Thesis, ANNs are used to attempt quantitatively estimate enantioresolution of chiral molecules from their structural information.

As stated in section I.3, ANNs are robust and adaptive machine learning techniques that can model complex and/or non-linear $\mathbf{y-X}$ or $\mathbf{Y-X}$ relationships. An ANN learns from a training dataset until its predictive ability across a validation dataset improves. The architecture of an ANN comprises interconnected neurons arranged in multiple layers that has to be optimised (see Figure IV.11). In the feed-forward method, the ANN architecture has: (i) an input layer (first layer) in which the \mathbf{X} variables are organised in the N_V neurons, (ii) an output layer (final layer) in which the known response variable(s) (\mathbf{y} or \mathbf{Y}) are also organised and (iii) the so-called hidden layers in the middle that must also be arranged. During the learning process, the weights (W_i) that connect all the neurons are adjusted by means of linear or non-linear functions (activation functions). Once the architecture is optimised, the ANN is ready to estimate response(s) for new compounds.

Because of the internal complexity of ANNs, the $\mathbf{y-X}$ relationship is not easily known. This lack of transparency is often referred to as the "black box" problem in ANN research. Although several methods have been proposed to estimate the importance of \mathbf{X} variables in predicting responses, they are not without limitations [222-224]. Moreover, there is currently no means to verify the quality of such estimates.

The ANN methodology has a wide range of applications in various research areas. However, at our knowledge, in the literature there are only four applications of ANNs for QSPR modelling in chiral HPLC (see Table I.9). These QSPR models have been derived for structurally related compounds using amylose-based [111], donor-acceptor-based [116], cellulose-based [127], and macrocyclic antibiotics [129] CSPs. At our knowledge, ANNs have never used to predict R_s values for structurally unrelated compounds.

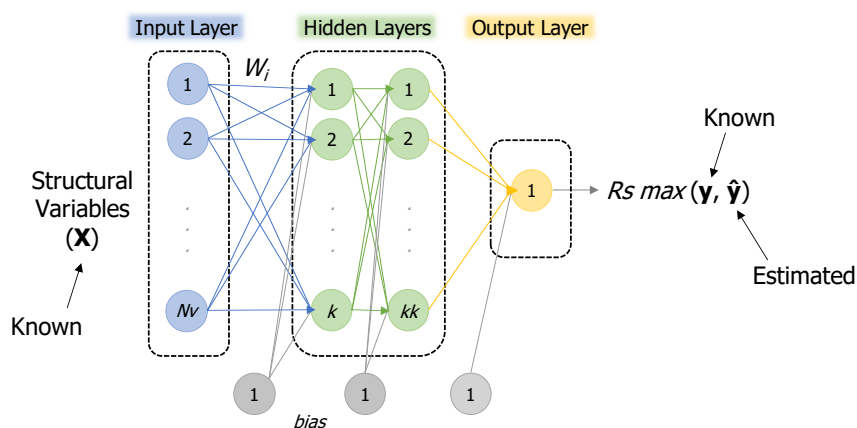


Figure IV.11.- Architecture of ANNs tested in this work.

The aim of this work was to design, for the first time, a strategy exclusively based on ANNs for FS and QSPR modelling of quantitative R_s values of structurally unrelated chiral compounds in a given chromatographic system. The proposed strategy was tested for the prediction of the $R_s \max$ values of 56 chiral compounds from 14 different chemical families chromatographed in Cell1 CSP and aqueous ACN mobile phases (nearly the same compounds and ACN mobile phases studied in section IV.2 and Paper II) from selected structural information. An approximation of the relative importance of the selected variables to quantitatively predict $R_s \max$ was also suggested.

IV.3.2.- Results and discussion

The 56 structurally unrelated compounds studied were nearly the same studied in section IV.2 (Paper II). The experimental $R_s \max$ values used as \mathbf{y} variable are those corresponding to ACN: NH_4HCO_3 (5 mM, $\text{pH} = 8$), 10:90 - 98:2 (v/v), mobile phases studied in section IV.2 (Paper II) for Cell1 CSP. The 56 structural variables used as \mathbf{X} variables were nearly the same studied in section IV.1 (Paper I). All variables (\mathbf{X} and \mathbf{y}) were autoscaled.

The 56 compounds studied were divided into three blocks: (i) the training block for learning with 49 compounds, (ii) the validation block for overfitting control with 7 compounds displaying a representative range of $R_s \max$ values, and (iii) the test block for improving robustness which included 9 sets of 5 different training compounds used for cross-validation, and as test compounds as well.

IV.3.2.1.- ANN architecture optimisation, feature selection and predictive ability

930 ANNs architectures were assayed that included the **X** variables in the input layer, the predicted *Rs max* values (\hat{y}) in the output layer, and up to two hidden layers with up to 30 neurons in each hidden layer. For comparative purposes, some aspects of the ANNs that can generate different outputs were fixed. That is, all inner weights (W_i in Figure IV.11) were fixed to one and the same compounds subsets (training, validation and cross-validation) were utilised for every ANN assayed.

The code $Nv - [k - kk] - 1$ was used for ANNs identification, being Nv , k and kk the number of structural variables and of neurons in the first and second hidden layer, respectively. The code $Nv - [k] - 1$ was used for ANNs with just one hidden layer.

To compare ANNs, a new quality target indicator (Q) was introduced:

$$Q = pMSE_{train} + pMSE_v + W1 |pMSE_v - pMSE_{train}| + W2 ((1 - R) + |1 - b_1| + |b_0|) + W3((1 - R_v) + |1 - b_{1v}| + |b_{0v}|) \quad (\text{Eq. IV.2})$$

where $pMSE$ are the penalised mean squared errors, and b_0 , b_1 and R are the intercept, slope, and correlation coefficient values from the validation plot. The subscripts *train* and *v* denote the training and validation compounds. $W1 = 1$, $W2 = 10$ and $W3 = 5$ were used in Eq. IV.2 to provide an almost similar contribution of all the terms. The $pMSE$ values were obtained by adding the standard deviation to the mean value (obtained from 10-ANNs MSE outputs: one with the training block and nine in the cross-validation runs). According to its definition, ANN quality increases as Q values decrease.

The final ANN architecture chosen was the simplest ANN (i.e., with lower $k \times kk$ value) that passed the two following filters: (i) $R > 0.9$, and (ii) Q values below the 10th percentile. It was assumed that a simpler ANN, with a few connecting coefficients, would be more robust. The simplest architecture fitting the two filters was 56-[7]-1. This architecture was selected for FS process.

To reduce the number of **X** variables and simplify the interpretation of the QSPR model (see section I.3), a new FS strategy based on ANN outputs (FS-ANN) was proposed. In the FS-ANN process, the most informative variables (i.e., those providing the lowest Q values) were incorporated (forward mode) sequentially (one-by-one) in each run. Figure IV.12 shows the relative Q values respect to the Q value obtained using all variables through the FS-ANN process. As can be observed, a Q value lower than 0 % (the initial one obtained with 56 variables) was obtained after adding eight **X** variables. So, the final operative ANN architecture selected was 8-[7]-1.

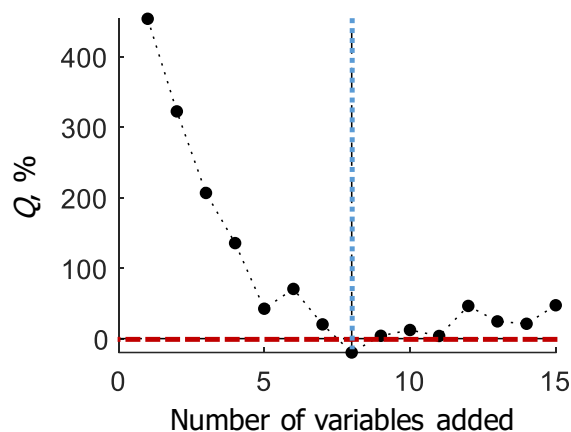


Figure IV.12.- Feature selection (FS-ANN) progress for Cell1 QSPR model: target indicator (Q) values (Eq. IV.2) obtained with the added variables relative to the Q value obtained with all the 56 X variables, expressed in percentage. (---) $Q = 0\%$ (using all the 56 X variables). (.....) Number of variables selected in the final operative ANN architecture.

The final operative ANN architecture selected 8-[7]-1 showed good performance (e.g., $MSE = 0.047$ and $R = 0.98$ for all the 56 compounds) in predicting $R_s max$ (see Figure IV.13).

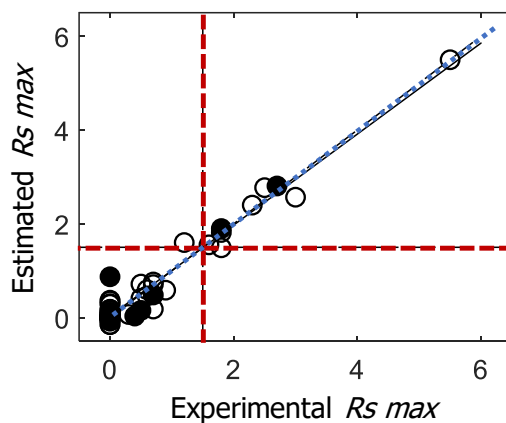


Figure IV.13.- $R_s max$ validation plot obtained from the operative ANN (8-[7]-1) for all 56 compounds studied. (O) Training and (●) validation block. (.....) Identity (i.e., slope = 1; intercept = 0) and (—) regression lines. (---) $R_s max = 1.5$.

IV.3.2.2.- Importance of variables

The importance of the eight selected structural variables in the ANN QSPR model was approximated using two approaches adapted from the literature [222,223]. Using these approaches, regression-like coefficients (one coefficient per variable) were obtained. These coefficients were normalised with respect to their maximum value to approximate the relative importance of each variable. Figure IV.14 shows the mean value of the relative importance together with their corresponding standard deviation uncertainty obtained from the results of the two adapted approaches for each selected variable.

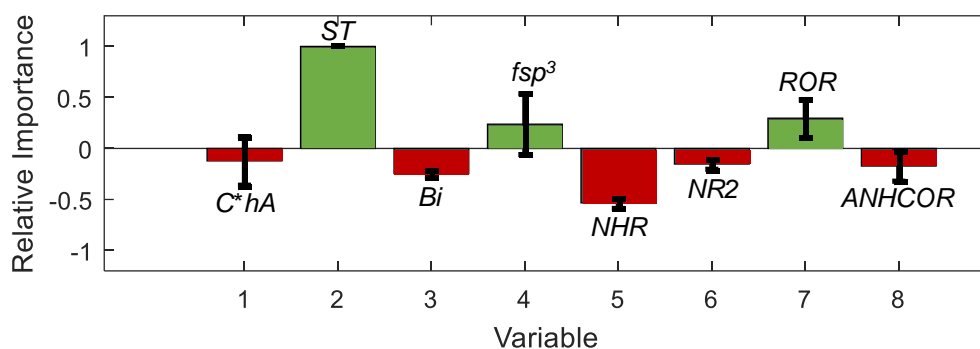


Figure IV.14.- Relative importance of the eight selected variables in the final ANN QSPR model. For each variable, the mean (bar) and the standard deviation (error bar) values obtained using two approaches are shown. (■) Positive and (■) negative contribution to $R_s \max$.

Variables selected: number of aromatic heterocycle groups bonded to the C^* (C^*hA); surface tension (ST); Balaban index (Bi); number of sp^3 hybridised carbons divided by the total carbon count (fsp^3), secondary amine (NHR), tertiary amine ($NR2$) and ether (ROR) groups in the molecule; and number of amide groups bonded to an aromatic ring ($ANHCOR$) in the molecule.

In a similar way to the regression coefficients in section IV.1 (Paper I), the approximated relative importance of variables in the ANN QSPR model can be used to explain the major operating forces in the modelled chromatographic systems. As can be observed in Figure IV.14, the presence of dipoles (ST) and ether groups (ROR) in the molecule enhance enantioresolution in the studied Cell1 chromatographic system. Therefore, van der Waals forces and hydrogen bonding interactions of enantiomers with the phenylcarbamate moiety of the CSP are of utmost importance on enantioseparation. Oppositely, steric factors (high Bi values), as well as the existence of amide ($ANHCOR$), secondary (NHR) and tertiary ($NR2$) amino groups in the compound molecule diminishes enantioresolution. For all compounds exhibiting some of these negative features in their structure (e.g., propafenone, fluoxetine, disopyramide, citalopram, brompheniramine among others, see Table III.1) $R_s \max < 1.5$ were obtained; except for orphenadrine ($R_s \max = 2.3$) and pindolol ($R_s \max = 1.6$) because of the presence of ether groups in their molecule (see Table III.1).

IV.3.3.- Conclusions

In this study, for the first time to our knowledge, ANNs were used for QSPR modelling of the quantitative enantioresolution of structurally unrelated chiral compounds. As a case study, experimental enantioresolution values of 56 chiral compounds from 14 diverse chemical families, obtained in Cell1 CSP and aqueous ACN mobile phases, were used as the response variable; and 56 structural parameters were tested as predictor variables.

The strategy proposed based on a new quality indicator (Q) calculated from 9 ANN outputs was designed to be suitable for the complexity of the data and the limited size of the dataset for ANN modelling purposes. This strategy allowed for the selection of an appropriate predictive ANN architecture (a single hidden layer of seven neurons) and for forward-stepwise FS-ANN process resulting in the selection of eight predictor variables.

Finally, the study of relative importance of the eight selected variables, which combined estimates from two different approaches, suggested that surface tension (positive contribution to enantioresolution) and the number of secondary amino groups in the molecule (negative contribution to enantioresolution) were the most important structural features of compounds for the prediction of their enantioresolution under the experimental conditions assayed.

This study demonstrates the potential of using ANNs for estimating enantioresolution from structural information, providing a valuable tool for predicting chiral separations. The ANN comparison strategy proposed in this study could also be applied to other datasets, offering a reliable and efficient method for selecting optimal ANN architectures and FS. Overall, this study provides a starting point for future research on the use of ANNs for enantioseparations and expands the knowledge of the relationship between molecular structure and chiral separation.

IV.4.- Modified Gaussian models applied to the description and deconvolution of peaks in chiral liquid chromatography. Paper IV

IV.4.1.- Brief introduction and objectives

As previously stated in the introduction chapter (section I.4), the profiles of chromatographic peaks, which can exhibit different peak characteristics such as efficiency and asymmetry, can be described by a huge variety of mathematical functions. Modified Gaussian models are a set of flexible functions with different complexity that stand out for the accuracy achieved when they are used to fit chromatographic peaks. In these models, the change in the variance (or standard deviation) of the chromatographic peaks over time is used to describe the deviation from an ideal Gaussian peak. In addition, they can be made dependent on experimental parameters as t_R , h_0 , A and B , which facilitates their practical application.

Among all modified Gaussian models proposed in Table I.10, the LMG, PVMG and PLMG models were chosen and used in this work. In LMG model, the peak standard deviation is explained by means of a linear function (see Eq. I.6, using the first-degree polynomial). However, a more elaborate model, such as PVMG model (see Eq. I.8), in which the variance follows a parabolic profile, is required to achieve more precise chromatographic peak fitting. In both models, for times that are significantly distant from the peak maximum, the parabolic growth of variance can result in non-zero values of the baseline. To prevent the function from growing beyond the peak region, PLMG model (see Eq. I.9) was proposed. PLMG model, which combines a parabola with a Lorentzian, has proven to be the most effective in fitting isolated asymmetric peaks.

In this work, the description of the enantiomeric peak profiles is studied by the application of the LMG, PVMG and PLMG models. The effectiveness of the approaches was verified by means of the simultaneous fitting of the peaks of the enantiomers. The deconvolution of the enantiomeric peaks, when they are not baseline separated ($R_s < 1.5$), is also studied with the aim of achieving the EF value.

IV.4.2.- Results and discussion

IV.4.2.1.- Fitting performance

Different approaches based on the selected modified Gaussian models (LMG, PVMG and PLMG models) have been proposed and compared (see Table IV.2). All models were applied unmodified (approach a). In addition, two modifications of the models (2 new approaches) were also applied to solve the problem of abnormal tail prediction. The tails models can be improved using exponential tails, specifically at 10 % of the peak height, beyond the peak region (approach b); or using a sigmoidal function that restricts the growth of the independent variable to obtain Gaussian tails (approach c). In order to simplify the application of the proposed approaches,

A and B parameters were measured at 10 % peak height, and the variance was kept positive and with a minimum value never lower than $1 \cdot 10^{-6}$. Least squares regression was used to optimize the peak parameters for each peak during the fitting process. Both enantiomeric peaks were simultaneously fitted, providing an assessment of the fitting quality independent of their R_s .

Table IV.2.- Nomenclature of the different approaches applied to modified Gaussian models.

Model/Approach	Unmodified (a)	Exponential function (b)	Sigmoidal function (c)
LMG (I)	Ia	Ib	Ic
PVMG (II)	IIa	IIb	IIc
PLMG (III)	IIIa	IIIb	IIIc

The enantiomeric peaks used for the application of the modified Gaussian models were chosen for their diverse shapes and skewness values. These enantiomeric peaks (20 chromatograms of eight chiral drugs from different families of interest: BUPI, FLU, IBU, KET, MET, OME, PRO, and TRI) were acquired using different chromatographic systems with different CSPs, mobile phases, pH values, and temperatures (see Table III.2 for additional information). The selected chromatograms present a wide range of peak parameters: t_R between 1.7 and 27.5 min, R_s values from 0.49 to 3.34, B/A between 0.84 and 3.13, and EF from 29.8 to 61.2 %.

The PLMG model achieved excellent results in the fitting of the studied enantiomeric peaks. Particularly, for KET4, IBU3 and MET2 chromatographic peaks that show a great diversity of values in peak asymmetry (B/A range from 0.84 to 2.81). When using the PLMG model, most of the compounds obtained errors below 1 % (mean relative error: 0.69 % for approach IIIa, 0.80 % for approach IIIb, and 0.71 % for approach IIIc). The PVMG model achieved acceptable results (mean relative error: 1.87 % for approach IIa, 1.52 % for approach IIb, and 1.58 % for approach IIc). While the LMG model achieved the worst results (mean relative error: 4.34 % for approach Ia, 4.12 % for approach Ib, and 4.54 % for approach Ic).

In overlapped peaks resolution, the unmodified models (approach a: Ia, IIa and IIIa) have a tendency to overfit and to transfer a fraction of area from one peak to another since doing so results in a better fit. While applying an exponential function (approach b: Ib, IIb and IIIb) can effectively address tail problems, it does not substantially enhance the fittings. The application of a sigmoidal function (approach c: Ic, IIc and IIIc) is a suitable option since it is easier to apply and provides acceptable results.

The LMG model can be only applied for peaks that are symmetric enough. The PVMG model provided satisfactory fittings for most peaks. However, it is worth noting the slight enhancement in fittings achieved with the modified PVMG models (approaches IIb and IIc). The PLMG model provided the best fittings, although it is possible to encounter problems of overfitting or

unsatisfactory tails in certain situations due to the high flexibility of the PLMG model (e.g., the reliability of the A and B parameters can be low) (see Figure IV.15). For example, in the KET4 chromatogram, the individual peaks obtained with the PLMG model, both applying and without applying restrictions (IIIa, IIIb and IIIc), are overlaid. Using approaches IIIa and IIIc, anomalous peak shapes were observed in regions with overlapped enantiomeric peaks, while approach IIIb addresses this problem by forcing an exponential decay in the peak tails. Therefore, it is not possible to apply the PLMG model for deconvoluting overlapped peaks, but it is advantageous for getting a peak function that precisely describes the experimental data for individual peaks that are perfectly defined, for determining peak parameters and for minimizing noise problems. However, for enantiomers that are partially separated, it is essential to perform a more exhaustive investigation into peak shape variations.

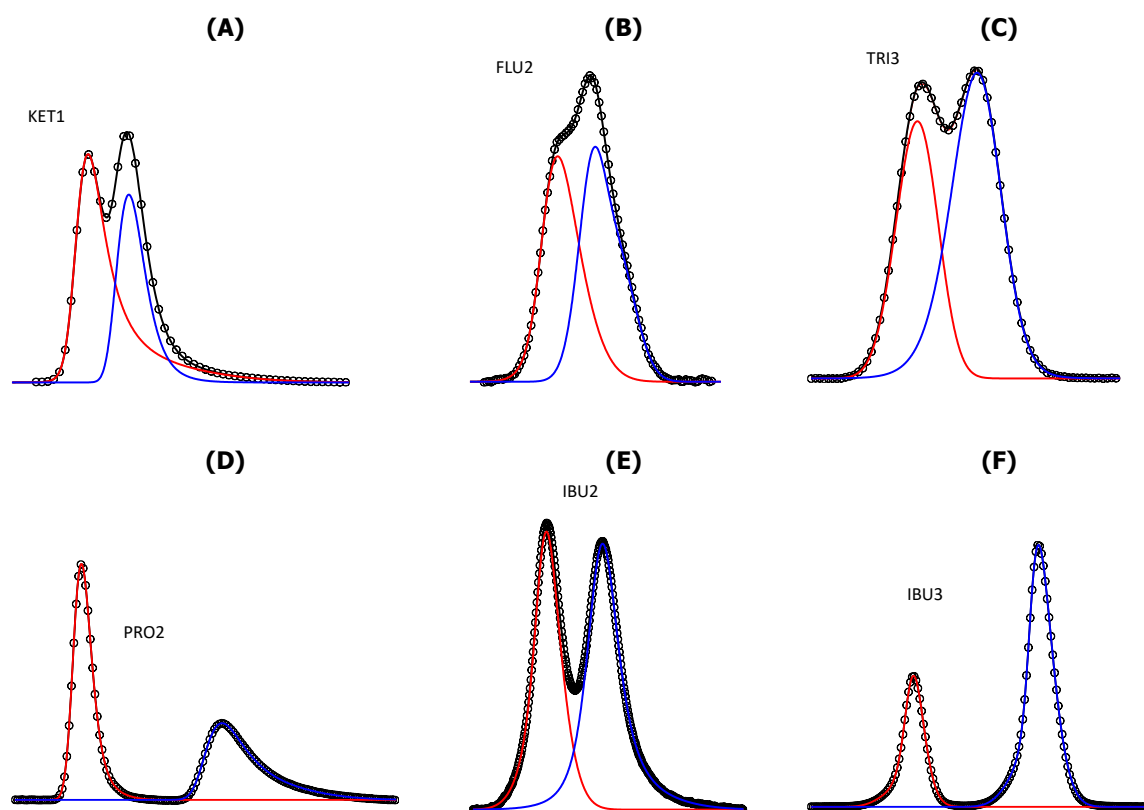


Figure IV.15.- Peaks adjusted with the PLMG function for **(A)** KET using Am2 CSP with ACN:HCOOH (0.1 %, v/v), 60:40 (v/v), at 15 °C; **(B)** FLU using Cell1 CSP with ACN:HCOONH₄ (10 mM, pH 3.0), 40:60 (v/v), + NaClO₄ (500 mM) at 15 °C; **(C)** TRI using Cell-SC CSP with ACN:CH₃COONH₄ (10 mM, pH 8.0), 45:55 (v/v), + DEA (0.1 %, v/v) at 25 °C; **(D)** PRO using Cell1 CSP with ACN:NaClO₄ (500 mM), 40:60 (v/v), at 25 °C; **(E)** IBU using Am2 CSP with ACN:HCOONH₄ (10 mM, pH 3.0), 40:60 (v/v), + NaClO₄ (500 mM) at 25 °C; and **(F)** IBU using Cell3 CSP with MeOH:HCOONH₄ (10 mM, pH 3.0), 80:20 (v/v), at 25 °C. Experimental (○), predicted (black solid line, —) and individual peaks (red and blue solid lines, — and — for E1 and for E2, respectively).

IV.4.2.2.- Peak deconvolution

Since both UV and MS spectra of the enantiomers of a racemic compound are identical, the application of multivariate techniques (e.g., multivariate curve resolution-alternating least squares) is not useful for the evaluation of the *EF*. Thus, the deconvolution of the peaks of the enantiomers of diverse chiral drugs was studied.

The stability of the PLMG and PVMG models (the models that exhibited the best results in chromatographic peak fitting) was compared. Both were applied to the overlapped peaks of KET4 ($R_s = 1.21$) at five concentration levels (2-100 mg L⁻¹) to subsequently calculate the *EF* by measuring the area of each peak. The reliability of the deconvolution process depends on the model's capability to correctly acquire the shape of each enantiomeric peak. Both models generated well-fitted peaks, with similar total areas and a mean relative error of 0.3 %. The same *EF* values should be obtained at different concentration levels since the shape of the peaks is expected to remain constant. However, the variation in *EF* values was measurably larger for the PLMG model than for the PVMG model. This may be because the significant uncertainties in the peak shapes obtained with PLMG model, which in turn leads to higher errors in the deconvolution.

It is obvious that the PLMG model incorrectly distributes the total area between the two enantiomeric peaks. Then, the PVMG model was used to fit the overlapped peaks of other chromatograms such as KET2 ($R_s = 0.73$) and KET3 ($R_s = 1.02$). Using approach IIc, the calculated *EF* was 38.3 % for KET2 and 46.4 % for KET3. In KET2, the width of the second peak grew, including a portion of the area from the first peak. This could be attributed to the fluctuation in width of one peak throughout the fitting iterations to counteract the reduction in width of the other peak. This phenomenon was not observed for KET3. The variability was higher with low enantioresolution (e.g., $R_s = 0.49$ for FLU2 and 0.62 for KET1). Nevertheless, when the enantioresolution was enough (e.g., $R_s = 1.19$ for BUP1 and 1.38 for PRO3), similar *EF* values were obtained using any approach studied. Therefore, the data set studied cannot be accurately deconvoluted using the PVMG model when attempting to fit all peak parameters and the enantioresolution is not sufficient ($R_s \leq 1.0$).

To address this problem, additional studies that reduce the peak shape variation should be performed. It is important to discover approaches to restrict the peak shape while maintaining a satisfactory level of fitting. Additionally, a protocol that maintain a constant *EF* value during the deconvolution process should be developed. The suggested models should be also evaluated even when the *EF* is significantly different from racemic.

IV.4.3.- Conclusions

Tested modified Gaussian peak models allowed the fitting of chromatographic peaks with a wide range of properties. LMG model only provides acceptable fittings for sufficiently symmetrical peaks. PVMG model provides satisfactory fittings, being the chosen model for compounds that present conventional profiles. PLMG model provides the best fittings, although overfitting problems or unsatisfactory tails may appear.

For overlapping peaks, it is necessary to constrain the models to establish the peak shape properly. If the models are applied without any restriction, they tend to overfit and transfer a fraction of the area between the overlapped peaks if this leads a better fit.

The application of exponential tails (approach b) can effectively eliminate tail problems, but it does not substantially enhance the fittings. The application of sigmoidal function (approach c) is a suitable option, it presents acceptable results and is easier to apply.

The deconvolution of insufficiently separated chromatographic peaks of enantiomers of a given chiral compound is also possible if resolution is not too low.

IV.5.- Trimeprazine is enantioselectively degraded by an activated sludge in ready biodegradability test conditions. Paper V

IV.5.1.- Brief introduction and objectives

As previously stated in the introduction chapter (sections I.1 and I.5), despite the recognized significance of stereochemistry in pharmacology, it has often been disregarded in the field of environmental research. The enantioselectivity in the ecotoxicity and biodegradation processes is obvious and parallel to that observed in the medical and biomedical fields.

The presence of chiral pollutants in the environment, particularly drugs, is a growing concern due to the different characteristics of enantiomers and their possible effects on both human health and the environment.

The OECD tests for assessing ready biodegradability (see section I.5.1) are designed to identify chemicals that can be easily degraded, thereby contributing to advances in water and environmental research. Therefore, monitoring the *EF* of chiral compounds during the biodegradation process is also crucial for assessing health and environmental risks.

TRI, also known as alimemazine, is a tricyclic antihistamine that shares structural similarities with phenothiazine antipsychotics but differs in ring-substitution and chain characteristics. Although TRI is not used clinically as an antipsychotic, it is commonly used as an antiemetic for motion sickness prevention, or as an antihistamine in combination with other medications for cough and cold relief. TRI is also used as an antipruritic agent, for insomnia, and as oral premedication in pediatric day surgery.

In this work, the enantioselective biodegradation of TRI enantiomers is examined by a biodegradability test under conditions similar to those recommended in OECD tests. The experiments were carried out in batch mode using a saline medium with an activated sludge inoculum from a local WWTP and spiked with *rac*-TRI at three concentration levels. A method for chiral separation of TRI enantiomers by RPLC was developed. This study aimed to provide the first evidence of enantioselective biodegradation of TRI and to relate it to microbial growth. In addition, a curve-fitting approach is proposed for *S*, *BD* and *EF* over time. Finally, a precision study on *S* and *EF* data, under intermediate precision conditions, is performed for the first time.

IV.5.2.- Results and discussion

IV.5.2.1.- Chiral chromatographic analysis

The effectiveness of various polysaccharide-based CSPs and mobile phases (see Table III.2 for additional information) in separating the enantiomers of TRI was evaluated. Partial enantioresolution was only achieved with Cell1 and Cell5 CSPs when using a mobile phase containing ACN:HCOONH₄ (10 mM, pH = 8.0), 60:40 (v/v), + DEA (0.1 %, v/v). To improve the separation, mobile phases containing ACN and chaotropic agents such as ACN:KPF₆ (100 mM), 40:60 (v/v), and ACN:NaClO₄ (500 mM), 40:60 (v/v), were tested.

By using Cell1 as CSP and a mobile phase composed of ACN:NaClO₄ (500 mM), 40:60 (v/v), the enantiomers of TRI were separated with satisfactory results ($R_s = 2.2$, $t_{R1} = 13.6$ min and $t_{R2} = 14.8$ min). Calibration curves were obtained for each enantiomer by injecting standard solutions containing *rac*-TRI in the concentration range of 1-30 mg L⁻¹ (5 concentration levels). Adequate results were obtained for both enantiomers ($R^2 > 0.99$). The limit of quantification was determined for a concentration of 1 mg L⁻¹ of *rac*-TRI (0.5 mg L⁻¹ of each enantiomer).

IV.5.2.2.- Enantioselective biodegradation results

Batch mode biodegradability assays were conducted in duplicate for TRI enantiomers at three concentration levels of *rac*-TRI (4.8, 9.0 and 18.0 mg L⁻¹) using the methodology outlined in section III.3.3. The inoculum activity was verified using benzoic acid (20 mg L⁻¹) as reference substance. It was observed that benzoic acid was completely biodegraded in less than 48 h, confirming the adequacy of the inoculum and therefore the validity of the TRI assays.

Figure IV.16 illustrates the changes in concentration ($S-t$, two replicates) of the enantiomers of TRI at an initial *rac*-TRI concentration of 9 mg L⁻¹ over the course of the experiment. As can be observed, both enantiomers experience a similar concentration depletion in the first few days, up to approximately day 4. However, different concentration profiles become apparent for the enantiomers during the following days up until the experiment is completed. Furthermore, the concentration profiles appear to stabilize at higher times, indicating that no further degradation is likely to occur. Similar outcomes were obtained for the other tested *rac*-TRI concentrations, which indicate that enantioselectivity is independent of the concentration. Abiotic assays showed relatively low degradation rates (< 20 %) compared to biotic assays, confirming that degradation was primarily driven by microbial communities.

OD_{600} values measure the turbidity of the solution, which can be considered proportional to biomass growth [225]. In Figure IV.16, the variation of OD_{600} measures over time was overlaid for comparison purposes. As can be observed, a typical microbial growth curve was obtained, including an initial lag phase (~ 2 days), a short exponential phase (~ 2 days), and a stationary/decline phase. This last phase may explain the stabilization observed in the concentration profiles. This behaviour was observed for all *rac*-TRI concentrations tested. Interestingly, by comparing the concentration and OD_{600} profiles, it can be concluded that the enantioselective biodegradation stage appears to coincide more with the stationary/decline phase than with the exponential phase.

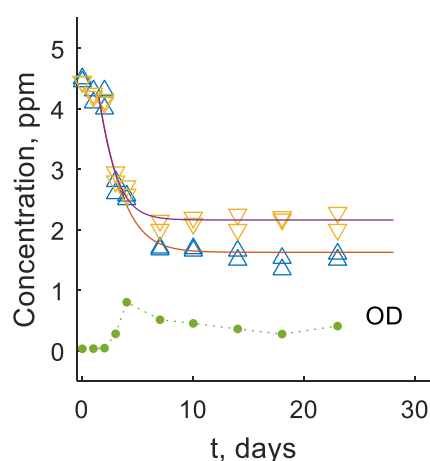


Figure IV.16.- Variation of concentration of TRI enantiomers (two replicates) during biodegradability assay. (Δ) First and (∇) second eluted enantiomers. Fitted curves (solid lines) were obtained by adjusting the experimental results to the simplified Monod model. OD_{600} values (\bullet , dashed line) are also shown. The results correspond to an initial concentration of *rac*-TRI of 9 mg L^{-1} .

Figure IV.17 depicts the variation of the *EF* values (Eq. I.1) together with the standard deviation over time for a *rac*-TRI concentration of 9 mg L^{-1} . Consistent with the results shown in Figure IV.16, *EF* values close to 0.5 (indicating no enantioselectivity) were obtained until approximately day 4. Subsequently, during the final phase of microbial growth, the *EF* values decreased and stabilized at around 0.40-0.45. Equivalent *EF* trends were noted for the other two *rac*-TRI concentration levels investigated. The grand mean of *EF* for the final five incubation times (where *EF* remained almost constant) were 0.44 ± 0.03 , 0.43 ± 0.04 , and 0.43 ± 0.05 for the low, intermediate, and high *rac*-TRI concentrations, respectively. These results show, for the first time, evidence of moderate enantioselectivity in the microbial degradation processes of TRI enantiomers using this activated sludge within the concentration range studied.

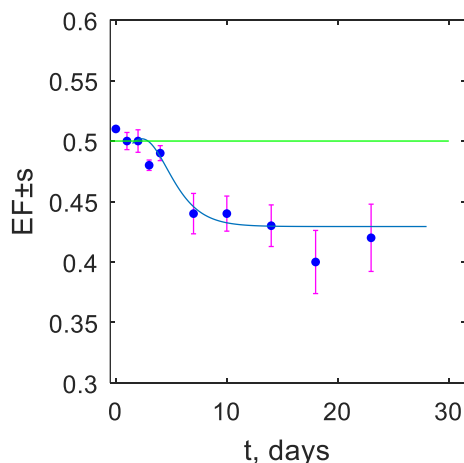


Figure IV.17.- Variation of mean $EF \pm s$ (●) over time obtained for a *rac*-TRI concentration of 9 mg L^{-1} . The solid line, $EF-t$ curve, was obtained by adjusting the experimental results to the simplified Monod model. The horizontal line at $EF = 0.5$ denotes no enantioselectivity in the biodegradation process.

IV.5.2.3.- Kinetic assessment of the data. Curve fitting

Regardless of the accuracy and reliability of the kinetic parameter estimates commented in section I.5.1, Monod and Michaelis-Menten-like models provide curves with a good fit (e.g., high R^2) to the experimental $S-t$ data in most cases.

In this work, the simplified Monod model (Eq. I.23) with an offset term was used to obtain $S-t$ curves. As can be observed in Figure IV.16, the resulting fitted models for both enantiomers (solid lines) shown an adequate agreement with experimental values. From these $S-t$ curves, the corresponding $EF-t$ curve was generated (solid line in Figure IV.17). Despite the presence of notable uncertainty in the EF data, the fitted curve agrees reasonably well with the experimental EF values. The curves obtained for the three concentration levels studied exhibited similar patterns.

Similarly, curves for BD (Eq. I.27) over time ($BD-t$ curves) were also obtained. These curves can be very useful to estimate the half-life time ($t_{1/2}$; $BD = 50\%$) as well as the BD at a given time. As can be observed in Figure IV.18, for the highest concentration level studied of *rac*-TRI (curves 5 and 6), both enantiomers have similar $t_{1/2}$ (~ 4.5 days), indicating a negligible degree of enantioselective biodegradation. At the intermediate concentration level studied (curves 3 and 4), $t_{1/2}$ differs between both enantiomers revealing an incipient enantioselective biodegradation (~ 4.5 and ~ 6 days for E1 and E2 enantiomers, respectively). For the lowest concentration level studied of *rac*-TRI (curves 1 and 2), $t_{1/2}$ is ~ 5 days for E1, but $t_{1/2}$ cannot be estimated for E2 because E2 never reach $BD = 50\%$. The observed differences in the outcomes obtained for the various substrate concentration levels could imply the existence of different biodegradation mechanisms for the TRI enantiomers. Furthermore, it can be observed that in all cases the maximum BD values increase as

rac-TRI concentration increases and that E1 reaches higher *BD* values than E2 during the enantioselective biodegradation phase, consistent with Figure IV.16.

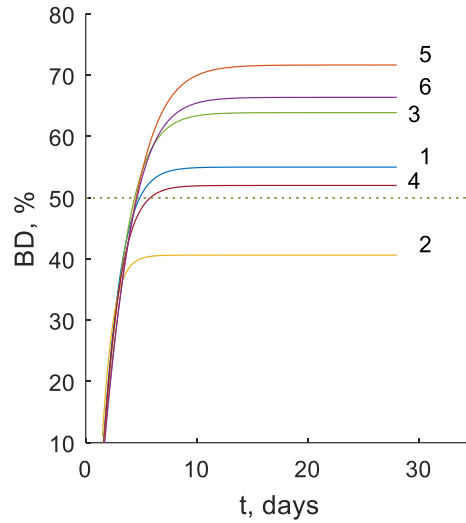


Figure IV.18.- Estimated *BD* values of TRI enantiomers according to the simplified Monod models. Initial *rac*-TRI concentrations: 4.8 mg L⁻¹ for curves 1 (E1) and 2 (E2); 9 mg L⁻¹ for curves 3 (E1) and 4 (E2); and 18 mg L⁻¹ for curves 5 (E1) and 6 (E2). (.....) *BD* = 50 %.

IV.5.2.4.- Precision study under intermediate precision conditions

In biodegradation studies, precision evaluation is frequently overlooked. In these studies, the uncertainty associated with both the analytical method and the biodegradation process contribute to overall precision. By providing precision data, it is possible to compare different biodegradation procedures and to assess the quality of the kinetic parameter estimates.

In this work, precision studies on *S* and *EF* values were performed to evaluate the repeatability and intermediate precision conditions, which included the factor of time. Duplicated results from biotic assays were placed in a matrix labelled $\mathbf{X}_{Nr \times Ns}$, with *Nr* and *Ns* representing the number of replicates (in this case, *Nr* = 2) and the number of series (incubation times). The data matrix was analysed with ANOVA. The repeatability standard deviation (*s_r*), between-run standard deviation (*s_{run}*), and standard deviation of the grand mean (*s_{mean}*) were calculated using equations IV.3 to IV.5, which were derived from the residual mean square (*MS_r*) and the between-run mean square (*MS_{run}*).

$$s_r^2 = MS_r \quad (\text{Eq. IV.3})$$

$$s_{run}^2 = \frac{(MS_{run} - MS_r)}{Nr} \quad (\text{Eq. IV.4})$$

$$s_{mean}^2 = \frac{MS_{run}}{Nr} \quad (\text{Eq. IV.5})$$

For precision estimation of S values, for each enantiomer, $\mathbf{X}_{2 \times 10}$ matrices (2 replicates, 10 days) were constructed and analysed using ANOVA. The ANOVA analysis indicated above, is valid for a single concentration level. But, in biodegradation data, S changes over time, therefore, only the s_r values are statistically consistent. From Eq. IV.3, the relative standard deviation values expressed as percentage (RSD_r) were calculated for each concentration level and enantiomer and ranged from 3.7 % to 8.7 %, which suggests moderate imprecision. These values reflect the overall method imprecision (biodegradation and analytical processes).

The precision study was extended, for the first time, to the EF values. In this case, since the EF can be considered almost constant in the last five times, the precision study could be performed including the factor time. For this purpose, for each concentration studied, ten EF data were used to construct $\mathbf{X}_{2 \times 5}$ matrices. From equations, IV.3 and IV.4, s_r and s_{run} values were calculated and expressed as RSD in percentages (RSD_r and RSD_{run} , respectively). RSD_r and RSD_{run} values of less than 5 and 13 %, respectively, were obtained for the concentrations studied. These values can be considered usual in the framework of a biodegradation process.

IV.5.3.- Conclusions

The results in this work provided the first evidence of enantioselective biodegradation of TRI enantiomers, with a maximum EF of 0.44 at concentrations of *rac*-TRI ranging from 5 to 20 mg L⁻¹.

The biomass growth, measured by OD_{600} , indicated that enantioselective biodegradation occurred mainly during the stationary/decline stage rather than the exponential stage.

The Michaelis-Menten-like approach with an offset term can be used to fit $S-t$ and $BD-t$ curves. Fitted curves accurately represented the experimental data and allowed the estimation of half-life times which were more secure than other estimations based on model parameters. In addition, for the first time, $EF-t$ fitted curves were also obtained. The results showed that enantioselectivity was found to be independent of concentration.

Moderate imprecision was observed in the precision study on S (repeatability conditions) and EF (intermediate precision conditions). Future works should consider the S imprecision when estimating kinetic parameters *via* Monod or alternative models.

The results obtained in this work suggest that TRI possesses the potential for moderate enantioselective biodegradation in diverse environments, in accordance with OECD guidelines. Nonetheless, additional studies are required to corroborate and extend these results using other substrates/biological materials.

IV.6.- Direct chromatographic study of the enantioselective biodegradation of ibuprofen and ketoprofen by an activated sludge. Paper VI

IV.6.1.- Brief introduction and objectives

To contribute to the advancement of knowledge of the risks and hazards of chiral pollutants, one of the objectives of this Doctoral Thesis, in this work, in a similar way to section IV.5, the enantioselective biodegradation of IBU and KET is studied.

IBU and KET are chiral NSAIDs that exhibit anti-inflammatory and analgesic properties. IBU is one of the most widely used drugs globally. The therapeutic benefits of these drugs are predominantly attributed to their (*S*)-enantiomers, with the (*R*)-enantiomers being weakly active or inactive. However, despite the differences in enantiomeric activity, IBU and KET are typically produced as racemic mixtures.

It has been reported the occurrence of IBU and KET enantiomers in influents and effluents from WWTPs. However, there is a controversy about the enantioselective biodegradation of IBU. (*S*)-IBU was found to be the predominant enantiomer in wastewater influents and preferentially degraded during wastewater treatment. Nonetheless, for constructed wetlands, the *EF* values exhibited significant variability, with (*R*)-IBU preferentially degraded in the final stage of the process. This behaviour has been attributed to changes in the aerobic and anaerobic conditions within the WWTP that could induce the chiral inversion of (*R*)-IBU. Additionally, the degree of chiral inversion seems to vary depending on the microorganisms present in the WWTP considered. No significant changes in *EF* values were reported for KET.

Laboratory-scale experiments have also been performed to investigate the enantioselectivity in the biodegradation of NSAIDs. The results obtained in these studies showed that (*S*)-IBU was the preferentially degraded enantiomer, and the degradation of (*R*)-KET was slightly higher than its antipode.

To summarize, alterations in the *EF* values of IBU and KET during biodegradation can be attributed not only to the faster degradation of one enantiomer compared to the other (enantioselective degradation), but also to the occurrence of chiral inversion resulting from enzymes that can vary in their ability to invert the degree and/or direction of chirality in different organisms, or due to the combination of both processes [177].

The objective of this work was to evaluate the biodegradation of IBU and KET enantiomers using ready biodegradability tests, compatible with OECD guidelines. To separate IBU and KET enantiomers, polysaccharide-based CSPs were tested under RPLC conditions and, under the chosen conditions, validation of the methods was performed.

In addition, this work describes a new approach for estimating significant parameters related to the biodegradation process using chromatographic peak areas of enantiomers. The approach is

designed to eliminate the uncertainty associated with the calibration step and to reduce experimental effort and cost. The article presents new equations to model $BD-t$ curves and $EF-t$ curves using enantiomer peak areas as dependent variables. The effectiveness of this approach is compared with conventional models and previous results for the biodegradation of IBU and KET enantiomers.

IV.6.2.- Results and discussion

IV.6.2.1.- Chiral chromatographic separation

The usefulness of various polysaccharide-based CSPs and mobile phases in separating the enantiomers of IBU and KET was evaluated. As mobile phases, binary mixtures of ACN or MeOH and aqueous formic acid solution (0.1 %, v/v), in varying proportions, at 15 and 25 °C were assayed (see Table III.2 for additional information). The identification of enantiomers of IBU and KET was performed by injecting (*S*)-IBU and (*S*)-KET standard solutions.

Using Cell3 CSP and a MeOH:HCOOH (0.1 %, v/v), 80:20 (v/v), mobile phase at 25 °C, adequate results ($R_s = 2.8$, $t_{R(R)}\text{-IBU} = 7.3$ min and $t_{R(S)}\text{-IBU} = 8.1$ min) were obtained. These conditions were selected for the enantioseparation of IBU in biodegradability assays.

For KET, the use of Am2 CSP and a mobile phase containing ACN:HCOOH (0.1 %, v/v), 35:65 (v/v), at 15 °C provides adequate results ($R_s = 1.6$, $t_{R(R)}\text{-KET} = 4.1$ min and $t_{R(S)}\text{-KET} = 5.2$ min) and was selected for the enantioseparation of KET in biodegradability assays. In the experimental conditions assayed no reversal elution order of IBU and KET enantiomers was observed.

IV.6.2.2.- Biodegradation assays and chromatographic information

Batch mode biodegradability assays were done by duplicate at 15.6 mg L⁻¹ of *rac*-IBU and 18.0 mg L⁻¹ of *rac*-KET following the procedure described in section III.3.3. The inoculum activity was verified using fluoxetine (20 mg L⁻¹) as reference compound (target value $BD_{7d} = 70 \pm 11$ %) [226]. In this work, a BD_{7d} of 69.3 % for fluoxetine was obtained, confirming the adequacy of the inoculum and therefore, the validity of the IBU and KET biodegradability assays.

In addition, the measurement of the OD_{600} values to control the biomass growth showed that, for both IBU and KET assays, the maximum biomass growth was obtained at 5 days, after which a stationary growth phase took place, followed by another decreasing phase.

In this study, an alternative method for calculating BD values, which involves using chromatographic information directly, specifically the peak area (A), instead of S data, was proposed:

$$BD = \frac{S_0 - S}{S} 100 = \frac{A_0 - A}{A_0 - b_0} 100 \approx \frac{A_0 - A}{A_0} 100 \quad (\text{Eq. IV.6})$$

where A_0 represents the peak area obtained at the beginning of the experiment ($t = 0$ days). This equation is valid assuming that the intercept of the calibration curve, b_0 , is statistically non-significant or negligible.

Moreover, the EF values at a given time were also calculated directly from the chromatographic information for IBU and KET enantiomers:

$$EF = \frac{S_{E1}}{S_{E1} + S_{E2}} = \frac{(A_{E1} - b_{0,E1})/b_{1,E1}}{(A_{E1} - b_{0,E1})/b_{1,E1} + (A_{E2} - b_{0,E2})/b_{1,E2}} \approx \frac{A_{E1}}{A_{E1} + A_{E2}} \quad (\text{Eq. IV.7})$$

where A_{E1} and A_{E2} correspond to the peak area obtained for E1 and E2 enantiomers, respectively, at a given time. This equation is valid assuming that the differences in the slopes ($b_{1,E1}$ and $b_{1,E2}$) are not statistically significant and the intercepts ($b_{0,E1}$ and $b_{0,E2}$) are statistically equal to zero.

In order to verify the indicated assumptions, methodological calibration for IBU and KET enantiomers was obtained under the selected chromatographic conditions. Satisfactory results were obtained for the enantiomers of both compounds studied ($R^2 = 0.998$). In both cases, b_0 values were statistically non-significant. In addition, the t -test used to compare the $b_{1,E1}$ and $b_{1,E2}$ slopes of the enantiomer calibration curves for IBU and KET indicated their statistical equality.

Figure IV.19 show the BD values calculated using the direct chromatographic approach for the enantiomers of IBU (Figure IV.19.A) and KET (Figure IV.19.B). Degradation was not detected for the enantiomers of IBU within the initial five days of incubation. Subsequently, the biodegradation process was initiated; however, even after 28 days of incubation, complete degradation of IBU enantiomers was not achieved. Furthermore, the biodegradation of (R)-IBU was found to be greater than that of (S)-IBU, suggesting enantioselectivity in the biodegradation process of IBU enantiomers.

Similar to IBU, degradation of KET was observed after five days of incubation. However, complete degradation of KET enantiomers was done within 25 days of incubation. As can be observed in Figure IV.19.B, the biodegradation of KET enantiomers was similar, therefore it appears not to be enantioselective.

In the abiotic assays, non-significant physicochemical degradation ($< 20\%$) was observed for IBU and KET enantiomers, confirming that degradation of these compounds was primarily driven by microbial community. From the results obtained and according to OECD guidelines, IBU and KET enantiomers exhibit ready biodegradability.

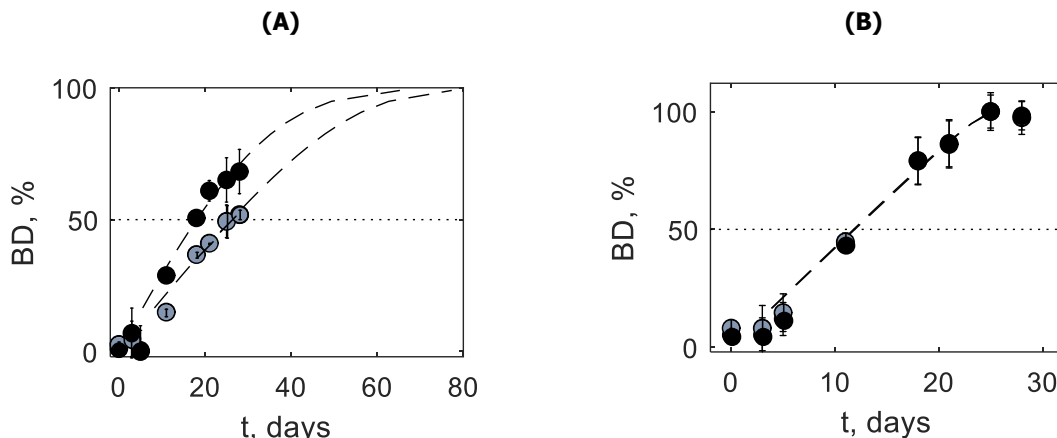


Figure IV.19.- Biodegradation values ($BD \pm s$), calculated from peak areas using the Eq. IV.6, in incubated samples during the biodegradation assay for: **(A)** (●) (*S*)-IBU and (○) (*R*)-IBU, and **(B)** (●) (*S*)-KET and (○) (*R*)-KET. Dashed lines represent the modelled $BD-t$ curves (Eq. IV.9).

For modelling $BD-t$ curves, the simplified Monod model (Eq. I.23), which relates S and t by means of the Lambert W function, has been adapted for chromatographic data ($A = W\{t\}$; Eq. IV.8). By substituting this model in Eq. IV.6, the following equation ($BD = W\{t\}$; Eq. IV.9) was obtained:

$$A = \frac{A_0}{S_0} \left\{ K_s \cdot W \left[\frac{S_0}{K_s} e^{\left(\frac{S_0 - V_m \cdot t}{K_s} \right)} \right] \right\} \quad (\text{Eq. IV.8})$$

$$BD = \frac{100}{S_0} \left\{ S_0 - K_s \cdot W \left[\frac{S_0}{K_s} e^{\left(\frac{S_0 - V_m \cdot t}{K_s} \right)} \right] \right\} \quad (\text{Eq. IV.9})$$

where V_m is the maximum specific growth rate and K_s is the half saturation constant for growth.

Dashed lines in Figures IV.19.A and IV.19.B represent the modelled $BD-t$ curves obtained according to Eq. IV.9 for IBU and KET enantiomers, respectively. As can be observed, a good agreement between the fitted curves and the experimental data points for BD exists (R^2 values of 0.94 and 0.95 for (*R*)- and (*S*)-IBU, respectively, and 0.99 for both (*R*)- and (*S*)-KET). By extrapolating these curves, it can conclude that the biodegradation process of (*R*)-IBU would be completed in approximately 60 days, while (*S*)-IBU would require around 80 days. In contrast, KET showed complete biodegradation within 25 days, as previously stated. Another significant advantage of the BD model is the capability to predict $t_{1/2}$ values. The $t_{1/2}$ values for (*R*)- and (*S*)-IBU were estimated to be 18 and 25 days, respectively. Whereas, the $t_{1/2}$ values for (*R*)- and (*S*)-KET were both 12 days.

Moreover, it is possible to model $EF-t$ curves from chromatographic data ($A-t$ curves) by combining $BD-t$ curves for the enantiomers E1 and E2 (BD_{E1} and BD_{E2} , respectively). From Eqs. IV.6 and IV.7, the following equation is obtained:

$$EF = \frac{100 - BD_{E1}}{200 - BD_{E1} - BD_{E2}} \quad (\text{Eq. IV.10})$$

Figures IV.20.A and IV.20.B show the modelled $EF-t$ curves for IBU and KET, respectively. As can be observed, a good agreement between the fitted curves and the experimental data points for EF exists. The models allow extrapolating EF values. For instance, the EF value of IBU decreased to approximately 0.4 at 28 days, and the expected minimum EF value is close to 0.2 at 60 days (i.e., at the time where (*R*)-IBU is almost completely biodegraded). These results show that the microorganisms present in the activated sludge used in this study show enantioselectivity towards IBU enantiomers. Specifically, the biodegradation of (*R*)-IBU was observed to be superior to that of (*S*)-IBU, as stated before. For KET, EF values close to 0.5 were observed throughout the biodegradation process, which confirms that the biodegradation process of KET is non-enantioselective, as anticipated. These results are in agreement with those described in the literature.

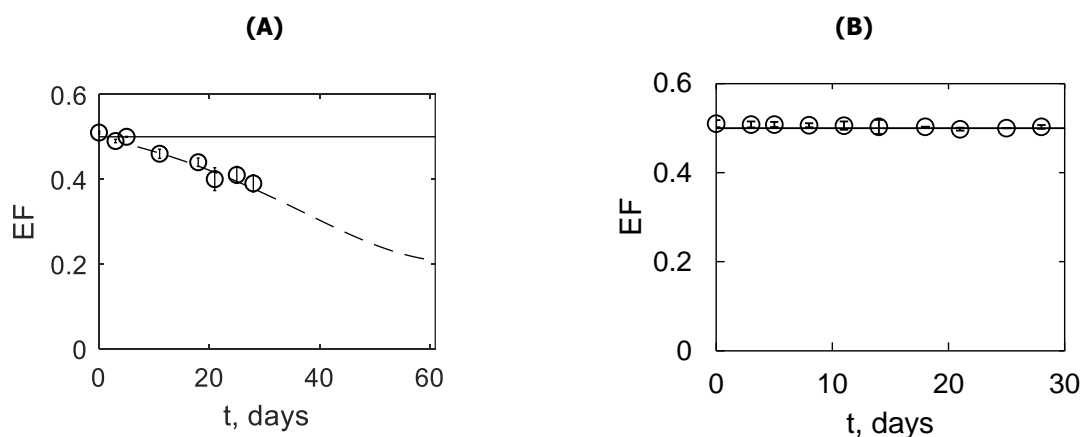


Figure IV.20.- Variation of EF values (mean \pm s) during the biodegradation assay for: **(A)** IBU and **(B)** KET. EF values were calculated from Eq. IV.7. Dashed lines represent the $EF-t$ fitted curves obtained from Eq. IV.10. The horizontal line ($EF = 0.5$) indicates the absence of enantioselective biodegradation.

The use of concentration data instead of peak areas provided similar BD and EF estimates. A maximum absolute difference of 2.3 was observed for BD , while EF exhibited relative differences below 1 %. Thus, both approaches can be applied indistinctly. However, using chromatographic peak

area data as input variables eliminates the uncertainty associated with using calibration curves and provides more precise *BD* and *EF* estimations.

Finally, although the purpose of the developed methods was not routine sample analysis, some established analytical features (precision and trueness) were obtained by processing two replicates of *rac*-IBU and *rac*-KET solutions prepared daily in MSM at two concentration levels (1.2 and 8 mg L⁻¹) for five days. Results for each enantiomer and compound were organised in a data matrix, $\mathbf{X}_{2 \times 5}$, and processed *via* ANOVA following the strategy showed in section IV.5. Relative standard deviations values and mean relative errors values lower than 6.9 and 9.5 % for IBU and 9.4 % and 9.5 % for KET, respectively, were obtained.

IV.6.3.- Conclusions

The assay to evaluate the biodegradability, following the OECD recommendations, of two commonly consumed drugs, IBU and KET, using an inoculum of activated sludge from a WWTP showed that both drugs were readily biodegradable with non-significant abiotic degradation. The outcomes of this study suggest that these drugs have the potential for degradation in various environments, according to the OECD guidelines. However, the extrapolation of these findings directly to environmental or wastewater treatment scales is not recommended.

The biodegradability of IBU enantiomers was enantioselective, being the *BD* of (*R*)-IBU higher than *BD* of (*S*)-IBU; while non-enantioselective biodegradation was observed for KET.

The chiral RPLC methods developed to monitor the enantiomers of IBU and KET were fast (analysis times lower than 10 min) and allow the complete separation of the enantiomers of both NSAIDs (*Rs* = 2.8 for IBU and *Rs* = 1.6 for KET).

The biodegradation process was confirmed by the biomass growth, which was measured by the *OD*₆₀₀. The maximum values of *OD*₆₀₀ were obtained on the fifth day of the biodegradation tests for both NSAIDs. During the stationary/declining growth phase, the differential behaviour of the IBU enantiomers was observed.

The proposed new equations using direct chromatographic information provided similar estimates to those obtained using *S* data. However, the use of *A* data as input variables eliminated the uncertainty associated with calculations derived from calibration curves and provided more precise *BD* and *EF* estimations. The use of *A* data allows for estimating significant parameters related to the biodegradation process: i) the *t*_{1/2} of (*R*)-IBU and (*S*)-IBU were estimated to be 18 and 25 days, respectively, while *t*_{1/2} values of 12 days were estimated for both KET enantiomers; ii) complete *BD* of IBU enantiomers required 60-80 days, meanwhile for KET enantiomers only 25 days are needed, and iii) the *EF* value of IBU decreased to approximately 0.4 at 28 days, being the expected minimum value of around 0.2 at 60 days.

IV.7.- Reversed phase liquid chromatography for the enantioseparation of local anaesthetics in polysaccharide-based stationary phases. Application to biodegradability studies. Paper VII

IV.7.1.- Brief introduction and objectives

LAs are commonly used analgesics that temporarily block the production and transmission of pain signals in nerve tissue. While LAs have a low risk of adverse effects, their systemic toxicity can cause serious harm, such as seizures, heart problems, and even death. The presence in the molecular structures of LAs of an aromatic ring, an ester or amide linkage, and a tertiary amine determines their therapeutic properties. Some of LAs (e.g., BUPI, MEPI, PRILO and PROPA) are chiral compounds. It has been reported differences in the pharmacokinetic, pharmacodynamic and toxicological properties of enantiomers of chiral LAs. For example, the (*R*)-BUPI enantiomer is more potent and toxic than the (*S*)-BUPI enantiomer. Similarly, it has been reported that the (*S*)-PRILO enantiomer exhibits higher toxicity, whereas the (*R*)-PRILO enantiomer is metabolized more efficiently in the liver.

LAs are widely present in the environment, mainly due to their extensive use in hospitals. Previous studies have detected the presence of MEPI, lidocaine, BUPI, PRILO, procaine, and benzocaine in wastewater samples at concentrations of the ng L⁻¹ range. However, there is a lack of research in the literature investigating the possibility of enantioselective biodegradation of these compounds.

In this work, a comprehensive investigation into the chiral separation of four LAs: BUPI, MEPI, PRILO and PROPA, is performed using five cellulose-based and three amylose-based CSPs with hydro-organic MeOH or ACN mobile phases compatible with MS detection. The study compared retention and enantioresolution values obtained for each LA in different CSPs and mobile phases. The results of the study were used to propose the optimal chromatographic experimental conditions for determining the enantiomers of these LAs in aqueous samples using MS detection, in order to perform, for the first time, enantioselective biodegradability assays for *rac*-BUPI, *rac*-MEPI, *rac*-PRILO and *rac*-PROPA. For estimating significant parameters related to the biodegradation process, the direct chromatographic approach proposed in section IV.6 was used.

IV.7.2.- Results and discussion

IV.7.2.1.- Chiral chromatographic separation

The effectiveness of five cellulose-based CSPs (Cell1, Cell2, Cell3, Cell4 and Cell5) and three amylose-based CSPs (Am1, Am2 and Am3) using hydro-organic mobile phases compatible with MS detection, which consist of mixtures of ACN or MeOH and NH₄HCO₃ (5 mM, pH = 8.0) in varying proportion (10-100 % in volume of ACN and 30-90 % in volume of MeOH), at 15-40 °C in separating

the enantiomers of BUPI, MEPI, PRILO and PROPA was evaluated (see Table III.2 for additional information).

At the operational pH , the compounds exhibit a positive charge (+0.55, +0.33, +0.44, and +0.25 for BUPI, MEPI, PRILO and PROPA, respectively), as well as a varying degree of hydrophobicity ($1.6 \leq \log D \leq 4.5$).

The retention of compounds with hydro-organic mobile phases containing ACN or MeOH was quite different. As indicated in sections I.2.1 and IV.2.2.1, when MeOH (protic solvent) was used to prepare hydro-organic mobile phases, for all compounds and CSPs, a typical RPLC behaviour was observed. In contrast, for hydro-organic mobile phases containing ACN (aprotic solvent), dual retention behaviour (HILIC or RPLC) as a function of the water content in the mobile phase was observed. This dual retention behaviour was more pronounced for MEPI and PROPA when Cell3, Cell5 and Am1 CSPs were used. On the other hand, among all the CSPs tested, Cell5 and Am3 showed the highest k values for the four ALs studied.

Polysaccharide-based CSPs assayed exhibited distinct enantioselectivity towards the compounds studied. Figure IV.21 displays the R_s max values achieved with the corresponding mobile phase composition for separating BUPI, MEPI, PRILO, and PROPA enantiomers using the different CSPs and mobile phases investigated. As can be observed, under the tested conditions, baseline enantioresolution of the four ALs studied could not be achieved with a single CSP. In general, the cellulose-based CSPs showed better enantioselectivity for the LAs studied than the amylose-based CSPs. The Cell2 CSP exhibited the highest enantioselectivity, providing R_s max > 1.5 for three out of the four studied compounds (MEPI, PRILO, and PROPA). The Cell4 CSP provided R_s max > 1.5 for two analytes (PRILO and PROPA), while the Cell3, Cell5, and Am1 CSPs only provided R_s max > 1.5 for one of the LAs studied (BUPI, MEPI, and PRILO, respectively). The Cell1, Am2, and Am3 CSPs were not able to baseline enantioseparate any of the LAs studied.

Regarding the mobile phase composition, the use of ACN provided, in general, better R_s max values than MeOH. Except for BUPI where a complete enantioresolution was only achieved with Cell3 CSP and a mobile phase of MeOH:NH₄HCO₃ (5 mM, $pH = 8.0$), 70:30 (v/v).

From the results obtained, the chromatographic conditions for the chiral analysis of samples containing racemic mixtures of the LAs studied in the biodegradability assays were selected taking into account R_s and analysis times. For BUPI and MEPI, mobile phase flow rate and separation temperatures were adjusted to get most adequate conditions for routine analysis. In Table III.2, the selected chromatographic conditions for each compound are shown. Under these conditions, satisfactory R_s and t_R values were obtained for BUPI ($R_s = 1.5$, t_R (R)-BUPI = 7.8 min and t_R (S)-BUPI = 8.5 min), MEPI ($R_s = 2.0$, $t_{R1} = 6.9$ min and $t_{R2} = 7.5$ min), PRILO ($R_s = 1.8$, $t_{R1} = 6.8$ min and $t_{R2} = 7.3$ min) and PROPA ($R_s = 2.0$, $t_{R1} = 10.6$ min and $t_{R2} = 11.7$ min).

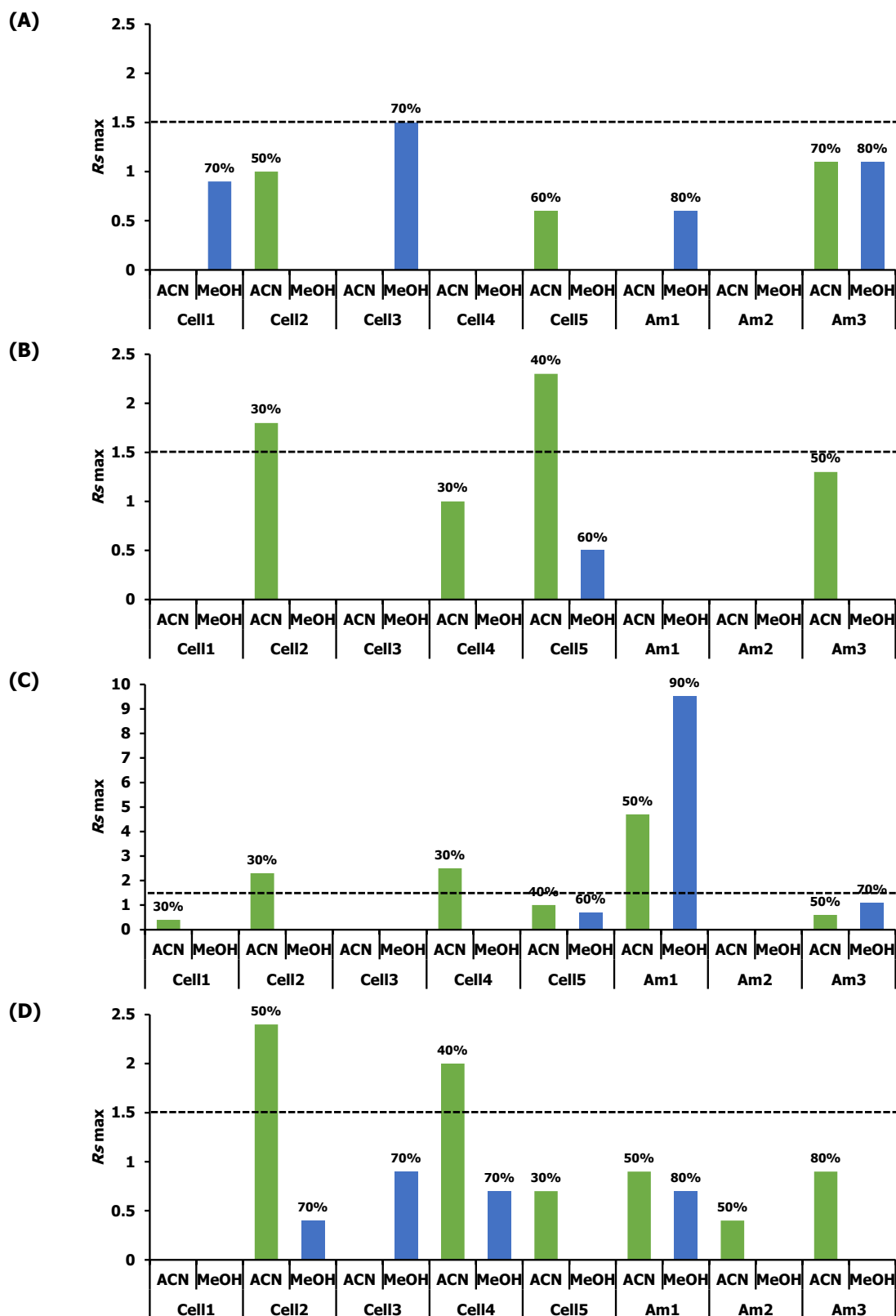


Figure IV.21.- Maximum enantioresolution values ($R_s \max$) obtained for the enantiomers of **(A)** BUPI, **(B)** MEPI, **(C)** PRILO and **(D)** PROPA using different CSPs (Cell1, Cell2, Cell3, Cell4, Cell5, Am1, Am2 and Am3) and mobile phases composed by binary mixtures of (■) ACN or (■) MeOH and NH_4HCO_3 (5 mM, $\text{pH} = 8.0$). The percentage of organic modifier that allows $R_s \max$ is indicated in the Figure. (---) $R_s = 1.5$.

IV.7.2.2.- Biodegradability assays

The biodegradability assays of *rac*-BUPI, *rac*-MEPI, *rac*-PRILO and *rac*-PROPA were performed following the procedure described in section III.3.3. The initial concentrations of the racemic compounds studied were 19.8 mg L⁻¹ for *rac*-BUPI, 20.6 mg L⁻¹ for *rac*-MEPI, 21.0 mg L⁻¹ for *rac*-PRILO and 21.0 mg L⁻¹ for *rac*-PROPA. Simultaneously to LAs assays, biodegradability assays were performed for fluoxetine as in section IV.6 (20 mg L⁻¹; target value $BD_{7d} = 70 \pm 11 \%$, in this work $BD_{7d} = 69 \pm 12 \%$). In view of the results obtained, the activity of the inoculum was considered adequate, and the biodegradability assays for *rac*-BUPI, *rac*-MEPI, *rac*-PRILO and *rac*-PROPA were valid. Measurements of OD_{600} values were also monitored to control the growth of microorganisms in the inoculum.

For estimating significant parameters related to the biodegradation process (S , BD and EF), the direct chromatographic approach proposed in section IV.6 was used. As it was indicated in that section, to apply this strategy it is necessary to verify some assumptions related with calibration curves of the enantiomers of a given compound.

Using the selected chromatographic conditions for each compound, methodological calibration (5 concentration levels, 1-30 mg L⁻¹ concentration range of racemic compound) was performed. The calibration statistics obtained for the enantiomers of the compounds studied showed adequate results ($R^2 > 0.997$) and the intercept ($b_{0,E1}$ and $b_{0,E2}$) values were statistically equal to 0, so Eq. IV.6 for BD calculations can be used. For both enantiomers of PRILO and PROPA, the slopes ($b_{1,E1}$ and $b_{1,E2}$) were statistically equivalent; therefore Eq. IV.7 for EF calculations can be used. However, for BUPI and MEPI enantiomers, differences statistically significant in the $b_{1,E1}$ and $b_{1,E2}$ values were found; so EF values were calculated from their concentration values (Eq. I.1).

Figure IV.22 shows the abiotic degradation (AD) and BD values estimated from the biodegradability assays for the enantiomers of BUPI, MEPI, PRILO and PROPA. Their EF values are also shown.

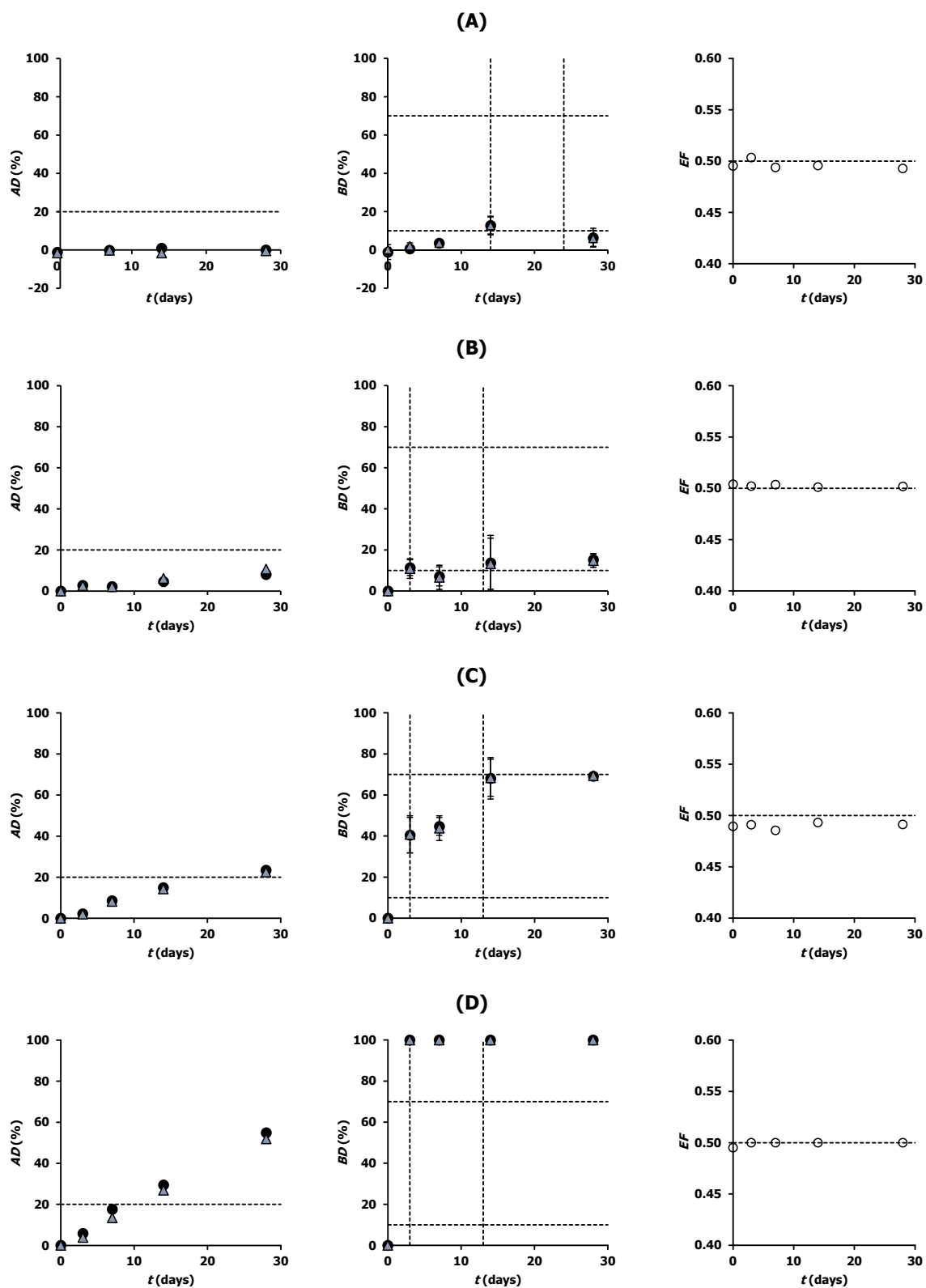


Figure IV.22.- AD (%), BD (mean \pm s , %) and EF values estimated during the biodegradability assays for **(A)** BUPI, **(B)** MEPI, **(C)** PRILO and **(D)** PROPA. (\bullet) less retained enantiomer; (Δ) most retained enantiomer. The dotted line at $AD = 20$ % represents the minimum value to consider significant abiotic degradation (OECD criterion). The dotted lines in the $BD - t$ plots represent the approximate 10-day window to assess persistence (OECD criterion). The dashed line at $EF = 0.5$ indicates non-enantioselective biodegradation.

For the enantiomers of BUPI (Figure IV.22.A) and MEPI (Figure IV.22.B), the estimated degradation at 28 days of incubation for the biotic and abiotic assays were lower than 20 %; consequently, the BUPI and MEPI enantiomers are “potentially persistent compounds” in agreement with the OECD guidelines. These results should be confirmed by simulation or inherent biodegradability (see section I.5.1).

In contrast, for PRILO enantiomers (Figure IV.22.C), microbiological and physicochemical degradation at 28 days was incomplete but notable (~ 69 % and 23 % for biotic and abiotic assays, respectively). For PROPA enantiomers (Figure IV.22.D), *BD* ~ 100 % was observed in three days. Regarding the abiotic tests, the physicochemical degradation was not significant (*AD* < 20 %) up to 14 days and reached ~ 53 % after 28 days of incubation. According to the OECD guidelines, the PRILO and PROPA enantiomers show “ready aerobic biodegradability”. For both compounds, the *EF* values were close to 0.5 during the course of the biodegradability assay, indicating the absence of enantioselective mechanisms in the biodegradation processes.

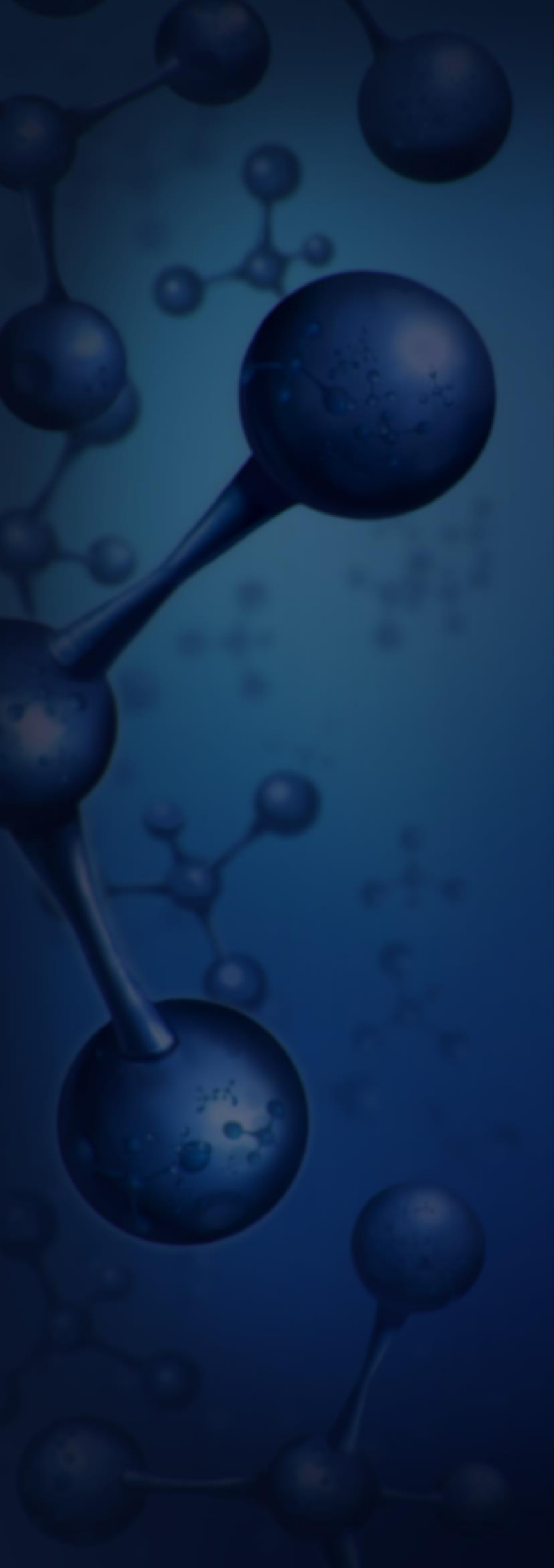
IV.7.3.- Conclusions

The study about the effectiveness of five cellulose-based CSPs (Cell1, Cell2, Cell3, Cell4 and Cell5) and three amylose-based CSPs (Am1, Am2, Am3) and hydro-organic mobile phases compatible with MS detection in separating the enantiomers of BUPI, MEPI, PRILO and PROPA revealed that for hydro-organic mobile phases containing MeOH, the compounds show a typical RPLC behaviour. Meanwhile for mobile phases containing ACN, the compounds shown HILIC- or RPLC-behaviour, as a function of water content in the mobile phase.

The enantioselectivity of the CSPs tested towards BUPI, MEPI, PRILO and PROPA enantiomers was different. The Cell2 CSP allows the complete enantioresolution of MEPI, PRILO and PROPA, while the CSPs Cell1, Am2 and Am3 did not allow the enantioresolution of the compounds studied.

From the systematic retention and enantioresolution study, the selected experimental conditions for the separation of BUPI, MEPI, PRILO and PROPA enantiomers in enantioselective biodegradation assays allow analysis times less than 15 min and the complete separation (*Rs* ≥ 1.5) of the enantiomers of the compounds studied.

From the biodegradability assays, in agreement with the OECD guidelines, the enantiomers of PRILO and PROPA exhibit ready aerobic biodegradability. However, the enantiomers of BUPI and MEPI are expected to be persistent compounds. Additionally, the enantiomers of BUPI, MEPI, PRILO and PROPA do not exhibit enantioselective biodegradation under the conditions assayed. The *EF* values were close to 0.50 during the whole biodegradation test.



V.- GENERAL CONCLUSIONS AND FUTURE STUDIES

- The studies presented in section IV.1 - IV.3 (Paper I - Paper III) comprise nearly 5300 experiments that include 53-56 structurally unrelated basic and neutral compounds, eight of the most commonly used commercial polysaccharide-based CSPs (three amylose derivatives: Am1, Am2 and Am3; and five cellulose derivatives: Cell1, Cell2, Cell3, Cell4 and Cell5) and hydro-organic mobile phases compatible with aqueous matrices and MS detection consisting of mixtures of NH_4HCO_3 (5 mM, $\text{pH} = 8.0$) and ACN or MeOH in varying proportions. From the results obtained in these studies, it is possible to draw the following general conclusions:

- Comparative exploratory studies on retention factor data as well as on enantioresolution data demonstrate that, under the experimental conditions assayed:

All compounds show a characteristic RPLC retention behaviour in all the CSPs studied, except when using mobile phases containing the aprotic solvent ACN in the range of 80-98 % and cellulose-based CSPs, where a HILIC retention behaviour exists, which in general significantly reduces the enantioresolution. This HILIC retention behaviour is not observed in the amylose-based CSPs studied, probably due to the lower ACN percentages used.

The ACN-Am1 and ACN-Am3 chromatographic systems show a reasonably broad and complementary enantioresolution ability, but the ACN-Am2 system do not.

The recommended screening sequence for cellulose-based chromatographic systems, taking into account the success rate and complementarity of the enantioresolution data obtained in these systems is as follows: ACN-Cell2 in the RPLC-domain as a first attempt, followed by MeOH-Cell3, then ACN-Cell5 in the RPLC-domain, next ACN-Cell1 in the RPLC-domain, and finally other chromatographic systems. HILIC-domain is not advisable, at least as a first attempt, taking into account the enantioresolution results obtained, as well as the cost and toxicity of the mobile phases.

- DPLS1 and ANNs have demonstrated to be successful multivariate chemometric tools for QSPR modelling of enantioresolution-related parameters, which are really complex data considering the relatively large dataset used, the diversity of compound structures and enantiomer-chromatographic system interactions, as well as the complexity of enantioresolution over other chromatographic parameters.

Moreover, these chemometric techniques have proven to be effective for the development of automated strategies for FS, an essential feature in QSPR studies for the sake of model simplicity and interpretability.

The QSPR models have been developed for categorical enantioresolution in ACN-Am1 and ACN-Am3 using FS-DPLS1; and for quantitative enantioresolution in ACN-Cell1 using FS-ANNs. The use of quantitative rather than categorical data demonstrates the superiority of ANNs over PLS for modelling complex data.

The fastest and most economical way to try to separate the enantiomers of a new basic or neutral chiral compound in the chromatographic systems studied in this Doctoral Thesis is first to use the QSPR models developed to estimate whether their baseline enantioresolution in the modelled chromatographic systems is *a priori* feasible or not.

The above conclusions have been derived from data on 53-56 structurally unrelated basic and neutral compounds and can, therefore, be considered to be of general applicability to this type of compounds in the chromatographic systems assayed. In our opinion, they represent a valuable contribution to the knowledge of chiral HPLC with polysaccharide-based CSPs, which can assist researchers in the rational selection of the most suitable chromatographic system to achieve satisfactory enantioresolution results for a new basic or neutral compound, which in turn could significantly reduce the cost and experimental effort required by the current trial-and-error methodologies.

However, extensive research is still needed to deepen the understanding of the enantiorecognition ability of polysaccharide-based CSPs. Currently, our research group has already obtained experimental data on amylose-based CSPs using MeOH mobile phases as well as ACN mobile phases in the HILIC domain. Exploratory comparative studies are underway to complete the screening sequence proposed above. In addition, FS-ANN QSPR models are being developed for other chromatographic systems.

- The results presented in section IV.4 (Paper IV) –involving the enantioseparation of eight chiral drugs (bupivacaine, flurbiprofen, ibuprofen, ketoprofen, metoprolol, omeprazole, propranolol and trimeprazine) under several chromatographic conditions (a total of 20 experiments carried out in five different polysaccharide-based CSPs using different ACN or MeOH hydro-organic mobile phases with different compositions, *pH* values and separation temperatures); and therefore, including chromatographic peaks with different efficiency, skewness and enantioresolution values– demonstrate that PVMG models with the proposed sigmoidal function correction for proper peak shape adjustment (approach IIc) is a simple and reliable strategy for the simultaneous fitting of chromatographic peaks (with a wide range of characteristics) of the enantiomers of chiral compounds. This suggests that the proposed approach could be an effective strategy for estimating chromatographic peak profiles at different retention times and peak overlapping. These estimations could be really useful in the decision making process on the mobile phase composition to achieve the maximum enantioresolution in a given chromatographic system (CSP/organic solvent combination) for a given chiral compound. Therefore, as in the above-indicated studies, it could be a valuable tool to save time and money in chiral HPLC research by contributing to a rational chromatographic system selection.

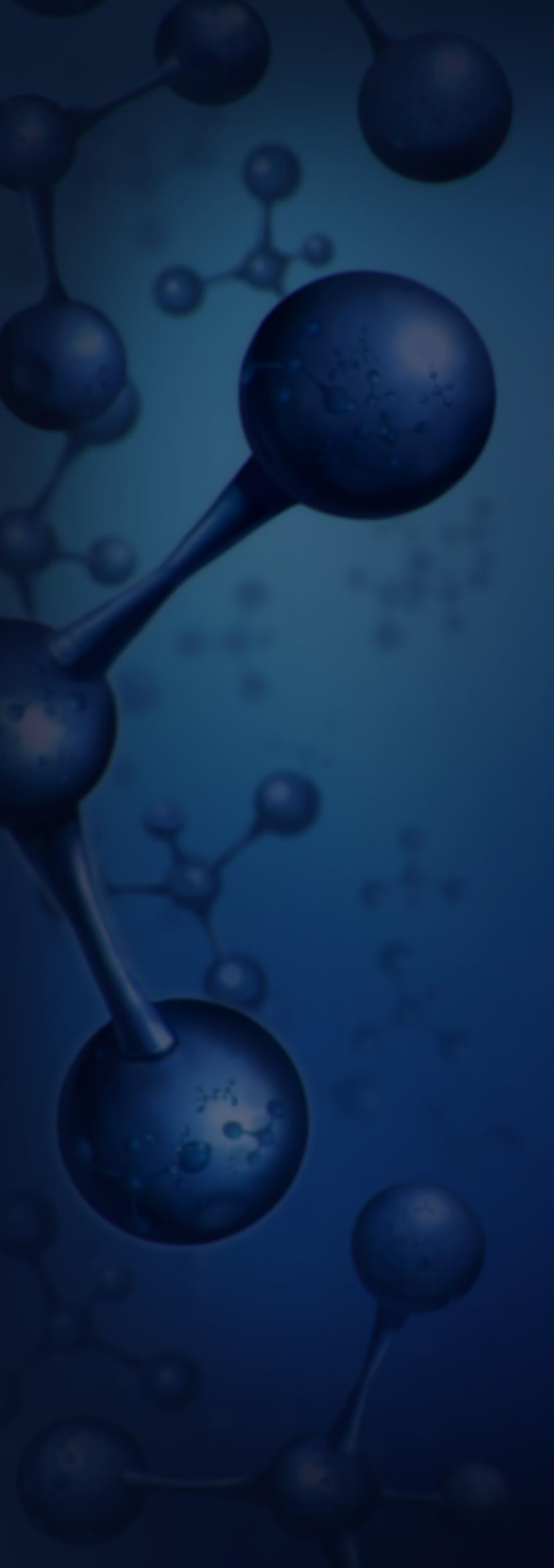
This approach has also proven to be useful to deconvolve partially overlapped peaks with non-marginal enantioresolution (i.e., $R_s \geq 1.0$). This makes it very helpful in chiral HPLC to achieve the mathematical resolution when the baseline resolution cannot be achieved experimentally.

Peaks with marginal enantioresolution require further investigation of peak shape variations. A procedure for keeping EF values constant in the deconvolution procedure should also be devised. The performance of the models should be further evaluated for non-racemic mixtures.

- The results of the OECD biodegradability tests using an activated sludge from Quart Benàger WWTP presented in section IV.5 - IV.7 (Paper V - VII) have proven that biodegradation is enantioselective for ibuprofen and, for the first time, for trimeprazine; but not for bupivacaine, ketoprofen, mepivacaine, prilocaine and propanocaine at least under the experimental conditions assayed. These results highlight the need for such studies for a reliable risk and hazard assessment of chiral pollutants.

Moreover, the enantiomers of ibuprofen, ketoprofen, prilocaine and propanocaine exhibited ready aerobic biodegradability ($BD > 70\%$ in a 10-day window within a 28-day test), whereas the enantiomers of bupivacaine, mepivacaine and trimeprazine are potentially persistent compounds ($BD < 70\%$ in a 10-day window within a 28-day test), although these results should be confirmed by simulation or inherent biodegradability tests.

Finally, the use of peak area instead of substrate concentration data in Michaelis-Menten-like kinetic models has proven to improve the precision of BD and EF estimates.



VI.- REFERENCES

- [1] N.M. Maier, P. Franco, W. Lindner, Separation of enantiomers: needs, challenges, perspectives, *J. Chromatogr. A* 906 (2001) 3-33. [https://doi.org/10.1016/S0021-9673\(00\)00532-X](https://doi.org/10.1016/S0021-9673(00)00532-X)
- [2] M. Friedman, Chemistry, nutrition, and microbiology of D-amino acids, *J. Agric. Food Chem.* 47 (1999) 3457-3479. <https://doi.org/10.1021/jf990080u>
- [3] M.L.R. del Castillo, M.M. Caja, M. Herraiz, G.P. Blanch, Rapid recognition of olive oil adulterated with hazelnut oil by direct analysis of the enantiomeric composition of Filbertone, *J. Agric. Food Chem.* 46 (1998) 5128-5131. <https://doi.org/10.1021/jf9807014>
- [4] F. Podebrad, M. Heil, S. Leib, B. Geier, T. Beck, A. Mosandl, A. C. Sewell, H. Böhles, Analytical approach in diagnosis of inherited metabolic diseases: Maple Syrup Urine Disease (MSUD)–simultaneous analysis of metabolites in urine by enantioselective multidimensional capillary gas chromatography-mass spectrometry (enantio-MDGC-MS), *J. High Resol. Chromatogr.* 20 (1997) 355-362. <https://doi.org/10.1002/jhrc.1240200703>
- [5] Z. Peng, L. Yuan, J. XuHong, H. Tian, Y. Zhang, J. Deng, X. Qi, Chiral nanomaterials for tumor therapy: autophagy, apoptosis, and photothermal ablation, *J. Nanobiotechnol.* 19 (2021) 1-13. <https://doi.org/10.1186/s12951-021-00965-7>
- [6] Y. Teng, C. Gu, Z. Chen, H. Jiang, Y. Xiong, D. Liu, D. Xiao, Advances and applications of chiral resolution in pharmaceutical field, *Chirality* 34 (2022) 1094-1119. <https://doi.org/10.1002/chir.23453>
- [7] G. Hancu, A. Modroiu, Chiral switch: between therapeutical benefit and marketing strategy, *Pharmaceuticals* 15 (2022) 240. <https://doi.org/10.3390/ph15020240>
- [8] I.W. Wainer, *Drug stereochemistry: analytical methods and pharmacology*, second ed., Marcel Dekker, New York, 1993.
- [9] E.J. Ariëns, Stereochemistry: a source of problems in medicinal chemistry, *Med. Res. Rev.* 6 (1986) 451-466. <https://doi.org/10.1002/med.2610060404>
- [10] D.R. Brocks, Drug disposition in three dimensions: an update on stereoselectivity in pharmacokinetics, *Biopharm. Drug Dispos.* 27 (2006) 387-406. <https://doi.org/10.1002/bdd.517>
- [11] M.M. Coelho, C. Fernandes, F. Remião, M.E. Tiritan, Enantioselectivity in drug pharmacokinetics and toxicity: pharmacological relevance and analytical methods, *Molecules* 26 (2021) 3113. <https://doi.org/10.3390/molecules26113113>
- [12] A.K. Pal, B. Bahadur, Chirality in nature and biomolecules: an overview, *LS-Int. J. Life Sci.* 9 (2020) 72-84. <https://doi.org/10.5958/2319-1198.2020.00004.4>

- [13] S. Grybinik, Z. Bosakova, An overview of chiral separations of pharmaceutically active substances by HPLC (2018–2020), *Mon. Chem.* 152 (2021) 1033-1043. <https://doi.org/10.1007/s00706-021-02832-5>
- [14] L.A. Nguyen, H. He, C. Pham-Huy, Chiral drugs: an overview, *Int. J. Biomed. Sci. (IJBS)* 2 (2006) 85-100. PMID: 23674971
- [15] J. Caldwell, Chiral pharmacology and the regulation of new drugs, *Chem. Ind.* 5 (1995) 176-178.
- [16] A.A. Basheer, Chemical chiral pollution: impact on the society and science and need of the regulations in the 21st century, *Chirality* 30 (2018) 402-406. <https://doi.org/10.1002/chir.22808>
- [17] B. Kasprzyk-Hordern, Pharmacologically active compounds in the environment and their chirality, *Chem. Soc. Rev.* 39 (2010) 4466-4503. <https://doi.org/10.1039/C000408C>
- [18] A.R. Ribeiro, L.H.M.L.M. Santos, A.S. Maia, C. Delerue-Matos, P.M.L. Castro, M.E. Tiritan, Enantiomeric fraction evaluation of pharmaceuticals in environmental matrices by liquid chromatography-tandem mass spectrometry, *J. Chromatogr. A* 1363 (2014) 226-235. <https://doi.org/10.1016/j.chroma.2014.06.099>
- [19] I. Ali, H.Y. Aboul-Enein, M.M. Sanagi, W.A.W. Ibrahim, Chirality and its role in environmental toxicology, in: A. Luch (Eds.), *Molecular, clinical and environmental toxicology. Experientia supplementum*, Springer Basel AG, Basel, 2012, pp. 413-436.
- [20] K. Möller, H. Hühnerfuss, D. Wölfle, Differential effects of the enantiomers of α -hexachlorocyclohexane (α -HCH) on cytotoxicity and growth stimulation in primary rat hepatocytes, *Organohalogen Compds.* 29 (1996) 357-360.
- [21] A. Miyazaki, T. Hotta, S. Marumo, M. Sakai, Synthesis, absolute chemistry, and biological activity of optically active cyclodiene insecticides, *J. Agric. Food Chem.* 26 (1978) 975-977. <https://doi.org/10.1021/jf60218a017>
- [22] A. Miyazaki, M. Sakai, S. Marumo, Synthesis and biological activity of optically active heptachlor, 2-chloroheptachlor, and 3-chloroheptachlor, *J. Agric. Food Chem.* 28 (1980) 1310-1311. <https://doi.org/10.1021/jf60232a036>
- [23] M. Blanco, I. Valverde, Choice of chiral selector for enantioseparation by capillary electrophoresis, *TrAC-Trends Anal. Chem.* 22 (2003) 428-439. [https://doi.org/10.1016/S0165-9936\(03\)00705-2](https://doi.org/10.1016/S0165-9936(03)00705-2)
- [24] T.J. Ward, D.M. Hamburg, Chiral separations, *Anal. Chem.* 76 (2004) 4635-4644. <https://doi.org/10.1021/ac040093t>

- [25] G.K.E. Scriba, Chiral recognition in separation science-an update, *J. Chromatogr. A* 1467 (2016) 56-78. <https://doi.org/10.1016/j.chroma.2016.05.061>
- [26] G.K.E. Scriba, Recognition mechanisms of chiral selectors: an overview, in: G.K.E. Scriba (Eds.), *Chiral separations. Methods in molecular biology*, Humana, New York, 2019, pp. 1-33.
- [27] J.H. Zhang, S.M. Xie, L.M. Yuan, Recent progress in the development of chiral stationary phases for high-performance liquid chromatography, *J. Sep. Sci.* 45 (2022) 51-77. <https://doi.org/10.1002/jssc.202100593>
- [28] S. Ahuja, *Chiral separation methods for pharmaceutical and biotechnological products*, first ed., John Wiley & Sons Inc., Hoboken, 2011.
- [29] I. Ali, H.Y. Aboul-Enein, *Chiral pollutants: distribution, toxicity and analysis by chromatography and capillary electrophoresis*, first ed., John Wiley & Sons, Chichester, 2004.
- [30] M. Lämmerhofer, Chiral recognition by enantioselective liquid chromatography: mechanisms and modern chiral stationary phases, *J. Chromatogr. A* 1217 (2010) 814-856. <https://doi.org/10.1016/j.chroma.2009.10.022>
- [31] J. Teixeira, M.E. Tiritan, M.M.M. Pinto, C. Fernandes, Chiral stationary phases for liquid chromatography: recent developments, *Molecules* 24 (2019) 865. <https://doi.org/10.3390/molecules24050865>
- [32] G. D'Orazio, Chiral analysis by nano-liquid chromatography, *TrAC-Trends Anal. Chem.* 125 (2020) 115832. <https://doi.org/10.1016/j.trac.2020.115832>
- [33] M. Del Bubba, L. Checchini, L. Lepri, Thin-layer chromatography enantioseparations on chiral stationary phases: a review, *Anal. Bioanal. Chem.* 405 (2013) 533-554. <https://doi.org/10.1007/s00216-012-6514-5>
- [34] R. Dubey, R. Bhushan, Enantioseparation by thin-layer chromatography, in: G.K.E. Scriba (Eds.), *Chiral separations. Methods in molecular biology*, Humana, New York, 2019, pp. 35-44.
- [35] S.M. Xie, J.H. Zhang, L.M. Yuan, Enantioseparations by gas chromatography using porous organic cages as stationary phase, in: G.K.E. Scriba (Eds.), *Chiral separations. Methods in molecular biology*, Humana, New York, 2019, pp. 45-55.
- [36] G. Betzenbichler, L. Huber, S. Kräh, M.L.K. Morkos, A. F. Siegle, O. Trapp, Chiral stationary phases and applications in gas chromatography, *Chirality* 34 (2022) 732-759. <https://doi.org/10.1002/chir.23427>
- [37] G. Roskam, B. van de Velde, A. Gargano, I. Kohler, Supercritical fluid chromatography for chiral analysis, part 1: theoretical background, *LCGC Europe* 35 (2022) 83-92.

- [38] G. Roskam, B. van de Velde, I. Kohler, Supercritical fluid chromatography for chiral analysis, part 2: applications, *LCGC Europe* 35 (2022) 118-129.
- [39] S. Bernardo-Bermejo, E. Sánchez-López, M. Castro-Puyana, M.L. Marina, Chiral capillary electrophoresis, *TrAC-Trends Anal. Chem.* 124 (2020) 115807. <https://doi.org/10.1016/j.trac.2020.115807>
- [40] C. Fanali, Enantiomers separation by capillary electrochromatography, *TrAC-Trends Anal. Chem.* 120 (2019) 115640. <https://doi.org/10.1016/j.trac.2019.115640>
- [41] S. Krait, M.L. Konjaria, G.K.E. Scriba, Advances of capillary electrophoresis enantioseparations in pharmaceutical analysis (2017–2020), *Electrophoresis* 42 (2021) 1709-1725. <https://doi.org/10.1002/elps.202000359>
- [42] S.A. Shamsi, F. Akter, Capillary electrophoresis mass spectrometry: developments and applications for enantioselective analysis from 2011–2020, *Molecules* 27 (2022) 4126. <https://doi.org/10.3390/molecules27134126>
- [43] G.M. Henderson, H.G. Rule, A new method of resolving a racemic compound, *Nature* 141 (1938) 917-918. <https://doi.org/10.1038/141917b0>
- [44] L. Escuder-Gilabert, Y. Martín-Biosca, M.J. Medina-Hernández, S. Sagrado, Cyclodextrins in capillary electrophoresis: recent developments and new trends, *J. Chromatogr. A* 1357 (2014) 2-23. <https://doi.org/10.1016/j.chroma.2014.05.074>
- [45] G.K.E. Scriba, Chiral recognition in separation sciences. Part I: polysaccharide and cyclodextrin selectors, *TrAC-Trends Anal. Chem.* 120 (2019) 115639. <https://doi.org/10.1016/j.trac.2019.115639>
- [46] P. Peluso, B. Chankvetadze, Native and substituted cyclodextrins as chiral selectors for capillary electrophoresis enantioseparations: structures, features, application, and molecular modelling, *Electrophoresis* 42 (2021) 1676-1708. <https://doi.org/10.1002/elps.202100053>
- [47] A. Harada, M. Furue, S.I. Nozakura, Optical resolution of mandelic acid derivatives by column chromatography on crosslinked cyclodextrin gels, *J. Polym. Sci.: Polym. Chem. Ed.* 16 (1978) 189-196. <https://doi.org/10.1002/pol.1978.170160119>
- [48] D.W. Armstrong, Y. Tang, S. Chen, Y. Zhou, C. Bagwill, J.R. Chen, Macrocyclic antibiotics as a new class of chiral selectors for liquid chromatography, *Anal. Chem.* 66 (1994) 1473-1484. <https://doi.org/10.1021/ac00081a019>
- [49] G.K.E. Scriba, Chiral recognition in separation sciences. Part II: macrocyclic glycopeptide, donor-acceptor, ion-exchange, ligand-exchange and micellar selectors, *TrAC-Trends Anal. Chem.* 119 (2019) 115628. <https://doi.org/10.1016/j.trac.2019.115628>

- [50] W.H. Pirkle, D.W. House, Chiral high-pressure liquid chromatographic stationary phases. 1. Separation of the enantiomers of sulfoxides, amines, amino acids, alcohols, hydroxy acids, lactones, and mercaptans, *J. Org. Chem.* 44 (1979) 1957-1960. <https://doi.org/10.1021/jo01326a014>
- [51] C. Fernandes, Y.Z. Phyto, A.S. Silva, M.E. Tiritan, A. Kijjoa, M.M.M. Pinto, Chiral stationary phases based on small molecules: an update of the last 17 years, *Sep. Purif. Rev.* 47 (2018) 89-123. <https://doi.org/10.1080/15422119.2017.1326939>
- [52] C. Rosini, C. Bertucci, D. Pini, P. Altemura, P. Salvadori, Cinchona alkaloids for preparing new, easily accessible chiral stationary phases.I. 11-(10,11-Dihydro-6'-methoxy-cinchonan-9-OL)-tiopropylsilanized silica, *Tetrahedron Lett.* 26 (1985) 3361-3364. [https://doi.org/10.1016/S0040-4039\(00\)98298-4](https://doi.org/10.1016/S0040-4039(00)98298-4)
- [53] M. Lämmerhofer, W. Lindner, Quinine and quinidine derivatives as chiral selectors I. Brush type chiral stationary phases for high-performance liquid chromatography based on cinchonan carbamates and their application as chiral anion exchangers, *J. Chromatogr. A* 741 (1996) 33-48. [https://doi.org/10.1016/0021-9673\(96\)00137-9](https://doi.org/10.1016/0021-9673(96)00137-9)
- [54] I. Ilisz, A. Bajtai, W. Lindner, A. Péter, Liquid chromatographic enantiomer separations applying chiral ion-exchangers based on *Cinchona* alkaloids, *J. Pharm. Biomed. Anal.* 159 (2018) 127-152. <https://doi.org/10.1016/j.jpba.2018.06.045>
- [55] V.A. Davankov, S.V. Rogozhin, Ligand chromatography as a novel method for the investigation of mixed complexes: stereoselective effects in α -amino acid copper(II) complexes, *J. Chromatogr. A* 60 (1971) 280-283. [https://doi.org/10.1016/S0021-9673\(00\)95566-3](https://doi.org/10.1016/S0021-9673(00)95566-3)
- [56] F. Ianni, L. Pucciarini, A. Carotti, S. Natalini, G.Z. Raskildina, R. Sardella, B. Natalini, Last ten years (2008–2018) of chiral ligand-exchange chromatography in HPLC: an updated review, *J. Sep. Sci.* 42 (2019) 21-37. <https://doi.org/10.1002/jssc.201800724>
- [57] G. Dotsevi, Y. Sogah, D.J. Cram, Chromatographic optical resolution through chiral complexation of amino ester salts by a host covalently bound to silica gel, *J. Am. Chem. Soc.* 97 (1975) 1259-61. <https://doi.org/10.1021/ja00838a059>
- [58] J.P. Behr, J.M. Girodeau, R.C. Hayward, J.M. Lehn, J.P. Sauvage, Molecular receptors. Functionalized and chiral macrocyclic polyethers derived from tartaric acid, *Helv. Chim. Acta* 63 (1980) 2096-2111. <https://doi.org/10.1002/hlca.19800630736>
- [59] R. Berkecz, G. Némethi, A. Péter, I. Ilisz, Liquid chromatographic enantioseparations utilizing chiral stationary phases based on crown ethers and cyclofructans, *Molecules* 26 (2021) 4648. <https://doi.org/10.3390/molecules26154648>

- [60] K.K. Stewart, R.F. Doherty, Resolution of DL-tryptophan by affinity chromatography on bovine-serum albumin-agarose columns, *Proc. Natl. Acad. Sci. U.S.A.* 70 (1973) 2850-2852. <https://doi.org/10.1073/pnas.70.10.2850>
- [61] J. Haginaka, Progress in chiral stationary phases based on proteins and glycoproteins, *Chem. Pharm. Bull.* 70 (2022) 458-468. <https://doi.org/10.1248/cpb.c22-00269>
- [62] J. Shen, Y. Okamoto, Efficient separation of enantiomers using stereoregular chiral polymers, *Chem. Rev.* 116 (2016) 1094-1138. <https://doi.org/10.1021/acs.chemrev.5b00317>
- [63] M. Kotake, T. Sakan, N. Nakamura, S. Senoh, Resolution into optical isomers of some amino acids by paper chromatography, *J. Am. Chem. Soc.* 73 (1951) 2973-2974. <https://doi.org/10.1021/ja01150a548>
- [64] Y. Okamoto, M. Kawashima, K. Hatada, Useful chiral packing materials for high-performance liquid chromatographic resolution of enantiomers: phenylcarbamates of polysaccharides coated on silica gel, *J. Am. Chem. Soc.* 106 (1984) 5357-5359. <https://doi.org/10.1021/ja00330a057>
- [65] A. Ichida, T. Shibata, I. Okamoto, Y. Yuki, H. Namikoshi, Y. Toda, Resolution of enantiomers by HPLC on cellulose derivatives, *Chromatographia* 19 (1984) 280-284. <https://doi.org/10.1007/BF02687754>
- [66] Y. Okamoto, M. Kawashima, K. Hatada, Chromatographic resolution : XI. Controlled chiral recognition of cellulose triphenylcarbamate derivatives supported on silica gel, *J. Chromatogr. A* 363 (1986) 173-186. [https://doi.org/10.1016/S0021-9673\(01\)83736-5](https://doi.org/10.1016/S0021-9673(01)83736-5)
- [67] Y. Okamoto, R. Aburatani, T. Fukumoto, K. Hatada, Useful chiral stationary phases for HPLC. Amylose tris(3,5-dimethylphenylcarbamate) and tris(3,5-dichlorophenylcarbamate) supported on silica gel, *Chem. Lett.* 16 (1987) 1857-1860. <https://doi.org/10.1246/cl.1987.1857>
- [68] Y. Okamoto, Y. Kaida, R. Aburatani, K. Hatada, Chromatographic optical resolution on polysaccharide carbamate phases, in: S. Ahuja (Eds.), *Chiral separations by liquid chromatography*, ACS Symposium Series, Washington D.C., 1991, pp. 101-113.
- [69] Y. Okamoto, J. Noguchi, E. Yashima, Enantioseparation on 3,5-dichloro- and 3,5-dimethylphenylcarbamates of polysaccharides as chiral stationary phases for high-performance liquid chromatography, *React. Funct. Polym.* 37 (1998) 183-188. [https://doi.org/10.1016/S1381-5148\(97\)00135-1](https://doi.org/10.1016/S1381-5148(97)00135-1)

- [70] T. Ikai, C. Yamamoto, M. Kamigaito, Y. Okamoto, Enantioseparation by HPLC using phenylcarbonate, benzoylformate, p-toluenesulfonylcarbamate, and benzoylcarbammates of cellulose and amylose as chiral stationary phases, *Chirality* 17 (2005) 299-304. <https://doi.org/10.1002/chir.20168>
- [71] B. Chankvetadze, Recent developments on polysaccharide-based chiral stationary phases for liquid-phase separation of enantiomers, *J. Chromatogr. A* 1269 (2012) 26-51. <https://doi.org/10.1016/j.chroma.2012.10.033>
- [72] P. Peluso, V. Mamane, S. Cossu, Liquid chromatography enantioseparations of halogenated compounds on polysaccharide-based chiral stationary phases: role of halogen substituents in molecular recognition, *Chirality* 27 (2015) 667-684. <https://doi.org/10.1002/chir.22485>
- [73] X. Chen, C. Yamamoto, Y. Okamoto, Polysaccharide derivatives as useful chiral stationary phases in high-performance liquid chromatography, *Pure Appl. Chem.* 79 (2007) 1561-1573. <https://doi.org/10.1351/pac200779091561>
- [74] J.M. Padró, S. Keunchkarian, State-of-the-art and recent developments of immobilized polysaccharide-based chiral stationary phases for enantioseparations by high-performance liquid chromatography (2013–2017), *Microchem. J.* 140 (2018) 142-157. <https://doi.org/10.1016/j.microc.2018.04.017>
- [75] P. Peluso, V. Mamane, R. Dallochio, A. Dessì, S. Cossu, Noncovalent interactions in high-performance liquid chromatography enantioseparations on polysaccharide-based chiral selectors, *J. Chromatogr. A* 1623 (2020) 461202. <https://doi.org/10.1016/j.chroma.2020.461202>
- [76] T. Ikai, Y. Okamoto, Structure control of polysaccharide derivatives for efficient separation of enantiomers by chromatography, *Chem. Rev.* 109 (2009) 6077-6101. <https://doi.org/10.1021/cr8005558>
- [77] P. Peluso, V. Mamane, E. Aubert, S. Cossu, Insights into the impact of shape and electronic properties on the enantioseparation of polyhalogenated 4,4'-bipyridines on polysaccharide-type selectors. Evidence for stereoselective halogen bonding interactions, *J. Chromatogr. A* 1345 (2014) 182-192. <https://doi.org/10.1016/j.chroma.2014.04.040>
- [78] P. Peluso, V. Mamane, E. Aubert, A. Dessì, R. Dallochio, A. Dore, P. Pale, S. Cossu, Insights into halogen bond-driven enantioseparations, *J. Chromatogr. A* 1467 (2016) 228-238. <https://doi.org/10.1016/j.chroma.2016.06.007>
- [79] P. Peluso, C. Gatti, A. Dessì, R. Dallochio, R. Weiss, E. Aubert, P. Pale, S. Cossu, V. Mamane, Enantioseparation of fluorinated 3-arylthio-4,4'-bipyridines: insights into chalcogen and π -hole bonds in high-performance liquid chromatography, *J. Chromatogr. A* 1567 (2018) 119-129. <https://doi.org/10.1016/j.chroma.2018.06.060>

- [80] R. Geryk, K. Kalíková, J. Vozka, E. Tesařová, Immobilized polysaccharide-based stationary phases for enantioseparation in normal versus reversed phase HPLC, *Chromatographia* 78 (2015) 909-915. <https://doi.org/10.1007/s10337-014-2804-8>
- [81] B. Chankvetadze, Recent trends in preparation, investigation and application of polysaccharide-based chiral stationary phases for separation of enantiomers in high-performance liquid chromatography, *TrAC-Trends Anal. Chem.* 122 (2020) 115709. <https://doi.org/10.1016/j.trac.2019.115709>
- [82] B. Chankvetadze, Polysaccharide-based chiral stationary phases for enantioseparations by high-performance liquid chromatography: an overview, in: G.K.E. Scriba (Eds.), *Chiral separations. Methods in molecular biology*, Humana, New York, 2019, pp. 93-126.
- [83] B. Chankvetadze, C. Yamamoto, Y. Okamoto, Enantioseparation of selected chiral sulfoxides using polysacchride-type chiral stationary phases and polar organic, polar aqueous-organic and normal-phase eluents, *J. Chromatogr. A* 922 (2001) 127-137. [https://doi.org/10.1016/S0021-9673\(01\)00958-X](https://doi.org/10.1016/S0021-9673(01)00958-X)
- [84] I. Matarashvili, D. Ghughunishvili, L. Chankvetadze, N. Takaishvili, T. Khatiashvili, M. Tsintsadze, T. Farkas, B. Chankvetadze, Separation of enantiomers of chiral weak acids with polysaccharide-based chiral columns and aqueous-organic mobile phases in high-performance liquid chromatography: typical reversed-phase behavior?, *J. Chromatogr. A* 1483 (2017) 86-92. <https://doi.org/10.1016/j.chroma.2016.12.064>
- [85] G. Jibuti, A. Mskhiladze, N. Takaishvili, M. Karchkhadze, L. Chankvetadze, T. Farkas, B. Chankvetadze, HPLC separation of dihydropyridine derivatives enantiomers with emphasis on elution order using polysaccharide-based chiral columns, *J. Sep. Sci.* 35 (2012) 2529-2537. <https://doi.org/10.1002/jssc.201200443>
- [86] L. Peng, S. Jayapalan, B. Chankvetadze, T. Farkas, Reversed-phase chiral HPLC and LC/MS analysis with tris(chloromethylphenylcarbamate) derivatives of cellulose and amylose as chiral stationary phases, *J. Chromatogr. A* 1217 (2010) 6942-6955. <https://doi.org/10.1016/j.chroma.2010.08.075>
- [87] B. Chankvetadze, Application of enantioselective separation techniques to bioanalysis of chiral drugs and their metabolites, *TrAC-Trends Anal. Chem.* 143 (2021) 116332. <https://doi.org/10.1016/j.trac.2021.116332>
- [88] M. Arenas, J. Martín, J.L. Santos, I. Aparicio, E. Alonso, An overview of analytical methods for enantiomeric determination of chiral pollutants in environmental samples and biota, *TrAC-Trends Anal. Chem.* 143 (2021) 116370. <https://doi.org/10.1016/j.trac.2021.116370>

- [89] S. Materazzo, S. Carradori, R. Ferretti, B. Gallinella, D. Secci, R. Cirilli, Effect of the water content on the retention and enantioselectivity of albendazole and fenbendazole sulfoxides using amylose-based chiral stationary phases in organic-aqueous conditions, *J. Chromatogr. A* 1327 (2014) 73-79. <https://doi.org/10.1016/j.chroma.2013.12.051>
- [90] R. Cirilli, HPLC enantioseparations with polysaccharide-based chiral stationary phases in HILIC conditions, in: G.K.E. Scriba (Eds.), *Chiral separations. Methods in molecular biology*, Humana, New York, 2019, pp. 127-146.
- [91] I. Matarashvili, A. Chelidze, G. Dolidze, G. Kobidze, N. Zaqashvili, A. Dadianidze, I. Bacskay, A. Felinger, T. Farkas, B. Chankvetadze, Separation of enantiomers of chiral basic drugs with amylose- and cellulose-phenylcarbamate-based chiral columns in acetonitrile and aqueous-acetonitrile in high-performance liquid chromatography with a focus on substituent electron-donor and electron-acceptor effects, *J. Chromatogr. A* 1624 (2020) 461218. <https://doi.org/10.1016/j.chroma.2020.461218>
- [92] Z. Shedania, R. Kakava, A. Volonterio, T. Farkas, B. Chankvetadze, Separation of enantiomers of chiral sulfoxides in high-performance liquid chromatography with cellulose-based chiral selectors using acetonitrile and acetonitrile-water mixtures as mobile phases, *J. Chromatogr. A* 1609 (2020) 460445. <https://doi.org/10.1016/j.chroma.2019.460445>
- [93] J. Shen, T. Ikai, Y. Okamoto, Synthesis and application of immobilized polysaccharide-based chiral stationary phases for enantioseparation by high-performance liquid chromatography, *J. Chromatogr. A* 1363 (2014) 51-61. <https://doi.org/10.1016/j.chroma.2014.06.042>
- [94] P. Ding, B.S. Chang, G.Y. Qing, T.L. Sun, New approach for chiral separation: from polysaccharide-based materials to chirality-responsive polymers, *Sci. China-Chem.* 57 (2014) 1492-1506. <https://doi.org/10.1007/s11426-014-5206-8>
- [95] Z. Song, J. Li, W. Lu, B. Li, G. Yang, Y. Bi, M. Arabi, X. Wang, J. Ma, L. Chen, Molecularly imprinted polymers based materials and their applications in chromatographic and electrophoretic separations, *TrAC-Trends Anal. Chem.* 146 (2022) 116504. <https://doi.org/10.1016/j.trac.2021.116504>
- [96] Y. Zhang, X. Jin, X. Ma, Y. Wang, Chiral porous organic frameworks and their application in enantioseparation, *Anal. Methods* 13 (2021) 8-33. <https://doi.org/10.1039/D0AY01831G>
- [97] A.M. Stalcup, Chiral separations, *Annu. Rev. Anal. Chem.* 3 (2010) 341-363. <https://doi.org/10.1146/annurev.anchem.111808.073635>
- [98] Y. Okamoto, T. Ikai, Chiral HPLC for efficient resolution of enantiomers, *Chem. Soc. Rev.* 37 (2008) 2593-2608. <https://doi.org/10.1039/b808881k>

- [99] P. De Gauquier, K. Vanommeslaeghe, Y. Vander Heyden, D. Mangelings, Modelling approaches for chiral chromatography on polysaccharide-based and macrocyclic antibiotic chiral selectors: a review, *Anal. Chim. Acta* 1198 (2022) 338861. <https://doi.org/10.1016/j.aca.2021.338861>
- [100] P. Peluso, A. Dessì, R. Dallochio, V. Mamane, S. Cossu, Recent studies of docking and molecular dynamics simulation for liquid-phase enantioseparations, *Electrophoresis* 40 (2019) 1881-1896. <https://doi.org/10.1002/elps.201800493>
- [101] R. Sardella, E. Camaioni, A. Macchiarulo, A. Gioiello, M. Marinozzi, A. Carotti, Computational studies in enantioselective liquid chromatography: forty years of evolution in docking- and molecular dynamics-based simulations, *TrAC-Trends Anal. Chem.* 122 (2020) 115703. <https://doi.org/10.1016/j.trac.2019.115703>
- [102] R.B. Kasat, S.Y. Wee, J.X. Loh, N.-H.L. Wang, E.I. Franses, Effect of the solute molecular structure on its enantioresolution on cellulose tris(3,5-dimethylphenylcarbamate), *J. Chromatogr. B* 875 (2008) 81-92. <https://doi.org/10.1016/j.jchromb.2008.06.045>
- [103] P. Peluso, B. Chankvetadze, The molecular bases of chiral recognition in 2-(benzylsulfinyl)benzamide enantioseparation, *Anal. Chim. Acta* 1141 (2021) 194-205. <https://doi.org/10.1016/j.aca.2020.10.050>
- [104] A. Del Rio, Exploring enantioselective molecular recognition mechanisms with chemoinformatic techniques, *J. Sep. Sci.* 32 (2009) 1566-1584. <https://doi.org/10.1002/jssc.200800693>
- [105] C. Altomare, A. Carotti, S. Cellamare, F. Fanelli, F. Gasparrini, C. Villani, P.A. Carrupt, B. Testa, Enantiomeric resolution of sulfoxides on a DACH-DNB chiral stationary phase: a quantitative structure–enantioselective retention relationship (QSERR) study, *Chirality* 5 (1993) 527-537. <https://doi.org/10.1002/chir.530050709>
- [106] A. Carotti, C. Altomare, S. Cellamare, A.M. Monforte, G. Bettoni, F. Loiodice, N. Tangari, V. Tortorella, LFER and CoMFA studies on optical resolution of α -alkyl α -aryloxy acetic acid methyl esters on DACH-DNB chiral stationary phase, *J. Comput.-Aided. Mol. Des.* 9 (1995) 131-138. <https://doi.org/10.1007/BF00124403>
- [107] J.V. de Julian-Ortiz, R. Garcia-Domenech, J.G. Alvarez, R.S. Roca, F.J. Garcia-March, G.M. Antón-Fos, Use of topological descriptors in chromatographic chiral separations, *J. Chromatogr. A* 719 (1996) 37-44. [https://doi.org/10.1016/0021-9673\(95\)00401-7](https://doi.org/10.1016/0021-9673(95)00401-7)
- [108] C. Altomare, S. Cellamare, A. Carotti, M.L. Barreca, A. Chimirri, A.M. Monforte, F. Gasparrini, C. Villani, M. Cirilli, F. Mazza, Substituent effects on the enantioselective retention of anti-HIV 5-aryl- Δ^2 -1,2,4-Oxadiazolines on *R,R*-DACH-DNB chiral stationary phase, *Chirality* 8 (1996) 556-566. [https://doi.org/10.1002/\(SICI\)1520-636X\(1996\)8:8<556::AID-CHIR4>3.0.CO;2-7](https://doi.org/10.1002/(SICI)1520-636X(1996)8:8<556::AID-CHIR4>3.0.CO;2-7)

- [109] T.D. Booth, I.W. Wainer, Investigation of the enantioselective separations of α -alkylarylcarboxylic acids on an amylose tris(3,5-dimethylphenylcarbamate) chiral stationary phase using quantitative structure-enantioselective retention relationships. Identification of a conformationally driven chiral recognition mechanism, *J. Chromatogr. A* 737 (1996) 157-169. [https://doi.org/10.1016/0021-9673\(96\)00011-8](https://doi.org/10.1016/0021-9673(96)00011-8)
- [110] T.D. Booth, I.W. Wainer, Mechanistic investigation into the enantioselective separation of mexiletine and related compounds, chromatographed on an amylose tris(3,5-dimethylphenylcarbamate) chiral stationary phase, *J. Chromatogr. A* 741 (1996) 205-211. [https://doi.org/10.1016/0021-9673\(96\)00208-7](https://doi.org/10.1016/0021-9673(96)00208-7)
- [111] T.D. Booth, K. Azzaoui, I.W. Wainer, Prediction of chiral chromatographic separations using combined multivariate regression and neural networks, *Anal. Chem.* 69 (1997) 3879-3883. <https://doi.org/10.1021/ac9702150>
- [112] V. Andrisano, T.D. Booth, V. Cavrini, I.W. Wainer, Enantioselective separation of chiral arylcarboxylic acids on an immobilized human serum albumin chiral stationary phase, *Chirality* 9 (1997) 178-183. [https://doi.org/10.1002/\(SICI\)1520-636X\(1997\)9:2<178::AID-CHIR19>3.0.CO;2-K](https://doi.org/10.1002/(SICI)1520-636X(1997)9:2<178::AID-CHIR19>3.0.CO;2-K)
- [113] T.D. Booth, W.J. Lough, M. Saeed, T.A.G. Noctor, I.W. Wainer, Enantioselective separation of enantiomeric amides on three amylose-based chiral stationary phases: effects of backbone and carbamate side chain chiralities, *Chirality* 9 (1997) 173-177. [https://doi.org/10.1002/\(SICI\)1520-636X\(1997\)9:2<173::AID-CHIR18>3.0.CO;2-K](https://doi.org/10.1002/(SICI)1520-636X(1997)9:2<173::AID-CHIR18>3.0.CO;2-K)
- [114] C.A. Montanari, Q.B. Cass, M.E. Tiritan, A.L.S. de Souza, A QSERR study on enantioselective separation of enantiomeric sulphoxides, *Anal. Chim. Acta* 419 (2000) 93-100. [https://doi.org/10.1016/S0003-2670\(00\)00962-4](https://doi.org/10.1016/S0003-2670(00)00962-4)
- [115] J. Huang, H. Chen, R. Gao, Q. Wang, R. Chen, Retention and chiral recognition mechanism of organo-phosphorus compounds in high-performance liquid chromatography, *Sci. China Ser. B-Chem.* 44 (2001) 147-153. <https://doi.org/10.1007/BF02879532>
- [116] T. Suzuki, S. Timofei, B.E. Iuoras, G. Uray, P., Verdino, W.M.F. Fabian, Quantitative structure–enantioselective retention relationships for chromatographic separation of arylalkylcarbinols on Pirkle type chiral stationary phases, *J. Chromatogr. A* 922 (2001) 13-23. [https://doi.org/10.1016/S0021-9673\(01\)00921-9](https://doi.org/10.1016/S0021-9673(01)00921-9)
- [117] E. Calleri, E. De Lorenzi, D. Siluk, M. Markuszewski, R. Kaliszan, G. Massolini, Riboflavin binding protein—Chiral stationary phase: investigation of retention mechanism, *Chromatographia* 55 (2002) 651-658. <https://doi.org/10.1007/BF02491778>

- [118] W.M. Fabian, W. Stampfer, M. Mazur, G. Uray, Modeling the chromatographic enantioseparation of aryl- and hetarylcarbinols on ULMO, a brush-type chiral stationary phase, by 3D-QSAR techniques, *Chirality* 15 (2003) 271-275. <https://doi.org/10.1002/chir.10197>
- [119] W. Du, G. Yang, X. Wang, S. Yuan, L. Zhou, D. Xu, C. Liu, Enantioseparation of 15 organic phosphonate esters on the cellulose tris(3,5-dimethylphenyl carbamate) chiral stationary phase by HPLC, *Talanta* 60 (2003) 1187-1195. [https://doi.org/10.1016/S0039-9140\(03\)00231-5](https://doi.org/10.1016/S0039-9140(03)00231-5)
- [120] G.S. Yang, S.L. Yuan, X.J. Lin, Z.N. Qi, C.B. Liu, H.Y. Aboul-Enein, G. Felix, The study of chiral discrimination of organophosphonate derivatives on pirkle type chiral stationary phase by molecular modeling, *Talanta* 64 (2004) 320-325. <https://doi.org/10.1016/j.talanta.2004.02.040>
- [121] M.L.C. Montanari, Q.B. Cass, A. Leitão, A.D. Andricopulo, C.A. Montanari, The role of molecular interaction fields on enantioselective and nonselective separation of chiral sulfoxides, *J. Chromatogr. A* 1121 (2006) 64-75. <https://doi.org/10.1016/j.chroma.2006.04.072>
- [122] M. Lämmerhofer, P. Franco, W. Lindner, Quinine carbamate chiral stationary phases: systematic optimization of steric selector-selectand binding increments and enantioselectivity by quantitative structure-enantioselectivity relationship studies, *J. Sep. Sci.* 29 (2006) 1486-1496. <https://doi.org/10.1002/jssc.200600111>
- [123] S. Caetano, Y. Vander Heyden, Modelling the quality of enantiomeric separations based on molecular descriptors, *Chemometrics Intell. Lab. Syst.* 84 (2006) 46-55. <https://doi.org/10.1016/j.chemolab.2006.04.010>
- [124] A. Del Rio, P. Piras, C. Roussel, Enantiophore modeling in 3D-QSAR. A data mining application on Whelk-O1 chiral stationary phase, *Chirality* 18 (2006) 498-508. <https://doi.org/10.1002/chir.20281>
- [125] S. Caetano, C. Krier, M. Verleysen, Y.V. Heyden, Modelling the quality of enantiomeric separations using Mutual Information as an alternative variable selection technique, *Anal. Chim. Acta* 602 (2007) 37-46. <https://doi.org/10.1016/j.aca.2007.08.048>
- [126] A. Del Rio, J. Gasteiger, Simple method for the prediction of the separation of racemates with high-performance liquid chromatography on Whelk-O1 chiral stationary phase, *J. Chromatogr. A* 1185 (2008) 49-58. <https://doi.org/10.1016/j.chroma.2008.01.034>
- [127] M. Szaleniec, A. Dudzik, M. Pawul, B. Kozik, Quantitative structure enantioselective retention relationship for high-performance liquid chromatography chiral separation of 1-phenylethanol derivatives, *J. Chromatogr. A* 1216 (2009) 6224-6235. <https://doi.org/10.1016/j.chroma.2009.07.002>

- [128] B. Rasulev, M. Turabekova, M. Gorska, K. Kulig, A. Bielejewska, J. Lipkowski, J. Lleszczynski, Use of quantitative structure–enantioselective retention relationship for the liquid chromatography chiral separation prediction of the series of pyrrolidin-2-one compounds, *Chirality* 24 (2012) 72-77. <https://doi.org/10.1002/chir.21028>
- [129] K. Boronová, J. Lehotay, K. Hroboňová, D.W. Armstrong, Study of physicochemical interaction of aryloxyaminopropanol derivatives with teicoplanin and vancomycin phases in view of quantitative structure–property relationship studies, *J. Chromatogr. A* 1301 (2013) 38-47. <https://doi.org/10.1016/j.chroma.2013.05.046>
- [130] H. Barfeii, Z. Garkani-Nejad, A comparative QSRR study on enantioseparation of ethanol ester enantiomers in HPLC using multivariate image analysis, quantum mechanical and structural descriptors, *J. Chin. Chem. Soc.* 64 (2017) 176-187. <https://doi.org/10.1002/jccs.201600253>
- [131] P. Piras, R. Sheridan, E.C. Sherer, W. Schafer, C.J. Welch, C. Roussel, Modeling and predicting chiral stationary phase enantioselectivity: an efficient random forest classifier using an optimally balanced training dataset and an aggregation strategy, *J. Sep. Sci.* 41 (2018) 1365-1375. <https://doi.org/10.1002/jssc.201701334>
- [132] L. Pisani, M. Rullo, M. Catto, M. de Candia, A. Carrieri, S. Cellamare, C.D. Altomare, Structure-property relationship study of the HPLC enantioselective retention of neuroprotective 7-[(1-alkylpiperidin-3-yl)methoxy]coumarin derivatives on an amylose-based chiral stationary phase, *J. Sep. Sci.* 41 (2018) 1376-1384. <https://doi.org/10.1002/jssc.201701442>
- [133] Y. Martín-Biosca, L. Escuder-Gilabert, M.J. Medina-Hernández, S. Sagrado, Modelling the enantioresolution capability of cellulose tris (3,5-dichlorophenylcarbamate) stationary phase in reversed phase conditions for neutral and basic chiral compounds, *J. Chromatogr. A* 1567 (2018) 111-118. <https://doi.org/10.1016/j.chroma.2018.06.061>
- [134] C. Luo, G. Hu, M. Huang, J. Zou, Y. Jiang, Prediction on separation factor of chiral arylhydantoin compounds and recognition mechanism between chiral stationary phase and the enantiomers, *J. Mol. Graph.* 94 (2020) 107479. <https://doi.org/10.1016/j.jmkgm.2019.107479>
- [135] T. Puzyn, J. Leszczynski, M.T.D. Cronin, *Recent advances in QSAR studies*, first ed., Springer, Dordrecht, 2010.
- [136] J. Zupan, J. Gaisteiger, *Neural networks in chemistry and drug design*, second ed., John Wiley & Sons Inc., New York, 1999.
- [137] J.N. Miller, J.C. Miller, *Statistics and chemometrics for analytical chemistry*, fifth ed., Pearson Education, Harlow, 2005.
- [138] ChirBase, Chemical database of chiral HPLC/SFC separations. <https://chirbase.u-3mrs.fr/> (accessed 4 November 2022).

- [139] J.R. Torres-Lapasió, J.J. Baeza-Baeza, M.C. García-Álvarez-Coque, Modeling of peak shape and asymmetry, in: Ł. Komsta, Y. Vander Heyden, J. Sherma (Eds.), *Chemometrics in Chromatography*, CRC Press, Boca Raton, 2017, pp. 217-238.
- [140] B.J. Asher, L.A. D'Agostino, J.D. Way, C.S. Wong, J.J. Harynuk, Comparison of peak integration methods for the determination of enantiomeric fraction in environmental samples, *Chemosphere* 75 (2009) 1042-1048. <https://doi.org/10.1016/j.chemosphere.2009.01.041>
- [141] V. Guillén-Casla, J. Magro-Moral, N. Rosales-Conrado, L.V. Pérez-Arribas, M.E. León-González, L.M. Polo-Díez, Direct chiral liquid chromatography determination of aryloxyphenoxypropionic herbicides in soil: deconvolution tools for peak processing, *Anal. Bioanal. Chem.* 400 (2011) 3547-3560. <https://doi.org/10.1007/s00216-011-4969-4>
- [142] T.T. Handlovic, M.F. Wahab, D.W. Armstrong, Symmetrization of peaks in chiral chromatography with an area-invariant resolution enhancement method, *Anal. Chem.* 94 (2022) 16638-16646. <https://doi.org/10.1021/acs.analchem.2c02683>
- [143] J. Verdú-Andrés, R. Herráez-Hernández, P. Campíns-Falcó, Analysis of enantiomers giving partially overlapped peaks by using different treatments of the chromatographic ultraviolet signals: quantification of pseudoephedrine enantiomers, *J. Chromatogr. A* 930 (2001) 95-107. [https://doi.org/10.1016/S0021-9673\(01\)01141-4](https://doi.org/10.1016/S0021-9673(01)01141-4)
- [144] N. Rosales-Conrado, V. Guillén-Casla, L.V. Pérez-Arribas, M.E. León-González, L.M. Polo-Díez, Simultaneous enantiomeric determination of acidic herbicides in apple juice samples by liquid chromatography on a teicoplanin chiral stationary phase, *Food Anal. Meth.* 6 (2013) 535-547. <https://doi.org/10.1007/s12161-012-9482-7>
- [145] V.B. Di Marco, G.G. Bombi, Mathematical functions for the representation of chromatographic peaks, *J. Chromatogr. A* 931 (2001) 1-30. [https://doi.org/10.1016/S0021-9673\(01\)01136-0](https://doi.org/10.1016/S0021-9673(01)01136-0)
- [146] J. Li, Development and evaluation of flexible empirical peak functions for processing chromatographic peaks, *Anal. Chem.* 69 (1997) 4452-4462. <https://doi.org/10.1021/ac970481d>
- [147] J.J. Baeza-Baeza, M.C. García-Álvarez-Coque, Characterization of chromatographic peaks using the linearly modified Gaussian model. Comparison with the bi-Gaussian and the Foley and Dorsey approaches, *J. Chromatogr. A* 1515 (2017) 129-137. <https://doi.org/10.1016/j.chroma.2017.07.087>
- [148] J. Olivé, J.O. Grimalt, Gram-Charlier and Edgeworth-Cramér series in the characterization of chromatographic peaks, *Anal. Chim. Acta* 249 (1991) 337-348. [https://doi.org/10.1016/S0003-2670\(00\)83005-6](https://doi.org/10.1016/S0003-2670(00)83005-6)

- [149] J.P. Foley, J.G. Dorsey, A review of the exponentially modified gaussian (EMG) function: evaluation and subsequent calculation of universal data, *J. Chromatogr. Sci.* 22 (1984) 40-46. <https://doi.org/10.1093/chromsci/22.1.40>
- [150] J.J. Baeza-Baeza, C. Ortiz-Bolsico, M.C. García-Álvarez-Coque, New approaches based on modified Gaussian models for the prediction of chromatographic peaks, *Anal. Chim. Acta* 758 (2013) 36-44. <https://doi.org/10.1016/j.aca.2012.10.035>
- [151] G. Vivó-Truyols, J.R. Torres-Lapasió, A.M. van Nederkassel, Y. Vander Heyden, D.L. Massart, Automatic program for peak detection and deconvolution of multi-overlapped chromatographic signals: Part II: peak model and deconvolution algorithms, *J. Chromatogr. A* 1096 (2005) 146-155. <https://doi.org/10.1016/j.chroma.2005.03.072>
- [152] J.J. Baeza-Baeza, M.C. García-Álvarez-Coque, Prediction of peak shape as a function of retention in reversed-phase liquid chromatography, *J. Chromatogr. A* 1022 (2004) 17-24. <https://doi.org/10.1016/j.chroma.2003.09.059>
- [153] R.D. Caballero, M.C. García-Alvarez-Coque, J.J. Baeza-Baeza, Parabolic-Lorentzian modified Gaussian model for describing and deconvolving chromatographic peaks, *J. Chromatogr. A* 954 (2002) 59-76. [https://doi.org/10.1016/S0021-9673\(02\)00194-2](https://doi.org/10.1016/S0021-9673(02)00194-2)
- [154] S. Kotz, S. Nadarajah, *Extreme value distributions: theory and applications*, first ed., Imperial College Press, London, 2000.
- [155] J.O. Grimalt, J. Olivé, Log-normal derived equations for the determination of chromatographic peak parameters from graphical measurements, *Anal. Chim. Acta* 248 (1991) 59-70. [https://doi.org/10.1016/S0003-2670\(00\)80869-7](https://doi.org/10.1016/S0003-2670(00)80869-7)
- [156] R.A. Vaidya, R.D. Hester, Deconvolution of overlapping chromatographic peaks using constrained non-linear optimization, *J. Chromatogr. A* 287 (1984) 231-244. [https://doi.org/10.1016/S0021-9673\(01\)87700-1](https://doi.org/10.1016/S0021-9673(01)87700-1)
- [157] T.L. Pap, Zs. Pápai, Application of a new mathematical function for describing chromatographic peaks, *J. Chromatogr. A* 930 (2001) 53-60. [https://doi.org/10.1016/S0021-9673\(01\)01163-3](https://doi.org/10.1016/S0021-9673(01)01163-3)
- [158] A. Losev, A new lineshape for fitting x-ray photoelectron peaks, *Surf. Interface Anal.* 14 (1989) 845-849. <https://doi.org/10.1002/sia.740141207>
- [159] J. Li, Comparison of the capability of peak functions in describing real chromatographic peaks, *J. Chromatogr. A* 952 (2002) 63-70. [https://doi.org/10.1016/S0021-9673\(02\)00090-0](https://doi.org/10.1016/S0021-9673(02)00090-0)
- [160] M.C. García-Alvarez-Coque, E.F. Simó-Alfonso, J.M. Sanchis-Mallols, J.J. Baeza-Baeza, A new mathematical function for describing electrophoretic peaks, *Electrophoresis* 26 (2005) 2076-2085. <https://doi.org/10.1002/elps.200410370>

- [161] C. Baker, P.S. Johnson, W.F. Maddams, The characterization of infrared absorption band shapes. II. Experimental studies, *Spectroc. Acta Pt. A-Molec. Spectr.* 34 (1978) 683-691. [https://doi.org/10.1016/0584-8539\(78\)80019-1](https://doi.org/10.1016/0584-8539(78)80019-1)
- [162] J.C. Giddings, H. Eyring, A molecular dynamic theory of chromatography, *J. Phys. Chem.* 59 (1955) 416-421.
- [163] J.M. Davis, J.C. Giddings, Statistical theory of component overlap in multicomponent chromatograms, *Anal. Chem.* 55 (1983) 418-424. <https://doi.org/10.1021/ac00254a003>
- [164] S. Pous-Torres, J.J. Baeza-Baeza, J.R. Torres-Lapasió, M.C. García-Álvarez-Coque, Peak capacity estimation in isocratic elution, *J. Chromatogr. A* 1205 (2008) 78-89. <https://doi.org/10.1016/j.chroma.2008.07.088>
- [165] D. Barceló, M.J. López de Alda, Contaminación y calidad química del agua: el problema de los contaminantes emergentes, in: *Jornadas de presentación de resultados: el estado ecológico de las masas de agua. Panel Científico-Técnico de seguimiento de la política de aguas*, Sevilla, 2008, pp. 1-27.
- [166] B. Petrie, R. Barden, B. Kasprzyk-Hordern, A review on emerging contaminants in wastewaters and the environment: current knowledge, understudied areas and recommendations for future monitoring, *Water Res.* 72 (2015) 3-27. <https://doi.org/10.1016/j.watres.2014.08.053>
- [167] N.H. Tran, K.Y.-H. Gin, Occurrence and removal of pharmaceuticals, hormones, personal care products, and endocrine disrupters in a full-scale water reclamation plant, *Sci. Total Environ.* 599-600 (2017) 1503-1516. <https://doi.org/10.1016/j.scitotenv.2017.05.097>
- [168] K. Liao, Y. Bai, Y. Huo, Z. Jian, W. Hu, C. Zhao, J. Qu, Integrating microbial biomass, composition and function to discern the level of anthropogenic activity in a river ecosystem, *Environ. Int.* 116 (2018) 147-155. <https://doi.org/10.1016/j.envint.2018.04.003>
- [169] C. García-Gómez, P. Gortáres-Moroyoqui, P. Drogui, Contaminantes emergentes: efectos y tratamientos de remoción. *Química Viva* 10 (2011) 96-105.
- [170] K. Kümmerer, The presence of pharmaceuticals in the environment due to human use-present knowledge and future changes, *J. Environ. Manage.* 90 (2009) 2354-2366. <https://doi.org/10.1016/j.jenvman.2009.01.023>
- [171] C. Fernández, M. González-Doncel, J. Pro, G. Carbonell, J.V. Tarazona, Occurrence of pharmaceutically active compounds in surfacewaters of the Henares-Jarama-Tajo river system (Madrid, Spain) and a potential risk characterization, *Sci. Total Environ.* 408 (2010) 543-551. <https://doi.org/10.1016/j.scitotenv.2009.10.009>

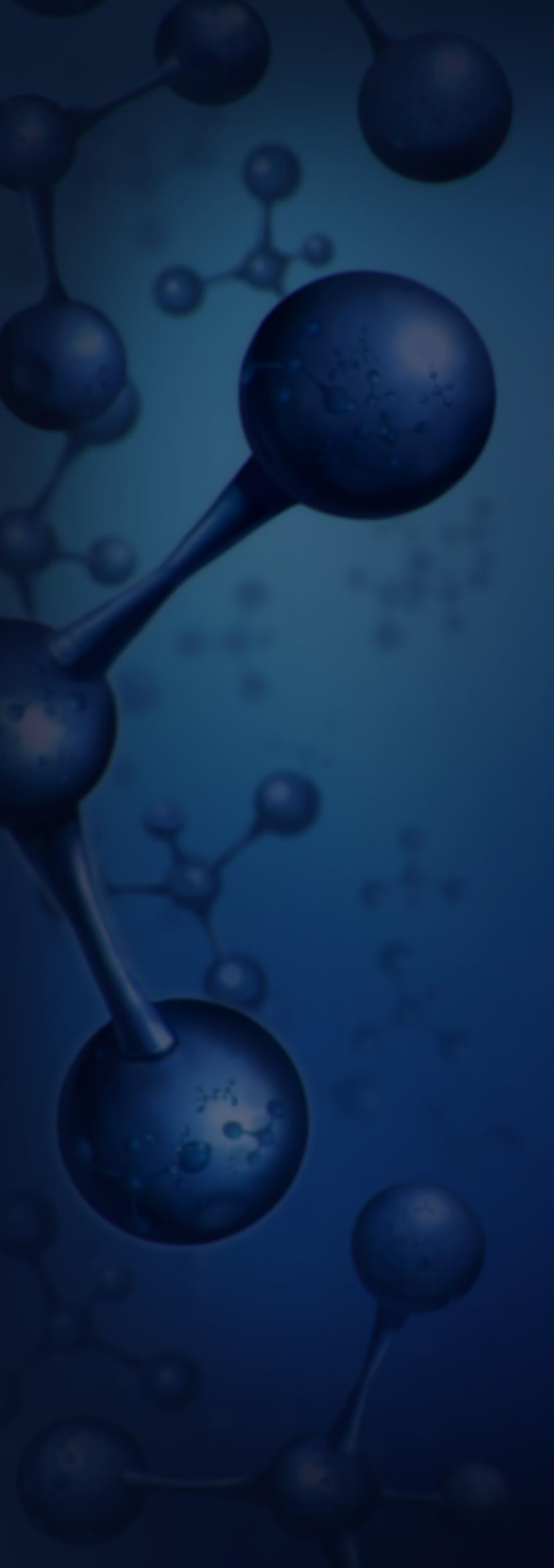
- [172] S. Ortiz de García, G. Pinto Pinto, P. García-Encina, R. Irusta-Mata, Consumption and occurrence of pharmaceutical and personal care products in the aquatic environment in Spain, *Sci. Total Environ.* 444 (2013) 451-465. <https://doi.org/10.1016/j.scitotenv.2012.11.057>
- [173] A.R. Ribeiro, P.M.L. Castro, M.E. Tiritan, Chiral pharmaceuticals in the environment, *Environ. Chem. Lett.* 10 (2012) 239-253. <https://doi.org/10.1007/s10311-011-0352-0>
- [174] V. Geissen, H. Mol, E. Klumpp, G. Umlauf, M. Nadal, M. van der Ploeg, S.E.A.T.M. van de Zee, C.J. Ritsema, Emerging pollutants in the environment: a challenge for water resource management, *Int. Soil Water Conserv. Res.* 3 (2015) 57-65. <https://doi.org/10.1016/j.iswcr.2015.03.002>
- [175] Y. Valcárcel, S. González Alonso, J.L. Rodríguez-Gil, A. Gil, M. Catalá, Detection of pharmaceutically active compounds in the rivers and tap water of the Madrid Region (Spain) and potential ecotoxicological risk, *Chemosphere* 84 (2011) 1336-1348. <https://doi.org/10.1016/j.chemosphere.2011.05.014>
- [176] A.J. Ebele, M.A.-E. Abdallah, S. Harrad, Pharmaceuticals and personal care products (PPCPs) in the freshwater aquatic environment, *Emerg. Contam.* 3 (2017) 1-16. <https://doi.org/10.1016/j.emcon.2016.12.004>
- [177] E. Sanganyado, Z. Lu, Q. Fu, D. Schlenk, J. Gan, Chiral pharmaceuticals: a review on their environmental occurrence and fate processes, *Water Res.* 124 (2017) 527-542. <https://doi.org/10.1016/j.watres.2017.08.003>
- [178] Y. Fu, F. Borrull, R.M. Marcé, N. Fontanals, Enantiomeric fraction determination of chiral drugs in environmental samples using chiral liquid chromatography and mass spectrometry, *Trends Environ. Anal. Chem.* 29 (2021) e00115. <https://doi.org/10.1016/j.teac.2021.e00115>
- [179] C.S. Wong, Environmental fate processes and biochemical transformations of chiral emerging organic pollutants, *Anal. Bioanal. Chem.* 386 (2006) 544-558. <https://doi.org/10.1007/s00216-006-0424-3>
- [180] A.R. Ribeiro, P.M.L. Castro, M.E. Tiritan, Environmental fate of chiral pharmaceuticals: determination, degradation and toxicity, in: E. Lichtfouse, J. Schwarzbauer, D. Robert (Eds.), *Environmental chemistry for a sustainable world*, Springer, Dordrecht, 2012, pp. 3-45.
- [181] Organisation for economic co-operation and development (OECD), OECD Guidelines for testing of chemicals: section 3. <https://www.oecd.org/chemicalsafety/testing/oecdguidelinesforthetestingofchemicals.htm>, 2023 (accessed 20 January 2023).
- [182] G. Vázquez-Rodríguez, R.I. Beltrán-Hernández, Pruebas normalizadas para la evaluación de la biodegradabilidad de sustancias químicas. Una revision, *Interciencia* 29 (2004) 578-573.

- [183] OECD (1992), *Test No. 301: Ready biodegradability*, OECD Guidelines for the testing of chemicals, section 3, OECD Publishing, Paris, <https://doi.org/10.1787/9789264070349-en>
- [184] OECD (1992), *Test No. 302B: Inherent biodegradability: Zahn-Wellens/ EVPA test*, OECD Guidelines for the testing of chemicals, section 3, OECD Publishing, Paris, <https://doi.org/10.1787/9789264070387-en>
- [185] OECD (2008), *Test No. 314: Simulation tests to assess the biodegradability of chemicals discharged in wastewater*, OECD Guidelines for the testing of chemicals, section 3, OECD Publishing, Paris, <https://doi.org/10.1787/9789264067493-en>
- [186] L. Escuder-Gilabert, Y. Martín-Biosca, S. Sagrado, M.J. Medina-Hernández, Anticipating the impact of pitfalls in kinetic biodegradation parameter estimation from substrate depletion curves of organic pollutants, *Environ. Pollut.* 252 (2019) 128-136. <https://doi.org/10.1016/j.envpol.2019.05.080>
- [187] J.A. Robinson, J.M. Tiedje, Nonlinear estimation of Monod growth kinetic parameters from a single substrate depletion curve, *Appl. Environ. Microbiol.* 45 (1983) 1453-1458. <https://doi.org/10.1128/aem.45.5.1453-1458.1983>
- [188] C.T. Goudar, An explicit expression for determining cometabolism kinetics using progress curve analysis, *J. Biotechnol.* 159 (2012) 56-60. <https://doi.org/10.1016/j.jbiotec.2012.02.009>
- [189] C. Liu, J.M. Zachara, Uncertainties of Monod kinetic parameters nonlinearly estimated from batch experiments, *Environ. Sci. Technol.* 35 (2001) 133-141. <https://doi.org/10.1021/es001261b>
- [190] C.T. Goudar, S.K. Harris, M.J. McInerney, J.M. Sufflita, Progress curve analysis for enzyme and microbial kinetic reactions using explicit solutions based on the Lambert W function, *J. Microbiol. Methods* 59 (2004) 317-326. <https://doi.org/10.1016/j.mimet.2004.06.013>
- [191] C.T. Goudar, T.G. Ellis, Explicit oxygen concentration expression for estimating extant biodegradation kinetics from respirometric experiments, *Biotechnol. Bioeng.* 75 (2001) 74-81. <https://doi.org/10.1002/bit.1166>
- [192] R.M. Corless, G.H. Gonnet, D.E.G. Hare, D.J. Jeffrey, D.E. Knuth, On the Lambert W function, *Adv. Comput. Math.* 5 (1996) 329-359. <https://doi.org/10.1007/BF02124750>
- [193] C. Her, A.P. Alonzo, J.Y. Vang, E. Torres, V.V. Krishnan, Real-time enzyme kinetics by quantitative NMR spectroscopy and determination of the Michaelis-Menten constant using the Lambert-W function, *J. Chem. Educ.* 92 (2015) 1943-1948. <https://doi.org/10.1021/acs.jchemed.5b00136>

- [194] N.H. Hashim, S. Shafie, S.J. Khan, Enantiomeric fraction as an indicator of pharmaceutical biotransformation during wastewater treatment and in the environment - a review, *Environ. Technol.* 31 (2010) 1349-1370. <https://doi.org/10.1080/09593331003728022>
- [195] S.L. MacLeod, C.S. Wong, Loadings, trends, comparisons, and fate of achiral and chiral pharmaceuticals in wastewaters from urban tertiary and rural aerated lagoon treatments, *Water Res.* 44 (2010) 533-544. <https://doi.org/10.1016/j.watres.2009.09.056>
- [196] P. Vazquez-Roig, B. Kasprzyk-Hordern, C. Blasco, Y. Picó, Stereoisomeric profiling of drugs of abuse and pharmaceuticals in wastewaters of Valencia (Spain), *Sci. Total Environ.* 494-495 (2014) 49-57. <https://doi.org/10.1016/j.scitotenv.2014.06.098>
- [197] A.R.L. Ribeiro, A.S. Maia, C. Ribeiro, M.E. Tiritan, Analysis of chiral drugs in environmental matrices: current knowledge and trends in environmental, biodegradation and forensic fields, *TrAC-Trends Anal. Chem.* 124 (2020) 115783. <https://doi.org/10.1016/j.trac.2019.115783>
- [198] B. Kasprzyk-Hordern, D.R. Baker, Enantiomeric profiling of chiral drugs in wastewater and receiving waters, *Environ. Sci. Technol.* 46 (2012) 1681-1691. <https://doi.org/10.1021/es203113y>
- [199] V. Matamoros, M. Hijosa, J.M. Bayona, Assessment of the pharmaceutical active compounds removal in wastewater treatment systems at enantiomeric level. Ibuprofen and naproxen, *Chemosphere* 75 (2009) 200-205. <https://doi.org/10.1016/j.chemosphere.2008.12.008>
- [200] N.H. Hashim, R.M. Stuetz, S.J. Khan, Enantiomeric fraction determination of 2-arylpropionic acids in a package plant membrane bioreactor, *Chirality* 25 (2013) 301-307. <https://doi.org/10.1002/chir.22151>
- [201] C. Caballo, M.D. Sicilia, S. Rubio, Enantioselective determination of representative profens in wastewater by a single-step sample treatment and chiral liquid chromatography–tandem mass spectrometry, *Talanta* 134 (2015) 325-332. <https://doi.org/10.1016/j.talanta.2014.11.016>
- [202] S.J. Khan, L. Wang, N.H. Hashim, J.A. McDonald, Distinct enantiomeric signals of ibuprofen and naproxen in treated wastewater and sewer overflow, *Chirality* 26 (2014) 739-746. <https://doi.org/10.1002/chir.22258>
- [203] Y. Fu, F. Borrull, R.M. Marcé, N. Fontanals, Enantiomeric determination of cathinones in environmental water samples by liquid chromatography-high resolution mass spectrometry, *J. Chromatogr. A* 1626 (2020) 461359. <https://doi.org/10.1016/j.chroma.2020.461359>
- [204] A.S. Maia, M.E. Tiritan, P.M.L. Castro, Enantioselective degradation of ofloxacin and levofloxacin by the bacterial strains *Labrys portucalensis* F11 and *Rhodococcus* sp. FP1, *Ecotox. Environ. Safe.* 155 (2018) 144-151. <https://doi.org/10.1016/j.ecoenv.2018.02.067>

- [205] S.E. Evans, J. Bagnall, B. Kasprzyk-Hordern, Enantioselective degradation of amphetamine-like environmental micropollutants (amphetamine, methamphetamine, MDMA and MDA) in urban water, *Environ. Pollut.* 215 (2016) 154-163. <https://doi.org/10.1016/j.envpol.2016.04.103>
- [206] J. Bagnall, L. Malia, A. Lubben, B. Kasprzyk-Hordern, Stereoselective biodegradation of amphetamine and methamphetamine in river microcosms, *Water Res.* 47 (2013) 5708-5718. <https://doi.org/10.1016/j.watres.2013.06.057>
- [207] S. Evans, J. Bagnall, B. Kasprzyk-Hordern, Enantiomeric profiling of a chemically diverse mixture of chiral pharmaceuticals in urban water, *Environ. Pollut.* 230 (2017) 368-377. <https://doi.org/10.1016/j.envpol.2017.06.070>
- [208] A.R. Ribeiro, A.S. Maia, I.S. Moreira, C.M. Afonso, P.M.L. Castro, M.E. Tiritan, Enantioselective quantification of fluoxetine and norfluoxetine by HPLC in wastewater effluents, *Chemosphere* 95 (2014) 589-596. <https://doi.org/10.1016/j.chemosphere.2013.09.118>
- [209] Z. Li, E. Gomez, H. Fenet, S. Chiron, Chiral signature of venlafaxine as a marker of biological attenuation processes, *Chemosphere* 90 (2013) 1933-1938. <https://doi.org/10.1016/j.chemosphere.2012.10.033>
- [210] I.S. Moreira, A.R. Ribeiro, C.M. Afonso, M.E. Tiritan, P.M.L. Castro, Enantioselective biodegradation of fluoxetine by the bacterial strain *Labrys portucalensis* F11, *Chemosphere* 111 (2014) 103-111. <https://doi.org/10.1016/j.chemosphere.2014.03.022>
- [211] A.R. Ribeiro, C.M. Afonso, P.M.L. Castro, M.E. Tiritan, Enantioselective HPLC analysis and biodegradation of atenolol, metoprolol and fluoxetine, *Environ. Chem. Lett.* 11 (2013) 83-90. <https://doi.org/10.1007/s10311-012-0383-1>
- [212] A.R. Ribeiro, C.M. Afonso, P.M.L. Castro, M.E. Tiritan, Enantioselective biodegradation of pharmaceuticals, alprenolol and propranolol, by an activated sludge inoculum, *Ecotox. Environ. Safe.* 87 (2013) 108-114. <https://doi.org/10.1016/j.ecoenv.2012.10.009>
- [213] M. Lv, C. Lo, C.C. Hsu, Y. Wang, Y.R. Chiang, Q. Sun, Y. Wu, Y. Li, L. Chen, C.P. Yu, Identification of enantiomeric byproducts during microalgae-mediated transformation of metoprolol by MS/MS spectrum based networking, *Front. Microbiol.* 9 (2018) 2115. <https://doi.org/10.3389/fmicb.2018.02115>
- [214] H.R. Buser, T. Poiger, M.D. Müller, Occurrence and environmental behavior of the chiral pharmaceutical drug ibuprofen in surface waters and in wastewater, *Environ. Sci. Technol.* 33 (1999) 2529-2535. <https://doi.org/10.1021/es981014w>
- [215] S. Chen, W. Liu, Enantioselective degradation of metalaxyl in anaerobic activated sewage sludge, *Bull. Environ. Contam. Toxicol.* 82 (2009) 327-331. <https://doi.org/10.1007/s00128-008-9559-6>

- [216] W.G. Birolli, M.S. Arai, M. Nitschke, A.L.M. Porto, The pyrethroid (\pm)-lambda-cyhalothrin enantioselective biodegradation by a bacterial consortium, *Pest. Biochem. Physiol.* 156 (2019) 129-137. <https://doi.org/10.1016/j.pestbp.2019.02.014>
- [217] N.H. Al-Shaalan, I. Ali, Z.A. AlOthman, L.H. Al-Wahaibi, H. Alabdulmonem, Enantioselective degradation of dufulin pesticide in water: uptake, thermodynamics, and kinetics studies, *Chirality* 31 (2019) 1060-1069. <https://doi.org/10.1002/chir.23150>
- [218] Z. Sun, M. Dzakpasu, D. Zhang, G. Liu, Z. Wang, M. Qu, R. Chen, X.C. Wang, Y. Zheng, Enantioselectivity and mechanisms of chiral herbicide biodegradation in hydroponic systems, *Chemosphere* 307 (2022) 135701. <https://doi.org/10.1016/j.chemosphere.2022.135701>
- [219] M. Youness, M. Sancelme, B. Combourieu, P. Besse-Hoggan, Identification of new metabolic pathways in the enantioselective fungicide tebuconazole biodegradation by *Bacillus* sp. 3B6, *J. Hazard. Mater.* 351 (2018) 160-168. <https://doi.org/10.1016/j.jhazmat.2018.02.048>
- [220] L. Fang, Q. Shi, L. Xu, T. Shi, X. Wu, Q.X. Li, R. Hua, Enantioselective uptake determines degradation selectivity of chiral profenofos in *Cupriavidus nantongensis* X1^T, *J. Agric. Food Chem.* 68 (2020) 6493-6501. <https://doi.org/10.1021/acs.jafc.0c00132>
- [221] W. Zhai, L. Zhang, H. Liu, C. Zhang, D. Liu, P. Wang, Z. Zhou, Enantioselective degradation of prothioconazole in soil and the impacts on the enzymes and microbial community, *Sci. Total Environ.* 824 (2022) 153658. <https://doi.org/10.1016/j.scitotenv.2022.153658>
- [222] J. Pizarroso, J. Portela, A. Muñoz, NeuralSens: sensitivity analysis of neural networks. <https://arxiv.org/abs/2002.11423> (accessed 7 March 2023).
- [223] J.D. Olden, M.K. Joy, R.G. Death, An accurate comparison of methods for quantifying variable importance in artificial neural networks using simulated data, *Ecol. Modell.* 178 (2004) 389-397. <https://doi.org/10.1016/j.ecolmodel.2004.03.013>
- [224] S. Lek, M. Delacoste, P. Baran, I. Dimopoulos, J. Lauga, S. Aulagnier, Application of neural networks to modeling nonlinear relationships in ecology, *Ecol. Modell.* 90 (1996) 39-52. [https://doi.org/10.1016/0304-3800\(95\)00142-5](https://doi.org/10.1016/0304-3800(95)00142-5)
- [225] M.L. Shuler, F. Kargi, *Bioprocess engineering: basic concepts*, second ed., Prentice Hall PTR, Upper Saddle River, 2002.
- [226] Y. Martín-Biosca, L. Escuder-Gilabert, M. Perez-Baeza, S. Sagrado, M.J. Medina-Hernández, Biodegradability features of fluoxetine as a reference compound for monitoring the activity of activated sludges in drug biodegradation studies, *Int. J. Adv. Res. Chem. Sci. (IJARCS)* 6 (2019) 16-23. <https://doi.org/10.20431/2349-0403.0601003>



VII.- APPENDIX: PUBLICATIONS



PAPER I

Comparative modelling study on enantioresolution of structurally unrelated compounds with amylose-based chiral stationary phases in reversed phase liquid chromatography-mass spectrometry conditions

**Mireia Pérez-Baeza^a, Laura Escuder-Gilabert^a, Yolanda Martín-Biosca^a,
Salvador Sagrado^{a,b}, María José Medina-Hernández^a**

^a Departamento de Química Analítica, Universitat de València, Burjassot, Valencia, Spain

^b Instituto Interuniversitario de Investigación de Reconocimiento Molecular y Desarrollo Tecnológico (IDM), Universitat Politècnica de València, Universitat de València, Valencia, Spain

Journal of Chromatography A 1625 (2020) 461281



Comparative modelling study on enantioresolution of structurally unrelated compounds with amylose-based chiral stationary phases in reversed phase liquid chromatography-mass spectrometry conditions

Mireia Pérez-Baeza^a, Laura Escuder-Gilabert^{a,**}, Yolanda Martín-Biosca^a, Salvador Sagrado^{a,b}, María José Medina-Hernández^{a,*}

^aDepartamento de Química Analítica, Universitat de València, Burjassot, Valencia, Spain

^bInstituto Interuniversitario de Investigación de Reconocimiento Molecular y Desarrollo Tecnológico (IDM), Universitat Politècnica de València, Universitatde València, Valencia, Spain

ARTICLE INFO

Article history:

Received 2 March 2020

Revised 23 May 2020

Accepted 25 May 2020

Available online 29 May 2020

Keywords:

Amylose-based chiral stationary phases. Reversed phase liquid chromatography. Enantioresolution modelling and description. Discriminant partial least squares. Feature selection

ABSTRACT

Polysaccharide-based chiral stationary phases (CSPs) are the most used chiral selectors in HPLC. These CSPs can be used in normal, polar organic and aqueous-organic mobile phases. However, normal and polar organic mobile phases are not adequate for chiral separation of polar compounds, for the analysis of aqueous samples and for MS detection. In these situations, reversed phase conditions, without the usual non-volatile additives incompatible with MS detection, are preferable. Moreover, in most of the reported chiral chromatographic methods, retention is too large for routine work. In this paper, the chiral separation of 53 structurally unrelated compounds is studied using three commercial amylose-based CSPs -coated amylose tris(3,5-dimethylphenylcarbamate) (*Am1*), coated amylose tris(5-chloro-2-methylphenylcarbamate) (*Am2*), and immobilised amylose tris(3-chloro-5-methylphenylcarbamate) (*Am3*)-. Chiral separations are carried out using acetonitrile/ammonium bicarbonate (pH = 8.0) mixtures, reversed mobile phases compatible with MS detection. To provide realistic conditions for routine analysis, maximum retention factors are set to 15. Retention and enantioresolution behaviour of compounds in those CSPs are compared. On the other hand, to compare and describe the resolution ability of these CSPs, 58 structural variables of the compounds are tested to model for the first time a categorical enantioresolution (CRs) for *Am1* and *Am3* CSPs. Discriminant partial least squares, for one response categorical variable (DPLS1) is used for feature selection, modelling. The final DPLS1 models showed good descriptive ability.

© 2020 Elsevier B.V. All rights reserved.

1. Introduction

High-performance liquid chromatography (HPLC) with chiral stationary phases (CSPs) is one of the most widely used analytical techniques for the separation of enantiomers of chiral compounds. Among the large number of CSPs commercially available, amylose and cellulose polysaccharide derivatives coated or immobilised onto the stationary support represent by far the most widely used CSPs in HPLC. This is due to their broad chiral recognition capacity that confers extensive applicability for a large structural diversity of compounds and compatibility with all of the most relevant

chromatographic mobile phase regimes: normal, polar organic and aqueous-organic mobile phases [1–7].

Mobile phase composition with polysaccharide-based CSPs strongly modulates the stereorecognition process. Different chromatographic behaviours, even reversals in the elution order of enantiomers, are observed depending on the nature and composition of the mobile phase, as a consequence of changes produced in the intra-molecular hydrogen bonds of the polysaccharide structure [5,6]. Selector-selectand complexes formation is mediated via hydrogen bonds involving the CO or NH groups of the carbamate moieties, π - π and Van der Waals interactions with the phenyl rings, and steric factors [3,7]. Halogen bonds have been also described to contribute to selector-selectand complexation as electrostatic interactions [4,8]. In aqueous-organic mobile phases, although water can compete for hydrogen-bond interaction sites with the chiral compound and the CSP, hydrophilic interac-

* Corresponding Author. Tel.: 34 96 386 4899, Fax: 34 96 386 4953.

** Corresponding Author.

E-mail addresses: lescuder@uv.es (L. Escuder-Gilabert), maria.j.medina@uv.es (M.J. Medina-Hernández).

tions (residing in carbamate or ester moieties) and hydrophobic interactions (associated with phenyl moieties) between the analytes and the polysaccharide-based CSPs exist [5–7, 9–12, 14]. In fact, the combination of polysaccharide-based CSPs and aqueous-organic mobile phases has proven to be useful for the separation of enantiomers [7,9–14].

Aqueous-organic mobile phases are of special importance for the separation of polar compounds poorly soluble in alkanes low molecular weights alcohols or acetonitrile, as well as for the analysis of aqueous matrix samples such as biological and environmental samples. Also, they are useful for chiral HPLC-MS detection because aqueous-organic mobile phases improve the analyte ionization [11]. Unfortunately, most of the additives used in reversed phase conditions to improve resolution, to control the ionic strength and the pH of the mobile phase are non-volatile or suppress analyte response and therefore they are incompatible with MS detection.

Despite the large number of analytical applications of polysaccharides-based stationary phases in HPLC, the fundamental mechanisms responsible for the observed chiral separations are not fully understood because of the inherent complexity of these selectors. To elucidate the chiral recognition mechanism of polysaccharide chiral selectors, analytical separation techniques in combination with spectroscopic techniques and molecular modelling have been used [3,6,7,15–21].

Chemometric methods can be helpful to extract valuable information on molecular recognition [22,23]. Among these, quantitative structure-property relationships (QSPRs), which correlate enantioresolution-related information (retention or selectivity values) with different molecular properties of compounds, are a powerful option. Different QSPR studies have been reported for modelling data in enantioselective chromatography using polysaccharides-based stationary phases, [22–30]. These studies are usually carried out for structurally related compounds using amylose and cellulose-based CSPs and normal or polar mobile phases. In these studies, information about the functional groups responsible for enantioresolution is usually obtained.

In a previous paper [31], the enantioresolution level (categorical variable) of structurally unrelated basic compounds, obtained in HPLC using immobilised cellulose tris(3,5-dichlorophenylcarbamate) CSP and hydro-organic mobile phases, was modelled as a function of structural and physicochemical parameters of the compounds. Similar studies in electrokinetic chromatography using sulfated β - and γ -cyclodextrins as chiral selectors were also performed [32,33]. The parameters used in the modelling processes include molecular properties obtained from a free on-line database and classical topological parameters, as well as new topological parameters connected to the chiral carbon (C^* -parameters). Variables were selected by means of a discriminant partial least squares on one single response (DPLS1) refinement process. The models obtained presented adequate descriptive and predictive capacity.

In this work, the chiral separation of 53 structurally unrelated compounds (47 drugs belonging to 13 therapeutic families and 5 fungicides) is studied using three amylose-based CSPs (coated amylose tris(3,5-dimethylphenylcarbamate), coated amylose tris(5-chloro-2-methylphenylcarbamate) and immobilised amylose tris(3-chloro-5-methylphenylcarbamate)). Chromatographic separations are carried out using reversed mobile phases compatible with MS detection consisting of mixtures of acetonitrile/ammonium bicarbonate buffer ($pH = 8.0$). Maximum retention factors are set to 15, in order to provide realistic conditions for routine analysis. Retention and enantioresolution behaviour of compounds in those amylose-based CSPs are compared. On the other hand, to compare and describe the resolution ability of these CSPs, 58 structural and physicochemical parameters of the compounds are tested to

model a categorical enantioresolution (CRs) for each column. DPLS1 is used for feature selection and modelling purposes. At our knowledge, this is the first time that these studies have been carried out under these strict and realistic chromatographic conditions and for a large dataset of structurally unrelated compounds.

2. Experimental

2.1. Instrumentation

An Agilent Technologies 1100 chromatograph (Palo Alto, CA, USA) with a binary pump, an UV-visible diode array detector, a mass spectrometer equipped with electrospray and atmospheric pressure chemical ionization (ESI / APCI) sources and single quadrupole, a column thermostat and an autosampler was used. Data acquisition and processing were performed by means of the LC/MSD ChemStation software (B.04.02 SP1 [208], ©Agilent Technologies 2001–2010).

An Agilent Technologies 1100 chromatograph (Palo Alto, CA, USA) with a quaternary pump, a UV-visible variable wavelength detector, a column thermostat and an autosampler was also used. In this case, data acquisition and processing were performed by means of the Chemstation software (A.09.03 [1417], ©Agilent Technologies 1990–2002).

Prior to injection into the chromatographic system, analyte solutions were filtered through disposable 0.22 μm Nylon® syringe filters (Análisis Vínicos, S.L., Tomelloso, Ciudad Real, Spain). Mobile phase solutions were vacuum-filtered through 0.22 μm Nylon membranes (Micron Separations, Westboro, MA, USA) and were degassed in an Elmasonic S60 ultrasonic bath (Elma, Singen, Germany) prior to use. A Crison MicropH 2000 pHmeter (Crison Instruments, Barcelona, Spain) was employed to adjust the pH of the aqueous mobile phase solutions.

2.2. Chemicals and solutions

All reagents were of analytical grade. Ammonium bicarbonate, ammonia, acetonitrile (ACN) and methanol (©Multisolvent, HPLC grade) were from Scharlau, S.L. (Barcelona, Spain). 5 mM Ammonium bicarbonate buffer solution was prepared by dissolving the appropriate amount of ammonium bicarbonate in water and adjusting the pH to 8.0 with 1 M ammonium hydroxide. Ultra Clear TWF UV deionised water (SG Water, Barsbüttel, Germany) was used to prepare solutions.

Bicalutamide, brompheniramine maleate, bupropion hydrochloride carbinoxamine maleate, chlorpheniramine maleate, clemastine fumarate, clenbuterol hydrochloride, doxylamine succinate, ethopropazine hydrochloride, fexofenadine hydrochloride, methadone hydrochloride, methotrimeprazine maleate, nomifensine maleate, orphenadrine hydrochloride, pantoprazole sodium, pindolol, procyclidine hydrochloride, rabeprazole sodium, terfenadine, thioridazine hydrochloride, trimeprazine hemi(+)-tartrate and verapamil hydrochloride were from Sigma-Aldrich (©Merck KGaA, Darmstadt, Germany). Atenolol, cinildipine, isoprenaline hydrochloride, mexiletine hydrochloride and propranolol hydrochloride were from Acros (Acros Organics, Geel, Belgium). Citalopram hydrobromide was from Tokyo Chemical Industry (Tokyo, Japan). Disopyramide was from MP Biomedicals (Irvine, CA, USA). Felodipine and oriprenaline sulfate were from EDQM (Strasbourg, France). Hydroxyzine hydrochloride was from Guinama (Valencia, Spain). Propafenone hydrochloride and terbutaline hemisulfate were from Abcam (Cambridge, United Kingdom). Bambuterol hydrochloride, bupivacaine, cetirizine hydrochloride, trimipramine maleate and warfarin were from Cayman Chemical Co (Ann Arbor, MI, USA). Acebutolol hydrochloride, aminoglutethimide, metoprolol tartrate, mianserin hydrochloride and salbutamol sulfate were from Alfa

Table 1

Enantioresolution data (R_s) obtained with the different amylose-based CSPs studied. Compounds are identified by their name and numbered order (No). Categorical enantioresolution (CRs) levels are assigned according to the experimental observations: $RsC = 1$ if $R_s > 2$; otherwise, $RsC = 0$. ϕ is the percentage of acetonitrile selected. See further details in Section 3.1.

Name	No	Family ^a	Am1			Am2			Am3		
			$Rs1_{max}$	ϕ	$CRs1$	$Rs2_{max}$	ϕ	$CRs2$	$Rs3_{max}$	ϕ	$CRs3$
Disopyramide	1	1	0.7	50	0	0	10	0	2.8	60	1
Mexiletine	2	1	0.6	50	0	0	10	0	0	50	0
Propafenone	3	1	2.0	50	1	4.0	60	1	1.0	70	0
Warfarin	4	2	5.5	50	1	0	50	0	5.3	60	1
Bupropion	5	3	6.7	50	1	0	30	0	2.4	50	1
Citalopram	6	3	0	40	0	0.5	30	0	0	60	0
Fluoxetine	7	3	0	40	0	0	40	0	0	60	0
Mianserin	8	3	8.3	60	1	0	40	0	3	60	1
Nomifensine	9	3	3.0	60	1	1.3	30	0	8.4	60	1
Trimipramine	10	3	0	50	0	0	50	0	0	60	0
Viloxazine	11	3	1.5	20	0	0	10	0	1.9	50	0
Benalaxyl	12	4	4.1	60	1	1.6	50	0	6.6	60	1
Hexaconazole	13	4	5.6	60	1	0	40	0	0	50	0
Imazalil	14	4	1.1	50	0	1.2	40	0	1.2	50	0
Metalaxyl	15	4	1.8	40	0	0	20	0	1.5	40	0
Myclobutanil	16	4	0	40	0	0	30	0	2.0	50	1
Penconazole	17	4	1.0	50	0	0	40	0	3.5	60	1
Brompheniramine	18	5	1.2	60	0	1.6	60	0	1.4	60	0
Carbinoxamine	19	5	1.8	50	0	0	20	0	0	60	0
Cetirizine	20	5	0	30	0	0	20	0	0	60	0
Chlorpheniramine	21	5	0.9	60	0	2.0	60	1	1.3	60	0
Clemastine	22	5	0	60	0	0	50	0	0	70	0
Doxylamine	23	5	0	20	0	0.6	20	0	0	60	0
Fexofenadine	24	5	0	20	0	0	10	0	0	30	0
Hydroxyzine	25	5	2.9	60	1	0	30	0	0	60	0
Orphenadrine	26	5	0	40	0	0	30	0	0	60	0
Terfenadine	27	5	0	70	0	0	60	0	0	60	0
Bupivacaine	28	6	0	50	0	0	50	0	0	60	0
Mepivacaine	29	6	0	30	0	0	30	0	1.3	50	0
Propanocaine	30	6	0.9	50	0	0.4	50	0	0	40	0
Methadone	31	7	0	40	0	0	40	0	0	60	0
Aminoglutethimide	32	8	3.4	70	1	0	30	0	1.5	60	0
Bicalutamide	33	8	3.7	50	1	3.3	40	1	2.4	60	1
Acebutolol	34	9	0.7	50	0	0	10	0	0.3	60	0
Metoprolol	35	9	0	30	0	0	10	0	0	60	0
Pindolol	36	9	0.5	40	0	0	10	0	0	60	0
Salbutamol	37	9	0	10	0	0	10	0	0	10	0
Timolol	38	9	0	20	0	0	10	0	0	60	0
Bambuterol	39	10	0	20	0	0	10	0	1.2	60	0
Clenbuterol	40	10	0.4	50	0	0	20	0	0.6	60	0
Isoprenaline	41	10	0	10	0	0	10	0	0.7	10	0
Orciprenaline	42	10	0	10	0	0	10	0	0	10	0
Terbutaline	43	10	0	10	0	0	10	0	0	10	0
Cinildipine	44	11	0	50	0	1.5	60	0	0	50	0
Felodipine	45	11	0	50	0	0	40	0	0	50	0
Verapamil	46	11	0.6	50	0	0	40	0	0	60	0
Procyclidine	47	12	0	50	0	0	50	0	0	60	0
Ethopropazine	48	13	1.4	60	0	0	50	0	0	50	0
Methotrimeprazine	49	13	0	50	0	0	50	0	0	60	0
Thioridazine	50	13	0	60	0	0	60	0	0.7	70	0
Trimeprazine	51	13	0	50	0	0	40	0	0.6	60	0
Pantoprazole	52	14	0.5	40	0	0.8	20	0	2.0	60	1
Rabeprazole	53	14	2.6	50	1	2.0	30	1	5.1	60	1

^a Drug/Pesticide families: 1 (antiarrhythmic drugs), 2 (anticoagulants), 3 (antidepressants), 4 (fungicides), 5 (antihistamines), 6 (local anaesthetics), 7 (analgesics), 8 (antineoplastics), 9 (β -blockers), 10 (bronchodilators), 11 (calcium channel blockers), 12 (anticholinergic drugs), 13 (antipsychotic drugs) and 14 (proton pump inhibitors).

Aesar (Thermo Fisher Scientific Inc., Karlsruhe, Germany). All the rest of drugs tested were kindly donated by several pharmaceutical laboratories: fluoxetine hydrochloride by Alter (Madrid, Spain) and mepivacaine hydrochloride by Laboratorios Inibsa (Barcelona, Spain); propanocaine by Laboratorio Seid (Barcelona, Spain); timolol maleate by Merck Sharp & Dohme (Madrid, Spain) and viloxazine hydrochloride by Astra Zeneca (Cheshire, UK). All racemic pesticides (benalaxyl, hexaconazole, imazalil, metalaxyl, myclobutanil, and penconazole) were from Dr. Ehrenstorfer GmbH (Augsburg, Germany).

Stock standard solutions of compounds used in this study were prepared by dissolving 10 mg of the racemate in 10 mL of methanol. Working solutions were prepared by dilution of the stock standard solutions using the mobile phase solution. The solutions were stored under refrigeration at 5°C.

2.3. Methodology for the chiral separation of compounds

The experimental maximum enantioresolution (Rs_{max}) values of the compounds listed in Table 1 were obtained using the fol-

lowing polysaccharide-based chiral columns: Lux Amylose-1 (amylose tris(3,5-dimethylphenylcarbamate); 3 μm , 150 \times 4.6 mm i.d.; Phenomenex, Torrance, CA, USA), *Am1*; Lux Amylose-2 (amylose tris(5-chloro-2-methylphenylcarbamate); 3 μm , 150 \times 2.0 mm i.d.; Phenomenex), *Am2* and i-Lux Amylose-3 (amylose tris(3-chloro-5-methylphenylcarbamate); 3 μm , 150 \times 4.6 mm i.d.; Phenomenex), *Am3*. Except for warfarin, mobile phases were prepared as binary mixtures of ammonium bicarbonate buffer (5 mM, pH 8) and ACN in varying proportion (10–80 % in volume of ACN). For warfarin, formic acid 0.1% (v) was used instead ammonium bicarbonate buffer. The mobile phase flow rate was 1.0 mL min⁻¹ in all cases except when using the Lux Amylose-2. In this last column, the mobile phase flow rate was 0.5 mL min⁻¹. In all of the experiences, the injection volume was 2 μL . The detection was performed in the UV at 220 nm for all the compounds, except for ethopropazine, methotrimeprazine and trimeprazine whose detection was performed at 254 nm. The column was thermostatted at 25°C.

2.4. Software and calculations

In this paper 58 structural variables of the compounds have been used (see Table S1 and S2 in Supplementary Data). Most of them were taken from the online ChemSpider chemical structure database [34] and were also tested in previous papers [31–33] related to the chiral carbon (C*), for instance, C*X (C*-heteroatoms), C*a (C*-aliphatic), C*H (C*-H) and C*C=O (C*-carbonyl), among others [32,33]. Variables \mathbf{x}_8 to \mathbf{x}_{15} correspond to predicted molecular descriptors from ACD/Labs and ChemAxon calculations: molecular weight (MW), octanol-water partition coefficient (log *P*), hydrogen bonding acceptor (HBA) and donor (HBD), minimal (*zmin*) and maximal *z* length (*zmax*), polar surface area (PSA), among others. Variable \mathbf{x}_{16} , the apparent log*P* at working pH (log*D*), was estimated as in reference [31].

Variables \mathbf{x}_{17} to \mathbf{x}_{33} correspond to molecular topological parameters predicted by ChemAxon; for example, aliphatic bond account (*abc*), aromatic bond count (*Abc*), bond count (bond count), ring bond count (*Rbc*), fused ring count (*frc*), hetero ring count (*Hrc*), heteroaliphatic ring count (*Harc*), ring count (*Rc*) and Balaban index (*Bi*). Finally, variables \mathbf{x}_{34} to \mathbf{x}_{58} are obtained as the count of atoms/groups present in the entire molecule; for instance, number of oxygen (*O*) and fluoride (*F*) atoms, hydroxyl (*OH*), tertiary amine (*NR₂*), ether (*ROR*), CH₃ groups (*ACH3*) and Cl atoms (*ACl*) bonded to aromatic rings, aromatic ring-C-aromatic (*ACA*) moieties, 1,2- (*A12*) and 1,2,3- (*A123*) substituted aromatic rings, aromatic nitrogen (*NA*), tertiary amine in aliphatic cycles (*NRC*) and sulphur aliphatic cycles (*Sc*) groups among others.

Discriminant partial least squares, for one response categorical variable (DPLS1) models have been performed using The Unscrambler® v.9.2 multivariate analysis software [35].

For DPLS1 modelling, categorised *R_s* (*CRs*) values (see Table 1) were used as response variable (*y*). For compounds showing baseline enantioresolution (*R_s* \geq 2.0), *CRs* = 1 (class-1) was assigned. The rest of compounds were assigned to *CRs* = 0 (class-0). As predictor matrix (*X*), the structural variables of the compounds (see section 2.4 and Table S2) were used. All *y-X* data were autoscaled before DPLS1. The corresponding coefficients (scaled), directly measures the importance of the variables [31–33, 36].

Feature selection (FS) was done using a leave-one-variable-out (or sequential) strategy equivalent to that used in the sequentialfs.m code available from MATLAB® R2019a (Mathworks®) web site [37]. The outputs from the DPLS1 were used to eliminate the worst variable on each run (the process was called FS-DPLS1). The variable whose elimination provokes the highest improvement of a target indicator (*TI*) function is removed for the next run. The following function (not previously reported) was considered to select

the variable to be eliminated each run:

$$TI = W1dD + (1 - W1)dDcv - W2mUrb - W3SSclass \quad (1)$$

where, *W1*, *W2* and *W3* are parameters in the 0–1 range to be optimised. *dD* is the lowest discriminant distance between the outputs from the two classes (i.e. the distance between the lowest *y*-predicted of class-1 and the highest *y*-predicted of class-0 data from DPLS1) and *dDcv* is as *dD* but for cross-validated predicted *y*-values. *mUrb* is the mean of the relative uncertainty of the DPLS1 coefficients (related to the importance of the variables). *SSclass* is the sum of squares for difference between predicted and actual DL values for compounds (i.e. *y*-predicted values from DPLS1 equal or higher than the lowest *y*-predicted of class-1 are assigned to DL = 1 and *y*-predicted values equal or lower than the highest *y*-predicted of class-1 are assigned to DL = 0; otherwise, DL = 0.5 is assigned).

Since *dD* represent the lowest distance between the classes, *dD* > 0 (the two groups are fully separated) can be considered an acceptable descriptive ability. Moreover, *dDcv* > 0 would correspond to an acceptable predictive ability. Low *mUrb* (i.e. low absolute coefficient uncertainty and/or high coefficient value) values mean more confidence on the model coefficients, thus more reliable variable, while low *SSclass* values indicate high classification ability, both aspects indirectly increase the descriptive ability of the model.

The parameters (*W1*, *W2*, *W3*) were optimized for each CSP, combining SIMPLEX optimization, from *fminsearch.m* [38], design of experiments (DOE), from *bbdesign.m* [39] and manual refinement strategies (manually varying one parameter value, previously optimized, to confirm that it is the adequate one).

3. Results and discussion

3.1. Retention behaviour and enantioresolution of compounds in amylose-based CSPs in reversed-phase conditions

The aim of this study is to explore the ability of *Am1*, *Am2* and *Am3* to enantioresolve chiral compounds using reversed phase conditions compatible with MS detection for their use in routine analysis (*k* value for the most retained enantiomer lower than 15). Table 1 shows the chiral compounds studied, which belong to 14 therapeutic families: antiarrhythmic drugs, anticoagulants, antidepressants, fungicides, antihistamines, local anaesthetics, analgesics, antineoplastics, β -blockers, bronchodilators, calcium channel blockers, anticholinergic drugs, antipsychotic drugs and proton pump inhibitors. Table S1 in Supplementary Data shows the chemical structure and the molecular weight, *pK_a*, log *P* and log *D* (estimated at pH 8.0) values for compounds under study. At working pHs, most of the compounds studied present positive net charge. Cetirizine (*No* = 20) has negative net charge; and warfarin (*No* = 4), fexofenadine (*No* = 24), aminoglutethimide (*No* = 32), cinildipine (*No* = 44), felodipine (*No* = 45) and fungicides (*No* = 12–17) have zero net charge. Compounds studied presents variable hydrophobic character (log *D* values ranged between -1.6 and 5.2).

For each analyte and CSP, the mobile phase that provided maximum *R_s* and *k* < 15 values was selected. Table 1 shows the maximum resolution values (*R_{smax}*) obtained for each compound and CSP together with the content of ACN in the mobile phase.

As can be observed in Table 1, 16 compounds of the 53 studied were fully resolved (30 %) and 19 were partially resolved (36 %) at least in one of the CSPs studied and the reversed phase conditions assayed. *Am1* allowed the complete resolution (baseline resolution) of 11 compounds whereas 16 were partially resolved. Similar results were obtained for *Am3* enabling the complete and partial res-

olution of 11 and 14 compounds, respectively. The worst results were obtained for *Am2* which only allowed the baseline resolution of 4 compounds while 9 remained partially resolved. Although the experimental resolution values were close or higher than 1.5 for some compounds (i.e. viloxazine, metalaxyl, brompheniramine, carbinoxamine and ethopropazine), baseline resolution was not observed. In these cases, the quality of the separation was affected by the high peak width obtained. The best resolution values in each column were obtained for mianserine ($Rs_{1max} = 8.3$; $No = 8$) in *Am1*, propafenone ($Rs_{2max} = 4.0$; $No = 8$) in *Am2* and nomifensine ($Rs_{3max} = 8.4$; $No = 9$) in *Am3*.

Bicalutamide and rabeprazole were baseline resolved in all three columns. Warfarin, bupropion, mianserin, nomifensine, benalaxyl, bicalutamide and rabeprazole were completely resolved in both *Am1* and *Am3* columns; for the rest of compounds, differences in enantioselectivity between *Am1* and *Am3* columns were observed, indicating differences in the interactions between the compounds and the CSPs.

It is known that polysaccharide-based CSPs may behave either as RP-like or HILIC-like stationary phases depending on compounds characteristics and separation conditions, especially when using ACN mobile phases with low water contents (<30%) [6–10]. In the experimental conditions assayed in this paper which include mobile phases with a water content in the range 20–90% (v/v), for all compounds and CSPs, typical chromatographic reversed phase behaviour was observed. The increase in the water content in the mobile phase produced an increase in the retention time of the compounds. Different behaviour was observed for resolution values. In most cases, resolution improved as the percentage of ACN in the mobile phase decreased (retention increased), as observed in Figure 1A for rabeprazole in the column *Am2*. However, for other compounds, e.g. brompheniramine in *Am1* (see Figure 1B), better resolutions were achieved when using higher percentages of ACN in the mobile phase for all the CSPs studied. This can be due to the existence of two opposite effects: thermodynamic and kinetic processes. For some compounds, resolution is mostly affected by the thermodynamics of the process (separation factor increased as retention increased), while for other compounds, the kinetics contribution (efficiency decreased as retention increased) prevails over the others [5].

On the other hand, for the same ACN content in the mobile phase, in general terms, *Am3* provided the highest k values. This behaviour might be due to the different electronic features of the polymers, along with the type CSP, that is immobilised vs coated [5].

Figure 2 shows the relationships between the logarithm of retention factors for the less retained enantiomers ($\log k_1$) and their corresponding $\log D$ values for each CSP. As can be observed, retention increased as hydrophobicity increased for *Am1* (Figure 2A) and *Am2* (Figure 2B) columns, as expected in reversed-phase conditions. Besides, a linear trend is observed for *Am1* column. In contrast, retention of analytes seems to be independent of their hydrophobicity in *Am3* column (Figure 2C).

3.2. Structure-categorical enantioresolution relationships in amylose-based CSPs

In this paper, an attempt has been performed to detect the effect of the structural variables of compounds on the resolution values obtained for each amylose-based CSPs in the chromatographic conditions assayed. In this paper, the experimental Rs values were also converted into categorised CRs values (see section 2.4 and Table 1).

DPLS1 modelling was selected to relate the structural data (X -matrix) (see section 2.4) to the $CRs1$ and $CRs3$ data (y -vectors) for *Am1* and *Am3*, respectively. *Am2* was not included in the analy-

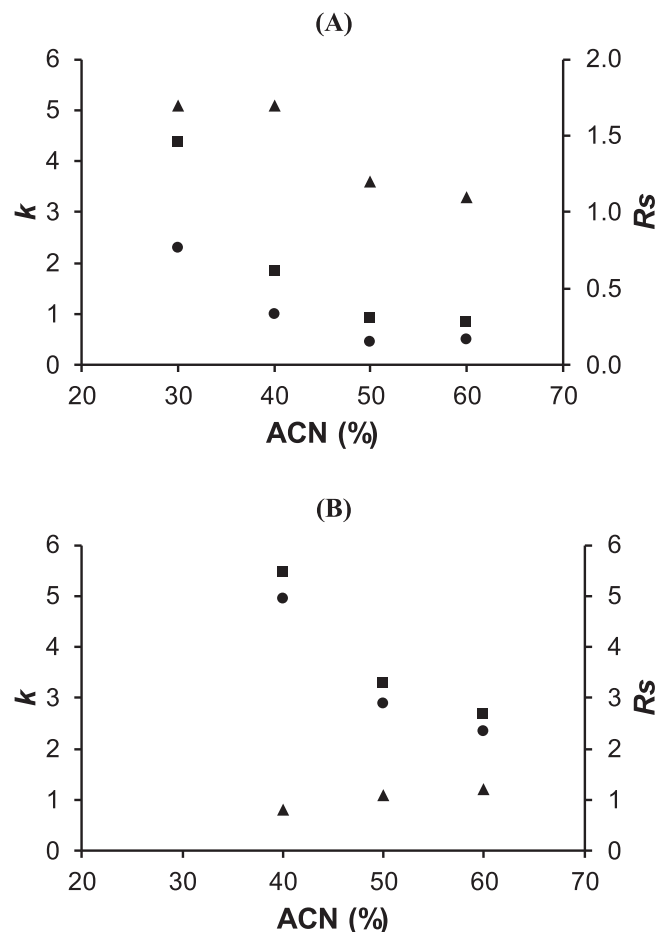


Figure 1. Resolution values, (\blacktriangle) Rs , and retention factors, k , for the less (\bullet) and the most retained enantiomer (\blacksquare) versus the percentage of acetonitrile (ACN, %) in the mobile phase. (A) Rabeprazole in *Am2* and (B) brompheniramine in *Am1*. See further details in section 2.3.

sis because the low number of class =1 data (just 4 compounds, see Table 1). Table 2 shows some outputs corresponding to the initial DPLS1 models (all variables) and the final model after the FS-DPLS1 process for *Am1* and *Am3*. For both columns, the initial DPLS1 model with 57 variables showed a poor descriptive ability, since $Dd < 0$. Thus such models become risky to define the importance of the variables. After an exhaustive of optimization study of the coefficients in Eq. 1, satisfactory models, with a considerable reduction of the number of the (irrelevant), variables were found. As can be seen in Table 2, for both columns, the results after FS-DPLS1 can be used to compare the importance of the remaining variables ($dD > 0$), which fits with the aim of this paper.

Comparing the two columns in Table 2, apparently, the results for *Am1* are better (higher dD ; with similar $dDcv$ value), but the DPLS1 model is more complex (7 latent variables) compared with the one for *Am3* (2 latent variables) and also in the case of *Am3*, the final mean uncertainty of the selected coefficients ($mUrb$) is lower. As an example, Figure 3 shows the feature selection progress in the case of column *Am1*.

Figure 4 shows the DPLS1 regression coefficients (scaled) for the selected variables for the columns *Am1* and *Am3*. Their absolute value indicates the importance of the variable to discriminate between the classes. Their sign indicates a positive or negative contribution on CRs . As can be observed, in both cases, variables related to atoms/groups bonded to the chiral carbon (C^*) or present in the entire molecule and molecular topological parameters were

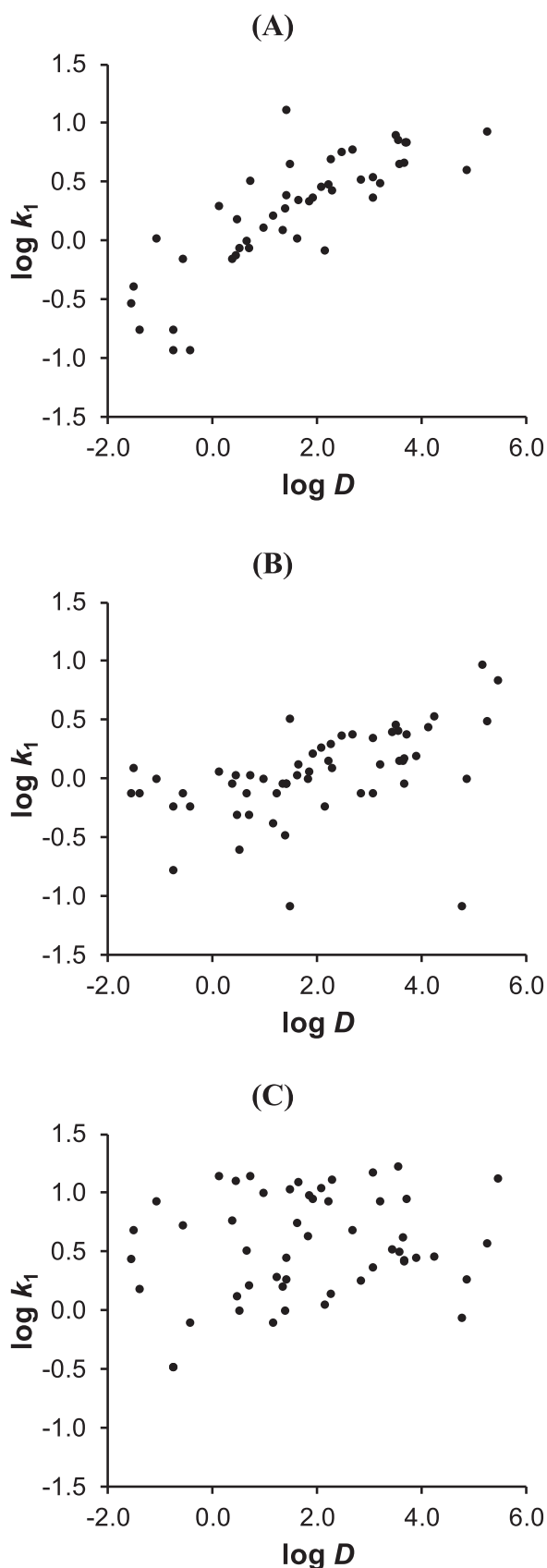


Figure 2. Representation of the logarithm of retention factor for less retained enantiomer ($\log k_1$) versus the logarithm of the distribution coefficient ($\log D$) at pH = 8 for the CSPs studied: (A) *Am1*, (B) *Am2* and (C) *Am3*. The mobile phases used for this data were 5 mM ammonium bicarbonate (pH 8)/acetonitrile (50/50, v/v) for *Am1* and 5 mM ammonium bicarbonate buffer (pH 8)/acetonitrile (40/60, v/v) for *Am2* and *Am3*.

selected. For a given compound and a given CSP, the balance between positive and negative contributions determines enantioresolution in that CSP.

For *Am1* column (Figure 4A), among the variables linked to the chiral center (C^* -parameters), $C^*C=O$ is the most important variable that favours enantioresolution. Additionally, the absence of heteroatoms (C^*X variable) or hydrogen (C^*H variable) substituents in C^* favours enantioresolution. The presence of carbonyl groups in amides ($-C(=O)NR_1R_2$), ketones ($-C(=O)-R$) and esters ($-C(=O)-OR$) linked to the chiral center is of great importance in the enantioresolution process ($C^*C=O$ variable). This is the case, for example, of bupropion ($No = 5$ in Table 1), benalaxyl ($No = 12$), aminoglutethimide ($No = 32$) and bicalutamide ($No = 33$). The amides have a conjugate system on the atoms of O, C, N, consisting of molecular orbitals occupied by delocalised electrons and therefore, selector-selectand $\pi-\pi$ interactions can exist. Amides, esters and ketones are hydrogen-bond acceptors and can provide hydrogen-bond interactions with the selector.

The presence of aromatic bonds in the molecule that favours $\pi-\pi$ interactions also favours the enantioresolution (*Abc* variable) in *Am1* column, as in the case of warfarin ($No = 4$). Nevertheless, the position and nature of the substituents in the aromatic ring can favour (e.g., *ACI*, *A12* and *A123* variables) or disfavour (e.g., *ACH3*, *ACA*) enantioresolution. The absence of aliphatic bonds in the molecule (*abc* and *bc* variables) also favours enantioresolution. On the other hand, for *Am1* column, the presence of a ternary amine (hydrogen-bond acceptor) in an aliphatic cyclic group also favours enantioresolution (*NRC* variable).

For *Am3* column (Figure 4B), $C^*C=O$ is the most important variable, among C^* -parameters, that favours enantioresolution; so selector-selectand $\pi-\pi$ interactions and hydrogen-bond interactions are of utmost importance for chiral separation. Moreover, the absence of heteroatoms (C^*X variable, as in *Am1* column) or aliphatic (C^*a variable) substituents in C^* favours enantioresolution. As in the case of *Am1* column, aromatic bonds (*Abc* variable) favours enantioresolution. Additionally, the presence of fused rings (*frc* variable) also improves resolution, as in the case of mianserin ($No = 8$), nomifensine ($No = 9$), pantoprazole ($No = 52$) or rabeprazole ($No = 53$). This is probably due to the fact that they confer rigidity to the molecule.

On the other hand, the presence of nitrogen in aromatic rings (*NA* variable) is also important to favour enantioresolution on *Am3* (e.g., for disopyramide ($No = 1$), myclobutanil ($No = 16$), penconazole ($No = 17$), pantoprazole ($No = 52$), rabeprazole ($No = 53$), oppositely to *Am1* column. In the basic aromatic rings (e.g. pyridinic rings), in which the nitrogen atom is not connected to a hydrogen atom, the lone pair of electrons is not part of the aromatic system and it is responsible for the basicity of these nitrogenous bases, similar to the nitrogen atom in amines. Therefore, they are hydrogen bonding acceptors. In the non-basic rings, in which the nitrogen atom is connected to a hydrogen atom, the lone pair of electrons of the nitrogen atom is delocalised and contributes to the aromatic π -electron system favouring selector-selectand $\pi-\pi$ interactions. The combination of these interactions together with the formation of a Lewis adduct between the aromatic amines (Lewis bases) and the chlorine atom in 3-position of the phenylcarbamate moiety in *Am3* column (Lewis acid) and/or between the aromatic amines and the acidic proton of the carbamate moiety of *Am3*, which hydrogen-bond donor character is exalted by the 3-chloro substitution, could explain the opposite selectivity to *Am1* column. Disopyramide ($No = 1$), myclobutanil ($No = 16$) and penconazole ($No = 17$) are examples of aromatic amines exhibiting this opposite enantioselectivity between *Am1* and *Am3* columns (see Table 1).

Table 2
Comparison of models

Column	DPLS1	Variables	<i>mUrb</i>	<i>dD</i>	<i>dDcv</i>	Descriptive ability	Predictive ability
<i>Am1</i>	Initial	57	10.9	-1.67	-2.85	Poor	Limited
	Final	22	1.2	0.56	-0.62	Acceptable	Limited
<i>Am3</i>	Initial	57	4.2	-0.88	-1.31	Poor	Limited
	Final	16	1.2	0.22	-0.67	Acceptable	Limited

Parameters, [*W1 W2 W3*], for Eq. 1 were: [0.53 0.49 0.48] for *Am1*; [1.0 0.083 0.62] for *Am3*.

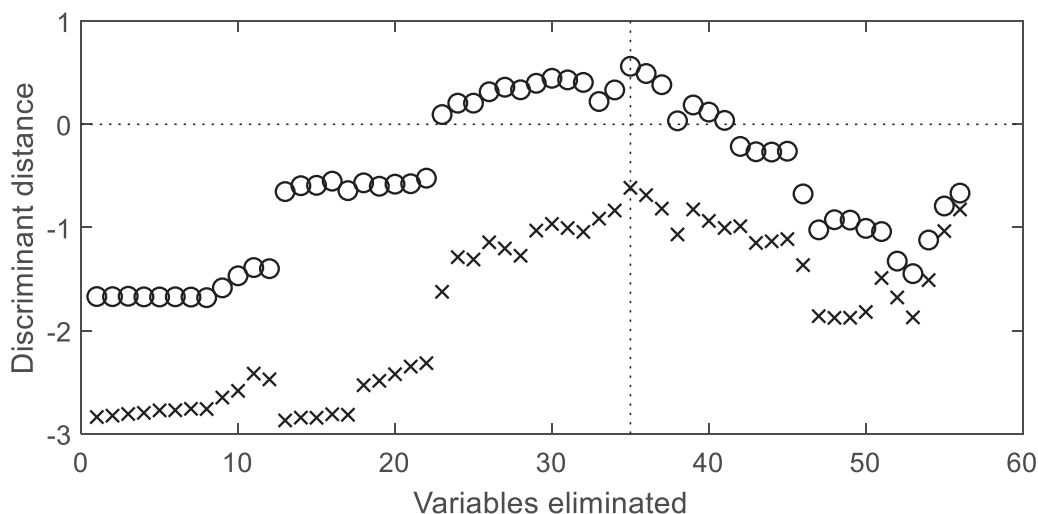


Figure 3. Feature selection progress in the case of *Am1* column. (o) Discriminant distance (*dd*); (x) Discriminant distance in cross-validation (*dDcv*). A discriminant distance above zero (dotted horizontal line) implies fully discrimination between classes. Elimination of 35 variables (vertical dashed line) provides a suitable DPLS1 model (with 22 remaining variables), providing *dd* > 0 (the highest value during the FS-DPLS1 process), which suggests acceptable descriptive ability.

4. Conclusions

In this paper, the resolution ability of three commercial amylose-based chiral stationary phases (*Am1*, *Am2* and *Am3*) is studied using acetonitrile/ammonium bicarbonate mobile phases compatible with MS detection. On the other hand, maximum retention factor are set to 15, so the chiral chromatographic methods developed are directly transferable to routine work. Studies are conducted for 53 structurally unrelated chiral compounds.

In the experimental conditions assayed which include mobile phases with a water content in the range 20–90% (v/v), for all the compounds studied and CSPs, typical chromatographic reversed phase behaviour was observed. On the other hand, resolution improved as the percentage of acetonitrile in the mobile phase decreased (retention increased) for most compounds. However, for some compounds better resolutions were achieved when using higher percentages of acetonitrile in the mobile phase for all the CSPs studied.

Hydrophobicity of compounds was an important property determining their retention in *Am1* and in a lesser extent in *Am2*. In contrast, retention of analytes was found to be independent of their hydrophobicity in *Am3* column.

Am1 and *Am3* CSPs allowed baseline resolution for a similar number of compound. Nevertheless, differences in chiral selectivities between both columns were observed. *Am2* provided the worst results, although its selectivity is also complementary to the other CSPs.

FS-DPLS1 modelling for 58 structural variables provided reduced set of variables with positive and negative contributions for

categorical enantioresolution in *Am1* and *Am3* CSPs. For a given compound in a given CSP, the balance of such contributions determines enantioresolution in that CSP.

For *Am1* and *Am3* CSPs, the presence of carbonyl groups linked to the chiral centre ($C^*C=O$ variable) as well as the presence of aromatic bonds (*Abc* variable) are of great importance in the enantio-recognition process. This suggests that selector-selectand π - π and hydrogen-bond interactions could play determinant role. In the case of *Am1*, the position and nature of the substituents in the aromatic ring can favour or disfavour enantioresolution. For *Am1* column, the presence of a ternary amine (hydrogen-bond acceptor) in an aliphatic cyclic group also favours enantioresolution (*NRC* variable).

For *Am3* column the presence of fused rings (*frc* variable) also improves resolution. This is probably due to the fact that they confer rigidity to the molecule.

On the other hand, the presence of nitrogen in aromatic rings (*NA* variable) is also important for enantioselectivity. Although, this variable presents an opposite effect for each column, i.e. favourable for *Am3* and unfavourable for *Am1*. The combination of selector-selectand π - π and hydrogen bonding interactions together with the formation of a Lewis adduct between the aromatic amines (Lewis bases) and the chlorine atom in 3-position of the phenyl-carbamate moiety in *Am3* column (Lewis acid) and/or between the aromatic amines and the acidic proton of the carbamate moiety of *Am3*, which hydrogen-bond donor character is exalted by the 3-chloro substitution could explain this opposite selectivity to *Am1* column.

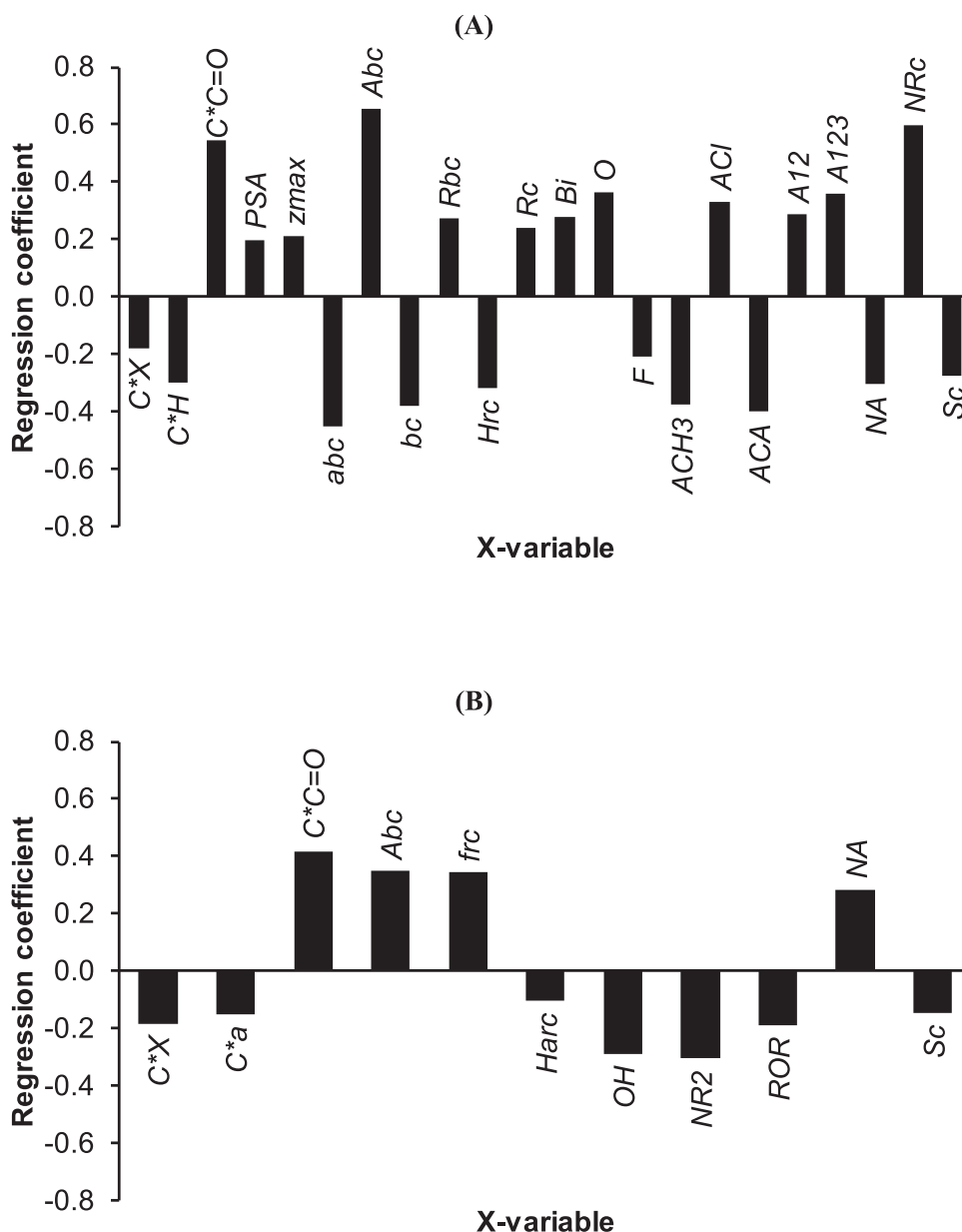


Figure 4. Regression coefficients obtained by FS-DPLS1 for: (A) Am1 and (B) Am3. See section 2.4 for further details.

Declaration of Competing Interest

The authors declare no conflict of interest.

CRediT authorship contribution statement

Mireia Pérez-Baeza: Investigation, Validation. **Laura Escuder-Gilbert:** Conceptualization, Supervision, Writing - original draft, Writing - review & editing. **Yolanda Martín-Biosca:** Methodology, Visualization, Writing - review & editing. **Salvador Sagrado:** Methodology, Software, Formal analysis, Data curation. **María José Medina-Hernández:** Conceptualization, Supervision, Project administration, Writing - review & editing.

Acknowledgements

The authors acknowledge the Spanish Ministerio de Economía y Competitividad (MINECO) and the European Regional Development Fund (ERDF) for the financial support (Project CTQ2015-70904-R,

MINECO/FEDER, UE). Mireia Pérez Baeza is grateful to the Generalitat Valenciana and the European Social Fund for the financial support (ACIF/2019/158 research contract).

Supplementary materials

Supplementary material associated with this article can be found, in the online version, at [doi:10.1016/j.chroma.2020.461281](https://doi.org/10.1016/j.chroma.2020.461281).

References

- [1] R.B. Yu, J.P. Quirino, Chiral liquid chromatography and capillary electrochromatography: Trends from 2017 to 2018, *Trends Anal. Chem.* 118 (2019) 779–792.
- [2] J.M. Padró, S. Keunchkarian, State-of-the-art and recent developments of immobilized polysaccharidebased chiral stationary phases for enantioseparations by high-performance liquid chromatography (2013–2017), *Microchem. J.* 140 (2018) 142–157.
- [3] G.K.E. Scriba, Chiral recognition in separation sciences. Part I: Polysaccharide and cyclodextrin selectors, *Trends Anal. Chem.* 120 (2019) 115639.
- [4] J. Teixeira, M.E. Tiritan, M.M.M. Pinto, C. Fernandes, Chiral stationary phases for liquid chromatography: recent developments, *Molecules* 24 (2019) 865.

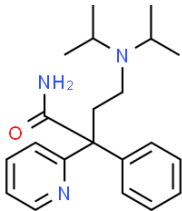
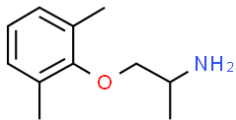
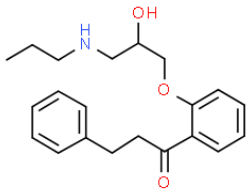
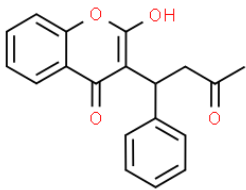
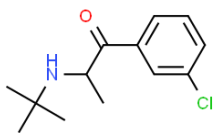
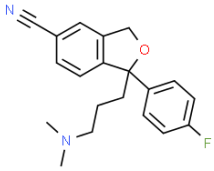
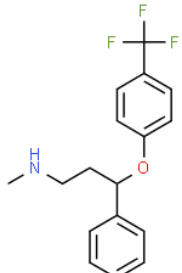
- [5] B. Chankvetadze, Recent trends in preparation, investigation and application of polysaccharide-based chiral stationary phases for separation of enantiomers in high-performance liquid chromatography, *Trends Anal. Chem.* 122 (2020) 115709.
- [6] B. Chankvetadze, Recent developments on polysaccharide-based chiral stationary phases for liquid-phase separation of enantiomers, *J. Chromatogr. A* 1269 (2012) 26–51.
- [7] B. Cerra, A. Macchiarulo, A. Carotti, E. Camaioni, I. Varfaj, R. Sardella, A. Gioliello, Enantioselective HPLC Analysis to Assist the Chemical Exploration of Chiral Imidazolines, *Molecules* 25 (2020) 640–651.
- [8] P. Peluso, V. Mamane, E. Aubert, S. Cossu, Insights into the impact of shape and electronic properties on the enantioseparation of polyhalogenated 4,4'-bipyridines on polysaccharide-type selectors. Evidence for stereoselective halogen bonding interactions, *J. Chromatogr. A* 1345 (2014) 182–192.
- [9] R. Geryk, K. Kalíková, J. Vozka, E. Tesařová, Immobilized Polysaccharide-Based Stationary Phases for Enantioseparation in Normal Versus Reversed Phase HPLC, *Chromatographia* 78 (2015) 909–915.
- [10] I. Matarashvili, D. Ghughunishvili, L. Chankvetadze, N. Takaishvili, T. Khatishvili, M. Tsintsadze, T. Farkas, B. Chankvetadze, Separation of enantiomers of chiral weak acids with polysaccharide-based chiral columns and aqueous-organic mobile phases in high-performance liquid chromatography: Typical reversed-phase behavior? *J. Chromatogr. A* 1483 (2017) 86–92.
- [11] L. Peng, S. Jayapalan, B. Chankvetadze, T. Farkas, Reversed-phase chiral HPLC and LC/MS analysis with tris(chloromethylphenylcarbamate) derivatives of cellulose and amylose as chiral stationary phases, *J. Chromatogr. A* 1217 (2010) 6942–6955.
- [12] A. Ghanem, C. Wang, Enantioselective separation of racemates using CHIRAL-PAK IG amylose-based chiral stationary phase under normal standard, non-standard and reversed phase high performance liquid chromatography, *J. Chromatogr. A* 1532 (2018) 89–97.
- [13] G. D'Orazio, C. Fanali, S. Fanali, A. Gentili, B. Chankvetadze, Comparative study on enantiomer resolving ability of amylose tris(3-chloro-5-methylphenylcarbamate) covalently immobilized onto silica in nano-liquid chromatography and capillary electrochromatography, *J. Chromatogr. A* 1606 (2019) 460425.
- [14] Z. Shedania, R. Kakava, A. Volonterio, T. Farkas, B. Chankvetadze, Separation of enantiomers of chiral sulfoxides in high-performance liquid chromatography with cellulose-based chiral selectors using acetonitrile and acetonitrile-water mixtures as mobile phases, *J. Chromatogr. A* 1609 (2020) 460445.
- [15] M. Lämmerhofer, Chiral recognition by enantioselective liquid chromatography: Mechanisms and modern chiral stationary phases, *J. Chromatogr. A* 1217 (2010) 814–856.
- [16] G.K.E. Scriba, Chiral recognition mechanisms in analytical separation sciences, *Chromatographia* 75 (2012) 815–838.
- [17] J. Shen, Y. Okamoto, Efficient separation of enantiomers using stereoregular chiral polymers, *Chem. Rev.* 116 (2016) 1094–1138.
- [18] Y. Okamoto, T. Ikai, Chiral HPLC for efficient resolution of enantiomers, *Chem. Soc. Rev.* 37 (2008) 2593–2608.
- [19] T. Ikai, Y. Okamoto, Structure control of polysaccharide derivatives for efficient separation of enantiomers by chromatography, *Chem. Rev.* 109 (2009) 6077–6101.
- [20] J. Shen, T. Ikai, Y. Okamoto, Synthesis and application of immobilized polysaccharide-based chiral stationary phases for enantioseparation by high-performance liquid chromatography, *J. Chromatogr. A* 1363 (2014) 51–61.
- [21] R.B. Kasat, S.Y. Wee, J.X. Loh, E.I. Franses, N.-H.L. Wang, Effect of the solute molecular structure on its enantioresolution on cellulose tris(3,5-dimethylphenylcarbamate), *J. Chromatogr. B* 875 (2008) 81–92.
- [22] A. Del Rio, Exploring enantioselective molecular recognition mechanisms with cheminformatic techniques, *J. Sep. Sci.* 32 (2009) 1566–1584.
- [23] R. Sheridan, W. Schafer, P. Piras, K. Zawatzky, E.C. Sherer, C. Roussel, C.J. Welch, Toward structure-based predictive tools for the selection of chiral stationary phases for the chromatographic separation of enantiomers, *J. Chromatogr. A* 1467 (2016) 206–213.
- [24] T.D. Booth, I.W. Wainer, Mechanistic investigation into the enantioselective separation of mexiletine and related compounds, chromatographed on an amylose tris(3,5-dimethylphenylcarbamate) chiral stationary phase, *J. Chromatogr. A* 741 (1996) 205–211.
- [25] C.A. Montanari, Q.B. Cass, M.E. Tiritan, A.L. Soares de Souza, A QSERR study on enantioselective separation of enantiomeric sulphoxides, *Anal. Chim. Acta* 419 (2000) 93–100.
- [26] L. Pisani, M. Rullo, M. Catto, M. de Candia, A. Carrieri, S. Cellamare, C.D. Altomare, Structure–property relationship study of the HPLC enantioselective retention of neuroprotective 7-[(1-alkylpiperidin-3-yl)methoxy]coumarin derivatives on an amylose-based chiral stationary phase, *J. Sep. Sci.* 41 (2018) 1376–1384.
- [27] B. Rasulev, M. Turabekova, M. Gorska, K. Kulig, A. Bielejewska, J. Lipkowski, J. Lleszczynski, Use of quantitative structure–enantioselective retention relationship for the liquid chromatography chiral separation prediction of the series of pyrrolidin-2-one compounds, *Chirality* 24 (2012) 72–77.
- [28] S. Khater, M.A. Lozac'h, I. Adam, E. Francotte, C. West, Comparison of liquid and supercritical fluid chromatography mobile phases for enantioselective separations on polysaccharide stationary phases, *J. Chromatogr. A* 1467 (2016) 463–472.
- [29] M. Szaleniec, A. Dudzik, M. Pawul, B. Kozik, Quantitative structure enantioselective retention relationship for high-performance liquid chromatography chiral separation of 1-phenylethanol derivatives, *J. Chromatogr. A* 1216 (2009) 6224–6235.
- [30] S. Carradori, M. Pierini, S. Menta, D. Secci, R. Fioravanti, R. Cirilli, 3-(Phenyl-4-oxy)-5-phenyl-4,5-dihydro-(1H)-pyrazole: A fascinating molecular framework to study the enantioseparation ability of the amylose (3,5-dimethylphenylcarbamate) chiral stationary phase. Part I. Structure–enantioselectivity relationships, *J. Chromatogr. A* 1467 (2016) 221–227.
- [31] Y. Martín-Biosca, L. Escuder-Gilabert, S. Sagrado, M.J. Medina-Hernández, Modelling the enantioresolution capability of cellulose tris(3,5-dichlorophenylcarbamate) stationary phase in reversed phase conditions for neutral and basic chiral compounds, *J. Chromatogr. A* 1567 (2018) 111–118.
- [32] L. Asensi-Bernardi, L. Escuder-Gilabert, Y. Martín-Biosca, M.J. Medina-Hernández, S. Sagrado, Modeling the chiral resolution ability of highly sulfated- β -cyclodextrin for basic compounds in electrokinetic chromatography, *J. Chromatogr. A* 1308 (2013) 152–160.
- [33] L. Escuder-Gilabert, Y. Martín-Biosca, M.J. Medina-Hernández, S. Sagrado, Enantioresolution in electrokinetic chromatography-complete filling technique using sulfated gamma-cyclodextrin. Software-free topological anticipation, *J. Chromatogr. A* 1467 (2016) 391–399.
- [34] ChemSpider Database. Royal Society of Chemistry. <http://www.chemspider.com/> (accessed 21.2.18).
- [35] CAMO Software AS. <http://www.camo.com/> (accessed 21.2.18).
- [36] D.L. Massart, B.G.M. Vandeginste, L.M.C. Buydens, S. De Jong, P.J. Lewi, J. Smeyers-Berbeke, *Handbook of Chemometrics and Qualimetrics, Part A*, Elsevier, Amsterdam, 1997.
- [37] MATLAB® R2019a (Mathworks®) web site. <https://www.mathworks.com/help/stats/sequentialfs.html>. (accessed 21.4.20).
- [38] MATLAB® R2019a (Mathworks®) web site. <https://www.mathworks.com/help/matlab/ref/fminsearch.html>. (accessed 21.4.20).
- [39] MATLAB® R2019a (Mathworks®) web site. <https://www.mathworks.com/help/stats/bbdesign.html>. (accessed 21.4.20).

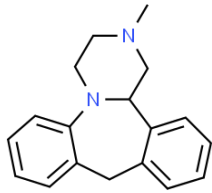
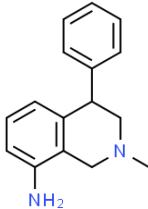
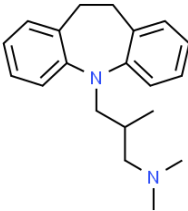
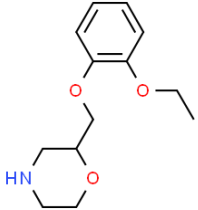
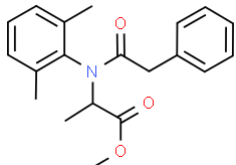
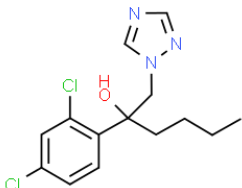
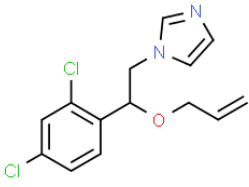
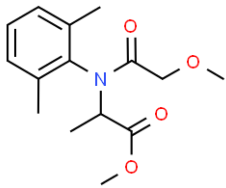
Supplementary data

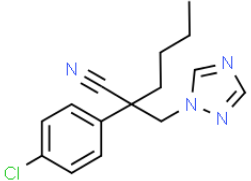
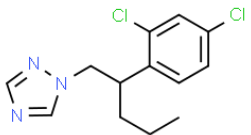
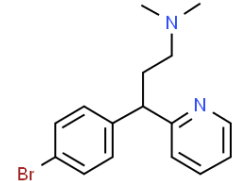
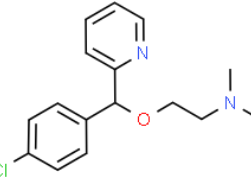
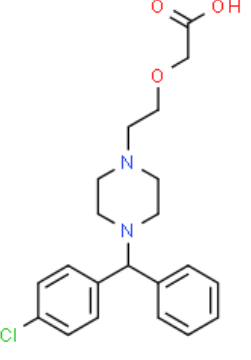
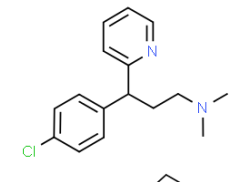
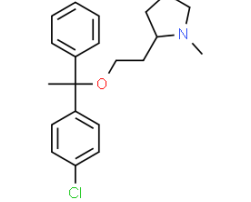
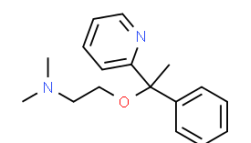
Comparative study on enantioresolution of neutral and basic drugs with amylose-based chiral stationary phases in reversed phase liquid chromatography-mass spectrometry conditions

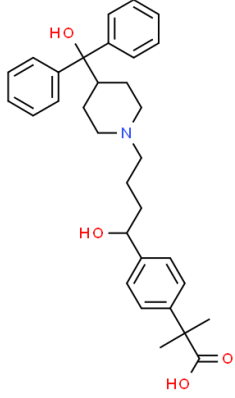
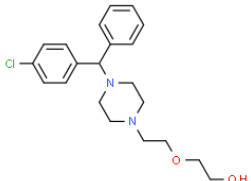
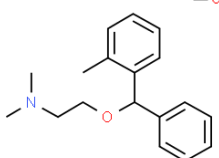
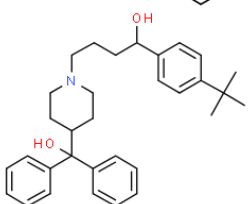
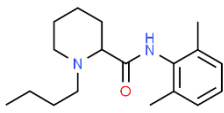
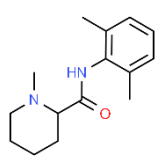
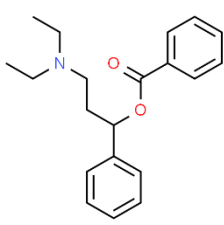
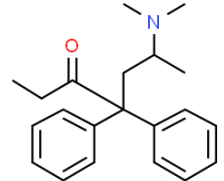

Mireia Pérez-Baeza ^a, Laura Escuder-Gilabert ^{a,*}, Yolanda Martín-Biosca ^a, Salvador Sagrado ^{a,b}, María José Medina-Hernández ^{a,*}

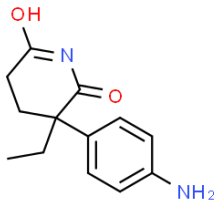
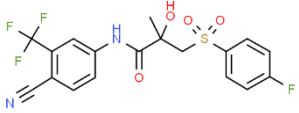
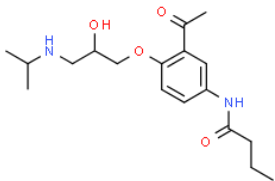
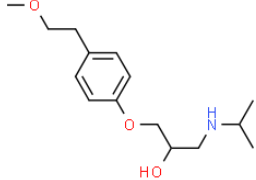
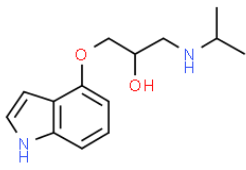
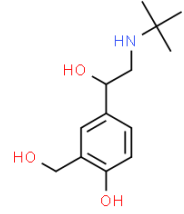
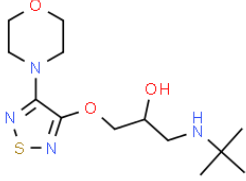
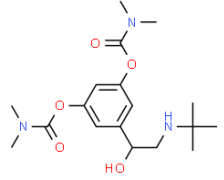
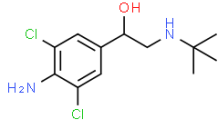
Table S1.- Chemical structure, molecular weight, the minus logarithm of the acidity constant (pK_a), the logarithm of the *n*-octanol-water partition coefficient ($\log P$) and the logarithm of the distribution coefficient ($\log D$) at pH=8 of the compounds under study.

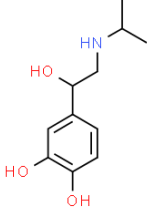
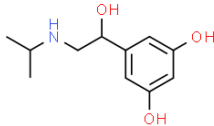
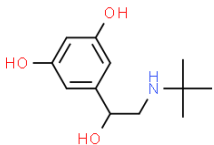
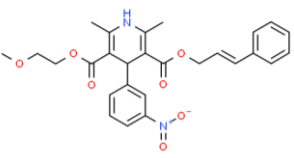
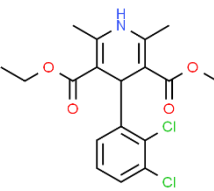
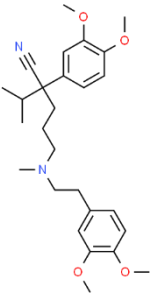
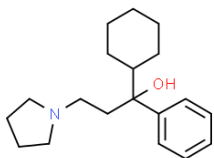
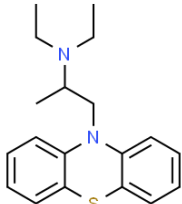
Compound	Structure	M_r (g/mol)	pK_a^a	$\log P^a$	$\log D$
Disopyramide		339.5	2.7; 10.4	2.86	0.44
Mexiletine		179.3	9.5	2.16	0.63
Propafenone		341.4	9.6; 14.0	3.10	1.46
Warfarin		308.3	5.6	3.42	3.42*
Bupropion		239.7	8.2	3.47	3.05
Citalopram		324.4	-	2.51	0.72
Fluoxetine		309.3	9.8	4.09	2.28

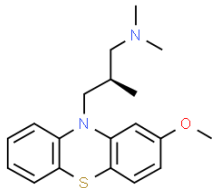
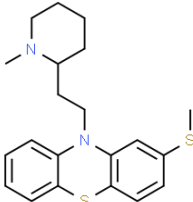
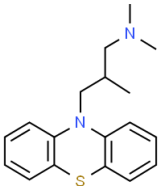
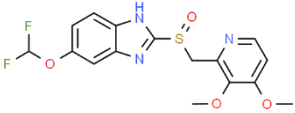
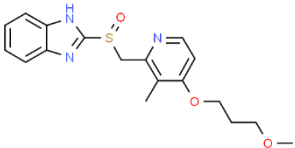
Compound	Structure	M_r (g/mol)	pK_a^a	$\log P^a$	$\log D$
Mianserin		264.4	6.9	3.67	3.64
Nomifensine		238.3	8.8	2.15	1.22
Trimipramine		294.4	9.4	5.15	3.71
Viloxazine		237.3	8.2	1.10	0.69
Benalaxyl		325.4	-	3.88	3.88
Hexaconazole		314.2	2.0, 13.3	3.66	3.66
Imazalil		297.2	-	3.58	3.56
Metalaxyl		279.3	-	2.15	2.15

Compound	Structure	M_r (g/mol)	pK_a^a	$\log P^a$	$\log D$
Myclobutanil		288.8	-	2.82	2.82
Penconazole		284.2	-	3.66	3.66
Brompheniramine		319.2	-	3.57	2.08
Carbinoxamine		290.8	8.9	2.76	1.84
Cetirizine		388.9	3.6; 4.6; 7.4	2.16	1.48
Chlorpheniramine		274.8	-	3.39	1.91
Clemastine		343.9	9.6	5.69	4.13
Doxylamine		270.4	8.9	2.52	1.60

Compound	Structure	M_r (g/mol)	pK_a^a	$\log P^a$	$\log D$
Fexofenadine		501.7	4.0; 9.0; 13.2; 14.5	4.80	4.77
Hydroxyzine		374.9	7.5; 15.1	2.03	1.81
Orphenadrine		269.4	-	4.12	3.20
Terfenadine		471.7	9.0; 13.2	6.51	5.45
Bupivacaine		288.4	8.0	3.64	2.68
Mepivacaine		246.3	7.3	2.04	1.40
Propanocaine		311.4	9.8	5.43	2.26
Methadone		309.4	-	4.20	3.05
Aminoglutethimide		232.3	4.3; 11.7	1.41	1.41

Compound	Structure	M_r (g/mol)	pK_a^a	$\log P^a$	$\log D$
					
Bicalutamide		430.4	11.8; 13.2; 15.1	4.94	1.14
Acebutolol		336.4	9.6	1.95	0.37
Metoprolol		267.4	9.7	1.79	0.11
Pindolol		248.3	9.7	1.97	-0.57
Salbutamol		239.3	9.4; 10.1	0.01	-1.41
Timolol		316.4	9.8	0.68	-1.09
Bambuterol		367.4	9.5; 13.9	0	-1.53
Clenbuterol		277.2	1.4; 9.6; 14.1	2.61	0.97

Compound	Structure	M_r (g/mol)	pK_a^a	$\log P^a$	$\log D$
Isoprenaline		211.3	9.0; 9.8; 12.7; 14.4	0.25	-0.76
Orciprenaline		211.3	8.8; 9.7; 10.6; 14.4	0.13	-0.77
Terbutaline		225.3	8.9; 9.8; 10.6; 14.4	0.48	-0.44
Cinildipine		492.5	-	5.36	5.36
Felodipine		384.3	-	4.83	4.83
Verapamil		454.6	-	3.90	2.21
Procyclidine		287.4	9.5; 13.8	3.93	2.46
Ethopropazine		312.5	-	5.84	4.23

Compound	Structure	M_r (g/mol)	pK_a ^a	$\log P$ ^a	$\log D$
Methotrimeprazine		328.5	-	4.94	3.50
Thioridazine		370.6	8.9	6.13	5.15
Trimeprazine		298.4	-	4.98	3.54
Pantoprazole		383.4	1.3; 3.6; 9.2	1.69	0.51
Rabeprazole		359.4	1.1; 4.2; 9.4	1.83	0.46

^a Estimated values obtained from <http://www.chemspider.com>

Table S2.- Structural variables used for DPLS1 modelling.

Number	Symbol	Description
x ₁	<i>C*X</i>	Number of heteroatoms bonded to the chiral carbon (C*-heteroatoms)
x ₂	<i>C*XH</i>	Number of –OH or NHR groups bonded to the chiral carbon (C*-OH or C*-NHR)
x ₃	<i>C*hA</i>	Number of aromatic heterocycles groups bonded to the chiral carbon (C*-aromatic heterocycles)
x ₄	<i>C*a</i>	Number of aliphatic groups bonded to the chiral carbon (C*-aliphatic)
x ₅	<i>C*H</i>	Number of hydrogen atoms bonded to the chiral carbon (C*-H)
x ₆	<i>C*C=O</i>	Number of carbonyl groups bonded to the chiral carbon C*-amide (–C(=O)NR ₁ R ₂), carbonyl (–C(=O)–R) and ester (–C(=O)–OR) groups
x ₇	<i>C*A</i>	Number of aromatic groups bonded to the chiral carbon (C*-aromatic)
x ₈	<i>Mr</i>	Molecular weight
x ₉	<i>logP</i>	Logarithm of the partition coefficient
x ₁₀	<i>HBA</i>	H-bond acceptors: number of hydrogen bond acceptors in the molecule
x ₁₁	<i>HBD</i>	H-bond donors: number of hydrogen bond donors in the molecule
x ₁₂	<i>PSA</i>	Polar surface area
x ₁₃	<i>ST</i>	Surface tension
x ₁₄	<i>zmin</i>	Minimal z length
x ₁₅	<i>zmax</i>	Maximal z length
x ₁₆	<i>logD</i>	log <i>P</i> at working pH
x ₁₇	<i>abc</i>	Aliphatic bond count: number of non-aromatic bonds in the molecule (excluding bonds of hydrogen atoms)
x ₁₈	<i>Abc</i>	Aromatic bond count: number of aromatic bonds in the molecule
x ₁₉	<i>bc</i>	Bond count: number of bonds in the molecule including hydrogens
x ₂₀	<i>Rbc</i>	Ring bond count: number of ring bonds
x ₂₁	<i>arc</i>	Aliphatic ring count: number of those rings in the molecule, which have non-aromatic bonds
x ₂₂	<i>Arc</i>	Aromatic ring count: number of aromatic rings in the molecule
x ₂₃	<i>Crc</i>	Carbo ring count: number of those rings in the molecule, which contain carbon atoms only
x ₂₄	<i>fArc</i>	Fused aromatic ring count: number of aromatic rings having common bonds with other rings
x ₂₅	<i>frc</i>	Fused ring count: number of fused rings in the molecule (having common bonds)
x ₂₆	<i>Hrc</i>	Hetero ring count: number of rings in the molecule, which contain hetero atoms
x ₂₇	<i>Harc</i>	Heteroaliphatic ring count: number of aliphatic heterocycles in the molecule
x ₂₈	<i>HArc</i>	Heteroaromatic ring count: number of aromatic heterocycles in the molecule

Number	Symbol	Description
X29	<i>Rc</i>	Ring count: number of rings in the molecule
X30	<i>Rsc</i>	Ring system count: number of disjunct ring systems
X31	<i>srss</i>	Smallest ring system size: number of rings in the smallest ring system
X32	<i>Bi</i>	Balaban index: Balaban distance connectivity of the molecule, which is the average distance sum connectivity
X33	<i>fsp3</i>	number of sp ³ hybridized carbons divided by the total carbon count
X34	<i>C</i>	Number of carbon atoms in the molecule
X35	<i>O</i>	Number of oxygen atoms in the molecule
X36	<i>S</i>	Number of sulfur atoms in the molecule
X37	<i>Cl</i>	Number of chlorine atoms in the molecule
X38	<i>F</i>	Number of fluor atoms in the molecule
X39	<i>OH</i>	Number of -OH groups in the molecule
X40	<i>NHR</i>	Number of -NHR groups in the molecule
X41	<i>NR2</i>	Number of -NR ₂ groups in the molecule
X42	<i>ROR</i>	Number of R-O-R groups in the molecule
X43	<i>tB</i>	Number of tert-butyl groups in the molecule
X44	<i>iP</i>	Number of iso-propyl groups in the molecule
X45	<i>ACH3</i>	Number of -CH ₃ groups bonded to an aromatic ring in the molecule
X46	<i>ACl</i>	Number of Cl atoms bonded to an aromatic ring in the molecule
X47	<i>AOH</i>	Number of -OH groups bonded to an aromatic ring in the molecule
X48	<i>AOR</i>	Number of -OR groups bonded to an aromatic ring in the molecule
X49	<i>ACOOR</i>	Number of -COOR groups bonded to an aromatic ring in the molecule
X50	<i>ANHCO-R</i>	Number of -NHCO-R groups bonded to an aromatic ring in the molecule
X51	<i>ACA</i>	Number of moieties Ar-C-Ar
X52	<i>A12</i>	Number of aromatic groups with 1,2 substitution.
X53	<i>A14</i>	Number of aromatic groups with 1,4 substitution
X54	<i>A123</i>	Number of aromatic groups with 1,2,3 substitution
X55	<i>A124</i>	Number of aromatic groups with 1,2,4 substitution
X56	<i>NA</i>	Number of nitrogen aromatic groups
X57	<i>NRC</i>	Number of tertiary amines in aliphatic cycles
X58	<i>Sc</i>	Number of S atoms in aliphatic cycles



PAPER II

Comparative study on retention behaviour and enantioresolution of basic and neutral structurally unrelated compounds with cellulose-based chiral stationary phases in reversed phase liquid chromatography-mass spectrometry conditions

**Mireia Pérez-Baeza^a, Laura Escuder-Gilabert^a, Yolanda Martín-Biosca^a,
Salvador Sagrado^{a,b}, María José Medina-Hernández^a**

^a Departamento de Química Analítica, Universitat de València, Burjassot, Valencia E-46100, Spain

^b Instituto Interuniversitario de Investigación de Reconocimiento Molecular y Desarrollo Tecnológico (IDM), Universitat Politècnica de València, Universitat de València, Valencia, Spain

Journal of Chromatography A 1673 (2022) 463073



Comparative study on retention behaviour and enantioresolution of basic and neutral structurally unrelated compounds with cellulose-based chiral stationary phases in reversed phase liquid chromatography-mass spectrometry conditions



Mireia Pérez-Baeza^a, Laura Escuder-Gilabert^{a,*}, Yolanda Martín-Biosca^a, Salvador Sagrado^{a,b}, María José Medina-Hernández^{a,*}

^a Departamento de Química Analítica, Universitat de València, Burjassot, Valencia E-46100, Spain

^b Instituto Interuniversitario de Investigación de Reconocimiento Molecular y Desarrollo Tecnológico (IDM), Universitat Politècnica de València, Universitat de València, Valencia, Spain

ARTICLE INFO

Article history:

Received 27 February 2022

Revised 12 April 2022

Accepted 15 April 2022

Available online 22 April 2022

Keywords:

Cellulose-based chiral stationary phases

Chiral HPLC

Hydro-organic mobile phases compatible with MS detection

Retention behaviour

Hydrophilic interaction liquid chromatography

Enantioresolution ability

ABSTRACT

A comparative study on the retention behaviour and enantioresolution of 54 structurally unrelated neutral and basic compounds using five commercial cellulose-based chiral stationary phases (CSPs) and hydro-organic mobile phases compatible with MS detection is performed. Four phenylcarbamate-type cellulose CSPs (cellulose tris(3,5-dimethylphenylcarbamate), Cell1; cellulose tris(3-chloro-4-methylphenylcarbamate), Cell2; cellulose tris(4-chloro-3-methylphenylcarbamate), Cell4 and cellulose tris(3,5-dichlorophenylcarbamate), Cell5) and one benzoate-type cellulose CSP (cellulose tris(4-methylbenzoate), Cell3) are assayed. Mobile phases consist of binary mixtures of methanol (30–90% MeOH) or acetonitrile (10–98% ACN) with 5 mM ammonium bicarbonate (pH = 8.0).

The existence of reversed phase (RPLC) and hydrophilic interaction liquid chromatography (HILIC) retention behaviour domains is explored. In MeOH/H₂O mobile phases, for all compounds and CSPs, the typical RPLC retention behaviour is observed. When using ACN/H₂O mobile phases, for all compounds in all CSPs (even in the non-chlorinated CSPs) a U-shaped retention behaviour depending on the ACN/H₂O content is observed which indicates the coexistence of the RPLC- (< 80% ACN) and HILIC- (~80–98% ACN) domains. The magnitude of retention changes in both domains is related to the hydrophobicity of the compound as well as to the nature of the CSP.

The study of the effect of the nature and concentration of the organic solvent, as well as the nature of the CSP on the enantioresolution reveals that: (i) the use of MeOH/H₂O or ACN/H₂O greatly affects the enantioselectivity and enantioresolution degree of the chromatographic systems, being, in general, better the results obtained with ACN/H₂O mobile phases. (ii) The ACN-RPLC-domain provides much better enantioresolution than HILIC-domain. (iii) Cell2, especially with ACN/H₂O mobile phases, is the CSP that allows baseline enantioresolution for a higher number of compounds. (iv) Phenylcarbamate-type CSPs do not offer clear complementary enantioselectivity to that of Cell2. (v) Cell3 is the only CSP that provides marked complementary enantioselectivity to that of Cell2, almost orthogonal in MeOH/H₂O mobile phases.

© 2022 The Author(s). Published by Elsevier B.V.

This is an open access article under the CC BY-NC-ND license (<http://creativecommons.org/licenses/by-nc-nd/4.0/>)

* Corresponding authors.

E-mail addresses: lescuder@uv.es (L. Escuder-Gilabert), maria.j.medina@uv.es (M.J. Medina-Hernández).

1. Introduction

High-performance liquid chromatography (HPLC) in combination with chiral stationary phases (CSPs) based on amylose or cellulose polysaccharide derivatives (coated or immobilised) is the preferential choice for the separation of the enantiomers of chiral compounds [1–6]. In these systems, separation is based on the formation of a transitory enantiomer-polysaccharide CSP complex, which is mediated by hydrophobic, electrostatic, hydrogen bonding and van der Waals interactions and steric factors [3,7–9].

Amylose and cellulose polysaccharide derivative CSPs are polymers in which the hydroxyl groups of the glucose molecules are derivatised with benzoate or phenylcarbamate groups. These benzoate or phenylcarbamate moieties can be functionalised with electron-withdrawing and electron-donating substituents, such as methyl groups and chlorine atoms, in various positions on the aromatic ring. The nature and position of substituent(s) on the phenyl moiety of polysaccharides are key factors in chiral recognition [2,3,5,6,10–12].

Polysaccharide-based CSPs are compatible with all mobile phase chromatographic regimes: apolar organic (normal phase HPLC), polar organic (polar organic HPLC), and hydro-organic (RPLC: reversed phase HPLC, and more recently HILIC: hydrophilic interaction liquid chromatography) [2,5,6,12].

The chiral recognition mechanism is modulated by the CSP and also by the nature and composition of the mobile phase. Different mobile phases can lead to differences in the enantioresolution and chromatographic behaviour of the enantiomers of chiral compounds [12–15], and even provoke reversals in their elution order [16–19].

Hydro-organic mobile phases are particularly relevant for the analysis of aqueous matrix samples, such as biological and environmental samples, which require mass spectrometry (MS) detection [20–21]. These mobile phases improve analyte ionisation, and thus the sensitivity in MS detection. However, most of the additives used in this HPLC-mode are incompatible with MS detection [22].

One aspect to be considered when using hydro-organic mobile phases is that the retention of compounds with polysaccharide derivative CSPs may follow a dual behaviour (RPLC or HILIC) depending on the protic or aprotic character of the organic solvent and the water content in the mobile phase [6,15–19,23–29]. It has been proposed that the balance between hydrophilic (hydrogen-bond interactions with carbamate or ester moieties) and hydrophobic (with phenyl moieties) enantiomer-CSP interactions can explain this dual behaviour [6,16–18,29].

For protic solvents, such as methanol the addition of water to the mobile phase promotes hydrophobic interactions between the analyte and the polysaccharide CSPs. This fact may increase the analyte retention (RPLC behaviour) and eventually lead to an enhancement of enantioseparation [6,16–18].

For aprotic solvents, such as acetonitrile, the addition of water to the mobile phase also increases analyte-polysaccharide CSPs hydrophobic interactions leading to an increase in retention (RPLC behaviour) but decreases hydrophilic interactions. The latter effect reduces analyte retention (HILIC behaviour) and may decrease enantioresolution. The overall effect observed is the sum of both contributions. The first contribution prevails in mobile phases with high water content and the second one in mobile phases with low water content [6,16–18]. This behaviour has been reported for chlorinated polysaccharide-based CSPs which show a great ability to form strong hydrogen bonds [29].

In the literature there are several studies on the enantioselectivity, enantioresolution and retention behaviour with different polysaccharide-based CSPs using hydro-organic mobile phases [16–18,30–36] and there are also several works that in-

volve the use of mobile phases compatible with MS detection [22,31,33,37,38].

In a previous work [31], a comprehensive study on the retention and enantioresolution behaviour of 53 structurally unrelated compounds using three commercial amylose-based CSPs and acetonitrile/ammonium bicarbonate (pH = 8.0) mixtures as mobile phases was performed.

In this paper, a comparative study on the retention behaviour and enantioresolution of 54 structurally unrelated neutral and basic compounds using five commercial cellulose-based CSPs and mixtures consisting of organic solvent (methanol or acetonitrile) and 5 mM ammonium bicarbonate (pH = 8.0) in varying proportion as MS-compatible mobile phases is performed. The structurally unrelated chiral compounds studied, belong to 13 drug/pesticides families: antiarrhythmic drugs, antidepressants, fungicides, antihistamines, local anaesthetics, analgesics, antineoplastics, β -blockers, bronchodilators, calcium channel blockers, anticholinergic drugs, antipsychotic drugs, and proton pump inhibitors.

2. Experimental

2.1. Chemicals and solutions

Acetonitrile (ACN) and methanol (MeOH) (©Multisolvent, HPLC grade), ammonium bicarbonate, and ammonia 32% were from Scharlau, S.L. (Barcelona, Spain). These reagents were all of the analytical grade. The appropriate amount of ammonium bicarbonate was dissolved in ultra-pure water to prepare a 5 mM ammonium bicarbonate buffer solution. 1 M ammonium hydroxide was used to adjust the pH to 8.0.

Racemic drugs were acquired from different suppliers: propafenone hydrochloride and terbutaline hemisulfate were from Abcam (Cambridge, United Kingdom); atenolol, cilnidipine, isoprenaline hydrochloride, mexiletine hydrochloride and propranolol hydrochloride were from Acros (Acros Organics, Geel, Belgium); acebutolol hydrochloride, aminoglutethimide, metoprolol tartrate, mianserin hydrochloride and salbutamol sulfate were from Alfa Aesar (Thermo Fisher Scientific Inc., Karlsruhe, Germany); bambuterol hydrochloride, bupivacaine, cetirizine hydrochloride and trimipramine maleate were from Cayman Chemical Co (Ann Arbor, MI, USA); felodipine and orciprenaline sulfate were from EDQM (Strasbourg, France); hydroxyzine hydrochloride was from Guinama (Valencia, Spain); disopyramide was from MP Biomedicals (Irvine, CA, USA); citalopram hydrobromide was from Tokyo Chemical Industry (Tokyo, Japan); and bicalutamide, brompheniramine maleate, bupropion hydrochloride, carbinoxamine maleate, chlorpheniramine maleate, clenbuterol hydrochloride, doxylamine succinate, ethopropazine hydrochloride, lansoprazole, methadone hydrochloride, nomifensine maleate, orphenadrine hydrochloride, pantoprazole sodium, pindolol, procyclidine hydrochloride, promethazine hydrochloride, rabeprazole sodium, terfenadine, thioridazine hydrochloride, trimeprazine hemi(+)-tartrate and verapamil hydrochloride were from Sigma-Aldrich (©Merck KGaA, Darmstadt, Germany). The rest of the drugs studied were kindly donated by various pharmaceutical laboratories: fluoxetine hydrochloride was kindly donated by Alter (Madrid, Spain); mepivacaine hydrochloride and prilocaine hydrochloride by Laboratorios Inibsa (Barcelona, Spain); propanocaine by Laboratorio Seid (Barcelona, Spain); timolol maleate by Merck Sharp & Dohme (Madrid, Spain) and viloxazine hydrochloride by Astra Zeneca (Cheshire, UK). All racemic pesticides, such as benalaxyl, hexaconazole, imazalil, metalaxyl, myclobutanil, and penconazole were from Dr. Ehrenstorfer GmbH (Augsburg, Germany).

Stock standard solutions of 1000 mg L⁻¹ of each compound were prepared by dissolving 10 mg of the racemic mixture in 10

mL of methanol. Working solutions of 100 mg L⁻¹ were prepared by dilution of the stock standard solutions using methanol. The solutions were stored under refrigeration at 4°C until usage.

2.2. Instrumentation

An Agilent Technologies 1100 chromatograph (Palo Alto, CA, USA) with a quaternary pump, a column thermostat, a UV-visible variable wavelength detector, and an autosampler was used. Data acquisition and processing were performed by means of the Chemstation software (A.09.03 [1417], ©Agilent Technologies 1990–2002).

Analytes solutions were filtered through disposable 0.22 µm Nylon® syringe filters (Análisis Vínicos, S.L., Tomelloso, Ciudad Real, Spain) before injection into the chromatographic system. Mobile phase solutions were vacuum-filtered through 0.22 µm Nylon membranes (Micron Separations, Westboro, MA, USA) and degassed in an Elmasonic S60 ultrasonic bath (Elma, Singen, Germany) before use. Ultra Clear TWF UV deionised water (SG Water, Barsbüttel, Germany) was used to prepare solutions and a Crison MicropH 2000 pHmeter (Crison Instruments, Barcelona, Spain) was employed to adjust the pH of the buffer solutions.

2.3. Methodology for the chiral separation of compounds

The following commercial polysaccharide-based CSPs: Lux Cellulose-1 (cellulose tris(3,5-dimethylphenylcarbamate), Cell1; Lux Cellulose-2 (cellulose tris(3-chloro-4-methylphenylcarbamate), Cell2; Lux Cellulose-3 (cellulose tris(4-methylbenzoate), Cell3; Lux Cellulose-4 (cellulose tris(4-chloro-3-methylphenylcarbamate), Cell4; and immobilised Lux Cellulose-5 (cellulose tris(3,5-dichlorophenylcarbamate), Cell5 were used. All columns (3 µm, 150 × 4.6 mm i.d.) were purchased from Phenomenex (Phenomenex, Torrance, CA, USA).

Binary mixtures consisting of ACN in varying proportions (10–98% in volume of ACN) and ammonium bicarbonate buffer (5 mM, pH 8) were used as mobile phases. Binary mixtures consisting of MeOH in varying proportions (30–90% in volume of MeOH) and ammonium bicarbonate buffer (5 mM, pH 8) were also used as mobile phases. The mobile phase flow rate was 1.0 mL min⁻¹, the column was thermostatted at 25°C, and the injection volume was 2 µL, for all the experiences. The detection was performed at 220 nm for all compounds, except for ethopropazine, promethazine, and trimeprazine whose detection was performed at 254 nm.

The retention factors (*k*), selectivity factors (*α*), experimental enantioresolution (*R_s*), plate number (*N*) and asymmetry factors (*B/A*) values were obtained using the following equations:

$$k = \frac{t_R - t_0}{t_0} \quad (1)$$

$$\alpha = \frac{k_2}{k_1} \quad (2)$$

$$R_s = 1.18 \frac{t_{R2} - t_{R1}}{W_1 + W_2} \quad (3)$$

$$N = 5.54 \frac{t_R^2}{W^2} \quad (4)$$

$$\text{Asymmetry factor} = \frac{B}{A} \quad (5)$$

where subindices 1 and 2 refer to the least and most retained enantiomer, respectively; *t_R* is the retention time, *t₀* is the gross hold-up time estimated from the first perturbation on the chromatogram, *W* is the peak width at half-height; and *A* and *B* correspond to the left and right half-widths at 10% peak height (Foley-Dorsey asymmetry).

3. Results and discussion

This paper aims to study the retention behaviour and explore the ability of the Cell1, Cell2, Cell3, Cell4, and Cell5 cellulose-based CSPs to enantioseparate structurally unrelated chiral compounds using hydro-organic mobile phases consisting of binary mixtures of 5 mM NH₄HCO₃ (pH 8) and ACN (ACN/H₂O) or MeOH (MeOH/H₂O) compatible with MS detection. The CSPs used in this work include one benzoate-type (Cell3) and four phenylcarbamate-type (Cell1, Cell2, Cell4, and Cell5) cellulose derivatives. The phenylcarbamate cellulose derivatives differ in the nature and position of the substituents on the phenyl moiety.

Table 1 shows the 54 structurally unrelated chiral compounds studied, which belong to 13 drug/pesticide families: antiarrhythmic drugs, antidepressants, fungicides, antihistamines, local anaesthetics, analgesics, antineoplastics, β-blockers, bronchodilators, calcium channel blockers, anticholinergic drugs, antipsychotic drugs, and proton pump inhibitors. All these compounds have only one asymmetric center. Table 1 also shows the logarithm of octanol-water distribution coefficients (*logD*) at pH 8 and the minus logarithm of the acidity constants (*pK_a*) of the compounds [39]. These compounds exhibit variable hydrophobic character with *logD* values ranging between -1.4 and 5.4 at pH 8. At the working pH, most of them have a positive net charge, except cetirizine (*No* = 19) which has a negative net charge; and aminoglutethimide (*No* = 30), cilnidipine (*No* = 44), felodipine (*No* = 45), and fungicides (*No* = 11–16) which exhibit net zero charge.

3.1. Retention behaviour of compounds with cellulose-based CSPs with hydro-organic mobile phases

The retention behaviour of compounds with polysaccharide derivative CSPs when using hydro-organic mobile phases depends on the nature of the compound, the nature of the organic solvent, and the water content.

To study the retention behaviour of the tested compounds with the different cellulose-based CSPs, ACN/H₂O mobile phases, with water content in the range 2–90% (v/v), were assayed. For most of the compounds and CSPs studied, a HILIC/RPLC dual retention behaviour was observed as a function of the water content. However, the observed changes in retention strongly depend on the nature of the compound and the CSP.

Fig. 1, left part, shows, as an example, the retention factor (*k*) values of the least retained enantiomer as a function of ACN content in the mobile phase for compounds with different hydrophobicity: atenolol (*No* = 33, *logD* = -1.41, Fig. 1.A), brompheniramine (*No* = 17, *logD* = 2.29, Fig. 1.B), myclobutanil (*No* = 15, *logD* = 3.22, Fig. 1.C), and bupivacaine (*No* = 25, *logD* = 3.99, Fig. 1.D) in all Cell-based CSPs studied.

As can be observed in Fig. 1.A and B, retention of atenolol and brompheniramine showed the typical U-shaped curves. Retention of both compounds was high for the mobile phase with the lowest water content (2%) in all the CSPs. The increase of the proportion of water in the mobile phase up to 20% (98–80% ACN, HILIC-domain) led to a large decrease in the retention of both compounds. On the other hand, for water contents above 20–30% (ACN content lower than 80%, RPLC-domain), retention was generally lower, especially for atenolol. For both compounds, the retention increased as the water content in the mobile phase increased.

On the contrary, as expected, compounds with high hydrophobic character (e.g. myclobutanil and bupivacaine, Fig. 1.C and Fig. 1D, respectively), in the RPLC-domain, showed large changes in their *k* values, which increased as the water content in the mobile phase increased. Oppositely, these compounds had very low *k* values in the HILIC domain, so changes in the retention were al-

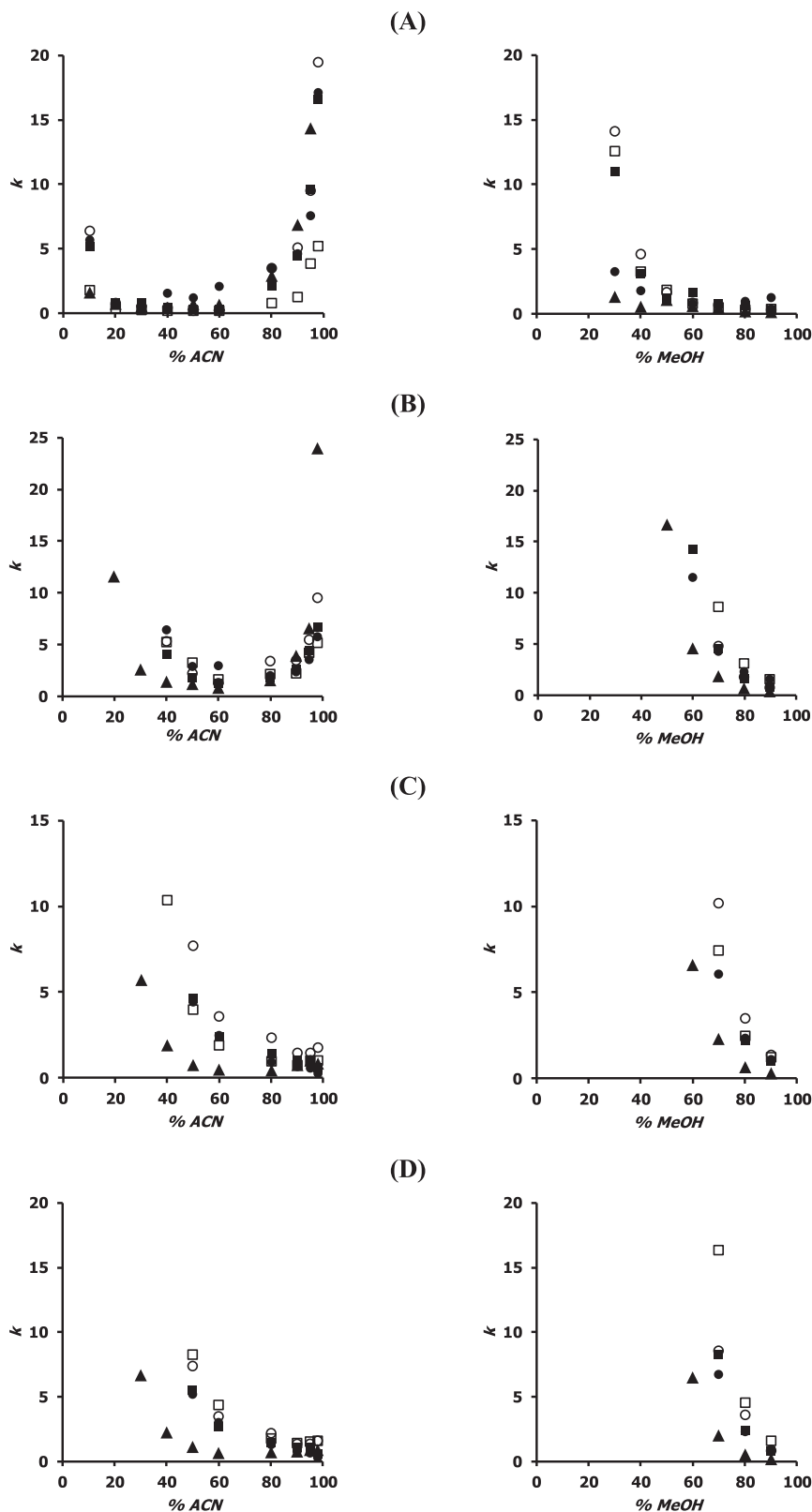


Fig. 1. Retention behaviour of (A) atenolol, (B) brompheniramine, (C) myclobutanil, and (D) bupivacaine with (●) Cell1, (○) Cell2, (▲) Cell3, (■) Cell4 and (□) Cell5 using mobile phases of 5 mM ammonium bicarbonate (pH = 8.0) and variable amounts of ACN and MeOH.

Table 1

Logarithm of the distribution coefficient ($\log D$) at $\text{pH}=8$ and the minus logarithm of the acidity constant ($\text{p}K_a$) values of the compounds under study. Compounds are identified by their name and numbered order (No).

No	Compound	FAM ^a	$\log D^b$	$\text{p}K_a^b$	No	Compound	FAM ^a	$\log D^b$	$\text{p}K_a^b$
1	Disopyramide	AAD	1.12	2.7; 10.4	28	Propanocaine	LA	2.95	9.8
2	Mexiletine	AAD	0.97	9.4	29	Methadone	ANAL	4.23	9.1
3	Propafenone	AAD	1.38	9.7	30	Aminoglutethimide	ANP	1.59	4.3; 11.7
4	Bupropion	AD	2.33	8.2	31	Bicalutamide	ANP	2.52	11.8; 13.2
5	Citalopram	AD	1.77	9.8	32	Acebutolol	BB	-0.50	9.7; 13.9
6	Fluoxetine	AD	2.39	9.8	33	Atenolol	BB	-1.41	9.7
7	Mianserin	AD	3.96	6.9	34	Metoprolol	BB	-0.18	9.7
8	Nomifensine	AD	1.89	1.9; 8.8	35	Pindolol	BB	-0.07	9.7
9	Trimipramine	AD	3.07	0.1; 9.4	36	Propranolol	BB	0.83	9.7
10	Viloxazine	AD	0.82	8.2	37	Salbutamol	BB+BD	-1.06	9.4; 10.1
11	Benalaxyl	AF	4.03	-	38	Timolol	BB	-0.60	-0.3; 9.8
12	Hexaconazole	AF	2.99	2.0; 13.3	39	Bambuterol	BD	-0.36	9.5; 13.9
13	Imazalil	AF	3.45	6.5	40	Clenbuterol	BD	0.35	1.4; 9.6
14	Metalaxyl	AF	1.91	15.8	41	Isoprenaline	BD	-0.50	9.0; 9.8; 12.7
15	Myclobutanil	AF	3.22	2.3	42	Orciprenaline	BD	-0.47	8.8; 9.7; 10.6
16	Penconazole	AF	3.77	2.1	43	Terbutaline	BD	-0.48	8.9; 9.8; 10.6
17	Brompheniramine	AH	2.29	3.6; 9.5	44	Cilnidipine	CaB	4.03	-
18	Carbinoxamine	AH	2.17	3.3; 8.9	45	Felodipine	CaB	3.07	-
19	Cetirizine	AH	0.00	1.6; 3.6; 7.4	46	Verapamil	CaB	2.87	9.7
20	Chlorpheniramine	AH	2.02	3.6; 9.5	47	Procyclidine	ACD	1.81	9.5; 13.8
21	Doxylamine	AH	1.88	3.2; 8.9	48	Ethopropazine	APD	3.47	9.6
22	Hydroxyzine	AH	3.09	1.6; 7.5	49	Promethazine	APD	3.31	9.1
23	Orphenadrine	AH	3.16	8.9	50	Thioridazine	APD	4.51	8.9
24	Terfenadine	AH	5.39	9.0; 13.2	51	Trimeprazine	APD	3.10	9.4
25	Bupivacaine	LA	3.99	8.0	52	Lansoprazol	PPI	2.90	1.1; 4.2; 9.4
26	Mepivacaine	LA	3.02	7.3	53	Pantoprazol	PPI	1.81	1.3; 3.6; 9.2
27	Prilocaine	LA	1.82	8.8	54	Rabeprazol	PPI	1.81	1.1; 4.2; 9.4

^a Drug/Pesticide family: AAD (antiarrhythmic drugs), AD (antidepressants), AF (antifungals), AH (antihistamines), LA (local anaesthetics), ANAL (analgesics), ANP (antineoplastics), BB (β -blockers), BD (bronchodilators), CaB (calcium channel blockers), ACD (anticholinergic drugs), APD (antipsychotic drugs), and PPI (proton pump inhibitors).

^b Estimated values obtained from ChemSpider [39]

most negligible, but perceptible. Therefore, the U-shaped retention curves were not so evident as for less hydrophobic compounds.

To visualise the HILIC behaviour with cellulose-based CSPs, Fig. 2 represents the differences between the k values for the least retained enantiomer obtained with ACN/H₂O mobile phases containing 2 and 10% of water (98–90% ACN) for each compound, in the Cell1, Cell2, Cell3, Cell4, and Cell5 columns. The compounds are shown in increasing order of $\log D$ values. In general, positive or zero values were obtained in all cellulose-based CSPs, indicating that in these experimental conditions these CSPs are operating in HILIC mode. It must be pointed out that, for the majority of compounds, the retention factors obtained using a mixture of 5 mM ammonium bicarbonate ($\text{pH } 8$)/ACN (2/98, v/v) as mobile phase followed the order $k \text{ Cell3} > k \text{ Cell2} > k \text{ Cell4} \approx k \text{ Cell1} \gg k \text{ Cell5}$ (results not shown).

As can be observed in Fig. 2, for all CSPs, the largest differences in retention factors were generally obtained for compounds with low to medium $\log D$ values whereas hydrophobic compounds showed mostly low retention (so differences close to 0), which is the typical behaviour with HILIC columns. The Cell3 CSP (Fig. 2.C) showed the highest differences in retention values for a large number of compounds, especially for compounds No = 6, 17, 18 and 20. These compounds present medium $\log D$ values (~ 2) and present in their molecular structure tertiary or secondary amine groups, halogen atoms, and high aromaticity which could favour π - π , hydrogen bonding and van der Waals interactions. These interactions could be important for 2% H₂O mobile phases (the lowest water content), and are drastically reduced when increasing the water content in the mobile phase. In contrast, for the Cell5 CSP (Fig. 2.E), the differences in k values were minimal due to the lower retention of the compounds under these experimental conditions. Cell1 and Cell4 CSPs presented similar results, while Cell2 showed larger differences in k values for a large number of compounds.

Fig. 3 shows the most remarkable results found when compared the k values for the first eluted enantiomer of compounds for mobile phases containing 5 mM NH₄HCO₃ ($\text{pH } 8$)/ACN (50/50, v/v) ($k_{50\%}$, RPLC-domain) in each CSP. For comparative purposes, the identity line of slope and intercept equal to 1 and 0, respectively has been included. When comparing the $k_{50\%}$ values obtained in each CSP, except for the Cell2 and Cell4 CSPs, there is a random distribution of the $k_{50\%}$ values and do not they fit the identity line for most compounds, which points out the differences between selectivities and retention extent of the CSPs.

The effect of the position of the substituents of the phenylcarbamate moiety on the retention can be observed in Fig. 3.A. As could be expected, the Cell2 and Cell4 CSPs showed similar $k_{50\%}$ values because of their close structure; the only difference between them being that the methyl and chlorine substituents in the 3,4 position of the phenyl moiety are interchanged. On the other hand, the Cell1 and Cell5 CSPs differ in the nature of the substituents (two methyl groups in Cell1 and two chlorine atoms in Cell5), not in their position (3,5) on the phenyl moiety. As can be observed in Fig. 3.E, these CSPs showed different selectivity, although it must be also taken into account that Cell5 is the only immobilised polysaccharide-based CSP.

In general, for most of the compounds, the $k_{50\%}$ values was higher in phenylcarbamate-type than in benzoate-type CSPs (Fig. 3.C), opposite behaviour to that described for the HILIC mode.

The retention behaviour of compounds using MeOH/H₂O mobile phases (in the range of 30–90%) was also studied. For all compounds and CSPs studied, it was observed that an increase in the water proportion in the mobile phase led to an increase in retention, which is the typical RPLC-behaviour. As an example, Fig. 1 (right part) shows the retention of atenolol, brompheniramine, myclobutanil, and bupivacaine with mobile phases containing different amounts of MeOH. By comparing the retention behaviour of these compounds with mobile phases containing the

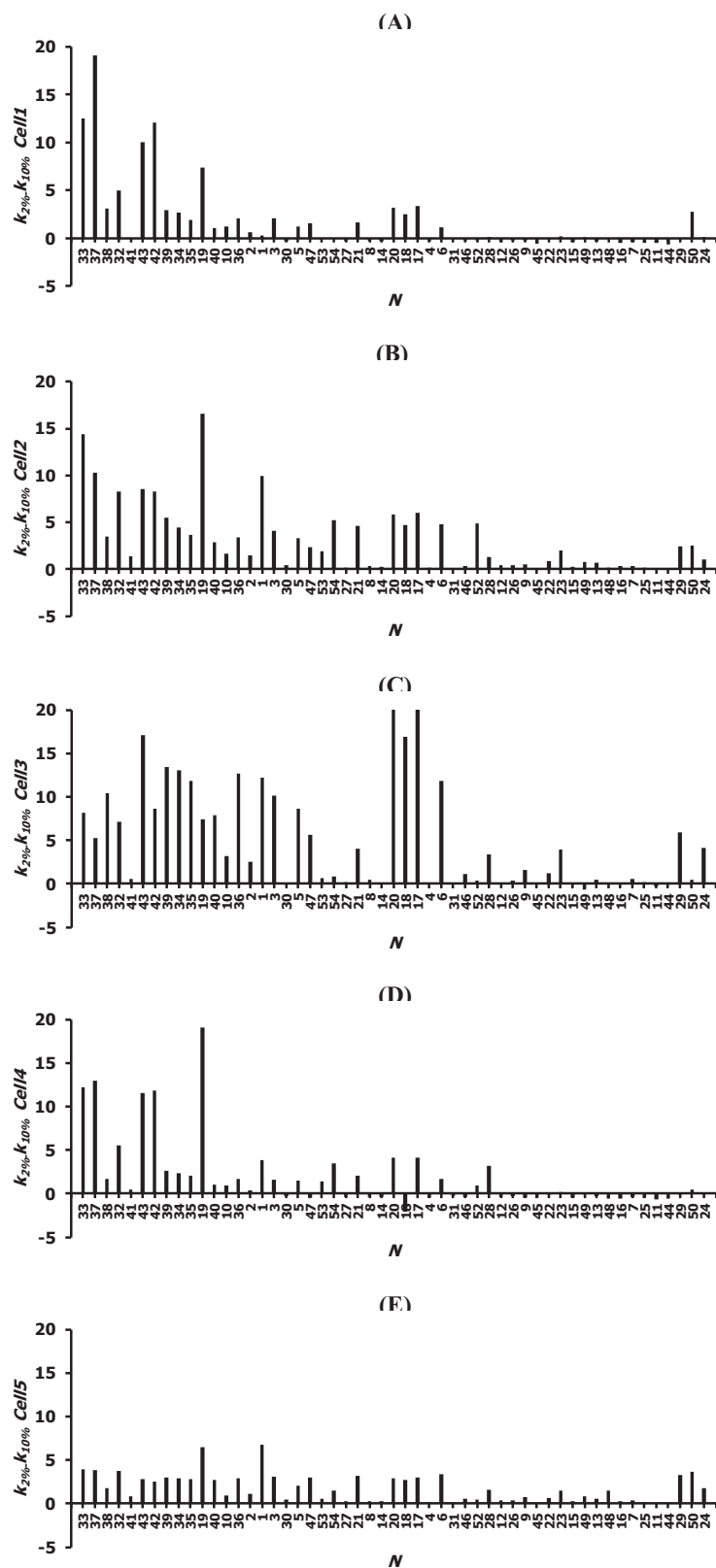


Fig. 2. Differences between the retention factors obtained for the least retained enantiomer with mobile phases of 5 mM $\text{NH}_4\text{HCO}_3/\text{ACN}$ (2/98, v/v) and 5 mM $\text{NH}_4\text{HCO}_3/\text{ACN}$ (10/90, v/v) ($k_{2\%} - k_{10\%}$) in each cellulose-based chiral stationary phase studied: (A) Cell1, (B) Cell2, (C) Cell3, (D) Cell4, (E) Cell5. The compounds are shown in increasing order of hydrophobicity. See No in Table 1

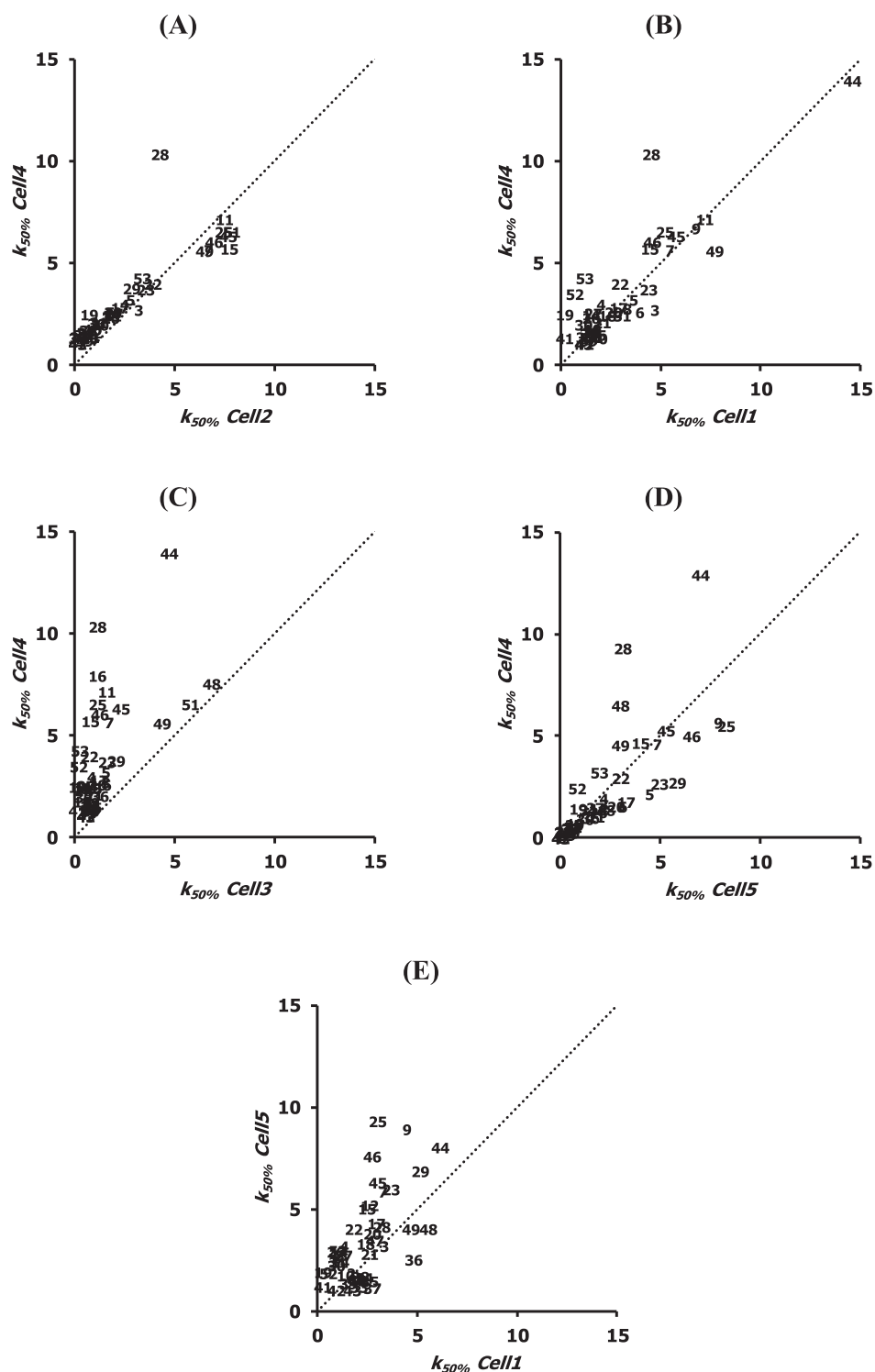


Fig. 3. Comparison of the retention factors of compounds using 5 mM $\text{NH}_4\text{HCO}_3/\text{ACN}$ (50/50, v/v) mobile phases and the following cellulose chiral stationary phases: (A) Cell4 vs. Cell2, (B) Cell4 vs. Cell1, (C) Cell4 vs. Cell3, (D) Cell4 vs. Cell5, and (E) Cell5 vs. Cell1. The diagonal dotted line represents the identity line of slope equal to unity and intercept zero.

same percentage of ACN and MeOH in the RPLC-domain, it can be concluded that in all cases the retention in MeOH/ H_2O is higher than in ACN/ H_2O and that MeOH presents lower eluent strength than ACN, as occurs in achiral RPLC systems. This behaviour was observed for all compounds.

3.2. Enantioresolution study

Table 2 shows, for each compound, the chromatographic system that provided the maximum enantioresolution value ($R_s \text{ max}$) for the ACN/ H_2O and MeOH/ H_2O mobile phases studied taking into account all CSPs data jointly. Table 2 also shows the correspond-

Table 2
Maximum enantioresolution (*Rs max*) values obtained with ACN and MeOH hydro-organic mobile phases for each compound taking into account the data from all CSPs jointly. The chromatographic system (CSP and percentage of organic solvent) corresponding to each *Rs max* value are included. The retention factor (*k*), selectivity (α), efficiency and (*N*) asymmetry factor (*B/A*) values for the least (1) and most (2) retained enantiomer are shown.

No	ACN					MeOH					Chromatographic system
	<i>k</i> ₁ / <i>k</i> ₂	α	<i>Rs max</i>	<i>N</i> ₁ / <i>N</i> ₂	(<i>B/A</i>) ₁ / ₂ (<i>B/A</i>) ₂	<i>k</i> ₁ / <i>k</i> ₂	α	<i>Rs max</i>	<i>N</i> ₁ / <i>N</i> ₂	(<i>B/A</i>) ₁ / ₂ (<i>B/A</i>) ₂	
1	3.9/4.4	1.11	1.2	3320/2320	2.1/2.0	0.6/0.7	1.18	0.7	1070/809	1.2/1.7	Cell2 - 90% MeOH
2	3.7/3.8	1.05	0.6	7170/6210	0.5/2.5	- b	1.00	0.0	- b	- b	- b
3	7.5/8.0	1.07	1.3	7310/6920	1.5/1.7	8.1/9.0	1.11	1.3	3220/3033	1.9/1.5	Cell2 - 70% MeOH
4	5.2/5.6	1.07	1.3	8630/8620	1.1/0.8	5.5/7.3	1.31	1.8	2350/2390	1.1/1.0	Cell3 - 60% MeOH
5	8.4/9.0	1.08	1.8	11300/11200	1.3/1.3	11.1/12.1	1.09	0.9	3190/3060	1.3/1.1	Cell2 - 70% MeOH
6	- a	1.00	0.0	- a	- a	6.8/7.9	1.17	1.2	1620/944	2.7/1.3	Cell4 - 60% MeOH
7	1.7/2.1	1.21	3.2	9470/9080	1.0/0.9	0.9/2.0	2.29	7.2	4290/4100	1.4/1.2	Cell3 - 90% MeOH
8	0.8/1.3	1.60	6.0	11500/11100	1.3/1.3	0.9/1.7	2.00	6.5	5090/4800	1.7/1.3	Cell3 - 90% MeOH
9	1.5/1.9	1.25	4.0	9930/9800	1.3/1.1	- b	1.00	0.0	- b	- b	- b
10	7.8/8.5	1.09	1.6	6020/5890	1.2/1.2	4.0/5.2	1.29	2.7	3110/2300	1.2/1.4	Cell4 - 60% MeOH
11	2.8/3.2	1.16	2.9	11500/11300	1.2/1.1	5.5/6.3	1.14	1.7	3930/3560	1.3/1.3	Cell5 - 80% MeOH
12	3.1/4.6	1.50	8.0	10100/10600	1.1/1.1	2.3/2.9	1.24	2.8	5200/4970	1.3/1.2	Cell2 - 80% MeOH
13	2.7/3.4	1.24	3.5	6990/6900	1.1/1.1	1.7/2.7	1.56	4.9	4650/4490	0.9/0.9	Cell3 - 80% MeOH
14	1.5/3.4	2.25	5.5	1930/1820	1.8/1.8	1.5/3.4	2.30	4.6	1550/886	1.4/1.9	Cell1 - 80% MeOH
15	4.4/5.8	1.30	3.0	2910/3100	1.7/1.6	2.2/2.9	1.33	3.3	4010/4090	1.2/1.1	Cell4 - 80% MeOH
16	5.3/6.4	1.20	4.4	12500/12700	1.1/1.1	1.7/2.1	1.23	2.3	6190/6350	1.4/1.3	Cell5 - 90% MeOH
17	- a	1.00	0.0	- a	- a	- b	1.00	0.0	- b	- b	- b
18	8.1/8.4	1.04	0.6	6370/3900	0.7/2.8	9.2/9.9	1.07	0.5	1970/539	0.4/3.5	Cell3 - 50% MeOH
19	3.2/3.8	1.17	2.3	5390/5300	0.9/0.8	1.7/2.4	1.39	0.6	161/101	1.3/3.6	Cell3 - 50% MeOH
20	- a	1.00	0.0	- a	- a	12.2/13.0	1.06	0.3	1970/633	0.9/3.8	Cell3 - 50% MeOH
21	5.2/5.7	1.10	2.0	9760/9610	1.6/1.5	2.9/3.2	1.09	0.9	3300/4060	1.3/0.9	Cell2 - 70% MeOH
22	5.3/6.6	1.24	2.9	3570/3540	0.9/1.0	1.7/2.8	1.67	2.6	1180/797	1.0/1.2	Cell3 - 80% MeOH
23	4.4/5.4	1.24	2.3	2810/3440	0.7/0.7	8.0/9.4	1.17	1.5	1770/1620	1.4/1.4	Cell1 - 70% MeOH
24	4.9/5.8	1.17	1.7	3660/2750	2.5/2.7	7.3/9.3	1.27	1.2	585/511	1.5/1.3	Cell3 - 80% MeOH
25	7.4/7.7	1.04	1.0	12400/12200	0.9/1.2	2.0/2.5	1.24	1.5	1530/1620	1.4/1.2	Cell3 - 70% MeOH
26	3.5/3.9	1.13	2.3	8750/8540	1.4/1.4	10.3/10.9	1.05	0.5	2710/1370	0.5/3.8	Cell5 - 60% MeOH
27	8.7/9.6	1.10	2.5	11800/11800	1.1/1.1	6.9/7.3	1.06	0.7	2960/2370	0.8/1.8	Cell5 - 60% MeOH
28	4.2/4.8	1.13	2.4	11100/10800	1.2/1.1	7.2/8.3	1.16	0.9	723/884	2.2/1.8	Cell3 - 70% MeOH
29	2.1/3.0	1.46	4.2	3840/3660	1.9/1.4	0.6/1.2	1.92	3.1	2120/1530	1.7/1.3	Cell3 - 90% MeOH
30	1.9/2.5	1.27	8.7	6700/5700	0.8/0.7	0.7/2.0	3.08	9.4	4220/4190	1.3/1.0	Cell3 - 90% MeOH
31	4.6/5.0	1.10	2.4	12600/12200	1.2/1.2	13.6/15.8	1.16	0.9	702/539	1.2/1.7	Cell5 - 60% MeOH
32	- a	1.00	0.0	- a	- a	- b	1.00	0.0	- b	- b	- b
33	0.8/1.0	1.29	0.8	701/1650	2.0/1.1	- b	1.00	0.0	- b	- b	- b
34	22.5/24.9	1.11	1.1	1800/1680	2.5/3.6	7.2/8.0	1.12	0.6	740/477	1.5/5.7	Cell3 - 50% MeOH
35	2.9/4.1	1.41	2.2	2170/621	2.0/4.5	8.8/12.3	1.40	2.3	993/905	2.2/2.0	Cell2 - 40% MeOH
36	3.9/4.3	1.08	0.5	1820/800	0.8/4.2	7.7/9.6	1.25	1.3	635/724	3.9/3.1	Cell3 - 60% MeOH
37	- a	1.00	0.0	- a	- a	- b	1.00	0.0	- b	- b	- b
38	32.7/40.5	1.24	1.2	617/423	2.9/2.2	- b	1.00	0.0	- b	- b	- b
39	5.8/6.6	1.12	0.7	831/587	1.0/3.5	3.8/4.9	1.29	0.6	129/139	1.0/2.6	Cell2 - 60% MeOH
40	4.4/5.1	1.14	2.3	5940/6200	2.0/1.9	12.8/15.3	1.19	1.1	800/630	1.9/2.3	Cell2 - 40% MeOH
41	1.6/2.7	1.67	5.4	3690/4730	5.5/4.1	1.0/1.9	1.94	5.1	3050/2900	1.7/1.4	Cell2 - 80% MeOH
42	0.3/0.6	2.20	3.3	2990/3660	2.0/2.3	0.4/0.5	1.50	0.8	543/1130	2.5/2.8	Cell3 - 70% MeOH
43	0.3/0.5	1.67	1.9	959/670	2.2/1.0	0.4/0.5	1.29	0.8	512/1320	2.6/2.8	Cell3 - 70% MeOH
44	5.1/5.4	1.07	1.4	10200/9810	1.2/1.1	3.9/4.5	1.14	1.7	4380/4150	1.4/1.3	Cell5 - 90% MeOH
45	7.6/8.2	1.08	1.8	11630/11500	1.0/1.1	12.9/18.7	1.45	1.8	307/298	2.2/2.3	Cell3 - 70% MeOH
46	15.9/16.7	1.05	0.7	3370/3320	0.7/2.8	14.0/17.1	1.22	1.2	291/272	1.9/1.9	Cell3 - 70% MeOH
47	6.3/6.4	1.02	0.4	15500/11000	0.3/3.5	4.3/4.7	1.11	0.7	1570/943	1.3/1.8	Cell4 - 70% MeOH

(continued on next page)

Table 2 (continued)

No	ACN				MeOH				Chromatographic system		
	k_1/k_2	α	$R_s \max$	N_1/N_2	$(B/A)_1/(B/A)_2$	k_1/k_2	α	$R_s \max$		N_1/N_2	$(B/A)_1/(B/A)_2$
48	6.8/8.1	1.19	3.0	5810/6390	1.5/1.4	7.8/8.2	1.05	0.6	2290/3490	0.7/2.3	Cell3 - 80% MeOH
49	1.2/1.5	1.31	2.7	4750/5020	1.5/1.1	2.2/3.4	1.52	4.2	3610/3360	1.1/1.1	Cell3 - 90% MeOH
50	7.3/8.4	1.15	1.5	2140/2510	2.7/2.3	4.6/5.2	1.13	1.0	1590/1440	1.1/1.5	Cell3 - 90% MeOH
51	7.8/7.9	1.02	0.5	12900/13800	0.5/2.7	2.4/4.0	1.65	5.5	3750/3350	1.3/1.2	Cell3 - 90% MeOH
52	1.4/2.2	1.56	5.0	4870/5410	1.5/1.5	4.7/7.4	1.56	4.0	1830/1840	1.0/0.9	Cell4 - 70% MeOH
53	2.4/4.7	1.93	9.5	7600/5160	1.6/2.1	1.0/1.3	1.32	2.5	4240/4490	1.5/1.4	Cell4 - 90% MeOH
54	3.2/5.4	1.67	8.5	7380/7010	1.2/1.3	2.1/3.3	1.59	6.0	5040/5190	1.3/1.2	Cell4 - 90% MeOH

^a Compound with $R_s = 0$ in all ACN/5 mM NH_4HCO_3 (pH=8) chromatographic systems

^b Compound with $R_s = 0$ in all MeOH/5 mM NH_4HCO_3 (pH=8) chromatographic systems

ing k , N and B/A values obtained for the first (1) and second (2) eluted enantiomers as well as the α values (Eqs. (1)–(5)). Additionally, Table 3 shows the count of compounds showing baseline ($R_s \max \geq 1.5$) and partial ($0 < R_s \max < 1.5$) enantioresolution in at least one of the experimental conditions assayed in each chromatographic system; as well as the count of those compounds showing null ($R_s \max = 0$) enantioresolution in all experimental conditions assayed in the indicated chromatographic system. Compounds are identified as indicated in Table 1.

As can be observed in Tables 2 and 3 (last row), the enantiomers of 38 of the 54 chiral compounds studied were baseline separated in at least one of all the chromatographic systems assayed. In addition, the enantiomers of five ($No = 2, 18, 20, 39$ and 47) of the 13 compounds partially separated showed marginal $R_s \max$ values ($0 < R_s \max \leq 0.7$); and three chiral compounds ($No = 17, 32$ and 37) showed $R_s = 0$ in any of the chromatographic systems studied. The highest $R_s \max$ value (9.4) was found for compound $No = 30$ (aminoglutethimide) in the Cell3 CSP and a 90% MeOH mobile phase.

The effect of the nature and concentration of the organic solvent, as well as the nature of the CSP on the enantioresolution is studied in depth in the sub-sections below.

3.2.1. Effect of the nature of the organic solvent used in the mobile phase on the enantioresolution

As stated in the introduction section, the mobile phase composition can modulate the enantioresolution ability of a given CSP [12–19]. As can be observed in Tables 2 and 3, ACN/ H_2O allowed baseline enantioresolution of a higher number of compounds than MeOH/ H_2O ($R_s \max \geq 1.5$ for 34 and 24 compounds in ACN/ H_2O and MeOH/ H_2O , respectively). It must be noted that, in most cases, the percentage of MeOH in the mobile phase allowing baseline enantioresolution was much higher than the corresponding one of ACN/ H_2O .

Fig. 4 shows the $R_s \max$ values obtained with MeOH/ H_2O vs. ACN/ H_2O mobile phases for each CSP studied (Fig. 4.A–E), as well as, taking into account all CSP results jointly (Fig. 4.F). The identity line (dotted line) has been included for comparative purposes. When compared the results obtained with both solvents in each CSP (Fig. 4.A–E), there is no correlation between the $R_s \max$ -ACN and $R_s \max$ -MeOH values, nor do they fit the identity line for most compounds, which means that the use of MeOH/ H_2O or ACN/ H_2O leads to a different enantioselectivity and enantioresolution degree of the chromatographic systems. Although in some cases MeOH/ H_2O mobile phases provided much better $R_s \max$ values than ACN/ H_2O mobile phases, the use of MeOH/ H_2O instead of ACN/ H_2O decreased enantioresolution for most compounds (i.e., compounds are below the identity line in Fig. 4) in all CSPs. This effect was less noticeable in Cell3-MeOH. The MeOH-Cell1 and MeOH-Cell5 chromatographic systems displayed very poor enantioresolution ability. The lower enantioresolution ability of the MeOH/ H_2O chromatographic systems could be attributed to its ability to exert hydrogen bonds with the CSP that can displace the enantiomer from the enantiomer-CSP complex. In addition, the efficiency (N) of the chromatographic peaks was always lower in MeOH/ H_2O than in ACN/ H_2O chromatographic systems while asymmetry (B/A) of the peaks was similar in both systems (see Table 2).

From a practical perspective, taking into account the results obtained for all CSPs (see Fig. 4.F and Tables 2 and 3), MeOH/ H_2O mobile phases became indispensable only for the baseline enantioresolution of four compounds: $No = 4$ (bupropion), $No = 25$ (bupivacaine), $No = 44$ (cilnidipine) and $No = 51$ (trimeprazine; see Fig. 5). For these compounds, baseline enantioresolution was only obtained with MeOH/ H_2O mobile phases.

Table 3

Compound count with baseline ($R_s \max \geq 1.5$) and partial ($0 < R_s \max < 1.5$) enantioresolution in at least one of the experimental conditions assayed in each chromatographic system; and compound count with null ($R_s \max = 0$) enantioresolution in all experimental conditions assayed in the indicated chromatographic system. See *No* in Table 1

Chromatographic system	$R_s \max$	Count	<i>No</i>
ACN-Cell1	$R_s \max \geq 1.5$	9	7, 8, 12, 14, 15, 22, 23, 30, 35
	$0 < R_s \max < 1.5$	14	9-11, 13, 16, 24, 27, 36, 40, 41, 44, 46, 52, 54
	$R_s \max = 0$	31	1-6, 17-21, 25, 26, 28, 29, 31-34, 37-39, 42, 43, 45, 47-51, 53
ACN-Cell2	$R_s \max \geq 1.5$	21	5, 7-10, 12-14, 16, 21, 26-28, 30, 35, 40, 41, 45, 52-54
	$0 < R_s \max < 1.5$	17	1-4, 11, 15, 22, 24, 25, 29, 33, 34, 39, 44, 47, 49, 51
	$R_s \max = 0$	16	6, 17-20, 23, 31, 32, 36-38, 42, 43, 46, 48, 50
ACN-Cell3	$R_s \max \geq 1.5$	16	7-9, 12-15, 19, 22, 29, 30, 42, 48, 49, 50, 53
	$0 < R_s \max < 1.5$	6	4, 16, 23, 24, 44, 45
	$R_s \max = 0$	32	1-3, 5, 6, 10, 11, 17, 18, 20-21, 25-28, 31-41, 43, 46, 47, 51, 52, 54
ACN-Cell4	$R_s \max \geq 1.5$	18	7, 8, 11-16, 27, 28, 30, 31, 35, 40, 41, 52-54
	$0 < R_s \max < 1.5$	17	1-5, 9, 10, 18, 21, 24, 26, 29, 34, 38, 42, 44, 45
	$R_s \max = 0$	19	6, 17, 19, 20, 22, 23, 25, 32, 33, 36, 37, 39, 43, 46-51
ACN-Cell5	$R_s \max \geq 1.5$	15	8, 11-14, 16, 24, 26, 30, 31, 41, 43, 52-54
	$0 < R_s \max < 1.5$	7	4, 9, 15, 25, 27, 28, 43
	$R_s \max = 0$	32	1-3, 5-7, 10, 17-23, 29, 32-40, 42, 45-51
ACN-All CSPs	$R_s \max \geq 1.5$	34	5, 7-16, 19, 21-24, 26-31, 35, 40-43, 45, 48, 49, 50, 52-54
	$0 < R_s \max < 1.5$	15	1-4, 18, 25, 33, 34, 36, 38, 39, 44, 46, 47, 51
	$R_s \max = 0$	5	6, 17, 20, 32, 37
MeOH-Cell1	$R_s \max \geq 1.5$	4	14-16, 23
	$0 < R_s \max < 1.5$	11	7, 10, 12, 13, 22, 25, 30, 35, 48, 52, 54
	$R_s \max = 0$	39	1-6, 8, 9, 11, 17-21, 24, 26-29, 31-34, 36-47, 49-51, 53
MeOH-Cell2	$R_s \max \geq 1.5$	13	8, 10, 12-16, 30, 35, 45, 52-54
	$0 < R_s \max < 1.5$	14	1, 3-5, 7, 11, 21, 28, 31, 36, 39, 40, 44, 45
	$R_s \max = 0$	27	2, 6, 9, 17-20, 22-27, 29, 32-34, 37, 38, 42, 43, 46-51
MeOH-Cell3	$R_s \max \geq 1.5$	11	4, 7, 8, 13, 22, 25, 29, 30, 45, 49, 51
	$0 < R_s \max < 1.5$	28	3, 6, 10, 11, 14-16, 18-20, 23, 24, 28, 31, 34-36, 39-44, 46, 48, 50, 52-54
	$R_s \max = 0$	15	1, 2, 5, 9, 12, 17, 21, 26, 27, 32, 37, 38, 47, 54
MeOH-Cell4	$R_s \max \geq 1.5$	10	8, 10, 12, 13, 15, 30, 41, 52-54
	$0 < R_s \max < 1.5$	16	1, 3-7, 11, 14, 21, 28, 37, 39, 40, 44, 45, 47
	$R_s \max = 0$	28	2, 9, 16-20, 22-27, 29, 31-34, 36-38, 42, 43, 46, 48-51
MeOH-Cell5	$R_s \max \geq 1.5$	7	8, 11, 13, 16, 41, 44, 54
	$0 < R_s \max < 1.5$	9	10, 12, 14, 24, 26, 27, 31, 52, 53
	$R_s \max = 0$	38	1-7, 9, 15, 17-23, 25, 28-30, 32-40, 42, 43, 45-51
MeOH-All CSPs	$R_s \max \geq 1.5$	24	4, 7, 8, 10-16, 22, 23, 25, 29, 30, 35, 41, 44, 45, 49, 51-54
	$0 < R_s \max < 1.5$	23	1, 3, 5, 6, 18-20, 21, 24, 26-28, 31, 34, 36, 39, 40, 42, 43, 46-48, 50
	$R_s \max = 0$	7	2, 9, 17, 32, 33, 37, 38
All (overall data from all mobile phases and CSPs)	$R_s \max \geq 1.5$	38	4, 5, 7-16, 19, 21-31, 35, 40-45, 48, 49-54
	$0 < R_s \max < 1.5$	13	1-3, 6, 18, 20, 33, 34, 36, 38, 39, 46, 47
	$R_s \max = 0$	3	17, 32, 37

In view of the results obtained, to try to separate the enantiomers of a new chiral compound in the cellulose CSPs studied we recommend using ACN/H₂O mobile phases as a first attempt and testing MeOH/H₂O only in those cases where ACN/H₂O fails. It must be pointed out that the MeOH-Cell3 system can provide interesting complementary results (see Section 3.2.2).

3.2.2. Effect of the percentage of organic solvent used in the mobile phase on the enantioresolution

For most of the compounds and CSPs, with MeOH/H₂O and ACN/H₂O in the RPLC-domain mobile phases, enantioresolution increased as the percentage of organic solvent in the mobile phase decreased. Different behaviour was observed for enantioresolution in the ACN HILIC-domain (98-80% ACN). For some compounds and some CSPs, enantioresolution decreased as the ACN content decreased (e.g. *No* = 53 in Cell2, Cell4, and Cell5) while for other cases CSPs, the opposite behaviour was observed (e.g. *No* = 29 in Cell3). Finally, in other cases, the enantioresolution decreased as the ACN content decreased up to a minimum were enantioresolution increased as the ACN content decreased (e.g. *No* = 8, 9, 12-14 in Cell2 and Cell4). This behaviour could be attributed to reversals in the elution order of enantiomers. Although this statement must be confirmed by injecting pure enantiomers.

The enantioresolution in the HILIC- and RPLC-domain were also compared. Table 4 shows compound count with baseline and partial enantioresolution in at least one of the experimental condi-

tions assayed in the HILIC- (80-98% ACN) and RPLC- (< 80%) domains in at least one of the experimental conditions assayed in each chromatographic system. As can be observed in Table 4 (last row) (see also Fig. S1.F in Supplementary materials), in the RPLC-domain, the baseline enantioresolution of almost twice as many compounds as in HILIC was obtained (32 and 17 compounds, respectively).

On the other hand, when comparing the $R_s \max$ values obtained in the HILIC-domain with the corresponding values in the RPLC-domain for each of the CSPs studied (Fig. S1.A-S1.E), it was observed that for most of the compounds, worse $R_s \max$ values were obtained in HILIC. As can be observed in Table 4 (last row) (and Fig. S1.F), the enantiomers of *No* = 49 (promethazine) were the only ones that were baseline separated in the HILIC-domain but partially resolved in the RPLC-domain (with ACN/H₂O, in MeOH/H₂O mobile phases baseline enantioresolution was achieved, see Tables 2 and 3). Moreover, all the other compounds that were baseline enantioresolved in HILIC also did so in RPLC and with higher $R_s \max$ values (Fig. S1.F), except for the enantiomers of pin-dolol (*No* = 35), and isoprenaline (*No* = 41) whose $R_s \max$ values were higher in the HILIC-domain.

As is well known, the HILIC mode in achiral HPLC is of particular interest for the separation of hydrophilic compounds, so it would not be illogical to suppose that this mode could be advantageous for the separation of the enantiomers of chiral hydrophilic compounds in chiral HPLC. In contrast, 3 (*No* = 35, 36, and 41) of

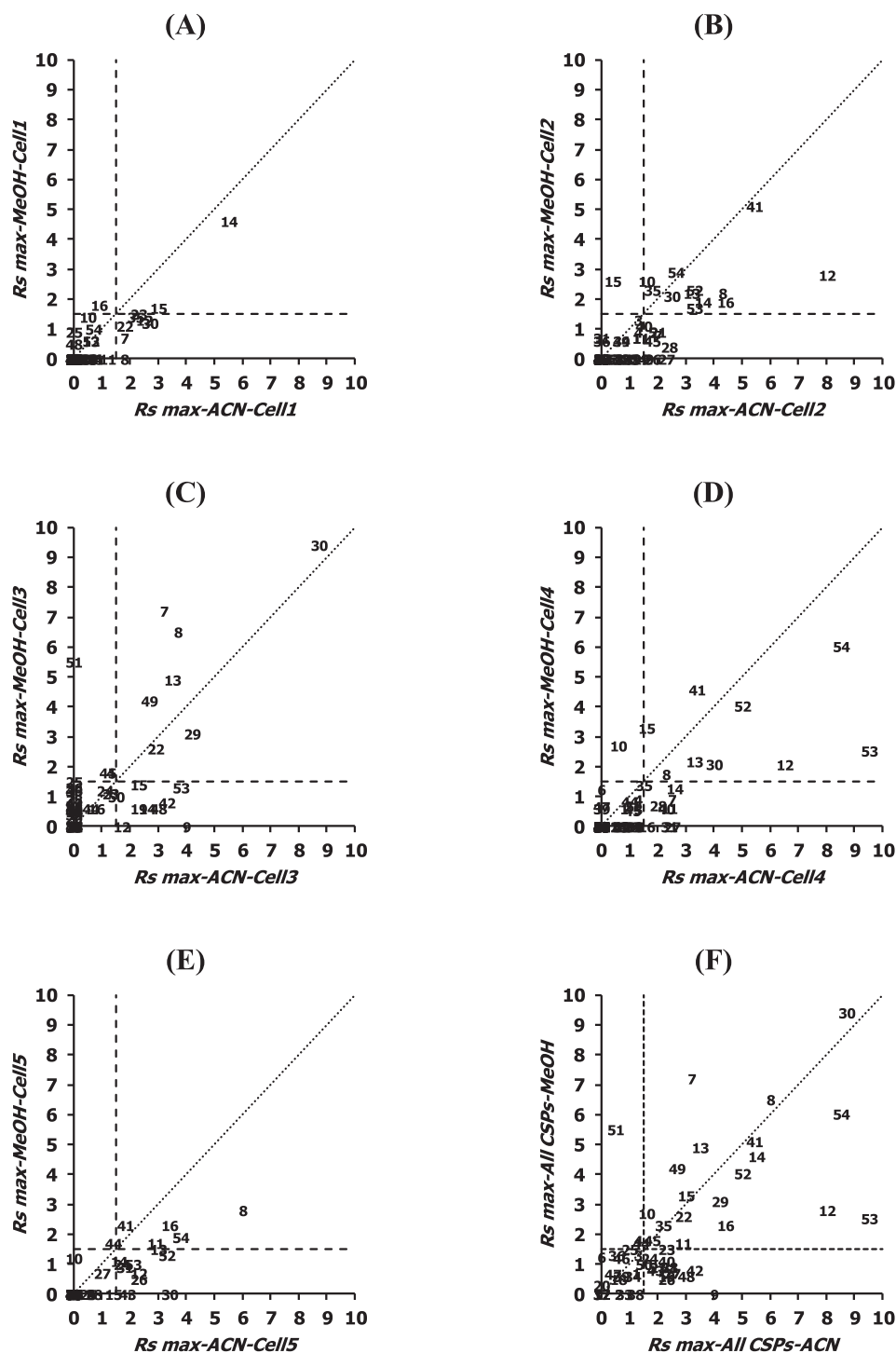


Fig. 4. Maximum enantioresolution values (R_s max) obtained for the MeOH/H₂O vs. ACN/H₂O mobile phases in each cellulose chiral stationary phase studied: (A) Cell1, (B) Cell2, (C) Cell3, (D) Cell4, (E) Cell5 and (F) all chiral stationary phases. The diagonal dotted line represents the identity line of slope equal to unity and intercept zero. The horizontal and vertical dashed lines indicate R_s max = 1.5.

the 30 chiral compounds for which some degree of enantioresolution was observed under the HILIC conditions assayed have $\log D$ values lower than 1.0.

In view of the results obtained, and taking into account the higher cost and toxicity of the HILIC mobile phases used, to try to separate the enantiomers of a new chiral compound in the cellulose CSPs studied we recommend using the RPLC mode.

3.2.3. Effect of the nature of the CSP on the enantioresolution

As can be seen in Table 3, with ACN/H₂O mobile phases, Cell2 is the CSP that allowed the separation (baseline and partial) of the enantiomers of the highest number of chiral compounds, followed by Cell4, then Cell3, Cell5, and finally Cell1. ACN-Cell2 is also the chromatographic system among all the assayed (including MeOH/H₂O systems) that provided the baseline enantioseparation

Table 4

Compound count with baseline ($R_s \max \geq 1.5$) and partial ($0 < R_s \max < 1.5$) enantioresolution in at least one of the experimental conditions assayed in each chromatographic system in the HILIC (80–98% ACN) and RPLC (<80%) domains. See No in Table 1

Chromatographic system	$R_s \max$	Domain	Count	No
ACN-Cell1	$R_s \max \geq 1.5$	HILIC	3	14, 15, 35
	$0 < R_s \max < 1.5$	RPLC	9	7, 8, 12, 14, 15, 22, 23, 30, 35
		HILIC	9	7, 8, 11, 12, 16, 22, 23, 30, 36
ACN-Cell2	$R_s \max \geq 1.5$	HILIC	10	8, 12–14, 16, 30, 41, 52–54
	$0 < R_s \max < 1.5$	RPLC	21	5, 7–10, 12–14, 16, 21, 26–28, 30, 35, 40, 41, 45, 52–54
		HILIC	9	1, 7, 9, 11, 24, 26–28, 45
ACN-Cell3	$R_s \max \geq 1.5$	RPLC	17	1–4, 11, 15, 22, 24, 25, 29, 33, 34, 39, 44, 47, 49, 51
	$R_s \max \geq 1.5$	HILIC	4	8, 9, 29, 49
		RPLC	15	7–9, 12–15, 19, 22, 29, 30, 42, 48, 50, 53
ACN-Cell4	$R_s \max \geq 1.5$	HILIC	4	7, 13, 30, 50
	$0 < R_s \max < 1.5$	RPLC	6	4, 16, 23, 24, 44, 45
		HILIC	6	12, 13, 41, 52–54
ACN-Cell5	$R_s \max \geq 1.5$	RPLC	17	7, 8, 11–16, 27, 28, 30, 31, 35, 40, 52–54
	$0 < R_s \max < 1.5$	HILIC	10	1, 7, 8, 11, 14, 16, 18, 27, 28, 30
		RPLC	17	1–5, 9, 10, 18, 21, 24, 26, 29, 34, 38, 42, 44, 45
ACN-Cell5	$R_s \max \geq 1.5$	HILIC	9	8, 11, 13, 16, 26, 30, 41, 52, 54
	$0 < R_s \max < 1.5$	RPLC	13	8, 11–14, 16, 24, 26, 30, 31, 52–54
		HILIC	7	12, 14, 15, 24, 25, 44, 53
ACN-All CSPs	$R_s \max \geq 1.5$	RPLC	7	4, 9, 15, 27, 28, 41, 44
	$R_s \max \geq 1.5$	HILIC	17	8, 9, 11–16, 26, 29, 30, 35, 41, 49, 52–55
		RPLC	32	5, 7–16, 19, 21–24, 36–31, 35, 40–42, 45, 48, 50, 52–54
$0 < R_s \max < 1.5$	HILIC	13	1, 7, 18, 22–25, 27, 28, 36, 44, 45, 50	
	RPLC	15	1–4, 18, 25, 33, 34, 38, 39, 44, 46, 47, 49, 51	

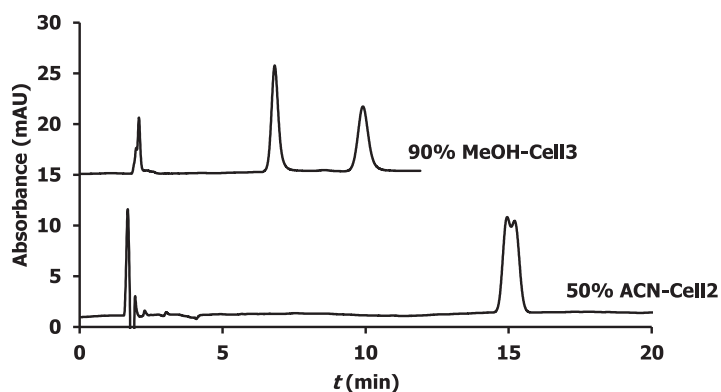


Fig. 5. Chromatograms obtained for trimeprazine ($No = 51$) in the ACN/H₂O and MeOH/H₂O chromatographic systems, which provided the maximum enantioresolution values. See further experimental details in Section 2.3.

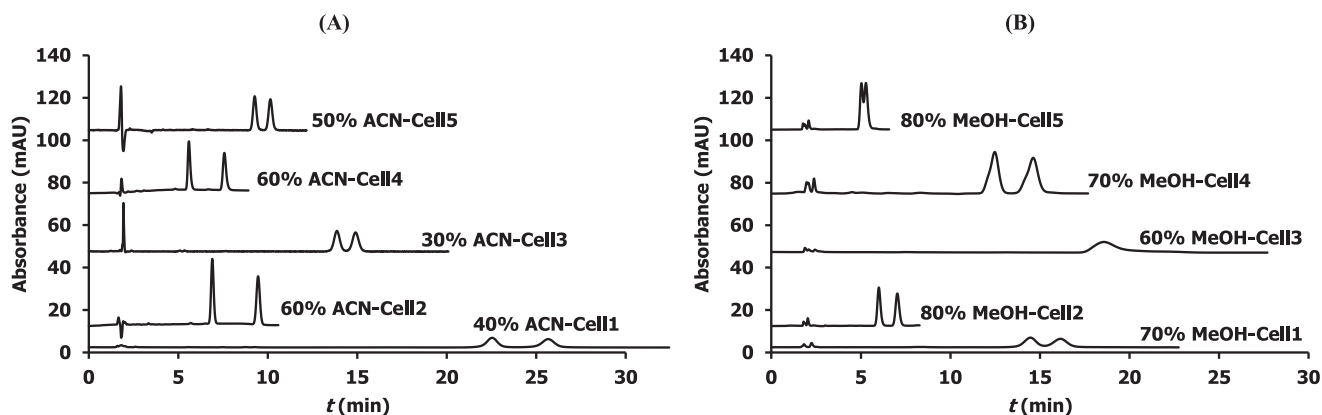


Fig. 6. Chromatograms obtained for hexaconazole ($No = 12$) in the chromatographic systems, which provided the maximum enantioresolution values using: (A) ACN/H₂O and (B) MeOH/H₂O mobile phases. See further experimental details in Section 2.3.

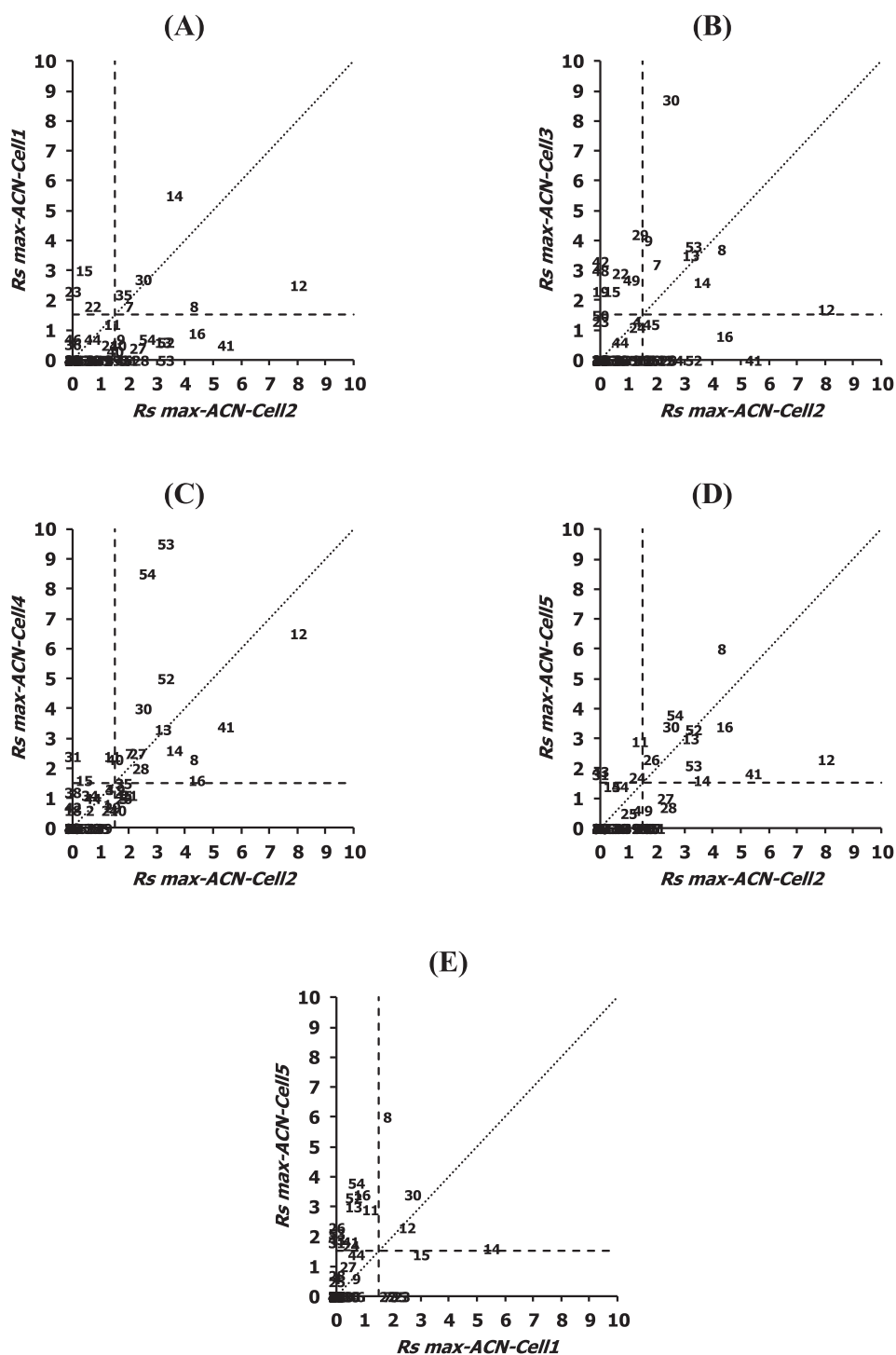


Fig. 7. Comparison of maximum enantioresolution values ($R_s \max$) obtained for ACN/H₂O mobile phases in the cellulose chiral stationary phase studied: (A) Cell1 vs. Cell2, (B) Cell3 vs. Cell2, (C) Cell4 vs. Cell2, (D) Cell5 vs. Cell2, and (E) Cell5 vs. Cell1. The diagonal dotted line represents the identity line of slope equal to unity and intercept zero. The horizontal and vertical dashed lines indicate $R_s \max = 1.5$.

of the highest number of compounds. In this system, the $R_s \max$ values, for compounds with baseline enantioresolution, were between 1.5 ($N_o = 40$, clenbuterol) and 8.0 (hexaconazole, $N_o = 12$, maximum value obtained among all compounds and ACN/H₂O conditions tested, see Fig. 6).

In Fig. 7 the $R_s \max$ -ACN values obtained with each CSP vs. those obtained with Cell2 are plotted. These graphs can be very useful to compare the enantioresolution of the CSPs and also to

establish if any of them have complementary/advantageous enantioselectivity with respect to that of the Cell2 with ACN/H₂O mobile phases.

As discussed above, Cell2 and Cell4 are the CSPs with the closest structure. The ACN-Cell4 system did not show clear enantioselectivity complementary to that of ACN-Cell2 (data show a random distribution around the identity line in Fig. 7.C). Thus, in general, the enantiomers of most compounds that separated (baseline or

partially) in the ACN-Cell4 system also did in the ACN-Cell2 system; except for the enantiomers of compounds $No = 18, 31, 38,$ and 42 which only showed some enantioresolution degree in ACN-Cell4. For other compounds ($No = 7, 11, 15, 30, 34, 40, 44, 52, 53$ and 54) better $R_s \text{ max-ACN-Cell4}$ values were also obtained. However, from a practical point of view, the use of ACN-Cell4 was advantageous over ACN-Cell2 only for the separation of the enantiomers of benalaxyl ($No = 11$) and bicalutamide ($No = 31$) that only showed baseline enantioresolution in ACN-Cell4 (although also in other systems, see Table 3). These results show that the position of the substituents of the phenylcarbamate moiety, although not exerting a marked effect on the enantioselectivity of the CSP, does affect the enantioresolution degree.

The other phenylcarbamate-type CSPs (Cell1 and Cell5) also did not clearly show complementary enantioselectivity to Cell2 with ACN/H₂O mobile phases. As can be seen in Fig. 7.D, among the compounds ($No = 8, 11, 24, 26, 30, 31, 42, 43,$ and 54) with baseline enantioresolution in ACN-Cell5 and with $R_s \text{ max}$ values higher than in ACN-Cell2, this system was only advantageous over the ACN-Cell2 system and also over all the systems studied (including the MeOH/H₂O systems) for the separation of the enantiomers of terfenadine ($No = 24$) and terbutaline ($N = 43$) whose baseline enantioresolution was only achieved in ACN-Cell5 (see Table 3). On the other hand, for enantiomers of $No = 14, 15, 22, 23, 30,$ and 35 baseline enantioresolution in ACN-Cell1 was found with higher $R_s \text{ max}$ values than in ACN-Cell2 (Fig. 7.A); but, among these compounds, only for the separation of orphenadrine enantiomers ($No = 23$), the ACN-Cell1 system was clearly advantageous over ACN-Cell2 and also over the rest of the systems in practical terms (see Table 3). As can be observed in Fig. 7.E, the ACN-Cell5 and ACN-Cell1 systems showed almost orthogonal enantioselectivity, highlighting the great impact of the nature of the CSP substituents on the enantioresolution.

Cell3 is the unique benzoate-type CSP assayed and is the only CSP that clearly showed complementary enantioselectivity to that of Cell2 and the other CSPs with ACN mobile phases. As can be seen in Fig. 7.B, the enantiomers of $No = 15, 19, 22, 29, 42, 48,$ $49,$ and 50 were baseline enantioresolved in Cell3-ACN but not in Cell2-ACN (see Table 3). Cell3-ACN was the unique system among all the studied systems (including the MeOH/H₂O systems) that allowed the baseline enantioresolution of the enantiomers of cetirizine ($No = 19$), orciprenaline ($No = 42$), ethopropazine ($No = 48$) and thioridazine ($No = 50$).

As can be seen in Table 3, with MeOH/H₂O mobile phases, Cell2 was also the CSP that allowed the baseline separation of the enantiomers of the highest number of chiral compounds, followed by Cell3, then Cell4, Cell5, and finally Cell1 CSP. On the other hand, Cell3 showed almost orthogonal enantioselectivity to that of Cell2 (see Fig. S2.A) in MeOH/H₂O. Moreover, in MeOH/H₂O mobile phases, Cell2 and Cell4 CSPs showed similar enantioselectivities as in ACN/H₂O mobile phases, but also similar enantioresolution degrees (Fig. S2.B). Finally, as stated in Section 3.2.1, the MeOH-Cell1 and MeOH-Cell5 chromatographic systems displayed very poor enantioresolution ability (Fig. S2.C).

For the aforementioned reasons, to try to enantioseparate a new basic or neutral chiral compound in the cellulose-CSPs studied we recommend using the following chromatographic system order: (i) ACN-Cell2, (ii) MeOH-Cell3, (iii) ACN-Cell5, (iv) ACN-Cell1 and (v) other systems.

4. Conclusions

In this paper, the retention behaviour and the enantioresolution of 54 structurally unrelated basic and neutral chiral compounds are studied using five commercial cellulose-based chiral stationary phases (Cell1, Cell2, Cell3, Cell4, and Cell5) and acetoni-

trile (10–98%) or methanol (30–90%)/5 mM ammonium bicarbonate ($pH = 8$) mobile phases.

In the experimental conditions assayed, for all compounds and CSPs in MeOH/H₂O mobile phases a typical RPLC retention behaviour was observed. Whereas for ACN/H₂O mobile phases, two different domains according to water content and retention behaviour were distinguished: the RPLC-domain, for the water content of 20–90% (ACN content below 80%), where RPLC behaviour prevails; and the HILIC-domain, for a water proportion in the mobile phase below 20% (ACN content of 80–98%), in which HILIC retention behaviour prevails.

This dual HILIC/RPLC retention behaviour was observed for all compounds and all (chlorinated and non-chlorinated) CSPs. However, the magnitude of retention changes was different for each compound and each CSP. HILIC behaviour was more noticeable for hydrophilic compounds with all CSPs.

The use of MeOH/H₂O or ACN/H₂O leads to different enantioselectivities and enantioresolution degrees of the chromatographic systems. For most compounds in all CSPs, ACN/H₂O provided much better enantioresolution than MeOH/H₂O mobile phases. This effect was less noticeable in Cell3-MeOH chromatographic system. The MeOH-Cell1 and MeOH-Cell5 chromatographic systems displayed very poor enantioresolution ability. The lower enantioresolution ability of the MeOH/H₂O chromatographic systems could be attributed to its competition with the enantiomer for hydrogen-bonding interactions with the CSP.

For ACN/H₂O mobile phases, much better enantioresolution was obtained in the RPLC-domain for most of the compounds. Except the enantiomers of promethazine, all the compounds that were baseline enantioresolved in HILIC also did so in RPLC.

Among all the chromatographic systems assayed, ACN-Cell2 allowed the separation of the enantiomers of the highest number of chiral compounds. Phenylcarbamate-type CSPs did not clearly show complementary enantioselectivity to that of Cell2 with ACN/H₂O mobile phases. Comparing enantioresolution of Cell2 vs. Cell4, it can be concluded that the position of the substituents of the phenyl moiety, although not exerting a marked effect on the enantioselectivity of the CSP, does affect the enantioresolution degree in ACN/H₂O but not in MeOH/H₂O mobile phases. On the other hand, comparing the enantioresolution of Cell1 vs. Cell5, it can be concluded that the nature of the CSP substituents has a significant effect on the enantioresolution with ACN/H₂O mobile phases. Cell3 is the only CSP that clearly showed complementary enantioselectivity to that of Cell2, mainly with MeOH/H₂O mobile phases.

From the results obtained, to try to separate the enantiomers of a new basic or neutral chiral compound in the cellulose-CSPs studied, we recommend using the ACN-Cell2 chromatographic system in the RPLC-domain as a first attempt, then MeOH-Cell3, ACN-Cell5, ACN-Cell1 both in the RPLC-domain, and finally other systems.

Declaration of Competing Interest

The authors declare that they have no known competing financial interests or personal relationships that could have appeared to influence the work reported in this paper.

CRediT authorship contribution statement

Mireia Pérez-Baeza: Investigation, Validation, Visualization, Formal analysis, Writing – original draft. **Laura Escuder-Gilabert:** Conceptualization, Methodology, Supervision, Formal analysis, Writing – original draft, Writing – review & editing. **Yolanda Martín-Biosca:** Conceptualization, Methodology, Supervision, Formal analysis, Writing – original draft, Writing – review & editing. **Salvador Sagrado:** Conceptualization, Methodology, Supervision,

Formal analysis, Writing – original draft, Writing – review & editing, Software, Data curation. **María José Medina-Hernández:** Conceptualization, Methodology, Supervision, Formal analysis, Writing – original draft, Writing – review & editing, Software, Data curation, Project administration, Funding acquisition.

Acknowledgments

Mireia Pérez Baeza is grateful to the Generalitat Valenciana and the **European Social Fund** for the financial support (ACIF/2019/158 research contract).

Supplementary materials

Supplementary material associated with this article can be found, in the online version, at doi:[10.1016/j.chroma.2022.463073](https://doi.org/10.1016/j.chroma.2022.463073).

References

- [1] B.Y. Raymond, J.P. Quirino, Chiral liquid chromatography and capillary electrochromatography: Trends from 2017 to 2018, *Trends Anal. Chem.* 118 (2019) 779–792, doi:[10.1016/j.trac.2019.07.011](https://doi.org/10.1016/j.trac.2019.07.011).
- [2] J. Teixeira, M.E. Tiritan, M.M.M. Pinto, C. Fernandes, Chiral stationary phases for liquid chromatography: recent developments, *Molecules* 24 (2019) 865, doi:[10.3390/molecules24050865](https://doi.org/10.3390/molecules24050865).
- [3] G.K.E. Scriba, Chiral recognition in separation sciences. Part I: Polysaccharide and cyclodextrin selectors, *Trends Anal. Chem.* 120 (2019) 115639, doi:[10.1016/j.trac.2019.115639](https://doi.org/10.1016/j.trac.2019.115639).
- [4] J.M. Padró, S. Keunchkarian, State-of-the-art and recent developments of immobilized polysaccharide based chiral stationary phases for enantioseparations by high-performance liquid chromatography (2013–2017), *Microchem. J.* 140 (2018) 142–157, doi:[10.1016/j.microc.2018.04.017](https://doi.org/10.1016/j.microc.2018.04.017).
- [5] B. Chankvetadze, Recent developments on polysaccharide-based chiral stationary phases for liquid-phase separation of enantiomers, *J. Chromatogr. A* 1269 (2012) 26–51, doi:[10.1016/j.chroma.2012.10.033](https://doi.org/10.1016/j.chroma.2012.10.033).
- [6] B. Chankvetadze, Recent trends in preparation, investigation and application of polysaccharide-based chiral stationary phases for separation of enantiomers in high-performance liquid chromatography, *Trends Anal. Chem.* 122 (2020) 115709, doi:[10.1016/j.trac.2019.115709](https://doi.org/10.1016/j.trac.2019.115709).
- [7] P. Peluso, V. Mamane, E. Aubert, S. Cossu, Insights into the impact of shape and electronic properties on the enantioseparation of polyhalogenated 4,4'-bipyridines on polysaccharide-type selectors. Evidence for stereoselective halogen bonding interactions, *J. Chromatogr. A* 1345 (2014) 182–192, doi:[10.1016/j.chroma.2014.04.040](https://doi.org/10.1016/j.chroma.2014.04.040).
- [8] P. Peluso, B. Chankvetadze, The molecular bases of chiral recognition in 2-(benzylsulfinyl) benzamide enantioseparation, *Anal. Chim. Acta* 1141 (2021) 194–205, doi:[10.1016/j.aca.2020.10.050](https://doi.org/10.1016/j.aca.2020.10.050).
- [9] A. Dessi, B. Sechi, R. Dallochio, B. Chankvetadze, M. Pérez-Baeza, S. Cossu, V. Mamane, P. Pale, P. Peluso, Comparative enantioseparation of planar chiral ferrocenes on polysaccharide-based chiral stationary phases, *Chirality* (2022) 1–11, doi:[10.1002/chir.23417](https://doi.org/10.1002/chir.23417).
- [10] B. Chankvetadze, E. Yashima, Y. Okamoto, Chloromethylphenylcarbamate derivatives of cellulose as chiral stationary phases for high-performance liquid chromatography, *J. Chromatogr. A* 670 (1994) 39–49, doi:[10.1016/0021-9673\(94\)80278-5](https://doi.org/10.1016/0021-9673(94)80278-5).
- [11] B. Chankvetadze, E. Yashima, Y. Okamoto, Dimethyl-, dichloro- and chloromethylphenylcarbamate derivatives of amylose as chiral stationary phases for high-performance liquid chromatography, *J. Chromatogr. A* 694 (1995) 101–109, doi:[10.1016/0021-9673\(94\)00729-5](https://doi.org/10.1016/0021-9673(94)00729-5).
- [12] G. D'Orazio, C. Fanali, S. Fanali, A. Gentili, B. Chankvetadze, Comparative study on enantiomer resolving ability of amylose tris(3-chloro-5-methylphenylcarbamate) covalently immobilized onto silica in nano-liquid chromatography and capillary electrochromatography, *J. Chromatogr. A* 1606 (2019) 460425, doi:[10.1016/j.chroma.2019.460425](https://doi.org/10.1016/j.chroma.2019.460425).
- [13] R. Geryk, K. Kalíková, J. Vozka, E. Tesařová, Immobilized polysaccharide-based stationary phases for enantioseparation in normal versus reversed phase HPLC, *Chromatographia* 78 (2015) 909–915, doi:[10.1007/s10337-014-2804-8](https://doi.org/10.1007/s10337-014-2804-8).
- [14] A. Ghanem, C. Wang, Enantioselective separation of racemates using CHIRAL-PAK IG amylose-based chiral stationary phase under normal standard, non-standard and reversed phase high performance liquid chromatography, *J. Chromatogr. A* 1532 (2018) 89–97, doi:[10.1016/j.chroma.2017.11.049](https://doi.org/10.1016/j.chroma.2017.11.049).
- [15] B. Chankvetadze, C. Yamamoto, Y. Okamoto, Enantioseparation of selected chiral sulfoxides using polysaccharide-type chiral stationary phases and polar organic, polar aqueous-organic and normal-phase eluents, *J. Chromatogr. A* 922 (2001) 127–137, doi:[10.1016/S0021-9673\(01\)00958-X](https://doi.org/10.1016/S0021-9673(01)00958-X).
- [16] I. Matarashvili, D. Ghughunishvili, L. Chankvetadze, N. Takaishvili, M. Tsintsadze, T. Khatishvili, T. Farkas, B. Chankvetadze, Separation of enantiomers of chiral weak acids with polysaccharide-based chiral columns and aqueous mobile phases in high performance liquid chromatography: typical reversed-phase behavior? *J. Chromatogr. A* 1483 (2017) 86–92, doi:[10.1016/j.chroma.2016.12.064](https://doi.org/10.1016/j.chroma.2016.12.064).
- [17] Z. Shedania, R. Kakava, A. Volonterio, T. Farkas, B. Chankvetadze, Separation of enantiomers of chiral sulfoxides in high-performance liquid chromatography with cellulose-based chiral selectors using acetonitrile and acetonitrile-water mixtures as mobile phases, *J. Chromatogr. A* 1609 (2020) 460445, doi:[10.1016/j.chroma.2019.460445](https://doi.org/10.1016/j.chroma.2019.460445).
- [18] I. Matarashvili, A. Chelidze, G. Dolidze, G. Kobidze, N. Zaqashvili, A. Dadianidze, I. Bacska, A. Felinger, T. Farkas, B. Chankvetadze, Separation of enantiomers of chiral basic drugs with amylose- and cellulose-phenylcarbamate-based chiral columns in acetonitrile and aqueous-acetonitrile in high-performance liquid chromatography with a focus on substituent electron-donor and electron-acceptor effects, *J. Chromatogr. A* 1624 (2020) 461218, doi:[10.1016/j.chroma.2020.461218](https://doi.org/10.1016/j.chroma.2020.461218).
- [19] G. Jibuti, A. Mskhiladze, N. Takaishvili, L. Chankvetadze, M. Karchkhadze, T. Farkas, B. Chankvetadze, HPLC separation of dihydropyridine derivatives enantiomers with emphasis on elution order using polysaccharide-based chiral columns, *J. Sep. Sci.* 35 (2012) 2529–2537, doi:[10.1002/jssc.201200443](https://doi.org/10.1002/jssc.201200443).
- [20] B. Chankvetadze, Application of enantioselective separation techniques to bioanalysis of chiral drugs and their metabolites, *Trends Anal. Chem.* 143 (2021) 116332, doi:[10.1016/j.trac.2021.116332](https://doi.org/10.1016/j.trac.2021.116332).
- [21] M. Arenas, J. Martín, J.L. Santos, I. Aparicio, E. Alonso, An overview of analytical methods for enantiomeric determination of chiral pollutants in environmental samples and biota, *Trends Anal. Chem.* 143 (2021) 116370, doi:[10.1016/j.trac.2021.116370](https://doi.org/10.1016/j.trac.2021.116370).
- [22] L. Peng, S. Jayapalan, B. Chankvetadze, T. Farkas, Reversed-phase chiral HPLC and LC/MS analysis with tris(chloromethylphenylcarbamate) derivatives of cellulose and amylose as chiral stationary phases, *J. Chromatogr. A* 1217 (2010) 6942–6955, doi:[10.1016/j.chroma.2010.08.075](https://doi.org/10.1016/j.chroma.2010.08.075).
- [23] R. Cirilli, R. Ferretti, B. Gallinella, L. Zanitti, Retention behavior of proton pump inhibitors using immobilized polysaccharide derived chiral stationary phases with organic aqueous mobile phases, *J. Chromatogr. A* 1304 (2013) 147–153, doi:[10.1016/j.chroma.2013.07.021](https://doi.org/10.1016/j.chroma.2013.07.021).
- [24] B. Gallinella, L. Bucciarelli, L. Zanitti, R. Ferretti, R. Cirilli, Direct separation of the enantiomers of oxaliplatin on a cellulose-based chiral stationary phase in hydrophilic interaction liquid chromatography mode, *J. Chromatogr. A* 1339 (2014) 210–213, doi:[10.1016/j.chroma.2014.02.071](https://doi.org/10.1016/j.chroma.2014.02.071).
- [25] S. Materazzo, S. Carradori, R. Ferretti, B. Gallinella, D. Secci, R. Cirilli, Effect of the water content on the retention and enantioselectivity of albendazole and fenbendazole sulfoxides using amylose-based chiral stationary phases in organic-aqueous conditions, *J. Chromatogr. A* 1327 (2014) 73–79, doi:[10.1016/j.chroma.2013.12.051](https://doi.org/10.1016/j.chroma.2013.12.051).
- [26] R. Ferretti, S. Carradori, P. Guglielmi, M. Pierini, A. Casulli, R. Cirilli, Enantiomers of triclofenazole sulfoxide: analytical and semipreparative HPLC separation, absolute configuration assignment, and transformation into sodium salt, *J. Pharm. Biomed. Anal.* 140 (2017) 38–44, doi:[10.1016/j.jpba.2017.03.021](https://doi.org/10.1016/j.jpba.2017.03.021).
- [27] Ch. Thirupathi, K. Nagesh Kumar, G. Srinivasu, Ch. Lakshmi Narayana, Ch. Parameswara Murthy, Development and validation of stereo selective method for the separation of razoxane enantiomers in hydrophilic interaction chromatography, *J. Chromatogr. Sci.* 56 (2018) 147–153, doi:[10.1093/chromsci/bmx094](https://doi.org/10.1093/chromsci/bmx094).
- [28] M. Pérez-Baeza, L. Escuder-Gilabert, Y. Martín-Biosca, S. Sagrado, M.J. Medina-Hernández, Reversed phase liquid chromatography for the enantioseparation of local anaesthetics in polysaccharide-based stationary phases. Application to biodegradability studies, *J. Chromatogr. A* 1625 (2020) 461334, doi:[10.1016/j.chroma.2020.461334](https://doi.org/10.1016/j.chroma.2020.461334).
- [29] R. Cirilli, G.K.E. Scriba, HPLC Enantioseparations with Polysaccharide-Based Chiral Stationary Phases in HILIC Conditions, in: *Chiral Separations. Methods in Molecular Biology, Humana, New York, 2019*, pp. 127–146, doi:[10.1007/978-1-4939-9438-0_7](https://doi.org/10.1007/978-1-4939-9438-0_7). vol 1985.
- [30] Z. Shedania, R. Kakava, A. Volonterio, T. Farkas, B. Chankvetadze, Separation of enantiomers of novel chiral sulfoxides in high-performance liquid chromatography with polysaccharide-based chiral selectors and aqueous-methanol as mobile phases, *J. Chromatogr. A* 1557 (2018) 62–74, doi:[10.1016/j.chroma.2018.05.002](https://doi.org/10.1016/j.chroma.2018.05.002).
- [31] M. Pérez-Baeza, L. Escuder-Gilabert, Y. Martín-Biosca, S. Sagrado, M.J. Medina-Hernández, Comparative modelling study on enantioresolution of structurally unrelated compounds with amylose-based chiral stationary phases in reversed phase liquid chromatography-mass spectrometry conditions, *J. Chromatogr. A* 1625 (2020) 461281, doi:[10.1016/j.chroma.2020.461281](https://doi.org/10.1016/j.chroma.2020.461281).
- [32] T. Zhang, D. Nguyen, P. Franco, Y. Isobe, T. Michishita, T. Murakami, Cellulose tris(3,5-dichlorophenylcarbamate) immobilised on silica: a novel chiral stationary phase for resolution of enantiomers, *J. Pharm. Biomed. Anal.* 46 (2008) 882–891, doi:[10.1016/j.jpba.2007.06.008](https://doi.org/10.1016/j.jpba.2007.06.008).
- [33] T. Zhang, D. Nguyen, P. Franco, Reversed-phase screening strategies for liquid chromatography on polysaccharide-derived chiral stationary phases, *J. Chromatogr. A* 1217 (2010) 1048–1055, doi:[10.1016/j.chroma.2009.11.040](https://doi.org/10.1016/j.chroma.2009.11.040).
- [34] M.E.D. Merino, R.N. Echevarría, E. Lubomirsky, J.M. Padró, C.B. Castells, Enantioseparation of the racemates of a number of pesticides on a silica-based column with immobilized amylose tris(3-chloro-5-methylphenylcarbamate), *Microchem. J.* 149 (2019) 103970, doi:[10.1016/j.microc.2019.103970](https://doi.org/10.1016/j.microc.2019.103970).
- [35] M.E.D. Merino, C. Lancioni, J.M. Padró, C.B. Castells, Chiral separation of several pesticides on an immobilized amylose tris(3-chloro-5-methylphenylcarbamate) column under polar-organic conditions. Influence of mobile phase and temperature on enantioselectivity, *J. Chromatogr. A* 1624 (2020) 461240, doi:[10.1016/j.chroma.2020.461240](https://doi.org/10.1016/j.chroma.2020.461240).
- [36] M.E.D. Merino, C. Lancioni, J.M. Padró, C.B. Castells, Study of enantioseparation of β -blockers using amylose tris(3-chloro-5-methylphenylcarbamate) as chiral

- stationary phase under polar-organic, reversed-phase and hydrophilic interaction liquid chromatography conditions, *J. Chromatogr. A* 1634 (2020) 461685, doi:[10.1016/j.chroma.2020.461685](https://doi.org/10.1016/j.chroma.2020.461685).
- [37] P. Zhao, Z. Wang, K. Li, X. Guo, L. Zhao, Multi-residue enantiomeric analysis of 18 chiral pesticides in water, soil and river sediment using magnetic solid-phase extraction based on amino modified multiwalled carbon nanotubes and chiral liquid chromatography coupled with tandem mass spectrometry, *J. Chromatogr. A* 1568 (2018) 8–21, doi:[10.1016/j.chroma.2018.07.022](https://doi.org/10.1016/j.chroma.2018.07.022).
- [38] P. Zhao, Z. Wang, X. Gao, X. Guo, L. Zhao, Simultaneous enantioselective determination of 22 chiral pesticides in fruits and vegetables using chiral liquid chromatography coupled with tandem mass spectrometry, *Food Chem.* 277 (2019) 298–306, doi:[10.1016/j.foodchem.2018.10.128](https://doi.org/10.1016/j.foodchem.2018.10.128).
- [39] ChemSpider Database, Royal Society of Chemistry, 2022. <http://www.chemspider.com/>. (Accessed 26 April 2022).

Supplementary materials

Comparative study on retention behaviour and enantioresolution of basic and neutral structurally unrelated compounds with cellulose-based chiral stationary phases in reversed phase liquid chromatography-mass spectrometry conditions

Mireia Pérez-Baeza^a, Laura Escuder-Gilabert^{a,**}, Yolanda Martín-Biosca^a, Salvador Sagrado^{a,b},
María José Medina-Hernández^{a,*}

^a *Departamento de Química Analítica, Universitat de València, E-46100, Burjassot, Valencia, Spain*

^b *Instituto Interuniversitario de Investigación de Reconocimiento Molecular y Desarrollo Tecnológico (IDM), Universitat Politècnica de València, Universitat de València, Valencia, Spain*

*Corresponding autor: M.J. Medina-Hernández (maria.j.medina@uv.es) Phone: 34-963544899

** Corresponding autor: L. Escuder-Gilabert (lescuder@uv.es) Phone: 34-963544901

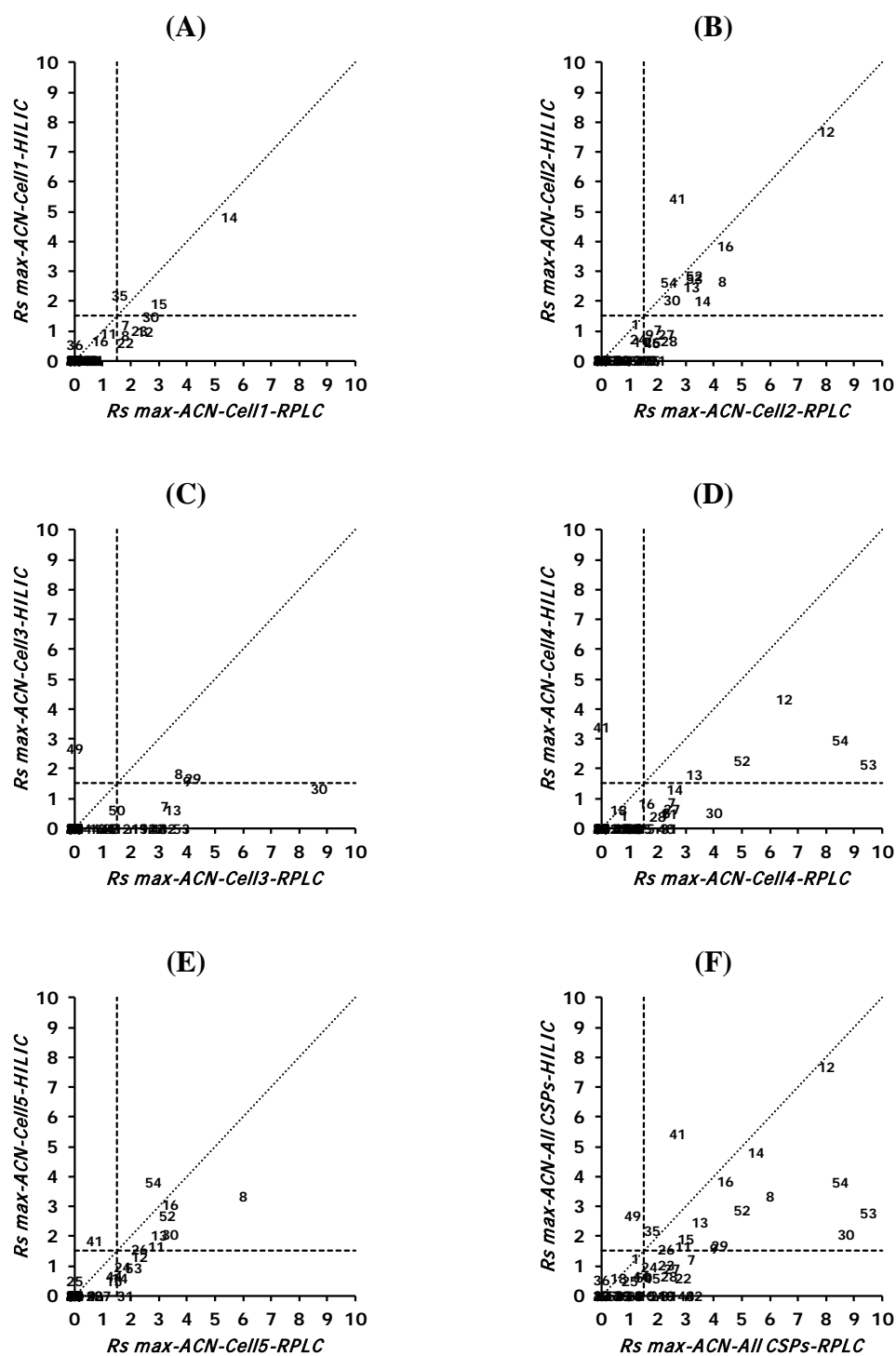


Fig. S1. M. Pérez-Baeza et al.

Maximum enantioselectivity values ($R_s \max$) obtained for the HILIC vs. RPLC domains with ACN/H₂O mobile phases in each cellulose chiral stationary phase studied: (A) Cell1, (B) Cell2, (C) Cell3, (D) Cell4, (E) Cell5 and (F) all chiral stationary phases. The diagonal dotted line represents the identity line of slope equal to unity and intercept zero. The horizontal and vertical dashed lines indicate $R_s \max = 1.5$.



PAPER III

**Artificial neural networks to model the
enantioresolution of structurally unrelated neutral
and basic compounds with cellulose
tris(3,5-dimethylphenylcarbamate) chiral stationary
phase and aqueous-acetonitrile mobile phases**

**Mireia Pérez-Baeza^a, Yolanda Martín-Biosca^a, Laura Escuder-Gilabert^a,
María José Medina-Hernández^a, Salvador Sagrado^{a,b}**

^a Departamento de Química Analítica, Universitat de València E-46100 Burjassot, Valencia, Spain

^b Instituto Interuniversitario de Investigación de Reconocimiento Molecular y Desarrollo Tecnológico (IDM), Universitat Politècnica de València, Universitat de València, Valencia, Spain

Journal of Chromatography A 1672 (2022) 463048



Artificial neural networks to model the enantioresolution of structurally unrelated neutral and basic compounds with cellulose tris(3,5-dimethylphenylcarbamate) chiral stationary phase and aqueous-acetonitrile mobile phases

Mireia Pérez-Baeza^a, Yolanda Martín-Biosca^{a,**}, Laura Escuder-Gilabert^a,
María José Medina-Hernández^a, Salvador Sagrado^{a,b,*}

^a Departamento de Química Analítica, Universitat de València E- 46100 Burjassot, Valencia, Spain

^b Instituto Interuniversitario de Investigación de Reconocimiento Molecular y Desarrollo Tecnológico (IDM), Universitat Politècnica de València, Universitat de València, Valencia, Spain

ARTICLE INFO

Article history:

Received 28 February 2022

Revised 5 April 2022

Accepted 8 April 2022

Available online 11 April 2022

Keywords:

Enantioresolution

Cellulose chiral stationary phase

Heterogeneous dataset

Artificial neural networks

Feature selection

Relative variable importance

ABSTRACT

Artificial neural networks (ANN; feed-forward mode) are used to quantitatively estimate the enantioresolution (R_s) in cellulose tris(3,5-dimethylphenylcarbamate) of chiral molecules from their structural information. To the best of our knowledge, for the first time, a dataset of structurally unrelated compounds is modelled using ANN, attempting to approach a model of general applicability. After setting a strategy compatible with the data complexity and their relatively limited size (56 molecules), by prefixing initial ANN inner weights and the validation and cross-validation subsets, the ANN optimisation based on a novel quality indicator calculated from 9 ANN outputs allows selecting a proper (predictive) ANN architecture (a single hidden layer of 7 neurons) and performing a forward-stepwise feature selection process (8 variables are selected). Such relatively simple ANN offers reasonable good general performance in predicting R_s (e.g. validation plot statistics: mean squared error = 0.047 and $R = 0.98$ and 0.92 , for all or just the validation molecules, respectively). Finally, a study of the relative importance of the selected variables, combining the estimation from two approaches, suggests that the surface tension (positive overall contribution to R_s) and the -NHR groups (negative overall contribution to R_s) are found to be the main variables explaining the enantioresolution in the current conditions.

© 2022 The Authors. Published by Elsevier B.V.

This is an open access article under the CC BY-NC-ND license (<http://creativecommons.org/licenses/by-nc-nd/4.0/>)

1. Introduction

Chiral stationary phases (CSPs) based on amylose and cellulose polysaccharide derivatives are by far the preferred choice for the enantioseparation of chiral compounds in high-performance liquid chromatography (HPLC). Besides the wide availability of commercially CSPs, their broad chiral recognition capacity enables the separation of the enantiomers of a high variety of compounds [1]. When using polysaccharide-based CSPs in HPLC, separations can be carried out in normal phase (NPLC), in reversed phase (RPLC)

as well as in polar organic mode [1]. For the analytical scale, RPLC has some advantages in the analysis of pharmaceuticals and aqueous biological samples and coupling with mass spectrometry detection [2].

There are numerous studies on the fundamentals of enantioseparation mechanisms involving polysaccharide-based CSPs [3–13]. Spectroscopic methods and molecular modelling approaches have contributed to elucidating the chiral recognition mechanism [3–13]. Despite the insight provided by these studies, finding the right CSP/mobile phase (MP) combination that allows the separation of a given pair of enantiomers remains a very challenging task. Different strategies have been proposed for this purpose. The most common consists of screening a series of CSP/MP combinations, a trial-and-error approach that often requires a considerable experimental and economical effort [14–20]. Alternatively, quantitative structure-enantioselective retention relationships (QSERR), which

* Corresponding author.

** Corresponding author.

E-mail addresses: yolanda.martin@uv.es (Y. Martín-Biosca), sagrado@uv.es (S. Sagrado).

correlate relevant separation parameters with molecular descriptors derived from molecular structure, have emerged as a useful strategy to select a suitable CSP/MP combination in chiral RPLC optimisation processes [21,22].

For polysaccharide-based CSPs, QSERR have been built using chemometric tools, like multiple linear regression (MLR) [23–26], partial least squares regression (PLS) [25,27] or random forest approach [28,29]. These models, most of them constructed using chromatographic data of structurally related compounds, allow the prediction of retention times [25], logarithm of the retention factor ($\log k$) [22,26,27], separation factor α [28,29] and $\log \alpha$ [26–28].

In previous papers, our research group modelled the enantioresolution (as a categorical variable) of structurally unrelated compounds in some commercial cellulose- and amylose-based stationary phases using data in RPLC mode [30,31]. 56 structural variables, including chiral topological parameters, molecular descriptors and molecular topological parameters were used. Discriminant partial least squares for one categorical response variable (DPLS1) was used for feature selection and modelling purposes. The models obtained for the different CSPs presented adequate predictive and descriptive capacity. The descriptive ability (importance – contribution – of structural variables to explain enantioresolution) was explored in two stages: (i) feature selection, FS, (eliminating unnecessary variables) and (ii) calculation of the normalised regression coefficients of variables.

Artificial neural networks (ANN) methodology is a flexible machine learning (artificial intelligence) approach capable of modelling complex/non-linear relationships between input and response variable(s) [32,33]. ANN were designed to learn from a training dataset (until the predictive ability of a different validation dataset improves) by using a neural architecture that consists of interconnected neurons arranged in several layers. In the so-called feed-forward modality, the architecture comprises an input layer (independent variables), one or more hidden layers, and an output layer (response variable(s)). The ANN behaviour depends on the weights of the connections. During ANN training, these weights are optimised using an iterative algorithm to obtain a final model that provides the minimal prediction error on the response variable(s) [34].

However, due to the inner complexity of ANN, it is difficult to extract information on how models work to predict the output from input variables (in ANN, the difficulty in establishing the relationship between input-output variables is commonly referred to as a black box). Different approaches have been developed to approximate the relative importance of the input variables to predict the response, although all of them have limitations [34]. For instance, the approach from Olden et al. comprises the sum of the product of the inner weights connecting the input-response variables through the hidden layer [35] but is sensitive to the neural architecture and the initial starting inner weights [34]. The Lek et al. approach changes the value of one input variable while maintaining the other variables at a constant value (at different quantiles) [36], but it could provide different data compared to those used for training [34]. However, we have found no evidence on which approach could provide a correct estimation of the importance of variables, due to the lack of a way to verify the estimation quality up to now.

After an exhaustive search, only three ANN applications to predict enantioselective parameters in chiral liquid chromatography have been found [37–39]. All these QSERR studies have been carried out for a limited number of structurally related compounds using macrocyclic antibiotics [37], cellulose [38] and brush-type [39] CSPs. The homogeneity (simplicity) of the data sets used probably allows performing standard conditions for ANN (that normally applies to big datasets) as well as a comparison with a conventional regression model.

The main objectives of this work can be summarised as designing a global strategy, based entirely on ANN, able to select a (preferably short) set of structural variables capable of satisfactorily estimating enantioresolution in cellulose tris(3,5-dimethylphenylcarbamate) chiral stationary phase and aqueous-acetonitrile mobile phases, working with a relatively limited dataset of 56 compounds from 14 different chemical families. An additional aim is to approximate the relative importance of the selected variables to quantitatively predict R_s . To the best of our knowledge, ANN have not been used to directly predict the enantioresolution values (R_s) of structurally unrelated chemical compounds nor to perform a selection of the more relevant structural parameters describing R_s in such a complex situation due to the heterogeneity of the dataset.

2. Experimental

2.1. ANN nomenclature

Fig. 1 depicts the scheme of ANN used in this work. For all compounds, the known structural variables (\mathbf{X}) are set as the input layer and the predicted R_s values (\mathbf{y}) are the output layer (to be compared with the known experimental R_s data (\mathbf{t}) during the training process). In the middle, we arranged up to 2 hidden layers and tried up to 30 neurons in each layer; so, a total of 930 ANN were evaluated. Each ANN architecture was identified by N_v -[k - kk]-1, where N_v is the number of structural variables and k and kk are the number of neurons in the first and second hidden layer, respectively. In the case of only one hidden layer, $kk=0$, the ANN were identified by N_v -[k]-1. Note that k and kk should be optimised, that N_v could be reduced after a feature selection process, and finally, from the ANN information (e.g. W_i , \mathbf{y}) the relative importance of the N_v input variables could be approximated.

2.2. Structural and chromatographic data

To study the structure-enantioresolution relationships for each compound under study, 56 structural variables (\mathbf{X}) were used. These variables include chiral carbon-related parameters, molecular descriptors and topological parameters predicted by software (ChemSpider Database) [40], and calculated hydrophobicity parameters as the octanol-water partition coefficient ($\log P$) and the apparent $\log P$ at pH = 8 ($\log D$) [30]. These structural variables were described in detail in previous papers [30,41,42]. Briefly, variables \mathbf{x}_1 to \mathbf{x}_7 correspond to chiral carbon (C^*) related parameters (e.g. number of aromatic heterocycles groups bonded to the chiral carbon (C^*hA) as \mathbf{x}_3); variables \mathbf{x}_8 to \mathbf{x}_{12} correspond to predicted molecular descriptors from ACD/Labs and ChemAxon calculations [40] (e.g. surface tension (ST , $\text{dyn}\cdot\text{cm}^{-1}$) as \mathbf{x}_{12}); variables \mathbf{x}_{13} to \mathbf{x}_{29} correspond to molecular topological parameters predicted by ChemAxon (e.g. Balaban index (Bi) and number of sp^3 hybridized carbons divided by the total carbon count (fsp^3) as \mathbf{x}_{28} and \mathbf{x}_{29} , respectively), variables \mathbf{x}_{30} to \mathbf{x}_{54} are obtained as the count of atoms/groups present in the compound (e.g. number of -NHR and -NR₂ amino groups in the molecule (NHR , NR_2), number of R-O-R ether groups in the molecule (ROR) and number of -NHCOR amide groups bonded to an aromatic ring in the molecule ($ANHCOR$) as \mathbf{x}_{36} , \mathbf{x}_{37} , \mathbf{x}_{38} and \mathbf{x}_{46} , respectively), while variables \mathbf{x}_{55} - \mathbf{x}_{56} are the hydrophobicity parameters.

Experimental R_s values of 56 structurally unrelated chemical compounds under study were obtained as described in [31] using the chiral column Lux Cellulose-1 (cellulose tris(3,5-dimethylphenylcarbamate) and mobile phases consisting of binary mixtures of ammonium bicarbonate buffer (5 mM, pH 8) and acetonitrile (ACN) in varying proportions (10–98% in volume of ACN).

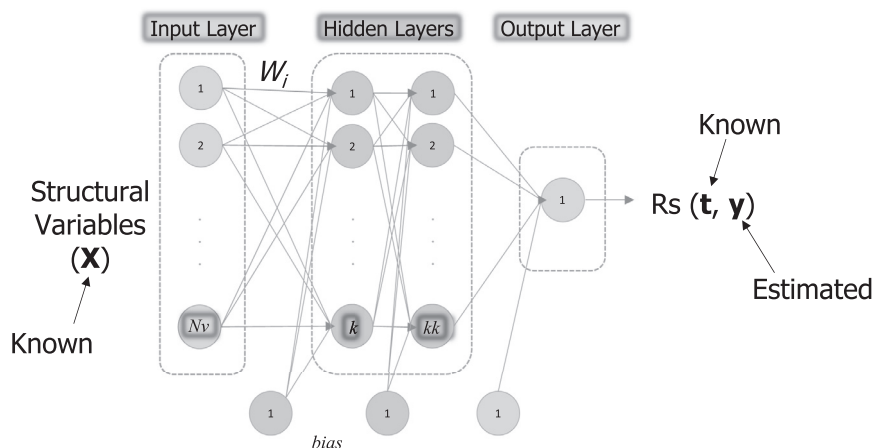


Fig. 1. Architecture of the artificial neural networks (ANN) in this work. The known structural variables (\mathbf{X}) are set in the N_v neurons of the input layer. The resolution (R_s) estimated values (\mathbf{y}) will be obtained in a single neuron (output layer). In the middle, the so-called hidden layers must be arranged, defining the complete architecture. ANN architectures assayed (930) include up to 2 hidden layers and up to 30 neurons (k , kk) in each layer. Sigmoid (hidden layers) and linear (output layer) activation functions are used. The weights (W_i ; connecting all the neurons, including those side neurons introducing bias) are adjusted during the learning process, minimising the differences between \mathbf{y} and the known experimental R_s values (\mathbf{t}). Once an ANN has been trained is able to estimate \mathbf{y} -values for novel compounds.

For each compound, amongst the various R_s values obtained using the different mobile phases tested, the maximum R_s value was chosen to be used as the response variable (\mathbf{t}). Other separations conditions were: flow-rate, $1 \text{ mL} \cdot \text{min}^{-1}$ and temperature, $25 \text{ }^\circ\text{C}$. These R_s values are shown in Table 1. Both \mathbf{X} and \mathbf{t} were autoscaled as pretreatment.

2.3. Software and calculations

The global approach developed in this paper includes three automatic strategies based on ANN outputs: (i) architecture optimisation, (ii) feature selection (FS) and (iii) approximation of the relative importance of variables. The first two strategies involve the comparison of the results from different ANN. To ensure a reliable ANN comparison, all aspects that could lead to different outputs due to the limited number of compounds, combined with the presumable complexity of the \mathbf{t} - \mathbf{X} relationship, were prefixed in ANN calculations. So, all the inner weights (W_i in Fig. 1) were set to one, and the same subsets of compounds (training, validation and cross-validation) were used in all ANN. The validation subset for overfitting control includes 7 compounds covering a representative range of R_s values (see Table 1). The rest of the 49 compounds corresponds to the training block (for learning). Additionally, 9 sets of 5 different training compounds were used in a cross-validation process implemented to improve robustness. Training compounds in these cross-validation subsets were punctually converted into test compounds, i.e., they did not participate in the training nor the validation task and were just predicted by the ANN as external compounds.

To compare the performance of any ANN tested, a quality indicator Q (Eq. (1)) was introduced. Q depends on 9 different statistics related to the differences between the estimated (\mathbf{y}) and experimental (\mathbf{t}) R_s values, in terms of mean squared errors (MSE) and regression statistics of the validation plot (correlation coefficient, R ; slope b_1 , and intercept, b_0), for all, training (subscript *train*) and validation (subscript *v*) compounds. MSE statistics were 'penalised' (identified using p before the statistic), adding to the mean the standard deviation, both estimated from 10 ANN outputs (one with 49 training compounds plus 9 cross-validation runs).

$$Q = pMSE + pMSE_v + W1|pMSE_v - pMSE_{train}| + W2((1 - R) + |1 - b_1| + |b_0|) + W3((1 - R_v) + |1 - b_{1v}| + |b_{0v}|) \quad (1)$$

The term $|pMSE_v - pMSE_{train}|$ characterises the (penalised) overfitting degree. Note that penalised values aim to take decisions in ANN comparisons including both the estimation of external compounds (test) as well as the uncertainty arising from the different cross-validated outputs. Note also that the regression terms in Eq. (1) were set in a format where lower values mean better quality (as MSE does intrinsically); thus, lower Q values imply higher ANN quality. The Q -weights ($W1$, $W2$ and $W3$) in Eq. (1) were set at values 1, 10 and 5, respectively, to provide an almost similar contribution of all the terms in Eq. 1.

Algorithms were written in MATLAB® R2019a (Mathworks®) [43]. MATLAB has a Toolbox containing algorithms and tools for creating and training artificial neural networks, called Deep Learning Toolbox. The programs used in this work include routines provided by this Toolbox: `feedforwardnet.m`, which generates a feed-forward (regression-focused) ANN from a defined $[k-kk]$ hidden layers architecture; `train.m`, that trains a shallow ANN from given \mathbf{X} - \mathbf{t} data and architecture and `net.m`, which predicts response values (\mathbf{y}) from a trained ANN. To carry out the different strategies, novel algorithms were also developed, such as `fANN.m`, a MATLAB function that builds and trains an ANN from \mathbf{X} - \mathbf{t} data with a defined $[k-kk]$ hidden layers architecture by prefixing validation and test blocks and initial W_i and, optionally, eliminates variables or objects (the last allows to perform cross-validation studies); `Stu-ANN.m`, which numerically and graphically compares Q values (and their parameters) of different ANN architectures up to k and kk neurons in the hidden layers.

The ANN final architecture was chosen from the 930 studied, in two steps. First, selecting those ANN showing $R > 0.9$ (filter-1), and from them, those whose Q values were below the 10th percentile (filter-2). Finally, a visual inspection of the validation plots (\mathbf{y} vs. \mathbf{t}) and the statistics of Eq. (1) allowed to select the definitive architecture, preferably one with a lower $k \times kk$ value (see Fig. 1), assuming that simpler ANN, with a lower number of connecting coefficients (W_i) should be more robust.

The optimal ANN architecture was chosen to conduct the subsequent FS process. The function `sequentialsfs.m` (part of the Machine Learning/Artificial Intelligence suite of MATLAB®) was employed. This function uses a sequential strategy (i.e. adds or removes one variable in each run). In this case, a forward mode (adding variables) was used. As before, the variables selected in

Table 1

Compounds of different families, with their maximum enantioresolution values (R_s) obtained in cellulose tris(3,5-dimethylphenylcarbamate) CSP using aqueous-acetonitrile mobile phases. Compounds are identified by their name and numbered order (N). Validation set compounds (indicated by +) and test compounds (in 9 cross-validation subsets indicated by its number in parenthesis) are shown.

N	Family ^a	Compound	R_s^b	Validation	Test
1	AAD	Disopyramide	0.0		(1)
2	AAD	Mexiletine	0.0		(2)
3	AAD	Propafenone	0.0		(3)
4	ACO	Warfarin	0.0	+	
5	AD	Nomifensine	1.8		(4)
6	AD	Citalopram	0.0		(4)
7	AD	Fluoxetine	0.0		(5)
8	AD	Viloxazine	0.5		(3)
9	AD	Trimipramine	0.7		(7)
10	AD	Bupropion	0.0		(6)
11	AD	Mianserin	1.8	+	
12	AF	Benalaxyl	1.2		(2)
13	AF	Imazalil	0.6		(5)
14	AF	Penconazole	0.9		(1)
15	AF	Hexaconazole	2.5		(7)
16	AF	Myclobutanil	3.0		(8)
17	AF	Metalaxyl	5.5		
18	AH	Doxylamine	0.0		(7)
19	AH	Brompheniramine	0.0		(8)
20	AH	Chlorpheniramine	0.0		
21	AH	Orphenadrine	2.3		(6)
22	AH	Carbinoxamine	0.0		(9)
23	AH	Hydroxyzine	1.8		(5)
24	AH	Terfenadine	0.5		(4)
25	AH	Cetirizine	0.0		(1)
26	AH	Fexofenadine	0.0		(2)
27	LA	Mepivacaine	0.0		(3)
28	LA	Propanocaine	0.0		(4)
29	LA	Prilocaine	0.4	+	
30	LA	Bupivacaine	0.0		(5)
31	ANP	Aminoglutethimide	2.7	+	
32	ANP	Bicalutamide	0.0		(6)
33	BB	Pindolol	1.6		(3)
34	BB	Propranolol	0.0		(7)
35	BB	Metoprolol	0.0		(8)
36	BB	Acebutolol	0.0		(9)
37	BB	Atenolol	0.0		
38	BB+BD	Salbutamol	0.0		
39	BB	Timolol	0.0		
40	BD	Bambuterol	0.0		(9)
41	BD	Isoprenaline	0.5	+	
42	BD	Orciprenaline	0.0		(2)
43	BD	Clenbuterol	0.3		(1)
44	BD	Terbutaline	0.0		(1)
45	CaB	Verapamil	0.7		(8)
46	CaB	Felodipine	0.0		(2)
47	CaB	Cilnidipine	0.7	+	
48	ACD	Procyclidine	0.0		(3)
49	APD	Trimeprazine	0.0		(4)
50	APD	Ethopropazine	0.0	+	
51	APD	Promethazine	0.0		(6)
52	APD	Thioridazine	0.0		(7)
53	PPI	Pantoprazol	0.0		(8)
54	ANAL	Methadone	0.0		(9)
55	PPI	Rabeprazol	0.7		(9)
56	PPI	Lansoprazol	0.6		(6)

^a Drug/Pesticide families: AAD (antiarrhythmic drugs), ACO (anticoagulants), AD (antidepressants), AF (antifungals), AH (antihistamines), LA (local anaesthetics), ANP (antineoplastics), BB (β -blockers), BD (bronchodilators), CaB (calcium channel blockers), ACD (anticholinergic drugs), APD (antipsychotic drugs), PPI (proton pump inhibitors), and ANAL (analgesics).

^b Maximum R_s value obtained using the mobile phases tested consisting of binary mixtures of ammonium bicarbonate buffer (5 mM, pH 8) and acetonitrile (ACN) in varying proportions (10–98% in volume of ACN).

each run were those that provided the lowest Q . Since FS is based on ANN outputs, the whole process can be called ANN-FS process.

To approximate the relative importance of the selected variables two approaches adapted from [35,36] were used. They are based on the use of connecting weights (ANNcw) and \mathbf{y} -estimates to calculate the variable effect (ANNef). Since there is no literature evidence on which approach could provide correct (and the best) estimations, we used the mean and standard deviation of the outputs from these two approaches. Both approaches include as a first step the estimation of a vector of regression-like coefficients (\mathbf{b} ; one coefficient per variable as occurs e.g., in PLS). In the ANNcw case, \mathbf{b} was calculated by multiplying the W_i -inner matrices (hidden-output layers and input-hidden layers) calculated by the ANN algorithm. In the ANNef case, \mathbf{b} was estimated, creating two 'artificial extreme molecules' per \mathbf{X} variable, using the maximum and minimum values of this variable and the mean value for the rest of the variables. The half difference between \mathbf{y} -estimations associated with the 'extreme molecules' was an estimation of \mathbf{b} . Finally, the \mathbf{b} -vector was normalised with respect to its maximum value (b_{max}) as:

$$\mathbf{I} = \mathbf{b}/b_{max} \quad (2)$$

We calculated the \mathbf{I} vectors using Eq. (2) for both approaches. Then, the mean \mathbf{I} and the standard deviation were used as an approximation of the relative importance of the variables (including the sign) on the R_s estimation.

3. Results and discussion

3.1. Previous results and data complexity

The use of a PLS model for predicting R_s values did not provide satisfactory results. Only by dividing the compounds into two categories (resolved and non-resolved) and using a discriminant approach (DPLS1 model) adequate predicted categories were found (results not shown). In our opinion, the data complexity is too high to be solved by this model (despite that, in general, PLS can deal with moderate non-linear problems). This was the main reason to try ANN to reach a quantitative level of prediction.

ANN is intrinsically less robust than PLS (since much more weights must be estimated). Moreover, ANN outputs can vary depending on the complexity of the ANN architecture, but also on the initial W_i values and validation and test subsets, mainly when the number of objects (here compounds) is limited. Thus, fixing the initial W_i values (Fig. 1) and pre-fixing the validation (see Table 1), as well as the cross-validation subsets (see Table 1), was necessary for consistently comparing the ANN results (i.e., architecture comparison and FS-ANN process). An extra element of complexity is the fact that the R_s values present a very asymmetric distribution (e.g. 62% of the R_s values are 0). Consequently, a random selection of subsets could be inadequate. As can be seen in Table 1, the validation set contains R_s values ($t = 0, 0, 0.4, 0.5, 0.7, 1.8$ and 2.7), while the entire data set ranges between 0 and 4.86.

3.2. ANN architecture optimisation

ANN architecture optimisation was carried out according to the procedure described in the experimental section based on the application of two consecutive filters. Fig. 2 shows the quality values (Q ; Eq. (1)) for the 930 architectures assayed. As it can be seen, the ANN architecture has a notable influence on the quality of the ANN outputs. In the plot, dots show the ANN architectures that pass filter-1 ($R > 0.9$), while circles indicate which of these also pass filter-2 (Q below 10th percentile). This last group exhibit similar Q -values, close to the target line ($Q = 0$). The simplest architecture

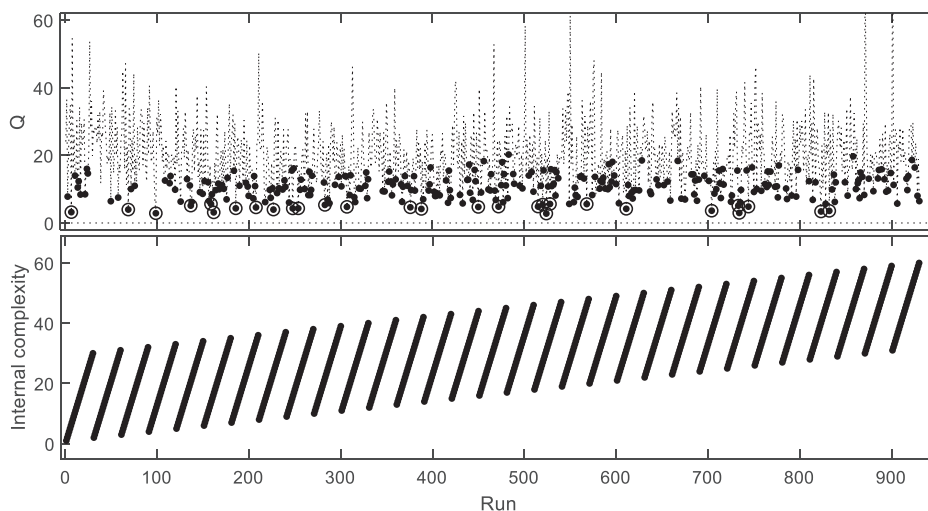


Fig. 2. Quality (Q ; upper part) values (Eq. (1)) through the ANN architecture study, where the runs correspond to different ANN architectures obtained by increasing the number of neurons in the first hidden layer (k , from 1 to 30; See Fig. 1) for a given number of neurons in the second hidden layer (kk , increasing from 0 (no layer) to 30, See Fig. 1). Thus, runs 1–30 correspond to ANN with a hidden layer with k from 1 to 30 neurons; runs 31–60 values correspond to ANN with two hidden layers with $kk = 1$ with k from 1 to 30 neurons, and so on. Internal ANN complexity (number of hidden neurons, $k + kk$, units; lower part) of each run. Symbols: dotted line = Q values for the 930 architectures assayed; dot = ANN architectures that pass filter-1 ($R > 0.9$). Circle = ANN architectures that pass both filter-1 and filter-2 (Q below 10th percentile). $Q = 0$ (target line) is also included as a horizontal dotted line.

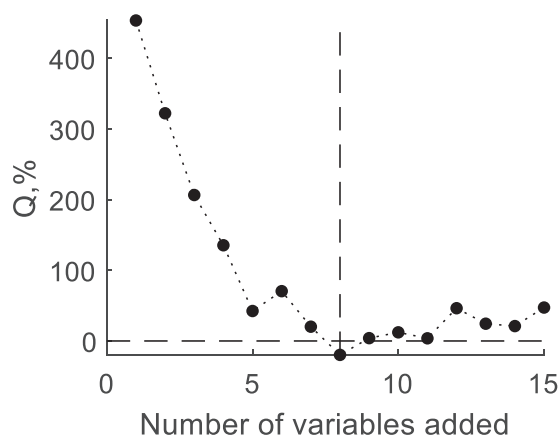


Fig. 3. Quality (Q) values (Eq. (1)), in percentage respect to the Q value obtained with the initial 56 variables (horizontal dotted line; $Q = 0\%$), through the ANN-based feature selection (FS-ANN) process, where input variables are sequentially added. The vertical dashed line indicates the number of variables added that provides a $Q < 0\%$.

fitting the two filters corresponds to run 7 ($Q = 3.2$). This architecture consists of 7 neurons in a single hidden layer (56-[7]-1) and was selected and used in the next step (FS-ANN process). The minimum Q value (2.8) was found at run 524, which corresponds to an ANN with two-hidden layers (56-[14 17]-1). However, as could be expected, this more complex ANN showed a higher penalised overfitting (0.49; i.e. extremely good prediction for training but worse prediction of the validation set) than the selected one (penalised overfitting 0.13). Thus, this ANN was not considered for the next step (feature selection).

3.3. Feature selection

The FS-ANN process, applied to the previously chosen ANN, aimed to reduce the current N_v value (56 variables) to (i) improve the current performance and (ii) be a first stage in defining the importance of variables by eliminating the unnecessary ones. Fig. 3 shows the evolution of the FS-ANN process, as variables are added (forward mode, 1 variable added in each run) by means of the Q -

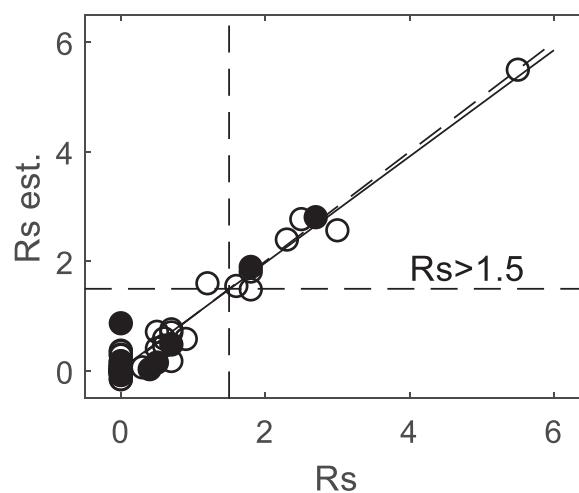


Fig. 4. R_s validation plot of the ANN: 8-[7]-1. Selected variables are: x_3 , C^*hA ; x_{12} , ST ; x_{28} , Bi ; x_{29} , fsp^3 ; x_{36} , NHR ; x_{37} , $NR2$; x_{38} , ROR and x_{46} , $ANHCOR$ (See Section 2.2), including all the compounds (empty circles). Validation compounds are highlighted using full circles. Vertical and horizontal dashed lines indicate $R_s = 1.5$. The diagonal dashed line reflects the target line while the solid line is the regression line.

values (Eq. (1)), calculated in percentage respect the Q value obtained using all the variables (previous section). After adding only 8 variables we observed a Q value lower than the initial one obtained with 56 variables (a satisfactory result). Since this fact fitted the main aim of this work, i.e., to select a reduced set of variables able to estimate the enantioresolution, we stopped the search for a higher number of variables at this point. Thus, the final architecture becomes 8-[7]-1. The selected variables are: x_3 , C^*hA ; x_{12} , ST ; x_{28} , Bi ; x_{29} , fsp^3 ; x_{36} , NHR ; x_{37} , $NR2$; x_{38} , ROR and x_{46} , $ANHCOR$ (see Section 2.2).

3.4. Performance of the ANN (predictive ability)

Fig. 4 shows the validation plot (y vs. t ; rescaled values representing R_s) obtained with ANN 8-[7]-1 for all compounds (the validation set is highlighted by full circles). As can be observed, a good agreement between experimental and predicted values was

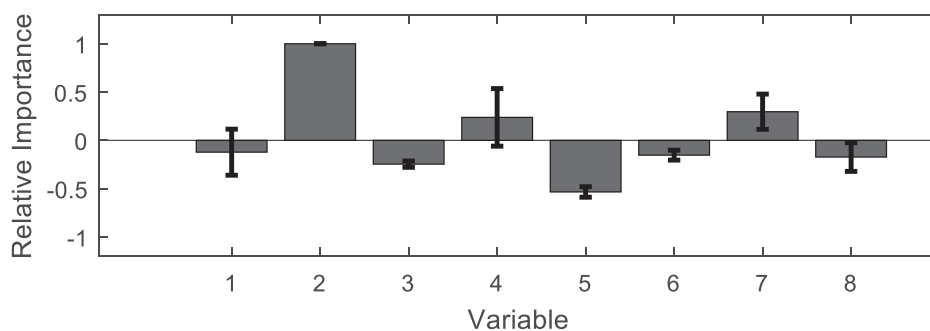


Fig. 5. Relative importance of selected variables (**I**; Eq. (2)) to estimate R_s of the ANN: 8-[7]-1. Selected variables in the order: 1- x_3 , C^*hA ; 2- x_{12} , ST ; 3- x_{28} , Bi ; 4- x_{29} , fsp^3 ; 5- x_{36} , NHR ; 6- x_{37} , $NR2$; 7- x_{38} , ROR and 8- x_{46} , $ANHCOR$. Data include the mean (bar) and standard deviation (error bar) of two strategies (ANNcw, based on inner connecting weights and ANNef, based on the variable effect).

obtained, according to the low Q value found for this relatively simple architecture. Only for one compound, with experimental $R_s = 0$, a low R_s estimate is observed, still sufficiently below the $R_s = 1.5$ critical line (indicating full enantioresolution). A good agreement is also visible between the regression line and the target (diagonal) line of the validation plot. These observations fit well with the first aim fixed for the present work since a relatively simple ANN (architecture, few structural variables) becomes capable of satisfactorily estimating enantioresolution in the current conditions.

On the other hand, to check the final ANN performance, it is advisable to use not only a validation subset (mandatory) but also a test (external) subset. When using a big dataset (the conventional situation in ANN models), this option normally does not result in a loss of representativeness of the remaining training data to build the ANN (due to the large number of cases). However, if the amount of data available is not high (as in many situations in the scientific context), separating an extra test subset (probably with particular structural information) would likely affect the representativeness in the learning process, providing a less general ANN.

3.5. Importance of variables

The importance of the variables (also known as sensitivity analysis) for describing the R_s data is an important issue in all the QSERR models. Fig. 5 shows an approximation of the relative importance (**I**; Eq. (2)) of the 8 selected variables in predicting the enantioresolution. **I** is the mean of the results of two adapted/simplified approaches, ANNcw and ANNef [35,36]. **I** absolute magnitude and sign approximate the importance of the variable and the positive or negative overall contribution to R_s , respectively. It must be pointed out that **I** values do not act as real regression coefficients. On the other hand, all the selected variables are necessary to obtain the R_s -estimations (Fig. 4), however, not all should be equally important (Fig. 5).

The standard deviation is an indication of the uncertainty arising from the two different approaches. The uncertainty for some variables was low, which could confer more reliability of their **I**-estimations. Fig. 5 results suggest that the contribution of variables x_3 (C^*hA) and x_{29} (fsp^3) is unclear since the error bar is higher than their magnitude. On the other hand, x_{12} (ST) is the most important, with a global positive effect on the enantioresolution. The second important variable is x_{36} (NHR), which should globally inversely affect R_s . Other less important variables are: x_{38} (ROR), positive overall contribution to R_s , and x_{28} (Bi), x_{37} ($NR2$) and x_{46} ($ANHCOR$), negative overall contribution to R_s .

For a given compound, the balance between positive and negative contributions determines enantioresolution in that CSP. The

results suggest that the presence of dipoles (variable ST) and ether groups (variable ROR) in the molecule (e.g. compounds $N = 13, 17, 21, 22, 23, 25, 33, 35, 47, 55$; Table 1) favours enantioresolution, which indicates the importance of van der Waals forces and hydrogen-bond interactions with the phenylcarbamate moiety in the CSP on enantiomer separation.

On the other hand, high steric factors (high values of Babalan index), together with the presence of secondary ($N = 3, 7, 10, 29, 33-44$), tertiary amines ($N = 1, 6, 9, 18-22, 28, 45, 49-51, 54$) and amide groups ($N = 27, 29, 30, 32, 36$) in the molecule decrease enantioresolution. As can be observed in Table 1, this second group of compounds, except $N = 21$ and 33, show null or partial resolution. However, both compounds present ether groups in their molecules and are fully enantioresolved.

3.6. Additional remarks

Since this work constitutes the first attempt to obtain ANN models to estimate R_s of a heterogeneous group of chiral compounds, we focused on adapting conventional ANN strategies to the current complex problem. Considering the introductory context of this work, we opted for simple fit-for-purpose strategies instead of more sophisticated ones. For instance, in a problem with a large number of input variables, an independent criterion to perform a previous feature selection is a logical strategy. However, in our case, in addition to the limited number of variables, we were interested in performing the feature selection based on the ANN outputs themselves (as an alternative to other approaches described [44]); thus, we preferred to initiate the FS-ANN process with a suitable ANN (architecture optimized; note that many architectures provide inadequate outputs; probably connected with the complexity of the current data; Fig. 2). Then, in FS, variables were added progressively until an improved ANN with a reduced number of variables was obtained (8 input variables; Fig. 3), which also facilitates establishing the relative importance of variables. On the other hand, after the ANN-FS process, to verify the consistency of the previous optimized architecture ($k = 7$), an additional (focused) architecture optimization was performed, now using the 8 input variables selected (probing architectures with k from 1 to 7 combined with kk from 0 to 3). The results were comparable to those obtained previously with 56 variables, and again, a single hidden layer of 7 neurons provided the best Q value, which supports the validity of our strategy.

In the same context, there are more sophisticated strategies proposed for the data division on subsets, e.g. those based on a clustering approach [44], that uses both descriptors and the response variable to divide compounds into subsets. A k-means neighbour clustering approach was used to separate 7 subgroups of compounds using the autoscaled y and X variables, followed by a

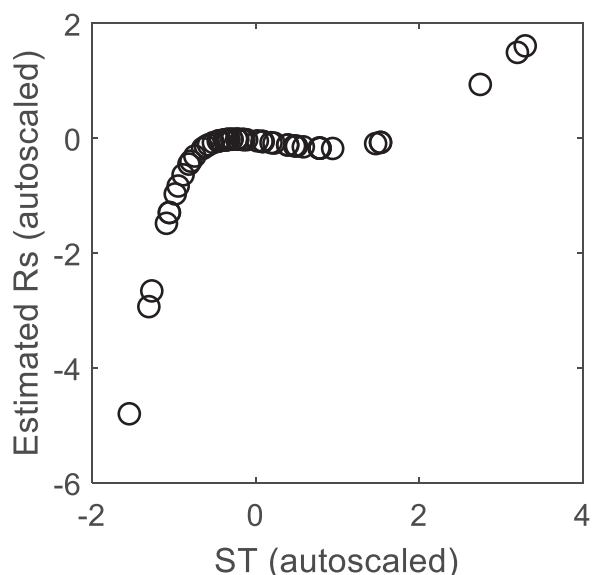


Fig. 6. Estimated autoscaled R_s response curve for variable x_{12} (Surface tension; ST). The autoscaled ST values are used to derive the curve, keeping the rest of the autoscaled variables in Fig. 5 in their mean value.

principal component analysis (PCA). The main (PC1-PC2) PCA plots were evaluated. The PCA score plot showed rough segregation between the clusters. On the other hand, the R_s variable was located close to the origin of coordinates in the PCA loading plot (negligible contribution), suggesting that it is not well represented by the clusters. Thus, taking into account the extreme asymmetry of the R_s data, we have prioritized the selection of the subsets based only on the response variable, for simplicity and representativeness of the current available R_s -space.

One of the approaches used in Section 3.5 (ANNef approach) for evaluating the impact of a single descriptor on the response variable uses the extreme values of the descriptor under study. A more sophisticated strategy, involving the whole range under examination, provides a response curve [44]; broadening the ANNef approach. In this work, five of the selected variables in Fig. 5 are binary (so a response curve can not be obtained) and only variables 2–4 are continuous. For the most important variable, ST , a response curve was obtained (Fig. 6). As it can be observed, the autoscaled R_s - ST data corresponding to the current ANN model show a complex-non linear relationship, which indicates (in the extremes of the ST data) the overall positive contribution of ST to R_s already shown in Fig. 5.

Conclusion

For the first time (to the best of our knowledge), ANN have been used to quantitatively estimate the enantioresolution (R_s) of a heterogeneous dataset of chiral molecules from their structural information. Furthermore, the relative importance of a reduced number of predicting variables was established. The strategy has been designed for consistently comparing different ANN (architecture, feature selection) for a relatively short dataset (here 56 compounds), which implies prefixing some parameters (ANN initial inner weights, validation and cross-validation subsets) to strengthen the decision-making process.

The proposed strategy has been tested in the prediction of enantioresolution values of the 56 chiral compounds from 14 different chemical families chromatographed in cellulose tris(3,5-dimethylphenylcarbamate) and aqueous-acetonitrile mobile phases, from selected structural information. The entire approach only uses outputs provided by ANN. The key of the ANN comparison strategy

is a novel 9-parameters quality indicator (Q) which relies on penalised (by the cross-validated uncertainty) MSE statistics (including an overfitting level) as well as on regression statistics.

After selecting the optimum architecture (first ANN comparison stage), it was used to reduce the X dimension (sequential FS-ANN approach; second ANN comparison stage). The final ANN is ready to: (i) estimate further enantioresolution data for novel non-chromatographed compounds and (ii) establish the relative importance of the selected variables. For the current dataset used, a simple architecture of 8 structural variables input layer and 7 neurons in a single hidden layer previous to the response variable layer (8-[7]-1), offers good general performance (e.g. $MSE = 0.047$ or $R = 0.98$ and 0.92 , for all or just the validation compounds, respectively) in predicting R_s . The analysis of the relative importance of the selected variables in this final ANN suggests that the surface tension (positive overall contribution to R_s) and the groups $-NHR$ in the molecule (negative overall contribution to R_s) are the most relevant for enantioresolution prediction.

Declaration of Competing Interest

The authors declare that they have no known competing financial interests or personal relationships that could have appeared to influence the work reported in this paper.

CRediT authorship contribution statement

Mireia Pérez-Baeza: Investigation, Validation, Visualization, Formal analysis, Writing – original draft. **Yolanda Martín-Biosca:** Conceptualization, Methodology, Supervision, Formal analysis, Writing – original draft, Writing – review & editing. **Laura Escuder-Gilbert:** Conceptualization, Methodology, Supervision, Formal analysis, Writing – original draft, Writing – review & editing. **María José Medina-Hernández:** Conceptualization, Methodology, Supervision, Formal analysis, Writing – original draft, Writing – review & editing. **Salvador Sagrado:** Conceptualization, Methodology, Supervision, Formal analysis, Writing – original draft, Writing – review & editing, Software, Data curation.

Acknowledgments

Mireia Pérez Baeza is grateful to the Generalitat Valenciana and the European Social Fund for the financial support (ACIF/2019/158 research contract).

References

- [1] B. Chankvetadze, Polysaccharide-Based Chiral Stationary Phases for Enantioseparations by High-Performance Liquid Chromatography: an Overview, in: G.K.E. Scriba (Ed.), Chiral Separations, Humana, New York, NY, 2019 Methods in Molecular Biology, vol 1985.
- [2] A. Tarafder, L. Miller, Chiral chromatography method screening strategies: past, present and future, J. Chromatogr. A 1638 (2021) 461878.
- [3] G.K.E. Scriba, Chiral recognition in separation sciences. Part I: polysaccharide and cyclodextrin selectors, Trends Anal. Chem. 120 (2019) 115639.
- [4] B. Chankvetadze, Recent developments on polysaccharide-based chiral stationary phases for liquid-phase separation of enantiomers, J. Chromatogr. A 1269 (2012) 26–51.
- [5] B. Cerra, A. Macchiarulo, A. Carotti, E. Camaioni, I. Varfaj, R. Sardella, A. Gioiello, Enantioselective HPLC Analysis to Assist the Chemical Exploration of Chiral Imidazolines, Molecules 25 (2020) 640–651.
- [6] M. Lämmerhofer, Chiral recognition by enantioselective liquid chromatography: mechanisms and modern chiral stationary phases, J. Chromatogr. A 1217 (2010) 814–856.
- [7] G.K.E. Scriba, Chiral recognition mechanisms in analytical separation sciences, Chromatographia 75 (2012) 815–838.
- [8] J. Shen, Y. Okamoto, Efficient separation of enantiomers using stereoregular chiral polymers, Chem. Rev. 116 (2016) 1094–1138.
- [9] Y. Okamoto, T. Ikai, Chiral HPLC for efficient resolution of enantiomers, Chem. Soc. Rev. 37 (2008) 2593–2608.

- [10] T. Ikai, Y. Okamoto, Structure control of polysaccharide derivatives for efficient separation of enantiomers by chromatography, *Chem. Rev.* 109 (2009) 6077–6101.
- [11] J. Shen, T. Ikai, Y. Okamoto, Synthesis and application of immobilized polysaccharide-based chiral stationary phases for enantioseparation by high-performance liquid chromatography, *J. Chromatogr. A* 1363 (2014) 51–61.
- [12] R.B. Kasat, S.Y. Wee, J.X. Loh, E.I. Franses, N.-H.L. Wang, Effect of the solute molecular structure on its enantioresolution on cellulose tris(3,5-dimethylphenylcarbamate), *J. Chromatogr. B* 875 (2008) 81–92.
- [13] A.Di Michele I.Varfaj, F. Ianni, M. Saletti, M. Anzini, C. Barola, B. Chankvetadze, R. Sardella, A. Carotti, Enantioseparation of novel anti-inflammatory chiral sulfoxides with two cellulose dichlorophenylcarbamate-based chiral stationary phases and polar-organic mobile phase(s), *J. Chromatogr. Open* 1 (2021) 100022.
- [14] C. Perrin, N. Matthijs, D. Mangelings, C. Granier-Loyaux, M. Maftouh, D. Massart, Y.V. Heyden, Screening approach for chiral separation of pharmaceuticals part II. Reversed-phase liquid chromatography, *J. Chromatogr. A* 966 (2002) 119–134.
- [15] L. Zhou, C. Welch, C. Lee, X. Gong, V. Antonucci, Z. Ge, Development of LC chiral methods for neutral pharmaceutical related compounds using reversed phase and normal phase liquid chromatography with different types of polysaccharide stationary phases, *J. Pharm. Biomed. Anal.* 49 (2009) 964–969.
- [16] M.E. Andersson, D. Aslan, A. Clarke, J. Roeraade, G. Hagman, Evaluation of generic chiral liquid chromatography screens for pharmaceutical analysis, *J. Chromatogr. A* 1005 (2003) 83–101.
- [17] J. Lin, C. Tsang, R. Lieu, K. Zhang, Method screening strategies of stereoisomers of compounds with multiple chiral centers and a single chiral center, *J. Chromatogr. A* 1624 (2020) 461244.
- [18] V.S. Sharp, N. Hicks, J. Stafford, A multimodal liquid and supercritical fluid chromatography chiral separation screening and column maintenance strategy designed to support molecules in pharmaceutical development (Part 1), *LCGC Europe* 26 (2013) 608–618.
- [19] C.L. Barhate, L.A. Joyce, A.A. Makarov, K. Zawatzky, F. Bernardoni, W.A. Schafer, D.W. Armstrong, C.J. Welch, E.L. Regalado, Ultrafast chiral separations for high throughput enantiopurity analysis, *Chem. Commun.* 53 (2017) 509.
- [20] A. Tarafder, L. Miller, Chiral chromatography method screening strategies: past, present and future, *J. Chromatogr. A* 1638 (2021) 461878.
- [21] P. De Gauquier, K. Vanommeslaeghe, Y. Vander Heyden, D. Mangelings, Modelling approaches for chiral chromatography on polysaccharide-based and macrocyclic antibiotic chiral selectors: a review, *Anal. Chim. Acta* 1198 (2022) 338861.
- [22] N.M. Maier, P. Franco, W. Lindner, Separation of enantiomers: needs, challenges, perspectives, *J. Chromatogr. A* 906 (2001) 3–33.
- [23] S. Khater, M.A. Lozac'h, I. Adam, E. Francotte, C. West, Comparison of liquid and supercritical fluid chromatography mobile phases for enantioselective separations on polysaccharide stationary phases, *J. Chromatogr. A* 1467 (2016) 463–472.
- [24] J. Shen, T. Ikai, Y. Okamoto, Synthesis and application of immobilized polysaccharide-based chiral stationary phases for enantioseparation by high-performance liquid chromatography, *J. Chromatogr. A* 1363 (2014) 51–61.
- [25] H. Barfeii, Z. Garkani-Nejad, A comparative QSRR study on enantioseparation of ethanol ester enantiomers in HPLC using multivariate image analysis, quantum mechanical and structural descriptors, *J. Chin. Chem. Soc.* 64 (2017) 176–187.
- [26] L. Pisani, M. Rullo, M. Catto, M. de Candia, A. Carrieri, S. Cellamare, C.D. Altomare, Structure–property relationship study of the HPLC enantioselective retention of neuroprotective 7-[(1-alkylpiperidin-3-yl) methoxy] coumarin derivatives on an amylose-based chiral stationary phase, *J. Sep. Sci.* 41 (2018) 1376–1384.
- [27] C. Luo, G. Hu, M. Huang, J. Zou, Y. Jiang, Prediction on separation factor of chiral arylhydantoin compounds and recognition mechanism between chiral stationary phase and the enantiomers, *J. Mol. Graph. Model.* 94 (2020) 107479.
- [28] R. Sheridan, W. Schafer, P. Piras, K. Zawatzky, E.C. Sherer, C. Roussel, C.J. Welch, Toward structure-based predictive tools for the selection of chiral stationary phases for the chromatographic separation of enantiomers, *J. Chromatogr. A* 1467 (2016) 206–213.
- [29] P. Piras, R. Sheridan, E.C. Sherer, W. Schafer, C.J. Welch, C. Roussel, Modeling and predicting chiral stationary phase enantioselectivity: an efficient random forest classifier using an optimally balanced training dataset and an aggregation strategy, *J. Sep. Sci.* 41 (2018) 1365–1375.
- [30] Y. Martín-Biosca, L. Escuder-Gilbert, M.J. Medina-Hernández, S. Sagrado, Modelling the enantioresolution capability of cellulose tris(3,5-dichlorophenylcarbamate) stationary phase in reversed phase conditions for neutral and basic chiral compounds, *J. Chromatogr. A* 1567 (2018) 111–118.
- [31] M. Pérez-Baeza, L. Escuder-Gilbert, Y. Martín-Biosca, S. Sagrado, M.J. Medina-Hernández, Comparative modelling study on enantioresolution of structurally unrelated compounds with amylose-based chiral stationary phases in reversed phase liquid chromatography-mass spectrometry conditions, *J. Chromatogr. A* 1625 (2020) 461281.
- [32] J. Zupan, J. Gaisteiger, *Neural Networks in Chemistry and Drug Design*, 2nd ed., Wiley, Weinheim, 1999.
- [33] J.N. Miller, J.C. Miller, *Statistics and Chemometrics for Analytical Chemistry*, Pearson Education Limited, Harlow, 2005.
- [34] J. Pizarroso, J. Portela, A. Muñoz, NeuralSens: sensitivity Analysis of Neural Networks. <https://arxiv.org/abs/2002.11423> (accessed 28 February 2022).
- [35] J.D. Olden, M.K. Joy, R.G. Death, An Accurate Comparison of Methods for Quantifying Variable Importance in Artificial Neural Networks Using Simulated Data, *Ecol. Modell.* 178 (2004) 389–397.
- [36] S. Lek, Delacoste M, P. Baran, I. Dimopoulos, J. Lauga, S. Aulagnier, Application of Neural Networks to Modeling Nonlinear Relationships in Ecology, *Ecol. Modell.* 90 (1996) 39–52.
- [37] K. Boronová, J. Lehotay, K. Hroboňová, D.W. Armstrong, Study of physicochemical interaction of aryloxyaminopropanol derivatives with teicoplanin and vancomycin phases in view of quantitative structure-property relationship studies, *J. Chromatogr. A* 1301 (2013) 38–47.
- [38] M. Szaleniec, A. Dudzik, M. Pawul, B. Kozik, Quantitative structure enantioselective retention relationship for high-performance liquid chromatography chiral separation of 1-phenylethanol derivatives, *J. Chromatogr. A* 1216 (2009) 6224–6235.
- [39] T. Suzuki, S. Timofei, B.E. Iuoras, G. Uray, P. Verdino, W.M.F. Fabian, Quantitative structure-enantioselective retention relationships for chromatographic separation of arylalkylcarbinols on Pirkle type chiral stationary phases, *J. Chromatogr. A* 922 (2001) 13–23.
- [40] ChemSpider Database. Royal Society of Chemistry. <http://www.chemspider.com/> (accessed 28 February 2022).
- [41] L. Asensi-Bernardi, L. Escuder-Gilbert, Y. Martín-Biosca, M.J. Medina-Hernández, S. Sagrado, Modelling the chiral resolution ability of highly sulfated- β -cyclodextrin for basic compounds in electrokinetic chromatography, *J. Chromatogr. A* 1308 (2013) 152–160.
- [42] L. Escuder-Gilbert, Y. Martín-Biosca, M.J. Medina-Hernández, S. Sagrado, Enantioresolution in electrokinetic chromatography-complete filling technique using sulfated gamma-cyclodextrin. Software-free topological anticipation, *J. Chromatogr. A* 1467 (2016) 391–399.
- [43] MATLAB®R2019a (Mathworks®). <https://matlab.mathworks.com/> (accessed 28 March 2022).
- [44] M. Szaleniec, Prediction of enzyme activity with neural network models based on electronic and geometrical features of substrates, *Pharmacol. Rep.* 64 (2012) 761–781.



PAPER IV

**Modified Gaussian models applied to the description
and deconvolution of peaks in chiral liquid
chromatography**

**M. Pérez-Baeza^a, L. Escuder-Gilabert^a, M.J. Medina-Hernández^a,
J.J. Baeza-Baeza^a, M.C. García-Alvarez-Coque^a**

^a Department of Analytical Chemistry, University of Valencia, c/Dr. Moliner 50, 46100 Burjassot
Spain

Journal of Chromatography A 1625 (2020) 461273



Modified Gaussian models applied to the description and deconvolution of peaks in chiral liquid chromatography

M. Pérez-Baeza, L. Escuder-Gilabert, M.J. Medina-Hernández, J.J. Baeza-Baeza, M.C. García-Alvarez-Coque*

Department of Analytical Chemistry, University of Valencia, c/Dr. Moliner 50, 46100 Burjassot Spain

ARTICLE INFO

Article history:

Received 18 March 2020

Revised 18 May 2020

Accepted 22 May 2020

Available online 29 May 2020

Keywords:

Liquid chromatography

Enantiomeric analysis

Peak fitting

Modified Gaussian models

Peak deconvolution

ABSTRACT

The description of the profiles of chromatographic peaks has been studied extensively, with a large number of proposed mathematical functions. Among them, the accuracy achieved with modified Gaussian models that describe the deviation of an ideal Gaussian peak as a change in the peak variance or standard deviation over time, has been highlighted. These models are, in fact, a family of functions of different complexity with great flexibility to adjust chromatographic peaks over a wide range of asymmetries and shapes. However, an uncontrolled behaviour of the signal may occur outside the region being fitted, forcing the use of different strategies to overcome this problem. In this work, the performance of the LMG (Linear Modified Gaussian), PVMG (Parabolic Variance Modified Gaussian), and PLMG (Parabolic-Lorentzian Modified Gaussian) models is compared with variants obtained by combination of the modified Gaussian models with an equation that adds an exponential tail and with other functions that limit the growth of the independent variable. The behaviour of the approaches is checked through the simultaneous fitting of enantiomeric peaks showing a wide range of characteristics, obtained in the separation of drugs with chiral activity by liquid chromatography using enantioselective columns. The study is also carried out with the purpose of performing the deconvolution of the peaks of the enantiomers, when these are not completely resolved, in order to evaluate the enantiomeric fraction.

© 2020 Elsevier B.V. All rights reserved.

1. Introduction

In order to forecast the experimental conditions that best resolve the components of a sample by liquid chromatography, in the shortest analysis time, it is convenient to make realistic predictions of the expected chromatograms. A reliable methodology to make such predictions is based on the use of models that describe the retention and shape of chromatographic peaks exhibiting different widths and asymmetries [1–5]. The parameters of the function used to fit the peaks should offer information about their position (t_R), height (H_0), and left (A) and right (B) half-widths [6,7]. Also, models able to predict the peak half-widths as a function of the experimental conditions are very useful for the simulation of chromatograms [8,9].

A large number of mathematical functions have been proposed to describe chromatographic peaks with different success [10–19]. Of special interest is the compilation of equations by Di Marco and

Bombi [16]. The exponentially modified Gaussian function has been especially popular and served Foley and Dorsey as a basis to obtain different equations to calculate parameters that characterise asymmetric chromatographic peaks, depending on the values of the left and right half-widths, and the retention times [20,21]. Our research group has proposed modified Gaussian models [6,13,22], which have demonstrated very good performance to describe peaks with diverse asymmetry, where the model parameters can be expressed as a function of the half-widths [7].

The simplest model (the linearly modified Gaussian, LMG model) uses a linear function to describe the peak standard deviation [13]:

$$h(t) = H_0 \exp \left[-\frac{1}{2} \left(\frac{t_c}{\sigma_0 + m t_c} \right)^2 \right] \quad (1)$$

being

$$\sigma_0 = 0.932 \frac{AB}{A+B} \quad (2)$$

$$m = 0.466 \frac{B-A}{A+B} \quad (3)$$

* Corresponding author.

E-mail address: celia.garcia@uv.es (M.C. García-Alvarez-Coque).

where $t_c = t - t_R$, and the half-widths are measured at 10% peak height. According to Foley and Dorsey [11,12], measurements at this height are most convenient, since peak asymmetry is more evident and the baseline noise is not disturbing. In the LMG model, σ_0 describes the standard deviation of a Gaussian that behaves as the asymmetric peak at the maximum [7]. This model is ideal for predicting peaks with moderate asymmetries.

For more accurate fitting of chromatographic peaks, a more complex model, such as the modified Gaussian with a parabolic function (PVMG model) [6] is needed:

$$h(t) = H_0 \exp \left[-\frac{1}{2} \frac{t_c^2}{\sigma_0^2 + b t_c + c t_c^2} \right] \quad (4)$$

where

$$b = \frac{B - A}{BA} \sigma_0^2 \quad (5)$$

$$c = 0.217 - \frac{\sigma_0^2}{BA} \quad (6)$$

The main disadvantage of the above models (Eqs. (1) and (4)) is that the parabolic growth of the variance can lead to non-null values of the baseline for times far from the peak maximum. Thus, for example, for the PVMG model:

$$h(\infty) = H_0 \exp \left[-\frac{1}{2c} \right] \quad (7)$$

With the purpose of avoiding the function growth outside the peak region, a modified Gaussian model formed by a combination of a parabola with a Lorentzian (PLMG model) was further proposed [22]:

$$h(t_c) = H_0 \exp \left(-\frac{1}{2} \frac{1 + w t_c + z t_c^2}{\sigma_0^2 + b t_c + c t_c^2} t_c^2 \right) \quad (8)$$

which has demonstrated the best performance in the fitting of isolated asymmetric peaks [7]:

All modified Gaussian models require accurate enough estimations of the height and time at the peak maximum to assure convergence in the fitting process [22,23]. In order to improve the applicability of the model, negative values of the variances should be avoided. It should be also noted that the high flexibility of the PLMG model could give rise to peaks exhibiting more than one maximum.

A large number of common drugs have at least one chiral centre, and the enantiomers may have different pharmacological and toxicological properties. Therefore, the quantification of the enantiomeric fraction, in both commercial and environmental samples, is of great importance [24–26]. The application of all the above models to the description of the peaks obtained in a chiral separation is an important challenge, since the peak characteristics for the enantiomers can be very different and their overlapping degree variable.

The aim of this work is to study the performance of the LMG, PVMG and PLMG models to get reliable fittings of experimental chromatographic peak profiles for several drugs with chiral activity, eluted with enantioselective columns. A main objective is to study how these models succeed in the deconvolution of the chromatographic peaks, when the enantiomers are not completely resolved. This is relevant for a proper evaluation of the enantiomeric fraction of the chiral samples. In this case, the application of multivariate techniques, such as multivariate curve resolution-alternating least squares is not helpful, since both enantiomers in a racemic mixture have the same UV and MS spectra.

2. Experimental

2.1. Reagents

The mobile phases were prepared with acetonitrile (ACN) or methanol (MeOH) (HPLC/LC-MS grade) from VWR International EuroLab (Barcelona, Spain). The following reagents were added to adjust the pH of the mobile phases: ammonium acetate, ammonium bicarbonate, hydrochloric acid (37%), sodium hydroxide all from Scharlau (Barcelona), and ammonium formate from Acros Organics (Geel, Belgium). In some separations, formic acid (98%) and sodium perchlorate monohydrate from Scharlau, and potassium perchlorate, diethylamine (DEA) and potassium hexafluorophosphate from Acros Organics, were used as additives. All reagents were of analytical grade.

Ultra Clear TWF (tap water feed) UV deionised water (SG Water, Barsbüttel, Germany) was used to prepare the following aqueous solutions: 10 mM ammonium acetate and 20 mM ammonium bicarbonate buffers at pH 8.0 adjusted with 2.5 M sodium hydroxide, 10 mM ammonium formate at pH 3.0 adjusted with 1 M hydrochloric acid, 100 mM potassium hexafluorophosphate, and 500 mM sodium or potassium perchlorate. All these solutions were mixed with the organic modifier to obtain the working concentration of the mobile phase. Ternary mixtures of the above aqueous solutions, pure organic modifier and 0.1% (v/v) formic acid or DEA were also used as mobile phases.

The following drugs were analysed: bupivacaine (BUP) from Cayman Chemical Company (Michigan, USA), flurbiprofen (FLU), ibuprofen (IBU), ketoprofen (KET), and trimeprazine (TRI) from Sigma-Aldrich (St. Louis, MO, USA), metoprolol (MET) from Alfa Aesar (Thermo Fisher Scientific, Karlsruhe, Germany), and omeprazole (OME) and propranolol (PRO) from Acros Organics. All the standards used in the experiments were racemates ((±)-analyte). Stock standard solutions of 1000 mg L⁻¹ for all the compounds in the study were prepared by dissolving the adequate amount of each drug in MeOH. From these, 100 mg L⁻¹ solutions were prepared by dilution in MeOH.

Prior to injection into the chromatographic system, samples were filtered through disposable 0.22 µm polyethersulphone syringe filters (Frisenette, Knebel, Denmark). Mobile phase solutions were vacuum-filtered through 0.22 µm Nylon membranes (Micron Separations, Westboro, MA, USA), and degassed in an Elmasonic S60 ultrasonic bath (Elma, Singen, Germany) prior to use.

2.2. Apparatus and columns

Two chromatographic systems were used. The first system was an Agilent Technologies 1100 chromatograph (Palo Alto, CA, USA), equipped with a binary pump, a UV-visible diode array detector, a mass spectrometer provided with a source of atmospheric pressure chemical electrospray/ionisation (ESI/APCI) and simple quadrupole, a column thermostat and an autosampler. Data acquisition and processing were performed by means of the LC/MSD ChemStation software (B.04.02 SP1 [208], ©Agilent Technologies 2001–2010).

The second system was an Agilent Technologies 1100 chromatograph, equipped with a quaternary pump, a UV-visible variable wavelength detector, a column thermostat and an autosampler. In this case, data acquisition and processing were performed by means of the Chemstation software (A.09.03 [1417], ©Agilent Technologies 1990–2002).

For the separation of the enantiomers of the drugs under study, several polysaccharide-based chiral stationary phases were used: Lux Cellulose-1 (cellulose tris(3,5-dimethylphenylcarbamate), 3 µm, 150 × 4.6 mm i.d. from Phenomenex, Torrance, CA, USA; Lux Cellulose-2 (cellulose tris(3-chloro-4-methylphenylcarbamate), 3 µm, 150 × 2.0 mm i.d. from Phenomenex; Lux Cellulose-

Table 1

Columns and experimental conditions used in the separation of the enantiomers of eight drugs. The retention times (t_R) of the peaks of each enantiomer, their resolution (R_S), asymmetry factor (B/A) for the peak of each enantiomer, and enantiomeric fraction (EF%) (see Section 4.1) are given.

Chromatogram ^a	Column	Experimental conditions ^b	t_R	R_S	B/A	EF (%)
BUP1	LuxCell-3	MeOH : NH ₄ HCO ₃ + DEA (70:30), 40 °C	7.8, 8.5	1.19	1.11, 1.04	48.6
FLU1	LuxAm-2	ACN : ammonium formate + NaClO ₄ (40:60), 25 °C	4.9, 7.9	3.34	1.96, 1.74	50.1
FLU2	LuxCell-1	ACN : ammonium formate + NaClO ₄ (40:60), 15 °C	15.4, 15.8	0.49	1.20, 1.54	40.0
IBU1	LuxCell-3	MeOH : ammonium formate (85:15), 25 °C	7.0, 7.8	2.98	1.08, 1.07	50.0
IBU2	LuxAm-2	ACN : ammonium formate + NaClO ₄ (40:60), 25 °C	8.9, 9.6	0.59	2.14, 1.98	61.2
IBU3	LuxCell-3	MeOH : ammonium formate (80:20), 25 °C	7.3, 8.1	2.29	0.84, 1.09	29.8
KET1	LuxAm-2	ACN : formic acid (60:40), 15 °C	1.7, 1.9	0.62	1.59, 2.31	47.8
KET2	LuxAm-2	ACN : formic acid (50:50), 15 °C	1.8, 2.0	0.73	1.17, 1.70	38.4
KET3	LuxAm-2	ACN : formic acid (40:60), 15 °C	2.7, 3.2	1.02	1.79, 1.45	54.4
KET4	LuxAm-2	ACN : formic acid (35:65), 15 °C	4.0, 4.7	1.21	1.39, 1.27	50.3
MET1	LuxCell-1	ACN : ammonium acetate (40:60), 25 °C	3.5, 3.7	1.08	1.27, 1.30	49.5
MET2	LuxCell-1	ACN : ammonium acetate (30:70), 25 °C	5.0, 5.6	2.03	1.49, 2.81	51.1
OME1	Cell-SC	ACN : ammonium acetate + DEA (35:65), 25 °C	7.2, 8.0	1.15	2.36, 2.35	49.0
OME2	LuxCell-2	ACN : NH ₄ HCO ₃ (50:50), 25 °C	4.5, 6.3	2.06	1.54, 1.43	49.4
PRO1	LuxCell-1	ACN : ammonium acetate (40:60), 25 °C	19.8, 21.5	1.88	1.18, 1.14	49.9
PRO2	LuxCell-1	ACN : NaClO ₄ (40:60), 25 °C	6.7, 8.1	2.41	1.64, 3.13	54.2
PRO3	LuxAm-2	ACN : ammonium acetate + DEA (40:60), 25 °C	4.7, 5.5	1.38	1.65, 1.51	49.2
TRI1	LuxCell-1	ACN : KClO ₄ (40:60), 25 °C	11.5, 12.5	1.94	1.22, 1.24	48.4
TRI2	LuxCell-1	ACN : KPF ₆ (40:60) 15 °C	26.3, 27.5	1.01	1.20, 1.20	48.0
TRI3	Cell-SC	ACN : ammonium acetate + DEA (45:55), 25 °C	20.0, 20.5	0.62	1.06, 1.13	51.0

^a Bupivacaine (BUP), flurbiprofen (FLU), ibuprofen (IBU), ketoprofen (KET), metoprolol (MET), omeprazole (OME), propranolol (PRO), and trimeprazine (TRI).

^b The concentration of the aqueous solutions of the reagents mixed with the organic modifiers is given in Section 2.1. BUP1 and OME2 were detected using both mass spectrometric and UV detection. All other analyses were carried out using UV detection exclusively.

3 (cellulose tris(4-methylbenzoate), 3 μ m, 150 \times 4.6 mm i.d. from Phenomenex; Chiralart Cellulose-SC (cellulose tris(3, 5-dichlorophenylcarbamate), 3 μ m, 150 \times 4.6 mm i.d. from YMC Separation Technology from Tokyo, Japan; and Lux Amylose-2 (amylose tris(5-chloro-2-methylphenylcarbamate), 3 μ m, 150 \times 2.0 mm i.d. from Phenomenex.

The mobile phase flow rate was 1.0 mL min⁻¹ in all cases, except when using the Lux Cellulose-2 and Lux Amylose-2 columns, for which the flow rate was 0.5 mL min⁻¹. In most cases, column temperature was set at 25 °C (see Table 1 for more information). The injection volume was 2 μ L, and UV detection was performed at 220 nm, except for trimeprazine for which the absorbance was measured at 254 nm. Mass spectrometric detection for bupivacaine and omeprazole was performed using an m/z ratio of 289 and 346, respectively, which corresponded to the [M+H]⁺ ions.

A MicropH 2000 pHmeter (Crison Instruments, Barcelona) was employed to adjust the pH of the buffer solutions.

3. Theory

3.1. Approaches for the prediction of peak profiles

New approaches were developed to eliminate the problem of the prediction of abnormal tails when the chromatographic peaks of enantiomers are fitted using the modified Gaussian models. The approaches are based on the three models described in Section 1 (LMG, PVMG and PLMG). To allow tails tending to zero asymptotically, two modifications of these models are proposed: (i) Replacing the model with exponential tails at 10% peak height outside the peak region, and (ii) applying a sigmoidal function so that the variance tends to a constant value when the time is far from the maximum, giving rise to Gaussian tails. All models should include the half-width values (A and B) as parameters [1]. In this work, parameters A and B were measured at 10% peak height to facilitate the application of the proposed modifications.

The different modifications are described below in detail. In all approaches, the variance is forced to be always positive and above 1×10^{-6} .

3.1.1. Approach I: LMG model

Approach Ia: The LMG model is applied directly using Eqs. (1) to (3), without any modification. In this model, the fitted parameters are t_R , H_0 , A and B .

Approach Ib: The peak tails are exponentially modified. The LMG model is substituted by an exponential function below height p .

$$p = \frac{h_p}{H_0} \quad (9)$$

To avoid discontinuities, the slope of the LMG function and the slope of the added exponential must be the same at the point of substitution. To simplify, we will write the modified Gaussian function using the general expression:

$$h = H_0 e^{-\frac{1}{2}q^2} \quad (10)$$

whose derivative is:

$$\frac{dh}{dt} = \frac{dh}{dq} \frac{dq}{dt} = -qh \frac{dq}{dt} \quad (11)$$

Meanwhile, the equation of the added exponential is:

$$h = H_0 e^{-kt} \quad (12)$$

and its derivative:

$$\frac{dh}{dt} = -kH_0 e^{-kt} = -kh \quad (13)$$

Matching Eqs. (11) and (13) at point p , the decay constant of the exponential function is obtained:

$$k = q \frac{dq}{dt} \quad (14)$$

For the LMG model:

$$q^2 = \frac{t^2}{(\sigma_0 + mt)^2} \quad (15)$$

whose derivative is:

$$q \frac{dq}{dt} = \frac{t\sigma_0}{(\sigma_0 + mt)^3} = \frac{\sigma_0 q^3}{t^2} \quad (16)$$

By substituting Eq. (16) in Eq. (14), the decay constant of the exponential function is as follows:

$$k = \frac{\sigma_0}{t^2} q^3 \quad (17)$$

We will arbitrarily take $p = 0.1$ (10% peak height) as the point of change of the LMG function to an exponential. Therefore, from Eq. (10):

$$q = \sqrt{-2 \times \ln \left(\frac{h_{0.1}}{H_0} \right)} = \sqrt{-2 \times \ln(0.1)} = 2.146 \quad (18)$$

In this point ($p = 0.1$), for the left side of the peak ($t_{0.1} = -A$), the exponential function will be:

$$h = p H_0 e^{k(A+t_c)} = 0.1 \times H_0 \times e^{9.883 \times \frac{\sigma_0}{A^2} (A+t_c)} \quad (19)$$

and for the right side ($t_{0.1} = B$):

$$h = p H_0 e^{k(B-t_c)} = 0.1 \times H_0 \times e^{9.883 \times \frac{\sigma_0}{B^2} (B-t_c)} \quad (20)$$

Approach Ic: The temporal variable of the variance is replaced by a sigmoidal function:

$$x = \frac{t_c}{1 + 0.2 \frac{|t_c|}{A+B}} \quad (21)$$

the final peak model being:

$$h(t) = H_0 \exp \left[-\frac{1}{2} \left(\frac{t_c}{\sigma_0 + mx} \right)^2 \right] \quad (22)$$

This assures that when $t_c = \infty$, then $x = (A+B)/0.2$ and $h = 0$.

3.1.2. Approach II: PVMG model

Approach IIa: The PVMG model is first applied without modifications, using Eqs. (4) to (6). The fitted parameters are t_R , H_0 , σ_0 , A and B .

Approach IIb: The exponential substitution is applied to the PVMG model, as in Approach Ib. In this case:

$$q^2 = \frac{t^2}{\sigma_0^2 + bt + ct^2} \quad (23)$$

whose derivative is:

$$q \frac{dq}{dt} = \frac{1}{2} \frac{2t \times (\sigma_0^2 + bt + ct^2) - t^2(b + 2ct)}{(\sigma_0^2 + bt + ct^2)^2} = \frac{1}{2} \frac{2\sigma_0^2 t + bt^2}{t^4} q^4 \quad (24)$$

Matching Eqs. (14) and (24), and working out:

$$k = \frac{1}{2} \frac{|2\sigma_0^2 t + bt^2|}{t^4} q^4 \quad (25)$$

where the absolute value has been taken to ensure a positive value of the decay exponential constant (k). Finally, considering that at 10% peak height, $p = 0.1$ and $q = 2.146$, the equation for the exponential left tail will be:

$$h = 0.1 \times H_0 \times e^{10.604 \times \frac{|bA^2 - 2\sigma_0^2 A|}{A^4} (A+t_c)} \quad (26)$$

and for the right tail:

$$h = 0.1 \times H_0 \times e^{10.604 \times \frac{|bB^2 - 2\sigma_0^2 B|}{B^4} (B-t_c)} \quad (27)$$

Approach IIc: As in Approach Ic, the temporal variable of the variance is replaced by Eq. (21). The final peak model will be:

$$h(t) = H_0 \exp \left[-\frac{1}{2} \frac{t_c^2}{\sigma_0^2 + bx + cx^2} \right] \quad (28)$$

3.1.3. Approach III: PLMG model

Approach IIIa: The PLMG approach is applied according to Eq. (8). However, the same as in Approaches I and II, in order to be able to implement Approaches IIIb and IIIc, the half-width values should be known. For this purpose, first of all, parameters b and c will be related to the half-widths as shown below.

From Eq. (8):

$$q^2 = \frac{1 + wt + zt^2}{\sigma_0^2 + bt + ct^2} t^2 \quad (29)$$

At 10% peak height, $q^2 = 4.605$, and by substituting the time for each half-width ($t_{0.1} = -A$ and $t_{0.1} = B$), we can get two equations from Eq. (29):

$$\sigma_0^2 - bA + cA^2 = 0.217 (A^2 - wA^3 + zA^4) \quad (30)$$

$$\sigma_0^2 + bB + cB^2 = 0.217 (B^2 + wB^3 + zB^4) \quad (31)$$

Dividing each equation by the corresponding half-width, and adding Eqs. (30) and (31) to eliminate b :

$$\sigma_0^2 \frac{A+B}{AB} + c(A+B) = 0.217 \times [A+B + w(B^2 - A^2) + z(B^3 + A^3)] \quad (32)$$

from which:

$$c = 0.217 \times [1 + w(B-A) + z(B^2 + A^2 - AB)] - \frac{\sigma_0^2}{AB} \quad (33)$$

Dividing Eqs. (30) and (31) by the corresponding squared half-width, and subtracting to eliminate parameter c , the following is obtained:

$$-\sigma_0^2 \frac{B^2 - A^2}{A^2 B^2} + b \frac{A+B}{AB} = 0.217 \times [w(A+B) + z(B^2 - A^2)] \quad (34)$$

which yields to:

$$b = \sigma_0^2 \frac{B-A}{AB} + 0.217 \times [w + z(B-A)] AB \quad (35)$$

Eqs. (8), (33) and (35) constitute Approach IIIa, where the model parameters to be fitted are t_R , H_0 , σ_0 , A , B , w and z . To avoid negative or close to zero values for the peak variance, the parabolas in the numerator and denominator of Eq. (8) will be limited to positive values above 1×10^{-6} .

Approach IIIb: In this approach, exponential tails are added to Approach IIIa. The equations that describe the exponential tails are obtained by deriving Eq. (29):

$$q \frac{dq}{dt} = \frac{1}{2} \frac{2t + 3wt^2 + 4zt^3 - q^2(b + 2ct)}{\sigma_0^2 + bt + ct^2} \quad (36)$$

The decay constant is obtained by matching Eqs. (14) and (36). The left tail is described by:

$$h = 0.1 \times H_0 \times \exp \left[\frac{1}{2} \times \left| \frac{-2A + 3wA^2 - 4zA^3 - 4.605 \times (b - 2cA)}{\sigma_0^2 - bA + cA^2} \right| \times (A + t_c) \right] \quad (37)$$

and the right tail by:

$$h = 0.1 \times H_0 \times \exp \left[\frac{1}{2} \times \left| \frac{2B + 3wB^2 + 4zB^3 - 4.605 \times (b + 2cB)}{\sigma_0^2 + bB + cB^2} \right| \times (B - t_c) \right] \quad (38)$$

Approach IIIc: As in Approach Ic, the temporal variable in the variance is replaced by Eq. (21). The final peak model is:

$$h(t) = H_0 \exp \left[-\frac{1}{2} \frac{1 + wx + zx^2}{\sigma_0^2 + bx + cx^2} t_c^2 \right] \quad (39)$$

4. Results and discussion

4.1. Characteristics of the experimental peaks

In order to check the performance of the proposed approaches, 20 chromatograms obtained in the analysis of chiral drugs were selected from our data base. The experimental peaks were obtained using different chromatographic modes, columns, mobile phase compositions, temperatures, and pH values, as indicated in Table 1. The peaks correspond to eight drugs with different pharmacological uses: bupivacaine (BUP1), flurbiprofen (FLU1 and FLU2), ibuprofen (IBU1, IBU2 and IBU3), ketoprofen (KET1, KET2, KET3 and KET4), metoprolol (MET1 and MET2), omeprazole (OME1 and OME2), propranolol (PRO1, PRO2 and PRO3), and trimeprazine (TRI1, TRI2 and TRI3). Peaks of the enantiomeric compounds with diverse efficiency and skewness values were selected. The peaks for BUP1 and OME2 were monitored using mass spectrometry detection, which decreased the noise in the chromatograms. All other peaks were monitored using UV detection.

Table 1 gives information about:

- (i) The retention times of the peaks for the two enantiomers of each drug.
- (ii) The resolution of the two peaks, calculated according to:

$$R_S = \frac{t_{R2} - t_{R1}}{B_1 + A_2} \quad (40)$$

where t_{R2} and t_{R1} are the retention times for the peaks at longer (peak 2) and shorter (peak 1) retention, and A_2 and B_1 are the corresponding left and right half-widths measured at 10% peak height.

(iii) The peak asymmetry for each peak (B/A , where peaks are tailing for $B/A > 1$ and fronting for $B/A < 1$).

(iv) The enantiomeric fraction (EF%), measured as the percentage area of peak 1 [25], calculated as:

$$EF\% = \frac{\text{area}_1}{\text{area}_1 + \text{area}_2} \times 100 \quad (41)$$

where area_1 and area_2 correspond to peaks 1 and 2, respectively.

The ranges of the above parameters for the peaks chosen for this work were: 1.7–27.5 min for the retention times, 0.49–3.34 for peak resolution, 0.84–3.13 for peak asymmetry, and 29.8–61.2% for the enantiomeric fraction of the first eluted enantiomer. All values were measured from the individual peaks obtained from the fittings according to Approach IIIb. In Fig. S1 in the Supplementary material, the chromatograms for the probe compounds are shown.

4.2. Fitting performance

The approaches described in Section 3 (LMG, PVMG and PLMG, without and with restrictions) were applied to fit the peaks in the chromatograms for the enantiomeric compounds (Fig. 1). It should be noted that the peaks of the two enantiomers were fitted simultaneously:

$$\hat{h}_i = h_1(t_i) + h_2(t_i) \quad (42)$$

h_1 and h_2 being the height of peaks 1 and 2, respectively at time t_i , and \hat{h}_i the predicted signal at this time, which is the summation of the contribution of both peaks. The fitting is performed using least squares regression by optimising the peak parameters of each peak. For instance, for the LMG model, eight parameters were optimised: t_{R1} , H_{01} , A_1 and B_1 for peak 1, and t_{R2} , H_{02} , A_2 and B_2 for peak 2.

When the peaks of the enantiomers are overlapped, they can only be resolved by making the simultaneous fitting of the functions of both enantiomers (Eq. (42)). Of course, there is no advantage in doing so when the peaks are perfectly spaced, more than saving time. However, this allows obtaining a measurement of the

quality of the fittings common to all peak pairs, independently of their resolution.

The fitting performance was assessed by calculating the mean relative errors according to:

$$\varepsilon_r(\%) = \frac{\sum_{i=1}^N |h_i - \hat{h}_i|}{\sum_{i=1}^N |h_i|} \times 100 \quad (43)$$

where h_i and \hat{h}_i are the experimental and predicted heights for each point in the chromatogram (at different times), and N is the number of experimental points.

Fig. 1 illustrates the performance of the different approaches based on the LMG, PVMG and PLMG models, without any restriction (Approaches Ia, IIa and IIIa), and after applying the restrictions described in Section 3 (Approaches Ib, IIb and IIIb, and Approaches Ic, IIc and IIIC). The excellent fitting achieved by applying the PLMG model for the enantiomeric peaks in KET4, IBU3 and MET2 (which show a large diversity in peak tailing, from $B/A = 0.84$ to 2.81), is remarkable. Similar behaviour was observed for the other peaks studied in this work.

The errors obtained in the fitting of the chromatograms of the chiral drugs studied in this work, according to each approach for the LMG, PVMG and PLMG models (without and with restrictions), are indicated in Table 2. As observed, the errors for the PLMG model were below 1% for most compounds. Approaches IIIa, IIIb and IIIc showed a mean relative error of 0.69%, 0.80% and 0.71%, considering the 20 studied peak-pairs, respectively. These errors were significantly smaller than the errors yielded by fitting the peaks according to the LMG and PVMG models. The behaviour was acceptable when the PVMG model was applied, with mean relative errors of 1.87%, 1.52% and 1.58% for Approaches IIa, IIb and IIc, respectively. The worst results were obtained with the LMG model, which is the simplest among those studied, with mean relative errors in the fitting of the chromatograms of 4.34%, 4.12% and 4.54% for Approaches Ia, Ib and Ic, respectively. Note also that for all studied cases, there was a notable improvement in the performance of the fittings, when the PVMG model was used instead of the LMG model.

The slight improvement in the fittings obtained with the PVMG model when exponential tails were added (Approach IIb), or the growth of the independent variable was limited (Approach IIc), should be also highlighted. Meanwhile, Approach b causes also a slight improvement for the LMG model, and a slight worsening for the PLMG model. For Approach c, the results of the LMG and PLMG models are worse.

However, in spite of the apparent better performance of the PLMG model, it should be indicated that this model is too flexible and may incur in overfitting in those regions where the peaks of the enantiomers are overlapped. This is observed in Fig. 2, where the experimental chromatogram for KET4 is overlaid with the individual peaks obtained through the fitting with the PLMG model, without restrictions (IIIa) and using the two proposed restrictions (IIIb and IIIc). Approaches IIIa and IIIc gave rise to anomalous peak shapes in regions where the peaks of the enantiomers were overlapped. Approach IIIb solved this anomaly by forcing the peak tails to follow an exponential decay.

The lack of reliability could persist if the overlap occurs above 10% peak height, a situation where the model may even predict peaks showing two maximums. It should be noted that the flexibility of the PLMG model is excessive for overlapped compounds, and the reliability of the fitted parameters A and B is low. Therefore, the PLMG model cannot be used for the deconvolution of overlapped peaks, without being constrained to a proper peak shape. However, it is useful for the fitting of perfectly defined individual

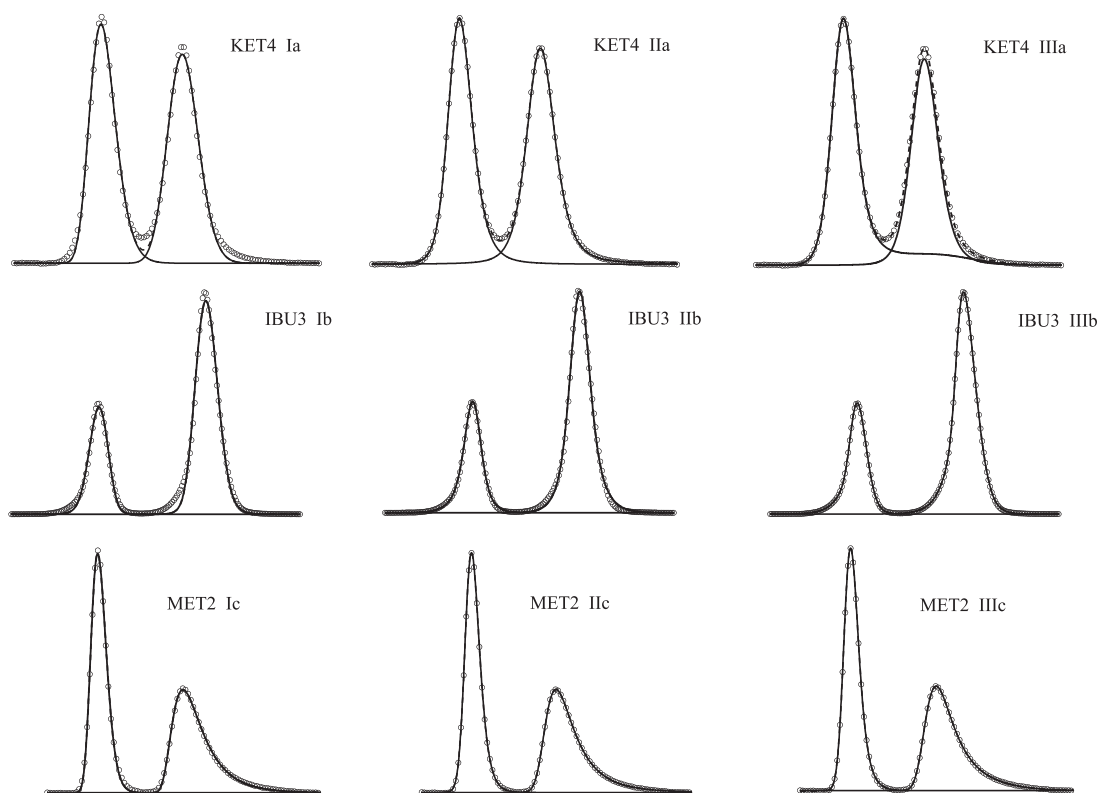


Fig. 1. Experimental (°) and predicted chromatograms (dashed line - - -) for ketoprofen (KET4), ibuprofen (IBU3), and metoprolol (MET2). Predicted peaks (black line, --) obtained by applying the studied approaches are overlaid. Only a few experimental points are shown.

Table 2

Fitting performance (percentage) according to Eq. (43) of the approaches (see Section 3.1) applied to the chromatograms described in Table 1.

Chromatograms	Ia	Ib	Ic	IIa	IIb	IIc	IIIa	IIIb	IIIc
BUP1	2.77	2.56	2.78	1.53	1.71	1.69	0.78	0.91	0.82
FLU1	7.60	7.57	8.57	3.35	2.35	2.08	1.92	2.15	1.95
FLU2	3.43	3.34	3.10	2.40	2.23	2.36	0.72	0.71	0.77
IBU1	2.73	2.33	2.74	2.28	2.10	2.35	1.07	1.36	1.06
IBU2	7.22	7.14	7.54	2.60	1.07	1.37	0.75	1.16	0.75
IBU3	9.98	9.49	9.99	6.47	5.67	5.81	1.22	0.67	1.09
KET1	3.62	4.08	4.72	1.34	1.18	1.24	0.34	0.43	0.46
KET2	4.21	4.57	4.22	1.75	1.10	1.26	0.70	0.38	0.61
KET3	7.74	7.43	7.96	1.63	1.24	1.08	0.66	0.76	0.73
KET4	7.80	7.39	7.90	1.33	1.06	1.07	0.47	0.62	0.54
MET1	2.77	2.48	2.84	0.54	0.74	0.77	0.22	0.38	0.20
MET2	2.85	2.37	3.26	1.47	1.03	0.97	0.62	0.63	0.59
OME1	3.33	2.87	3.74	2.55	1.85	1.66	0.47	0.44	0.48
OME2	2.08	1.89	2.27	2.07	1.74	2.26	1.25	1.80	1.36
PRO1	1.72	1.24	1.76	0.77	0.57	0.86	0.37	0.47	0.38
PRO2	3.40	3.04	3.46	1.99	1.93	1.82	0.67	1.00	0.63
PRO3	10.5	10.2	10.9	1.96	1.36	1.42	0.53	0.82	0.57
TRI1	1.94	1.45	2.02	0.73	0.74	0.85	0.59	0.66	0.59
TRI2	0.72	0.56	0.75	0.38	0.35	0.38	0.30	0.27	0.30
TRI3	0.37	0.31	0.39	0.23	0.32	0.33	0.23	0.31	0.34
Mean error	4.34	4.12	4.54	1.87	1.52	1.58	0.69	0.80	0.71

peaks, to get a peak function describing accurately the experimental data. Outside the peak region, the function value should be set to zero to avoid problems with the baseline. This function can be thus used without restrictions to obtain peak parameters or reduce noise problems.

From the results obtained, it can be seen that Approaches IIb and IIc provide very similar results, Approach IIc being easier to apply. This approach will be used in the next section to study the deconvolution of overlapped peaks, together with the PLMG model (Approach IIIa).

4.3. Peak deconvolution

As commented, the PLMG model is the best to obtain the characteristics of an isolated peak [1]. It is very flexible and can fit very satisfactorily perfectly profiled peaks in a wide range of peak shapes, inside specific time intervals. However, it could be not reliable enough to deconvolve overlapped peaks (as could be the case of some enantiomeric compounds), or to make predictions at times outside the fitted range.

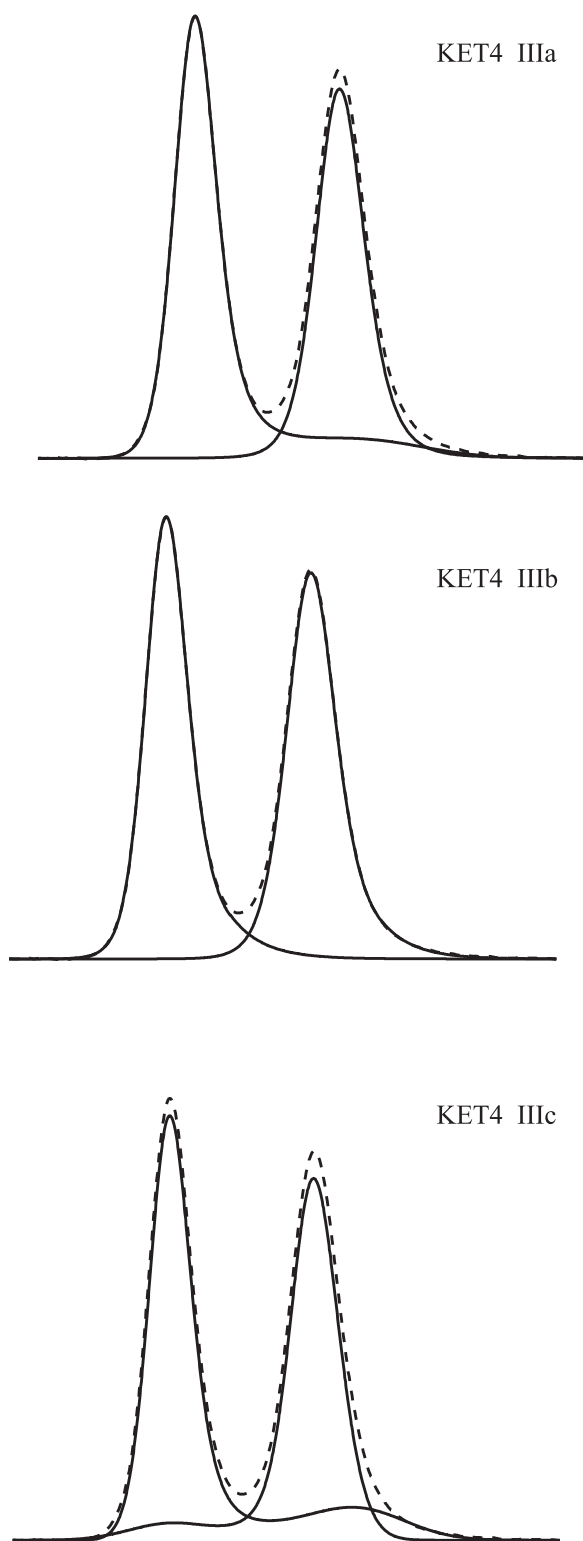


Fig. 2. Performance of the PLMG model in the fitting of the experimental signal of ketoprofen (KET4) (dashed line - - -). Predicted peaks (black line, ---) obtained by applying Approaches IIIa, IIIb and IIIc are overlaid.

Once the baseline effects have been removed, for example with the exponential decay of Approaches Ib, IId and IIIb, the difference in the reliability of the deconvolution depends on the capability of the model to extract the correct peak shape of each enantiomer. This is possible if the experimental errors are random Gaussian and the peak shape is maintained identical to the individual peaks [22].

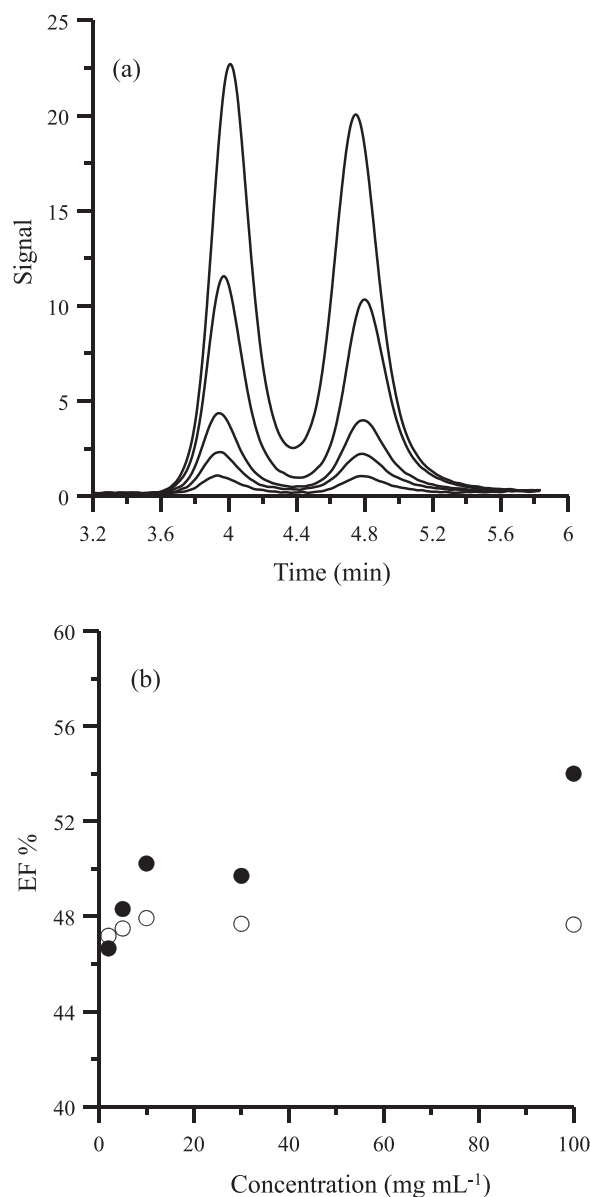


Fig. 3. (a) Deconvolution of KET4 data eluted at several concentrations: 2, 5, 10, 30 and 100 mg L⁻¹ (from bottom to top). (b) Enantiomeric fraction obtained with Approach IIIa (model PLMG) (●) and Approach IIIc (model PVMG) (○).

However, in the case of enantiomeric mixtures, the individual peak information is not easy to obtain.

We will first compare the stability of the two models that showed the best performance in the fitting of chromatographic peaks (PLMG and PVMG). In this study, both models were used to fit the overlapped peaks of KET4, for samples injected at different concentrations (2, 5, 10, 30 and 100 mg L⁻¹). In Fig. 3a, the experimental chromatograms are shown. With the information obtained in the deconvolution, the area of each peak was measured in order to calculate the enantiomeric fraction.

The deconvolution of the peaks for the chromatograms obtained at different concentrations should show the same enantiomeric fraction, since the peak shape is not expected to change. Fig. 3b compares the results obtained using Approaches IIIc (PVMG model) and IIIa (PLMG model) to fit the chromatograms. The plot shows the large stability in the values of enantiomeric fraction when the PVMG model was applied (i.e., the change in the calculated fraction for chromatograms at different concentrations was rather small).

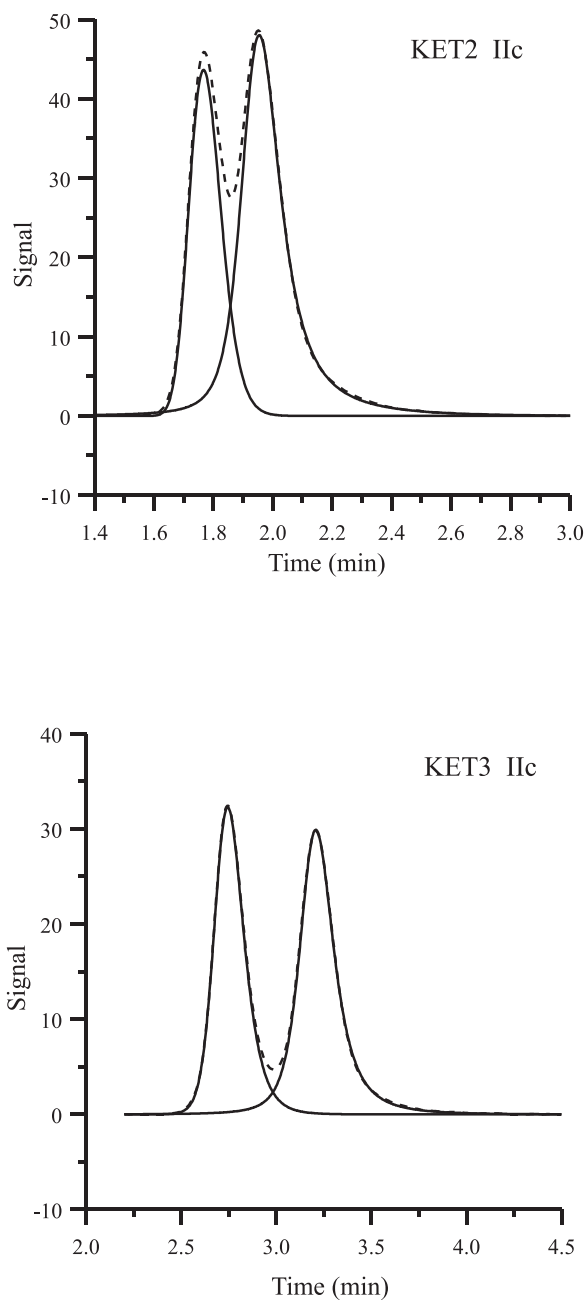


Fig. 4. Performance of the PVMG model in the fitting of the experimental signals of ketoprofen (KET2 and KET3) (dashed line - - -). Predicted peaks (black line, —) obtained by applying Approach IIc are overlaid.

Instead, the variation in the calculated enantiomeric fraction for the same chromatograms was appreciably larger for the PLMG model. This can be explained by the large uncertainties in the peak shapes with this model, and consequently, the larger errors in the deconvolution of the overlapped peaks. In contrast, both PVMG and PLMG models yielded good fitting of the chromatograms, resulting in similar total areas with a mean relative error of 0.3%. Therefore, it is evident that the PLMG model makes an incorrect distribution of the total area between the two individual peaks.

Finally, we considered interesting to study the behaviour of the PVMG model when it is applied to chromatograms containing overlapped peaks. Fig. 4 shows the chromatograms obtained for KET2 ($R_S = 0.73$) and KET3 ($R_S = 1.02$), together with the predicted individual peaks obtained with the PVMG model. It should be noted

that the evaluated enantiomeric fractions, using Approach IIc is 38.3% for KET2 and 46.4% for KET3, the latter being better resolved. As observed, peak 2 increased its width in KET2, incorporating part of the area of peak 1. This may be due to the variation in the width of one peak along the fitting iterations to compensate the decrease in the width of the other, to get a better fit. On the other hand, significant changes could occur in the individual peaks when eluted overlapped along the chiral column. For KET3, this effect was not observed owing to the better resolution.

This shows that the PVMG model does not yield reliable deconvolutions when all peak parameters are fitted and the resolution is poor (below $R_S = 1.0$ for the data set studied in this work). Further study should be done to overcome this problem, limiting the peak shape variation. For example, if we keep fixed the parameters of the PLMG model, except for t_R , H_0 , A and B , we would have a model with four parameters with a fairly stable peak shape as in Approach I. This can also be observed in Figs. S2 to S5 depicted in the Supplementary material. When the resolution is sufficient (1.19 and 1.38 for Figs. S2 and S5, respectively), all the approaches give similar EF values. However, in Figs. S3 and S4 with resolutions of 0.49 and 0.62, respectively, the variability is larger. Again, Approaches I (where only the shape parameters A and B are fitted) show greater similarity, and Approaches III (where five shape parameters are fitted, give rise to larger variability. Obviously, it is necessary to find ways to limit the peak shape with Approach III, without losing goodness of fit.

5. Conclusions

In this work, modifications of some modified Gaussian models are proposed and evaluated. We have seen that in order to obtain adequate results for overlapping peaks, it is necessary to restrict the models to set the peak shape in a proper way. The family of functions of modified Gaussian peaks allow the fitting of chromatographic peaks with a wide range of properties, from symmetric to highly asymmetric. The deconvolution of the components of a mixture of enantiomeric compounds, insufficiently resolved with a chiral column, is also possible. In this work, different approaches based on the LMG, PVMG and PLMG models were applied to fit a variety of peaks of enantiomeric compounds of eight drugs, separated with several chiral columns. The simplest function (LMG) provided satisfactory fittings only for sufficiently symmetric peaks. The PVMG function gave rise to adequate fittings for most peaks, being the model of choice for compounds eluted in the optimal conditions, when the peaks show conventional profiles. However, the best fittings were obtained with the PLMG model, although in some situations overfitting problems or unsatisfactory tails may arise. Even eliminating the tails by adding an exponential function, the overfitting did not disappear, which may be problematic for the deconvolution of overlapped peaks.

The application of exponential tails (Approaches Ib, IIb and IIIb) is an appropriate option to eliminate problems, but does not significantly improve the fittings. On the other hand, the LMG and PVMG models using a sigmoidal function to limit the growth of the temporal variable in the variance (Approaches Ic and IIc) provide acceptable results and are easier to apply.

We have observed that in order to obtain adequate results for overlapping peaks, it is necessary to restrict the models to set the peak shape. When the models are used without restrictions, they tend to overfitting, and transfer an area fraction from one peak to another if this yields a better fit. A more extensive study of the peak shape variations is necessary for poorly resolved enantiomers. Also, a procedure should be developed to keep the enantiomeric fraction constant in the deconvolution procedure, which will be the purpose of future work. The proposed models should be still tested when the enantiomeric fraction is far from racemic.

Declaration of Competing Interest

None

Acknowledgements

This work was supported by Projects CTQ2015-70904-R (Ministerio de Economía y Competitividad, Spain), CTQ2016-75644-P (Ministerio de Economía, Industria y Competitividad, Spain), and PID2019-106708GB-I00 (Ministerio de Ciencia, Innovación y Universidades), and FEDER funds, and PROMETEO/2016/128 (Direcció General d'Universitat, Investigació i Ciència, Generalitat Valenciana, Spain). Mireia Pérez-Baeza acknowledges Generalitat Valenciana and European Social Fund for the contribution to the pre-doctoral contract ACIF/2019/158.

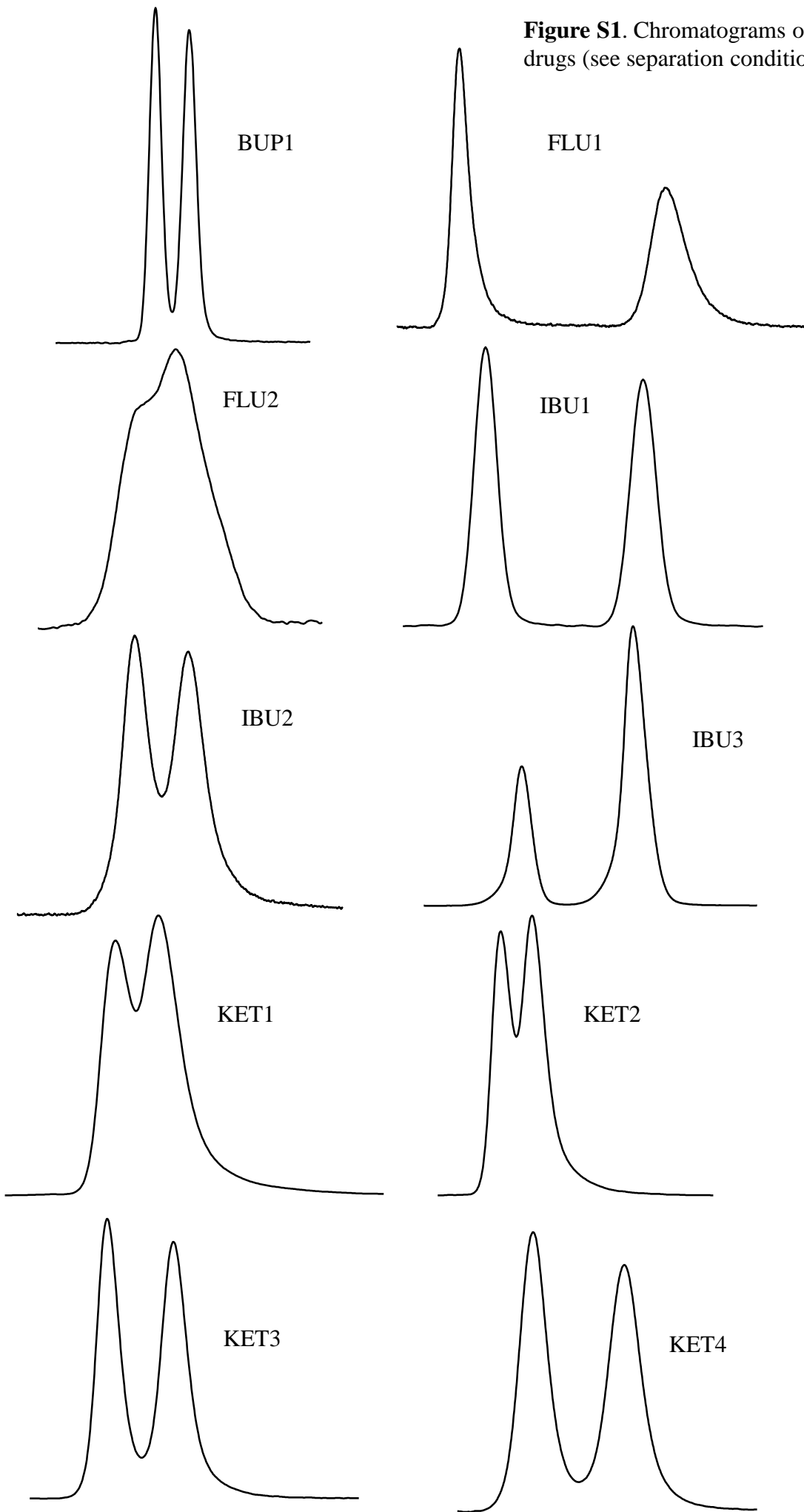
Supplementary materials

Supplementary material associated with this article can be found, in the online version, at [doi:10.1016/j.chroma.2020.461273](https://doi.org/10.1016/j.chroma.2020.461273).

References

- [1] M.C. García-Alvarez-Coque, J.R. Torres-Lapasió, J.J. Baeza-Baeza, Models and objective functions for the optimisation of selectivity in reversed-phase liquid chromatography, *Anal. Chim. Acta* 579 (2006) 125–145.
- [2] J.R. Torres-Lapasió, M.C. García-Alvarez-Coque, Levels in the interpretive optimisation of selectivity in high-performance liquid chromatography: a magical mystery tour, *J. Chromatogr. A* 1120 (2006) 308–321.
- [3] R. Cela, E.Y. Ordoñez, J.B. Quintana, R. Rodil, Chemometric-assisted method development in RPLC, *J. Chromatogr. A* 1287 (2013) 2–22.
- [4] A. Periat, D. Guillaume, J.L. Veuthey, J. Boccard, S. Moco, D. Barron, A. Grand-Guillaume-Perrenoud, optimized selection of liquid chromatography conditions for wide range analysis of natural compounds, *J. Chromatogr. A* 1504 (2017) 91–104.
- [5] J.A. Navarro-Huerta, E.J. Carrasco-Correa, J.R. Torres-Lapasió, J.M. Herrero-Martínez, M.C. García-Alvarez-Coque, Modelling retention and peak shape of small polar solutes analysed by nano-HPLC using methacrylate-based monolithic columns, *Anal. Chim. Acta* 1086 (2019) 142–155.
- [6] J.J. Baeza Baeza, M.C. García-Alvarez-Coque, Prediction of peak shape as a function of retention in reversed-phase liquid chromatography, *J. Chromatogr. A* 1022 (2004) 17–24.
- [7] J.J. Baeza-Baeza, C. Ortiz-Bolsico, M.C. García-Alvarez-Coque, New approaches based on modified Gaussian models for the prediction of chromatographic peaks, *Anal. Chim. Acta* 758 (2013) 36–44.
- [8] M.J. Ruiz-Angel, S. Carda-Broch, M.C. García-Alvarez-Coque, Peak half-width plots to study the effect of organic solvents on the peak performance of basic drugs in micellar liquid chromatography, *J. Chromatogr. A* 1217 (2010) 1786–1798.
- [9] J.J. Baeza-Baeza, M.J. Ruiz-Angel, M.C. García-Alvarez-Coque, S. Carda-Broch, Half-width plots, a simple tool to predict peak shape, reveal column kinetics and characterise chromatographic columns in liquid chromatography: state of the art and new results, *J. Chromatogr. A* 1314 (2013) 142–153.
- [10] E. Grushka, Characterization of exponentially modified Gaussian peaks in chromatography, *Anal. Chem.* 44 (1972) 1733–1738.
- [11] J.P. Foley, J.G. Dorsey, Equations for calculation of chromatographic figures of merit for ideal and skewed peaks, *Anal. Chem.* 55 (1983) 730–737.
- [12] J.P. Foley, Equations for chromatographic peak modeling and calculation of peak area, *Anal. Chem.* 59 (1987) 1984–1987.
- [13] J.R. Torres-Lapasió, J.J. Baeza-Baeza, M.C. García-Alvarez-Coque, A model for the description, simulation, and deconvolution of skewed chromatographic peaks, *Anal. Chem.* 69 (1997) 3822–3831.
- [14] P. Nikitas, A. Pappa-Louisi, A. Papageorgiou, On the equations describing chromatographic peaks and the problem of the deconvolution of overlapped peaks, *J. Chromatogr. A* 912 (2001) 13–29.
- [15] K. Lan, J.W. Jorgenson, A hybrid of exponential and Gaussian functions as a simple model of asymmetric chromatographic peaks, *J. Chromatogr. A* 915 (2001) 1–13.
- [16] V.B. Di Marco, G.G. Bombi, Mathematical functions for the representation of chromatographic peaks, *J. Chromatogr. A* 931 (2001) 1–30.
- [17] J. Li, Comparison of the capability of peak functions in describing real chromatographic peaks, *J. Chromatogr. A* 952 (2002) 63–70.
- [18] S.V. Romanenko, A.G. Stromberg, T.N. Pushkareva, Modeling of analytical peaks: peak properties and basic peak functions, *Anal. Chim. Acta* 580 (2006) 99–106.
- [19] edited by J.R. Torres-Lapasió, J.J. Baeza-Baeza, M.C. García-Alvarez-Coque, Modeling of peak shape and asymmetry, in *Chemometrics in Chromatography*, in: L. Komsta, Y. Vander Heyden, J. Sherma (Eds.), Vol. 111 de *Chromatographic Science Series*, CRC Press, Boca Raton, 2018, pp. 217–238. edited by FL.
- [20] J.P. Foley, J.G. Dorsey, Equations for calculation of chromatographic figures of merit for ideal and skewed peaks, *Anal. Chem.* 55 (1983) 730–737.
- [21] J.P. Foley, J.G. Dorsey, A review of the exponentially modified Gaussian (EMG) function: evaluation and subsequent calculation of universal data, *J. Chromatogr. Sci.* 22 (1984) 40–46.
- [22] R.D. Caballero, M.C. García-Alvarez-Coque, J.J. Baeza-Baeza, Parabolic-Lorentzian modified Gaussian model for describing and deconvolving chromatographic peaks, *J. Chromatogr. A* 954 (2002) 59–76.
- [23] P.G. Stevenson, F. Gritti, G. Guiochon, Automated methods for the location of the boundaries of chromatographic peaks, *J. Chromatogr. A* 1218 (2011) 8255–8263.
- [24] Lien Ai Nguyen, Hua He, Chuong Pham-Huy, chiral drugs: an overview, *Int. J. Biomed. Sci.* 2 (2006) 85–100.
- [25] A.R. Ribeiro, L.H.M.L.M. Santos, A.S. Maia, C. Delerue-Matos, P.M.L. Castro, M.E. Tiritan, Enantiomeric fraction evaluation of pharmaceuticals in environmental matrices by liquid chromatography-tandem mass spectrometry, *J. Chromatogr. A* 1363 (2014) 226–235.
- [26] L. Escuder-Gilabert, Y. Martín-Biosca, M. Pérez-Baeza, S. Sagrado, M.J. Medina-Hernández, Direct chromatographic study of the enantioselective biodegradation of ibuprofen and ketoprofen by an activated sludge, *J. Chromatogr. A* 1568 (2018) 140–148.

Figure S1. Chromatograms of the studied chiral drugs (see separation conditions in Table 1).



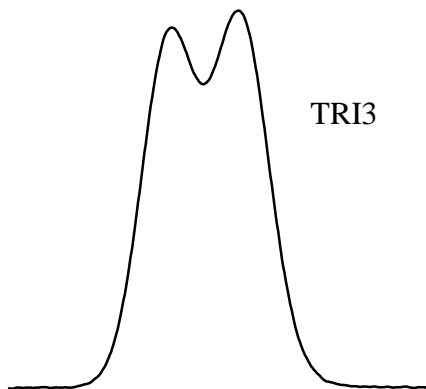
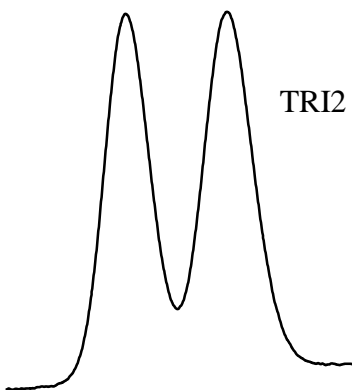
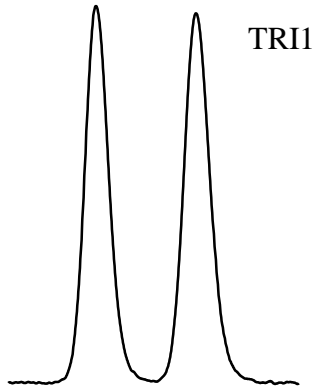
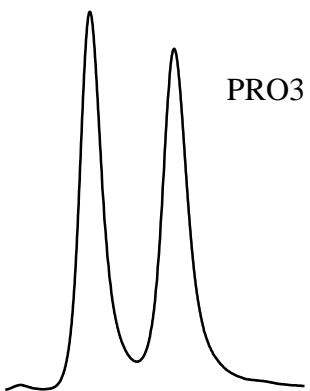
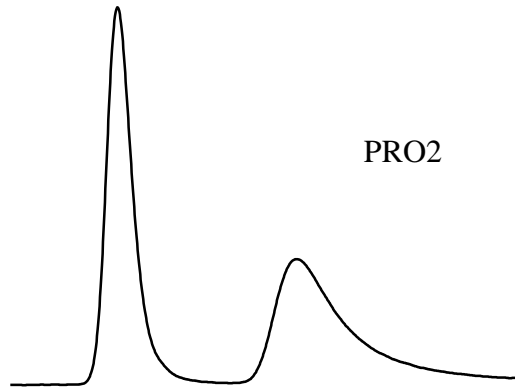
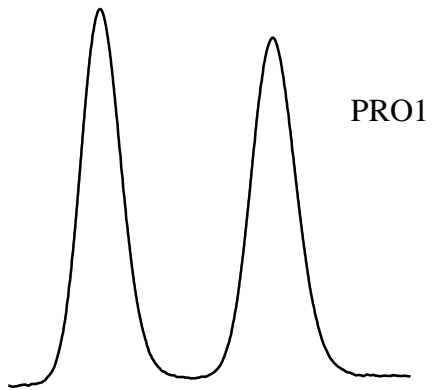
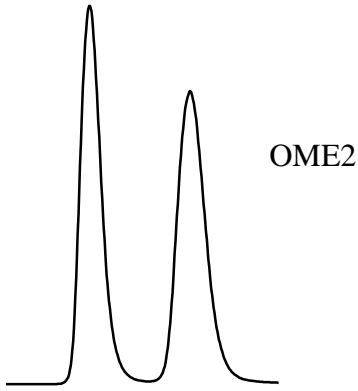
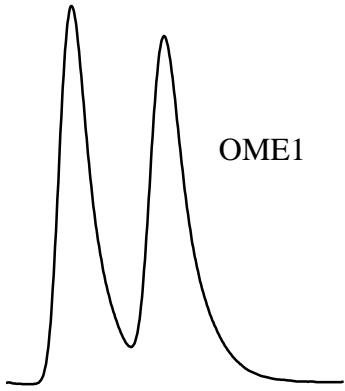
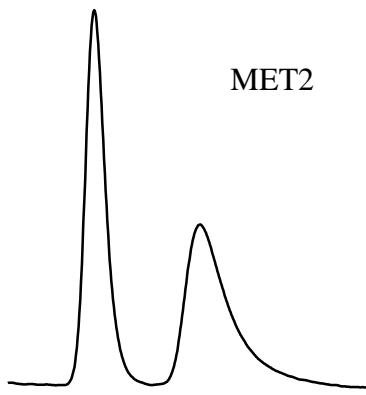
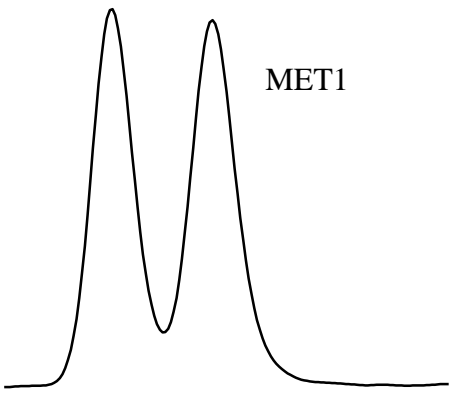


Figure S2. Chromatographic peaks for bupivacaine (BUP1). Experimental (\circ), predicted (dashed line, ---) and individual peaks (black line, —)

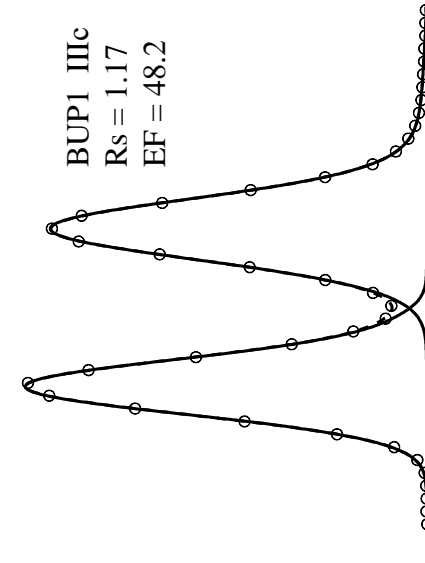
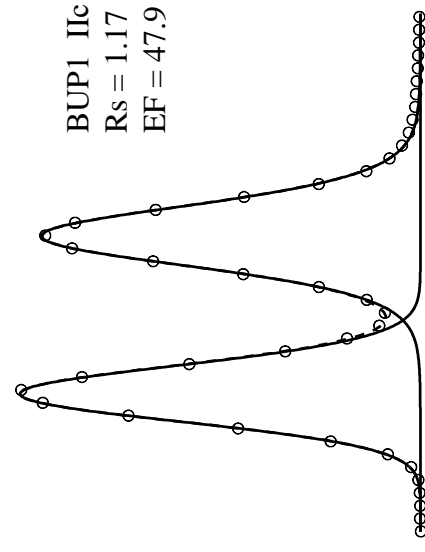
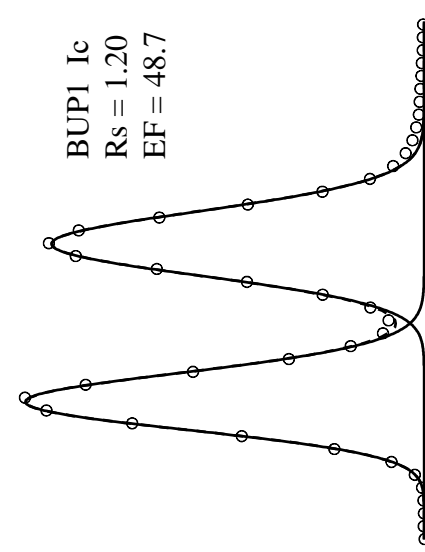
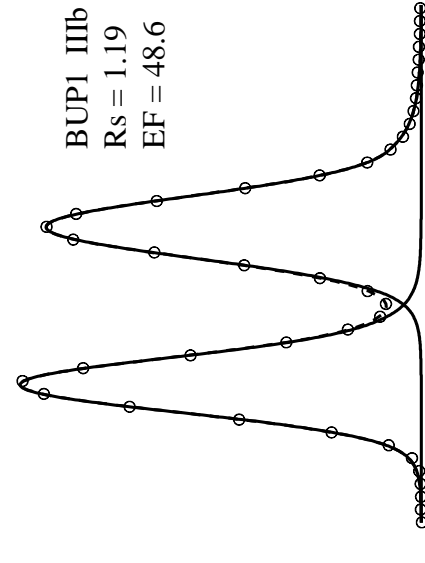
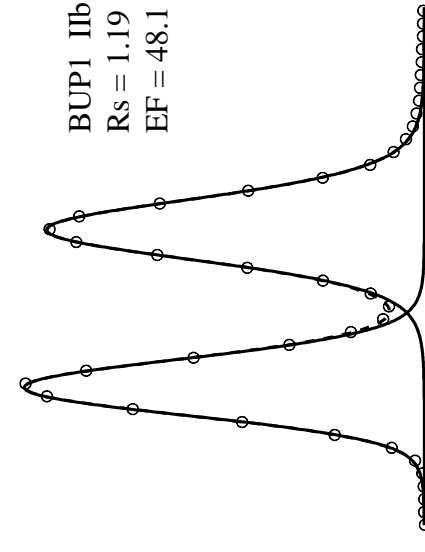
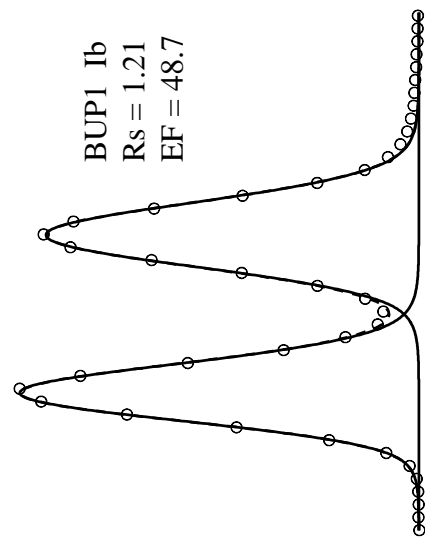
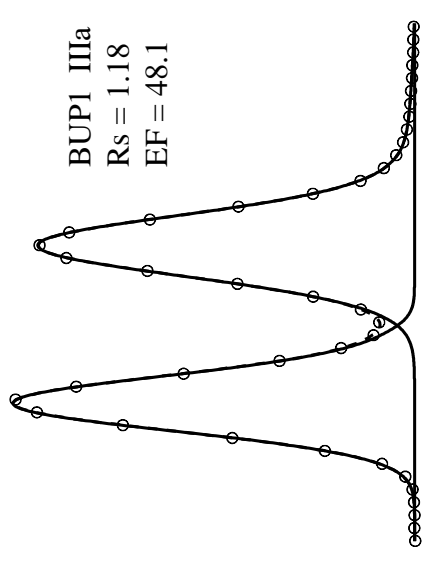
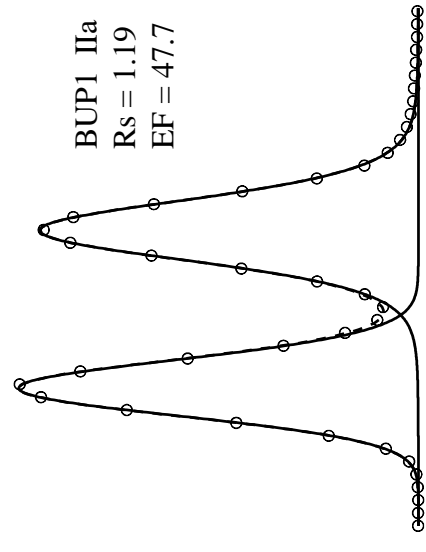
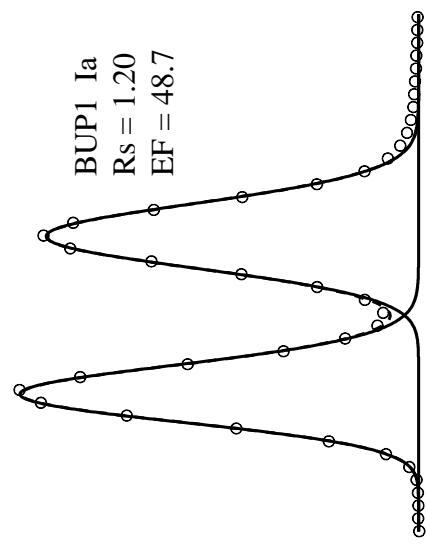


Figure S3. Chromatographic peaks for flurbiprofen (FLU2). Experimental (○), predicted (dashed line, - - -) and individual peaks (black line, —)

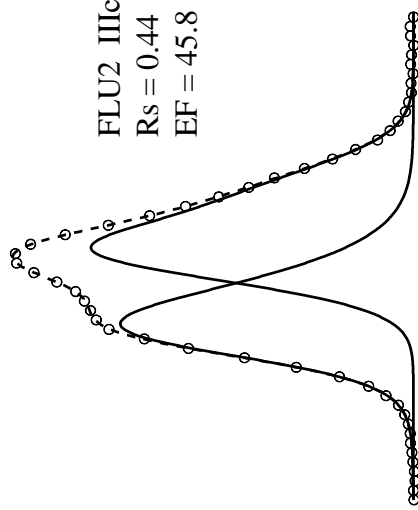
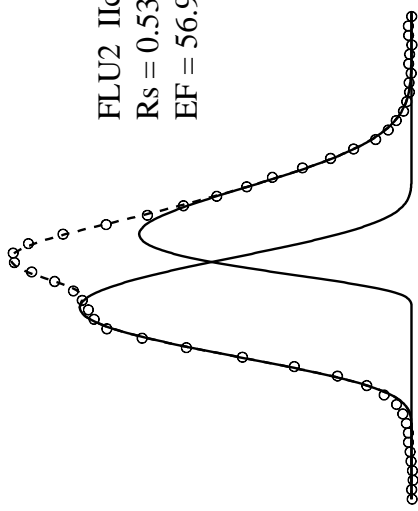
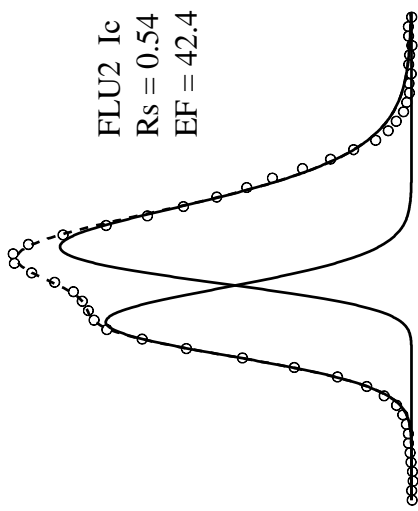
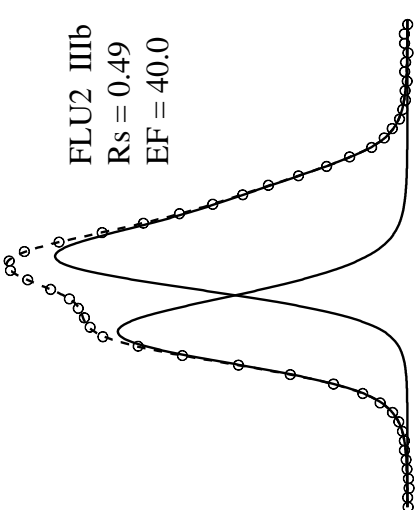
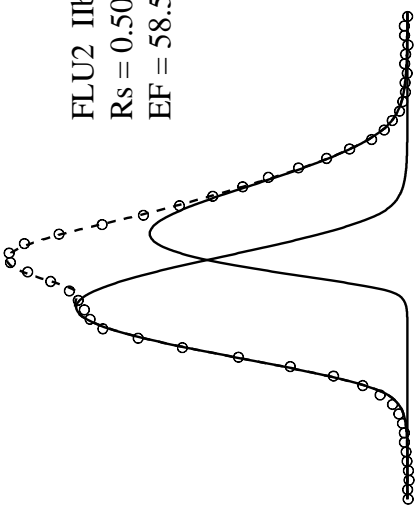
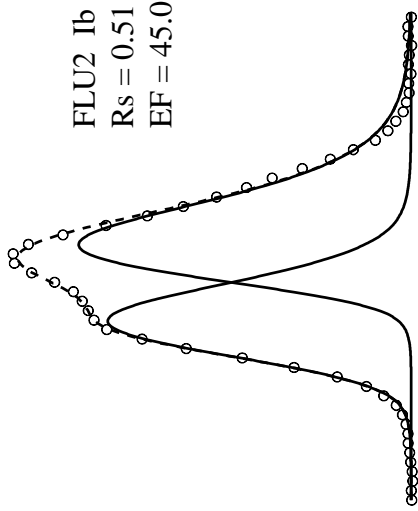
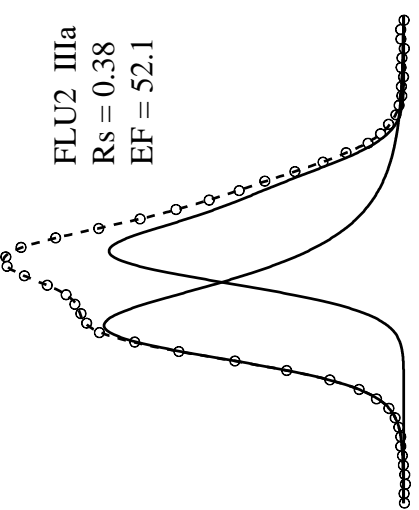
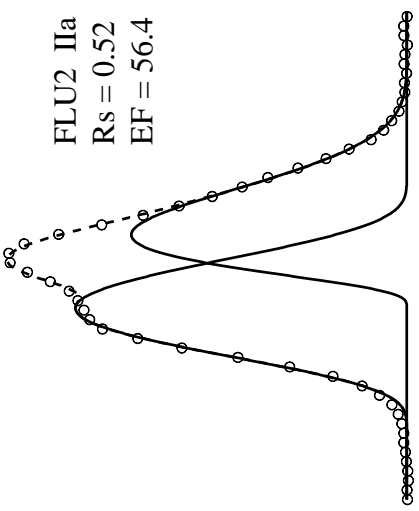
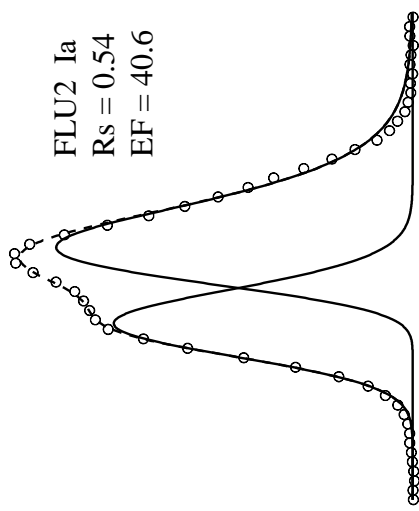


Figure S4. Chromatographic peaks for ketoprofen (KET1). Experimental (\circ), predicted (dashed line, ---) and individual peaks (black line, —)

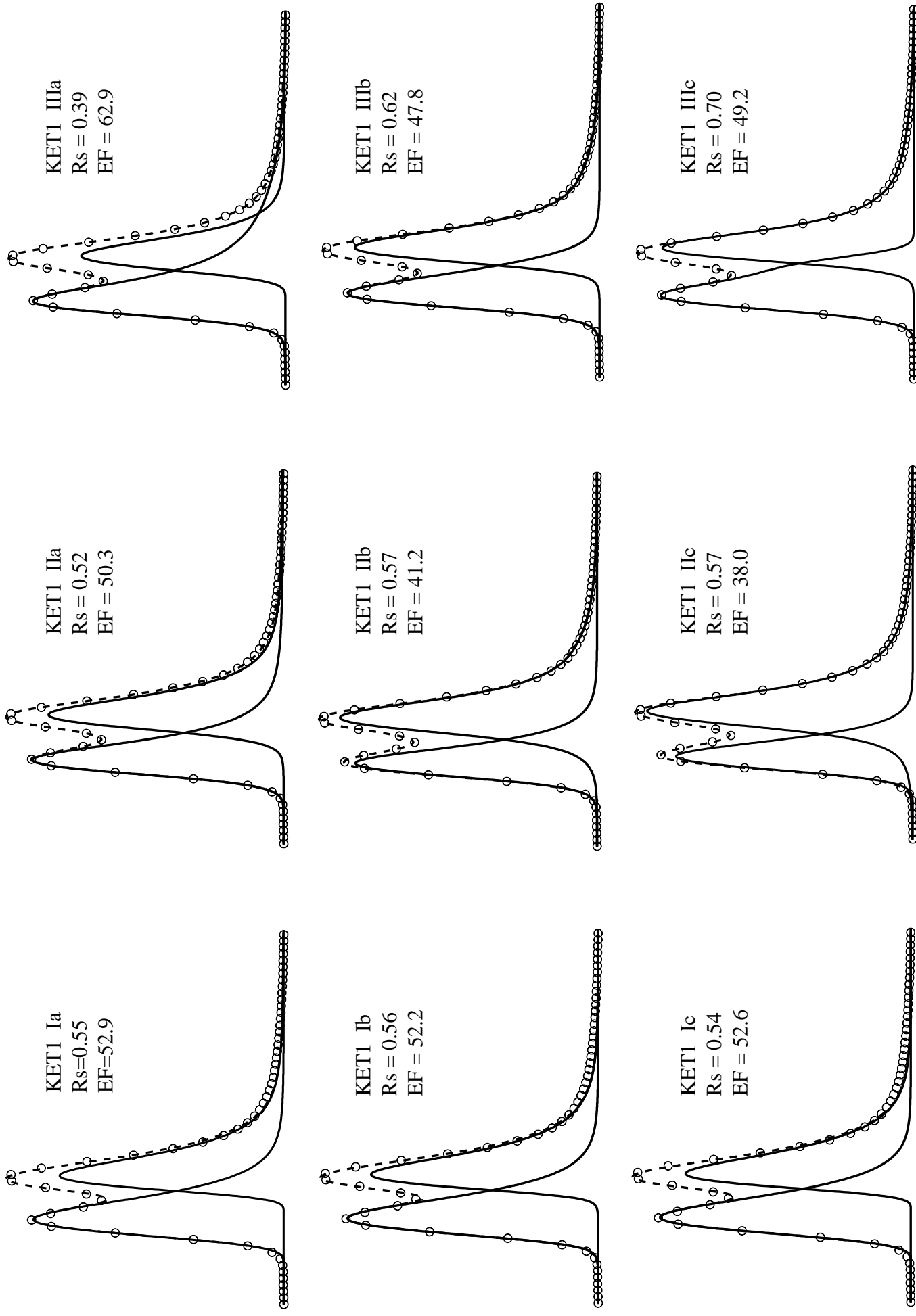
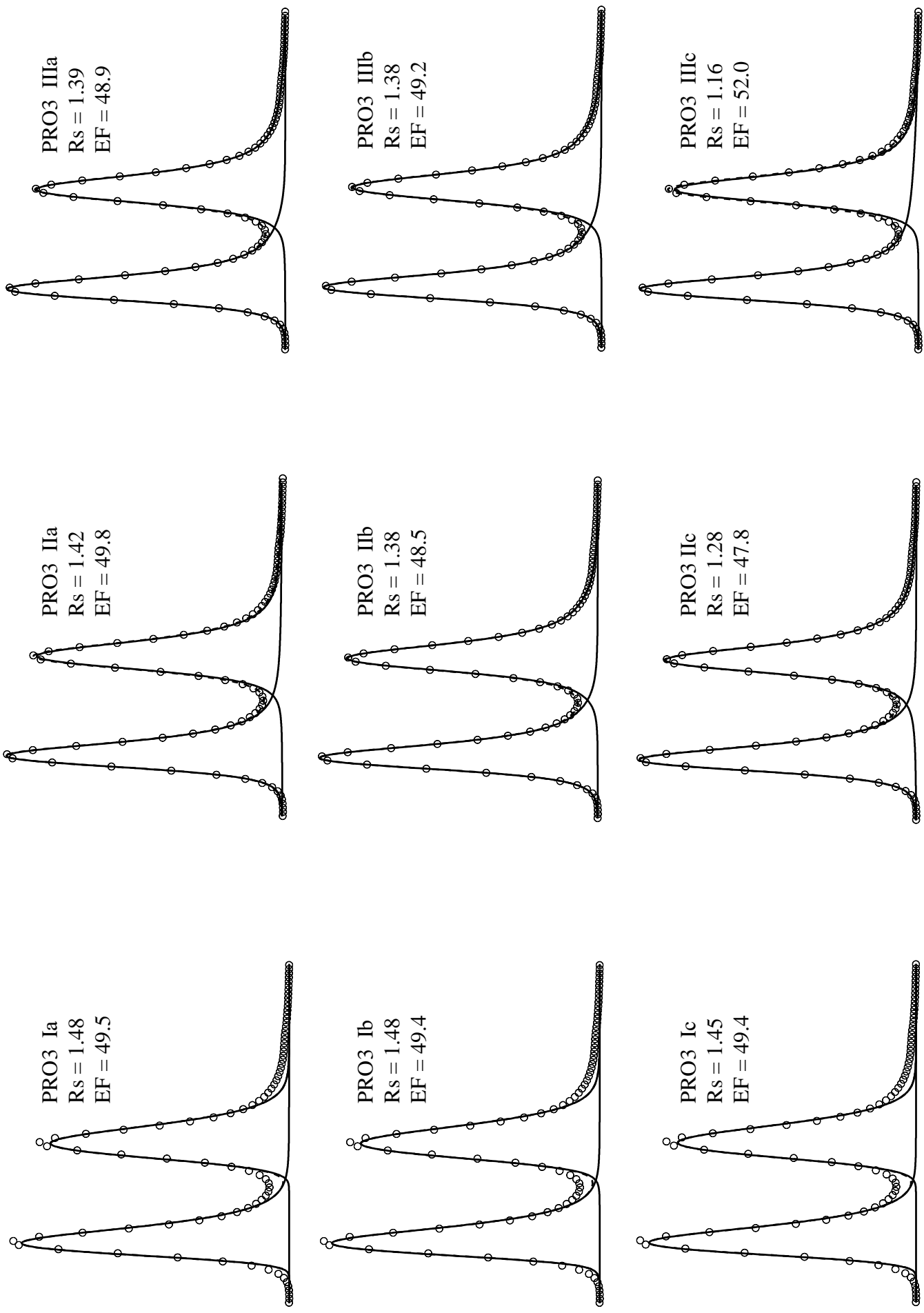


Figure S5. Chromatographic peaks for propranolol (PRO3). Experimental (○), predicted (dashed line, - - -) and individual peaks (black line, —)





PAPER V

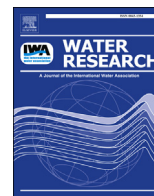
**Trimeprazine is enantioselectively degraded by an
activated sludge in ready biodegradability test
conditions**

**Laura Escuder-Gilabert^a, Yolanda Martín-Biosca^a, Mireia Perez-Baeza^a,
Salvador Sagrado^{a,b}, María José Medina-Hernández^a**

^a Departamento de Química Analítica, Universitat de València, Burjassot, Valencia, Spain

^b Instituto Interuniversitario de Investigación de Reconocimiento Molecular y Desarrollo Tecnológico (IDM), Universitat Politècnica de València, Universitat de València, Valencia, Spain

Water Research 141 (2018) 57-64



Trimeprazine is enantioselectively degraded by an activated sludge in ready biodegradability test conditions

Laura Escuder-Gilabert ^a, Yolanda Martín-Biosca ^{a, **}, Mireia Perez-Baeza ^a, Salvador Sagrado ^{a, b}, María José Medina-Hernández ^{a, *}

^a Departamento de Química Analítica, Universitat de València, Burjassot, Valencia, Spain

^b Instituto Interuniversitario de Investigación de Reconocimiento Molecular y Desarrollo Tecnológico (IDM), Universitat Politècnica de València, Universitat de València, Burjassot, Valencia, Spain

ARTICLE INFO

Article history:

Received 22 December 2017
Received in revised form
2 May 2018
Accepted 5 May 2018
Available online 9 May 2018

Keywords:

Biodegradability test
Batch experiment
Enantioselectivity
Trimeprazine
Curve fitting
Precision

ABSTRACT

A great number of available pharmaceuticals are chiral compounds. Although they are usually manufactured as racemic mixtures, they can be enantioselectively biodegraded as a result of microbial processes. In this paper, a biodegradability assay in similar conditions to those recommended in OECD tests of enantiomers of trimeprazine (a phenothiazine employed as a racemate) is carried out. Experiments were performed in batch mode using a minimal salts medium inoculated with an activated sludge (collected from a Valencian Waste Water Treatment Plant, WWTP) and supplemented with the racemate. The concentration of the enantiomers of trimeprazine were monitored by means of a chiral HPLC method using a cellulose-based chiral stationary phase and 0.5 M NaClO₄/acetonitrile (60:40, v/v) mobile phases. Experiments were performed at three concentration levels of the racemate. In parallel, the optical density at 600 nm (OD₆₀₀) was measured to control the biomass growth and to connect it with enantioselectivity. The calculated enantiomeric fractions (EF) offer the first evidence of enantioselective biodegradation of trimeprazine. A simplified Monod equation was used as a curve fitting approach for concentration (S), biodegradation (BD), and for the first time, EF experimental data in order to expand the usefulness of the results. Precision studies on S (repeatability conditions) and, for the first time, EF (intermediate precision conditions) were also performed.

© 2018 Elsevier Ltd. All rights reserved.

1. Introduction

Among emerging pollutants, drugs are probably the main concern of regulatory authorities due to their huge consume. Drugs, their metabolites and their degradation products could reach the environment mainly due to poor removal rates in Waste Water Treatment Plants (WWTP), and by improper disposal of unused medicines (Kümmerer, 2009). The presence of these compounds in the environment has been extensively reported (Petrie et al., 2015; Geissen et al., 2015; Ebele et al., 2017; Sanganyado et al., 2017). However, although the great efforts made by regulatory authorities

and scientific community, not much is known about the impact of this kind of compounds on the environment and human health (Wong, 2006; Stanley et al., 2006, 2007; Kasprzyk-Hordern, 2010; Ribeiro et al., 2012).

A great number of currently available drugs are chiral compounds and many of these are marketed as racemates. Enantiomers have different interactions with physiological chiral molecules leading to different biological responses that affect living organisms in different ways. The enantioselectivity in ecotoxicity and biodegradation processes is evident and comparable to the events in medical/biomedical fields (Kasprzyk-Hordern, 2010; Ribeiro et al., 2014a).

The biodegradability, defined as the capacity of a molecule to be degraded by microorganisms forming more simple final products, is an essential parameter to know the risk that involves the dispersion of a compound into the environment. This property depends on the chemical structure of the compound as well as on the physicochemical conditions under which the degradation

* Corresponding author. Departamento de Química Analítica, Facultat de Farmàcia, Universitat de València, Avda. Vicent Andrés Estellés, s/n, E-46100 Burjassot, Valencia, Spain.

** Corresponding author.

E-mail addresses: yolanda.martin@uv.es (Y. Martín-Biosca), maria.j.medina@uv.es (M.J. Medina-Hernández).

process takes place. Biodegradability assays are designed to test a chemical substance as the sole carbon source in a mixed inoculum (Thouand, 2014). The OECD tests for ready biodegradability have been devised as screening methods to determine whether a chemical is potentially easily biodegradable, which contribute to gain knowledge in the field of water and environmental research. There are evidences of enantioselective biodegradation of chiral compounds in the environment. The quantification of the enantiomeric fractions (EF) during the biodegradation process is of key importance to evaluate the health and environmental risk. However, there is not much research done on this subject.

Some studies have been focused on the EF evaluation directly in wastewaters. They involve drugs of abuse and pharmaceuticals (Vázquez-Roig et al., 2014; Kasprzyk-Hordem and Baker, 2012), amphetamines (Evans et al., 2016) and seven selected chiral pharmaceuticals in WWTP influents and effluents (Ribeiro et al., 2014b). Other approaches have been based on *in vitro* biodegradability assays. They simulate the degradation processes of chemicals in soils, surface waters or in activated sludge, generally in the presence of oxygen (Kowalczyk et al., 2015). The subsequent separation and determination of the individual enantiomers of the original compound (or its metabolites) in the test solution by analytical techniques, mainly liquid chromatography, allow the estimation of EF. Using this laboratory scale methodology, enantioselective evaluation of biodegradation for fluoxetine and norfluoxetine (Ribeiro et al., 2014b; Moreira et al., 2014), amphetamine based compounds (Evans et al., 2016; Bagnall et al., 2013), atenolol, metoprolol and fluoxetine (Ribeiro et al., 2013a), alprenolol and propranolol (Ribeiro et al., 2013b) and venlafaxine (Li et al., 2013) have been reported. Recently, S. Evans et al. reported an enantioselective biodegradation study involving chiral pharmaceuticals (amphetamines, beta-blockers and antidepressants) (Evans et al., 2017).

Trimeprazine or alimemazine is a tricyclic antihistamine, similar in structure to the phenothiazine antipsychotics, but differing in the ring-substitution and chain characteristics. Trimeprazine is not used clinically as an anti-psychotic. It is used principally as an antiemetic, to prevent motion sickness, or as an anti-histamine in combination with other medications in cough and cold preparations. Trimeprazine is largely used as antipruritic agent, but also for insomnia and oral premedication in paediatric day surgery (Drug Information Portal, 2017).

In this paper, the enantioselective biodegradation of trimeprazine enantiomers is studied by means of a biodegradability assay in similar conditions to those recommended in OECD tests. For this purpose, experiments at three concentration levels of racemic trimeprazine are performed in batch conditions using an activated sludge inoculum from a local WWTP. A RPLC method for chiral separation of trimeprazine enantiomers is developed. In the literature, some references about the chiral separation of enantiomers of trimeprazine using electrophoretic (Lin et al., 2005; Martínez-Gómez et al., 2007) and liquid chromatographic methods using chiral stationary phases (Van Overbeke et al., 1997; Oguni et al., 1995; Sanchez et al., 2012) have been reported. Complete separations of enantiomers of trimeprazine have been obtained using a α_1 -glycoprotein (AGP) column and hydroorganic mobile phases containing 20 mM phosphate buffer pH 3.5:2-propanol 99:1 (v/v) (Sanchez et al., 2012); a cellulose tris(3,5-dimethylphenylcarbamate) (Chiralcel OD-R) stationary phase and mobile phases containing 0.1 M sodium hexafluorophosphate: acetonitrile 60:40 (v/v) (Oguni et al., 1995) and a cellulose tris(4-methylbenzoate) (Chiralcel OJ-R) stationary phase and mobile phases containing 1 M sodium chlorate: acetonitrile: methanol 40:15:45 (v/v) (Van Overbeke et al., 1997).

To the best of our knowledge, neither biodegradation nor

enantioselective biodegradation for trimeprazine has been reported in the literature. Thus, one aim of this work is to provide the first evidence of enantioselective biodegradation of this emergent contaminant. Additional objectives are: (i) to connect the enantioselective biodegradation with the microbial growth; (ii) to apply a curve fitting approach for concentration, biodegradation, and also for the first time, enantiomeric fraction data over time in order to expand the usefulness of the results; (iii) to perform a precision study on S and EF data and, for the first time, under intermediate precision conditions.

2. Material and methods

2.1. Instrumentation

An Agilent Technologies 1100 chromatograph (Palo Alto, CA, USA) with a quaternary pump, a UV-visible variable wavelength detector, a column thermostat and an autosampler was used. Data acquisition and processing were performed by means of the Chemstation software (A.09.03 [1417], ©Agilent Technologies 1990–2002). For the determination of the enantiomers of trimeprazine, several polysaccharide-based chiral stationary phases were tested: Chiralart Cellulose-SC (cellulose tris(3,5-dichlorophenylcarbamate); 3 μ m, 150 \times 4.6 mm i.d.; YMC Separation Technology Co., Ltd., Tokyo, Japan); Lux Cellulose-1 (cellulose tris(3,5-dimethylphenylcarbamate); 3 μ m, 150 \times 4.6 mm i.d.; Phenomenex, Torrance, CA, USA); Lux Cellulose-3 (cellulose tris(4-methylbenzoate); 3 μ m, 150 \times 4.6 mm i.d.; Phenomenex, Torrance, CA, USA) and Lux Amylose-2 (amylose tris(5-chloro-2-methylphenylcarbamate); 3 μ m, 150 \times 2.0 mm i.d.; Phenomenex). The mobile phases flow rate was 1.0 mL min⁻¹ in all cases except when using the Lux Amylose-2. In this last column the mobile phases flow rate was 0.4 mL min⁻¹. The injection volume was 2 μ L, the detection was performed in the UV at 254 nm. The columns were thermostatted at 25 °C.

For samples mixtures preparation, 15 mL conical sterile polypropylene tubes (Deltalab, S.L., Barcelona, Spain) were used. Disposable sterile filter pipette tips (Capp Expell, Odense, Denmark) were also used. For the biodegradability assays, a shaking incubator with temperature control (WiseCube® Wis-30, Witeg Labortechnik GmbH, Wetheim, Germany) was used. Prior to the measurement of the microbial growth, incubated samples were subjected to agitation in a vortex mixer (Velp Scientific Vortex, Usmate, Italy). Microbial growth was monitored by measuring the optical density (OD) of the cultures at 600 nm with an Epoch 2 microplate reader (Biotek Instruments Inc., Vermont, USA) and 96-well plates with UV transparent flat bottom (Corning, Kennebunk, ME, USA). Samples were stored at -80 °C in an ultra-low temperature freezer (U570 Premium, New Brunswick Scientific, Herts, UK) until chromatographic analysis.

Prior to injection into the chromatographic system, samples were centrifuged (Hettich Lab Technology, EBA 20, Tuttlingen, Germany) and filtered through disposable 0.22 μ m polyethersulphone syringe filters (Frisenette, Knebel, Denmark). Mobile phase solutions were vacuum-filtered through 0.22 μ m Nylon membranes (Micron Separations, Westboro, MA, USA) and were degassed in an Elmasonic S60 ultrasonic bath (Elma, Singen, Germany) prior to use. A Crison MicropH 2000 pHmeter (Crison Instruments, Barcelona, Spain) was employed to adjust the pH of the buffer solutions.

2.2. Chemicals and solutions

All reagents were of analytical grade. Ammonium acetate, hydrochloric acid (37%), sodium hydroxide, sodium perchlorate

monohydrate, acetonitrile and methanol ([®]Multisolvent, HPLC grade) were from Scharlau, S.L. (Barcelona, Spain). Ammonium formate, diethylamine and potassium hexafluorophosphate were from Acros Organics (Geel, Belgium).

Ultra Clear TWF UV deionized water (SG Water, Barsbüttel, Germany) was used to prepare solutions. Different solutions were tested for the preparation of the mobile phases. Ammonium acetate buffer (10 mM, pH 8.0) was prepared in the same way from ammonium acetate. 100 mM hexafluorophosphate and 500 mM perchlorate solutions were prepared by dissolving in water the appropriate amount of potassium hexafluorophosphate and sodium perchlorate monohydrate, respectively. The mobile phases were prepared by mixing aqueous or buffer solutions with the tested organic modifier to obtain the working concentration.

The minimal salts medium (MSM) solution used in the biodegradability assays was prepared with the following composition per liter (Ribeiro et al., 2013a; b): 2.1 g Na₂HPO₄ (Panreac Química, S.A., Barcelona, Spain); 1.4 g KH₂PO₄ (Panreac); 0.2 g MgSO₄·7H₂O (Scharlau Chemie S.A., Barcelona, Spain); 0.5 g (NH₄)₂SO₄ (Scharlau), and 10 mL of a trace elements solution with the following composition per liter: 2.0 g NaOH (Scharlau); 12.0 g Na₂EDTA₂·2H₂O (Scharlau); 1.4 g FeSO₄·2H₂O (Panreac); 1.3 g CaCl₂·2H₂O (Panreac); 10 g Na₂SO₄ (Panreac); 0.7 g ZnSO₄·7H₂O (Merck, Darmstadt, Germany); 0.3 g MnSO₄·H₂O (Panreac); 0.1 g CuSO₄·5H₂O (Merck); 0.1 g Na₂MoO₄·2H₂O (Merck); 0.5 mL H₂SO₄ (98%) (Scharlau).

The activated sludge sample was kindly donated by General de Análisis Materiales y Servicios, S.L (GAMASER, S.L., Valencia, Spain), a laboratory and inspection entity of the Group “Aguas de Valencia”. They were obtained from the aerated tanks of a municipal WWTP (Quart Benàger, Valencia, Spain), which receives domestic, agricultural, livestock and industrial wastewater from eight Valencian towns with a surface area of 164,171 ha and a population of approximately 1 million. Its average flow rate is 30,318 m³/day. The plant operates on activated sludge/nitrification/phosphorous removal process (where phosphate is biologically removed), with a hydraulic retention time of 24 h. The activated sludge sample was collected in plastic flasks and stored at 4 °C until usage.

Trimeprazine hemi (+)-tartrate was from Sigma (St. Louis, MO, USA). Stock standard solutions of 1000 mg L⁻¹ of *rac*-trimeprazine were prepared by dissolving the adequate amount of the compound in methanol. To prepare the calibration standards, an intermediate stock solution of 100 mg L⁻¹ of *rac*-trimeprazine was prepared by dilution of the corresponding 1000 mg L⁻¹ stock solution in the MSM. Calibration solutions of approximately 2, 5, 10, 20 and 30 mg L⁻¹ were prepared by dilution of the intermediate stock solution of 100 mg L⁻¹ in the MSM. For the biodegradability assays, working solutions of approximately 5, 10 and 20 mg L⁻¹ of *rac*-trimeprazine were prepared by dilution of the 1000 mg L⁻¹ stock solution in the MSM. The solutions were stored under refrigeration at 5 °C.

2.3. HPLC method

The enantiomers of trimeprazine were separated using the Lux Cellulose-1 column. The optimized mobile phase was 500 mM sodium perchlorate/acetonitrile (60:40, v/v). In both cases, the separation temperature was set at 25 °C and the mobile phase flow rate was 1.0 mL min⁻¹.

2.4. Biodegradability assays

The biodegradability assays for the enantiomers of trimeprazine were performed in batch mode at three concentration levels (4.8, 9 and 18 mg L⁻¹ of *rac*-trimeprazine in the incubation tubes). For the

preparation of the samples mixtures, 15 mL uncovered sterile tubes were used. Samples mixtures containing 3000 µL of the corresponding working solution of *rac*-trimeprazine inoculated with 100 µL of the activated sludge (total sample volume of 3100 µL) were prepared. Independent samples were prepared for each concentration level and each incubation time studied. All experiments were done in duplicate, using tubes of a volume five-fold superior to guarantee the aeration of the cultures. The samples were incubated on a shaking incubator (150 rpm) at 20 °C under natural light cycles. At ten prefixed incubation times (0, 1, 2, 3, 4, 7, 10, 14, 18 and 23 days), two test tubes of each concentration level were taken, and when necessary to compensate solvent evaporation ultrapure water was added to get a total volume of 3100 µL. Then, mixtures were vortex mixed for 20 s and an aliquot of 200 µL of each tube was taken to measure the OD of the cultures at 600 nm. After OD measurement, samples were frozen at -80 °C until HPLC analysis (described in section 2.3). Abiotic degradation of the enantiomers of trimeprazine was evaluated using 100 µL of ultrapure water instead of the activated sludge inoculum, under the same conditions as samples. Prior to HPLC analysis, the samples were centrifuged at 6000 rpm for 15 min and the supernatant was filtered. Experimental conditions used (i.e., trimeprazine concentration and volume of inoculum) were chosen according to OECD guidelines (OECD, 1992).

2.5. Precision studies

Precision statistics considering repeatability and intermediate precision conditions (including the factor time) were used according to an approach described elsewhere (Bonet-Domingo et al., 2006; Maroto et al., 1999). Duplicated results obtained from biotic assays were organized in a matrix X_{NrXNs}, where Nr are the number of replicates (Nr = 2) and Ns are the number of series or ‘runs’ (in this case, incubation times). The approach analyses the X_{NrXNs} data matrix by means of analysis of variance (ANOVA). From the residual mean square (MS_r) and the between-run mean square (MS_{run}), the repeatability standard deviation (s_r), between-run standard deviation (s_{run}) and standard deviation of the run mean or grand mean (s_{mean}), can be calculated using the following equations (Eqs. (1)–(3)):

$$s_r^2 = MS_r \quad (1)$$

$$s_{run}^2 = \frac{(MS_{run} - MS_r)}{Nr} \quad (2)$$

$$s_{mean}^2 = \frac{MS_{run}}{Nr} \quad (3)$$

2.6. Biodegradation kinetics

Common biodegradation models proposed in the literature (the nonlinear Monod equation and its simplified version, the Michaelis-Menten-like equation) are unreliable approaches in terms of kinetic parameters accuracy. This is due to the linear parameter correlation (Robinson and Tiedje, 1983; Liu and Zachara, 2001). This is particularly evident for imprecise data, low substrate concentration (S) and few incubation times (t). Despite this, both Monod and Michaelis-Menten-like equations often provide good fit between the model (S vs. t fitted curve) and the experimental data (S vs. t experimental data; discrete points), even with wrong estimates. The aim in this work is not to estimate kinetic parameters (that anyway could be unreliable), but to be able to model the

substrate concentration vs. time (S vs. t) experimental data in order to approach biodegradation vs. time (BD vs. t) or the enantiomeric fraction vs. time (EF vs. t) fitted curves. The Michaelis Menten-like equation does not account to the biomass concentration and the microbial yield coefficient, necessary for the Monod equation. Thus, this equation was used as a simplified Monod model in this work (Eq. (4)).

$$\frac{dS}{dt} \sim \left(-\frac{V_m S}{K_s + S} \right) \quad (4)$$

Where V_m approaches is the maximum specific growth rate and K_s approaches the half saturation constant for growth. In the simplified approach, V_m is assumed constant (strictly speaking it depends on the biomass concentration, which in general varies with t). An explicit solution for Eq. (4) can be written (Goudar and Strevelt, 2000), based on the Lambert W function (S as a function of the time, t ; $S = W\{t\}$; (Corless et al., 1993)):

$$S = K_s \cdot W \left\{ \frac{S_0}{K_s} e^{\left(\frac{S_0 - V_m \cdot t}{K_s} \right)} \right\} + \text{offset} \quad (5)$$

Where S_0 is the initial concentration of the compound. Eq. (5) could provide estimations of V_m and K_s by nonlinear parameter estimation. If degradation profiles do not reach zero, an offset term can be considered for fitting the function to the experimental data (Her et al., 2015).

2.7. Software and data processing

For curve fitting purposes, the NLINFIT.m function in MATLAB® R2016b (MathWorks, Natick, Massachusetts) has been used. It estimates the coefficients of a nonlinear regression function using iterative least squares estimation. Algorithmic details of the explicit Lambert W function (Eq. (5)) can be found in (Her et al., 2015).

3. Results and discussion

3.1. Chiral chromatographic analysis

For the separation of enantiomers of trimeprazine, different polysaccharides stationary phases Chiralart Cellulose-SC, Lux Cellulose-1, Lux Cellulose-3 and Lux Amylose-2 were assayed (see experimental section). Using an ammonium acetate pH 8/acetonitrile (40:60) + 0.1% diethylamine mobile phase, only partial resolution of trimeprazine enantiomers were obtained using/with Chiralart Cellulose-SC and Lux Cellulose-1 stationary phases (R_s values of 0.5 and 0.3, respectively). Using these columns, different chaotropic agents, like potassium hexafluorophosphate and sodium perchlorate solutions, were assayed. The use of 100 mM potassium hexafluorophosphate and acetonitrile 60:40 (v:v) mobile phases did not provide the separation of trimeprazine enantiomers in spite of the results reported by Oguni and coworkers using a stationary phase similar to Lux Cellulose-1 (Oguni et al. 1995). Adequate resolution value ($R_s = 2.2$) and retention times (13.6 and 14.8 min for the first (E1) and the second (E2) eluted enantiomers, respectively) for the enantiomers of trimeprazine were obtained using a Lux Cellulose-1 column as stationary phase and a 500 mM sodium perchlorate/acetonitrile (60:40, v/v) mobile phase (See Fig. 1).

Using these experimental conditions, a concentration value of 1 mg L^{-1} of racemic trimeprazine (0.5 mg L^{-1} of each enantiomer) was considered the limit of quantification. Peak areas below this concentration level were too low for quantification purposes; i.e.

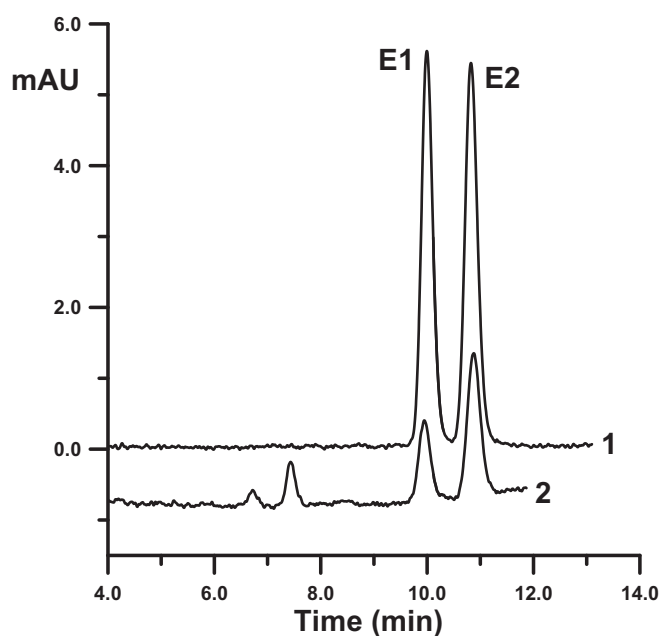


Fig. 1. Chromatograms corresponding to a sample solution containing 9 mg L^{-1} of trimeprazine, after 0 (curve 1) and 18 days of incubation (curve 2). E1 and E2 refer to the first and second eluting enantiomer.

they provide signal to noise ratio values below 10. For the present work, the noise was measured from chromatograms of blank samples in the same regions as the peaks of trimeprazine enantiomers (Ribani et al., 2007). The calibration curves of each enantiomer were obtained by injection of standard solutions containing racemic trimeprazine in the $1\text{--}30 \text{ mg L}^{-1}$ range (5 concentration levels) (see section 2.2). Table 1 shows the calibration statistics obtained for each enantiomer. As can be observed, for both enantiomers, satisfactory results were obtained ($R^2 > 0.99$).

3.2. Enantioselective biodegradation results

The biodegradability assays for the enantiomers of trimeprazine were performed in batch mode by duplicate at three concentration

Table 1
Method statistics.

Method Calibration				
Enantiomer	Interval ^a , mg L^{-1}	Regression curve equation	R^2	
E1	1–30	$y = -3.65 + 8.29 x$	0.994	
E2		$y = -4.04 + 8.83 x$	0.994	
Method precision		Concentration ^b	Enantiomeric fraction (EF) ^c	
Enantiomer	Level ^a , mg L^{-1}	RSD _r %	RSD _r %	RSD _{run} %
E1	4.8	6.7	4.9	7.3
E2		6.2		
E1	9	4.2	3.5	9.8
E2		8.7		
E1	18	5.9	3.6	12.4
E2		3.7		

E1 and E2 refer to the first and second eluted enantiomers, respectively. R^2 is the coefficient of determination. RSD_r is the relative standard deviation in repeatability conditions. RSD_{run} is the relative standard deviation in intermediate precision conditions (including the factor time).

^a Racemate concentration.

^b Concentration data for the whole time period evaluated; eq. (7).

^c EF data for the last five days; eqs. (8) and (9).

levels (section 2.2). Sample tubes containing trimeprazine and inoculum in MSM medium were collected and analysed at different times (0, 1, 2, 3, 4, 7, 10, 14, 18 and 23 days). Similarly, samples tubes containing trimeprazine in MSM medium (abiotic assays) were analysed at the same times. According to OECD (OECD, 1992), benzoic acid was used as reference substance to ensure that the microbial community in the test system is active. A complete biodegradation of benzoic acid (20 mg L^{-1}) was achieved in less than 48 h in the experimental conditions used, indicating the adequacy of the inoculum and thus, the validity of the trimeprazine assays.

Fig. 1 shows two chromatograms corresponding to $t = 0$ and 18 days. As can be observed, the peak areas of the first (E1) and second (E2) eluting enantiomers of trimeprazine are lower in the second case. This fact indicates that a degradation process has occurred. Moreover, in the second chromatogram the peak area of E1 seems lower than those of E2. This suggests that an enantioselective biodegradation process has occurred.

Fig. 2 shows the concentration profiles (S vs. t experimental data; two replicates) of enantiomers at initial trimeprazine racemate concentration of 9 mg L^{-1} (i.e. $S_0 = 4.5 \text{ mg L}^{-1}$). As can be seen, a similar concentration decay is observed during the first days for E1 and E2 enantiomers until day ~4. However, different profiles for the enantiomers are evident during the following days until the end of the experiment. This behaviour could be attributed to a shift in the microbial communities during the biodegradation of trimeprazine. Biodegradation in communities of diverse microorganisms is a complex process (combination of different effects, kinetics), especially when enantiomers are present (competition, enantio-merization, etc.) where several degradation pathways could sequentially operate, some being enantioselective and others not. Similar behaviour has been previously described for other compounds and it was attributed to time-dependent changes in the composition of the microbial community (Evans et al., 2017).

Anyway, the enantioselective biodegradation mechanism is confirmed in Fig. 2. The results also indicate that the concentration profiles are stabilized at higher times; so, no further degradation is expected. Similar results (not shown) were obtained for the other concentration trimeprazine racemate concentrations assayed.

On the other hand, abiotic assays indicate relatively low

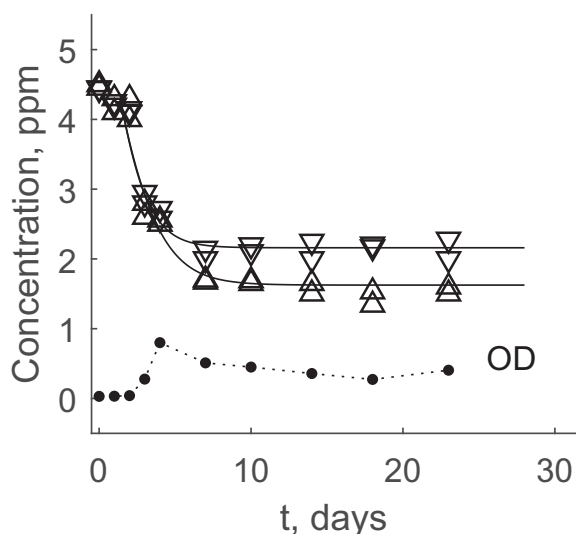


Fig. 2. Concentration versus time experimental data (two replicates) of trimeprazine enantiomers. First (Δ) and second (∇) eluted enantiomers. Fitted curves (solid lines) from the simplified Monod model (Eq. (5)). Optical density at 600 nm (OD, \bullet , dashed line). Initial trimeprazine racemate concentration: 9 mg L^{-1} .

degradation in absence of inoculum (<20%) for the concentration levels studied. These results indicates that abiotic elimination of the compound can be considered non-significant [ISO 9888:1999] and the degradation estimated in biotic assays can be considered as biodegradation.

In order to control to the biomass growth, the optical density (OD, at 600 nm; OD_{600}) profile was obtained. The OD_{600} can be considered proportional to the biomass growth (Shuler and Kargi, 2002). The OD_{600} values (in the range 0–1) were superimposed in Fig. 2, just for comparison purposes. Individual phases of the typical batch growth curve (Shuler and Kargi, 2002) can be perceived, bearing in mind the experimental design used. After an initial lag growth phase (~2 days), a short exponential phase (~2 days) is observed, to continue with a stationary/decline phase. The last phase could explain the stabilization in the concentration profiles. Similar results were obtained with the other trimeprazine racemate concentrations. Interestingly, when comparing both the concentration with OD_{600} profiles, it can be deduced that the stage of enantioselective biodegradation mainly coincides with the last growth phase, more than with the exponential phase.

To obtain the enantiomeric fraction profiles of trimeprazine enantiomers the enantiomeric fraction (EF) was calculated for each incubation time according to (Bagnall et al., 2012):

$$EF = \frac{S_{E1}}{S_{E1} + S_{E2}} \quad (6)$$

Where S_{E1} and S_{E2} refers to the estimated concentration of enantiomers at a given incubation time (e.g. S values in Fig. 2). Fig. 3 shows the mean EF values together with their standard deviation ($EF \pm s$) for each time during the biodegradation process. The horizontal line at $EF = 0.5$ represents no enantioselectivity. Consistently with conclusions of Fig. 2, until day ~4, EF values close to 0.5 are obtained (differences could be attributed to the method imprecision). Only during the last growth phase, EF values below 0.5 are observed and they are stabilized around 0.4–0.45.

The results in Fig. 3 correspond to the intermediate concentration level (9 mg L^{-1}) evaluated in this work. Comparable EF patterns were observed for the other two trimeprazine concentration levels studied. In fact, the grand mean of the EF values, considering the five last incubation times (where EF is almost constant), were 0.44 ± 0.03 , 0.43 ± 0.04 and 0.43 ± 0.05 , for the low, intermediate and high trimeprazine concentration levels studied, respectively (The error terms correspond to s_{mean} ; Eq. (3)). This represents a

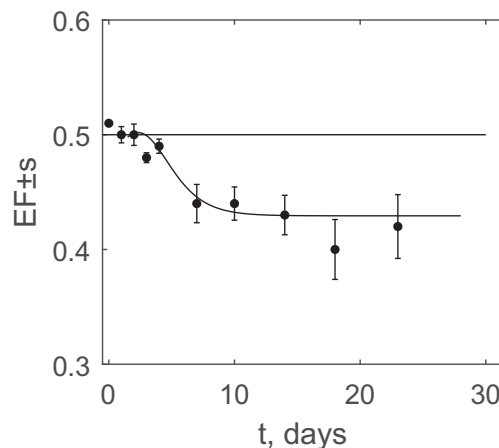


Fig. 3. Mean enantiomeric fraction and standard deviation ($EF \pm s$, points with error bars). EF vs. time fitted curve (solid line) consistent with the simplified Monod models. The horizontal line at $EF = 0.5$ represents no enantioselective biodegradation.

clear evidence on a moderate enantioselectivity in the biodegradation process of trimeprazine, with this activated sludge, with a minimum EF (i.e. maximum enantioselectivity) around 0.44, independent of S_0 . Further verification with sludges from other plants would be necessary to confirm if the results could be generalized.

3.3. Kinetic assessment of the data. Curve fitting

In this work, the model kinetic parameters (the maximum specific growth rate, V_m , and the half saturation constant for growth, K_s) estimated from Eq. (5) were not taken into account, since they cannot be considered accurate due to their linear correlation. Moreover, errors can increase depending on the S_0/K_s ratio (Liu and Zachara, 2001); and K_s is *a priori* unknown. In addition, when the degradation profiles do not reach zero (as in this work), an offset term in Eq. (5) has been proposed to model the entire profile (Her et al., 2015). It is important to realize that this fact should alter the estimated parameters. Moreover, it is possible that the experiment is conducted while the sludge is in an adaptation phase to the current conditions, which could difficult the mathematical treatment of the data. Finally, it is impossible to guarantee a unique kinetic behaviour during the entire process since communities of diverse microorganisms exist, as stated before. A deeper study on this matter is beyond the scope of this study.

The S vs. t experimental data were adjusted to Eq. (5) (including the offset term) just with the purpose to obtain S vs. t fitted curves that fit well the experimental data (a suitable objective as stated in section 2.6). Fig. 2 shows the fitted models (S vs. t fitted curves; solid lines). From the S vs. t fitted curves of two enantiomers derived using Eq. (5), an enantiomeric fraction versus time (EF vs. t) fitted curve can be obtained (considering Eq. (6)). The EF vs. t fitted curve is included in Fig. 3. Despite the noticeable uncertainty of the EF data, the fitted curve shows a reasonable agreement with the EF points. The curves at the three concentration levels were similar.

EF vs. t fitted curves provide a simple manner to estimate EF at different times or vice versa. For instance, the EF vs. t fitted curves confirm the minimum EF value at 0.44 (at the maximum t value). To the best of our knowledge, this is the first time that an EF vs. t fitted curve to the experimental data has been reported. Similarly, from the S vs. t fitted curves, curves for the percentage of biodegradation can also be estimated (considering the expression $BD = 100(S_0 - S)/S_0$). Fig. 4 shows the biodegradation versus time (BD vs. t) fitted curves obtained for each enantiomer at the three concentration levels evaluated (for clarity experimental values are not included). The time where the $BD = 50\%$ line cross a biodegradation versus time fitted curve is an estimate of $t_{1/2}$. BD vs. t fitted curves provide a simple manner to estimate $t_{1/2}$ values (independently from the parameters), as well as the BD estimates at different times or vice versa.

According to these plots, at the highest concentration level (curves 5 and 6), both enantiomers have similar half-life (~4.5 days), being still negligible the enantioselectivity of the biodegradation. For the intermediate concentration level (curves 3 and 4), $t_{1/2}$ differs between E1 and E2 (~4.5 and ~6 days, respectively), with an incipient enantioselective biodegradation. The most extreme situation occurs at the lowest concentration level (curves 1 and 2). While E1 has $t_{1/2}$ = 5 days, E2 never reach the 50% of biodegradation ($t_{1/2}$ cannot be estimated). The differences in the results obtained for the different substrate concentration levels could indicate that different mechanisms of biodegradation of trimeprazine enantiomers could exist. On the other hand, as can be observed in all cases, maximum BD values increase with the concentration studied, and as expected according to Figs. 1 and 2, E1 always reach higher BD values than E2 after the enantioselective biodegradation stage.

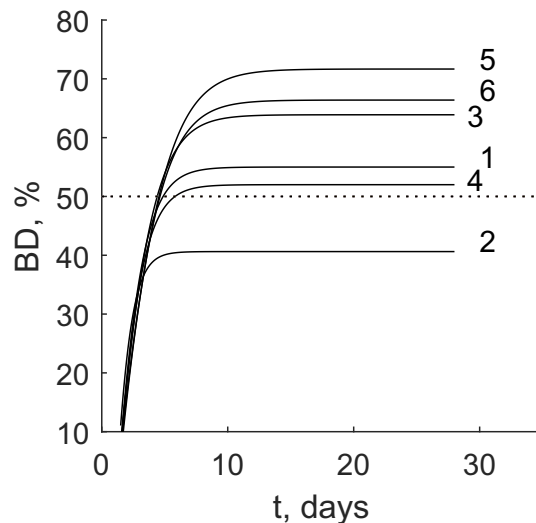


Fig. 4. Biodegradation (BD) in percentage of trimeprazine enantiomers estimated from the simplified Monod models. Initial racemate concentrations: 4.8 mg.L⁻¹ for curves 1 (E1) and 2 (E2); 9 mg.L⁻¹ for curves 3 (E1) and 4 (E2); 18 mg.L⁻¹ for curves 5 (E1) and 6 (E2). The dashed line at $BD = 50\%$ is included. E1 and E2 refer to the first and second eluted enantiomer.

3.4. Precision study under intermediate precision conditions

Precision is often forgotten in biodegradation studies. However, in our opinion, these data should be always provided. For instance, although beyond the aim of this work, the imprecision on S data is probably the most critical variable affecting the quality of kinetic parameters estimation. Also, it could serve to compare different biodegradation procedures. It should be noted that both the analytical method and the biodegradation process, as sources of uncertainty, contribute to the overall precision.

The typical design and initial statistics for assessing method precision in such conditions is summarised in section 2.5. The $X_{N \times N_s}$ design is consistent with a unique concentration level. However, in the case of biodegradation data, S changes with time due to the degradation process. In these conditions, only the s_r statistic makes sense (Eq. (1)). For each enantiomer, $X_{2 \times 10}$ matrices (2 replicates, 10 days) were built and processed via ANOVA. Considering Eq. (1), the relative standard deviation expressed in percentage (RSD_r) was then calculated according to Eq. (7):

$$RSD_r = \frac{100 \cdot \sqrt{MS_r}}{S_0} \quad (7)$$

The RSD_r results for each concentration level and enantiomer are shown in Table 1. As can be seen, the RSD_r values range from 3.7 to 8.7%. Those values account the overall method imprecision, including the biodegradation and the analytical processes. This value, habitually unreported, is more relevant than the simply analytical method precision (sometimes reported as part of a validation study).

The precision study can be extended to other variables different from concentrations. In this work, a precision study on EF, which accounts for the degree of enantioselective biodegradation, was performed. Considering the fact that the higher noise is concentrate in the last five times (see Fig. 3), and that EF can be considered almost constant in this period, the precision can be performed under intermediate precision conditions (including the factor time; section 2.5).

Thus, the last ten EF data (duplicate values), for each concentration level studied, was arranged into $X_{2 \times 5}$ matrices. Considering

Eqs. (1) and (2), repeatability and between-run standard deviations can be calculated, as RSD, according to Eqs. (8) and (9):

$$RSD_r = \frac{100 \cdot \sqrt{MS_r}}{EF} \quad (8)$$

$$RSD_{run} = 100 \cdot \frac{\sqrt{\frac{MS_{run} - MS_r}{Nr}}}{EF} \quad (9)$$

Where EF represents the grand mean of X (calculated in section 3.2). As X contain the lowest EF values and imprecise data (the worst case), this procedure provides the maximum EF impression associated with the proposed method. Table 1 shows the precision estimates obtained. To the best of our knowledge, this is the first time that a precision study, including between-days EF imprecision estimation, have been reported.

Table 1 reveals that $RSD_{run} > RSD_r$. Thus, the use of only RSD_r could provide a false idea of imprecision. On the other hand, the values of RSD_r (<5%) and RSD_{run} (<13%) could be considered reasonably normal in the context of a biodegradation process. They suggest that EF estimations can be satisfactorily used to evidence the magnitude of the enantioselectivity of the process.

4. Conclusions

Enantiomeric fractions and their standard deviation ($EF \pm s$), at the three concentration levels of trimeprazine studied, offer the first evidence of enantioselective biodegradation of trimeprazine. The maximum enantioselectivity observed (minimum EF value) at three trimeprazine initial racemate concentration (in the 5–20 range) is 0.44.

The biomass growth (indirectly established by optical density at 600 nm, OD_{600} , measurements), suggests that the enantioselective biodegradation process is produced during the stationary/decline stage (more than in the exponential stage). This is an interesting and novel outcome that deserves more attention. We suggest future work with other substrates/biological material to confirm this observation in order to establish if it's a non-isolated fact.

The curve fitting method by means of Michaelis-Menten-like approach (solved by the Lambert W function approximation), provides S vs. t fitted curves that fit well the S-t experimental data independently of the quality of the parameters. Furthermore, they enable to obtain BD vs. t and, for the first time, EF vs. t fitted curves. From BD vs. t fitted curves, a reasonable estimation of half-life times can be obtained. Such estimation should be more secure than other based on estimated model parameters (e.g. as usual when using first-order kinetics), which can be inaccurate. The similarity between the EF vs. t fitted curves at three concentration curves tested indicates that the enantioselectivity is independent from the concentration. We suggest future work with other substrates/biological material to confirm this observation.

The precision study on S (repeatability conditions) and, for the first time, on EF (intermediate precision conditions), suggests that moderate imprecision is observed. Future works focus on estimating the kinetic parameters via Monod (or simplified equations) or also alternative models, should take into account the S imprecision which affects the estimates accuracy. On the other hand, improvements in a biodegradation procedure could be controlled by precision studies by simply comparing the precision outputs.

The results obtained in this work correspond to ready biodegradability test obtained in a laboratory scale compatible with the OECD recommendations (whose analyte and microorganisms amounts differ from those in the environment). The moderate enantioselective biodegradation observed for trimeprazine can be

considered as indicative of its potential degradation in most environments including biological sewage treatment plants, according to OECD guidelines. On the other hand, a direct extrapolation of the results to the environmental or wastewater treatment scale should not be performed.

Conflicts of interest

None.

Acknowledgements

The authors acknowledge the Spanish Ministerio de Economía y Competitividad (MINECO) and the European Regional Development Fund for the financial support (Project CTQ2015-70904-R, MINECO/FEDER, UE).

References

- Bagnall, J., Malia, L., Lubben, A., Kasprzyk-Hordern, B., 2013. Stereoselective biodegradation of amphetamine and methamphetamine in river microcosms. *Water Res.* 47, 5708–5718.
- Bagnall, J.P., Evans, S.E., Wort, M.T., Lubben, A.T., Kasprzyk-Hordern, B., 2012. Using chiral liquid chromatography quadrupole time-of-flight mass spectrometry for the analysis of pharmaceuticals and illicit drugs in surface and wastewater at the enantiomeric level. *J. Chromatogr. A* 1249, 115–129.
- Bonet-Domingo, E., Escuder-Gilbert, L., Medina-Hernández, M.J., Sagrado, S., 2006. Uncertainty-based internal quality control. Harmonization considerations. *Anal. Chem.* 78, 8113–8120.
- Corless, R.M., Gonnet, G.H., Hare, D.E., Jeffrey, D.J., 1993. On the Lambert W Function. Technical Report Cs-93-03. Department of Computer Science, University of Waterloo, Waterloo, Canada.
- Drug Information Portal, 2017. Available at: <http://www.druglib.com/activeingredient/trimeprazine/>. Accessed November 29, 2017.
- Ebele, A.J., Abdallah, M.A.E., Harrad, S., 2017. Pharmaceuticals and personal care products (PPCPs) in the freshwater aquatic environment. *Emerging Contaminants* 3, 1–16.
- Evans, S., Bagnall, J., Kasprzyk-Hordern, B., 2017. Enantiomeric profiling of a chemically diverse mixture of chiral pharmaceuticals in urban water. *Environ. Pollut.* 230, 368–377.
- Evans, S.E., Bagnall, J., Kasprzyk-Hordern, B., 2016. Enantioselective degradation of amphetamine-like environmental micropollutants (amphetamine, methamphetamine, MDMA and MDA) in urban water. *Environ. Pollut.* 215, 154–163.
- Geissen, V., Mol, H., Klumpp, E., Umlauf, G., Nadal, M., van der Ploeg, M., van de Zee, S.E.A.T.M., Ritsema, C.J., 2015. Emerging pollutants in the environment: a challenge for water resource management. *International Soil and Water Conservation Research* 3, 57–65.
- Goudar, C.T., Strevett, K.A., 2000. Estimating in-situ Monod biodegradation parameters using a novel explicit solution of a one-dimensional contaminant transport equation. *Ground Water* 38, 894–898.
- Her, C., Alonzo, A.P., Vang, J.Y., Torres, E., Krishnan, V.V., 2015. Real-time enzyme kinetics by quantitative NMR spectroscopy and determination of the michaelis-menten constant using the Lambert-W function. *J. Chem. Educ.* 92, 1943–1948.
- ISO 9888:1999, 1999. Norma UNE-EN ISO 9888. Calidad del agua. Evaluación de la biodegradabilidad aerobia final de los compuestos orgánicos en medio acuoso. Ensayo estático (Método de Zahn-Wellens). AENOR, Madrid, España.
- Kasprzyk-Hordern, B., Baker, D.R., 2012. Enantiomeric profiling of chiral drugs in wastewater and receiving waters. *Environ. Sci. Technol.* 46 (3), 1681–1691.
- Kasprzyk-Hordern, B., 2010. Pharmacologically active compounds in the environment and their chirality. *Chem. Soc. Rev.* 39, 4466–4503.
- Kowalczyk, A., Martin, T.J., Price, O.R., Snape, J.R., van Egmond, R.A., Finnegan, C.J., Schäfer, H., Davenport, R.J., Bending, G.D., 2015. Refinement of biodegradation test methodologies and the proposed utility of new microbial ecology techniques. *Ecotoxicol. Environ. Saf.* 111, 9–22.
- Kümmerer, K., 2009. The presence of pharmaceuticals in the environment due to human use- present knowledge and future changes. *J. Environ. Manag.* 90, 2354–2366.
- Li, Z., Gomez, E., Fenet, H., Chiron, S., 2013. Chiral signature of venlafaxine as a marker of biological attenuation processes. *Chemosphere* 90 (6), 1933–1938.
- Lin, C.E., Liao, W.S., Cheng, H.T., Kuo, C.M., Liu, Y.C., 2005. Enantioseparation of phenothiazines in cyclodextrin-modified capillary zone electrophoresis using sulfated cyclodextrins as chiral selectors. *Electrophoresis* 26, 3869–3877.
- Liu, C., Zachara, J.M., 2001. Uncertainties of Monod Kinetic parameters nonlinearly estimated from batch experiments. *Environ. Sci. Technol.* 35, 133–141.
- Maroto, A., Riu, J., Boqué, R., Rius, F.X., 1999. Estimating uncertainties of analytical results using information from the validation process. *Anal. Chim. Acta* 391, 173–185.
- Martínez-Gómez, M.A., Sagrado, S., Villanueva-Camañas, R.M., Medina-

- Hernández, M.J., 2007. Enantioseparation of phenothiazines by affinity electrokinetic chromatography using human serum albumin as chiral selector: application to enantiomeric quality control in pharmaceutical formulations. *Anal. Chim. Acta* 582, 223–228.
- Moreira, I.S., Ribeiro, A.R., Afonso, C.M., Castro, Tiritan, M.E., P.M.L., 2014. Enantioselective biodegradation of fluoxetine by the bacterial strain *Labrys portuacensis* F11. *Chemosphere* 111, 103–111.
- OECD, 1992. Test No. 302B: Inherent Biodegradability: Zahn-wellens/evpa Test. OECD Publishing, Paris. <https://doi.org/10.1787/9789264070387-en>.
- Oguni, K., Oda, H., Ichida, A., 1995. Development of chiral stationary phases consisting of polysaccharide derivatives. *J. Chromatogr. A* 694, 91–100.
- Petrie, B., Barden, R., Kasprzyk-Hordern, B., 2015. A review on emerging contaminants in wastewaters and the environment: current knowledge, understudied areas and recommendations for future monitoring. *Water Res.* 72, 3–27.
- Ribani, M., Collins, C.H., Bottoli, C.B.G., 2007. Validation of chromatographic methods: evaluation of detection and quantification limits in the determination of impurities in omeprazole. *J. Chromatogr. A* 1156, 201–205.
- Ribeiro, A.R., Afonso, C.M., Castro, P.M.L., Tiritan, M.E., 2013a. Enantioselective HPLC analysis and biodegradation of atenolol, metoprolol and fluoxetine. *Environ. Chem. Lett.* 11 (1), 83–90.
- Ribeiro, A.R., Afonso, C.M., Castro, P.M.L., Tiritan, M.E., 2013b. Enantioselective biodegradation of pharmaceuticals, alprenolol and propranolol, by an activated sludge inoculum. *Ecotoxicol. Environ. Saf.* 87, 108–114.
- Ribeiro, A.R., Castro, P.M.L., Tiritan, M.E., 2012. Environmental fate of chiral pharmaceuticals: determination, degradation and toxicity. In: Lichtfouse, E., Schwarzbauer, J., Robert, D. (Eds.), *Environmental Chemistry for a Sustainable World*. Springer, Dordrecht.
- Ribeiro, A.R., Maia, A.S., Moreira, I.S., Afonso, C.M., Castro, P.M.L., Tiritan, M.E., 2014b. Enantioselective quantification of fluoxetine and norfluoxetine by HPLC in wastewater effluents. *Chemosphere* 95, 589–596.
- Ribeiro, A.R., Santos, L.H.M.L.M., Maia, A.S., Delerue-Matos, C., Castro, P.M.L., Tiritan, M.E., 2014a. Enantiomeric fraction evaluation of pharmaceuticals in environmental matrices by liquid chromatography-tandem mass spectrometry. *J. Chromatogr. A* 1363, 226–235.
- Robinson, J.A., Tiedje, J.M., 1983. Nonlinear estimation of Monod Growth kinetic parameters from a single substrate depletion curve. *Appl. Environ. Microbiol.* 45, 1453–1458.
- Sánchez, F.G., Navas Díaz, A., Sánchez Torreño, E., Aguilar, A., Medina Lama, I., Algarra, M., 2012. Determination of enantiomeric excess by chiral liquid chromatography without enantiomerically pure starting standards. *Biomed. Chromatogr.* 26, 1241–1246.
- Sanganyado, E., Lu, Z., Fu, Q., Schlenk, D., Gan, J., 2017. Chiral pharmaceuticals: a review on their environmental occurrence and fate processes. *Water Res.* 124, 527–542.
- Shuler, M.L., Kargi, F. (Eds.), 2002. *Bioprocess Engineering: Basic Concepts*, second ed. Prentice Hall, Upper Saddle River, NJ.
- Stanley, J.K., Ramirez, A.J., Chambliss, Brooks, B.W., 2007. Enantiospecific sublethal effects of the antidepressant fluoxetine to a model aquatic vertebrate and invertebrate. *Chemosphere* 69, 9–16.
- Stanley, J.K., Ramirez, A.J., Mottaleb, M., Chambliss, C.K., Brooks, B.W., 2006. Enantiospecific toxicity of the β -blocker propranolol to *Daphnia magna* and *Pimephales promelas*. *Environ. Toxicol. Chem.* 25, 1780–1786.
- Thouand, G., 2014. Biodegradability assessments of organic substances and polymers. *Environ. Sci. Pollut. Res.* 21, 9443–9444.
- Van Overbeke, A.A.L., Baeyens, W.R.G., Beyaert, A., Aboul-Enein, H.Y., Oda, H., 1997. Chiral resolution of several phenothiazine compounds and trimipramine, a dibenzazepine drug on chiralcel OJ-R. *J. Liq. Chromatogr. Relat. Technol.* 20, 693–705.
- Vazquez-Roig, P., Kasprzyk-Hordern, B., Blasco, C., Picó, Y., 2014. Stereoisomeric profiling of drugs of abuse and pharmaceuticals in wastewaters of Valencia (Spain). *Sci. Total Environ.* 494–495, 49–57.
- Wong, C.S., 2006. Environmental fate processes and biochemical transformations of chiral emerging organic pollutants. *Anal. Bioanal. Chem.* 386, 544–558.



PAPER VI

**Direct chromatographic study of the enantioselective
biodegradation of ibuprofen and ketoprofen
by an activated sludge**

**Laura Escuder-Gilabert^a, Yolanda Martín-Biosca^a, Mireia Perez-Baeza^a,
Salvador Sagrado^{a,b}, María José Medina-Hernández^a**

^a Departamento de Química Analítica, Universitat de València, Burjassot, Valencia, Spain

^b Instituto Interuniversitario de Investigación de Reconocimiento Molecular y Desarrollo Tecnológico (IDM), Universitat Politècnica de València, Universitat de València, Valencia, Spain

Journal of Chromatography A 1568 (2018) 140-148



Direct chromatographic study of the enantioselective biodegradation of ibuprofen and ketoprofen by an activated sludge[☆]

Laura Escuder-Gilabert^a, Yolanda Martín-Biosca^{a,*}, Mireia Perez-Baeza^a, Salvador Sagrado^{a,b}, María José Medina-Hernández^{a,*}

^a Departamento de Química Analítica, Universitat de València, Burjassot, Valencia, Spain

^b Instituto Interuniversitario de Investigación de Reconocimiento Molecular y Desarrollo Tecnológico (IDM), Universitat Politècnica de València, Universitat de València, Valencia, Spain



ARTICLE INFO

Article history:

Received 23 March 2018

Received in revised form 4 July 2018

Accepted 6 July 2018

Available online 7 July 2018

Keywords:

Batch experiment

Enantioselective biodegradation

Ibuprofen

Ketoprofen

Chiral separation

Peak area based estimates

ABSTRACT

The quantification of the enantiomeric fraction (*EF*) during the biodegradation process is essential for environmental risk assessment. In this paper the enantioselective biodegradation of ibuprofen, IBU, and ketoprofen, KET, two of the drugs most consumed, was evaluated. Biodegradation experiments were performed in batch mode using a minimal salts medium inoculated with an activated sludge (collected from a Valencian Waste Water Treatment Plant) and supplemented with the racemate of each compound. The inoculum activity was verified using fluoxetine as reference compound. The experimental conditions used (analyte concentration and volume of inoculum) were chosen according to OECD guidelines. In parallel, the optical density at 600 nm was measured to control the biomass growth and to connect it with enantioselectivity. Two RPLC methods for chiral separations of IBU and KET using polysaccharides-based stationary phases were developed. Novel calculations and adapted models, using directly the chromatographic peak areas as dependent variable, were proposed to estimate significant parameters related to the biodegradation process: biodegradation (*BD*) and *EF* values at given time, half-life times of (R)- and (S)-enantiomers, number of days to reach a complete *BD* and the minimum *EF* expected. The modelled *BD* and *EF* curves fitted adequately the data ($R^2 > 0.94$). The use of these new equations provided similar results to those obtained using concentration data. However, the use of chromatographic peak areas data, eliminates the uncertainty associated to the use of the calibration curves. The results obtained in this paper indicate that an enantioselective recognition towards IBU enantiomers by the microorganisms present in the activated sludge used in this study occurred, being the biodegradation of (R)-IBU higher than that of (S)-IBU. For KET, non-enantioselective biodegradation was observed.

© 2018 Elsevier B.V. All rights reserved.

1. Introduction

Public environmental awareness has increased notably in recent years, due to the adverse effects that pollutants can produce not only on the environment but also on the human health. Among the emerging pollutants, drugs are probably the main concern of regulatory authorities because of their huge consume. Drugs, their metabolites and their degradation products could reach the environment mainly due to poor removal rates in Waste Water

Treatment Plants (WWTP), and by improper disposal of unused medicines [1]. The presence of these compounds in the environment has been extensively reported [2–5]. However, although the great efforts made by regulatory authorities and scientific community, not much is known about the impact of this kind of compounds on the environment and the human health [6–10].

The majority of currently available drugs are chiral compounds and, even though the use of single enantiomers has increased during the last decades, many of these are marketed as racemates [11]. As a result of the enantioselective human metabolism, and also of the microbial biodegradation during the wastewater treatment process, these compounds are not present in the environment in their original racemic or enantiomeric form. For this reason, and due to the fact that enantiomers may have different toxicological and ecotoxicological properties compared to each other, the quantification of the enantiomeric fractions (*EF*) during the

[☆] Thematic Virtual Special Issue on “Enantioseparations-2018”.

* Corresponding authors at: Departamento de Química Analítica, Facultat de Farmàcia, Universitat de València, Avda. Vicent Andrés Estellés, s/n, Burjassot, E-46100, Valencia, Spain.

E-mail addresses: Yolanda.martin@uv.es (Y. Martín-Biosca), maria.j.medina@uv.es (M.J. Medina-Hernández).

biodegradation process is essential for environmental risk assessment. However, there is not much research done on this subject.

Some studies have been focused on the direct *EF* quantification in WWTP influents and effluents [12–15]. Other approaches have been based on *in vitro* biodegradability assays. The OECD tests for ready biodegradability have been devised as screening methods to determine whether or not a chemical is potentially easily biodegradable. They simulate the degradation processes of chemicals in soils, surface waters or in activated sludge, generally in the presence of oxygen. A high concentration of the test substance (2–100 mg L⁻¹) is used in these tests [16]. The subsequent separation and determination of the individual enantiomers of the original compound (or its metabolites) in the test solution by analytical techniques, mainly liquid chromatography, allow the estimation of *EF*. Using this methodology, the enantioselective evaluation of biodegradation (*BD*) for amphetamines [14,17,18], β -blockers [17,19,20] and antidepressants [15,17,19,21,22] have been reported.

Ibuprofen (IBU) and ketoprofen (KET) are non-steroidal anti-inflammatory (NSAIDs) chiral drugs with anti-inflammatory and analgesic activities, being IBU one of the most popular clinically used drugs in the world [23]. Their therapeutic effects have been observed to reside almost exclusively in the (*S*)-enantiomers while the (*R*)-enantiomers are weakly active or inactive (e.g. (*S*)-IBU has been reported to be 160 times more active than (*R*)-IBU) [24,25]. In spite of the differences in their enantiomers activity, IBU and KET are commonly manufactured, dispensed and consumed as racemic mixtures [25].

The occurrence of the NSAIDs IBU and KET in WWTP influents and effluents from WWTPs of Spain [26,27], Australia [25,28] and Switzerland [29] has been reported. In these studies, the enantioselective biodegradation was evaluated by comparison of the *EF* values obtained in influents and effluents. (*S*)-IBU was found to be predominant in wastewater influents due to chiral inversion during human metabolism [25–28] and preferentially degraded during wastewater treatment [27–29]. Matamoros et al. [26], in the evaluation of the biodegradation of IBU in different WWTPs, found high variability on the *EF* values for constructed wetlands, being in the final step of the process (*R*)-IBU preferentially degraded. The authors attributed this behaviour to the presence of microorganisms and changes in the aerobic and anaerobic conditions in the WWTP could induce the chiral inversion of (*R*)-IBU to its optical antipode. Moreover, the chiral inversion degree seems to depend on the WWTP considered [28]. For KET, no significant changes in *EF* were reported [25,27].

In order to study the enantioselectivity in the NSAIDs biodegradation, experiments under laboratory conditions have also been performed. In a laboratory-scale membrane bioreactor, the (*S*)-IBU was preferentially degraded, while for KET, a slightly higher degradation of (*R*)-KET was observed [30]. Buser et al. also found a faster degradation of (*S*)-IBU during the incubation in the laboratory of an influent from a WWTP containing IBU, with an activated sludge and under aerobic conditions [29]. Incubation of lake water fortified with racemic IBU also indicated a faster dissipation of the (*S*)-enantiomer [29].

Changes in the *EF* values during the biodegradation process have been mainly explained by the more rapid degradation of one enantiomer relative to the other (i.e. enantioselective degradation). However, it is well established that 2-arylpropionic acids undergo *in vivo* chiral inversion during mammalian metabolism, and also in several species of fungi and bacteria. Multiple enzymes are believed to play a role in the process, varying the degree and/or direction of chiral inversion in the different organisms [5,28]. Therefore, changes in the *EF* for ibuprofen and ketoprofen could be explained not only by enantioselective degradation, but also by chiral inversion or by the concurrence of both processes [5,28].

Chiral analysis of NSAIDs in the above-mentioned enantioselective studies was carried out mainly by gas chromatography-mass spectrometry after diastereomer formation with the chiral derivatising reagent (*R*)-1-phenylethylamine [25,28,30], or using a cyclodextrin-based chiral stationary phase [26,29]. Liquid chromatography-mass spectrometry has also been applied with a (*R*)-1-naphthylglycine based chiral stationary phase and a mixture of tetrahydrofuran- ammonium acetate in methanol as mobile phase [27]. In the literature, few references exist about chiral separations of IBU and KET in reversed phase conditions [31–36].

One of the main aims on this work is to evaluate the biodegradation of IBU and KET enantiomers to provide more information on this issue, due to the ambiguous results reported in the literature. For this purpose, a ready biodegradability test (compatible with the OECD guidelines) is performed. Experiments are carried out in batch conditions using an activated sludge inoculum from a local WWTP which receives domestic, agricultural, livestock and industrial wastewater. The inoculum activity is checked using fluoxetine as reference substance. Abiotic assays and biomass growth control assays are also performed. For the separation of the IBU and KET enantiomers, several polysaccharide based chiral stationary phases in RPLC conditions were tested. Using the selected conditions, fit-for-purpose validation of the methods is performed.

Another aim of this work is to develop a new strategy based on the direct use of chromatographic peak areas of enantiomers (instead of their concentrations) to estimate significant parameters related to the biodegradation process such as: *BD* of enantiomers and *EF* values at a given time, half-life times of enantiomers, number of days to reach a complete biodegradation and the maximum enantioselectivity degree (e.g. $|EF-0.5|$) expected. The purposes of this strategy are: (i) to eliminate the uncertainty source associated to the calibration stage and (ii) to reduce the experimental effort and cost due to the elimination of the calibration step. For this purpose, novel equations to calculate and model *BD* and *EF* data based on peak areas as dependent variables are developed. The results obtained are compared with those obtained using conventional calculations/models and with previous reported results for biodegradation of IBU and KET enantiomers.

2. Material and methods

2.1. Chemicals and solutions

Racemic Ibuprofen (*rac*-IBU), (*S*)-(+)-ibuprofen ((*S*)-IBU), racemic ketoprofen (*rac*-KET) and (*S*)-(+)-ketoprofen ((*S*)-KET) were from Sigma-Aldrich (St. Louis, MO, USA). Fluoxetine hydrochloride (FLX) was kindly donated by Alter (Madrid, Spain).

All reagents were of analytical grade. Formic acid (98%), sodium dihydrogen phosphate monohydrate, sodium hydroxide, acetonitrile (ACN), isopropanol, ethanol and methanol (MeOH) ([®]Multisolvent, HPLC grade) were from Scharlau, S.L. (Barcelona, Spain).

Ultra Clear TWF UV deionized water (SG Water, Barsbüttel, Germany) was used to prepare solutions. Different solutions were tested for the preparation of the mobile phases. Aqueous solutions of formic acid (0.1%, v/v, pH 3.0) were prepared. Phosphate buffer (10 mM, pH 8.0) was prepared by dissolving the appropriate amount of sodium dihydrogen phosphate monohydrate in water and adjusting the pH with 2.5 M sodium hydroxide. The mobile phases were prepared by mixing 0.1% formic or 10 mM phosphate solutions with the tested organic modifier to obtain the working concentration.

The minimal salts medium (MSM) solution used in the biodegradation assays was prepared with the following composition per litre [19,20]: 2.1 g Na₂HPO₄ (Panreac Química, S.A., Barcelona,

Spain); 1.4 g KH_2PO_4 (Panreac); 0.2 g $\text{MgSO}_4 \cdot 7\text{H}_2\text{O}$ (Scharlau Chemie S.A., Barcelona, Spain); 0.5 g $(\text{NH}_4)_2\text{SO}_4$ (Scharlau), and 10 mL of a trace elements solution with the following composition per litre: 2.0 g NaOH (Scharlau); 12.0 g $\text{Na}_2\text{EDTA}_2 \cdot 2\text{H}_2\text{O}$ (Scharlau); 1.4 g $\text{FeSO}_4 \cdot 2\text{H}_2\text{O}$ (Panreac); 1.3 g $\text{CaCl}_2 \cdot 2\text{H}_2\text{O}$ (Panreac); 10 g Na_2SO_4 (Panreac); 0.7 g $\text{ZnSO}_4 \cdot 7\text{H}_2\text{O}$ (Merck, Darmstadt, Germany); 0.3 g $\text{MnSO}_4 \cdot \text{H}_2\text{O}$ (Panreac); 0.1 g $\text{CuSO}_4 \cdot 5\text{H}_2\text{O}$ (Merck); 0.1 g $\text{Na}_2\text{MoO}_4 \cdot 2\text{H}_2\text{O}$ (Merck); 0.5 mL H_2SO_4 (98%) (Scharlau).

Activated sludge was kindly donated by General de Análisis Materiales y Servicios, S.L (GAMASER, S.L., Valencia, Spain), a laboratory and inspection entity of the Group "Aguas de Valencia". It was obtained from the aerated tanks of a municipal WWTP (Quart Benàger, Valencia, Spain), which receives domestic, agricultural, livestock and industrial wastewater from eight Valencian towns with a surface area of 164,171 ha and a population of approximately 1 million. Its average flow rate is 30,318 m^3/day . Activated sludge was collected in plastic flasks and stored at 5 °C until usage. The storage of the activated sludge before usage was lower than to 24 h.

Stock standard solutions of 1000 mg L^{-1} of *rac*-IBU, *rac*-KET and FLX were prepared by dissolving the adequate amount of each compound in methanol. To prepare the calibration standards, intermediate stock solutions of 100 mg L^{-1} of *rac*-IBU, *rac*-KET and FLX were prepared by dilution of the corresponding 1000 mg L^{-1} stock solution in the MSM. Solutions of 100 mg L^{-1} of *rac*-IBU and *rac*-KET were spiked with 50 mg L^{-1} of the corresponding (S)-enantiomer for the identification of the enantiomers peaks.

For each drug, calibration solutions of approximately 2, 5, 10, 20 and 30 mg L^{-1} were prepared by dilution of the corresponding intermediate stock solution of 100 mg L^{-1} in the MSM. For the biodegradability assays, working solutions of approximately 20 mg L^{-1} of *rac*-IBU, *rac*-KET and FLX were prepared by dilution of the 1000 mg L^{-1} stock solution in the MSM. The solutions were stored under refrigeration at 5 °C until usage (for less than 3 h).

2.2. Instrumentation

An Agilent Technologies 1100 chromatograph (Palo Alto, CA, USA) with a binary pump, an UV-vis diode array detector, a column thermostat and an autosampler was used. Data acquisition and processing were performed by means of the LC/MSD ChemStation software (B.04.02 SP1 [208], ©Agilent Technologies 2001–2010).

For the determination of FLX, an Halo C_{18} column (2.7 μm , 75 × 4.6 mm i.d.; Advanced Materials Technology, Wilmington, USA) and phosphate buffer (10 mM, pH 8.0):ACN (30:70, v/v) mobile phase were used. The injection volume was 2 μL . The detection was performed in the UV at 220 nm. The mobile phase flow rate was 1 mL min^{-1} and the separation temperature 25 °C.

For the separation of the IBU and KET enantiomers, several polysaccharide-based chiral stationary phases were tested: Chiralart Cellulose-SC (celulose tris(3,5-dichlorophenylcarbamate); 3 μm , 150 × 4.6 mm i.d.; YMC Separation Technology Co., Ltd., Tokyo, Japan); Lux Cellulose-1 (cellulose tris(3,5-dimethylphenylcarbamate); 3 μm , 150 × 4.6 mm i.d.; Phenomenex, Torrance, CA, USA); Lux Cellulose-3 (cellulose tris(4-methylbenzoate); 3 μm , 150 × 4.6 mm i.d.; Phenomenex, Torrance, CA, USA) and Lux Amylose-2 (amylose tris(5-chloro-2-methylphenylcarbamate); 3 μm , 150 × 2.0 mm i.d.; Phenomenex).

For the determination of IBU enantiomers the Lux Cellulose-3 column and a binary mixture of methanol:formic acid aqueous solution (0.1%, pH = 3) (80:20, v/v) as mobile phase were used. The separation temperature was set at 25 °C and the mobile phase flow rate was 1.0 mL min^{-1} . The injection volume was 2 μL . The detection was performed in the UV at 220 nm.

The separation of KET enantiomers was carried out using the Lux Amylose-2 column and a binary mixture of acetonitrile:formic

acid aqueous solution (0.1%, pH = 3) (35:65, v/v) as mobile phase. The separation temperature was set at 15 °C and the mobile phase flow rate was 0.5 mL min^{-1} . The injection volume was 2 μL . The detection was performed in the UV at 240 nm.

For samples mixtures preparation, 15 mL conical sterile polypropylene tubes (Deltalab, S.L., Barcelona, Spain) were used. Disposable sterile filter pipette tips (Capp Expell, Odense, Denmark) were also used. For the biodegradability assays, a shaking incubator with temperature control (WiseCube® Wis-30, Witeg Labor Technik GmbH, Wetheim, Germany) was used. Prior to the measurement of the microbial growth, incubated samples were subjected to agitation in a vortex mixer (Velp Scientific Vortex, Usmate, Italy). Microbial growth was monitored by measuring the optical density of the cultures at 600 nm (OD_{600}) with an Epoch 2 microplate reader (Biotek Instruments Inc., Vermont, USA) and 96-well plates with UV transparent flat bottom (Corning, Kennebunk, ME, USA). Samples were stored at -80 °C in an ultra-low temperature freezer (U570 Premium, New Brunswick Scientific, Herts, UK) until chromatographic analysis.

Prior to injection into the chromatographic system, samples were centrifuged (Hettich Lab Technology, EBA 20, Tuttlingen, Germany) and filtered through disposable 0.22 μm polyethersulphone syringe filters (Frisenette, Knebel, Denmark). Mobile phase solutions were vacuum-filtered through 0.22 μm Nylon membranes (Micron Separations, Westboro, MA, USA) and were degassed in an Elmasonic S60 ultrasonic bath (Elma, Singen, Germany) prior to use. A Crison MicropH 2000 pHmeter (Crison Instruments, Barcelona, Spain) was employed to adjust the pH of the buffer solutions.

2.3. Biodegradability assays

The biodegradability assays were performed in batch mode at 15.6 and 18.0 mg L^{-1} of *rac*-IBU and *rac*-KET, respectively. For the preparation of the samples mixtures, 15 mL uncovered sterile tubes were used. Samples mixtures containing 3000 μL of the corresponding working solution of *rac*-IBU and *rac*-KET inoculated with 100 μL of the activated sludge (total sample volume of 3100 μL) were prepared. Independent samples were prepared for each compound and each incubation time studied. All experiments were done in duplicate, using tubes of a volume five-fold superior to guarantee the aeration of the cultures. The samples were incubated on a shaking incubator (150 rpm) at 20 °C under natural light cycles. At eight prefixed incubation times (0, 3, 5, 11, 18, 21, 25 and 28 days), two test tubes of each compound were taken, and when necessary to compensate solvent evaporation, ultrapure water was added to get a total volume of 3100 μL . Then, mixtures were vortex mixed for 20 s and an aliquot of 200 μL of each tube was taken to measure the OD_{600} of the cultures. After OD_{600} measurement, samples were frozen at -80 °C until HPLC analysis (described in Section 2.2). Abiotic degradation of the enantiomers of IBU and KET was evaluated using 100 μL of ultrapure water instead of the activated sludge inoculum, under the same conditions as samples. Prior to HPLC analysis, the samples were centrifuged at 6000 rpm for 15 min and the supernatant was filtered. A similar procedure was used for the biodegradability assays of FLX at 20 mg L^{-1} .

2.4. Software and data processing

For modelling purposes, the NLINFIT.m function in MATLAB® R2016b (MathWorks, Natick, Massachusetts) was used. It estimates the coefficients of a nonlinear regression function using iterative least squares estimation. Details of the algorithm for the explicit Lambert W function can be found in [37].

Table 1

Retention factors (k_1 , k_2) selectivity (α) and resolution (R_s) values obtained for the separation of ibuprofen and ketoprofen enantiomers in different polysaccharide-based stationary phases and 0.1% (v/v) formic acid aqueous solution/organic modifier (v/v) mobile phases.

Compound	T ($^{\circ}$ C)	Flow rate (mL min $^{-1}$)	Modifier	% Modifier (v/v)	k_1 (R)	k_2 (S)	α	R_s
Ibuprofen ^a	25	1.0	MeOH	92	2.80	3.05	1.09	1.4
				90	2.85	3.17	1.11	1.6
				87	3.13	3.54	1.13	2.1
				85	3.38	3.85	1.14	2.3
				80	4.64	5.38	1.16	2.8
				75	7.31	8.61	1.18	2.9
Ketoprofen ^b	15	0.5	ACN	80	0.35	0.35	1.00	0.0
				60	0.56	0.71	1.26	0.6
				50	0.61	0.77	1.27	0.7
				40	1.50	1.92	1.28	1.4
				35	2.64	3.31	1.26	1.6
				30	5.33	6.42	1.20	1.5
				28	7.12	7.12	1.00	0.0
				25	11.91	11.91	1.00	0.0

See further details in Section 2.2.

^a Lux-Cellulose 3 column.

^b Lux-Amylose 2 column.

3. Results and discussion

3.1. Inoculum activity control

The microbial community of an activated sludge in a given WWTP could change over time and, therefore, its biodegradation activity against incoming compounds could also vary. In order to verify the biodegradation capacity of the activated sludge used as inoculum in a laboratory assay for a given compound, a reference substance has been recommended to be tested in parallel [38]. Fluoxetine (FLX, 20 mg L $^{-1}$) has been proposed as a rapid 'inoculum activity control' according to the results of previous experiments (results are pending of publication). Briefly, the study implied four inoculum collection dates from the same WWTP, different storage times of the inoculum in the laboratory and three different analysts performing the assay. The aim was to include usual sources of variation that could influence the results. As a result, it was concluded that if the biodegradation (BD) values after seven days of incubation (BD_{7d}) are within the $70 \pm 11\%$ range, the inoculum biodegradation capacity could be considered as normal. In the present case, a BD_{7d} of 69.3% for FLX was obtained. Therefore, the inoculum activity was considered in the normal range and, therefore, the assays for IBU and KET enantiomers were performed in adequate conditions.

3.2. Chiral chromatographic separation

For the separation of enantiomers of IBU and KET, different polysaccharide-based stationary phases (Chiralart Cellulose-SC, Lux Cellulose-1, Lux Cellulose-3 and Lux Amylose-2) were tested (see experimental section). Binary mixtures of formic acid aqueous solution (0.1%, v/v, pH 3) and different percentages of methanol or acetonitrile were assayed as mobile phases. Experiments were carried out at 15 or 25 $^{\circ}$ C.

The use of Chiralart Cellulose-SC and Lux Cellulose-1 stationary phases and a formic acid aqueous solution (0.1%, pH 3):ACN (40:60, v/v) mobile phase, at the temperatures assayed, did not provide resolution of IBU and KET enantiomers.

For IBU enantiomers partial or complete resolution was obtained using the Lux Cellulose-3 stationary phase and mobile phases containing different proportions of methanol, (see Table 1). As can be observed, the retention factors and resolution values of IBU enantiomers increased as the amount of water in the mobile phase increased. This fact indicates that the contribution of the hydrophobic interactions to analytes retention and enantiosepara-

tion becomes more important in these conditions [39]. With the mobile phases assayed, no reversal in enantiomer elution order was observed. Taking into account resolution and retention times, a mobile phase containing a formic acid aqueous solution (0.1%, pH 3):MeOH (20:80, v/v) was selected for the separation of IBU enantiomers in further experiments. Under these experimental conditions, adequate retention times (7.3 and 8.1 min for (R)- and (S)-IBU enantiomers, respectively) and resolution ($R_s = 2.8$) were obtained (see Fig. 1A chromatogram 2). In the conditions tested for IBU, no resolution of KET enantiomers was obtained.

In the case of KET, the use of Lux Amylose 2 stationary phase and mobile phases containing different proportions of ACN at 25 $^{\circ}$ C provided partial resolution of KET enantiomers. It was observed that resolution improved as the separation temperature decreased. As can be observed in Table 1, at 15 $^{\circ}$ C, the retention factors of KET enantiomers increased as the proportion of the aqueous solution in the mobile phase increased. As for IBU, this behaviour indicates that for mobile phases with high content in water, hydrophobic interactions are important for the retention and the enantioresolution [39]. With the mobile phases assayed, no reversal in enantiomer elution order of KET was observed. Adequate resolution values ($R_s = 1.6$) and retention times (4.1 and 5.2 min, for (R)- and (S)-KET enantiomers, respectively) were obtained using a mobile phase containing a formic acid aqueous solution (0.1%, pH 3):ACN (65:35, v/v), therefore it was selected for the separation of KET enantiomers in further experiments (see Fig. 1B chromatogram 2).

In Fig. 1A and B (chromatograms 1), the chromatogram corresponding to the S-enantiomer was included for identification purposes. As can be seen, for both compounds, the first eluted enantiomer (E1) is the (R)-form while the second one (E2) is the (S)-form. These identifications were also confirmed by the injection of spiked samples with the corresponding (S)-enantiomer.

Using the selected experimental conditions, it was observed that concentrations lower than 2 mg L $^{-1}$ of racemic IBU and KET (1 mg L $^{-1}$ of each enantiomer) did not provide adequate peak areas for quantification. So, the peak area at this concentration level was considered as the critical signal for quantification. Details on the calibration statistics are considered in Section 3.6.

3.3. Biodegradation assays and chromatographic information

The biodegradability assays for the enantiomers of IBU and KET were performed in batch mode by duplicate (Section 2.3). Sample tubes were collected at different times ($t = 0, 3, 5, 11, 18, 21, 25$

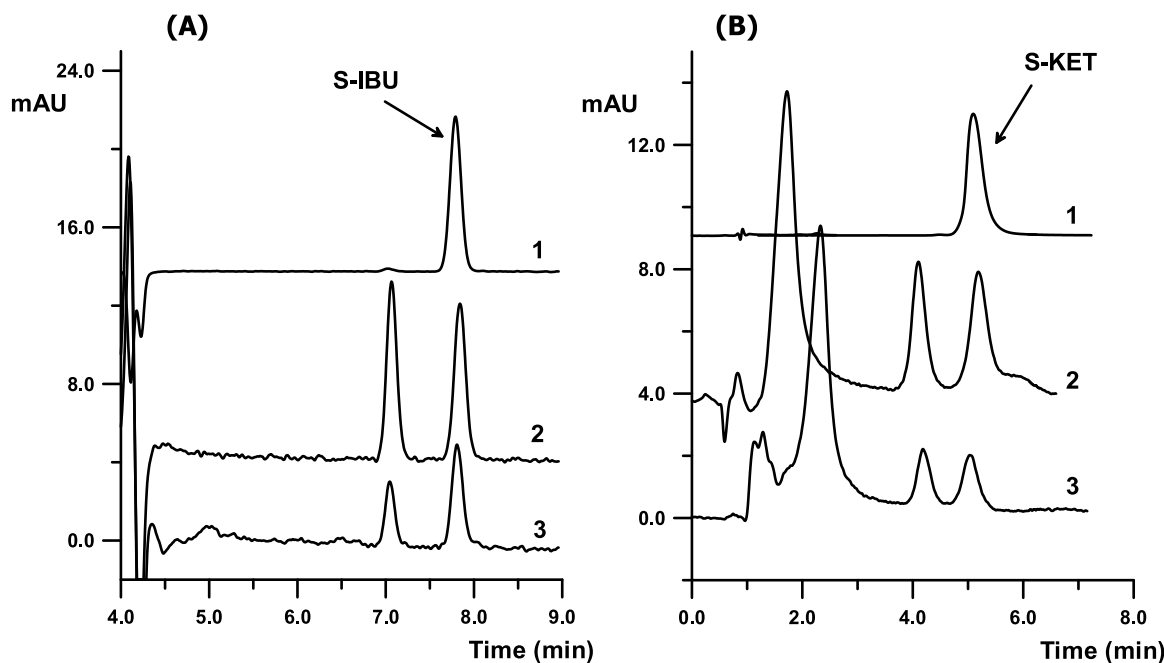


Fig. 1. Chromatograms of (A) ibuprofen (IBU) and (B) ketoprofen (KET) obtained using the experimental conditions detailed in Section 2.2. Chromatogram 1 corresponds to a standard solution of the (S)-enantiomer. Chromatograms 2 and 3 correspond to samples containing racemic mixtures at $t=0$ and $t=21$ days of incubation, respectively. Initial racemate concentrations were 15.6 and 18.0 mg L^{-1} for IBU and KET, respectively.

and 28 days) for the biotic and abiotic assays and analysed in the optimal chromatographic conditions.

Figs. 2A and 3A show the experimental peak area data (A ; mean \pm s from two replicates) obtained during the biodegradability assays for the enantiomers of IBU and KET, respectively. The initial concentration of each enantiomer (S_0) was 7.8 mg L^{-1} for IBU and 9.0 mg L^{-1} for KET.

Biodegradation, BD , is usually calculated from concentration data (S) obtained over time. In this work an alternative way to calculate BD directly from the chromatographic information (peak area, A) is proposed:

$$BD = \frac{A_0 - A}{A_0} \times 100 \quad (1)$$

where A_0 represents the area obtained at $t=0$. This equation could be obtained from the definition of BD and the linear calibration equation assuming that the intercept of the b_0 is statistically non-significant (i.e. confidence interval of b_0 includes zero; see Section 3.6) or negligible (i.e. $b_0 \ll A_0$), which is a logical situation:

$$BD = \frac{S_0 - S}{S} \times 100 = \frac{A_0 - A}{A_0 - b_0} \times 100 \quad (2)$$

Figs. 2B and 3B show the biodegradation (%) and the standard deviation (BD ; mean \pm s from two replicates) for IBU and KET enantiomers calculated using the Eq. (1).

For the IBU enantiomers, during the first days of incubation (from $t=0$ to $t=5$ days), no degradation was observed (see Fig. 2). After this period, the peak areas of enantiomers decreased indicating that a degradation process has occurred, although complete degradation of IBU enantiomers was not achieved at $t=28$ days. Moreover, higher peak areas were obtained for (S)-IBU enantiomers, which indicates that the biodegradation of (R)-IBU is higher than the one obtained for (S)-IBU (Fig. 2B). This suggests that an enantioselective biodegradation of IBU enantiomers has occurred. The same conclusion can be derived from the chromatograms shown in Fig. 1A.

For KET, like in the case of IBU, degradation seems to occur after $t=5$ days (see Fig. 3). In addition, complete degradation was

achieved after 25 days of incubation. As can be observed in Fig. 3A and B, similar peak areas and biodegradation values were obtained for both enantiomers, so the degradation of KET by the microorganisms seems not to be enantioselective. These conclusions are in agreement with the observations derived from the chromatograms shown in Fig. 1B.

For IBU and KET, the abiotic assays (in absence of inoculum) indicated low physicochemical degradation ($<20\%$). These results indicate that the abiotic elimination of IBU and KET can be considered non-significant [40] and the degradation estimated in the biotic assays can be considered as biodegradation.

In order to control the biomass growth during the biodegradation process, the optical density at 600 nm (OD_{600}) during the biotic assays was monitored. OD_{600} measures the solution turbidity and can be considered proportional to the biomass growth [41]. The OD_{600} values for IBU and KET (supplementary data Fig. S1) indicated a biomass growth during the biodegradation process. For both NSAIDs, the maximum biomass growth was observed at $t=5$ days, followed by a stationary/decline growth phase. In this last phase the differential behaviour for IBU enantiomers was observed.

3.4. Biodegradation kinetics

Different kinetic biodegradation models have been proposed in the literature. These models often provide good fit of the experimental data (S and t), despite estimating inaccurate kinetic parameters due to their linear correlation [42,43]. The simplified Monod equation, which resembles a Michaelis Menten equation [44,45], is one of the most used. It relates S and t by means of the Lambert W function ($S = W \{t\}$, see more details in the supplementary data; Eq. S2).

In this work, this model has been adapted for chromatographic data ($A = W \{t\}$):

$$A = \frac{A_0}{S_0} \left\{ K_s \cdot W \left[\frac{S_0}{K_s} e^{\left(\frac{S_0 - V_m \cdot t}{K_s} \right)} \right] \right\} \quad (3)$$

where V_m approaches the maximum specific growth rate and K_s is the half saturation constant for growth (the two parameters to be

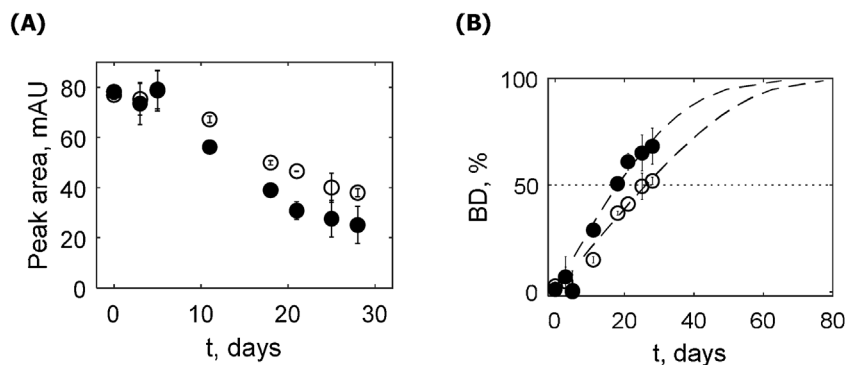


Fig. 2. (A) Experimental peak areas (A , mean \pm s from two replicates) obtained for (S)-IBU (\circ) and (R)-IBU (\bullet) in incubated samples during the biodegradation assay. (B) Biodegradation (BD , %, mean \pm s from two replicates) calculated from peak areas using the Eq. (1) for (S)-IBU (\circ) and (R)-IBU (\bullet). Dashed lines correspond to the modelled BD vs t curves according to Eq. (4).

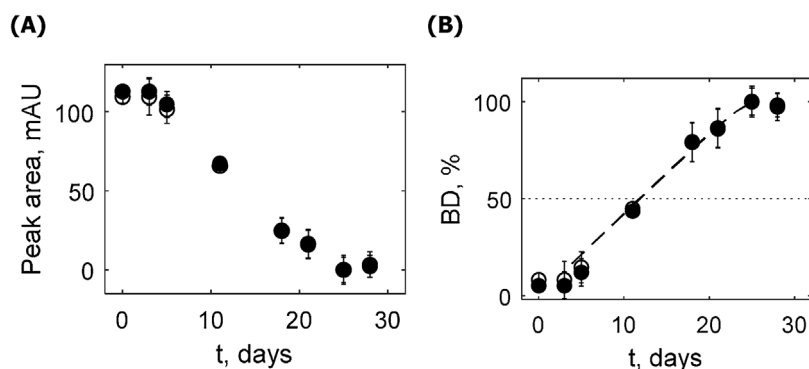


Fig. 3. (A) Experimental peak areas (A , mean \pm s from two replicates) obtained for (S)-KET (\circ) and (R)-KET (\bullet) in incubated samples during the biodegradation assay. (B) Biodegradation (BD , %, mean \pm s from two replicates) calculated from peak areas using the Eq. (1) for (S)-KET (\circ) and (R)-KET (\bullet). Dashed lines correspond to the modelled BD vs t curves according to Eq. (4).

estimated). By substituting this equation in Eq. (1) the following equation ($BD = W \{t\}$) is obtained:

$$BD = \frac{100}{S_0} \left\{ S_0 - K_s \cdot W \left[\frac{S_0}{K_s} e^{\left(\frac{S_0 - V_m \cdot t}{K_s} \right)} \right] \right\} \quad (4)$$

Eqs. (3) and (4), provide estimations of V_m and K_s by non-linear fitting of A vs. t experimental data. The complete algorithm is provided in supplementary data. To the best of our knowledge, this is the first time that these expressions have been proposed.

Figs. 2B and 3B (dashed lines) show the modelled BD vs. t curves according to Eq. (4), for IBU and KET enantiomers, respectively. The BD data at $t = 0, 3$, and 5 days, were excluded for modelling purposes since $BD \sim 0$. As can be seen, the curves fit reasonably well to the BD experimental points (R^2 values were 0.94 and 0.95 for (R)- and (S)-IBU, respectively and 0.99 for (R)- and (S)-KET). The extrapolation of the curves shown in Fig. 2B suggests that a complete biodegradation of (R)-IBU would require around 60 days, while 80 days would be required for complete degradation of (S)-IBU. Extrapolated values should be taken with caution and would require further experimental confirmation. For KET, the biodegradation is complete after 25 days, as stated before.

On the other hand, an advantage of modelling BD is the possibility of estimating the half-life times ($t_{1/2}$). For (R)- and (S)-IBU the $t_{1/2}$ values were 18 and 25 days, respectively, whereas for (R)- and (S)-KET were 12 days. It should be noted that the quality of the estimation of half-life times provided by Eq. (4) depends on the agreement between the data and the fitted curves. These $t_{1/2}$ estimates should be less risky than those based on first-order kinetics (an extra-simplified model of Eq. S2, [44]) usually used in literature, which could provide inaccurate estimations if the mathematical assumption for using this model ($S_0 \ll K_s$, [44]) is not confirmed.

3.5. Enantioselective biodegradation results. Direct chromatographic approach

The enantiomeric fraction (EF) at each incubation time was calculated for IBU and KET enantiomers. This calculation is usually obtained from the concentration data (S data) of E1 and E2 enantiomers ($EF = S_{E1} / (S_{E1} + S_{E2})$). According to the aim of this work, an easy way to calculate EF values, directly from the chromatographic information (peak area), is proposed:

$$EF = \frac{A_{E1}}{A_{E1} + A_{E2}} \quad (5)$$

where A_{E1} and A_{E2} represent the area obtained for E1 and E2 enantiomers, respectively. This equation could be obtained from the definition of EF and the linear calibration equations for both enantiomers assuming that the slopes ($b_{1,E1}$ and $b_{2,E2}$) are statistically equal and the intercepts ($b_{0,E1}$ and $b_{0,E2}$) are statistically non-significant (see Section 3.6):

$$EF = \frac{S_{E1}}{S_{E1} + S_{E2}} = \frac{(A_{E1} - b_{0,E1})/b_{1,E1}}{(A_{E1} - b_{0,E1})/b_{1,E1} + (A_{E2} - b_{0,E2})/b_{1,E2}} \quad (6)$$

In addition, from Eqs. (1) and (5), the following equation can be derived:

$$EF = \frac{100 - BD_{E1}}{200 - BD_{E1} - BD_{E2}} \quad (7)$$

where BD_{E1} and BD_{E2} values are the BD values for E1 and E2 obtained from Eq. (1). This expression enables modelling the enantiomeric fraction versus time (EF vs. t) by combining the BD vs. t fitted curves obtained for the two enantiomers (Eq. (4))

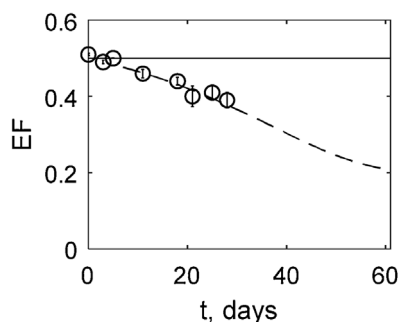


Fig. 4. Variation of the enantiomeric fraction (EF) of ibuprofen (mean \pm s from two replicates) during the biodegradation assay. EF values were calculated according to Eq. (5). Dashed line corresponds to the EF vs. t fitted curve. The horizontal line at $EF=0.5$ represents no enantioselective biodegradation.

Fig. 4 shows the experimental mean EF values together with their standard deviation ($EF \pm s$) obtained at each time during the biodegradation process for IBU. The horizontal line at $EF=0.5$ represents no enantioselectivity. In the same figure, the EF vs. t fitted curve (dashed line) is included. As can be observed, the fitted curve shows a reasonable agreement with the experimental EF values. For the first days ($t=0$ to $t=5$ days), EF values close to 0.5 were obtained that correspond to BD values close to zero for both enantiomers, as it was previously stated. After that, the EF values decreased to a value below 0.4 at $t=28$ days. The EF vs. t fitted curve in Fig. 4 allows extrapolating EF values at higher times. For instance, the EF expected at $t=60$ days (the time where (R)-IBU is nearly complete biodegraded) is around 0.2. This value is an extrapolation which should be taken with caution and would require an experimental confirmation.

The results obtained confirm that an enantiorecognition towards IBU enantiomers by the microorganisms present in the activated sludge used in this study has occurred, being the biodegradation of (R)-IBU higher than that of (S)-IBU. This enantiorecognition could be due to several mechanisms: enantioselective degradation, chiral inversion or the concurrence of both processes. These results agree with those obtained for constructed wetlands by Matamoros et al. [26] and with the most common behaviour observed in mammalian and some species of fungi for NSAIDs [28].

In the case of KET, as expected according to the previous sections, EF values close to 0.5 were obtained during the whole biodegradation process (not shown), confirming that its biodegradation process is not enantioselective. This result agrees with those reported in previous studies.

3.6. Additional remarks

BD and EF estimates were also calculated using the usual expressions based on concentration data (Eqs. (2) and (6)) for comparison purposes. The calibration curves of each IBU enantiomer were obtained by injection of standard solutions containing racemic IBU in the 2–30 mg L⁻¹ range (5 concentration levels). Table 2 shows the calibration statistics obtained for each enantiomer. As can be observed, satisfactory results ($R^2=0.998$) were obtained for both enantiomers. The 95% confidence intervals for the intercepts were 1 ± 9 and 2 ± 9 for (R)-IBU and (S)-IBU, respectively. This means that in both cases, b_0 is statistically equal to zero; which is the assumption considered in Eqs. (1) and (5). Moreover, slopes are comparable according to their confidence interval (10.0 ± 1.0 and 10.1 ± 1.0 , for (R)-IBU and (S)-IBU, respectively). A t -test was also used to compare both slopes [46]. The calculated t statistic (0.29) was lower than the critical value, $t_{0.025,8}$ (2.45), indicating the statistical equality of the slopes; which is the assumption considered in Eq. (5). When using

Table 2

Calibration statistics for ibuprofen (IBU) and ketoprofen (KET), (2–30 mg L⁻¹ racemate concentration range).

Method Calibration		
Enantiomer	Regression curve equation ($A = b_0 + b_1 S$) ^a	R^2
(R)-IBU	$A = 1.32 + 10.00 S$	0.998
(S)-IBU	$A = 1.84 + 10.13 S$	0.998
(R)-KET	$A = 5.28 + 12.71 S$	0.998
(S)-KET	$A = 7.12 + 13.61 S$	0.998
Selected regression statistics		
Enantiomer	CI (b_0), CI (b_1) ^b	S estimates (CI) ^c
(R)-IBU	$1 \pm 9, 10.0 \pm 1.0$	4.9 (3.6; 6.2)
(S)-IBU	$2 \pm 9, 10.1 \pm 1.0$	4.8 (3.4; 6.1)
(R)-KET	$5 \pm 12, 12.7 \pm 1.5$	3.5 (2.1; 5.0)
(S)-KET	$7 \pm 12, 13.6 \pm 1.5$	3.2 (1.7; 4.6)

^a A = peak area (mAU min); S = enantiomer concentration in the calibration standards; b_0 = intercept; b_1 = slope.

^b Confidence interval at 95% confidence level (CI) for b_0 and b_1 .

^c Concentration estimate and its CI (95%) corresponding to a peak area of $A = 50$ mAU min.

both A and S -data as dependent variables, very close values of BD and EF (at different times) were obtained. The maximum absolute BD difference was 2.3 whereas relative differences below 1% for EF were obtained. This indicates that, in general, both strategies could be used indistinctly.

However, when using S data obtained by interpolation into the calibration curves to calculate BD or EF data, the uncertainty associated to the interpolation should also be considered. As an example, Table 2 shows the confidence intervals for S_{E1} and S_{E2} estimates obtained by interpolation into the corresponding calibration curves of a peak area $A = 50$. Taking into account the associated confidence limits, the BD values for (R)-IBU would vary between 21 and 54% (values well below or above of the $t_{1/2}$ level). Therefore, the strategy of using direct A data instead of S as input variables provides less uncertain BD and EF estimations. Similar conclusions were obtained using the statistics for KET.

The purpose of the current methods is not routine sample analysis, but the estimation of the current biodegradation data of IBU and KET. For this reason, in our opinion, a full method validation seems to be unnecessary according to the concept of “fit-for-purpose”. Despite this, Table 3 shows some established analytical features obtained for the current methods used. Precision and trueness were investigated with two replicates of spiked solutions at two concentration levels (8 and 1.2 mg L⁻¹) in MSM, which were prepared on five different days. The selectivity was assessed for three biodegradation samples (at $t = 3, 11$ and 21 days) by means of an automated tool for evaluating peak purity of the Chemstation software (Section 2.1). Nine spectra per peak provided match factor values higher than 995 (over 1000) in all cases; thus, selectivity was considered satisfactory. R_s values were in the 2.8–2.9 and 1.6–1.8 ranges for IBU and KET enantiomers, respectively, at the concentrations levels of the calibration standards.

Finally, adapting accepted protocols used by ISO 17025-accredited laboratories, during the working analysis session (all samples were processed in the same day), one abiotic sample at $t = 0$ was used as a quality assurance stage to control the signal stability. This solution was injected at the start and the end of the working session (as a verification standard) and after each seven sample injections (as a quality control standard), totalling 6 times. The relative errors were calculated using the initial peak area values as references. Since all errors were below the $\pm 5\%$ (within the

Table 3

Validation parameters for ibuprofen (IBU) and ketoprofen (KET) enantiomers. For precision (intra- and inter-day relative standard deviation, RSD) and trueness (relative errors) evaluation, data matrices of 2 × 5 (replicates × days) results were obtained and processed by analysis of variance (ANOVA) [47].

Parameter	(R)-IBU	(S)-IBU	(R)-KET	(S)-KET
RSD, %	4.5, 6.0 ^a	4.3, 6.1 ^a	5.4, 3.7 ^a	6.4, 4.9 ^a
(Intra-day, Inter-day)	6.9, 6.5 ^b	6.7, 6.6 ^b	9.4, 7.8 ^b	9.1, 8.2 ^b
Mean relative errors, %	−1.4, 4.9, −9.0, 9.2, −0.3 ^a	−1.4, 4.9, −8.8, 8.7, −0.3 ^a	6.4, −1.1, −2.1, 4.4, −6.5 ^a	6.9, −1.2, −2.1, 4.1, −6.8 ^a
(during five days)	2.0, −9.1, 7.0, 9.5, −6.4 ^b	2.0, −9.2, 6.9, 9.1, −6.5 ^b	−0.2, −6.2, 7.0, 9.5, 1.8 ^b	−0.2, −6.7, 7.1, 8.9, 1.9 ^b
Limit of detection, mg L ^{−1c}	0.2	0.3	0.2	0.2
Limit of quantification, mg L ^{−1c}	0.8	0.9	0.7	0.7
Sensibility, mAU min L mg ^{−1d}	10.0	10.1	12.7	13.6

^a Spiked concentration level: 8 mg L^{−1}.

^b Spiked concentration level: 1.2 mg L^{−1}.

^c Standard solutions in MSM were used for determining the concentrations of each enantiomer that gave a signal/noise ratio of 3/1 and 10/1 for detection and quantification limits, respectively. The noise was measured from chromatograms of blank samples in the same regions as the peaks of enantiomers [48].

^d Sensibility was estimated as the slope of the calibration curve (Table 2).

± 10% prefixed level), it was considered that the peak areas of the biotic and abiotic samples were stable during the session.

4. Conclusions

An enantioselective biodegradability test of ibuprofen (IBU) and ketoprofen (KET), two of the drugs most consumed, was established using an inoculum (activated sludge from a waste water treatment plant) whose activity was verified using fluoxetine as reference compound. IBU and KET enantiomers were monitored using two chiral RPLC methods suitable for samples analysis. As a result of this test (compatible with the OECD guidelines), both compounds exhibited ready biodegradability, with no significant abiotic degradation. In addition, the results indicated that an enantiorecognition towards IBU enantiomers by the microorganisms present in the activated sludge used in this study occurred, being the biodegradation of (R)-IBU higher than that of (S)-IBU. For KET, non-enantioselective biodegradation was observed.

The biomass growth, indicated by the optical density at 600 nm, confirmed the biodegradation process. For both NSAIDs, the maximum biomass growth was observed at $t=5$ days, followed by a stationary/decline growth phase. In this last phase the differential behaviour for IBU enantiomers was observed.

In this work, new equations to estimate significant parameters related to the biodegradation process -biodegradation (*BD*), enantiomeric fraction (*EF*) and half-life time ($t_{1/2}$)- directly from the chromatographic information (peak area, *A*) have been proposed. The use of these equations provided similar estimates to those obtained using concentration data (*S*). However, the use of *A* data as input variable, instead of *S*, eliminates the uncertainty associated to the use of calibration curves and should provide less uncertain *BD* and *EF* estimations.

Thus, using the new equations proposed some relevant parameters related to the biodegradation process were estimated for IBU and KET: (i) Half-life times of (R)-IBU and (S)-IBU were 18 and 25 days, respectively; while for both KET enantiomers were 14 days. (ii) IBU enantiomers required 60–80 days to reach a complete biodegradation, while KET only needed 25 days. (iii) The enantiomeric fraction of IBU decreased to approximately 0.4 at 28 days and the expected minimum value could be around 0.2 at 60 days (extrapolated output).

The results obtained in this work correspond to ready biodegradability tests (laboratory scale) compatible with the OECD recommendations (whose analyte and microorganisms amounts differ from those in the environment). The data can be considered as indicative of its potential degradation in most environments including biological sewage treatment plants, according to OECD guidelines. In spite of this, a direct extrapolation of the results to the environmental or wastewater treatment scale should not be performed.

Conflicts of interest

The authors declare no conflict of interest.

Acknowledgements

The authors acknowledge the Spanish Ministerio de Economía y Competitividad (MINECO) and the European Regional Development Fund (ERDF) for the financial support (Project CTQ2015-70904-R, MINECO/FEDER, UE).

Appendix A. Supplementary data

Supplementary material related to this article can be found, in the online version, at doi:<https://doi.org/10.1016/j.chroma.2018.07.034>.

References

- [1] K. Kümmerer, The presence of pharmaceuticals in the environment due to human use- present knowledge and future changes, *J. Environ. Manag.* 90 (2009) 2354–2366.
- [2] B. Petrie, R. Barden, B. Kasprzyk-Hordern, A review on emerging contaminants in wastewaters and the environment: current knowledge, understudied areas and recommendations for future monitoring, *Water Res.* 72 (2015) 3–27.
- [3] V. Geissen, H. Mol, E. Klumpp, G. Umlauf, M. Nadal, M. van der Ploeg, S.E.A.T.M. van de Zee, C.J. Ritsema, Emerging pollutants in the environment: a challenge for water resource management, *Int. Soil Water Conserv. Res.* 3 (2015) 57–65.
- [4] A.J. Ebele, M.A.E. Abdallah, S. Harrad, Pharmaceuticals and personal care products (PPCPs) in the freshwater aquatic environment, *Emerg. Contam.* 3 (2017) 1–16.
- [5] E. Sanganyado, Z. Lu, Q. Fu, D. Schlenk, J. Gan, Chiral pharmaceuticals: a review on their environmental occurrence and fate processes, *Water Res.* 124 (2017) 527–542.
- [6] C.S. Wong, Environmental fate processes and biochemical transformations of chiral emerging organic pollutants, *Anal. Bioanal. Chem.* 386 (2006) 544–558.
- [7] J.K. Stanley, A.J. Ramirez, M. Mottaleb, C.K. Chambliss, B.W. Brooks, Enantiospecific toxicity of the β -blocker propranolol to *Daphnia magna* and *Pimephales promelas*, *Environ. Toxicol. Chem.* 25 (2006) 1780–1786.
- [8] J.K. Stanley, A.J. Ramirez, C.K. Chambliss, B.W. Brooks, Enantiospecific sublethal effects of the antidepressant fluoxetine to a model aquatic vertebrate and invertebrate, *Chemosphere* 69 (2007) 9–16.
- [9] B. Kasprzyk-Hordern, Pharmacologically active compounds in the environment and their chirality, *Chem. Soc. Rev.* 39 (2010) 4466–4503.
- [10] A.R. Ribeiro, P.M.L. Castro, M.E. Tiritan, Environmental fate of chiral pharmaceuticals: determination, degradation and toxicity, in: E. Lichtfouse, J. Schwarzbauer, D. Robert (Eds.), *Environmental Chemistry for a Sustainable World Volume 2: Remediation of Air and Water Pollution*, Springer, Dordrecht, 2012, pp. 3–45.
- [11] A.R. Ribeiro, L.H.M.L.M. Santos, A.S. Maia, C. Delerue-Matos, P.M.L. Castro, M.E. Tiritan, Enantiomeric fraction evaluation of pharmaceuticals in environmental matrices by liquid chromatography–tandem mass spectrometry, *J. Chromatogr. A* 1363 (2014) 226–235.
- [12] P. Vazquez-Roig, B. Kasprzyk-Hordern, C. Blasco, Y. Picó, Stereoisomeric profiling of drugs of abuse and pharmaceuticals in wastewaters of Valencia (Spain), *Sci. Total Environ.* 494–495 (2014) 49–57.
- [13] B. Kasprzyk-Hordern, D.R. Baker, Enantiomeric profiling of chiral drugs in wastewater and receiving waters, *Environ. Sci. Technol.* 46 (2012) 1681–1691.

- [14] S.E. Evans, J. Bagnall, B. Kasprzyk-Hordern, Enantioselective degradation of amphetamine-like environmental micropollutants (amphetamine, methamphetamine, MDMA and MDA) in urban water, *Environ. Pollut.* 215 (2016) 154–163.
- [15] A.R. Ribeiro, A.S. Maia, I.S. Moreira, C.M. Afonso, P.M.L. Castro, M.E. Tiritan, Enantioselective quantification of fluoxetine and norfluoxetine by HPLC in wastewater effluents, *Chemosphere* 95 (2014) 589–596.
- [16] OECD, Revised Introduction to the OECD Guidelines for Testing of Chemicals, Section 3, OECD Guidelines for the Testing of Chemicals, Section 3, OECD Publishing, Paris, 2006, <http://dx.doi.org/10.1787/9789264030213-en>.
- [17] S. Evans, J. Bagnall, B. Kasprzyk-Hordern, Enantiomeric profiling of a chemically diverse mixture of chiral pharmaceuticals in urban water, *Environ. Pollut.* 230 (2017) 368–377.
- [18] J. Bagnall, L. Malia, A. Lubben, B. Kasprzyk-Hordern, Stereoselective biodegradation of amphetamine and methamphetamine in river microcosms, *Water Res.* 47 (2013) 5708–5718.
- [19] A.R. Ribeiro, C.M. Afonso, P.M.L. Castro, M.E. Tiritan, Enantioselective HPLC analysis and biodegradation of atenolol, metoprolol and fluoxetine, *Environ. Chem. Lett.* 11 (2013) 83–90.
- [20] A.R. Ribeiro, C.M. Afonso, P.M.L. Castro, M.E. Tiritan, Enantioselective biodegradation of pharmaceuticals, alprenolol and propranolol, by an activated sludge inoculum, *Ecotoxicol. Environ. Saf.* 87 (2013) 108–114.
- [21] Z. Li, E. Gomez, H. Fenet, S. Chiron, Chiral signature of venlafaxine as a marker of biological attenuation processes, *Chemosphere* 90 (2013) 1933–1938.
- [22] I.S. Moreira, A.R. Ribeiro, C.M. Afonso, P.M.L. Castro, M.E. Tiritan, Enantioselective biodegradation of fluoxetine by the bacterial strain *Labrys portucalensis* F11, *Chemosphere* 111 (2014) 103–111.
- [23] S. Kane, The Top 200 Drugs of 2017? *Pharmacy Times*, 2017, march 20.
- [24] N.H. Hashim, S.J. Khan, Enantioselective analysis of ibuprofen, ketoprofen and naproxen in wastewater and environmental water samples *J. Chromatogr. A* 1218 (2011) 4746–4754.
- [25] N.H. Hashim, R.M. Stuetz, S.J. Khan, Enantiomeric fraction determination of 2-arylpropionic acids in a package plant membrane bioreactor, *Chirality* 25 (2013) 301–307.
- [26] V. Matamoros, M. Hijosa, J.M. Bayona, Assessment of the pharmaceutical active compounds removal in wastewater treatment systems at enantiomeric level. Ibuprofen and naproxen, *Chemosphere* 75 (2009) 200–205.
- [27] C. Caballo, M.D. Sicilia, S. Rubio, Enantioselective determination of representative profens in wastewater by a single-step sample treatment and chiral liquid chromatography–tandem mass spectrometry, *Talanta* 134 (2015) 325–332.
- [28] S.J. Khan, L. Wang, N.H. Hashim, J.A. McDonald, Distinct enantiomeric signals of ibuprofen and naproxen in treated wastewater and sewer overflow, *Chirality* 26 (2014) 739–746.
- [29] H.-R. Buser, T. Poiger, M.D. Müller, Occurrence and environmental behavior of the chiral pharmaceutical drug ibuprofen in surface waters and in wastewater, *Environ. Sci. Technol.* 33 (1999) 2529–2535.
- [30] N.H. Hashim, L.D. Nghiem, R.M. Stuetz, S.J. Khan, Enantiospecific fate of ibuprofen, ketoprofen and naproxen in a laboratory-scale membrane bioreactor, *Water Res.* 45 (2011) 6249–6258.
- [31] T.T. Chen, Q. Li, J.M. Lu, C. Yu, C. Chen, Z.P. Li, Determination of ibuprofen enantiomers in human plasma by HPLC–MS/MS: validation and application in neonates, *Bioanalysis* 8 (2016) 1237–1250.
- [32] J.M. Padró, J. Osorio-Grisales, J.A. Arancibia, A.C. Olivieri, C.B. Castells, Enantiomeric analysis of overlapped chromatographic profiles in the presence of interferences. Determination of ibuprofen in a pharmaceutical formulation containing homatropine, *J. Chromatogr. A* 1467 (2016) 255–260.
- [33] A. Imran, H. Iqbal, S. Kishwar, Y.A.E. Hassan, Enantiomeric resolution of ibuprofen and flurbiprofen in human plasma by SPE-chiral HPLC methods, *Comb. Chem. High Throughput Screen.* 15 (2012) 509–514.
- [34] J. Ye, W. Yu, G. Chen, Z. Shen, S. Zeng, Enantiomeric separation of 2-arylpropionic acid nonsteroidal anti-inflammatory drugs by HPLC with hydroxypropyl- β -cyclodextrin as chiral mobile phase additive, *Biomed. Chromatogr.* 24 (2010) 799–807.
- [35] A.R.M. De Oliveira, E.J. Cesarino, P.S. Bonato, Solid-phase microextraction and chiral HPLC analysis of ibuprofen in urine, *J. Chromatogr. B* 818 (2005) 285–291.
- [36] B. Vermeulen, J.P. Remon, Validation of a high-performance liquid chromatographic method for the determination of ibuprofen enantiomers in plasma of broiler chickens, *J. Chromatogr. B* 749 (2000) 243–251.
- [37] C. Her, A.P. Alonzo, J.Y. Vang, E. Torres, V.V. Krishnan, Real-time enzyme kinetics by quantitative NMR spectroscopy and determination of the Michaelis–Menten constant using the Lambert–W function, *J. Chem. Educ.* 92 (2015) 1943–1948.
- [38] OECD, Test No. 302B: Inherent Biodegradability: Zahn–Wellens/EVPA Test, OECD Publishing, Paris, 1992, <http://dx.doi.org/10.1787/9789264070387-en>.
- [39] I. Matarashvili, D. Ghughunishvili, L. Chankvetadze, N. Takaishvili, T. Khataishvili, M. Tsintsadze, T. Farkas, B. Chankvetadze, Separation of enantiomers of chiral weak acids with polysaccharide-based chiral columns and aqueous-organic mobile phases in high-performance liquid chromatography: typical reversed-phase behavior? *J. Chromatogr. A* 1483 (2017) 86–92.
- [40] ISO 9888:1999, Norma UNE-EN ISO 9888. Calidad del agua. Evaluación de la biodegradabilidad aerobia final de los compuestos orgánicos en medio acuoso. Ensayo estático (Método de Zahn–Wellens), AENOR, Madrid, 1999.
- [41] M.L. Shuler, F. Kargi (Eds.), *Bioprocess Engineering: Basic Concepts*, 2nd ed., Prentice Hall, Upper Saddle River, NJ, 2002.
- [42] J.A. Robinson, J.M. Tiedje, Nonlinear estimation of Monod growth kinetic parameters from a single substrate depletion curve, *Appl. Environ. Microbiol.* 45 (1983) 1453–1458.
- [43] C. Liu, J.M. Zachara, Uncertainties of Monod kinetic parameters nonlinearly estimated from batch experiments, *Environ. Sci. Technol.* 35 (2001) 133–141.
- [44] C.T. Goudar, K.A. Strevett, Estimating in-situ Monod biodegradation parameters using a novel explicit solution of a one-dimensional contaminant transport equation, *Ground Water* 38 (2000) 894–898.
- [45] R.M. Corless, G.H. Gonnet, D.E. Hare, D.J. Jeffrey, On the Lambert W Function. Technical Report Cs-93-03, Department of Computer Science, University of Waterloo, Waterloo, 1993.
- [46] D.L. Massart, B.G.M. Vandeginste, L.M.C. Buydens, S. De Jong, P.J. Lewi, J. Smeyers-Berbeke, *Handbook of Chemometrics and Qualimetrics, Part A*, Elsevier, Amsterdam, 1997, pp. 208.
- [47] A. Maroto, J. Riu, R. Boqué, F.X. Rius, Estimating uncertainties of analytical results using information from the validation process, *Anal. Chim. Acta* 391 (1999) 173–185.
- [48] M. Ribani, C.H. Collins, C.B.G. Bottoli, Validation of chromatographic methods: evaluation of detection and quantification limits in the determination of impurities in omeprazole, *J. Chromatogr. A* 1156 (2007) 201–205.

Supplementary data

(1) OD₆₀₀ for ibuprofen and ketoprofen during the biodegradation assays

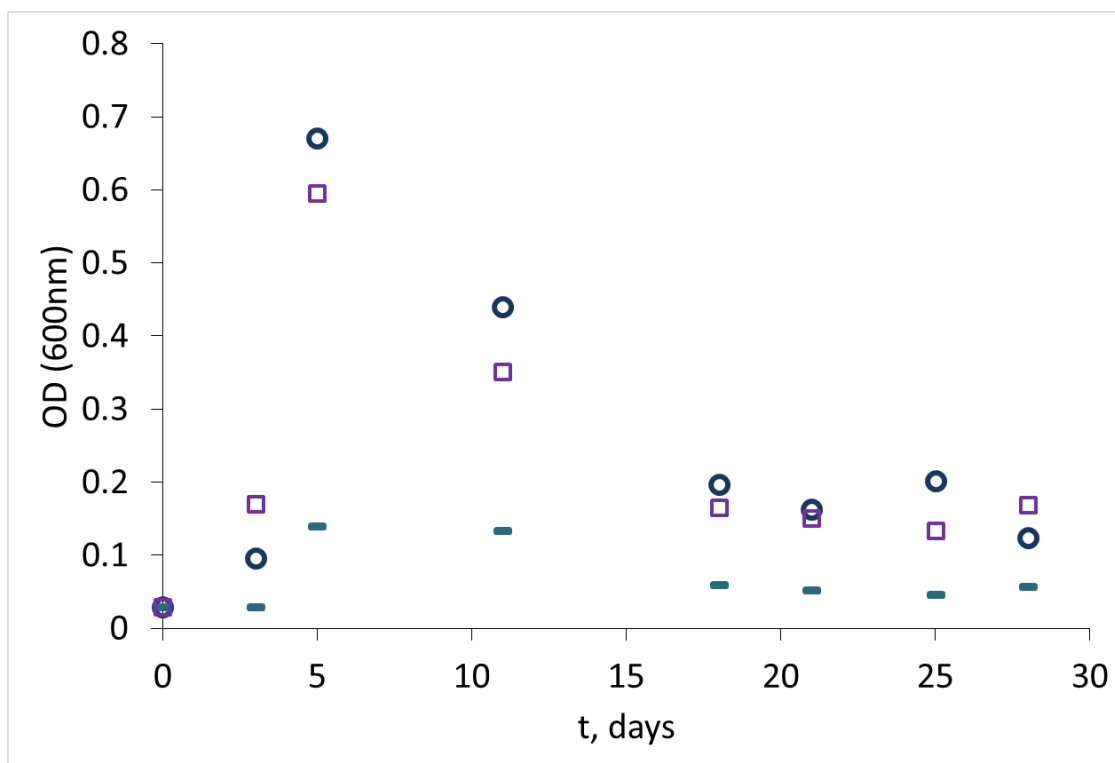


Fig. S1. Optical density at 600 nm (OD₆₀₀) for the biodegradation assays of (○) ibuprofen (15.6 mg L⁻¹), (□) ketoprofen (18.6 mg L⁻¹) and a blank (-). The OD₆₀₀ can be considered proportional to the biomass growth [41]. After an initial exponential growth phase until day 5, a stationary/decline growth phase is observed.

(2) Biodegradation models

Common biodegradation models proposed in the literature (the nonlinear Monod equation and its simplified version, the Michaelis-Menten-like equation) are unreliable approaches in terms of kinetic parameters accuracy. This is due to the linear correlation between the parameters [42,43] (see the main text). This is particularly evident for imprecise data (e.g. peak areas and estimated concentrations), low substrate concentration (S) and few incubation times (t). Despite this, both Monod and Michaelis-Menten-like equations often provide good fit of the model (S vs. t fitted curve) to the experimental data (S - t experimental data pairs), even with wrong parameter estimates. If the aim is just to obtain the fitted S vs. t curve any of these models can be used. The Michaelis-Menten-like equation does not account for the biomass concentration and the microbial yield coefficient, necessary for the Monod equation. Thus, the Michaelis-Menten-like equation is simpler. (eq. S1).

$$\frac{dS}{dt} \sim \left(- \frac{V_m S}{K_s + S} \right) \quad (\text{S1})$$

where V_m approaches the maximum specific growth rate and K_s approaches the half saturation constant for growth. In the simplified approach, V_m is assumed constant (which is only strictly true in the case of no (or negligible) biomass growth [44] (see the main text). An explicit solution for eq. S1 [44] is based on the Lambert W function (W relates S and t ; $S = W\{t\}$ [45] (see the main text):

$$S = K_s \cdot W \left\{ \frac{S_0}{K_s} e^{\left(\frac{S_0 - V_m \cdot t}{K_s} \right)} \right\} \quad (\text{S2})$$

where S_0 is the initial concentration of the compound. Eq. S2 could provide estimations of V_m and K_s by means of nonlinear regression. Since $BD = 100 (S_0 - S) / S_0$, eq. S2 can be adapted for BD (see Eq. 4 in the main text).

Algorithm used in MATLAB® for Eq. 4:

$$BD = 100/S0 * (S0 - [\text{betaBD}(2) * \log(1 + S0/\text{betaBD}(2) * \exp((S0 - \text{betaBD}(1) * t)/\text{betaBD}(2))) * (1 - \log(1 + \log(1 + S0/\text{betaBD}(2) * \exp((S0 - \text{betaBD}(1) * t)/\text{betaBD}(2)))))) / (2 + \log(1 + S0/\text{betaBD}(2) * \exp((S0 - \text{betaBD}(1) * t)/\text{betaBD}(2))))])$$

Where $\text{betaBD}(1)$ and $\text{betaBD}(2)$ are the estimates of V_m and K_s from BD vs. t experimental data.



PAPER VII

**Reversed phase liquid chromatography for the
enantioseparation of local anaesthetics in
polysaccharide-based stationary phases. Application
to biodegradability studies**

**Mireia Pérez-Baeza^a, Laura Escuder-Gilabert^a, Yolanda Martín-Biosca^a,
Salvador Sagrado^{a,b}, María José Medina-Hernández^a**

^a Departamento de Química Analítica, Universitat de València, Burjassot, Valencia, Spain

^b Instituto Interuniversitario de Investigación de Reconocimiento Molecular y Desarrollo Tecnológico (IDM), Universitat Politècnica de València, Universitat de València, Valencia, Spain

Journal of Chromatography A 1625 (2020) 461334



Reversed phase liquid chromatography for the enantioseparation of local anaesthetics in polysaccharide-based stationary phases. Application to biodegradability studies

Mireia Pérez-Baeza^a, Laura Escuder-Gilabert^a, Yolanda Martín-Biosca^{a,*}, Salvador Sagrado^{a,b}, María José Medina-Hernández^{a,*}

^aDepartamento de Química Analítica, Universitat de València, Burjassot, Valencia, Spain

^bInstituto Interuniversitario de Investigación de Reconocimiento Molecular y Desarrollo Tecnológico (IDM), Universitat Politècnica de València, Universitat de València, Valencia, Spain

ARTICLE INFO

Article history:

Received 3 March 2020

Revised 4 June 2020

Accepted 8 June 2020

Available online 10 June 2020

Keywords:

Local anaesthetics

Cellulose and amylose-based chiral stationary phases

Reversed phase conditions

Enantioselective biodegradation study

ABSTRACT

A comprehensive study on the chiral separation of bupivacaine, mepivacaine, prilocaine and propanocaine with eight commercial polysaccharide-based chiral stationary phases (CSPs) in reversed phase conditions compatible with MS detection is performed. Methanol and acetonitrile are used as organic modifiers. Retention and resolution values obtained for each compound in the different CSPs and mobile phases are compared. The polysaccharide-based CSPs tested present different enantioselectivity towards the analytes. From the results, the experimental conditions for determining the enantiomers of bupivacaine, mepivacaine, prilocaine and propanocaine in saline aqueous samples using MS detection are used, for the first time, to perform an enantioselective biodegradability study.

© 2020 Elsevier B.V. All rights reserved.

1. Introduction

Local anaesthetics are one of the most used analgesics. They are drugs that reversibly inhibit the production and conduction of the stimulus of any excitable membrane, particularly in nerve tissue. This action is used to produce loss of pain sensitivity in a particular area of the body. Adverse effects are infrequent; however, their systemic toxicity can result in serious patient harm, including seizure, cardiac compromise and death [1,2].

Local anaesthetics have in their molecular structure a lipophilic aromatic ring, an intermediate ester or amide linkage and a tertiary amine, which are responsible for the clinical properties of the molecule [1]. Furthermore, some local anaesthetics are chiral and their enantiomers show significant differences in pharmacological and toxicological properties. Thus, (*R*)-bupivacaine shows greater potency and toxicity in the cardiovascular and central nervous systems than (*S*)-bupivacaine. The enantiomers of prilocaine also show different toxicity. It has been found that the (*S*)-prilocaine enantiomer is the most toxic and the hepatic clearance of (*R*)-prilocaine is greater [3].

High-performance liquid chromatography (HPLC) with chiral stationary phases (CSPs) is widely used for the separation of chiral compounds. Among the large number of CSPs commercially available the polysaccharide-based chiral stationary phases are one of most commonly used, due to their broad applicability [4,5]. Separations with these CSPs are normally carrying out in normal and polar organic conditions and less frequently in reversed phase conditions [5]. Reversed phase conditions are adequate for chiral separation of polar compounds as well as for the analysis of aqueous matrix samples (e.g. biological and environmental samples), and can be compatible with MS detection if the usual non-volatile additives (e.g. hexafluorophosphate, phosphate buffers) or suppress analyte response (e.g. diethylamine) are avoided.

The separation of the enantiomers of local anaesthetics has been performed using polysaccharide-based CSPs in both normal and polar organic conditions [6–12]. However, as far as we know, only two applications on the use of reversed conditions have been reported for the separation of bupivacaine [13] and mepivacaine enantiomers [14]. The separation of bupivacaine enantiomers was achieved using cellulose tris(3,5-dimethylphenylcarbamate) and a mobile phase consisting of a mixture of methanol: 20 mM ammonium bicarbonate buffer 70:30 with 0.1% of diethylamine. For mepivacaine enantiomers, the use of immobilized cellulose tris(3,5-dichlorophenylcarbamate) and a mobile phase con-

* Corresponding author.

E-mail addresses: Yolanda.martin@uv.es (Y. Martín-Biosca), maria.j.medina@uv.es (M.J. Medina-Hernández).

sisting of a mixture of acetonitrile: 20 mM ammonium bicarbonate buffer 35:65 was proposed. No references were found in the literature for the other local anaesthetics under study (prilocaine and propanocaine).

Nowadays, the presence of drugs in the environment is a big issue because of the possible impact of these compounds not only in human health but also in the environment [15,16]. Of special concern is the occurrence of chiral drugs whose enantiomers may have different toxicological and ecotoxicological properties compared to each other [17–19]. They can be present in the environment in different proportions as a result of the enantioselective human metabolism, and also of the microbial biodegradation during the wastewater treatment process. In this context, the quantification of enantiomeric fraction (*EF*) during enantioselective studies about biodegradation is crucial for environmental risk assessment [20–22].

Local anesthetics are ubiquitous compounds in the environment due to their high hospital use [23]. In fact, the presence in wastewater of mepivacaine, lidocaine bupivacaine, prilocaine, procaine and benzocaine in concentrations in the ng L⁻¹ level has been reported [24,25]. Nevertheless, there are no references in the literature about the possible enantioselective biodegradation of local anesthetics.

In this paper a systematic study on the chiral separation of the local anaesthetics bupivacaine, mepivacaine, prilocaine and propanocaine using five cellulose based CSPs, (Lux® Cellulose 1, Lux® Cellulose 2, Lux® Cellulose 3, Lux® Cellulose 4 and immobilised Lux® Cellulose 5) and three amylose based CSPs (Lux® Amylose 1, Lux® Amylose 2 and immobilised Lux® Amylose 3), under reversed phase conditions compatible with MS detection is performed. Methanol and acetonitrile were used as organic modifiers. Retention and resolution values obtained for each compound in the different CSPs and mobile phases were compared. As far as we know, it is the first time that this kind of study is performed in the current experimental conditions. From the resolution values and the chromatographic retention times obtained the experimental conditions for determining the enantiomers of bupivacaine, mepivacaine, prilocaine and propanocaine in aqueous samples using MS detection were proposed. These conditions were applied to evaluate for the first time the biodegradability of bupivacaine, mepivacaine, prilocaine and propanocaine enantiomers according to the OECD ready biodegradability test [26,27].

2. Material and methods

2.1. Chemicals and solutions

Racemic bupivacaine (BUPI) was from Cayman Chemical Co (Ann Arbor, MI, USA) and (*S*)-bupivacaine hydrochloride (*S*-BUPI) was from Sigma-Aldrich (©Merck KGaA, Darmstadt, Germany). The rest of drugs tested were kindly donated by several pharmaceutical laboratories: fluoxetine hydrochloride (FLX) by Alter (Madrid, Spain); racemic mepivacaine hydrochloride (MEPI) and racemic prilocaine hydrochloride (PRILO) by Laboratorios Inibsa (Barcelona, Spain) and racemic propanocaine (PROPA) by Laboratorio Seid (Barcelona, Spain).

All reagents were of analytical grade. Ammonium acetate, ammonium bicarbonate, ammonium hydroxide, sodium azide, acetonitrile (ACN) and methanol (MeOH) (©Multisolvent, HPLC grade) were from Scharlau, S.L. (Barcelona, Spain). 5 mM ammonium bicarbonate buffer solution was prepared by dissolving the appropriate amount of ammonium bicarbonate in water and adjusting the pH to 8.0 with 1 M ammonium hydroxide. Ammonium acetate buffer solution (10 mM, pH 8.0) was prepared in the same way from ammonium acetate. Ultra Clear TWF UV ultrapure water (SG Water, Barsbüttel, Germany) was used to prepare solutions.

Binary mixtures consisting of different percentages of acetonitrile or methanol and ammonium bicarbonate buffer (5 mM, pH 8) (10–100% in volume of ACN or 30–90% in volume of MeOH) were tested as mobile phases for the separation of the chiral compounds. For the determination of FLX a mixture consisting of acetonitrile: ammonium acetate buffer (10 mM, pH 8.0) (60:40, v/v) was prepared as mobile phase.

The minimal salts medium (MSM) solution used in the biodegradability assays was prepared as previously described in references [21,22]. Activated sludge was kindly donated by General de Análisis Materiales y Servicios, S.L (GAMASER, S.L., Valencia, Spain). It was collected from the aerated tanks of the Quart Benàger WWTP (Valencia, Spain) [21,22] in plastic flasks and stored at 5 °C until usage. The storage time was lower than 24 h.

Stock standard solutions of 1000 mg L⁻¹ of BUPI, MEPI, PRILO, PROPA and FLX were prepared by dissolving the adequate amount of each compound in MeOH. To prepare the calibration standards, intermediate stock solutions of 100 mg L⁻¹ of BUPI, -MEPI, PRILO, PROPA and FLX were prepared by dilution of the corresponding 1000 mg L⁻¹ stock solution in MeOH. For each drug, calibration solutions in the concentration range 1–30 mg L⁻¹ were prepared by dilution of the corresponding intermediate stock solution of 100 mg L⁻¹ in the MSM. 10 mg L⁻¹ of *S*-BUPI in MSM was also prepared for the identification of the enantiomer peaks of BUPI. For the biodegradability assays, working solutions of approximately 20 mg L⁻¹ of BUPI, MEPI, PRILO, PROPA and FLX were prepared by dilution of the 1000 mg L⁻¹ stock solution in the MSM. The solutions were stored under refrigeration at 5 °C until usage.

2.2. Instrumentation

An Agilent Technologies 1100 chromatograph (Palo Alto, CA, USA) equipped with a binary pump, an UV–visible diode array detector, a mass spectrometer with a source of electrospray and atmospheric pressure chemical ionisation (ESI / APCI) and single quadrupole, a column thermostat and an autosampler was used. Data acquisition and processing were performed using the LC/MSD ChemStation software (B.04.02 SP1 [208], ©Agilent Technologies 2001–2010).

For the determination of FLX, an Halo C18 column (2.7 µm, 75 × 4.6 mm i.d.; Advanced Materials Technology, Wilmington, USA) was used. For the separation of the local anaesthetics enantiomers, eight polysaccharide-based chiral stationary phases were tested: Lux® Cellulose-1 (cellulose tris(3,5-dimethylphenylcarbamate); 3 µm, 150 × 4.6 mm i.d.; Phenomenex, Torrance, CA, USA); Lux® Cellulose-2 (cellulose tris(3-chloro-4-methylphenylcarbamate); 3 µm, 150 × 4.6 mm i.d.; Phenomenex); Lux® Cellulose-3 (cellulose tris(4-methylbenzoate); 3 µm, 150 × 4.6 mm i.d.; Phenomenex); Lux® Cellulose-4 (cellulose tris(4-chloro-3-methylphenylcarbamate); 3 µm, 150 × 4.6 mm i.d.; Phenomenex); immobilised Lux® Cellulose-5 (cellulose tris(3,5-dichlorophenylcarbamate); 3 µm, 150 × 4.6 mm i.d.; Phenomenex); Lux® Amylose-1 (amylose tris(3,5-dimethylphenylcarbamate); 3 µm, 150 × 4.6 mm i.d.; Phenomenex); Lux® Amylose-2 (amylose tris(5-chloro-2-methylphenylcarbamate); 3 µm, 150 × 2.0 mm i.d.; Phenomenex) and immobilised Lux® Amylose-3 (amylose tris(3-chloro-5-methylphenylcarbamate); 3 µm, 150 × 4.6 mm i.d.; Phenomenex).

The mobile phase flow rate was 1.0 mL min⁻¹ in all cases except for the Lux® Amylose-2. In this last column, the mobile phase flow rate was set at 0.5 mL min⁻¹. The separation temperature was set at 25 °C for fluoxetine and local anaesthetics. In some cases, temperatures of 15 and 40 °C were also assayed to improve the resolution of the enantiomers. The injection volume was 2 µL and the detection was performed in the UV at 220 nm.

In the mass detector, positive ESI mode was chosen under the following conditions: voltage, 3000 V; nebuliser pressure, 35 psig; N₂ flow, 12 L min⁻¹; drying temperature 350 °C. The total current ion chromatogram (TIC) with the mass/charge ratio range (*m/z*) of 100-500 was recorded. The selected ion monitoring mode (SIM), which corresponds to the [M+H]⁺ ion for each compound, was recorded too at the *m/z* values 289.2, 247.2, 221.2 and 312.2 for BUPI, MEPI, PRILO and PROPA, respectively.

For the preparation of sample mixtures, 15 mL conical sterile polypropylene tubes (Deltalab, S.L., Barcelona, Spain) were used. Disposable sterile filter pipette tips (Capp Expell, Odense, Denmark) were also used. For the biodegradability assays, a shaking incubator with temperature control (WiseCube@Wis-30, Witeg Labortechnik GmbH, Wetheim, Germany) was used. Prior to the measurement of the microbial growth, incubated samples were subjected to agitation in a vortex mixer (Velp Scientific Vortex, Usmate, Italy). Microbial growth was monitored by measuring the optical density of the cultures at 600 nm (OD₆₀₀) with an Epoch 2 microplate reader (Biotek Instruments Inc., Vermont, USA) and 96-well plates with UV transparent flat bottom (Corning, Kennebunk, ME, USA). Samples were stored at -80 °C in an ultra-low temperature freezer (U570 Premium, New Brunswick Scientific, Herts, UK) until chromatographic analysis.

Prior to injection into the chromatographic system, analyte solutions were filtered through disposable 0.22 μm Nylon® syringe filters (Análisis Vínicos, S.L., Tomelloso, Ciudad Real, Spain). Mobile phase solutions were vacuum-filtered through 0.22 μm Nylon® membranes (Micron Separations, Westboro, MA, USA) and were degassed in an Elmasonic S60 ultrasonic bath (Elma, Singen, Germany) prior to use. A Crison MicroPH 2000 pHmeter (Crison Instruments, Barcelona, Spain) was employed to adjust the pH of the buffer solutions.

2.3. Biodegradability assays

The biodegradability assays were performed in batch mode at approximately 20 mg L⁻¹ BUPI, MEPI, PRILO and PROPA. The incubation times of samples mixtures were prefixed a *t*=0, 3, 7, 14 and 28 days. The procedure followed to perform the biodegradability assays was similar to that used in previous papers [22]. In the present paper, sodium azide was added to prevent non-desirable microbial growth. In the abiotic assays, 0.1% NaN₃ solution in ultrapure water was used instead of the activated sludge to prepare sample mixtures. In the biotic assays, a small amount of NaN₃ was added to sample mixtures after incubation to stop the microbial activity. Biodegradability assays for FLX at 20 mg L⁻¹ were also performed to control inoculum activity [28] in parallel to those of local anaesthetics.

2.4. Calculations. Direct chromatographic approach

The values of biodegradation, *BD*, were calculated directly from the chromatographic information (peak area, *A*) according to a direct chromatographic approach recently published [22]:

$$BD = \frac{S_0 - S}{S_0} \times 100 = \frac{A_0 - A}{A_0} \times 100 \quad (1)$$

where *S* is the concentration data obtained over time, *S*₀ is the initial concentration and *A*₀ represents the area obtained at *t*=0.

The enantiomeric fraction (*EF*) at each incubation time was calculated either directly from the chromatographic peak area or using the concentration data obtained for each enantiomer [22]:

$$EF = \frac{S_{E1}}{S_{E1} + S_{E2}} = \frac{A_{E1}}{A_{E1} + A_{E2}} \quad (2)$$

where E1 and E2 represent the less and the most retained enantiomers, respectively.

Table 1

Chemical structure, molecular weight, the minus logarithm of the acidity constant (p*K*_a), the logarithm of the *n*-octanol-water partition coefficient (log*P*) and the logarithm of the *n*-octanol-water partition coefficient (log*D*) at pH 8 of local anesthetics.

Compound	Structure	<i>M</i> _r (g/mol)	p <i>K</i> _a ^a	log <i>P</i> ^a	log <i>D</i>
Bupivacaine		288.4	8.1	3.4	3.1
Mepivacaine		246.3	7.7	1.8	1.6
Prilocaine		220.3	7.9	2.1	1.9
Propanocaine		311.4	7.5	4.6	4.5

^a Estimated values obtained from reference [29].

For the estimation of the *BD* following this direct chromatographic approach it is assumed that the intercept (*b*₀) of the calibration lines of both enantiomers are equal to 0, i.e. statistically non-significant (logical situation in the absence of systematic error). To estimate *EF* values the assumption that the slopes (*b*₁) are statistically equal should also be met [22].

3. Results and discussion

3.1. Chiral chromatographic separation

The use of different polysaccharide-based CSPs in reversed phase conditions compatible with MS detection (i.e. aqueous-organic mobile phases in the absence of non-volatile reagents) for the separation of the enantiomers of local anaesthetics was investigated. Aqueous-organic mobile phases are preferable in the present study because of their compatibility with the saline aqueous matrix samples involved in the biodegradability assays. Table 1 shows the chemical structure, the molecular weight, *M*_r, the acidity constant, p*K*_a, the logarithm of the *n*-octanol-water partition coefficient, log*P*, and the log*D* (log*P* estimated at pH 8.0) for the studied compounds. At the working pH the compounds present positive charge (BUPI +0.55, MEPI +0.33, PRILO +0.44 and PROPA +0.25) and variable hydrophobic character (log*D* values range between 1.6 and 4.5).

For the separation of enantiomers of BUPI, MEPI, PRILO and PROPA five commercial cellulose-based CSPs [Lux® Cellulose-1 (Cell1), Lux® Cellulose-2 (Cell2), Lux® Cellulose-3 (Cell3), Lux® Cellulose-4 (Cell4) and Lux® Cellulose-5 (Cell5)] and three commercial amylose-based CSPs [Lux® Amylose-1 (Am1), Lux® Amylose-2 (Am2) and Lux® Amylose-3 (Am3)] (see experimental section) were tested. Several binary mixtures consisting of ammonium bicarbonate buffer (5 mM, pH 8) and different proportions of ACN (10-100%, v/v) or MeOH (30-90%, v/v) were assayed as mobile phases.

Tables 2 and 3 show the chromatographic data (retention and resolution data) obtained for BUPI, MEPI, PRILO and PROPA in all the reversed mobile phases assayed using cellulose and amylose-based chiral stationary phases, respectively. As can be observed, the separation results obtained for local anaesthetics in acetonitrile and methanol mobile phases were quite different.

When MeOH was used as organic modifier, for all the columns and compounds, retention decreased as the proportion of the organic modifier in the mobile phase increased (typical reverse-phase behavior). This behaviour has been previously reported for other compounds [4-5]. Methanol is a protic solvent and may compete with the analyte for hydrogen-bond interactions with the polysaccharide-based CSPs. The addition of water to methanol did not alter hydrogen-bond interactions, but hydrophobic interactions increase and therefore retention increase [4-5].

For aqueous-MeOH mobile phases, a linear trend between the logarithm of retention factors for the less retained enantiomers and their corresponding log*D* values for each CSP studied was ob-

Table 2

Chromatographic data obtained by HPLC-DAD for the enantioseparation of local anesthetics using cellulose-based chiral stationary phases and several mobile phases. Retention time (*t*), retention factor (*k*) of the second eluted enantiomer, and resolution (*R*_s) are shown. Mobile phases consist of mixtures of ammonium bicarbonate buffer (5 mM, pH 8) and different proportions of organic modifier.

Mobile phase		Bupivacaine			Prilocaine			Mepivacaine			Propanocaine			
Organic modifier	% (v/v)	<i>t</i> * (min)	<i>k</i> *	<i>R</i> _s	<i>t</i> * (min)	<i>k</i> *	<i>R</i> _s	<i>t</i> * (min)	<i>k</i> *	<i>R</i> _s	<i>t</i> * (min)	<i>k</i> *	<i>R</i> _s	
<i>Cell1</i>														
ACN	100	3.0	0.5	0	4.1	1.0	0	4.8	1.3	0	9.7	3.9	0	
	90	2.7	0.4	0	2.5	0.3	0	2.5	0.3	0	4.1	1.1	0	
	80	3.1	0.6	0	2.6	0.3	0	2.5	0.3	0	4.1	1.1	0	
	70	3.9	1.1	0	2.9	0.5	0	2.7	0.4	0	4.8	1.5	0	
	60	6.0	3.0	0	3.5	1.3	0	3.2	0.9	0	7.1	3.2	0	
	50	9.9	5.2	0	4.5	1.6	0	4.2	1.5	0	8.2	4.5	0	
	40	–	–	–	6.9	3.6	0	5.7	2.8	0	10.1	4.9	0	
	30	–	–	–	13.3	6.4	0.4	9.9	4.5	0	–	–	–	
	MeOH	90	3.3	0.9	0	2.7	0.6	0	2.6	0.5	0	4.8	1.8	0
		80	6.4	2.6	0.9	3.6	1.0	0	3.5	0.9	0	9.6	4.3	0
70		15.5	7.6	0.9	5.6	2.1	0	5.3	1.9	0	–	–	–	
60		–	–	–	11.5	5.4	0	10.8	5.0	0	–	–	–	
<i>Cell2</i>														
ACN	100	3.8	0.9	0.6	3.2	0.6	1.1	4.0	1.0	0.6	4.9	1.5	0	
	90	3.0	0.5	0	2.6	0.4	0.4	2.7	0.4	0	3.2	0.7	0	
	80	3.6	0.8	0	2.8	0.5	0.5	2.8	0.5	0	3.7	0.9	0	
	70	4.9	1.7	0	3.2	0.8	0.6	3.1	0.7	0.3	4.5	1.5	0.7	
	60	7.8	3.6	0.7	3.9	1.3	1.1	3.8	1.2	0.8	5.6	2.3	1.7	
	50	14.8	7.7	1.0	5.3	2.1	1.4	4.9	1.9	1.1	9.8	4.8	2.4	
	40	–	–	–	8.7	4.1	1.8	7.8	3.6	1.5	–	–	–	
	30	–	–	–	18.0	9.0	2.3	15.7	7.7	1.8	–	–	–	
	MeOH	90	3.3	0.8	0	2.6	0.4	0	2.7	0.5	0	3.9	1.2	0
		80	8.3	3.6	0	3.4	0.9	0	3.6	1.0	0	8.1	3.5	0
70		17.2	8.6	0	5.6	2.1	0	6.0	2.3	0	23.2	11.9	0.4	
60		–	–	–	11.0	5.1	0	12.4	5.9	0	–	–	–	
<i>Cell3</i>														
ACN	100	2.4	0.2	0	2.6	0.3	0	3.1	0.6	0	7.5	2.8	0	
	90	2.2	0.1	0	2.2	0.1	0	2.2	0.1	0	3.5	0.8	0	
	80	2.2	0.1	0	2.2	0.1	0	2.1	0.1	0	3.1	0.6	0	
	70	2.4	0.2	0	2.3	0.2	0	2.2	0.1	0	3.1	0.6	0	
	60	2.7	0.7	0	2.3	0.4	0	2.2	0.4	0	2.8	0.8	0	
	50	3.6	1.1	0	2.6	0.5	0	2.4	0.4	0	3.6	1.1	0	
	40	5.5	2.2	0	3.4	1.0	0	2.9	0.7	0	5.5	2.2	0	
	30	13.1	6.7	0	5.2	2.1	0	3.9	1.3	0	10.8	5.4	0	
	20	–	–	–	12.5	5.9	0	7.8	3.3	0	–	–	–	
	MeOH	90	2.4	0.3	0	2.4	0.3	0	2.2	0.2	0	3.6	0.9	0.7
80		3.3	0.7	0.5	2.9	0.5	0	2.5	0.3	0	6.5	2.4	0.6	
70		5.9	2.1	1.5	4.1	1.2	0	3.1	0.6	0	15.8	7.3	0.9	
60		17.3	8.1	1.4	7.8	3.1	0	5.2	1.7	0	–	–	–	
50		–	–	–	17.1	8.0	0	9.8	4.2	0	–	–	–	
40		–	–	–	–	–	–	17.9	8.4	0	–	–	–	
<i>Cell4</i>														
ACN	100	3.4	0.7	0	3.1	0.6	1.1	3.5	0.8	0.5	5.0	1.5	0	
	90	2.9	0.5	0	2.5	0.3	0	2.6	0.3	0	2.9	0.5	0	
	80	3.3	0.7	0	2.7	0.4	0.3	2.6	0.3	0	3.2	0.6	0.5	
	70	4.3	1.3	0	3.0	0.6	0.6	2.9	0.5	0	3.9	1.1	0.6	
	60	6.6	2.7	0	3.8	1.0	0.6	3.4	0.8	0	5.6	1.9	0.4	
	50	11.7	5.5	0	4.8	1.7	1.7	4.2	1.3	0.5	9.3	4.6	1.0	
	40	–	–	–	6.9	2.8	1.9	5.8	2.2	0.6	11.7	5.5	2.0	
	30	–	–	–	16.9	9.6	2.5	13.4	7.4	1.0	–	–	–	
	<i>Cell5</i>													
ACN	100	12.8	5.1	0	8.6	3.1	0	15.8	6.5	0	28.6	12.6	0	
	90	3.4	0.7	0	2.6	0.3	0	3.1	0.6	0.6	3.9	1.0	0	
	80	4.1	1.2	0	2.7	0.4	0	3.1	0.6	0.7	3.8	1.0	0	
	70	5.5	2.1	0.6	3.1	0.7	0	3.5	0.9	0.9	4.6	1.6	0	
	60	9.2	4.4	0.6	3.8	1.2	0	4.4	1.6	1.0	7.1	3.2	0	
	50	16.7	8.3	0	5.1	1.8	0.7	5.6	2.1	2.0	7.7	3.3	0.6	
	40	–	–	–	8.0	3.4	1.0	8.9	3.9	2.3	28.8	15.0	0.6	
	30	–	–	–	–	–	–	–	–	–	44.4	23.7	0.7	

*When *R*_s=0, the values correspond to the peak of the compound.

served, indicating that hydrophobicity of compounds plays a key role in the retention (e.g. PROPAs were the most retained according to its log*D*).

When ACN was used as organic modifier, for all the columns and compounds, the retention of compounds initially decrease for low water content in the mobile phase (HILIC behavior), while at the higher content (up to 20%(v/v) of water content) in the mo-

bile phase retention increase (reverse-phase behavior). This behaviour has been explained taking into account that, ACN, as a non-hydrogen-bond donor solvent, allows more hydrogen-bond interactions between the chiral analyte and the polysaccharide-based CSPs. The addition of water to the mobile phase provokes two opposite contributions in the retention of analytes. On one hand, water competes with analytes for hydrogen-bond interac-

Table 3

Chromatographic data obtained by HPLC-DAD for the enantioseparation of local anesthetics using amylose-based chiral stationary phases and several mobile phases. Retention time (t), retention factor (k) of the second eluted enantiomer, and resolution (R_s) are shown. Mobile phases consist of mixtures of ammonium bicarbonate buffer (5 mM, pH 8) and different proportions of organic modifier.

Mobile phase		Bupivacaine			Prilocaine			Mepivacaine			Propanocaine			
Organic modifier	%(v/v)	t^* (min)	k^*	R_s	t^* (min)	k^*	R_s	t^* (min)	k^*	R_s	t^* (min)	k^*	R_s	
<i>Am1</i>														
ACN	100	13.5	5.8	0	10.0	4.3	0	16.6	7.3	0	23.4	10.7	0	
	90	3.1	0.6	0	2.6	0.4	0	2.5	0.3	0	4.0	1.1	0	
	80	3.5	0.8	0	2.9	0.5	0.6	2.5	0.3	0	3.8	1.0	0	
	70	4.7	1.8	0	3.0	0.8	0	2.8	0.6	0	4.5	1.6	0	
	60	7.5	4.0	0	3.8	1.5	0	3.3	1.2	0	6.6	3.4	0.5	
	50	12.0	6.1	0	7.3	3.3	4.7	3.8	1.2	0	10.8	5.4	0.9	
	40	–	–	–	–	–	–	5.6	2.3	0	–	–	–	
	30	–	–	–	–	–	–	11.7	5.9	0	–	–	–	
	MeOH	90	2.7	0.8	0	6.2	3.1	9.5	2.2	0.5	0	4.6	2.1	0.5
		80	5.0	2.3	0.6	–	–	–	2.3	0.5	0	10.0	5.7	0.7
70		13.2	7.3	0.4	–	–	–	4.3	1.7	0	–	–	–	
60		–	–	–	–	–	–	11.6	4.5	0	–	–	–	
50		–	–	–	–	–	–	24.4	10.1	0	–	–	–	
<i>Am2</i>														
ACN	60	4.1	2.4	0	2.3	0.9	0	2.3	0.9	0	4.0	2.3	0.4	
	50	7.6	4.8	0	3.1	1.4	0	2.8	1.2	0	7.8	5.0	0.4	
	40	–	–	–	4.2	2.2	0	3.8	1.9	0	–	–	–	
	30	–	–	–	6.4	3.9	0	6.2	3.8	0	–	–	–	
MeOH	90	3.4	1.1	0	2.5	0.6	0	2.8	0.8	0	4.7	1.9	0	
	80	7.5	2.9	0	3.9	1.1	0	4.5	1.4	0	11.9	5.3	0	
	70	26.6	8.5	0	7.8	1.8	0	9.6	2.4	0	41.9	14.0	0	
<i>Am3</i>														
ACN	100	17.0	7.5	0	10.8	4.4	0	27.4	12.7	0	46.6	22.3	0	
	90	3.6	0.8	0.6	2.9	0.5	0	3.0	0.5	0	9.6	3.8	0.7	
	80	4.1	1.2	0.8	3.0	0.6	0	3.0	0.6	0.4	10.4	4.5	0.9	
	70	5.7	2.2	1.1	3.5	0.9	0	3.3	0.8	0.5	14.6	7.1	0.6	
	60	8.8	4.9	0	4.4	1.9	0.5	4.0	1.7	1.1	–	–	–	
	50	–	–	–	6.4	3.3	0.6	5.6	2.7	1.3	–	–	–	
	MeOH	90	4.4	1.9	1.3	3.6	1.4	0.6	3.0	1.0	0	16.6	10.1	0
80		8.8	4.5	1.1	5.0	2.1	0.8	4.0	1.5	0	41.9	25.2	0	
70		38.2	14.9	0.7	12.5	4.2	1.1	10.1	3.2	0	–	–	–	
60		–	–	–	24.9	9.4	1	20.2	7.4	0	–	–	–	

* When $R_s=0$, the values correspond to the peak of the compound.

tions with the polysaccharide-based-CSPs and reduces the analyte retention (HILIC like behavior). On the other hand, water promotes hydrophobic interactions between the analyte and the polysaccharide-based-CSPs and increases the analyte retention (reverse-phase like behavior) [4-5]. The explained effect is more evident for the column Cell3, Cell5 and Am1 for MEPI and PROPA.

Among the cellulose-based CSPs, the immobilised column Cell5 showed the highest retention values for all the studied compounds. In the case of amylose-based CSPs, the immobilised column Am3 showed the highest retention values for all the studied compounds.

The polysaccharide-based CSPs tested presented different enantioselectivity towards the analytes. As shown in Tables 2 and 3, in the conditions assayed, a single column was unable to completely resolve ($R_s > 1.5$) the enantiomers of the four studied compounds. The Cell2 CSP provided the best enantioselectivity, being able to resolve three of the four compounds under study (MEPI, PRILO and PROPA). The Cell4 allowed the resolution of two of the analytes (PRILO and PROPA), whereas the Cell3, Cell5 and Am1 CSPs only allowed the enantioseparation of one of the compounds (BUPI, MEPI and PRILO, respectively). The Cell1, Am2 and Am3 CSPs did not provide the complete resolution of any of the local anaesthetics, only the partial resolution of some of them. From the results, and in the experimental conditions tested, the cellulose-based CSPs showed better enantioselectivity towards the four analytes than the amylose-based CSPs.

The enantioselectivity of Cell2 and Cell4 for all the compounds was similar, although the resolution was generally better in Cell2. The only difference between these two stationary phases is the po-

sition of the chlorine and methyl substituents in the phenylcarbamate moieties. The Cell1 CSP contains two methyl groups in the positions 3 and 5 in the phenylcarbamate ring whereas the Cell5 has two chlorine atoms in these positions. As can be observed in Table 2, the R_s values obtained in Cell5 were in general better than in Cell1, especially for MEPI, which indicates that the presence of chlorine substituents has a deep impact on the enantioresolution. The nature and position of the substituents in Am1 and Cell1 are identical, however better resolution values were obtained with Am1, especially for PRILO. The inclusion of a chlorine atom at position 3 instead of a methyl group in Am3, compared with Am1, resulted in a slight improvement in resolution for BUPI and MEPI, but a worsening for PRILO and PROPA.

When it comes to the mobile phase, ACN as organic modifier provided, in most cases (see Tables 2 and 3), better enantioresolution than MeOH. However, the complete resolution of the BUPI enantiomers was only achieved using MeOH in the mobile phase (70%) and the Cell3 CSP. For this compound, in most cases, the use of ACN did not provide any enantioseparation; only partial resolution was achieved for the Cell2 CSP. It is also worth mentioning the excellent resolutions obtained for the enantioseparation of PRILO using the Am1 CSP and both MeOH and ACN as organic modifiers. The value of R_s value of 9.5 for the mobile phase consisting of MeOH: ammonium bicarbonate buffer (5 mM, pH 8) 90:10 (v/v) is by far the highest value obtained. In general, resolution improved as the percentage of ACN or MeOH decreased; for instance, for PRILO and MEPI in Cell2 using ACN, or PRILO using MeOH in Am3 (see Tables 2 and 3). However, in the case of BUPI in Am3 and MeOH as organic modifier the opposite behavior was observed; the

Table 4

Chiral separation conditions by HPLC-MS for biodegradation assays of local anesthetics. Chiral stationary phase, organic modifier, chromatographic conditions, retention times (t_R), resolution values (R_s) and calibration statistics are indicated for bupivacaine (BUPI), mepivacaine (MEPI), prilocaine (PRILO) and propanocaine (PROPA). Mobile phases consist of mixtures organic modifier: ammonium bicarbonate buffer 5 mM, pH=8.0.

Compound	Chiral SP	Organic modifier, %, v/v	T (°C)	Flow rate (mL min ⁻¹)	Enantiomer	t_R (min)	R_s	Calibration curve ^a		
								$b_0 \pm t \cdot s_{b_0}$	$b_1 \pm t \cdot s_{b_1}$	R^2
BUPI	Cell3	MeOH, 70%	40	0.5	R	7.8	1.5	$(1 \pm 4) \cdot 10^5$	$(3.48 \pm 0.07) \cdot 10^6$	0.9995
					S	8.5		$(1 \pm 4) \cdot 10^5$	$(3.77 \pm 0.08) \cdot 10^6$	0.9995
MEPI	Cell5	ACN, 50%	25	0.75	E1	6.9	2.0	$(1 \pm 14) \cdot 10^4$	$(5.02 \pm 0.15) \cdot 10^5$	0.9995
					E2	7.5		$(1 \pm 18) \cdot 10^4$	$(5.6 \pm 0.2) \cdot 10^5$	0.9992
PRILO	Cell4	ACN, 40%	25	1.0	E1	6.8	1.8	$(7 \pm 23) \cdot 10^4$	$(4.5 \pm 0.3) \cdot 10^5$	0.997
					E2	7.3		$(5 \pm 24) \cdot 10^4$	$(4.8 \pm 0.3) \cdot 10^5$	0.997
PROPA	Cell4	ACN, 40%	25	1.0	E1	10.6	2.0	$(-10 \pm 18) \cdot 10^4$	$(4.3 \pm 0.2) \cdot 10^5$	0.9990
					E2	11.7		$(-11 \pm 20) \cdot 10^4$	$(4.7 \pm 0.2) \cdot 10^5$	0.9990

^a b_0 , intercept and b_1 , slope of the calibration curve.

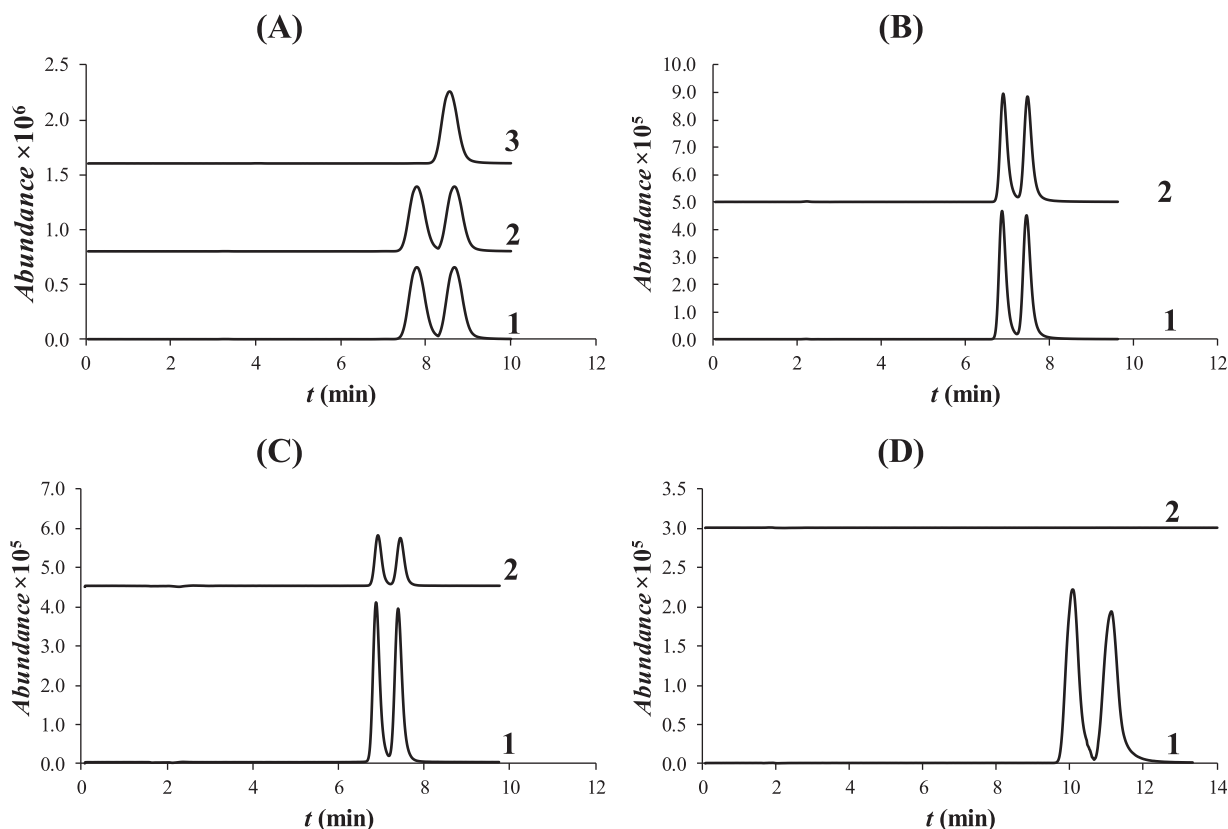


Figure 1. Chromatograms of (A) bupivacaine, (B) mepivacaine, (C) prilocaine and (D) propanocaine obtained by HPLC-MS using the experimental conditions detailed in Section 2.2. Chromatograms 1 and 2 correspond to samples containing racemic mixtures at $t=0$ and $t=28$ days of incubation, respectively. Chromatogram 3 corresponds to a standard solution of (*S*)-bupivacaine. Initial racemate concentrations were 19.8, 20.6, 21.0 and 21.0 mg L⁻¹ for BUPI, MEPI, PRILO and PROPA, respectively.

values of resolution were better when using higher proportions of MeOH in the mobile phase.

3.2. Chiral chromatographic analysis

Table 4 indicates the chromatographic conditions selected for each analyte to complete the chiral analysis of the samples in the subsequent biodegradability assays. These conditions were chosen considering both the enantioresolution and the retention times of the compounds obtained during the optimization process (see Tables 2 and 3). For BUPI and MEPI, the values of temperature and mobile phase flow rate were adjusted to obtain the most convenient conditions in terms of resolution and speed of analysis. Fig. 1 shows the chromatograms for the four local anesthetics obtained using the selected chromatographic conditions. The chromatograms correspond to some of the samples taken during the

biodegradability assay. In Fig. 1A, the chromatogram corresponding to the (*S*)-enantiomer of BUPI was included for identification purposes. In all cases, adequate separations were achieved in less than 12 min.

Methodological calibration for each enantiomer was performed under the chromatographic conditions selected. The calibration curves were obtained by injection of standard solutions containing the racemic compound in the 1–30 mg L⁻¹ range (5 concentration levels) (see Section 2.1). Table 4 shows the calibration statistics obtained for each enantiomer. Satisfactory results were obtained for the enantiomers of the four local anesthetics studied ($R^2 > 0.99$).

The confidence intervals for a 95% confidence level for the intercepts included the 0 value, which means that the values of b_0 are statistically equal to 0 (assumption made in Eq. (1)). These results proved the validity of the approach based on the direct use

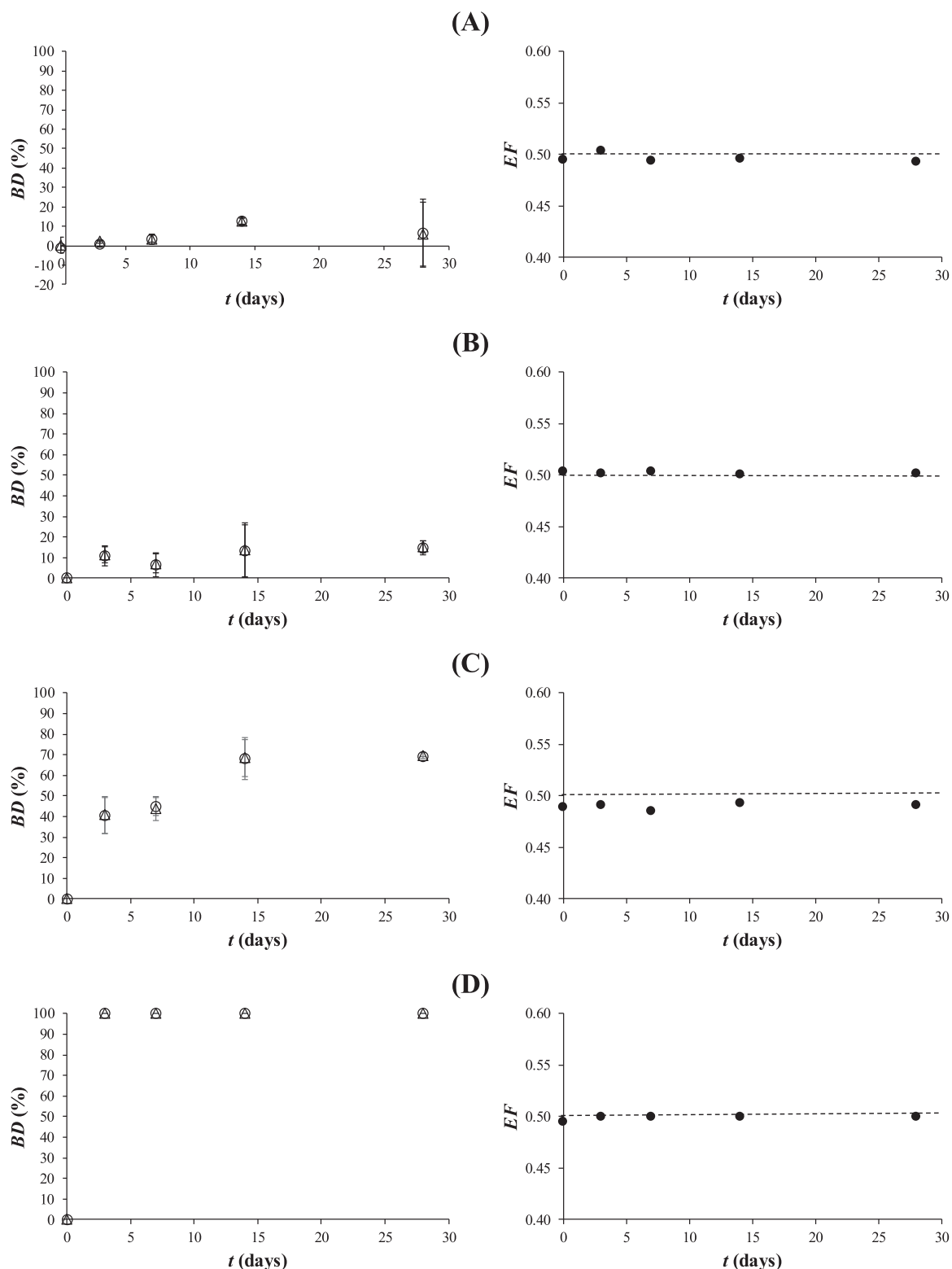


Fig. 2. Biodegradation (BD, %, mean \pm s from two replicates) calculated from peak areas using the Eq. (1) and enantiomeric fraction for (A) bupivacaine, (B) mepivacaine, (C) prilocaïne and (D) propanocaine by HPLC-MS. (\circ) BD for E1, less retained enantiomer; (Δ) BD for E2, most retained enantiomer; (\bullet) EF.

of the areas of chromatographic peaks to estimate the BD values in the present study. The slopes (b_1) of both enantiomers for PRILO and PROPA are statistically equal (assumption made in Eq. (2)), so the EF values could also be calculated using the direct chromatographic approach. However, for BUPI and MEPI, the values of b_1 were not statistically equal, and therefore, the EF could not be cal-

culated directly from the chromatographic peak areas, so concentration values were used instead.

According to the “fit-for-purpose concept”, full method validation of the current analytical method becomes unnecessary [28]. First, the method was not designed for routine sample analysis. Second, to obtain the biodegradation data, the estimation of con-

centrations is not necessarily required, since it is possible to use directly the peak areas measurements. Besides, performance features and quality assurance parameters of the same procedure have been established elsewhere for two drugs [22], and substantial differences are not expected.

3.3. Biodegradability assays

The OECD ready biodegradability tests have been thought as screening methods to determine whether a substance is or not potentially easily biodegradable or not [26,27]. The biodegradability assays for the enantiomers of local anaesthetics were performed in batch mode by duplicate (Section 2.3). Samples were incubated and collected at different times ($t=0, 3, 7, 14$ and 28 days) for the biotic and abiotic assays and analysed in the optimal chromatographic conditions (Table 4). Fluoxetine (FLX, 20 mg L⁻¹) was tested in parallel as reference substance to ensure the adequate activity of the microbial community in the test system [28]. According to the criteria established in a previous paper, if the biodegradation (BD) values after seven days of incubation (BD_{7d}) are within the 70 ± 11% range, the inoculum biodegradation capacity could be considered as normal. In the present case, a BD_{7d} of 69 ± 12% for FLX was obtained, indicating the adequacy of the inoculum and thus, the validity of the assays. The activity of the inoculum was also monitored by measuring the optical density at 600 nm.

Fig. 1 shows for each analyte two chromatograms corresponding to biotic samples taken at $t=0$ and 28 days. For BUPI and MEPI, there were only slight differences between the samples, which indicates a poor degree of degradation under the conditions assayed. Conversely, in the case of PRILO, there was a significant decrease in the peak areas of both enantiomers after 28 days of incubation. This decrease was even greater for PROPA, which was completely degraded during the assay (there were no peaks in the corresponding chromatogram, Fig. 1D). No appreciable differences between the areas of the chromatographic peaks of both enantiomers were observed for any compound, suggesting the non enantioselectivity of the processes involved in the degradation of the local anaesthetics.

Fig. 2 shows the BD values obtained during the biodegradability assays for the enantiomers of local anaesthetics (left part) as well as the corresponding EF (right part). The initial concentration of each enantiomer (S_0) was approximately 10 mg L⁻¹. Both BUPI and MEPI presented low values of biodegradation during the whole biodegradability assay. For the enantiomers of BUPI and MEPI, the maximum estimated degradation after 28 days of incubation in the biotic assay was approximately 10% and 15%, respectively. Regarding the abiotic assay (in the absence of inoculum), the degradation at the end of the test was around 5–10% for the enantiomers of both compounds. These results indicate that both, the biodegradation and the physicochemical degradation can be considered non-significant [26,27]. According to the criteria established in the OECD (Organization for Economic Co-operation and Development) guidelines, BUPI and MEPI enantiomers would not be readily biodegradable and could be considered as potentially persistent compounds. As expected due to lack of biodegradation, the values of EF remained constant and close to 0.5 (Fig. 2) during the biodegradability assays.

For both enantiomers of PRILO, the maximum estimated degradation at 28 days of incubation was approximately 69% and 23% in the biotic and abiotic assays, respectively. These results indicate that PRILO enantiomers exhibit incomplete but appreciable degradation, not only physicochemical but also microbiological ($BD - D > 20\%$). In the case of the enantiomers of PROPA, the complete degradation was achieved in only three (or less) days under biotic conditions. In the abiotic assay, the degradation remained not significant ($D < 20\%$) until $t=14$ days, which points out the major

contribution of the microbiological biodegradation to the degradation process. After 28 days of incubation, the values of degradation in abiotic conditions reached 53%, indicating that even in the absence of microorganisms, this compound is easily degraded by physico-chemical mechanisms.

According to the results obtained and the OECD guidelines [26,27], it can be concluded that PROPA and PRILO enantiomers exhibit ready aerobic biodegradability. For both PRILO and PROPA, the EF values remained close to 0.5 throughout the biodegradability assay, indicating the prevalence of non-enantioselective mechanisms in the degradation processes.

4. Conclusions

The comprehensive study on the chiral separation of bupivacaine, mepivacaine, prilocaine and propanocaine with eight polysaccharide-based chiral stationary phases in reversed phase conditions compatible with MS detection revealed that when using aqueous- MeOH mobile phases a typical reversed phase behaviour, i.e. the retention of compounds increased as the proportion of organic modifier in the mobile phase decreased. When ACN was used as organic modifier, for all the columns and compounds, the retention of compounds initially decrease for low water content in the mobile phase (HILIC behavior), while at the higher content (up to 20%(v/v) of water content) in the mobile phase retention increase (reverse-phase behavior). This explained effect is more evident for the column Cell3, Cell5 and Am1 for MEPI and PROPA.

In the conditions assayed, none of the columns provided the enantioselective separation of the four compounds studied. The polysaccharide-based CSPs tested presented different enantioselectivity towards the analytes. The Cell2 CSP allowed the baseline resolution of the enantiomers of mepivacaine, prilocaine and propanocaine. The Cell1, Am2 and Am3 CSPs were not able to completely resolve the enantiomers of any of the compounds. Except for bupivacaine, the use of acetonitrile as organic modifier in the mobile phase instead of methanol provided better resolution values. In general, the resolution increased as the retention increased. As far as we know, no references for the chiral separation of local anaesthetics in reversed phase conditions compatible with MS detection using polysaccharide-based stationary phases exist for bupivacaine, prilocaine and propanocaine.

The adequate mobile phases for the separation of the local anaesthetics studied were used to perform an enantioselective biodegradability study. Under the conditions tested, the enantiomers of bupivacaine and mepivacaine were not significantly degraded, so they can be considered potentially persistent. On the contrary, propanocaine and prilocaine exhibited ready biodegradability. No enantioselective biodegradation was observed for any local anesthetic studied. As far as we know, this is the first study on the enantioselective biodegradation reported for these compounds.

Declaration of Competing Interest

The authors declare no conflict of interest.

CRediT authorship contribution statement

Mireia Pérez-Baeza: Investigation, Validation. **Laura Escuder-Gilabert:** Methodology, Visualization, Writing - review & editing. **Yolanda Martín-Biosca:** Supervision, Writing - original draft, Writing - review & editing. **Salvador Sagrado:** Methodology, Software, Formal analysis, Data curation. **María José Medina-Hernández:** Supervision, Project administration, Writing - review & editing.

Acknowledgments

The authors acknowledge the Spanish Ministerio de Economía y Competitividad (MINECO) and the European Regional Development Fund (ERDF) for the financial support (Project CTQ2015-70904-R, MINECO/FEDER, UE). Mireia Pérez Baeza acknowledges to Generalitat Valenciana and European Social Fund for the contribution to the contract ACIF/2019/158.

References

- [1] D.E. Becker, K.L. Reed, Local Anesthetics, Review of pharmacological considerations, *Anesth. Prog.* 59 (2012) 90–102.
- [2] M. Gitman, M.R. Fettiplace, G.L. Weinberg, J.M. Neal, M.J. Barrington, Local anesthetic systemic toxicity: a narrative literature review and clinical update on prevention, diagnosis, and management, *Plastic Reconstruct. Surg.* 144 (2019) 783–795.
- [3] L.E. Mather, Stereochemistry in anesthetic and analgetic drugs, *Minerva Anesthesiol.* 71 (2005) 507–516.
- [4] Z. Shedania, R. Kakava, A. Volonterio, T. Farkas, B. Chankvetadze, Separation of enantiomers of chiral sulfoxides in high-performance liquid chromatography with cellulose-based chiral selectors using acetonitrile and acetonitrile-water mixtures as mobile phases, *J. Chromatogr. A* 1609 (2020) 460445.
- [5] B. Chankvetadze, Recent trends in preparation, investigation and application of polysaccharide-based chiral stationary phases for separation of enantiomers in high-performance liquid chromatography, *Trends Anal. Chem.* 122 (2020) 115709.
- [6] R.W. Stringham, K.Y. Yun, Chiral separation of amines by high-performance liquid chromatography using polysaccharide stationary phases and acidic additives, *J. Chromatogr. A* 1101 (2006) 86–93.
- [7] T. Zhang, D. Nguyen, P. Franco, Y. Isobe, T. Michishita, T. Murakami, Cellulose tris (3, 5-dichlorophenylcarbamate) immobilised on silica: a novel chiral stationary phase for resolution of enantiomers, *J. Pharm. Biomed. Anal.* 46 (2008) 882–891.
- [8] K.S.S. Dossou, P. Chiap, B. Chankvetadze, A.C. Servais, M. Fillet, J. Crommen, Enantioresolution of basic pharmaceuticals using cellulose tris (4-chloro-3-methylphenylcarbamate) as chiral stationary phase and polar organic mobile phases, *J. Chromatogr. A* 1216 (2009) 7450–7455.
- [9] K.S.S. Dossou, P. Chiap, B. Chankvetadze, A.C. Servais, M. Fillet, J. Crommen, Optimization of chiral pharmaceuticals enantioseparation using a coated stationary phase with cellulose tris (4-chloro-3-methyl-phenylcarbamate) as chiral selector and non-aqueous polar mobile phase, *J. Sep. Sci.* 33 (2010) 1699–1707.
- [10] K.S.S. Dossou, P. Chiap, A.C. Servais, M. Fillet, J. Crommen, Evaluation of chlorine containing cellulose-based chiral stationary phases for the LC enantioseparation of basic pharmaceuticals using polar non-aqueous mobile phases, *J. Sep. Sci.* 34 (2011) 617–622.
- [11] K.S.S. Dossou, P. Chiap, A.C. Servais, M. Fillet, J. Crommen, Development and validation of a LC method for the enantiomeric purity determination of S-ropivacaine in a pharmaceutical formulation using a recently commercialized cellulose-based chiral stationary phase and polar non-aqueous mobile phase, *J. Pharmaceut. Biomed.* 54 (2011) 687–693.
- [12] T. Zhang, P. Franco, D. Nguyen, R. Hamasaki, S. Miyamoto, A. Ohnishi, T. Murakami, Complementary enantio-recognition patterns and specific method optimization aspects on immobilized polysaccharide-derived chiral stationary phases, *J. Chromatogr. A* 1269 (2012) 178–188.
- [13] L. Peng, S. Jayapalan, B. Chankvetadze, T. Farkas, Reversed-phase chiral HPLC and LC/MS analysis with tris (chloromethylphenylcarbamate) derivatives of cellulose and amylose as chiral stationary phases, *J. Chromatogr. A* 1217 (2010) 6942–6955.
- [14] T. Zhang, D. Nguyen, P. Franco, Reversed-phase screening strategies for liquid chromatography on polysaccharide-derived chiral stationary phases, *J. Chromatogr. A* 1217 (2010) 1048–1055.
- [15] B. Petrie, R. Barden, B. Kasprzyk-Hordern, A review on emerging contaminants in wastewaters and the environment: current knowledge, understudied areas and recommendations for future monitoring, *Water Res.* 72 (2015) 3–27.
- [16] V. Geissen, H. Mol, E. Klumpp, G. Umlauf, M. Nadal, M. van der Ploeg, S.E.A.T.M. van de Zee, C.J. Ritsema, Emerging pollutants in the environment: a challenge for water resource management, *Int. Soil Water Conserv. Res.* 3 (2015) 57–65.
- [17] E. Sanganyado, Z. Lu, Q. Fu, D. Schlenk, J. Gan, Chiral pharmaceuticals: a review on their environmental occurrence and fate processes, *Water Res.* 124 (2017) 527–542.
- [18] C.S. Wong, Environmental fate processes and biochemical transformations of chiral emerging organic pollutants, *Anal. Bioanal. Chem.* 386 (2006) 544–558.
- [19] B. Kasprzyk-Hordern, Pharmacologically active compounds in the environment and their chirality, *Chem. Soc. Rev.* 39 (2010) 4466–4503.
- [20] A.R. Ribeiro, L.H.M.L.M. Santos, A.S. Maia, C. Delerue-Matos, P.M.L. Castro, M.E. Tiritan, Enantiomeric fraction evaluation of pharmaceuticals in environmental matrices by liquid chromatography-tandem mass spectrometry, *J. Chromatogr. A* 1363 (2014) 226–235.
- [21] L. Escuder-Gilabert, Y. Martín-Biosca, S. Sagrado, M. Pérez-Baeza, M.J. Medina-Hernández, Trimeprazine is enantioselectively degraded by an activated sludge in ready biodegradability test conditions, *Water Res.* 141 (2018) 57–64.
- [22] L. Escuder-Gilabert, Y. Martín-Biosca, M. Pérez-Baeza, S. Sagrado, M.J. Medina-Hernández, Direct chromatographic study of the enantioselective biodegradation of ibuprofen and ketoprofen by an activated sludge, *J. Chromatogr. A* 1568 (2018) 140–148.
- [23] O. Frédéric, P. Yves, Pharmaceuticals in hospital wastewater: their ecotoxicity and contribution to the environmental hazard of the effluent, *Chemosphere* 115 (2014) 31–39.
- [24] A.G. Asimakopoulos, P. Kannan, S. Higgins, K. Kannan, Determination of 89 drugs and other micropollutants in unfiltered wastewater and freshwater by LC-MS/MS: an alternative sample preparation approach, *Anal. Bioanal. Chem.* 409 (2017) 6205–6225.
- [25] P.C. Rúa-Gómez, W. Püttmann, Occurrence and removal of lidocaine, tramadol, venlafaxine, and their metabolites in German wastewater treatment plants, *Environ. Sci. Pollut. R.* 19 (2012) 689–699.
- [26] OECD, Test No. 302B, Inherent Biodegradability: Zahn-Wellens/EVPA Test, OECD Publishing, Paris, 1992 <http://dx.doi.org/>, doi:10.1787/9789264070387-en.
- [27] OECD, Revised Introduction to the OECD Guidelines for Testing of Chemicals, Section 3, OECD Guidelines for the Testing of Chemicals, Section 3, OECD Publishing, Paris, 2006 <http://dx.doi.org/>, doi:10.1787/9789264030213-en.
- [28] Y. Martín-Biosca, L. Escuder-Gilabert, M. Pérez-Baeza, S. Sagrado, M.J. Medina-Hernández, Biodegradability features of fluoxetine as a reference compound for monitoring the activity of activated sludges in drug biodegradation studies, *Int. J. Ad. Res. Chem. Sci.* 6 (2019) 16–23.
- [29] C. Hansch (Ed.), Comprehensive medicinal chemistry. Cumulative subject index & drug compendium, 6, Pergamon Press, Oxford, Reino Unido, 1990 vol.

